African Union
Scientific Technical Research Commission

African Scientific Research and Innovation Council

ASRIC journal

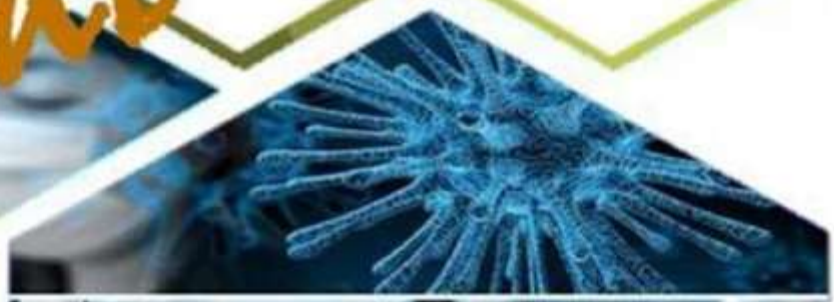

2023

Natural Sciences

Vol. 3, Issue 1

ASRIC JOURNAL ON NATURAL SCIENCES

Vol. 3, Issue 1 2023

African Scientific Research and Innovation Council

Copyright © African Scientific Research and Innovation Council, 2023
Published by: African Scientific Research and Innovation Council
Plot 114 Yakubu Gowon Crescent Asokoro
Abuja, Nigeria

asric_editor@yahoo.com
www.asric.africa

ISSN 2795-3610 (online), 2795-3629 (print))

The views expressed in the *ASRIC Scientific Journals* are those of the authors and not necessarily those of the African Scientific Research and Innovation Council; the African Union Scientific, Technical and Research Commission; or the organisations that they belong to.

EDITORIAL BOARD

Editor in Chief:

Prof Mosto Onuoha — University of Nigeria, Nsukka, Nigeria; mosto.onuoha@gmail.com

Editorial Board:

Prof. Lawrence Ezemonye — Igbinedion University, Okada, Nigeria; ezemslaw@yahoo.com

Prof. Kirk T. Semple — Lancaster University, UK; K.semple@lancaster.ac.uk

Dr Sammia Shahid — University of Management and Technology, Pakistan; res.dean@umt.edu.pk

The editorial correspondence should be sent to:
Editor-in-Chief, ASRIC Scientific Journals,
African Scientific Research and Innovation Council,
Plot 114 Yakubu Gowon Crescent Asokoro
Abuja, Nigeria

Table of Contents

Policy Framework for Managing Decommissioned Solar Power Systems in the Niger Delta: A Scientometric Report Okorhi Ojiyovwi Johnson, Richard John Azubuike, Uhunmwangho Roland…….….1

Cybersecurity Resilience Maturity Assessment Tool for Critical National Information Infrastructure Victor Emmanuel Kulugh, Uche M. Mbanaso and Gloria Chukwudebe…18

Urban Flood Vulnerability and Risk Mapping using Multi-Criteria Analysis in Mzuzu City, Malawi Donnex Chilonga, Mabvuto Tembo……..35

Improved Organically Treated Nanoclay-Polyurethane Nanocomposite Mona A. Ahmed, Ashraf M. El-Saeed, Hamdy M. Naguib…….42

Fencing Lands to Enhanced Climate Change Resilience, promoting Biodiversity Regeneration and Improved Livelihoods of Climate Change in Makueni County Frank Wesonga, Francis Keya……47

Isotherm, Kinetic and Thermodynamic Terms of Adsorption of Pyrimethamine from Binary Aqueous Solution Adesokan Saheed Ademola, Giwa Abdur-Rahim Adebisi……50

Phytochemical Analysis, Antibacterial and Antioxidant Activity of Stem Extracts of Azadirachta indica Yiketel Adege Chekol, Molla Zewdie Eshetu…….59

Comparative Evaluation of Glycemic index (GI) of some Traditional Dishes consumed in Enugu North Senatorial zone of Enugu State, Nigeria Umerah Nkemjika Nnedinso.66

High Performance Liquid Chromatography Assay of Cyclopiazonic Acid in Some Stored Cereals from the Agro-Ecological Zones of Nigeria Peter Francis Adikwu, Okibe Friday Godwin, Abgaji Edith Bolanle, Hussaini Makun Anthony……..78

Development Of Novel Commercial Production Protocol for High-Yielding Oyster Mushrooms (Pleurotus Species) Adebayo Elijah Adegoke ……..84

Influence of Rock Mass Properties and Discontinuity with Explosive Charge on Muck-Pile Size Distribution Adebayo Babatunde, Ajaka Ebenezer O. , Afeni Thomas B., Akinbinu Victor A., Okewale Ismail A., Lawal Abiodun I., Apena Waliu O., Ogunyemi Bidemi O., Amigun John O…….91

The Utilization of Solid Waste Transfer Stations in Managing Solid Waste in Rapidly Transforming Neighborhoods. The Case of Sinza Ward in Dar Es Salaam City, Tanzania. David Mihigo……101

Exploring the Efficacy of a Potent Corrosion Suppressant Derived from Trandescantia Pallida (Purpple Heart) Leaves: A Qualitative Assessment Cornelius C. Ahanotu, Kenneth C. Madu , Cynthia A. Ugochukwu …….113

Composition, antioxidant and antimicrobial activities of volatile oils from *Lantana camara* Linn Ayopo A. Sotade, Clement O. Ajiboye, Olapeju O. Aiyelaagbe……125

Fermentation Enhances the Attenuation of Oxidative Stress by Sugar Apple Cotyledon Polysaccharides Christianah Adebimpe Dare, Oluokun Oluboade Oyedapo……132

Cytotoxic Evaluation of the Aqueous Extract of some Selected Medicinal Plants Combinations on Lung Carcinoma Epithelial Cells A549 and Human Cervix Carcinoma HeLa S330194 Tossou Sandra Bénédicta Kadoukpè, Luka Carrol Domkat, Emmanuel Adeyemi, Jeffrey Matthew, Taiwo Emmanuel Alemika…….145

Revolutionizing Industrial Cleaning Techniques: Harnessing the Power of Algae and Sponge Iron to Combact Co2 in Biogas Production Julius Ibeawuchi Onyewudiala, Nnadikwe Johnson[1], Iheme Chigozie, Ibe Raymond Obinna, Alaka, Amarachi Chekosiba, Onuruka Anthony Uzodinma……..163

Advancing Environmental Technology Through Computational Fluid Dynamics (CFD) and Design Simulation Analysis for Enhanced Performance and Sustainability Ewelike Asterius Dozie, Nnadikwe Johnsone, Iheme Chigozie, Chikodi Daberechi Alaka, Wopara Onuoha Fidelis, Akuchie Justin Chukwuma……173

Ctgan Adversarial Attack on Network Intrusion Detection Based on Lstm Algorithm Ahmad Abubakar Yunusa, Fatima Umar. Zambuk, Badamasi Imam. Ya'u, Abubakar Umar, Abdulkadir Hassan Disina[5]……..182

Innovative Approaches to Achieving Dynamics Design in Biogas System: A Comprehensive Study on Integral Proceeding Emeribe Happiness Ebere, Nnadikwe Johnson, Obilor Meshack Chinaka, Ibe Raymond Obinna, Amarachi Chekosiba Alaka…194

Smart Bandage Plant: A report on Isolation of Trigonelline and Methoxy Quercetin from the Methanol Extract of Pennisetum Pedicellatum (Trin) (Poaceae) Malah Mohammed AJi, Abubakar Samaila, Danbature Wilson Lamayi……210

Identification of high Groundwater Potential Locations in the Atebubu Municipality of Ghana using the Electrical Resistivity Method Alfred K. Bienibuor, Kwasi Preko, Akwasi A. Aning, Aboagye Menyeh, David D. Wemegah……..220

Potential Applications of Débélé Clays (Guinea): Formulation of Ceramic Compositions and Hydraulic Binders Balde Mamadou Yaya, Sidibe Diaka, Simo Bakam Éric Severin, Djangang Njiomou Chantale, Blanchart Philippe……237

ASRIC JOURNAL ON NATURAL SCIENCES

Available online at www.asric.org
ASRIC Journal on Natural Sciences Vol 3(1) (2023) 1-17

Policy Framework for Managing Decommissioned Solar Power Systems in the Niger Delta: A Scientometric Report

Okorhi Ojiyovwi Johnson[1]*, Richard John Azubuike[2], Uhunmwangho Roland[3]

[1]Dennis Osadebay University, Asaba, Delta State, Nigeria
[2]Institute of Engineering, Technology and Innovation Management (METI),
University of Port Harcourt, Rivers State, Nigeria
[3]Electrical/Engineering Department, University of Port Harcourt, Rivers State, Nigeria

*Corresponding author: johnson.okorhi@dou.edu.ng

Abstract
The Niger Delta region has experienced substantial growth in the deployment of solar power systems (SPSs) to meet the energy requirements of its populace. As these systems reach their end-of-life, appropriate management strategies are crucial to minimize environmental footprints and maximize resource recovery. This scientometrics paper was aimed at assessing government regulations for managing decommissioned SPSs in the core Niger Delta. The study adopted a quantitative approach method using questionnaire as the research instrument. Thirty six (36) government officials from the strata of 3 States were investigated on the policy framework deployed for decommissioned SPSs. Both descriptive and inferential statistics were used in the analysis of data and discussion of results. Results revealed that government officials are inept with the policy instruments that promote renewable energy and green energy technologies in the setup of SPSs and its management at their end-of-life. Among others, it was recommended that these government agencies should embrace and domesticate the key 8 policy instruments, as well as implement sustainable management strategies therein for handling wastes from SPSs for the policy framework used in the study area.
Keywords: Solar power systems (SPSs), Niger Delta, Management Strategies, Solar PV panels

1.0 Introduction
The Niger Delta region covers nearly 75,000 km², making up 7.5% of Nigeria's land mass and regarded as one of the nine most difficult deltas globally (Nwogwugwu et al., 2012). From history and early cartography, it originally consists of today's Bayelsa, Delta and Rivers States. Of the nine coastal states of the Niger Delta, these three states remain referred to as the core Niger Delta (Benefit, *et al.*, 2014). With a population growth rate at 3.2%, the Niger Delta region has an estimated population of over 42 million people (National Bureau of Statistics, NBS, 2018). Consequent to the 3.2% growth rate, the core Niger Delta has an official population of 15,650,300 for 2022 (City Population, 2022). The region has reportedly remained a rugged terrain with grips of squalor, poor sanitation services, lack of basic infrastructure, habitat loss and environmental degradation (Sahara Reporters, 2022). Today, there are waste management reports indicating continuous and unaddressed threats to the Niger Delta region biodiversity (Ogolo, 2011; Benefit, et al., 2014; Donatus et al., 2021). Okorhi (2018) and Johnson, *et al*. (2019) had reported that one of the ways degradation set into the biodiversity of the Niger Delta is through the leaching of perilous wastes into the components of the environment. Environmental and health conditions were affected from air pollution through the burning of e-wastes, leaching of perilous compounds into ground and surface water at waste disposal sites, and the persistent organic pollutants (toxins) on soil. These were partly attributed to stakeholders' poor management practices and strategies deployed in handling solid wastes. The authors concluded by identifying a "disconnect between policy and practice" for waste management in the Nigeria.

Generally, the management of decommissioned solar power systems (SPSs) is an emerging research topic in Nigeria and beyond. Several empirical studies are focused on potential environmental impacts, general waste management issues, and the need for sustainable solutions. However, there is lack of comprehensive policies specifically tailored to the region of the Niger Delta because of its uniqueness. For instance, environmental impacts and challenges studies are characterized with highlights of various environmental concerns associated with decommissioned solar power systems, like the presence of toxins (e.g., lead and cadmium) in solar PV panels, improper disposal of wastes, and the release of greenhouse gases during the dismantling process leading to contamination of components of the environment. Besides, sparse recycling facilities, inadequate waste management infrastructure, and lack of awareness among stakeholders pose major challenges too. Secondly, resource recovery and circular economy approach which are efforts meant towards resource recovery from decommissioned SPSs were equally discussed in several studies. These researches emphasized the importance of adopting a circular economy approach to extract valuable materials and promote recycling. The recovery of metals, such as copper, silver, and silicon, is identified as economically viable and environmentally beneficial. However, all these studies fall short of specific policy perspective dedicated to the management of SPSs in the core Niger Delta. A scientometrics report on policies for managing decommissioned solar power systems in the Niger Delta would therefore add to the topic by bridging the disconnect between policy and practice.

The Africa Clean Energy (2021) had reported that Nigeria is among the 10 African countries (Egypt, Madagascar, Ivory Coast, Nigeria, Ghana, Cameroon, Rwanda, Kenya, South Africa, and Zambia) that have specific electronic waste or e-waste legislation (law, act, regulatory, statutory instruments etc.) that are legally binding for the management of end-of-life EEE. By implication, Nigeria remains considered as a leading proponent in Africa for handling disused EEE (or e-waste) because of its specific regulations targeted at several e-products. Secondly, because of some mitigating challenges in handling electronic waste from renewable facilities, the federal government of Nigeria (FGN) initiated the promotion of additional policy measures in the framework for renewable energy setups to avert wastes from the environment, and thereby improving living conditions of citizenry and the pursuit of sustainability. This paper is therefore aimed at assessing regulations of the government for managing decommissioned solar PV power systems in the Niger Delta region. We would also consider testing a null hypothesis for this study. The hypothesis (H_0) states that "The EEE regulations for handling wastes from solar power systems (SPSs) are inadequate". In particular, this study would assess the implementation of the National Environmental (Electrical/Electronics Sector) Regulations, 2022 along with other policy instruments use in the framework of renewable energy power systems in Nigeria. Also, the study intends to address reports indicating the continuous and unaddressed threats from solar power system wastes to the biodiversity of the Niger Delta region. This is in order to further ignite and reassure the citizenry that renewable energy pursuit by the FGN could be built upon and sustained.

2.0 Clean energy and the significance of solar power systems option for Nigeria.

From reports, the Federal Government of Nigeria (FGN) had ensured a progressive policy direction on the diversification of the country's energy mix to promote the acceptance and usage of renewable energy as a major energy source (Adeniyi et. al, 2020; Alternative Energy Store, 2022). The government demonstrated this by creating a level playing ground, political will and commitments in developing strategies for off-grid sub-sector powered by renewable energy setup (Africa Clean Energy, 2019). The report further stated that the Nigeria Renewable Energy and Energy Efficiency Policy (NREEEP), 2015 submitted that an estimated investment of US$3.5 billion is required to accelerate the projected 30GW by 2030. In another report, the Nigeria market was considered to be among the fastest growing solar power systems (SPSs) markets around the world. This is because of the erratic and inadequate supply of electricity from government national grids to its populace. According to its operators, the growing solar PV panels market in Nigeria has been valued to be more than US$39 million, and employing over 10,000 persons (Isaac, February 26, 2018). The market is partly driven by rapid innovations in solar power devices, efficiency and reduction in prices for components of SPSs (solar panels, batteries and associated peripherals) (Netherlands Enterprise Agency, 2021). Reports of solar photovoltaic (PV) power systems setups within Nigeria by

individuals, in rural dwellings and marketplaces, street lightings, etc. are overwhelming. A report by Isaac (April 6, 2018) confirmed that some of these set-ups are located in agricultural farmlands for processing, lightening and other rural purposes. An example is the Innotech 18 Meter Tunnel Solar Dryer which is said to have helped farmers in drying pepper faster within half the required normal time. With the introduction of this innovative solar dryer, farmers' production time was cut to nearly half the normal time, and saving 40% of products that would have gone into the waste stream on the account of weather conditions and rodents damages. The solar panel system installations are locations at Kadabo and Baawa, both communities in Makarfi, Kaduna State (Isaac, April 6, 2018). Lagos State is also reckoned with installations of revolutionary solar-powered kiosks in marketplaces. These kiosks were seen strategically positioned mostly in food markets, with the traders preserving fresh vegetables and fruits in compartments of the solar-powered kiosks, while reducing food wastes. The solar powered refrigerators in kiosks were capable of elongating the shelf-life of agricultural products for between 2 to 21 days. While the high installation charges demanded upfront have deterred many of these desiring consumers within the lower segment in Nigeria, the government has equally introduced combine strategies to ignite a renewable energy pursuit using solar power systems. Some of these strategies are contained in policy framework for energy options, usage, acquisition, decommissioning and handling of obsolete solar PV power systems. For the purpose of this study, we present in Table 1 relevant policy instruments and their promoters on solar PV power systems setup.

Table 1: Framework for solar PV power systems in Nigeria

Regulations/Laws/Legislations/Acts/ for Solar PV Power Systems Management in Nigeria		**Proponents**
i	National Environmental (Energy Sector) Regulations, 2014	National Environmental Standards and Regulations Enforcement Agency (NESREA)
ii	National Renewable Energy and Energy Efficiency Policy (NREEEP), 2015	Federal Ministry of Power
iii	National Energy Efficiency Action Plan, 2016 (NEEAP)	Federal Ministry of Power, Work and Housing
iv	National Renewable Energy Action Plan, 2016 (NREAP)	Federal Ministry of Power, Work and Housing
v	National Environmental (Sanitation and Wastes Control) Regulation S.I.28 of 2009	NESREA
vi	National Environmental (Electrical/Electronics Sector) Regulations, 2022	NESREA

Regardless of the framework represented in Table 1, Nigeria is still challenged with the implantation of policies in the renewable energy sector. By April, 2018, BusinessDay newspaper brought to the knowledge of the public that Nigeria's clean energy ambitions is been hampered with reported transboundary movement of decommissioned solar PV panels into Nigeria, the socioeconomic impacts, and government's huge tariffs on items for setting up renewable energy systems (Isaac, April 6, 2018). This report titled "New import duty on solar panels: How Nigeria preys on dreams" was another fact-finding article from Isaac Anyaogu. The report reckoned that the Nigerian Customs Service (NCS) had an imposed levy of 5% duty and another 5% value added tax (VAT) on all new solar PV panels imported into Nigeria. Until 2018, imported solar PV panels were exempted from duties payable to government base on Nigeria's HS Codes classification for imports. Hitherto, the NCS classified solar PV panels under the code: 85414000 classifications which attracted zero duty. In addition, the government appeared to be defiant in providing incentives for operators as part of its policy commitments for accelerating the energy transition as contained in sub-section 2.1.2, Supporting Policies and Measure, of the NREEEP (2015). These and other issues have become challenging to operators and lenders in the renewable energy sector, thereby reducing the pace for solar power systems set in Nigeria. This has equally hindering the policy drive for "generating 30% of its electricity through renewable energy and to the tune of 30GW target by 2030 from renewable energy sources, especially through solar power programme" in the Niger Delta and beyond (FMP,

2015; Isaac, April 6, 2018). Furthermore, stakeholders on the sector are apparently uninformed on the extended producer responsibility (EPR) programme for electrical and electronic equipment (EEE) at their end-of-life. The pursuit of EPR programme for solar PV devices is stipulated under Part II—General Provisions, sub-section 21 and in Schedule VI of the National Environmental (Energy Sector) Regulations, (2014). This is a key strategy to sound environmental management of decommissioned components of solar PV power systems and its peripherals (NESREA, 2014; Isaac, February 26, 2018).

3.0 Framework for Handling Waste from Solar Power Systems in the Niger Delta

Pursuant to assessing government regulations for managing decommissioned solar PV power systems in the Niger Delta region, we adopted a conceptual framework (Figure 1) for "Management Strategies for Handling E-Waste from Solar Devices in Selected Cities of the Niger Delta" by John (2022). It showcases the Scope, Proponents and Strategic aspects of the framework. It revealed "What" is involved, "Who" is a stakeholder and "How" the implementation of policy is dished out. In a nutshell, the management strategies for wastes from solar power systems (SPSs) could be systematically organized under six components viz.: legal and regulatory framework, institutional arrangements, strategic planning, sensitization and participation, waste scheme funding, as well as waste generation and handling (Okorhi, 2018). Because waste electrical and electronic equipment (WEEE) is a specialized waste type, the legal and regulation framework for handling waste from SPSs in the Niger Delta is mainly drawn from the policy instruments listed in Table 1. These policy instruments have sessions and stipulations that are dedicated to strategies for handling of disused devices from SPSs. These six regulations targeted at renewable energy and sustainability in power supply in Nigeria are summarized as follow:

a) The National Environmental (Energy Sector) Regulations, 2014 speaks to preventing or minimizing pollution as well as encouraging energy efficiency in all operations and ancillary undertakings of the energy sector toward achieving a sustainable economic development in Nigeria (NESREA, 2014). The sources for renewable energy should be obtained from solar, hydro, wave, wind, geothermal and biomass. Part II of the General Provisions of the regulation stipulates that the disposal of hazardous waste, like decommissioned SPSs, on land or water without prior treatment is strictly prohibited, and that every power generating facility should have a "sustainable community relations programme" as part of compliance to corporate social responsibility (CSR).

b) The National Renewable Energy and Energy Efficiency Policy (NREEEP), 2015 was designed to remove major barriers to renewable energy and energy efficiency pursuit in Nigeria at an economic, regulatory and institutional advantages compared to other forms of energy sources. It is intended that the policy would serve as a blue print for the sustainable expansion, supply and deployment of renewable energy resources within the Nigeria economy for on-grid and off-grid energy solutions (Federal Ministry of Power, 2015). The sources of renewable energy were targeted at solar energy, biomass, wind, small and medium hydro, tide, geothermal and wave energy. Solar energy resource intensity was considered to be generally high in Nigeria and should be harnessed for agricultural processing purposes, street, homes and park lightings, among others using solar energy conversion technologies, such as photovoltaic materials (cells or modules) for setting up SPSs. The idea is also to extend the plans to the informal sector and rural communities which are inadequately captured in the national accounts for electricity supply and thereby contributing to the national accounts a minimum electricity supply of 3% by year 2020 and 6% by year 2030.

c) The National Energy Efficiency Action Plan (NEEAP) 2016 is aimed at the effective and efficient energy use and proposes key areas for energy efficiency and conservation to be considered. Also, the policy hinge on pursuing the goal for the "Solar Thermal Program (SOLTRAIN) in West Africa" that meant at contributing to a switch over from the use of fossil fuel based energy supplies to a cleaner and sustainable energy supply system that is based on renewable energies from solar power systems (Federal Ministry of Power, Work and Housing, FMPWH, 2016a).

d) The National Renewable Energy Action Plan (NREAP), 2016 is drafted for strategy implementation of the National Renewable Energy and Energy Efficiency Policy (NREEEP) 2015. The policy provides a summary on concrete guidelines, regulations, laws, incentives and strategies to be implemented in achieving Nigeria's quest in renewable energy targets and sustainable energy supply for its citizenry. Also, Nigeria's contribution to renewable energies to achieving its national target under the ECOWAS Renewable Energy Policy (EREP) was target at 23% by 2020 and 31% by 2030 renewable energy (FMPWH, 2016b).

e) Part II of the General Provisions, sub-section 25 in the National Environmental (Energy Sector) Regulations, 2014 had stipulated that all power generating facility shall ensure that generated wastes should be handled and disposed as recommended in the National Environmental (Sanitation and Wastes Control) Regulation S.I.28 of 2009. Generally, strategies for solid waste management and environmental sanitation practices for all categories of wastes are primarily drawn from the National Environmental (Sanitation and Wastes Control) Regulation S.I.28 of 2009 (NESREA, 2009). In the policy document, Part 2 of the Environmental Sanitation Section, Sub-section 11(a) – (II. Duties and Obligations) promotes the stratification of hazardous wastes like decommissioned solar PV panels, batteries, inverters, etc. from non-hazardous municipal wastes. Besides, Sub-section III (44-53) – "Hazardous Waste Control" was particularly dedicated to strategies for handling and disposing hazardous wastes in Nigeria. It equally classified generated hazardous waste under Schedules 13 and 14 of the regulation.

f) The National Environmental (Electrical/Electronics Sector) Regulations, 2022 is a unique policy that is specifically dedicated to the managing waste from electrical and electronic equipment (EEE) in the Nigeria environment. It was first enacted in 2011 and then reviewed in 2022. The broad objective of the new regulation is to provide strategies for minimizing and preventing pollution operations and relative activities into the environment in the electrical and electronic sector (NESREA, 2022). It promoted strategies on extended producer responsibility (EPR), best practices for handling e-wastes or WEEE, restrictions on toxin effluent, WEEE handling, permit issuance and revocation, offences and penalties, among others. In the 1st Schedule [regulation 2(3)] EEE were classified into 10 categories of goods. Solar PV panel which is the principal device used in the installation of SPSs is classified under grey goods – ICT and telecommunication equipment. By implication the 2022 Electrical/Electronics Sector Regulations is the foremost guideline for handling end-of-life devices from decommissioned solar power systems (SPSs).

POLITICAL CONTEXT

	OBJECTIVES
Scope (What?)	**PLANNING AND MANAGEMENT** • Strategic planning • Legal and regulatory framework • Public participation • Financial management • Institutional arrangements • Disposal facility Siting
	SOLAR WASTE GENERATION • Solar waste characterisation • Solar waste minimisation and source separation
	SOLAR WASTE HANDLING • Solar waste collection • Solar waste transfer, intermediate storage, treatment and disposal
	GOVERNMENT AGENCIES • NESREA • State Environment Protection Agencies • LGA Environmental Health office

Proponents (Who?)	• Nigeria Customs Service • Standards Organisation of Nigeria (SON)
	BUSINESS SECTOR • Dealers/Marketers/Retailers
	INFORMAL SECTOR • Technicians/Refurbishers/Scavengers
	END-USERS • Households, Government Institutions, Industries, Private Offices, • Trading/Agricultural Businesses, • Banks, Educational & Health-Care Centres
	SUPPORT AGENCIES • National Environmental Standards and Regulations Enforcement Agency (NESREA), Abuja • Federal Ministry of Power, Abuja • European Union Commission, Europe • Basel Convention Secretariat, Switzerland
Strategic Aspects (How?)	**POLITICAL** • Formulation of goals and priorities, • Determination of roles and jurisdiction, and • Establishment of Legal and Regulatory Framework.
	INSTITUTIONAL • Arrangements and Sectorial Integration
	SOCIAL • Patterns of Solar waste usage, generation and disposal of the population, and the associated Solar waste management needs and demands, • End-user participation in Solar waste management activities, and the • Ethical issues on Solar waste workers, both formal and informal.
	FINANCIAL • Budgeting and cost accounting systems, • Resource mobilisation for Solar waste funding, • Cost recovery and operational financing, • Cost control
	ECONOMICAL • Impact of Solar waste management services on the productivity and development of the economy, • The economic effectiveness of Solar waste management systems, • Conservation and efficient use of materials and resources, and • Job creation and income generation in Solar waste management activities.
	TECHNICAL • technical planning and design of Solar waste management systems, • Solar waste collection systems, • Intermediate storage and transfer systems, • Solar waste recovery, repair, reuse, recycling and disposal management
ECONOMIC CONTEXT	

Figure 1: Conceptual framework for "Management Strategies for Handling E-Waste from Solar Devices in Selected Cities of the Niger Delta" in John, 2022

4.0 Materials and Methods

The study took place in selected local government areas (LGAs) in the core Niger Delta, comprising Delta, Rivers and Bayelsa States (Kimiebi, 2010). Table 2 represents a population of the 9 purposively selected LGAs in the Core Niger Delta. Of this population, three (3) stakeholders (monitoring/regulatory agencies, recycler/technicians/traders and end-users) involved in the pursuit of renewable energy setups and management. They were investigated using distinct questionnaires for each listed group. The sample size was determined as 400 using the Yamane formulae computation, while the distribution criterion for questionnaires was informed by Ogbuene (2014). However, this report presents results from government monitoring/regulatory agencies surveyed in the study area. In addition, Table 3 gives a schedule of questionnaire administered to these stakeholders, where government senior officials involved in policy planning and implementation for renewable energy pursuit and waste management were considered in eliciting information from the Regulatory/Monitoring Agencies sector. The choice of these officials was purposive because certain distinct data sets on the policies investigated were necessitated and could not be obtained from the other categories of respondents. For even spread, at least one urbanized LGA was picked from each strata of States in the study area. Hence, 4 questionnaires were administered to the respondents in each LGA. These 36 respondents were drawn from the federal and state environmental protection agencies, local government environmental offices and other government policing agencies. Both descriptive and inferential statistics were presented, analysed and discussed in the section that followed.

Table 2: Population of selected LGAs in the Core Niger Delta

Metropolis (City)	**State**	**Local Government Area**	**Population in 2006 (NBS, 2013)**	**Estimated population in 2022**	**Estimated population by City**	**Percentage**	**Number of Questionnaire**
Asaba	Delta	Oshimili South	150,032	214,846	214,846	06.08%	024
Warri metropolis	Delta	Warri South West	116,538	166,882	1,087,913	30.80%	123
	Delta	Warri South	311,970	446,741			
	Delta	Uvwie	188,728	270,259			
	Delta	Udu	142,480	204,031			
Port Harcourt metropolis	Rivers	Obio-Akpor	462,350	662,085	1,705,658	48.29%	193
	Rivers	Eleme	190,194	272,358			
	Rivers	Port Harcourt City	538,558	771,215			
Yenegoa	Bayelsa	Yenegoa	*(395,615)	523,794	523,794	14.83%	060
Total				**3,532,211**	**3,532,211**	**100%**	**400**

**Estimated population in 2010 for Yenegoa is 395,615*

Source: Extrapolated from National Bureau of Statistics, NBS (2013)

Table 3: Schedule of Questionnaire Administered

Stakeholders	Number Administered	Number Retrieved	% of Number Retrieved	Number of Valid Retrieved Questionnaire	% of Valid Retrieved Questionnaire
Regulatory/Monitoring Agencies	36	36	100.00	34	94.44
Distributors/ Recyclers	90	82	91.11	69	76.67
Consumers/End-Users	274	252	91.97	206	75.18
Total	**400**	**370**	**92.50%**	**309**	**77.25%**

Source: Field Survey, 2022

5.0 Results

Sequel to Table 2 representation of number of questionnaires administered (36), number of questionnaires retrieved (36) and number of valuable questionnaires retrieved (34), we present an analysis of the respondents with Table A1 and Figure A1. The respondents from the Regulatory and Monitoring Agencies were drawn from government agencies like the Federal Ministry of Environment, National Environmental Standards and Regulations Enforcement Agency (NESREA), State Environmental Protection Agencies from Bayelsa, Rivers and Delta, Local Government Area

Health Offices, Government/Private Waste Management Firms, Nigerian Custom Service, as well as Federal Ministry of Power.

Table A1: Analysis of the Respondents

Organization/ Occupation	**Frequency**	**Cumulative Frequency**	**%**
REGULATORS/MONITORING AGENCIES: (Federal Ministry of Environment, NESREA, State Environmental Protection Agencies, Local Government Health Offices, Government/Private Waste Management Firms, Nigerian Custom Service, Federal Ministry of Power)	34	34	100
Total	**34**		**100**

Source: Field Survey, 2022

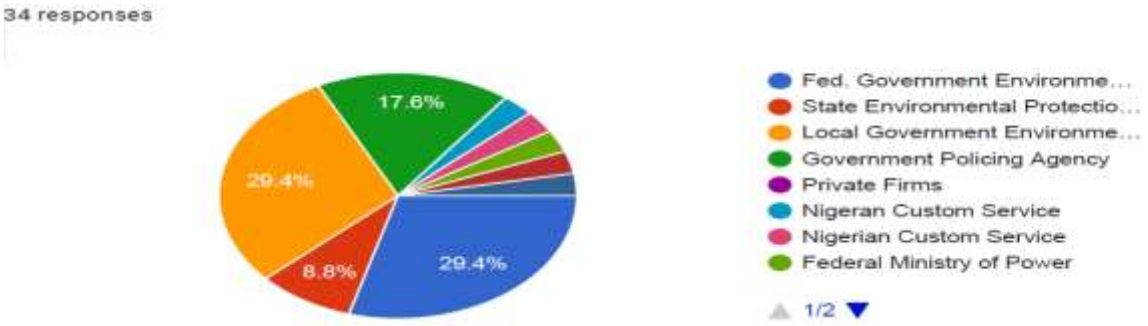

Figure A1: Schema of respondents (Regulatory and Monitoring Agencies (36))

The respondents for this study were primarily senior government officers who are responsible for the planning, execute, monitor and regulating strategies for the policy framework deployed for managing wastes from Solar PV Systems in the study area. These officials subsequently suggest improvements, adoption and promotion of frontier measures that are sustainable for the management of WEEE in Nigeria. We discuss this framework by first analysing the applicable guideline(s) adopted and promoted by these agencies for conducting routine management of wastes from SPSs, and thereafter assessing the strategies deployed for implementation in the Niger Delta region. Table 1 had a listing of six (6) national policy instruments approved for use by the regulatory and legislative agencies.

5.1 Waste management policies for solar power systems (SPSs) in the Niger Delta

From Table B1, it is revealed that 20 (59%) respondents opined that they deploy 2 state environmental edicts from Delta and Rivers in addition to the 6 FGN regulatory instruments in the management of decommissioned solar PV systems. Together, eight (8) regulations are deployed in the study area. The number of guidelines falls short of the waste management by-laws for Bayelsa State, owing to government officials' restriction, show of confidentiality and unwillingness to release the State's by-law before and during the survey.

Table B1: Policy instruments used by government officials in managing decommissioned solar PV systems in the Niger Delta

	Regulation/Law/Legislations/Acts/ in carrying out routine management of decommissioned solar PV systems	Very Great Extent	Great Extent	Small Extent	Very Small Extent	Not At ALL	Total No. of Respondents
I	National Environmental (Energy Sector) Regulations, 2014	9	11	11	2	1	34
Ii	National Energy Efficiency Action Plan, 2016 (NEEAP)	4	10	6	12	2	34
Iii	National Renewable Energy and Energy Efficiency Policy (NREEEP), 2015	1	13	7	11	2	34
Iv	National Renewable Energy Action Plan, 2016 (NREAP)	2	12	8	10	2	34

V	The National Environmental (Electrical/Electronics Sector) Regulations S.I. No. 23 of 2011	7	13	8	3	3	34
Vi	The National Environmental (Sanitation and Wastes Control) Regulation S.I.28 of 2009	11	12	6	3	2	34
Vii	Others	Delta State Waste Management law Rivers State Waste Management Authority Law					34

Statistics

		National Environmental (Energy Sector) Regulations, 2014	National Energy Efficiency Action Plan, 2016 (NEEAP)]	National Renewable Energy and Energy Efficiency Policy (NREEEP), 2015	National Renewable Energy Action Plan, 2016 (NREAP)	The National Environmental (Electrical/Electronics Sector) Regulations S.I. No. 23 of 2011	The National Environmental (Sanitation and Wastes Control) Regulation S.I.28 of 2009
N	Valid	34	34	34	34	34	34
	Missing	0	0	0	0	0	0
Mean		3.74	3.06	3.00	3.06	3.53	3.79
Median		4.00	3.00	3.00	3.00	4.00	4.00
Std. Deviation		1.024	1.179	1.044	1.071	1.187	1.175
Range		4	4	4	4	4	4
Minimum		1	1	1	1	1	1
Maximum		5	5	5	5	5	5

Other legislative provisions (including State edits) that form part of the policy framework adopted and applicable in managing disused wastes from solar devices in the Niger Delta

		Frequency	Percent	Valid Percent	Cumulative Percent
Valid	Rivers State Waste Management Authority Law	17	50.0	50.0	50.0
	Delta State Waste Management Board Law	3	8.8	8.8	58.8
	Nil	14	41.2	41.2	100.0
	Total	34	100.0	100.0	

Source: Field Survey, 2022

5.2 Waste management plans and strategies for decommissioned solar power systems (SPSs)

Table B2 further assessed the appropriateness of adopted regulations for the management of end-of-life solar PV system setups.

Table B2: Adequacy of adopted legislations deployed by government officials

Are these additional national guidelines - "Harmful Waste (Special Criminal Provisions) Act Cap H1 LFN 2004 and the National Environmental Protection (Waste Management) Regulations S.I.15 of 1991" relevant to decommissioned solar PV systems management

		Frequency	Percent	Valid Percent	Cumulative Percent
Valid	Not at all	1	2.9	2.9	2.9
	Very small	7	20.6	20.6	23.5
	Small	8	23.5	23.5	47.1
	Great	10	29.4	29.4	76.5
	Very Great	8	23.5	23.5	100.0
	Total	34	100.0	100.0	

Are the management strategies in the regulatory framework adequate for the effective handling of end-of-life solar PV systems?

		Frequency	Percent	Valid Percent	Cumulative Percent
Valid	Very small	5	14.7	14.7	14.7
	Small	12	35.3	35.3	50.0
	Great	15	44.1	44.1	94.1
	Very Great	2	5.9	5.9	100.0
	Total	34	100.0	100.0	

From the existing national regulations, is there a minimum collection targets and handling expertise defined for the States in the Niger Delta to be followed for the management of wastes from solar devices?

		Frequency	Percent	Valid Percent	Cumulative Percent
Valid	Not at all	12	35.3	35.3	35.3
	Very small	6	17.6	17.6	52.9
	Small	5	14.7	14.7	67.6
	Great	10	29.4	29.4	97.1
	Very Great	1	2.9	2.9	100.0
	Total	34	100.0	100.0	

Are there provisions in the policy documents that promotes cascaded application and second life for end-of-life solar PV devices?

		Frequency	Percent	Valid Percent	Cumulative Percent
Valid	Not at all	6	17.6	17.6	17.6
	Very small	8	23.5	23.5	41.2
	Small	11	32.4	32.4	73.5
	Great	9	26.5	26.5	100.0
	Total	34	100.0	100.0	

When it becomes necessary, do you adopt any foreign regulations in the management process of solar device wastes?

		Frequency	Percent	Valid Percent	Cumulative Percent
Valid	Not at all	8	23.5	23.5	23.5
	Very small	9	26.5	26.5	50.0
	Small	11	32.4	32.4	82.4
	Great	6	17.6	17.6	100.0
	Total	34	100.0	100.0	

Are there financing mechanisms or reward for formal recycling of solar PV systems included in the integrated policy framework?

		Frequency	Percent	Valid Percent	Cumulative Percent
Valid	Not at all	7	20.6	20.6	20.6
	Very small	9	26.5	26.5	47.1
	Small	8	23.5	23.5	70.6
	Great	6	17.6	17.6	88.2
	Very Great	4	11.8	11.8	100.0
	Total	34	100.0	100.0	

Statistics

		Are these additional national guidelines - Harmful Waste (Special Criminal Provisions) Act Cap H1 LFN 2004 and the National Environmental Protection (Waste Management) Regulations S.I.15 of 1991 â€“ relevant to decommissioned solar PV systems management	Are the management strategies in the regulatory framework adequate for the effective handling of end-of-life solar PV systems?	From the existing national regulations, is there a minimum collection targets and handling expertise defined for the States in the Niger Delta to be followed for the management of wastes from solar devices?	Are there provisions in the policy documents that promotes cascaded application and second life for end-of-life solar PV devices?	When it becomes necessary, do you adopt any foreign regulations in the management process of solar device wastes?	Are there financing mechanisms or reward for formal recycling of solar PV systems included in the integrated policy framework?
N	Valid	34	34	34	34	34	34
	Missing	0	0	0	0	0	0
Mean		3.50	3.41	2.47	2.68	2.44	2.74
Median		4.00	3.50	2.00	3.00	2.50	3.00
Std. Deviation		1.161	.821	1.331	1.065	1.050	1.310
Range		4	3	4	3	3	4
Minimum		1	2	1	1	1	1
Maximum		5	5	5	4	4	5

Source: Field Survey, 2022

Eighteen 18 (53%) respondents admitted that the national guidelines like the "Harmful Waste (Special Criminal Provisions) Act Cap H1 LFN 2004 and "National Environmental Protection (Waste Management) Regulations S.I.15 of 1991" were also pertinent to 6 FGN key policy instruments listed in Table B1 for the management of decommissioned SPSs in the Niger Delta. But half of the FGN respondents (17(50%)) admitted that the deployed management strategies in the policy framework for obsolete solar PV systems were inadequate or ineffective. Besides, it was revealed that the minimum set targets in the national regulations as management strategies for the collection of wastes for solar devices as well as handling expertise stipulated for States of the Niger Delta is not adhered to. Eighteen (18) (53%) respondents confirmed that set targets for collecting and handling of solar PV system wastes were not followed through. However, 11(32%) respondents admitted to a small extent that there are strategies in the policy framework that promotes the recovery and recycling of decommissioned solar PV devices, while another 8(24%) respondents debunked this position to be at a very small extent, and 6(18%) respondents further opined that the strategies promoting recovery and recycling for such wastes are not tenable in the study area. More so, 11 (32%) respondents agreed to a small extent that they adopt foreign regulations as part of the management strategies for solar device wastes generated. With 6(18%) respondents affirmed strongly to incorporating foreign management strategies during implementation. Nevertheless, there are close indifferences in adjudging inclusion of government financial mechanisms in the integrated policy framework to promote formal recycling of decommissioned SPSs. From Table B2, 7(21%) respondents strongly disagree, 9 (27%) respondents slightly disagreed, 8(24%) respondents agreed to a small extent, 6(18%) respondents agreed, and 4(14%) respondents totally agreed to the inclusion of financial mechanisms during the implementation process.

5.3 Hypothesis Test and Interpretation (H_o1)

A regression statistical was used to test the relationship between the dependent variable (response Y) and independent variables (predictors k) on the main research question: What are the standard government regulations deployed for managing decommissioned SPSs in the Niger Delta region? The null hypothesis H_o1 is stated as: "The EEE regulations for handling wastes from solar power systems

(SPSs) are inadequate". Here, the dependent variable is considered as "the extent of knowledge and participation of regulatory and monitoring agencies in the formulated policies, laws/legislatures, guidelines and regulations relating to wastes from SPSs". And the independent variables include the quantitative responses on management standards and disposal strategies deployed in the study area. Table B3 reveals analysis on questions for hypothesis H_0 (1). Here A linear multiple regression test was carried out on questions relating to government policies, regulations, laws, acts, legislations, edits, guidelines, standards etc. for handling wastes from SPSs.

Table B3: Linear multiple regression test for hypothesis $H_0$1

Regression

Notes		
Output Created		15-JAN-2023 18:40:05
Comments		
Input	Data	
	Active Dataset	DataSet1
	Filter	<none>
	Weight	<none>
	Split File	<none>
	N of Rows in Working Data File	34
Missing Value Handling	Definition of Missing	User-defined missing values are treated as missing.
	Cases Used	Statistics are based on cases with no missing values for any variable used.
Syntax		REGRESSION /MISSING LISTWISE /STATISTICS COEFF OUTS R ANOVA /CRITERIA=PIN(.05) POUT(.10) /NOORIGIN /DEPENDENT @1.AreyouawareofanyspecificRegulationsLawsLegislationsActsforsol /METHOD=ENTER @1.Amongtheprovisionslistedbelowticktheapplicableguidelinesusedb @1.Amongtheprovisionslistedbelowticktheapplicableguidelinesuse_A @1.Amongtheprovisionslistedbelowticktheapplicableguidelinesuse_B @1.Amongtheprovisionslistedbelowticktheapplicableguidelinesuse_C @1.Amongtheprovisionslistedbelowticktheapplicableguidelinesuse_D @1.Amongtheprovisionslistedbelowticktheapplicableguidelinesuse_E @2.Otherthanthoselistedinquestion1abovepleaseindicateotherlegisl v2.
Resources	Processor Time	00:00:00.03
	Elapsed Time	00:00:00.05
	Memory Required	38416 bytes
	Additional Memory Required for Residual Plots	0 bytes

Variables Entered/Removed[a]

Model	Variables Entered	Variables Removed	Method
1	Are these additional national guidelines â€“ Harmful Waste (Special Criminal Provisions). Act Cap H1 LFN 2004 and the National Environmental Protection (Waste Management) Regulations S.I.15 of 1991 â€“ relevant to decommissioned solar PV systems management, Among the provisions listed below, tick the applicable guideline(s) used by your firm/business in carrying out routine management of end-of-life lithium batteries: [National Environmental (Energy Sector) Regulations, 2014], Among the provisions listed below, tick the applicable guideline(s) used by your firm/business in carrying out routine management of end-of-life lithium batteries: [National Energy Efficiency Action Plan, 2016 (NEEAP)], Among the provisions listed below, tick the applicable guideline(s) used by your firm/business in carrying out routine management of end-of-life lithium batteries: [The National Environmental (Electrical/Electronics Sector) Regulations S.I. No. 23 of 2011, Other than those listed in question 1 above, please indicate other legislative provisions (including State edits) that form part of the policy framework adopted and applicable in managing disused wastes from solar devices in your jurisdiction of work, Among the provisions listed below, tick the applicable guideline(s) used by your firm/business in carrying out routine management of end-of-life lithium batteries: [National Renewable Energy Action Plan, 2016 (NREAP)], Among the provisions listed below, tick the applicable guideline(s) used by your firm/business in carrying out routine management of end-of-life lithium batteries: [The National Environmental (Sanitation and Wastes Control) Regulation S.I.28 of 2009], Among the provisions listed below, tick the applicable guideline(s) used by your firm/business in carrying out routine management of end-of-life lithium batteries: [National Renewable Energy and Energy Efficiency Policy (NREEEP), 2015][b]		Enter

a. Dependent Variable: Are you aware of any specific Regulations/Laws/Legislations/Acts for solar PV components management in the Niger Delta?
b. All requested variables entered.

Model Summary

Model	R	R Square	Adjusted R Square	Std. Error of the Estimate
1	.577[a]	.333	.120	1.297

a. Predictors: (Constant), Are these additional national guidelines “Harmful Waste (Special Criminal Provisions) Act Cap H1 LFN 2004 and the National Environmental Protection (Waste Management) Regulations S.I.15 of 1991“ relevant to decommissioned solar PV systems management, Among the provisions listed below, tick the applicable guideline(s) used by your firm/business in carrying out routine management of end-of-life lithium batteries: [National Environmental (Energy Sector) Regulations, 2014], Among the provisions listed below, tick the applicable guideline(s) used by your firm/business in carrying out routine management of end-of-life lithium batteries: [National Energy Efficiency Action Plan, 2016 (NEEAP)], Among the provisions listed below, tick the applicable guideline(s) used by your firm/business in carrying out routine management of end-of-life lithium batteries: [The National Environmental (Electrical/Electronics Sector) Regulations S.I. No. 23 of 2011, Other than those listed in question 1 above, please indicate other legislative provisions (including State edits) that form part of the policy framework adopted and applicable in managing disused wastes from solar devices in your jurisdiction of work, Among the provisions listed below, tick the applicable guideline(s) used by your firm/business in carrying out routine management of end-of-life lithium batteries: [National Renewable Energy Action Plan, 2016 (NREAP)], Among the provisions listed below, tick the applicable guideline(s) used by your firm/business in carrying out routine management of end-of-life lithium batteries: [The National Environmental (Sanitation and Wastes Control) Regulation S.I.28 of 2009], Among the provisions listed below, tick the applicable guideline(s) used by your firm/business in carrying out routine management of end-of-life lithium batteries: [National Renewable Energy and Energy Efficiency Policy (NREEEP), 2015]

ANOVA[a]

Model		Sum of Squares	df	Mean Square	F	Sig.
1	Regression	21.028	8	2.629	1.563	.186[b]
	Residual	42.030	25	1.681		
	Total	63.059	33			

a. Dependent Variable: Are you aware of any specific Regulations/Laws/Legislations/Acts for solar PV components management in the Niger Delta?

b. Predictors: (Constant), Are these additional national guidelines "Harmful Waste (Special Criminal Provisions) Act Cap H1 LFN 2004 and the National Environmental Protection (Waste Management) Regulations S.I.15 of 1991" relevant to decommissioned solar PV systems management, Among the provisions listed below, tick the applicable guideline(s) used by your firm/business in carrying out routine management of end-of-life lithium batteries: [National Environmental (Energy Sector) Regulations, 2014], Among the provisions listed below, tick the applicable guideline(s) used by your firm/business in carrying out routine management of end-of-life lithium batteries: [National Energy Efficiency Action Plan, 2016 (NEEAP)], Among the provisions listed below, tick the applicable guideline(s) used by your firm/business in carrying out routine management of end-of-life lithium batteries: [The National Environmental (Electrical/Electronics Sector) Regulations S.I. No. 23 of 2011, Other than those listed in question 1 above, please indicate other legislative provisions (including State edits) that form part of the policy framework adopted and applicable in managing disused wastes from solar devices in your jurisdiction of work, Among the provisions listed below, tick the applicable guideline(s) used by your firm/business in carrying out routine management of end-of-life lithium batteries: [National Renewable Energy Action Plan, 2016 (NREAP)], Among the provisions listed below, tick the applicable guideline(s) used by your firm/business in carrying out routine management of end-of-life lithium batteries: [The National Environmental (Sanitation and Wastes Control) Regulation S.I.28 of 2009], Among the provisions listed below, tick the applicable guideline(s) used by your firm/business in carrying out routine management of end-of-life lithium batteries: [National Renewable Energy and Energy Efficiency Policy (NREEEP), 2015]

Coefficients[a]

Model		Unstandardized Coefficients		Standardized Coefficients	t	Sig.
		B	Std. Error	Beta		
1	(Constant)	.450	2.647		.170	.866
	Among the provisions listed below, tick the applicable guideline(s) used by your firm/business in carrying out routine management of end-of-life lithium batteries: [National Environmental (Energy Sector) Regulations, 2014]	.583	.292	.432	1.997	.057
	Among the provisions listed below, tick the applicable guideline(s) used by your firm/business in carrying out routine management of end-of-life lithium batteries: [National Energy Efficiency Action Plan, 2016 (NEEAP)]	.211	.571	.180	.369	.715
	Among the provisions listed below, tick the applicable guideline(s) used by your firm/business in carrying out routine management of end-of-life lithium batteries: [National Renewable Energy and Energy Efficiency Policy (NREEEP), 2015]	-.260	.908	-.196	-.286	.777
	Among the provisions listed below, tick the applicable guideline(s) used by your firm/business in carrying out routine management of end-of-life lithium batteries: [National Renewable Energy Action Plan, 2016 (NREAP)]	.333	.515	.258	.647	.523
	Among the provisions listed below, tick the applicable guideline(s) used by your firm/business in carrying out routine management of end-of-life lithium batteries: [The National Environmental (Electrical/Electronics Sector) Regulations S.I. No. 23 of 2011	.189	.279	.162	.678	.504

Among the provisions listed below, tick the applicable guideline(s) used by your firm/business in carrying out routine management of end-of-life lithium batteries: [The National Environmental (Sanitation and Wastes Control) Regulation S.I.28 of 2009]	.063	.400	.053	.157	.876
Other than those listed in question 1 above, please indicate other legislative provisions (including State edits) that form part of the policy framework adopted and applicable in managing disused wastes from solar devices in your jurisdiction of work	.213	.339	.149	.630	.535
Are these additional national guidelines â€“ Harmful Waste (Special Criminal Provisions) Act Cap H1 LFN 2004 and the National Environmental Protection (Waste Management) Regulations S.I.15 of 1991 â€“ relevant to decommissioned solar PV systems management	-.605	.282	-.509	-2.144	.042

a. Dependent Variable: Are you aware of any specific Regulations/Laws/Legislations/Acts for solar PV components management in the Niger Delta?

Source: Field Survey, 2022

The Regression Criteria = $P < 0.05$ implies we reject the null hypothesis. The comparable values for regression inferential statistics are the Beta, β coefficients: $H_0 1$ are $\beta_1 = 0.432$; $\beta_2 = 0.180$; $\beta_3 = -0.196$; $\beta_4 = 0.258$; $\beta_5 = 0.162$; $\beta_6 = 0.053$; $\beta_7 = 0.149$ and $\beta_8 = -0.509$. The R-square is given as 0.333 or R^2 = (33%). The question "…the applicable guideline(s) used by your firm/business in carrying out routine management of end-of-life lithium batteries: [National Environmental (Energy Sector) Regulations, 2014]" has Beta (β_1) = 0.432 when compared with the tabulated p-value (P_1) = 0.057. This result reveals that the variable is significant. Next, the question "the applicable guideline(s) used by your firm/business in carrying out routine management of end-of-life lithium batteries: [National Energy Efficiency Action Plan, 2016 (NEEAP)]" has Beta (β_2) = 0.180 which is comparably (P_2) = 0.715. However, this result implies that the variable tested is insignificant. We compute and compare for the others as follow for $\beta_3 - \beta_8$ and $P_3 - P_8$: $\beta_3 = -0.196$: $P_3 = 0.777$, $\beta_4 = 0.258$: $P_4 = 0.523$, $\beta_5 = 0.162$: $P_5 = 0.504$, $\beta_6 = 0.053$: $P_6 = 0.876$, $\beta_7 = 0.149$: $P_7 = 0.535$, and $\beta_8 = -0.509$: $P_8 = 0.042$. From the above results, the P-values ($P_3 - P_8$) are found to be greater than the comparable Beta coefficient (β) significant values. Therefore the tested variables become insignificant. So, we are to accept the null hypothesis $H_0 1$: "The EEE regulations for handling wastes from solar power systems (SPSs) are inadequate", since most p-values (except P_8) were greater than P = 0.05. These findings agrees with field observations and anecdotal claims by stakeholders that there remain inadequate action of management functions that starts with proper planning, organising, leading, handling and control of wastes from decommissioned SPSs.

6.0 Conclusions and Recommendations

This scientometrics report highlights the emerging issue of managing decommissioned solar power systems (SPSs) in the core Niger Delta, and emphasizes the need for comprehensive policies to operate. Following data elicited, processed and analyzed for the study "…policies for managing decommissioned solar power systems in the Niger Delta", the discussions and tested hypothesis confirmed that officials from government regulatory/monitoring agencies are unaware of key regulations/guidelines that promotes renewable energy and green energy technologies, including SPSs setup and management at their end-of-life. Some of the important regulations listed in Table 1 remain key to promoting the setup of solar PV power systems and in handling wastes from decommission SPSs. To ensure environmental sustainability, resource use and recovery, as well as circular economy principles, it is pertinent for stakeholders to collaborate and implement recommended policies. Therefore, we recommend to the regulatory/monitoring agencies that they should urgently embrace, domesticate and implement sustainable management strategies in handling waste from SPSs as contained in the 6 policy instruments listed in Table 1, along with individual state environmental edicts (region-specific policies), the Harmful Waste (Special Criminal Provisions) Act Cap H1 LFN 2004, and the National Environmental (Sanitation and Wastes Control) Regulation S.I.28 of 2009.

Furthermore, additional research and continuous monitoring are needed to evaluate the effectiveness of these policies and refine them over time.

7.0 References

Africa Clean Energy Technical Assistance Facility, ACE TAC (2019). *Importation Guide for Solar PV Products and Technologies in Nigeria*. https://www.ace-taf.org/wp-content/uploads/2020/01/ACE-NIGERIAN-IMPORTATION-GUIDE-2019122001.pdf

Africa Clean Energy Technical Assistance Facility, ACE TAC (2021). *E-Waste Guide for Stand-Alone Solar in Nigeria.* Coffey International Development Ltd, United Kingdom. https://www.ace-taf.org/wp-content/uploads/2020/01/ACE-NIGERIAN-IMPORTATION-GUIDE-2019122001.pdf

Alternative Energy Store Inc (2022). *Components for Your Solar Panel (Photovoltaic) System*. https://www.altestore.com/diy-solar-resources/components-for-your-solar-panel-photovoltaic-system/

Benefit O., Suresh S., Surendran and Trevor P. (2014). Impact of Inadequate Urban Planning on Municipal Solid Waste Management in the Niger Delta Region of Nigeria. *Journal of Sustainable Development*. Vol. 7(6). ISSN 1913-9063 E-ISSN 1913-9071.

City Population (March 21, 2022). *NIGERIA: States & Cities Federal Republic of Nigeria*. https://www.citypopulation.de/en/nigeria/cities/

Donatus A. O., Marianna K. & Vladimir G. (2021). Proliferation of household waste irregular dumpsites in Niger Delta region (Nigeria): unsustainable public health monitoring and future restitution. *Sustainable Environment Research*. Vol 31(4). https://doi.org/10.1186/s42834-020-00077-1

Federal Ministry of Power (2015). *National Renewable Energy and Energy Efficiency Policy (NREEEP)*. Approved by FEC for the Electricity Sector. http://admin.theiguides.org/Media/Documents/NREEE%20POLICY%202015-%20FEC%20APPROVED%20COPY.pdf

Federal Ministry of Power, Work and Housing, FMPWH (2016a). *National Renewable Energy Action Plans (NREAP) (2015 – 2030)*. First Version Adopted by the Inter-Ministerial Committee on Renewable Energy. https://www.se4all-africa.org/fileadmin/uploads/se4all/Documents/Country_PANER/Nigeria_National_Renewable_Energy_Action_Plans_.pdf

FMPWH (2016b). *National Renewable Energy Action Plan (NREAP), 2016 (2015-2030)*. Approved by the National Council on Power (NACOP), July 14, 2016. https://www.all-on.com/media/publications/simplified-guides-to-nigerias-energy-access-policies-and-regulations/_jcr_content/par/textimage.stream/1595008848747/8d18c624aa6792e0c9afe79f1bd595831a7d0697/national-renewable-energy-action-plan-nreap.pdf

Isaac Anyaogu (April 6, 2018). New import duty on solar panels: How Nigeria preys on dreams. *BusinessDay*. https://businessday.ng/uncategorized/article/new-import-duty-solar-panels-nigeria-preys-dreams/

Isaac Anyaogu (February 26, 2018). INVESTIGATION: Nigeria's solar energy revolution stirs toxic battery waste management concern. *BusinessDay*. https://businessday.ng/investigations/article/investigation-nigerias-solar-energy-revolution-stirs-toxic-battery-waste-management-concern/

John Richard (2022). *Management Strategies for Handling E-Waste from Solar Devices in selected Cities of the Niger Delta*. (Reg. No. G2022/PHD/METI/CETM/FT/006). [Doctoral Thesis, University of Port Harcourt, River State, Nigeria].

Johnson O. O., Joe E. A., Helen O. A., Roland U. & Anthony C. O. (2019). Disconnect between policy and practice in developing countries: Evidence of managing e-waste from Nigeria. *African Journal of Science, Technology, Innovation & Development*. Vol. 11 (4). https://hdl.handle.net/10520/EJC-16f21c3121

Kimiebi, I. E. (2010). *Oil, Militancy and Political Opportunities in Niger Delta*. http://kimiebi.blogspot.com/2010/02/oil-militancy-and-amnesty-politics-in.html

Adeniyi A., Dolapo K., Muriel C., Olufolasewa S. & Uyiosa O. (2020). In review: renewable energy policy and regulation in Nigeria. An extract from The Renewable Energy Law Review, 3rd Edition. *The Law Reviews, Lexology*. https://www.lexology.com/library/detail.aspx?g=47feee75-9538-4500-ab77-54c9b64dfe1f

National Bureau of Statistics, NBS, (May, 2018). *2017 Demographic Statistics Bulletin. National Bureau of Statistics*. https://nigerianstat.gov.ng/download/1241121

National Environmental Standards and Regulations Enforcement Agency, NESREA (2009). *National Environmental (Sanitation and Wastes Control) Regulations 2009*. Federal Republic of Nigeria Official Gazette. N0.60 Abuja – 6th October, 2009 Vol.96. Government Notice No. 281. The Federal Government Printer, Lagos, Nigeria. FGP 112/102009/1,000 (0L 54)

NESREA (2022). National Environmental (Electrical/Electronic Sector) Regulations, 2022. Vol. 109. No. 142 of 2022, Federal Republic of Nigeria Official Gazette No. 50 Lagos – 5th September, 2022. Lagos: The Federal Government Printer, Lagos, Nigeria. FGP186/122022/105. B3451 – 3514.

NESREA (2022). *National Environmental (Electrical/Electronic Sector) Regulations 2022*. Federal Republic of Nigeria Official Gazette No. 160 Lagos – 5th September, 2022. Vol. 109, Government Notice No. 142. The Federal Government Printer, Lagos, Nigeria. FGP86/122022/150.

NESREA, (2014). *National Environmental (Energy Sector) Regulations, 2014*. No. 141 Lagos - 22nd December, 2014 Vol. 102. Government Notice No. 254. The Federal Government Printer, Lagos, Nigeria. FGP 153/102015/300.

Netherlands Enterprise Agency (2021). *Solar Report Nigeria*. https://www.rvo.nl/sites/default/files/2021/06/Solar-Report-Nigeria.pdf

Nwogwugwu, N., Alao O. E. a& Egwuonwu, C. (2012). Militancy and Insecurity in the Niger Delta: impact on the inflow of foreign direct investment to Nigeria. Kuwait Chapter of *Arabian Journal of Business and Management Review* Vol. 2(1); https://www.researchgate.net/publication/265426995_Militancy_and_Insecurity_in_the_Niger_Delta_impact_on_the_inflow_of_foreign_direct_investment_to_Nigeria

Ogolo, J. I. (2011, December). *Waste management development to protect water resources in the Niger Delta Region*. [WATER AND SOCIETY] WIT Transactions on Ecology and the Environment. Vol 153 (2011). DOI: 10.2495/WS110201

Okorhi Johnson (2018). *Assessment of Management Strategies for Waste Electrical and Electronic Equipment in South Eastern Nigeria* (Reg. No. G2012/PHD/METI/CETM/FT/013). [Doctoral Thesis, University of Port Harcourt, River State, Nigeria]

Sahara Reporters (September 28, 2022). *Niger Delta Communities Poorest In Nigeria, In Depressing Condition Despite Oil Wealth – Report*. Sahara Reporters. https://saharareporters.com/2022/09/28/niger-delta-communities-poorest-nigeria-depressing-condition-despite-oil-wealth-report

Available online at www.asric.org
ASRIC Journal on Natural Sciences Vol 3(1) (2023) 18-33

Cybersecurity Resilience Maturity Assessment Tool for Critical National Information Infrastructure

Victor Emmanuel Kulugh[1*], Uche M. Mbanaso[2] and Gloria Chukwudebe[3]

[1,2]Centre for Cyberspace Studies, Nasarawa State University, Keffi, Nigeria
[3]School of Information and Communication Technology, Federal University of Technology, Owerri, Nigeria

*Corresponding author: Kulughvictore@nsuk.edu.ng

Abstract
Cybersecurity resilience maturity assessment of critical national information infrastructure (CNII) is an important process in ensuring that organisations' capability for resilience are measured and gaps determined vis-à-vis targeted resilience for the purpose of improvements. However, existing solutions do not provide an automated quantitative tool to enable organisation conduct the assessment of their cybersecurity resilience posture at defined regular intervals. This paper presents the cybersecurity resilience maturity assessment tool (CRMAT). The CRMAT is built on the cybersecurity resilience maturity assessment framework and the cybersecurity resilience maturity assessment model (CRMAM). While the CRMAF and CRMAM provide requirements and computational algorithms for the tool respectively. The agile methodology of the software development life cycle (SDLC) was adopted with the MVC (model-view-controller) architectural pattern to implement the software. The software tool has two interfaces, namely; admin interface that enables the setup of the cybersecurity controls and other parameters that will form the basis for the assessment and a report generation interface for all the cybersecurity controls. CRMAT was demonstrated on 31 CNIII organisations and result showed its capability to successfully and accurately compute the CNII resilience index (CNIIRI) and the indexes of other cybersecurity controls indicated in the CRMAF. Comparative analysis of the results showed that 5 (16.13%) of the organisations are in Q4, 9 (29.03%) are in Q3 while 13 (41.94%) and 4 (12.90%) are in Q2 and Q1 respectively. The implication is that the organisations in Q4 has optimised resilience while those in Q1 have the weakest cybersecurity resilience.
Keywords: cybersecurity; maturity model; resilience; cybersecurity resilience; maturity assessment

Introduction
This paper is a software implementation of the cybersecurity resilience maturity assessment framework and model developed in [1]. Critical national information infrastructures (CNII) support nations and organisations to provide critical services and functions. As critical digital assets, their cybersecurity resilience has increasingly become important to sustain continuous operation of modern organisations and nations. The fact that CNII vulnerabilities are further expanding with increased application of existing and emerging technologies amidst a constantly evolving threat landscape [2] further enforces the need for increased assessment of their resilience for proactive actions, geared towards sustaining their resilience. Failure of critical digital assets have potentials for catastrophic outcomes as a result of cascading, escalating and common cause effects [3] that will be propagated through their interconnectedness and interdependencies created based on their networked nature [4]. The foregoing underpins the need to have a system that measures the resilience of CNII systems at regular intervals, especially that they are technology-based systems that are constantly evolving. However, attempts at providing solutions with respect to the maturity assessment of CNII assets fall short of providing tools that automate the process of assessment and maintain data that supports the tracking of progress made. Several works either defined the metrics, formulate frameworks and models and formulate maturity models but did not implement a software-based solution. Software-based solutions will potentially provide tools that organisations can use at set intervals to measure

their resilience, establish gaps and improve on those gaps to have better resilience system. Data obtained from previous measurements can be used to track progress in cybersecurity resilience assessment. Such tools can also be used by regulators to audit CNII organisations to ensure that they are resilient enough to support national security, economy and safety in the event of cyberattacks or other forms of failures. Consequently, this article presents the cybersecurity resilience maturity assessment tool (CRMAT) a software that is built on sound theoretical and methodological foundation. The CRMAT has the capability to support organisations' resilience assessments, compute various resilience indices based on defined metrics and indicators and compare organisations as well as compare the performance of indicators within the organisation. The rest of the paper presents the background and related works in section 2; section 3 features the methodology; conceptualization of CRMAT presented in section 4; while section 5 contains the software implementation of the CRMAT as section 6 presents the testing/results. Sections 7 and 8 present the evaluation of CRMAT and conclusion respectively.

2. Background and Related Works

Critical national information infrastructures support modern societies to provide vital functions and services to the population. However, they exposed to the vulnerabilities and threat landscape of their underlying information and operations technology. Thus, the compelling need for them to be resilient against cyberattacks. CNII resilience in this context refers to their capacity to resist cyberattacks, respond effectively to successful attacks without allowing system to degrade beyond tolerable levels and successfully recover to optimal service within set mean time to recovery (MTTR) [5]–[7]. To achieve resilience in terms of the afore mentioned capabilities (resistance, response and recovery), these capabilities have to be constantly measured [8], [9]. This can be achieved through the design and implementation of fit for purpose maturity models (MM). MMs provide data that potentially form the basis for organisations to appreciate the current state of the performance of their systems, identify gaps and point the path to closing these gaps for improved systems resilience [10]–[13]. There have been several research efforts geared towards providing solutions that constantly measure the cybersecurity resilience maturity of digital assets using maturity models (MM). For instance, [14], argued that the cyber-trust programme in the kingdom of Bahrain has the potentials to positively affect the cybersecurity resilience of organisation by increasing their compliance and implementation of cybersecurity controls. However, the work did not highlight any implementation of a process of measuring the maturity of cybersecurity resilience. Although, [15] discussed the measurement of the resilience of critical infrastructure that supports the smart city, the work was more concerned with addressing the physical threats to the physical elements of those CI and thus did not address the digital aspects of the CI. The work in [16] developed and organize effective resilience metrics for cyber systems using the resilience matrix framework developed in their earlier work. A matrix that recognises the interactions between each domain of an organisation (physical, information, cognitive and social) across each stage of the event management cycle (plan/prepare, absorb, recover and adopt) was generated for the purpose of managing the resilience of cyber systems. However, the work did not elaborate on how this matrix could be used to capture measurements of resilience in organisation that will lead to exposing the gaps in the resilience of cyber systems in the organisation. Consequently, no tool was developed, nor data generated to enable the testing of the proposed methodology. [17] illustrated how resilience could be assessed through the elucidation of indicators that might be useable in its assessment through the bridging of the gap between the theoretical and practical foundations of resilience by attempting to remove the definitional ambiguity of the concept of resilience. While the article defined a number of new resilience enhancing indicators, the authors failed to establish a relationship among these indicators that will lead to the development of a model for the assessment of resilience. [7] proposed a methodology for assessments of resilience of systems from assets/facility level, organisation and community or regional levels was proposed. However, the authors presented a basic framework for measuring resilience at the infrastructure level with a single survey. Although CI (inter)dependencies were discussed in the article, the debates did not link these dependencies and interdependencies to the underlying cyber infrastructure that are responsible for the quantum and sophistication of the interconnections leading to interdependencies with potentials for cascading and escalating failures. Consequently, the article failed to address resilience assessment at the cyber layer

which constitutes the epicentre of cyber risk in today's infrastructure and also form the core of this article.

In [18] the authors focused on identifying the key components of, and formulating the structure of a cybersecurity resilience maturity measurement framework for critical information infrastructure. The article identified pillars of measurement of cybersecurity resilience and combined them to formulate the resilience framework that led to the development of a mathematical model. Four cybersecurity resilience quadrants (CRQs) were proposed with a defined range of values for each quadrant to support the comparative viewing and ranking of the resilience of measured entities. Although, the authors emphasised the need for a software tool that will support the regular assessment of the cybersecurity resilience of CNI, the proposed methodology did not lead to a software tool. Thus, the framework was not tested with empirical data to evaluate its performance. The authors [19][20]emphasised the importance of resilience assessment in the security and reliability of critical infrastructure. They argued that it provides the basis for understanding the current level of CI Resilience (CIR) and planning to improve it to target levels. [21] further reinforced this argument by developing methods for evaluating the resilience of individual or isolated elements of critical infrastructure. This methodology was tested on the control room of an electricity distribution company. The results showed potentials for the computation of the resilience of the control room. However, the fact that this methodology was designed to assess the resilience of separate elements of a CI in isolation does not account for the networked nature of critical infrastructure systems nor the organisation or national level assessment. Thus, the isolated analysis in this model does not provide for comparative ranking of the elements within the organisation. Similarly, the methodology cannot be applied for cybersecurity resilience maturity assessment at sectoral or national levels. Debates in literature support the fact that CNII resilience requires current and historical data to thrive, such data will support risk analysis by tracking improvements or decline in resilience of nations or organisations' key digital assets [22]–[24]. However, [23] examine 183 articles published on the subject for a period of 10 years (2010 – 2020), the conclusion is that, there are currently no databases available for the explicit purpose of supporting risk analysis of CNII in nations. The foregoing points to the fact that existing cybersecurity resilience assessment methodologies did not achieve the development of a software tool that could be used by individual organisations, CNII owners or regulators to gauge the cybersecurity resilience maturity of CNII at designated intervals. The absence of such tools also affirms the fact that there is no existing data set for analyses that will expose patterns in the resilience maturity of CNII. Thus, this article addresses this gap by presenting the cybersecurity resilience maturity assessment tool (CRMAT), a tool that is built on the basis of defined cybersecurity metrics for the purpose of regularly gauging the cybersecurity resilience maturity of CNII.

3. Methodology

Figure 1 describes the process for the conceptualisation and development of the cybersecurity resilience maturity assessment tool (CRMAT). Processes A, B and C have been completed in an earlier work in [1]. Where the building blocks of the cybersecurity resilience maturity assessment framework (CRMAF) were identified and used to develop the framework. CRMAF formed the basis for the development of the cybersecurity resilience assessment model (CRMAM). These phases laid the foundation the data structures and algorithms for the development of the software tool referred to as the cybersecurity resilience maturity assessment tool (CRMAT), presented in this article.

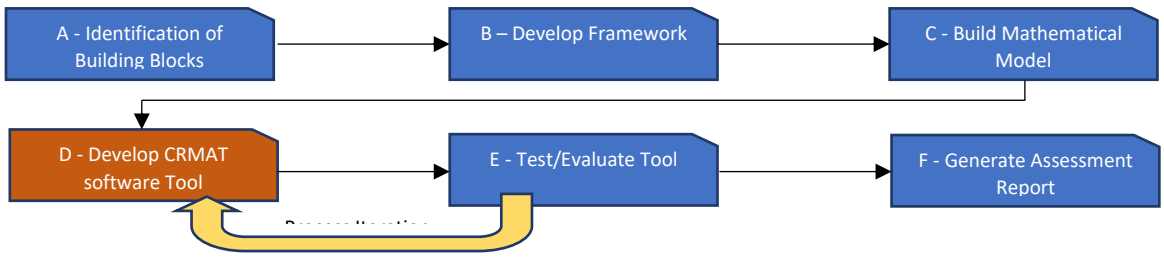

Figure 1: CRMAT Development Process

The development of CRMAT software tool (process – D) followed the agile methodology of the software development life cycle (SDLC). This is to support continuous iteration and refinement of

the tool as indicated in the process iteration between processes D and E. The MVC (Model – View – Controller) architectural pattern was adopted to support separation of concerns between the different elements of CRMAT. The detailed process of the development methodology is explained in section 5.

4. Conceptualisation of the Cybersecurity Resilience Maturity Assessment Framework

Figure 2 adopted from [1] shows the Cybersecurity Resilience Maturity Assessment Framework (CRMAF) core for Critical National Information Infrastructure (CNII). The framework derived from the national cyberspace operational structure described in [25], which describes three layers of national cyber operations, namely: government, organisation and the individual. In context, The CRMAF is designed for organisational cybersecurity resilience measurement. Nevertheless, the organisational cybersecurity resilience for key CNIIs can be aggregated and normalised to provide insights for national cybersecurity resilience. The CRMAF as illustrated in Figure 2 consists of three major components: the cybersecurity controls, cybersecurity resilience mathematical model (a computational algorithm) and the CNII resilience quadrant (CNIIRQ)

Cybersecurity controls: these are a set of functions and sub-functions that provide the basis for the measurement of the degree of maturity – that is, the cybersecurity resilience maturity of CNII. In the CRMAF, cybersecurity controls are broken down into five distinct but connected layers; namely resilience temporal dimensions (RTD) based on [5], [7], [26] which define resilience in terms of a system's ability to prevent an incident from occurring (pre-event); minimise the impact and duration of attack (event-management); and recover to optimal service after an attack (post-event). The other layers with each of the layer providing inputs to the layer immediately adjoining it from left to right. The theoretical concepts and cybersecurity frameworks described in this article were adopted to conceptualise the building blocks of the framework core. The components are described in details in the following sections.

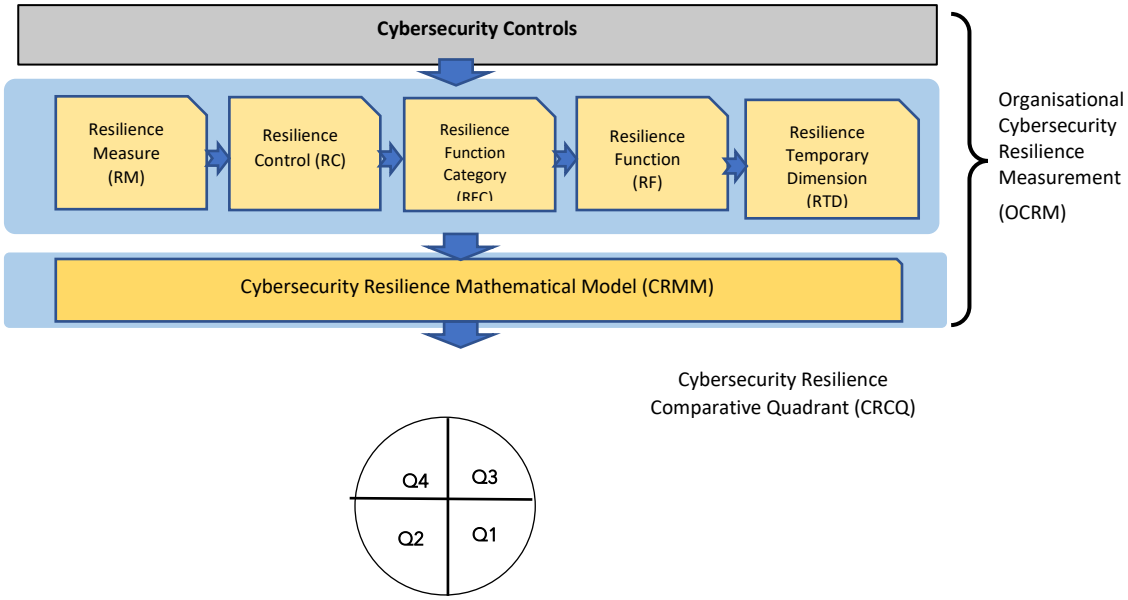

Figure 2:Cybersecurity Resilience Maturity Assessment Framework (CRMAF)
Redrawn from [1]

The RTDs are linked to the resilience functions (RFs), the resilience functions supply inputs into the RTDs. There are five RFs derived from the five pillars of the NIST cybersecurity framework [27] (i.e. identify, protect, detect, respond and recover) and mapped into the three resilience RTDs. Consequently, pre-event RTD has identify, detect and protect; respond and recover RFs are mapped onto the event-management and post-event RTDs respectively. Other cybersecurity controls are resilience functions category (RFCs) and the resilience controls (RCs), each providing inputs into their adjoining layers of the cybersecurity controls. Thus, RFCs are mapped into the relevant RFs and RCs are mapped into relevant RFCs,

Resilience Measure (RM) illustrated as the first of the cybersecurity controls on the CRMAF from the left in Figure 2 is the granular unit of measure of the actual cybersecurity practices against baseline cybersecurity controls described in the framework. Its quantitative weights are defined on a 5-level ratio scale between 0 – 4 and provides equal intervals between adjoining levels of the RM. This is appropriate as the ratio scale starts from zero (0) and advances to higher weights [28]; zero represents the absence of control, which is vital for the quantification of measurement. The weights of the resilience measure are described in Table 1.

Table 1: Cybersecurity Resilience Measure Scale adopted from [1]

Weight	Qualitative	Description
0	Not achieved	Complete absence of cybersecurity controls in place.
1	Loosely achieved	Negligible cybersecurity controls are in place and incoherently applied.
2	Partially achieved	Moderate cybersecurity controls are in place but not consistently and structurally organised; many and/or important elements are missing.
3	Largely achieved	Cybersecurity controls are structurally implemented but some elements are missing.
4	Fully achieved	Best practices in cybersecurity practices and controls are comprehensively implemented.

Based on the scale presented in Table 1, CNII organisations that apply the highest weight (4) in the assessment of their cybersecurity practices will be more resilient compared to those that apply 1, 2 or 3. Those that have zero (0) compliance, equally have zero (0) resilience. The RM is built into the CRMAT to enable the quantification of resilience during assessment.

Cybersecurity Resilience Mathematical Model (CRMM)

The CRMM derived from the cybersecurity controls presented in Figure 2 and described in the preceding section provides the algorithmic functions for the computational engine of the CRMAT that underpin the quantitative assessment of the cybersecurity resilience maturity of a CNII. the CRMM is presented in equation. The complete derivation of the CRMM is presented in [1].

$$CNIIRI = 0.55(PRTDI_N) + 0.30(EMRTDI) + 0.15(PoRTDI) \quad \text{.....Equation (1)}$$

Thus, *CIINRI*, which lies between 0.00 – 1.00 represents the composite *CNIIRI* value of a CNII organisation.

Cybersecurity Resilience Comparative Quadrant (CRCQ)

The CRCQ also referred to here as the CNII resilience quadrant (CNIIRQ) intuitively analyse and compare the Cybersecurity Resilience Maturity of organisations. CNII resilience index (CNIIRI) scores are grouped into a four-band scale called the cybersecurity resilience comparative quadrant (CRCQ). The CRCQ provides a mechanism for a single view of the CNIIRI of several CNII organisations for ranking and visualisation of the degree of resilience maturity of CNII organisation[29]. This comparative tool is also helpful in comparing the performance of the control metrics at different levels as a way of determining the effects of contributing elements relative to one another. For instance, the scores of the individual elements of the RTD (i.e., pre-event, during event and post-event) can be compared to determine their contributing effects in quantifying the Cybersecurity Resilience Maturity of a CNII organisation. Table 2 provides the scale range defined for the four quadrants, labelled Q1, Q2, Q3 and Q4 respectively. The table also provides a detailed interpretation of each quadrant.

Table 2: CNII Cybersecurity Resilience Comparative Quadrant (CNIICRCQ) [29].

Quadrant	Composite Value	Note
Q1	0.00 – 0.25	**Initial**: very low level of resilience resulting from a few resilience controls in place that are incoherently adopted.
Q2	0.26 – 0.51	**Defined**: This demonstrates a low level of resilience as a result of the inconsistent and unstructured application of resilience controls with many and/or important elements of resilience controls missing.
Q3	0.51 – 0.75	**Managed**: High resilience occasioned by a structured but inconsistent implementation of resilience controls with a few and/or minor elements missing.
Q4	0.76 – 1.00	**Optimised**: Optimal resilience achieved based on best practices and application of cybersecurity controls are comprehensively implemented.

5. Implementation of the (CRMAT)

The MVC architectural pattern was used for the implementation of the CRMAT– MVC separates an application into three major parts, namely; Model, View and controller. This architectural pattern supports separation of concerns that improves security and a modularised code-base that is easier to maintain. The model (M) represents the database, view (V) is the front end where users (administrator and organisations – respondents) interface with the application while the controller serves as the coordinating frame between the view and the model. The model (database), view (front end) and the controller (backend) were implemented using *MySQL,* React js and Laravel (PHP) respectively. This is detailed in the following section.

Data Model Domain

Figure 3 describes the entity relationship diagram (ERD) that represents the database structure upon which the CRMAT application is built. Two user roles are defined in the CRMAT database in the *crmatusers* entity in Figure 3, namely: administrator (*is_admin*) and respondent (which is represented as organisation: *org_id*) using the tool to assess their cybersecurity resilience. The role of the administrator spans the entire database entities. It is prominent in setting up all the values against the variables set in the entities. For instance, the administrator performs the following operations in the database entities: setup the quadrants and their ranges in *crmatquadrant* entity, add sectors in *crmatsectors*, organisations in *crmatorganisations*, resilience measures in *crmatresilience_measures*, resilience measure scales in *crmatresilient_measure_scales*, resilience temporal dimensions (RTD) in *crmatresilience_temporal_dimensions*, resilience controls in *crmatresilience_control*, etc. In the respondent/organisation role; the *crmatorganisation* entity is the central table that ties together most of the other entities in the model. It is connected to other entities through an associative entity called *crmatusers*. Note that the user table contains the two user roles as earlier explained in the preceding paragraph. The actions of the respondents (*crmatusers*) in performing the assessments generates the numerical data that is stored in the *resilience_measure_responses* entity. The values in this entity are used for the computation of other entities like: *crmatresilience_controls*, *crmatresilience_functions_categories*, *crmatresilience_functions*, *crmatcniir_indices*, and *crmatresilience_temporal_dimensions*

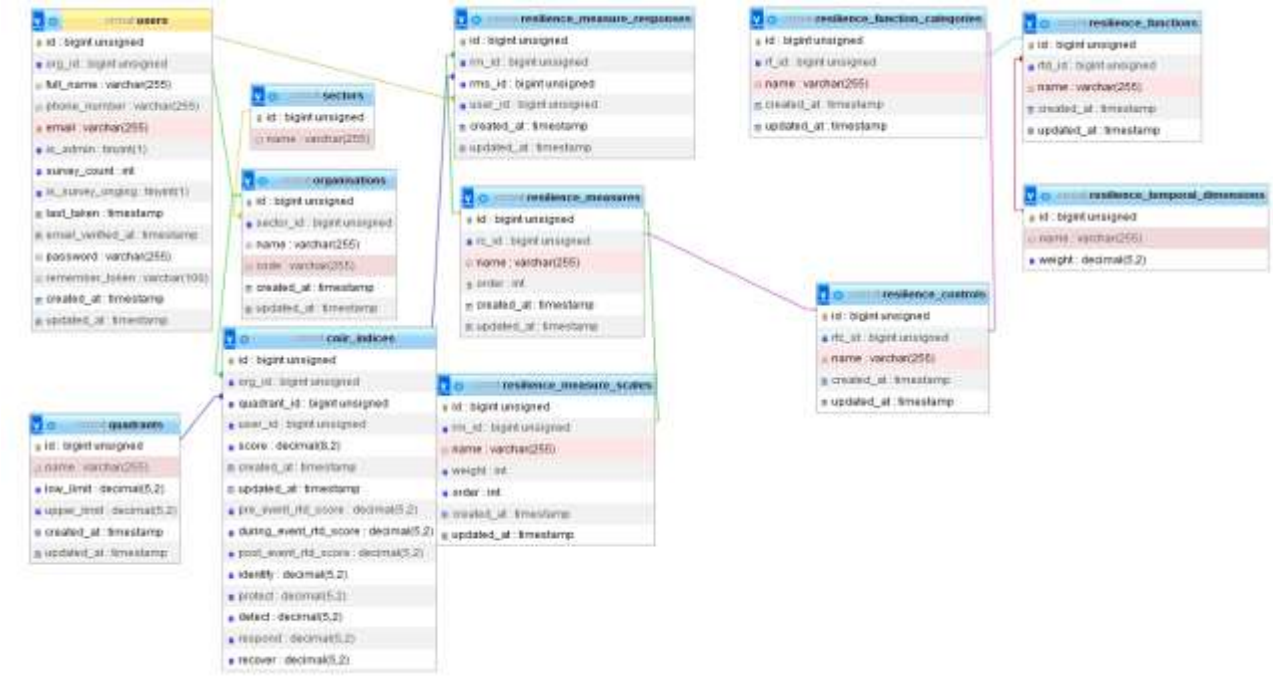

Figure 3: CRMAT Entity Relationship Diagram (ERD)

View Domain

The view domain describes the interfaces for interaction with the CRMAT application. Like the model domain, the two user roles are reflected in the view domain. For example, the administrator's interface supports administrative operations on the CRMAT at the backend while the organisation (respondents) interface enables organisations carryout cybersecurity resilience maturity assessment of their organisations and view summarised results of the assessments. Figure 5 describes the CRMAT domain view.

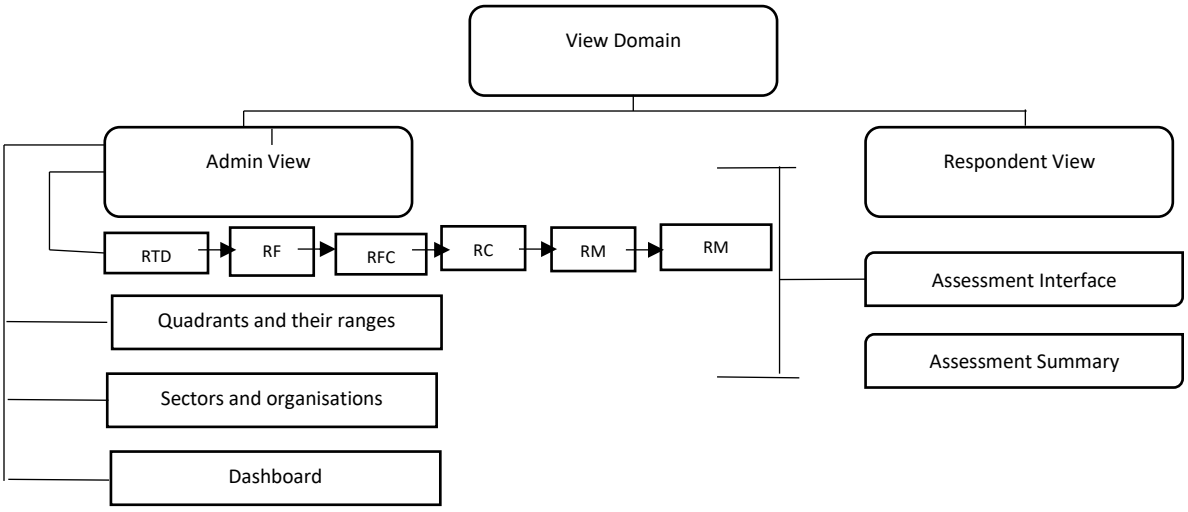

Figure 4: Description of Domain View

Figure 4 is the view domain design that shows the operations that can be done at the two interfaces of the view domain, namely admin view and the respondent view. At the admin view, the administrator setups the values of the resilience temporal dimensions (RTD), resilience functions (RF), resilience function categories (RFC), resilience controls (RC), resilience measure (RM) and the resilience measure scales (RMS). In addition, admin can setup CNIIRQ and their ranges (quadrants and ranges), add sectors and organisations. The dashboard at the administrator's view also provides comparative information on the performance of the assessed organisations and between other elements like the RTDs, RFs, RFCs, etc. The respondent view on the other hand provides for organisations through their

respondents to access the assessment interface and carry out their cybersecurity resilience maturity assessment and view the summary of the assessment as computed and presented from the system.

Control Domain

The control domain provides the business logic of the CRMAT that enables the computation of the various metrics and indicators ranging from the CNII resilience index (CNIIRI), resilience temporal dimensions (RTDs), resilience functions (RFs), resilience functions categories (RFCs) and resilience controls (RCs). The comparative logic illustrated in the CRCQ is powered in the control domain. The details of this logic are presented in the sub-section on Cybersecurity Resilience Mathematical Model (CRMM).

6. Test and Results

Figures 5 – 11 describe some key administrator's interfaces while Figures 12 – 14 describe organisations (respondents) interfaces. The CRMAT is coded to accommodate changes in requirements of system without necessarily re-programming the tool. This is taking into account the fact that requirements may change in the future. For example, the CRMAT currently has three temporal dimensions (RTDs), if and when the RTD increases or reduces, the administrator will only be required to add, delete or modify the RTD as the case may be. Consequently, the administrator's log-in page presented in Figure 6 authenticates access to the interface of the CRMAT that enables the administrator to configure the software tool based on organisations' requirements.

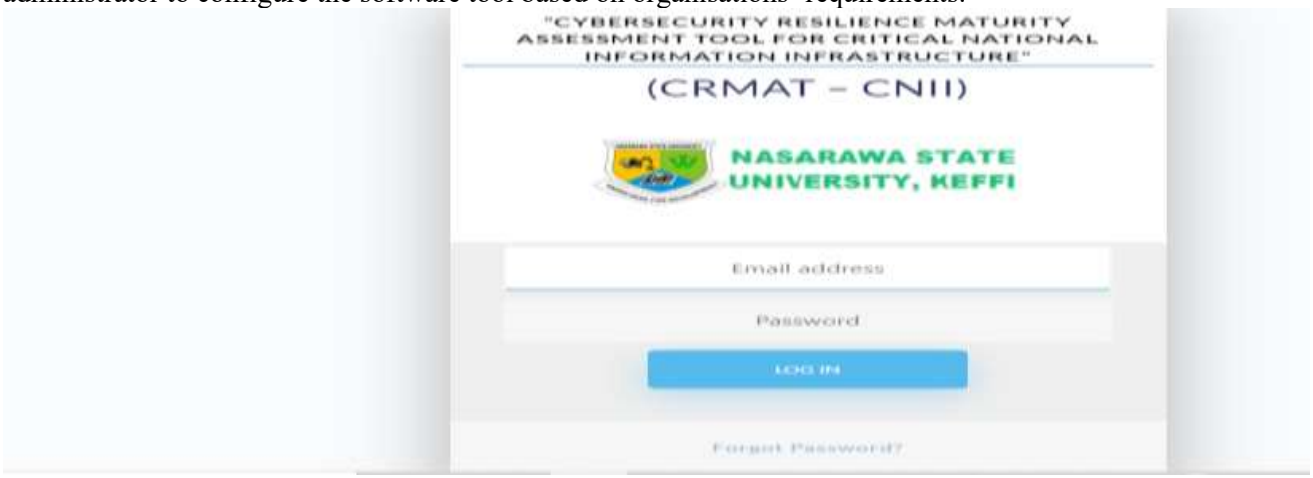

Figure 5: CRMAT Log in Page for Administrator Operations

Figure 6 presents the CRMAT dashboard where some key sets of information contained in the application's database are summarised for administrator's consumption.

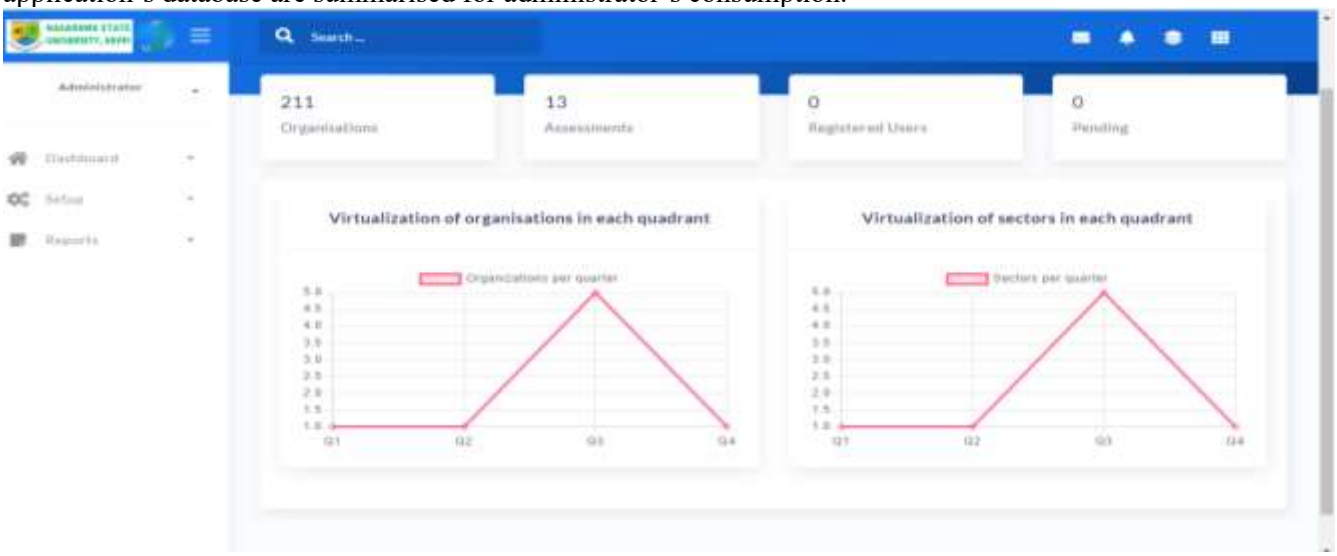

Figure 6: CRMAT Admin Dashboard

As can be seen in Figure 6, a summary of information on the number of organisations that can access the tool and carryout assessments, number of assessments already conducted, number of registered users. For example, the dashboard presented in Figure 6 shows that 211 organisations and 13 assessments currently exist in the database while there are zero users and pending assessments respectively. Figure 6 also provides a visualisation of how organisations place in the different quadrants of the CRMAM, that is, the number of organisations in Q1, Q2, Q3 or Q4 as well as how the measured metrics compare against each other. The left-hand pane of the dashboard contains the setup menu for all the cybersecurity controls defined in the in the framework in Figure 2.

Figure 7 presents the interface that enables the administrator to add, delete or edit resilience temporal dimensions (RTD) by clicking on the ***Add RTD*** (circled in yellow)***, delete or edit*** (circled in green) buttons. Note the three RTDs namely; pre-event, during-event (event management) and post-event have been added as circled in red.

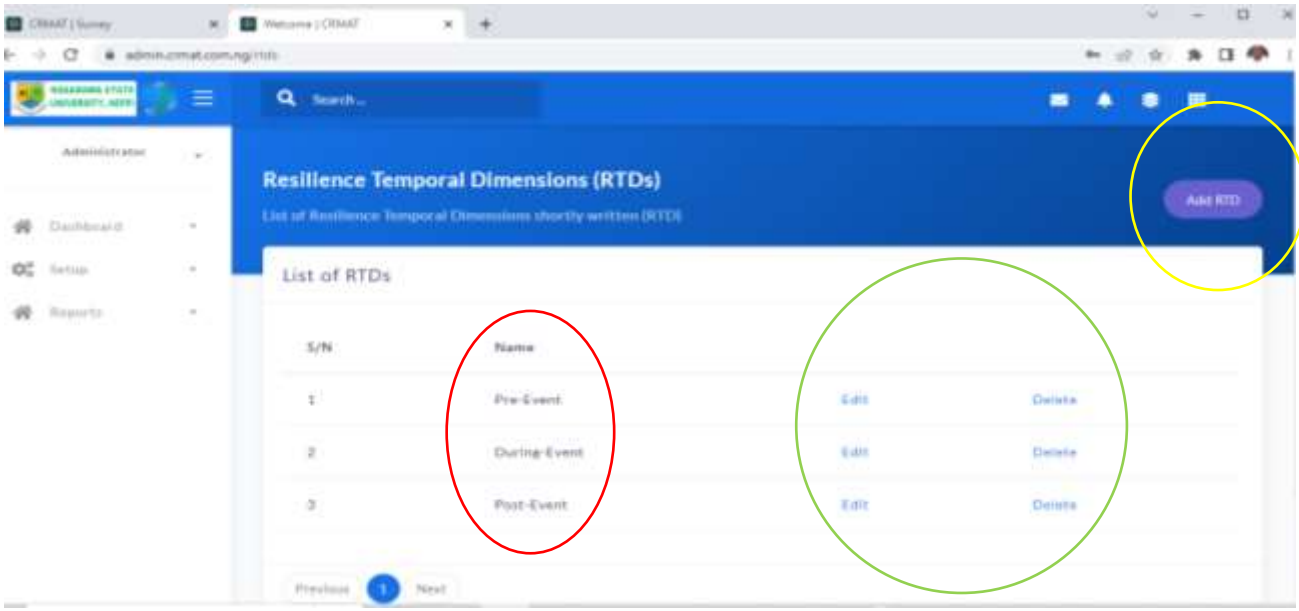

Figure 7: Add Resilience Temporal Dimensions (RTD)

Clicking on the *Add RTD* button opens up a dialog box that enables the admin to add more RTDs to the tool. Note that the delete/edit buttons allow for the deletion or edit of an already added RTD. Similar interfaces exist in the application to enable one add several elements of the.

Figure 8 is the interface that allows the administrator to add, delete or edit the quadrants defined in Table 2 and their respective ranges (low and upper limits).

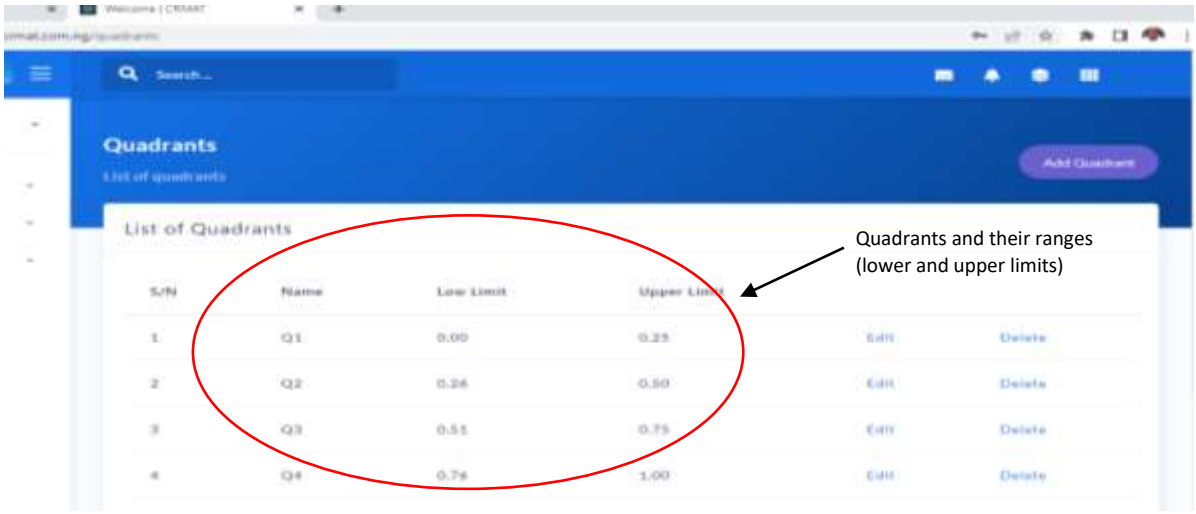

Figure 8: CNII Resilience Quadrants (CNIIRQ) Setup

These quadrants, labelled as Q1 – Q4 were exhaustively described in Table 2. The quadrants are the basis for ranking of the cybersecurity resilience index described as the CNIIRI and other metrics like the resilience function (RF), resilience function category (RFC) and resilience controls. Figure 9 is the resilience measure (RM) interface. The RMs are the questions that guide the process of the cybersecurity resilience maturity assessment. This interface enables the additions of RMs according to their resilience controls (RC).

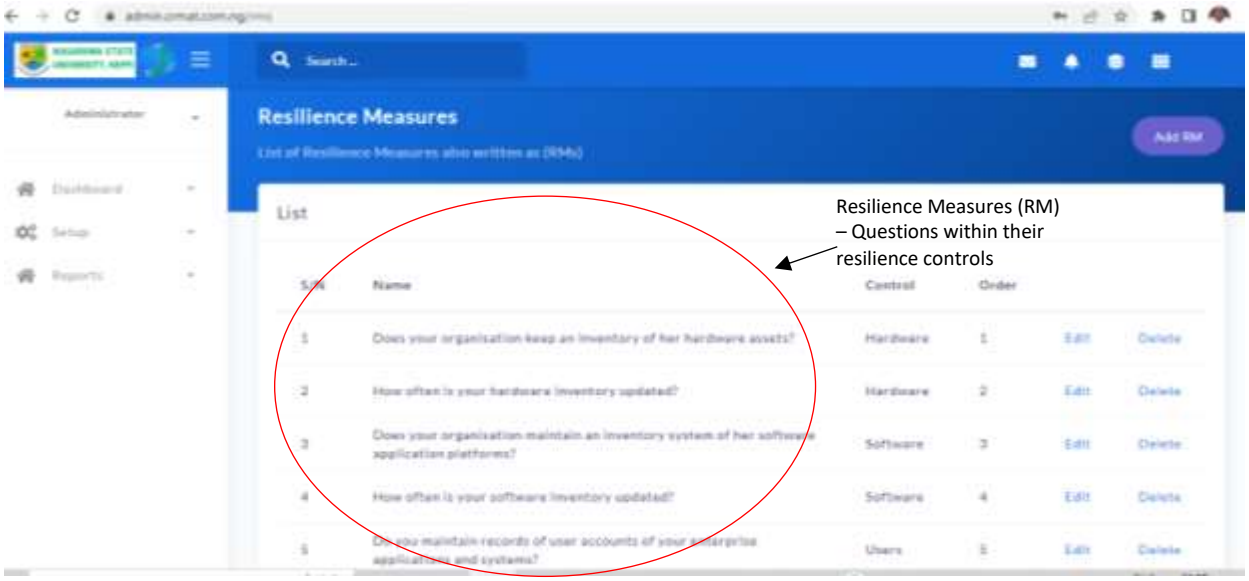

Figure 9: Resilience Measures Setup

Figure 10 shows the resilience measure responses (RMR) which provides the interface to add the possible options to each RM. There are five possible options (RMRs) to each RM, each of these options are mapped to their corresponding numerical weights between (0-4) which Figure 10 provides the capability for tying each option to its corresponding weight relative to its RM.

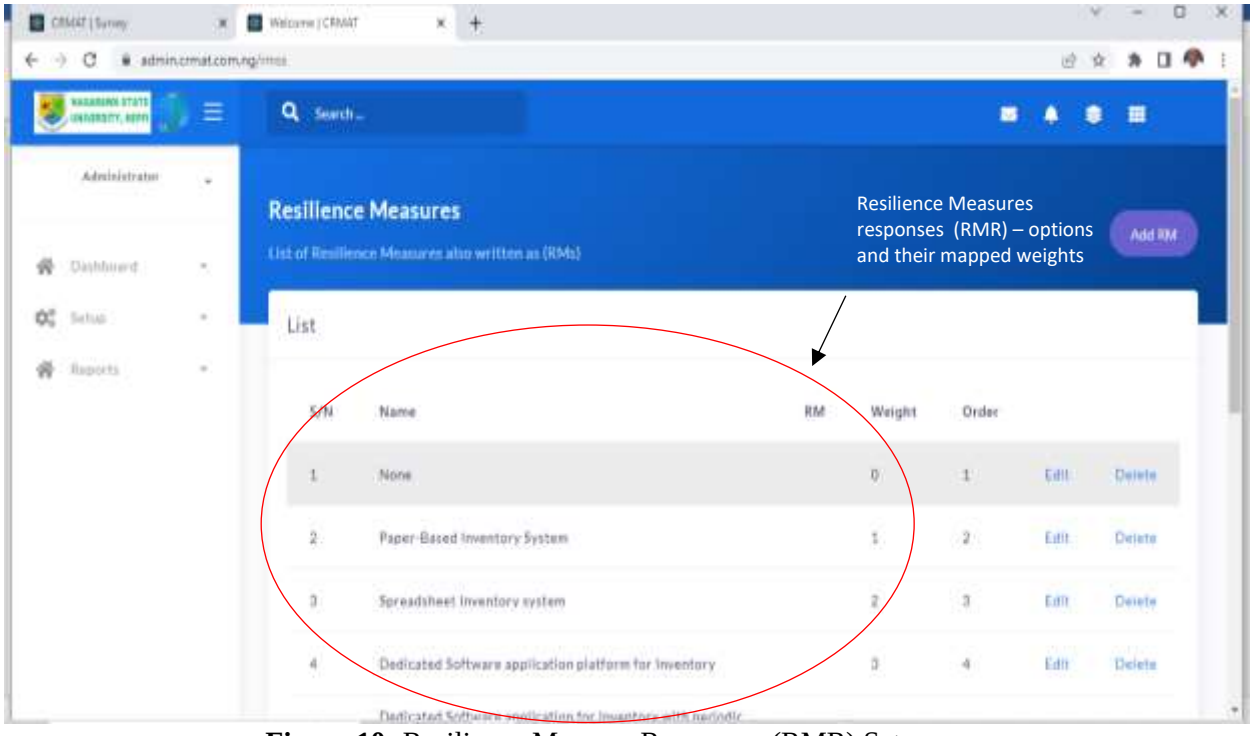

Figure 10: Resilience Measure Responses (RMR) Setup

Figure 11: Reports

Figure 11 is the sample CNIIRI report from the CRMAT, similar reports can be generated for the identify, protect, detect, respond and recover RFs as well as for the RFCs. The reports menu contains a download feature that enables users to export data from the CRMAT into other statistical tools for further analysis and visualisations.

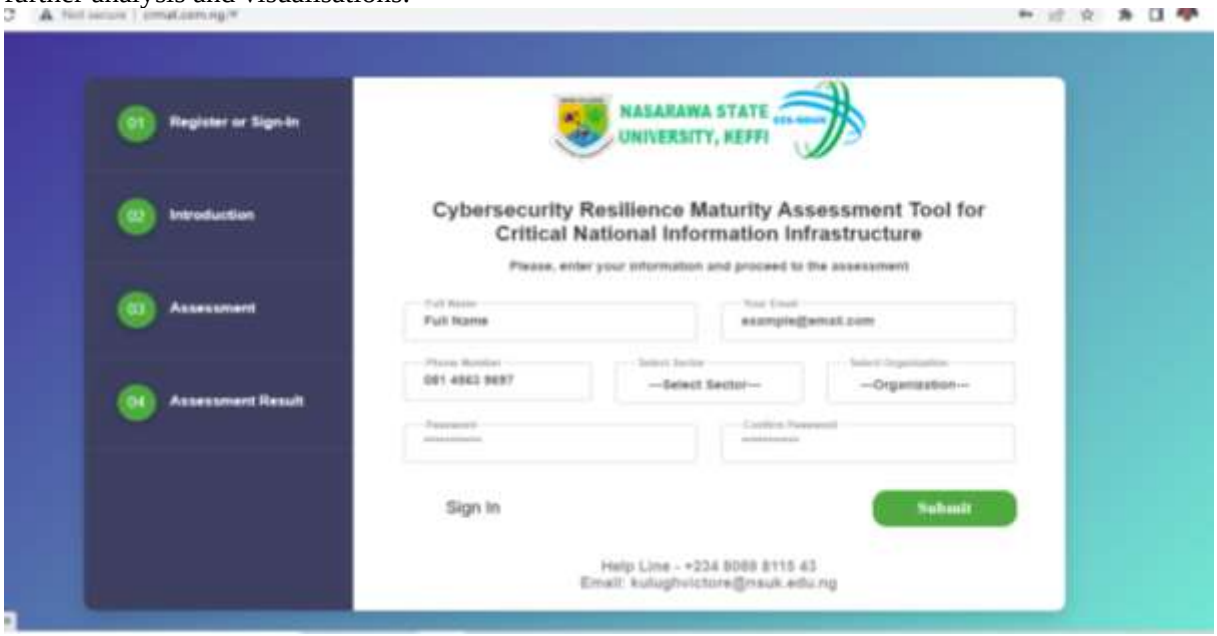

Figure 12: Organisation (Respondent) Login Page

Figure 12 presents the log-in page for organisations that use the tool for assessment. It requires users to provide their names, phone number, email, password, sector and organisations for registration. Figure 13 on the other hand shows the assessment interface where items are provided with options to be selected using radio buttons, each item selected here has it mapped quantitative value recorded in the database for computation of the various indices defined in the model. In Figure 14, the assessment summary is provided for organisations that use the CRMAT to conduct their resilience assessment. It provides the CNIIRI score of the organisation and the corresponding quadrant upon which they fall. This summary also present reports on the RTD scores namely; pre-event, event management and post-event scores.

Figure 13: Sample Assessment Interface

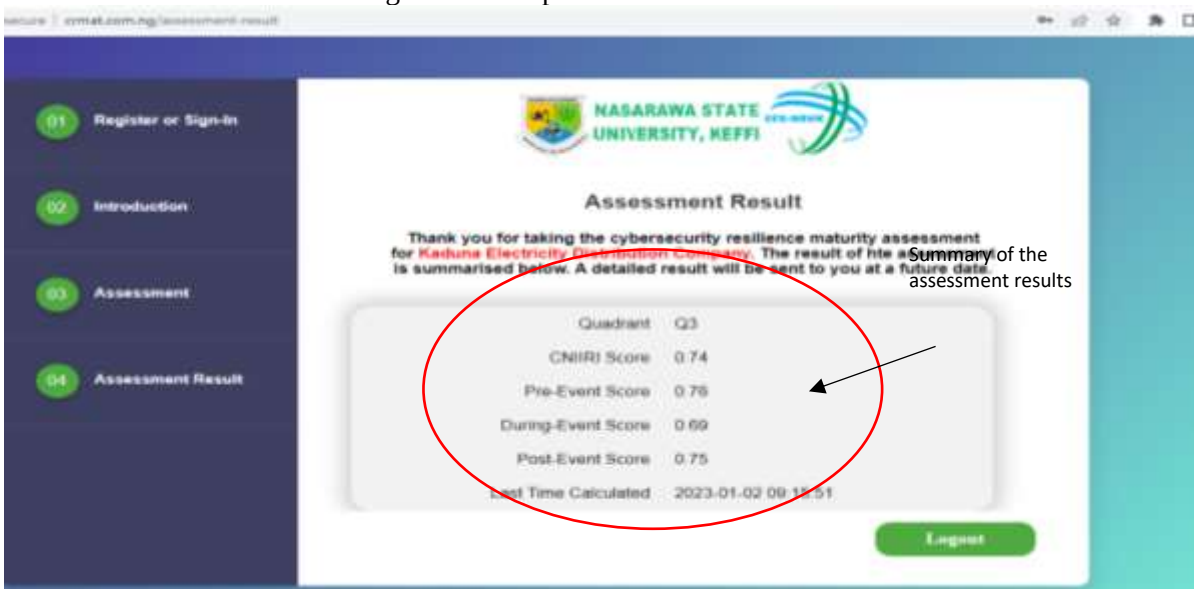

Figure 14: Sample Assessment Summary

7. Evaluation of CRMAT

The CRMAT was deployed to collect data from 31 CNII organisations representing 10 CNII sectors to carry out the two-fold exercises of evaluating the CRMAT and performing cybersecurity resilience assessment of the organisations based on data generated and computation carried out by CRMAT's computational engine. The names of the organisations and sectors were anonymised to address the inherent conflict between information sharing and security [23]. The evaluation took into account all three (3) Resilience Temporal Dimensions (RTDs); all five (5) Resilience Functions (RFs). Similarly, all five (5) resilience function categories (RFCs) in the identify, protect and respond RFs; and all three (3) RFCs in the detect and recover RFs respectively. Note that each RFC has several RCs and RCs have RMs (the numerical values at the granular levels that are mapped to actual cybersecurity practices at the organisational context). Data collected was based on organisations within the CNII sectors as defined in the Nigerian national cyber security strategy and policy (NCSSP) [30] document as presented in Table 3. It (Table 3) contains a summary of sectors, number of organisations per sector and number of respondents per organisation. To reduce the effect of the biases that will be introduced into the data by respondents, the CRMAT is designed with the capability to aggregate responses from multiple respondents per organisation, average them and report a single value for the organisation. Thus, organisations were encouraged to have a minimum of 2 respondents to participate in the assessment.

Table 3: Summary Responding CNII Sectors and Organisations

#	Sector	No. of Organisations	Respondents
1	SECT001	3	9
2	SECT002	2	5
3	SECT003	2	4
4	SECT004	6	12
5	SECT005	5	15
6	SECT006	3	6
7	SECT007	4	8
8	SECT008	2	4
9	SECT009	1	2
10	SECT010	3	6
	Total	**31**	**71**

Table 4 shows the CNIIRI scores of 31 CNII organisations and their distribution in the CNII resilience quadrant (CNIIRQ). The CNIIRI scores as distributed in the CNIIRQ show that 4(12.90%), 8(25.81%), 15(48.39%) and 4(12.90%) are in Q4, Q3, Q2 and Q1 respectively. The groupings reflect the overall resilience of these organisations with respect to the cybersecurity controls (resilience measures - RMs) applied in their computation. Consequently, it can be inferred from this distribution that organisations in Q4 are the most resilient while those in Q1 are the least resilient.
Table 5 presents the pre-event RTD index (PRTDI) of the 31 CNII organisation that participated in the assessment and their distribution in the CNIIRQ. The CNIIRQ distribution of the PRTDI shows that 5 (16.13%) of the organisations are in Q4, 9 (29.03%) are in Q3 while 13 (41.94%) and 4 (12.90%) are in Q2 and Q1 respectively.

Table 6 on the other hand represents the event management resilience temporal dimension index (EMRTDI) of the 31 CNII organisation and their distribution in the CNIIRQ. The distribution showed that 3(9.68%) of the organisations are in Q4, 9 (29.03%) are in Q3 while 13(41.94 and 6(19.35%) are in Q2 and Q1 respectively.

The post-event resilience temporal dimension index (PoRTDI) of the 31 CNII organisations are presented in Table 7. The distribution of the PoRTDI scores in the CNIIRQ shows that Q4 has 6(19.35) organisations, Q3 has 8 (25.81%), Q2 and Q1 have 13 (41.94%) and 4 (12.90%) respectively.

Table 4: CNIIRI Score

#	Code	CNIIRI	
1	URUJV	0.93	
2	JY6CE	0.85	Q4 = 4
3	GIDF8	0.78	
4	BTN8P	0.75	
5	AMAM6	0.73	
6	ZUPUH	0.68	Q3 = 8
7	UOUHN	0.67	
8	A4BR9	0.66	
9	KTJ0P	0.64	
10	1ANVE	0.62	
11	IHWER	0.57	
12	DAJZB	0.54	
13	NVKAR	0.48	
14	UHWK3	0.44	Q2 = 15
15	EM90M	0.44	
16	JKJ9Y	0.43	
17	IZVSC	0.42	
18	CAW6R	0.42	
19	ASDCD	0.42	
20	PYW4X	0.40	
21	8JSNN	0.39	
22	PXJK5	0.33	
23	L3O4X	0.33	
24	PPBBJ	0.30	
25	Y6BZW	0.27	
26	TCVKZ	0.25	
27	CYQNT	0.25	
28	L4FZP	0.20	
29	QW2MK	0.12	Q1 = 4
30	3JRFF	0.05	
31	NC23W	0.03	

Table 5: PRTDI Score

#	Code	Pre-Event	
1	URUJV	0.94	
2	JY6CE	0.88	Q4 = 5
3	GIDF8	0.81	
4	AMAM6	0.80	
5	ZUPUH	0.76	
6	UOUHN	0.72	
7	DAJZB	0.67	Q3 = 9
8	BTN8P	0.67	
9	KTJ0P	0.66	
10	IHWER	0.64	
11	1ANVE	0.62	
12	A4BR9	0.62	
13	IZVSC	0.52	
14	UHWK3	0.52	
15	CAW6R	0.46	Q2 = 13
16	NVKAR	0.46	
17	JKJ9Y	0.46	
18	PYW4X	0.44	
19	ASDCD	0.43	
20	EM90M	0.42	
21	PXJK5	0.41	
22	L3O4X	0.41	
23	8JSNN	0.39	
24	L4FZP	0.38	
25	Y6BZW	0.33	
26	PPBBJ	0.26	
27	CYQNT	0.25	
28	TCVKZ	0.21	
29	QW2MK	0.19	Q1 = 4
30	NC23W	0.07	
31	3JRFF	0.06	

Table 6: EMRTDI Score

#	Code	Event Mgt.	
1	URUJV	0.85	
2	BTN8P	0.81	Q4 = 3
3	JY6CE	0.78	
4	UOUHN	0.73	
5	GIDF8	0.73	Q3 = 9
6	ZUPUH	0.64	
7	A4BR9	0.63	
8	KTJ0P	0.63	
9	1ANVE	0.60	
10	AMAM6	0.59	
11	CAW6R	0.55	
12	IHWER	0.53	
13	IZVSC	0.49	
14	DAJZB	0.44	Q2 = 13
15	8JSNN	0.41	
16	EM90M	0.41	
17	NVKAR	0.40	
18	JKJ9Y	0.40	
19	PYW4X	0.39	
20	ASDCD	0.39	
21	PPBBJ	0.37	
22	UHWK3	0.36	
23	PXJK5	0.32	
24	L3O4X	0.27	
25	CYQNT	0.25	
26	Y6BZW	0.24	
27	L4FZP	0.23	Q1 = 6
28	TCVKZ	0.23	
29	QW2MK	0.10	
30	3JRFF	0.04	
31	NC23W	0.03	

Table 7: PoRTDI Scores

#	Code	Post-Event	
1	URUJV	1.00	
2	JY6CE	0.88	Q4 = 6
3	AMAM6	0.81	
4	GIDF8	0.80	
5	BTN8P	0.75	
6	A4BR9	0.75	
7	1ANVE	0.63	
8	ZUPUH	0.63	Q3 = 8
9	KTJ0P	0.63	
10	NVKAR	0.56	
11	UOUHN	0.56	
12	IHWER	0.53	
13	DAJZB	0.50	
14	EM90M	0.50	
15	UHWK3	0.44	Q2 = 13
16	JKJ9Y	0.44	
17	ASDCD	0.44	
18	8JSNN	0.38	
19	PYW4X	0.38	
20	TCVKZ	0.31	
21	L3O4X	0.31	
22	PPBBJ	0.28	
23	IZVSC	0.25	
24	CAW6R	0.25	
25	Y6BZW	0.25	
26	CYQNT	0.25	
27	PXJK5	0.25	
28	QW2MK	0.06	Q1 = 4
29	3JRFF	0.06	
30	L4FZP	0.00	
31	NC23W	0.00	

Distribution of CNIIRI and RTDs in the CNIIRQ

Table 8 summarises the distributions of the resilience parameters in the CNIIRQ as shown in Figures Tables 4-7. It shows that although, the CNIIRI is derivative of the cumulative effects of the RTDs; It values does not necessarily match the values of the RTDs upon which it is derived. For example, 4 organisations are in the Q4 quadrants based on CNIIRI. However, the RTDs presents unmatching patterns for the same quadrant, namely; PRTDI = 5, EMRTDI = 3 and PoRTDI = 6. This is similar to the distributions in other quads as shown in Table 4. The implication is that, organisations must explore further to establish the indicators that account for their high performance (and even low scores). This will expose indicators with low scores but which effects are compensated by high performing indicators, thus hiding the gaps.

Table 8: Distribution of CNIIRI and RTDs in the CNIIRQ

#	Indicator	Q4	Q3	Q2	Q1
1	CNIIRI	4	8	15	4
2	PRTDI	5	9	13	4
3	EMRTDI	3	9	13	6
4	PoRTDI	6	8	13	4

Comparison of RTDs and RFs

Figure 15 represents a comparison of the averages of the RTD computed by the CRMAT based on the 31 CNII organisation taken for the 3 RTDs (i.e., PRTDI, EMRTDI and PoRTDI). Similarly, Figure 16 is a representation of the averages of the 5 RFs (namely: identify, protect, detect, respond and

recover). These Figures compare the performance of these cybersecurity resilience controls based on data generated from the CRMAT.

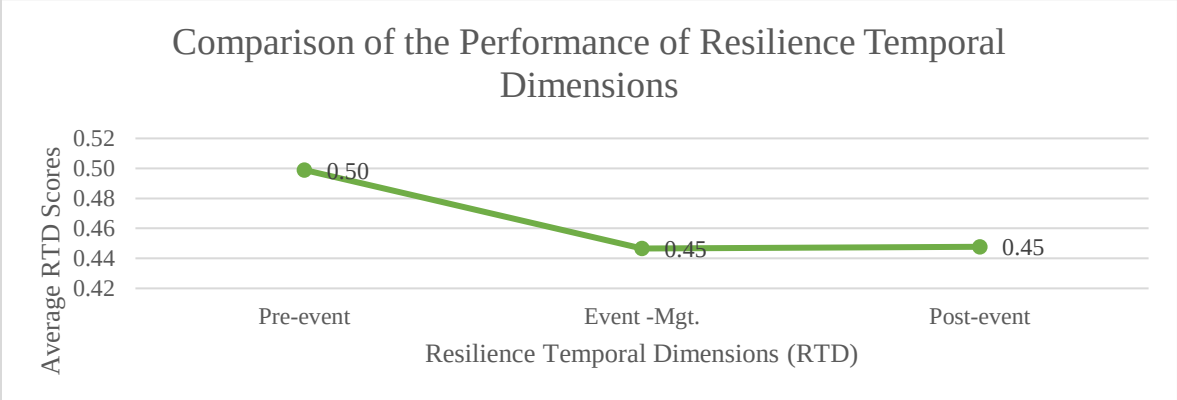

Figure 15: Comparison of the Performance of RTDs

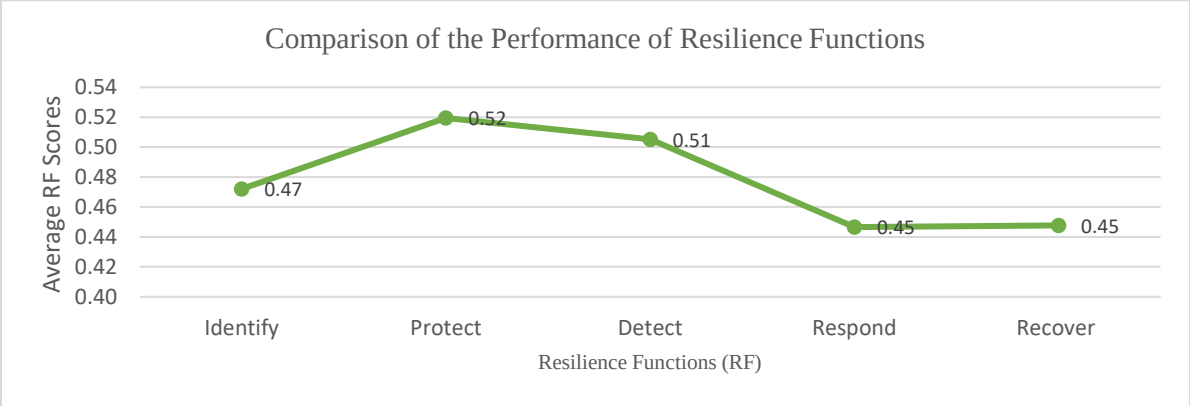

Figure 16: Comparison of the Performance of RFs

Figure 15 indicates a trend that showed higher average score on the pre-event RTD (0.50) as compared to the averages in event-management and post-event RTDs (0.45) respectively. Although, 0.50 averages place the organisations at the lowest boundary of Q3 quad, it indicates that organisations are generally more prepared to prevent cybersecurity incidents compared to their response and recovery efforts which scored average of 0.45 (i.e., a Q2 placements). Figure 16 presents a Q2 average value of 0.47 on the identify RF, indicating vulnerabilities in this phase as the resilience of unidentified assets cannot be optimised. Similarly, the protect and detect RFs are at the lowest boundary of the Q3, this combines with the identify RF generally make the pre-event RTD vulnerable. Again, the respond and recover RFs are weak at 0.45 both and depict the fact that these organisations have poor response and recovery mechanisms.

8. Conclusion

The economy, security, economic security, health and safety of citizens of modern societies will experience monumental disaster of catastrophic proportion if the CNII experience huge and sustained cyberattacks. To proactively address this concern, organisations and nations need to regularly and quantitatively gauge the maturity of their cybersecurity resilience to cyberattacks. Proposed solutions do not provide tools that simplify the process and maintain data so that organisations, CNII owners, operators and regulators can track improvements or decline in resilience of their digital assets. This paper presents the cybersecurity resilience maturity assessment tool (CRMAT) that addresses this gap. CRMAT was conceptualised from a theoretical and methodological background that provided the requirements (building blocks) that were further refined to formulate the computational algorithms. The software tool was built using the agile development process with the MVC architectural pattern. CRMAT has a built-in setup frame that allows organisation to add or drop cybersecurity controls on

the admin panel as per their needs. The data generated from the software can be exported into other data analytics tools for further analyses and insights. The CRMAT system stores data of assessment with timestamp to enable organisations track their resilience performance in terms of improvements on the revealed gaps. CRMAT relies solely on data provided by organisations for its computation, this data could be subjected to biases and thus, may not provide accurate insights into the resilience maturity of assessed organisations. However, an attempt has been made to address this by ensuring that more than one respondent participates per organisation and the scores aggregated and averaged, this will potentially limit the effects of any biases that may be introduced. Additionally, the assessment programme (questionnaire) has follow-up questions that checks biases that may be introduced by respondents. The software has been tested based on input data received from 31 organisations and has shown capability to accurately compute the performances of the various cybersecurity controls defined within the framework (CRMAF – Figure 2). A comparative analysis of the results on the CNIIRQ showed that 12.90% of the 31 assessed organisation fall within Q4 which depicts an optimised level of resilience, however, nearly half of these organisations (48.39%) and 12.90% fell in Q2 and Q1 respectively. Thus, depicting a generally weak cybersecurity resilience posture of the participating organisations. A comparison of the performance of the resilience temporal dimensions showed that majority of the organisations have more pre-event capabilities as compared to their ability to respond and recover from cybersecurity incidents. Overall, it can be inferred from the assessment of the organisation that the general cybersecurity resilience posture of the organisations is weak.

Acknowledgement

Conflict of Interest This article is part of the Cybersecurity and Critical National Infrastructure (CNI) research project which is supported by TETFund National Research Fund (NRF) research grant TETF/ DR&D/CE/NRF/UNI/KEFFI/VOL.1/B5 to Nasarawa State University, Keffi, Nigeria.

References

[1] V. E. Kulugh, U. M. Mbanaso, and G. Chukwudebe, "Cybersecurity Resilience Maturity Assessment Model for Critical National Information Infrastructure," *SN Comput Sci*, vol. 3, no. 3, May 2022, doi: 10.1007/s42979-022-01108-x.

[2] M. Panfili, A. Giuseppi, A. Fiaschetti, H. B. Al-jibreen, and A. Pietrabissa, "A Game-Theoretical Approach to Cyber-Security of Critical Infrastructures Based on Multi-Agent Reinforcement Learning," pp. 460–465, 2018.

[3] S. M. Rinaldi, J. P. Peerenboom, and T. K. Kelly, "Identifying, understanding, and analyzing critical infrastructure interdependencies," *IEEE Control Systems Magazine*, vol. 21, no. 6, pp. 11–25, 2001, doi: 10.1109/37.969131.

[4] B. Rød, D. Lange, M. Theocharidou, and C. Pursiainen, "From risk management to resilience management in critical infrastructure," *Journal of Management in Engineering*, vol. 36, no. 4:04020039, 2020, doi: DOI: 10.1061/(ASCE)ME.1943-5479.0000795.

[5] M. Bruneau *et al.*, "A Framework to Quantitatively Assess and Enhance the Seismic Resilience of Communities," *Earthquake Spectra*, vol. 19, no. 4. Earthquake Engineering Research Institute, pp. 733–752, 2003. doi: 10.1193/1.1623497.

[6] M. Bruneau and A. Reinhorn, "Overview of the Resilience Concept."

[7] J. L. Carlson *et al.*, "Resilience: Theory and Application.," Argonne, IL (United States), Feb. 2012. doi: 10.2172/1044521.

[8] G. Stergiopoulos, P. Kotzanikolaou, M. Theocharidou, G. Lykou, and D. Gritzalis, "Time-based critical infrastructure dependency analysis for large-scale and cross-sectoral failures," *International Journal of Critical Infrastructure Protection*, vol. 12, pp. 46–60, Mar. 2016, doi: 10.1016/j.ijcip.2015.12.002.

[9] S. Puuska *et al.*, "Nationwide critical infrastructure monitoring using a common operating picture framework," *International Journal of Critical Infrastructure Protection*, vol. 20, pp. 28–47, 2018, doi: 10.1016/j.ijcip.2017.11.005.

[10] G. Sharkov, "Assessing the Maturity of National Cybersecurity and Resilience," vol. 4, no. 4, pp. 5–24, 2020.

[11] M. Levesque, "Understanding Cybersecurity Maturity Models Within the Context of Energy Regulations," Europe and Eurasia, 2020.

[12] W. Miron and K. Muita, "Cybersecurity Capability Maturity Models for Providers of Critical Infrastructure," *Technology Innovation Mnagement Review*, vol. 4, no. 10, pp. 33–39, 2014.

[13] T. Mettler, "Maturity assessment models : a design science research approach," vol. 3, 2011.

[14] K. Shaheen and A. H. Zolait, “The impacts of the cyber-trust program on the cybersecurity maturity of government entities in the Kingdom of Bahrain,” *Information and Computer Security, Emerald Publishing Limited*, 2023.
[15] D. Rehak, T. Lovecek, M. Hromada, N. Walker, and I. Haring, “Critical Infrastructures Resilience in the Context of a Physical Protection System,” in *Advances in Engineering and Information Science Toward Smart City and Beyond*, R. Shinkuma, F. Xhafa, and T. Nishio, Eds., 5th ed.Springer , 2023, pp. 1–33.
[16] I. Linkov, D. A. Eisenberg, K. Plourde, T. P. Seager, J. Allen, and A. Kott, “Resilience metrics for cyber systems,” pp. 471–476, 2013, doi: 10.1007/s10669-013-9485-y.
[17] P. Tim, “Measuring Critical Infrastructure Resilience : Possible Indicators,” Zurich, 2014.
[18] U. M. Mbanaso, L. Abrahams, and O. Z. Apene, “Conceptual design of a cybersecurity resilience maturity measurement (CRMM) framework,” *The African Journal of Information and Communication*, vol. 23, no. 23, pp. 1–26, 2019, doi: 10.17159/2077-7213/2019/n23a2.
[19] D. Rehak and M. Hromada, “Failures in a Critical Infrastructure System,” in *System of System Failures*, InTech, 2018. doi: 10.5772/intechopen.70446.
[20] D. Rehak, M. Hromada, and J. Ristvej, “Indication of critical infrastructure resilience failure,” no. December, 2017.
[21] D. Rehak, P. Senovsky, M. Hromada, and T. Lovecek, “Complex approach to assessing resilience of critical infrastructure elements,” *International Journal of Critical Infrastructure Protection*, vol. 25, pp. 125–138, 2019, doi: 10.1016/j.ijcip.2019.03.003.
[22] A. Larsson and C. Groβe, “Data use and data needs in critical infrastructure risk analysis,” *J Risk Res*, 2023, doi: 10.1080/13669877.2023.2181858.
[23] C. Große, A. Larsson, and O. Björkqvist, “Information-flawing filters in critical infrastructure protection: the deficient information basis in a Swedish approach,” *International Journal of Critical Infrastructures, Inderscience Enterprises Ltd*, vol. 9, no. 1, pp. 40–57, 2023.
[24] C. Große, “Enhanced information management in inter-organisational planning for critical infrastructure protection: Case and framework,” in *ICISSP 2021 - Proceedings of the 7th International Conference on Information Systems Security and Privacy*, SciTePress, 2021, pp. 319–330. doi: 10.5220/0010186803190330.
[25] U. M. Mbanaso and R. A. Koleoso, “AN INVESTIGATION OF CYBERSECURITY VULNERABILITY LANDSCAPE,” in *International Conference on Emerging Application and Technologies for Industry 4.0*, 2020, pp. 110–123.
[26] A. Smith and A. Stirling, “Transitions Social-ecological resilience and socio-technical transitions: critical issues for sustainability governance,” 2008. [Online]. Available: www.steps-centre.org
[27] NIST, “Framework for Improving Critical Infrastructure Cybersecurity, Version 1.1,” Gaithersburg, MD, Apr. 2018. doi: 10.6028/NIST.CSWP.04162018.
[28] J. Uher, “Quantitative Data from Rating Scales :An Epistemological and Methodological Enquiry,” *Front Psychol*, vol. 9, no. 2599, 2018.
[29] U. M. Mbanaso and V. E. Kulugh, “Empirical Findings of Assessment of Critical Infrastructure Degree of Dependency on ICT,” in *First International Conference on Cybersecurity in Emerging Digital Era*, R. Agrawal, G. Sanyal, K. Curran, V. E. Balas, and M. S. Gaur, Eds., Greater Nodia: Communications in Computer and Information Science, Oct. 2020, pp. 3–17.
[30] ONSA, “NATIONAL CYBERSECURITY POLICY AND STRATEGY 2021,” ABUJA, Mar. 2021.

Available online at www.asric.org
ASRIC Journal on Natural Sciences Vol 3(1) (2023) 35-41

Urban Flood Vulnerability and Risk Mapping using Multi-Criteria Analysis in Mzuzu City, Malawi

Donnex Chilonga[1*], Mabvuto Tembo[2]

[1]Mzuzu University,P/Bag 201, Luwinga, Mzuzu 2, Malawi

*Corresponding author: donnexc@gmail.com; chilonga.d@mzuni.ac.mw

Abstract

This paper presents the results of the assessment of flood vulnerability of Mzuzu City using Multi-criteria analysis and GIS. Using a Weighted Overlay approach, physiogeographic variables that influence floods such as drainage density, elevation, slope, landuse/landcover and soil type, were integrated and ranked based on their importance. From this assessment, urban flood risk map for the City was derived. The results show that 12% of the total area (112 sq. km.) of Mzuzu City has very high risk of flooding, 29% has high risk, 41% has low risk and 18% has very low risk of flooding. Both very high- and high-risk zones are located in the low-lying and flat central part of the City. The Northern and Easterly parts are low risk zones while the southern part are very low risk areas. LU/LC changes have exacerbated the degree of vulnerability of the city. High population growth has led to changes in LU/LC patterns. Built-up Area/Settlement and Bareground/Paved have increased while Dense Vegetation and Dambo Land have reduced considerably. The adoption and use of the generated flood risk vulnerability map by authorities will help to quickly assess potential hazardous areas and the impact of flood hazard. It can further guide in the commencement of appropriate measures to reduce its impacts in pre-disaster and post-disaster situations.

Keywords: Analytical Hierarchical Process (AHP), Geographic Information System (GIS), Landsat Images, Multi-criteria analysis, Reclassification, Weighted Overlay, Urban texture typology.

1.0 Introduction

The nature of flooding events experienced in Mzuzu City is becoming dynamic in time and space. Due to urbanization and the subsequent increase in population, urban texture keeps on changing. Land meant for agricultural activities, natural vegetation and wetlands have been converted into built-up environments (Stewart and Oke, 2012). With the sporadic infrastructural developments taking place, Mzuzu is characterized by a highly distorted urban texture typology of built types as well as land cover types. The most devastating flood occurred in 2016 where 15 settlements were affected. During these floods 19,000 people were displaced and 7 people lost their lives (Kita, 2017). The most affected areas were Masasa, Chibanja, Ching'ambo and Chibavi. These are informal settlements characterized by poor service provision, congestion and poor sanitation. Such dwellings are developed in wetlands and seasonal dambo lands with poor drainage. These conditions, coupled with human-induced climate change, render Mzuzu City more vulnerable to flood risk necessitating the acquisition of accurate spatial and temporal information regarding possible hazards and flood risks.

1.1. Conceptual Framework of Urban Flood Risk

The analysis and assessment of flood risk in an urban setting requires the development of a theoretical framework that captures all the various components contributing to the generation of urban flood risk (Muller, 2013). Flood risk consists of hazard and vulnerability (Merz et al., 2010). Hazard refers to a threatening event, or probability of occurrence of a potentially damaging phenomena within a given time and area. The damage that ensues when a hazardous event occurs depends on the elements at risk which include population, building structures, economic activities, public services and infrastructure.

Therefore, when assessing the risk of damage due to natural hazards in general, at least two factors need to be taken into account. First is the probability and consequences. Second are the elements and their economic values (Estoque, 2010).

The second component of risk assessment which aims to quantify the damage potential (Merz et al., 2010), especially in complex and heterogeneous urban setups where elements at risk are affected unequally resulting into different types of damages, is vulnerability (Satterthwaite, et al., 2007). Muller (2013) defines vulnerability as the social and physical conditions that make parts of an urban system susceptible to experiencing damage from a flood event. People are the main actors in the generation of risk and its reduction. It is imperative therefore to identify the population characteristics as well as its associated urban infrastructure that lead to different levels of risk within an area. The better the knowledge about the amount and the capacities of people and values potentially affected, the more appropriate measures can be planned (Muller, 2013). Equation 1 considers risk as a product of three components i.e. hazard, elements at risk, and vulnerability (Muller, 2013).

$$\textbf{Risk} = \text{Hazard} \times \text{Elements at risk} \times \text{Vulnerability} \quad \text{……..…. (Equation 1)}$$

1.2. Multi-criteria Evaluation (MCE)

MCE is a decision theory of applying a decision rule to a set of alternatives whereas a 'decision rule' is a procedure by which criteria are combined to arrive at a particular evaluation, and by which evaluations are compared and acted upon (Eastman, 2001). A decision is a choice between alternatives while a criterion is a basis on which a decision is made. Two types of criteria may be identified thus factors and constraints (Estoque, 2010). The former is generally considered to be continuous in nature, and indicate the relative suitability of certain areas. The latter are Boolean in nature and serve to exclude certain areas from consideration. Using any Boolean method, factors and constraints can be combined in the MCE scheme (Estoque, 2010). MCE process aims at aggregating a set of criteria so as to realize one composite basis for decision making in line with a specific objective (Ouma and Ryutaro, 2014: Eastman, 2001).

1.3. Spatial Information and MCE for Flood Risk Mapping

Almost 80% of the data used by decision makers is geography-related (Bhadra et al., 2011). For one to ably prepare for a disaster, sufficient geographic information on hazards and vulnerable areas is a requirement. As such GIS, through its overlay process, is better placed to providing better information about situations that require decision making (Bhadra et al., 2011). The application of GIS in flood hazard analysis has many advantages. GIS does not only provide a visualization of the flooding, but it also provides room for probable estimation of damage caused by floods (Eastman, 2001). As opposed to the traditional mapping, GIS allows for multi-dimensional analyses of natural hazards. It allows comparisons across spatial units and across different spatial themes. GIS allows for performance of logical and/or numerical operations through merging of several spatial databases. GIS is time and cost-effective technology for extraction and provision of information of flood inundation magnitudes in hilly areas where conventional surveys is difficult to conduct (Ouma and Ryutaro, 2014).

2. Materials and Methods

2.1. Study Area

Mzuzu City is located in the northern Malawi between the boarders of Mzimba and Nkhatabay districts. It is the largest urban centre in the northern Malawi covering an area of 112km^2 and third largest urban centre in Malawi, after Blantyre and Lilongwe. Its population is 221,272, 60% of which lives in informal settlements (Malawi National Statistical Office, 2019). It is confined within the natural gap of Viphya Mountains where the terrain is generally flat with some gentle slopes dissected by some ridges and gullies. Main rivers that drain Mzuzu are Lunyangwa and Ching'ambo rivers which run from east to west and from north to south respectively. There are several streams that drain the southern part of the city and these include Katoto, Kavuzi and Kajiliwe (Leenaars, Dijkshoorn, Huting, & Kempen, 2016).

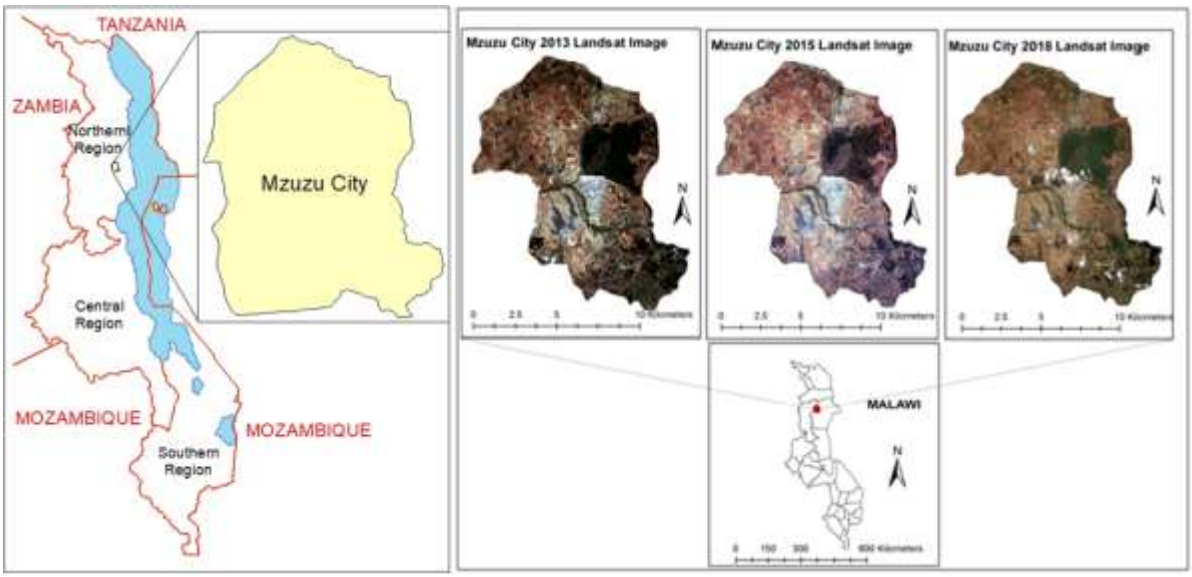

Figure 1: Map showing Mzuzu City and Multi-temporal Landsat 8 Images

2.2. Sources of data

Table 1 contains the data and material used for the study and their respective sources.

Table 1Data, Data Type and Data sources

	Data/Materials	Data Type	Source
1.	Mzuzu City boundary, drainage system, road network, soil.	Shapefiles	Surveys department, Ministry of Lands, Malawi
2.	Ground Truth and Accuracy Assessment Points	Point data	Global Positioning System (GPS) in Field survey
3.	Mzuzu City Slope and elevation	Raster map	Research generated from DEM
4.	Mzuzu City Landuse/landcover	Maps	Research generated from satellite imageries
5.	Landsat 8 Imageries	Satellite image	Online downloads @ http://earthexplorer.usgs.gov/
6.	Digital Elevation Model (DEM)	Raster	Online downloads @ http://earthexplorer.usgs.gov/
7.	ArcGIS 10.2, QGIS 3.2.1 & Google Earth Pro	GIS Software	Online downloads @ https://download.qgis.org, except for ArcGIS 10.2 which was purchased by the Geosciences department of Mzuzu University.

2.3. Parameter inputs for flood vulnerability analysis

Spatial Analyst and 3D Analyst extensions of ArcGIS 10.2 were used to analyze flood vulnerability using MCE. The selected flood variables of drainage density, landuse/landcover, elevation, slope, and soil were weighted using raster calculator.

Drainage density was generated in ArcMap using the *Line density* function of Spatial Analyst Tool. The streams were extracted from the DEM. *Stream buffering* was later done using the *proximity analysis* from the Analysis Tools. *LU/LC* layer was generated from the 2018 Landsat 8 image. Supervised maximum likelihood classification was done using the urban texture classes as adopted from Stewart and Oke (2012). These classes were collapsed into five main classes of Built up Area/Settlement, Dense trees, Light trees/Bush/Shrub, Bare ground/Paved and Dambo land. Calculation of the area coverage of the different classes of the image was done using the kernel density attribute table. Since the resolution of Landsat 8 image is 30m by 30m (NASA, 2019), the area of each pixel is thus 900 m^2. Therefore the area for each class was calculated by multiplying the observed count of all pixels in each class by 900 m^2.

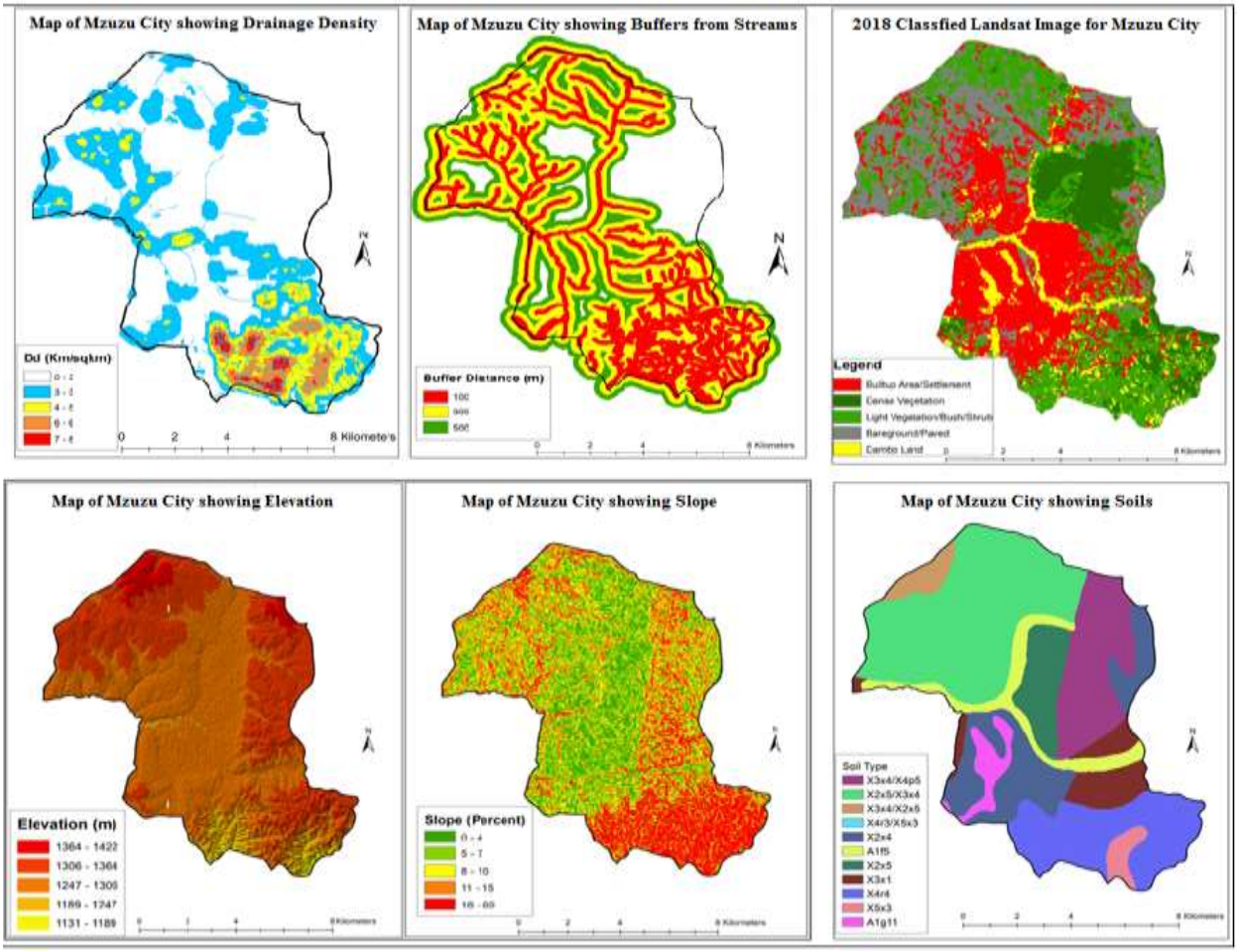

Figure 2: Maps showing Parameter inputs for flood vulnerability analysis

Elevation and *slope* layers were generated from the DEM using the *conversion* tool (i.e. from raster to TIN) of 3D Analyst and the *slope* Spatial Analyst Tool, respectively. Before the actual production of the elevation layer, elevation values for the pixels had to be extracted from the DEM layer via the *build raster attribute table* function from raster properties of Data Management Tools. Slope output layer was given in percentage. The *Soil* layer was obtained from the Surveys department, Ministry of Lands, Malawi.

2.4. Reclassification Process

Reclassification was done using the *inverse ranking method* in the ArcMap platform. The ranking was done for each of the five variables (i.e. drainage density, elevation, slope, landuse/landcover and soil type) in accordance to their degree of influence in flood induction (Njoku et al 2018; Bhadra, Choudhury, & Kar, 2011). A value of 1 was assigned to the class which was deemed to have least influence in flood initiation while class with next level of influence was assigned 2 and 3… in that order. Further, the ranks were grouped into index rating of high and low risk groups (see Table 2).

2.5. Weighting Process

The weighting process was done using the *Weighted Overlay* function of ArcMap's Spatial Analyst Tools. This process combines several raster layers using a common measurement scale and weighs each layer according to its attached significance. The final result of the weighting process is determined by the weight of each variable (Njoku et al 2018; Bhadra, Choudhury, & Kar, 2011). This study considered distance from the river, topography (i.e. elevation and slope), and LU/LC as the most significant variables for flood risk. This is because it was revealed during reconnaissance survey that floods in Mzuzu City typically ensue during rainy season and affect low lying areas covered by settlements. While rainfall has been considered another major variable in certain studies, its influence has been suppressed in this study (*see Table 2*).

The general weighted overlay process in MCA was guided by the equations below.

Scaling Range Formula $= \frac{X_i - X_{min}}{X_{max} - X_{min}}$

Overall Score Formula = [Criteria score 1 x Weight 1]+[Criteria score 2 x Weight 2]+[Criteria score 3 x Weight 3]+[Criteria score 4 x Weight 4]+...

Source: Maxwell (2018)

Table 2 Multi-criteria evaluation variables

Variables	Class	Reclass (Rates)	Rating Index	Weight (W)
Distance from Rivers (m)	<100	4	High risk	30
	100-300	3	Low risk	
	300-500	2	Low risk	
	>500	1	Low risk	
Elevation (m)	1131-1189	5	High risk	25
	1189-1247	4	High risk	
	1247-1306	3	Low risk	
	1306-1364	2	Low risk	
	1364-1422	1	Low risk	
Slope (%)	0-4	5	High risk	25
	5-7	4	High risk	
	8-10	3	Low risk	
	11-15	2	Low risk	
	16-69	1	Low risk	
Landuse/ Landcover	Built-up Area/Settlement	3	High risk	12
	Light Vegetation/Dambo Land/Shrub/Bareground	2	Low risk	
	Dense Vegetation	1	Low risk	
Soil Types	Eutric Fluvisols	2	High risk	8
	Haplic Lixisols	1	Low risk	

3. Results and Discussion

3.1. Flood risk vulnerability for Mzuzu City

The results of the weighted overlay process show that out of the total 112 sq. km that make up Mzuzu City, the very high flood risk vulnerability areas cover an area of 13.5 sq. km whereas 32.6 sq.km are high risk zones (see Table 3). The areas are in the central part of the city where Chiputula, Chibanja, Mzilawayingwe, Jombo and Mchengautuwa wards are located. These are generally flat dambo areas characterized by low elevation of 1247-1306m above sea level and gentle slopes with slope percentage range of 0–4. These zones fall within the outwash plains of Lunyangwa, Kang'ona and other small streams such as Katoto, Kavuzi and Kajiliwe. They have Eutric Fluvisols soils (*A1f5*) which are very deep and imperfectly drained hence allow very little water to infiltrate (Leenaars, et al 2016). During precipitation, run-off is downslope and water normally accumulates in low lying areas making such areas susceptible to flooding (Salami et. al., 2017).

Table 3Area Coverage of Flood Risk Zones

Rowid	Label	Pixel Count	Area Coverage (sq. km)	Percentage
1	Very High Risk	15051	13.5	12
2	High Risk	36222	32.6	29
3	Low Risk	51140	46.0	41
4	Very Low Risk	22611	20.0	18
Total		**125024**	**112.1**	**100.0**

The high vulnerability of the central part of the city is further compounded by the tremendous growth the city is currently experiencing in both intensity and extent. Due to this growth, landuse patterns of the City continue changing over time. High population growth has exerted pressure on the available

space and has led to the occupation of marginal lands for both settlements and commercial use. Spaces in the outskirts of the City which were meant for agricultural purposes have been turned into settlement areas thereby affecting agricultural productivity. Dambo lands along the streams and steep sloped areas have been encroached by people. During the past five years, Built-up area/Settlement has increased from 25.646 sq. km in 2013 to 32.988 sq. km. in 2015 and to 34.528 sq. km. in 2018. Light vegetation and Dambo areas have been decreasing (see Table 4). Such changes in LU/LC are a call for worry since they increase vulnerability of people to flood risk.

Table 4Area comparison for the classified Landsat images

		CLASS AREA (sq. km)		
Rowid	**CLASS NAME**	**2013**	**2015**	**2018**
1	Built-up Area/Settlement	25.646	32.998	34.528
2	Dense Vegetation	10.426	6.026	14.58
3	Light Vegetation/Bush/Shrub	41.345	35.344	32.752
4	Bareground/Paved	19.804	25.396	22.964
5	Dambo Land	14.856	12.313	7.253
Total Area		**112.077**	**112.077**	**112.077**

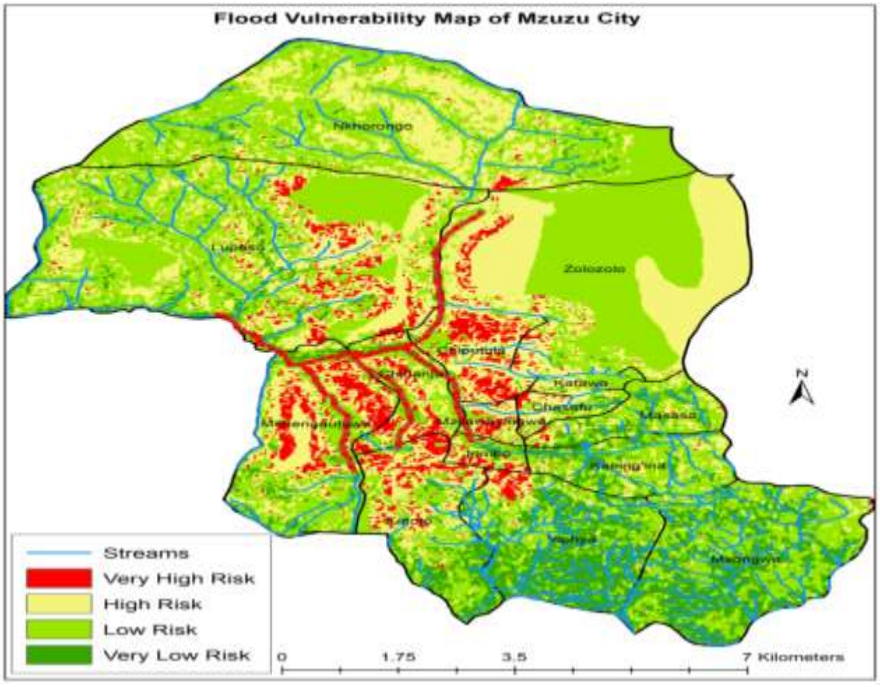

Figure 8: Flood Risk Vulnerability Map of Mzuzu City

Low risk zones are located to the northern and eastern part of the city where Lupaso, Nkhorongo and Zolozolo wards are found. Very low risk areas are in the southern part of the city where Kaning'ina, Masasa, Msongwe and Viphya wards are located. These zones cover an area of 46 sq. km. and 20 sq. km., respectively.

The terrain in this part of the city is rugged and is characterized by high elevation ranging from 1131-1189m above sea level, steep slopes with slope percentage of 16–69 and high drainage density of 7-8km/sqkm. These physical characteristics make the area less vulnerable to flood occurrences as they do not allow water to accumulate and cause flood. However, with the proliferation of informal settlements in these marginal zones, these areas are potential hazardous zones for landslides, mud flows and rock falls (Orok, 2011).

4. Conclusion

Flood vulnerability assessment is an important exercise for decision makers for planning and management purposes. While it is not possible to prevent floods from taking place, flood simulations

and risk assessment using MCA analysis in GIS environment are pragmatic tools to reducing flood risk and its impact. This paper presents work carried out in Mzuzu City. The generated composite map in Figure 8 is the resulting map of the assessment. It provides a platform for the quick assessment of potentially hazardous areas and the impact of flood hazard and can guide in the commencement of appropriate measures to reduce its impacts.

5. Acknowledgements

Sincere gratitude goes to my supervisor, Dr. Mavuto Tembo for the untiring effort he put in guiding me through the entire work. His constructive criticism and the consistent follow-ups were valuable in the entire period of working on this study. I am further indebted to Dr. Faith Taylor of Kings London College for the provision of the necessary guidance in the acquisition of spatial data. Colleagues in the Department of Geosciences at Mzuzu University, Mzuzu City Council, Ministry of Agriculture, Irrigation and Water Resources Development; you all deserve recognition for the various roles you played in this study. Many thanks to my wife, my children and those who made me feel challenged. You are the reason for the completion of this work. You gave me the urge to fight on for the best and look forward to many more challenges.

References Cited

Bhadra, A., Choudhury, S., Kar, D. (2011) Flood Hazard Mapping in Dikrong Basin of Arunachal Pradesh – Inida. World Acade. Sci. Eng. Technol..

Eastman, J.R. (2001) Guide to GIS and Image Processing. Volume 2, Manual Version 32.20. Clark University.

Estoque, R.C., Murayama, Y. (2010) Suitability Analysis for Beekeeping Sites in La Union, Philippines, Using GIS and Multi-criteria Evaluation Techniques. *Res. J. Appl. Sci. Vol 5*

Kita, S.M. (2017) Urban Vulnerability, Disaster Risk Reduction and Resettlement in Mzuzu City, Malawi. *Intern Journal of Disaster Risk Reduction* (22)

Leenaars, J.G.B., Dijkshoorn, J.A., Huting, J., & Kempen, B. (2016) Soil and Terrain database of the Republic of Malawi: Technical Report. ISRIC - World Soil Information. Wageningen.

Malawi National Statistical Office (2019) Malawi Population and Housing Census Report – 2018.

Merz, B., Hall, J., Disse, M., & Schumann, A. (2010) Fluvial Flood Risk Management in a Changing World. Journal for Natural Hazards Earth Syst Sci. Vol. 10.

Muller, A. (2013) Flood Risk in a Dynamic Urban Agglomeration: A Conceptual and Methodological Assessment Framework. Journal of Natural Hazards.

Njoku, C.G., Efiong, J, Uzoezie, A.C., Okeniyi, F.O. & Olagbe, A,O. (2018) A GIS Multi-Criteria Evaluation for Flood Risk Vulnerability Mapping of Ikom Local Government Area, Cross River State. Journal of Geography, Environment and Earth Science International.

NASA (2019) Landsat Science @ https://landsat.gsfc.nasa.gov/landsat-data-continuity-mission/ as retrieved on 11/2/2019

Orok, H.A. (2011) A GIS-Based Flood Risk Mapping for Kano City, Nigeria. University of East Anglia, Norwich, UK.

Ouma, Y.O.O. and Ryutaro T. (2014) Urban Flood Vulnerability and Risk Mapping Using Integrated Multi-Parametric AHP and GIS: Methodological Overview and Case Study Assessment.

Salami, R.O., Von Meding, J.K., and Giggins, H., (2017) Urban Settlements' Vulnerability of Flood Risks in African Cities: A Conceptual Framework. *J. of Disaster Risk Studies* (1)

Satterthwaite, D., Hug, S., Pelling, M., Reid, H., Romero Lankao, P. (2007) Adapting to Climate Change in Urban Areas. The Possibility and Constraints in Low and Mid income Nations. International Institute for Environment and Development (IIED). Human Settlement Discussion Paper: Climate Change and Cities, 1

Stewart, I.D., and Oke, T.R. (2012) Local Climate Zones for Urban Temperature Studies. British Columbia, Canada.

Available online at www.asric.org
ASRIC Journal on Natural Sciences Vol 3(1) (2023) 42-46

Improved Organically Treated Nanoclay-Polyurethane Nanocomposite

Mona A. Ahmed[1]*, Ashraf M. El-Saeed[1], Hamdy M. Naguib[1]

[1]Department of Petroleum Applications, Egyptian Petroleum Research Institute (EPRI), Nasr City, 11727 Cairo, Egypt.

* Corresponding author: mona_chemist17@yahoo.com

Abstract

Recently, nanocomposites are used in a wide range of applications; however the incompatibility between all components causes some drawbacks. Treatment of filler can solve this problem through formation of improved filler-matrix interface. The aim of this study is to investigate the effect of filling polyurethane matrix with (0.5, 1 and 1.5) wt.% layered double hydroxide nanoclay, as coating. Magnesium aluminium layered double hydroxide nanoclay (LDH) was firstly prepared via coprecipitation process, and then modified with palmitic acid via anion exchange to obtain the functionalized LDH (FLDH) nanoclay. The influence of treatment reaction on the synthesized polyurethane is studied. The treatment reaction was confirmed by FTIR; also the DLS and XRD data show dispersion of nanofillers, and amorphous structure after functionalization. TGA curves approve the performed functionalization reaction due to insertion of lower thermally stable fatty acid in nanoclay layers. Furthermore, the FLDH-polyurethane nanocomposite achieved enhanced mechanical properties, due to the strong interface between FLDH nanofiller and polyurethane matrix. The results reveal the improved characteristics after treatment, as a result of the compatibility between nanofiller and hydrophobic polyurethane matrix.

Keywords: Polyurethane, Layered double hydroxide, Nanocomposites.

1. Introduction

Thermosetting polyurethane (PU) is one of the most important engineering coatings. Due to its good processability, excellent chemical stability, high wear resistance and mechanical performance, it has been widely utilized towards protective coatings, wires and cables, automotive parts, and medical apparatus [i,ii]. Despite its advantages, PU is easily deformed, ignited, burns violently and release large amount of smoke and toxic gases due to it is rich in carbon and hydrogen, which have caused a great threat to human life and greatly limited its wide application in above fields [i,ii,iii,iv]. Therefore, in order to increase the mechanical and surface properties, some nanofillers can be used as additives. One of the recent nanofillers is layered double hydroxide (LDH) nanofiller. Incorporation of LDH into polymers to form LDH-polymer nanocomposites has gained increasing research interest, along with the improvement of their properties like surface and mechanical characteristics. LDHs, also known as hydrotalcite like materials, are anionic clays that are inexpensive and environment friendly [i,ii]. The introduction of long-chain organic anions into LDH leads to the formation of alternating metal hydroxide layer-organic anion layer hybrids, in which the intercalation of many long-chain anions and surfactants, including alkyl carboxylates, alkyl sulfate, alkyl sulfonates etc. have been reported [iii]. The interlayer anions can be exchanged by other organic anions, a process that leads to the functionalization to prepare functionalized LDH (FLDH). The compatibility of the polymer with LDH inorganic filler is increased by the surface modification of inorganic fillers with small organic compounds, which have polar groups [iv,v]. The harmonization of organically-modified Mg-Al-layered double hydroxides and polyurethane was carried out by homogenizing blend of polymers with LDH. This study aims to fabricate palmitate–LDH (FLDH) by an anion exchange method. Furthermore, FLDH was introduced to prepare a PU/FLDH nanocomposite by a solution of intercalation method. The obtained materials were characterized using dynamic light scattering (DLS) to ensure the nanosize particle, and thermo gravimetric analysis (TGA) to investigate the thermal

stability of nanofillers. X-ray diffraction (XRD) and infrared spectroscopy (IR) were used to characterize the LDH before and after functionalization. Finally, the mechanical properties were investigated using DMA for the performed LDH/FLDH-PU nanocomposites.

2. Experimental

Materials

Aluminum nitrate nonahydrate (Al $(NO_3)_3 \cdot 9H_2O$, assay ≥98 wt %), magnesium nitrate hexahydrate Mg $(NO_3)_2.6H_2O$, assay ≥99 wt %), and sodium nitrite ($NaNo_3$) were purchased from Fluka with high purity and used without any further purification. Sodium hydroxide (NaOH, Aldrich Chemical Co.). Deionized water was used in aqueous solution and in filtration. High Quality Two Components polyurethane Glossy Coating with mixing ratio 9A:1B Specific gravity (mix) 1. 3 ± 0.03 g/cm^3.

Preparation of MgAl-LDH (LDH)

The MgAl LDH nanoclay was prepared by the co-precipitation method. The starting materials were NaOH, $NaNO_3$, Mg $(NO_3)_2.6H_2O$ and Al $(NO_3)_3.9H_2O$. Under nitrogen atmosphere, 0.125 mol of Mg $(NO_3)_2.6H_2O$ and 0.0625 mol of Al $(NO_3)_3.9H_2O$ were dissolved in 125 ml of deionized water. This nitrate solution was then added dropwise to a solution containing 0.313 mol NaOH and 0.214 mol $NaNO_3$ dissolved in 140 ml deionized water. The pH of the solution was maintained at 10 using a solution of 1M NaOH. The reaction was aged for 24 h at 65 °C. Finally, the obtained white precipitate was filtrated, washed and dried at 55 °C, as LDH.

Preparation of Functionalized-LDH (FLDH)

Anion exchange method was used for the preparation of OM-LDH with a palmitate /LDH Firstly, (5g) of LDH were dispersed in (100ml) of (0.008M) anion solution prepared by dissolving the organic acid in a warm (water methanol) solution (1:1 volume ratio) containing (0.008M) NaOH under a steady flow of nitrogen to exclude (CO_2), the solution was vigorously stirred for 24hr at 50 °C. Then, filterate and washed several times with deionized water. Finally drying in a vaccum oven at (40 °C).

Preparation of (MgAl–NO_3 LDH) with Polyurethane Nanocomposites

Via in-situ polymerization, the desired amount of dispersed MgAl/NO3–LDHs was added to the MDI which was diluted with terahydrofuran (THF). The resulting suspension was dispersed with ultrasound at 22 kHz (UZD-22/44, Ukrrospribor, Ukraine) over 3 min for better distribution of LDHs in a polymer matrix and used for films preparation with adding its hardner. The formation of the polyurethane nanocomposite films was performed on Teflon substrates. The films were initially prepared by drying at 20–25 °C for 48 h, and then they were further dried at the same conditions for 3 days. The homogeneous transparent films without splicing and foaming were obtained. The amount of the introduced MgAl/ NO3–LDHs in PU nanocomposites was varied from 0.5 to 1.5wt%. For the characterization, every content of the nanofller three PU films were obtained.

3. Results and Discussion

Particle Size Distribution

The particle size distribution of prepared MgAl-LDH and FLDH are given by DLS. The average of particle sizes for LDH and FLDH are 89 nm and 142 nm, respectively. As DLS deals with the structure of a single molecule, and measures its whole size [vi]; the obtained data reveal the successful preparation of LDH and FLDH as separated nanostructures.

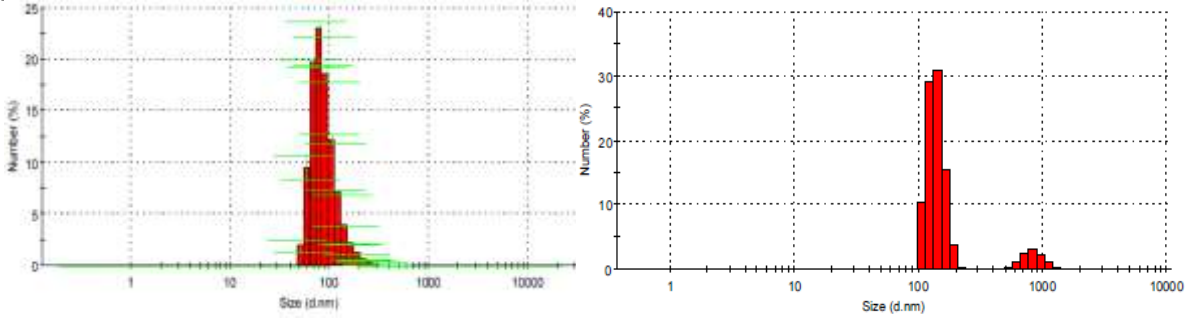

LDH FLDH

Fig 1: Particle Size Distribution

Fourier transforms infrared

The sharp peak at around 1375 cm^{-1} and the shoulder peak at 980 cm^{-1} indicate the nitrate ions in the interlayer spacing. Also, the absorption broad band near 3450 cm^{-1} is attributed to O-H stretching of hydroxyl group. The absorption peak near 1720 cm^{-1} is for C=O. The bands at lower wavenumber, below 800 cm^{-1} are related to O-metal bonds in naoclay [vii,viii]. It is noticed that the C=O to O-H peak ratio (C=O/O-H) is very low. After functionalization reaction in FLDH, the O-H peak has much lower intensity. For LDH, the C=O/O-H was small (< 1). However, in FLDH, it becomes higher (≥ 1); this confirms the functionalization reaction.

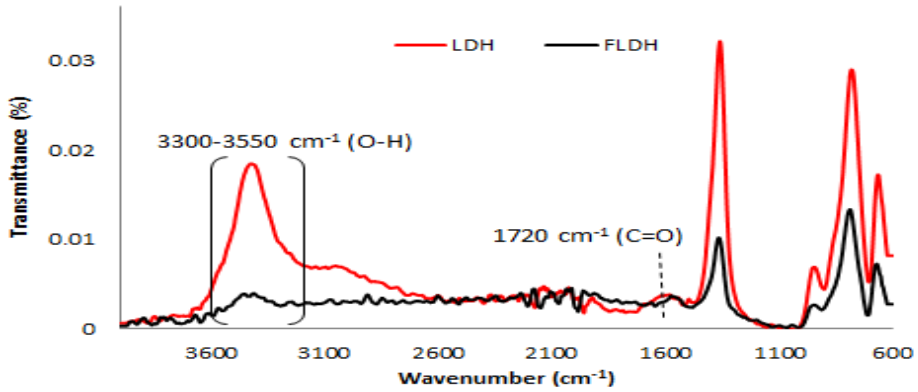

Fig 2: Fourier transforms infrared

X-ray diffraction

The XRD spectrum of the synthesized nanoclay shows that the MgAl nitrate LDH has highly crystalline nature and layered geometry. The pattern showed a series of peaks of 2θ at 11.5, 22.9, 34.8, 38.6, 45.8, 60.7 and 62 which relate to the LDH phase [ix,x]. The screened sharp and intense diffractions with low 2θ as well as the lower intensity and asymmetric diffractions at higher 2θ values illustrate the layered and well-crystallized structure of LDH. After treatment reaction, the spectrum of FLDH indicates amorphous structure compared with LDH, in addition to appearance of a new low 2θ peak at 7 due to increasing of d-spacing after functionalization.

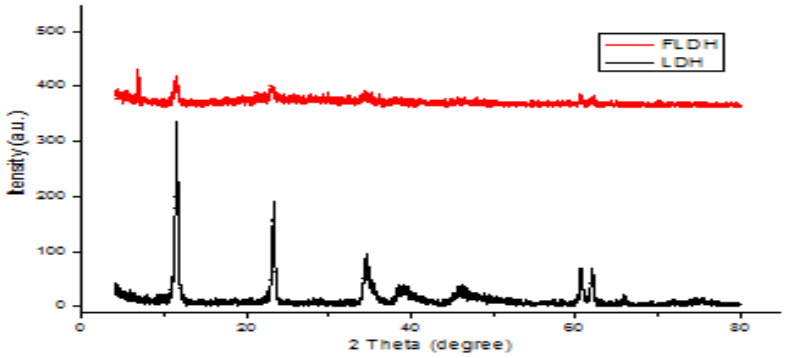

Fig 3: X-ray diffraction

Thermal gravimetric analysis

The TGA thermograms show losing of physically adsorbed water below 150 °C [xi], it demonstrates about 4% weight loss. Considering the weight losses from 150 °C to 600 °C, the LDH nanostructures showed 43% weight loss, which is attributed to the evaporation of interlayer water and dehydroxylation degradation of the metallic hydroxides and interlayer anions [xii,xiii]. However, the weight loss of FLDH was 52%. This matches with the performed functionalization reaction due to insertion of lower thermally stable fatty acid chains inside LDH layers. Both nanofillers are stable above 600 °C. The amount of residue after ignition is around 57% and 47% for LDH and FLDH, respectively.

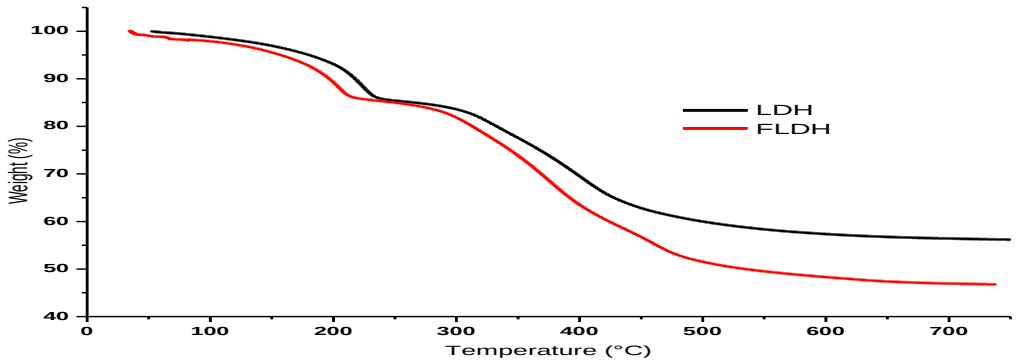

Fig 4: Thermal gravimetric analysis

Dynamic mechanical analysis

The mechanical properties of polyurethane nanocomposites filled with LDH and FLDH were investigated by DMA. The storage modulus of the blank polyurethane is 49 MPa. Addition of more concentrations of MgAl LDH led to increasing of modulus, within all temperature scale (from room temperature to 100 °C) as seen in the modulus-temperature curves. All nanocomposites show similar behavior regarding reducing of modulus as the temperature increases. As indicated in the columns of modulus values measured at room temperature, respectively, the 0.5%, 1% and 1.5% LDH-polyurethane nanocomposites achieved 68.5 MPa, 96.3 MPa and 169.9 MPa. However after treatment reaction, the modulus increased to 85.2 MPa, 113.6 MPa and 223.7 MPa, respectively. It is clear that the 1.5% nanocomposites has the highest modulus. Furthermore, the functionalization of nanofiller has achieved the maximum enhancement of modulus, especially with 1.5% FLDH through increasing by 356.5% and 31.7% compared with blank polyurethane and 1.5% LDH, respectively. This enhancement is due to the effective transferring of external load to the surrounding matrix by the modified LDH. However, the 0.5% nanocomposites have minor effect on modulus due to the insufficient concentration of used filler.

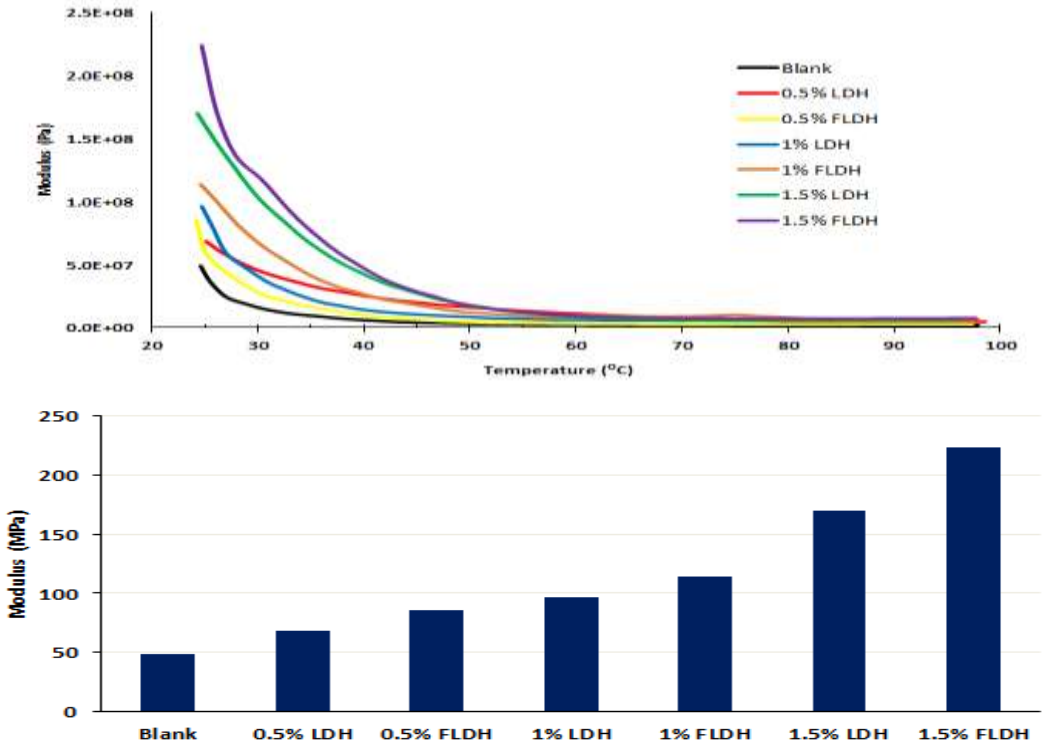

Fig 5: Dynamic mechanical analysis

4. Conclusion

Preparation of MgAl LDH and FLDH as separated nanostructures. TGA thermograms show successful grafting of palmitate into LDH nanoclay. XRD and IR peaks confirm formation of crystalline MgAl LDH, and its functionalization to amorphous FLDH. The functionalization of nanofiller achieved the maximum enhancement of modulus, especially with 1.5% FLDH nanocomposite, due to the effective treatment reaction.

References

1) Choi, J.; Moon, D. S.; Ja]ng, J. U.; Yin, W. B.; Lee, B.; Lee, K. J. Synthesis of highly functionalized thermoplastic polyurethanes and their potential applications. Polymer 2017, 116, 287–294.
2) Spontak, R. J.; Patel, N. P. Thermoplastic elastomers: Fundamentals and applications. Curr. Opin. Colloid Interface Sci. 2000, 5, 333–340.
3) Wei, W. C.; Deng, C.; Huang, S. C.; Wei, Y. X.; Wang, Y. Z. Nickel Schiff base decorated graphene for simultaneously enhancing the electro conductivity, fire resistance, and mechanical properties of a polyurethane elastomer. J. Mater. Chem. A 2018, 6, 8643–8654.
4) Shi, Y. Q.; Yu, B.; Zhou, K. Q.; Yuen, R. K. K.; Gui, Z.; Hu, Y.; Jiang, S. H. Novel CuCo2O4/graphitic carbon nitride nanohybrids: Highly effective catalysts for reducing CO generation and fire hazards of thermoplastic polyurethane nanocomposites. J. Hazard. Mater. 2015, 293, 87–96.
5) Liu, X. D.; Guo, J.; Tang, W. F.; Li, H. F.; Gu, X. Y.; Sun, J.; Zhang, S. Enhancing the flame retardancy of thermoplastic polyurethane by introducing montmorillonite nanosheets modified with phosphorylated chitosan. Composites, Part A 2019, 119, 291–298.
6) He, L. X.; Wang, J. L.; Wang, B. B.; Wang, X.; Zhou, X.; Cai, W.; Mu, X. W.; Hou, Y. B.; Hu, Y.; Song, L. Large-scale production of simultaneously exfoliated and functionalized Mxenes as promising flame retardant for polyurethane. Composites, Part B 2019, 179, 107486.
7) Xue LH, Gao B, Wan YS, et al. High efficiency and selectivity of MgFe-LDH modified wheat-straw biochar in the removal of nitrate from aqueous solutions. J Taiwan Inst Chem E. 2016;63:312–317. doi:10.1016/j. jtice.2016.03.021.
8) Wimalasiri Y, Fan R, Zhao XS, et al. Assembly of NiAl layered double hydroxide and graphene electrodes for supercapacitors. Electrochim Acta. 2014; 134:127– 135. doi:10.1016/j.electacta.2014.04.129
9) Zhang J, Wilkie CA. Polym. Degrad. Stab. 2003, 80, 163–169
10) Zoromba MSh, Bassyouni M, Abdel-Hamid SMS. Rubber Chem. Technol. 2015, 88, 449– 462.
11) Al-Qabandi O, De Silva A, Al-Enezi S, Bassyouni M. J. Reinf. Plast. Compos. 2014, 33, 2287–2299
12) C. Colombo, G. Palumbo, A. Ceglie, R. Angelico, Characterization of synthetic hematite (α-Fe_2O_3) nanoparticles using a multi-technique approach. Journal of Colloid and Interface Science 374 (2012), 118-126.
13) R.E. Daugherty, M.M. Zumbach, S.F. Sanders, T.D. Golden, Design challenges in electrodepositing metal-anionic clay nanocomposites: synthesis, characterization, and corrosion resistance of nickel-LDH nanocomposite coatings. Surface and Coatings Technology 349 (2018), 773-782.
14) M. Kaseem, Y.G. Ko, Benzoate intercalated mg-Al-layered double hydroxides (LDHs) as efficient chloride traps for plasma electrolysis coatings. Journal of Alloys and Compounds 787 (2019), 772-778.
15) F.R. Costa, M. Abdel-Goad, U. Wagenknecht, G. Heinrich, Nanocomposites based on polyethylene and Mg–Al layered double hydroxide. I. Synthesis and characterization. Polymer 46 (2005), 4447-4453.
16) E. Alibakhshi, E. Ghasemi, M. Mahdavian, B. Ramezanzadeh, S. Farashi, Active corrosion protection of mg-Al-PO43- LDH nanoparticle in silane primer coated with epoxy on mild steel. Journal of the Taiwan Institute of Chemical Engineers 75 (2017), 248-262.
17) A. Mohammadi, D. Hosseini, A.P. Isfahani, Z. Dehghani, E. Shams, Waterborne polyurethane nanocomposite incorporated with phytic acid intercalated layered double hydroxides: A highly stable aqueous dispersion with desired corrosion protection capability. Polymers for Advanced Technologies 32 (2021), 4014–4028.
18) N. Voyer, A. Soisnard, S.J. Palmer, W.N. Martens, R.L. Frostet, Thermal decomposition of the layered double hydroxides of formula Cu6Al2(OH)16CO3 and Zn6Al2(OH)16CO3. Journal of Thermal Analysis and Calorimetry 96 (2009), 481–485.
19) O.P. Ferreira, O.L. Alves, D.X. Gouveia, A.G.S. Filho, J.A.C. de Paiva, J.M. Filho, Thermal decomposition and structural reconstruction effect on Mg–Fe-based hydrotalcite compounds. Journal of Solid State Chemistry 177 (2004), 3058-3069.

Available online at www.asric.org
ASRIC Journal on Natural Sciences Vol 3(1) (2023) 47-49

Fencing Lands to Enhanced Climate Change Resilience, promoting Biodiversity Regeneration and Improved Livelihoods of Climate Change in Makueni County

Frank Wesonga[1*], Francis Keya[2]

[1]Project Manager, African Alliance for Health, Research and Economic Development (AAHRED) P.O. Box 11102 Nairobi Kenya
[2]National Non-Government Council (NGO) Kenya, P.O Box425, Kenya

* Corresponding author: Frankwesonga2016@gmail.com

Abstract
Kenya is a food insecure country, weather patterns are drastically changing and people are losing livelihoods and earnings when their lands dry, water for domestic supply lacks and livestock die further frustrating livelihoods of the poor. This paper briefly discusses Fencing of lands as prerequisite to biodiversity protection and faster water retention mechanism, through tree planting, enhancing CO2 sequestration as trees, shrubs and vegetation's find suitable environment to grow. Baringo and Makueni County are characterized by unsustainable agriculture, environmental degradation resulting from soil erosion, high poverty levels and food insecurity due to unpredictable dry spells and climate change. The present paper illustrates that Fencing of lands improves agricultural land management practices, biodiversity growth increased soil carbon sequestration.
Keywords, food security, soil carbon sequestration, climate change, soil erosion

Introduction,
The capacity to protect land from interference and planting trees play a crucial role in ameliorating climate change by CO2 sequestration, where CO2 from the atmosphere is stored as carbon in stems and roots, thereby reducing the greenhouse effect. Trees also influence hydrology by absorbing, intercepting and storing precipitation, and releasing water to the atmosphere through transpiration, maintaining ground water levels and reducing runoff. Trees are a source of food, shelter, and habitat for many organisms and soil erosion has contributed to desertification, growing water scarcity, and climate events such as flooding, storms and final loss of biodiversity. Fencing helps regeneration increasing soil biodiversity and organic matter, leading to more resilient soils that can better withstand climate change impacts like flooding and drought. It stops loss of the humus leading to healthy soils resulting to strong plant growth and nutrient-rich crops, diminishes erosion and runoff, leading to improved water quality on and off the farm and water sources and help us fight the climate crisis by pulling carbon from the atmosphere and sequestering it in the ground.

Scope and Main Objective
Against this background this paper analyses fencing of lands as a prerequisite to biodiversity protection and faster water mechanisms, through tree planting in Makuein and Baringo Counties in Kenya. These two notable counties have varying agro-climate zones needing varying conservative interventions. These agro zones contrast in relationships to soil moisture index, precipitation, plant life and agriculture patterns. High potential areas have a moisture index greater than 50% but account for only 12% of Kenya's land area (Kabudo & Kabara 2015).

Temperatures have average of 22.9c and an average rainfall is 450-900mm with evaporation rates of 16502300mm.Survival depends on the inflows from rivers originating from the humid hill slopes of the drainage basin (World Lakes Database-ILEC).

These areas are mainly suitable for livestock farming (mostly cattle and sheep and key food crops (maize, beans and wheat) (Kabudo & Kabara 2015).Climatic variations affect crop and livestock systems both directly and indirectly and could have severe socio-economic impacts such as shortages of food, water, energy and other essential basic commodities, as well as long-term food insecurity (Kabubo-Mariara 2008a)There is however a gap of literature between a correlationship between Climate Change and food security in Kenya. This paper tries to resolve the underlying gap.

The general objective of this study is to investigate the relationships between climate change and food Security in Kenya, by studying Climate change Resilience, promoting biodiversity regeneration and land fencing.

Methodology

The paper examines county level data. The research employed both qualitative and quantitative approaches of research. The data was composed by questionnaires and key informants. The research paper targeted small holder farmers, women and youth and the general community at large.

The study used random sampling to select the study themes and purposive sampling to select key informants. Soil data, climate variables was sourced from the Ministry of Agriculture. The sampling setting was of 300 participants drawn from different cross cutting sectors including small scale farmers, women and youth and the general community in the two counties.

Table 1.1 Sample Distribution

County	No.of participating populations	20%	Total participating populations
Baringo	180	180*20/100	36
Makueni	120	120*20/100	24

(Mugenda 2003) mentions a sample size of more than 30 or at least 10% is appropriate for social science. The selected sample of 20% of the participating populations formed the sample of the study. The study Used both quantitative and qualitative which included key informants small scale farmers, women, youth and the general community.

Table 1.2 Study methods, instruments and sources of information

Method	Tool	Source
Small holder Farmer, Women Youth, Community	Questionnaire	Participating smallholders farmer, women youth, community
	Key Informant Interview	Ministry of Agriculture, Agriculture extension officers

Results

Extreme change in precipitation was a major cause of crop failure. The majority of small holder farmers cited loss of crop as result of climate change due to the variability of precipitation. And this group cited precipitation as a major cause of crop failure. Hence it was reported a great loss of income and also loss of food security. These findings affected both women and youth as the most vulnerable groups. The study found that climate change caused a huge burden to the community as drought prolonged and the rainfall season shortened. Women were forced to go great distances in search of water both for households. As Agriculture declined the youth resorted to social misfits engaging in substance abuse and the rate of crime swelled. Boreholes dried and a record decline in available water and so sustainable agriculture became almost impossible given the prevailing circumstances.

Discussion

Fencing was introduced in four farms. This helped prevent soil erosion and increased land productivity. It was observed that fencing created a micro climate in the said farms. Reduced precipitation by 26% and observed stalks of the maize plant increased in diameter. Planted millet also proved to be stronger than before. Horticultural production was introduced and seemed to do very well especially tomatoes did very well. Onions yield per acre increased as precipitation reduced. Food insecurity was projected to reduce by 32% and community incomes and livelihoods were projected to increase to 54%.

Conclusion

The study findings demonstrated that climate change has been a real challenge in Kenya. Farmers affirmed that vagaries of climate change were real and this was confirmed by persistent droughts, dried boreholes, crop failure, and change in temperature, increased pests and diseases. Loss of livestock as result of droughts was reported as a result of climate change.

Acknowledgements

African Alliance for Health Research Economic Development and National NGOs Council of Kenya.

References

Jane KABADO-Mariara and Millicent Kabara March 2017, Climate change and Food Security in Kenya
Kennedy Mwangi 2017, Adapting to Climate Change in Kenya, A case study
Ministry of Agriculture 2015, A handbook depicting the impacts of climate change to small holder farmers.
World Lake Database-ILEC

Available online at www.asric.org
ASRIC Journal on Natural Sciences Vol 3(1) (2023) 50-58

Isotherm, Kinetic and Thermodynamic Terms of Adsorption of Pyrimethamine from Binary Aqueous Solution

Adesokan Saheed Ademola[1*], Giwa Abdur-Rahim Adebisi[1]

[1]Department of Pure and Applied Chemistry, Ladoke Akintola University of Technology, Ogbomoso

*Corresponding author: adesokansaheed@ymail.com

Abstract
The processing of under-utilized sawdust as adsorbent for removing contaminants like pharmaceuticals from aqueous solutions is a sustainable environmental management strategy. In this study, sawdust was carbonized, activated with $ZnCl_2$ and code-named Z-AC. Binary aqueous solutions of pyrimethamine containing paracetamol were treated with Z-AC; and effects of contact time, pH, temperature, adsorbent dose and adsorbate concentration were determined in batch adsorption experiments. The isotherm, kinetic and thermodynamic studies were conducted. The equilibrium was attained at 100 minutes. At pH 2.0 and 7.6, pyrimethamine load on Z-AC were 5.20 and 2.68 mg/g respectively. At 30 ^oC and 50 ^oC, pyrimethamine adsorbed were 1.68 and 2.52 mg/g respectively. Z-AC has monolayer adsorption capacity of 4.76 mg/g for pyrimethamine in binary solution. Load of pyrimethamine per unit mass of Z-AC decreased with increased dose of Z-AC. The best isotherm and kinetic fitting were Langmuir (0.98) and pseudo-first order (0.98) respectively. The process was endothermic (+18.5 kJ/mol/K) with increased degree of randomness (+48.52 J/mol/K). The process was feasible at higher temperatures. Higher pH and adsorbent doses de-enhanced the process while increased temperatures enhanced adsorption of pyrimethamine in binary aqueous media. Therefore, Z-AC could be utilized in adsorption process for remediating pharmaceutical contaminated aqueous media.
Keywords: pyrimethamine, binary solution, paracetamol, pharmaceuticals, isotherm, thermodynamics

Introduction

The availability of usable and potable water is on decline across the world. This is due to discharge of substances with range of sources into water bodies (Adesokan et al., 2022). These substances constitute contaminants and pollutants that impact water resources with negative attributes. These water contaminants and pollutants could be toxic at low concentration, persistent, bio-accumulate or alter the standard characteristics (colour, odour, taste, density, biological oxygen demand, chemical oxygen demand and pH) of water (Manisalidis et al., 2020). Human exposure to these pollutants in the environment could be primary where there would be direct contact through water. Pollutants in portable water could impair human health or worsen condition of vulnerable populations like sick and persons with compromised immune system. Also, presence of contaminants and pollutants could hinder direct usage of water resource for agricultural, e.g. irrigation, and industrial, e.g. cooling, purposes. Human could made secondary contact with pollutants in water through consumption of aquatic food resources. Some persistent, bio-accumulative, bio-magnified and transformed pollutants could enter food chains and wreck havocs (Fuller et al., 2022).

Some of the contaminants and pollutants are heavy metals, dyes, organic chemicals, detergents, pesticides, herbicides, hydrocarbons, flame retardants and industrial additives, plasticizers and pharmaceuticals and personal care products. These substances are generated by pharmaceutical, medical/health, agrochemicals, petrochemical, dyeing and agricultural industries/facilities (Akhtar et al., 2021). Drugs are neurological and physiological compounds administered to facilitate, maintain and sustain wellbeing. Pharmaceuticals/drugs are endocrine disruptive substances. Involuntary exposure to pharmaceuticals could lead to cancer, renal failure and other health infractions, especially among aged, children and ailing populations (Kusturica et al., 2022; Wilkinson et al., 2022).

Extensive profiling of levels of contaminants and pollutants in environment has been done, as well as their effects on ecosystem. However, pharmaceuticals are substances of emerging concerns. Methods of determining pharmaceuticals in the environment are emerging as well as their impacts. The contaminants from these sources enter into the environment through, majorly, discharge of effluents. Many wastewater treatment plants were not designed to deteriorate/remove emerging contaminants (Patel et al., 2019). One of the promising methods for treatment of pharmaceutical-bearing water/wastewater is adsorption. Adsorption, using low cost adsorbent, is comparatively cheap and effective (Vinayagam et al., 2022).

Pyrimethamine, a pharmaceutical, is a substance in anti-malarial drugs. Anti-malarial drugs are among most produced and dispensed in Nigeria and many global south countries, because of prevalence of malarial disease. The propensity of pyrimethamine in pharmaceutical wastewater is expected to be high. Therefore, in this study pyrimethamine was removed from aqueous solution using sawdust-based adsorbent.

Materials and Methods

Material and equipment

Sawdust was collected from a wood processing factory in Ogbomoso, Nigeria. $ZnCl_2$ HCl and NaOH of analytical grades were purchased from chemical store outlets in Ibadan. Pyrimethamine and paracetamol were donated by Bond Chemical Industry Limited, Awe, Oyo State for research purpose. Some of the equipment used were spectrometer (Pelkinlmer Spectrum BX), oven (Carbolite), ultraviolet-visible (UV) (B-UV 1800PC) spectrophotometer, furnace (Carbolite AAF 1100) and pH meter (Jenway 3520).

Preparation of Z-AC

A 300 g of sawdust was soaked in 300 mL of 1 M $ZnCl_2$ for 30 minutes in a clean crucible. The mixture was put in the furnace, the temperature rose to and maintained at 800 ^{0}C for 5 minutes. The sample was removed with the help of a probe, poured into cold (iced) water; excess water drained and allowed to stand at room temperature. The activated carbon generated was washed with warm distilled water to remove residual acid until pH of the supernatant was neutral. The sample was then dried in an oven at 110 ^{O}C overnight and sieved, 0.4 mm sizes retained and stored in air tight containers as Z-AC (Adesokan et al., 2021).

Batch adsorption experiments

The batch adsorption was conducted in 100 mL adsorption bottles containing 20 mL of equal concentrations of pyrimethamine and paracetamol. The adsorbent-adsorbate systems were oscillated on a mechanical shaker. The effects of adsorbent dosage (0.1– 1.0 g), pH (2.8, 3.8, 4.9, 7.6), contact time (0–200 min), initial adsorbate concentration (30 – 70 mg/L), and temperatures (30, 40, 50 ^{o}C) were evaluated. After the adsorption, the mixtures were filtered and the filtrates analysed with the ultraviolet-visible (UV) spectrometer to determine the amount of un-adsorbed adsorbates in solutions. The amount of adsorbate uptake at equilibrium was determined using:

$$q = \frac{V(C_i - C_e)}{m}$$

Where, q is amount of adsorbate adsorbed per unit mass of adsorbent (mg/g), V is the volume of solution (L), m is the amount of adsorbent (g), and C_i and C_e (mg/L) are the initial and equilibrium adsorbate concentrations in the solution, respectively.

Adsorption Isotherms

Table 1 contains selected isotherms used to process experimental data and then described the adsorption processes.

Table 1: Adsorption isotherm parameters

Model	Linearised Formulae	Reference
Langmuir	$\frac{C_e}{q_e} = \frac{1}{K.Q_o} + \frac{C_e}{Q_o}$	(Langmuir, 1918)
Freundlich	$lnq_e = lnK_F + \frac{1}{n} lnC_e$	(Freundlich, 1906)
Temkin	$q_e = BlnK_T + BlnC_e$	(Tempkin and Pyzhev, 1940)
Dubinin–Radushkevich	$\ln q_e = \ln(q_s) - (K_{ad}\varepsilon^2)$	(Rieman and Walton, 1974)

In Langmuir Model plot, C_e/q_e versus C_e gives a straight line with intercept: $1/K.Q_o$; and slope: $1/Q_0$. Langmuir isotherm equilibrium parameter, R_L: $R_L = \frac{1}{1+K_L C_i}$. (Rieman and Walton, 1974). C_i = highest initial adsorbate concentration (mg/L); R_L>1 = unfavourable; R_L=1=linear; favorable 0<R_L<1=favourable and R_L = 0 = irreversible. In Freundlich Model plot, lnq_e vs ln C_e yields an intercept of log K_F and a slope of 1/n. n defines isotherm shape; 1/n = 0 = irreversible; (0<1/n<1) = favourable; unfavourable (1/n>1); n = 1=linear; n > 1 = physical process and n < 1= chemical process. In Temkin Model, q_e was ploted against ln C_e. K_T =Temkin isotherm equilibrium binding constant (L/g); b_T (B) = Temkin isotherm constant; R= universal gas constant (8.314J/mol/K); T= Temperature at 298K; B = Constant related to heat of sorption (J/mol). In Dubinin–Radushkevich Model, ln qe was plotted against ε^2: $\varepsilon = RT\ln[1 + \frac{1}{C_e}]$; $E = [\frac{1}{\sqrt{2B_{DR}}}]$; $K_{ad} = B_{DR}$; E<8 kJ/mol (physical adsorption); E = 20–40 kJ/mol (chemical adsorption) (Tempkin and Pyzhev, 1940); E = 8–16 kJ/mol (ion-exchange) (Helfferich, 1962); q_e = amount of adsorbate on the adsorbent at equilibrium(mg/g); q_s = theoretical isotherm saturation capacity (mg/g); K_{ad} = Dubinin–Radushkevich isotherm constant (mol^2/kJ^2).

The Kinetic Study

Samples were taken from adsorption bottles at time intervals and the amounts of adsorbates were measured. The amount of adsorbed adsorbate at time, *t*, q_t (mg/g), was calculated using Equation:

$$q_t = \frac{(C_o - C_t)V}{m}$$

The kinetic parameters were calculated using kinetic equations presented in Table 2.

Table 2: Adsorption kinetic parameters

Kinetic	Equation	Reference
Pseudo-First Order	$\log(q_e - q_t) = \log q_e - \frac{k_1}{2.303}.t$	(Lagergren, 1898)
Pseudo-Second Order	$\frac{t}{q_t} = \frac{1}{h} + \frac{t}{q_e}$	(Ho & G. McKay, 1998)
Elovich	$q_t = \frac{1}{\beta}\ln(\alpha\beta) + \left(\frac{1}{\beta}\right)\ln t$	(Okiemen and Onyega, 1989; Sparks, 1986)
Intra-Particle Diffusion	$Q_t = k_{id}t^{0.5} + C_i$	(Weber and Morris, 1962)

In Pseudo-First Order equation, q_e and q_t are the amounts of the pyrimethamine adsorbed (mg/g) at equilibrium and at time t (min), respectively, and k_1 is the rate constant adsorption (min^{-1}). A plot of $\log(q_e - q_t)$ versus t gives a slope of $(-\frac{k_1}{2.303})$ and intercept of $\log q_e$. In Pseudo-Second Order equation, $h = (k_2\ q_e^2)$; q_e is the amount of the solute adsorbed at equilibrium per unit mass of adsorbent (mg g^{-1}) , q_t is the amount of solute adsorbed (mg g^{-1}) at any given time, *t* (min) and k_2 is the rate constant for pseudo-second-order adsorption (g $mg^{-1}min^{-1}$) and *h*, known as the initial sorption rate. In Elovich equation, plot of q_t vs *ln t* gives a straight line with intercept $\frac{1}{\beta}\ln(\alpha\beta)$ and slope $\left(\frac{1}{\beta}\right)$. α is the initial adsorption rate (mg/g. min), β is the desorption constant (g/mg) and q_t is the amount of solute adsorbed (mg/g) at any given time, t (min). In Intra-Particle Diffusion equation, graph of Q_t versus $t^{0.5}$ gives a straight line with slope, k_{id}, and intercept, C_i. C_i defines the thickness of the boundary layer. Q_t (mg/g) = quantity of adsorbate adsorbed at time, t and k_{id} ($mg/gh^{0.5}$) = intra-particle diffusion constant.

Thermodynamic Study

A series of experiments were performed at 30, 40 and 50 °C to establish the effect of temperature on the adsorption capacities of Z-AC for the pyrimethamine in binary solution. The thermodynamic parameters of the adsorption were determined using the equations:

$$log(\frac{C_{Ae}}{C_e}) = \frac{\Delta S^0}{2.303R} - \frac{\Delta H^0}{2.303RT}$$

C_{Ae} = (C_i – C_e) (mg/L) = amount of adsorbate adsorbed on adsorbent at equilibrium; C_e (mg/L) = amount of adsorbate in solution at equilibrium; R = gas constant (8.314 J/mol/K); T = temperature (K). The enthalpy change (ΔH), the entropy change (ΔS) and the change in standard free energy (ΔG) were calculated. The spontaneity of the processes was thereby determined using van't Hoff graph which is a plot of $log(\frac{C_{Ae}}{C_e})$ vs $\frac{1}{T}$.

Results and Discussion

Effect of Z-AC dose on adsorption of PYR from binary solution

In binary solution of PYR and paracetamol, at 0.1, 0.2, 0.3, 0.4 and 0.5 g of Z-AC, the q_e were 1.91, 1.34, 1.04, 0.68, 2.22 mg/g respectively (Figure 1). These q_e were comparable to those for single system (Giwa et al., 2021). As Z-AC dose increased, the q_e (mg/g) decreased (dose α $1/q_e$). As Z-AC dose increased, the adsorption sites per molecule of PYR in binary solution increased. The competition among the molecules in solution thereby reduced and there was dropped in repulsive drift towards the Z-AC surface.

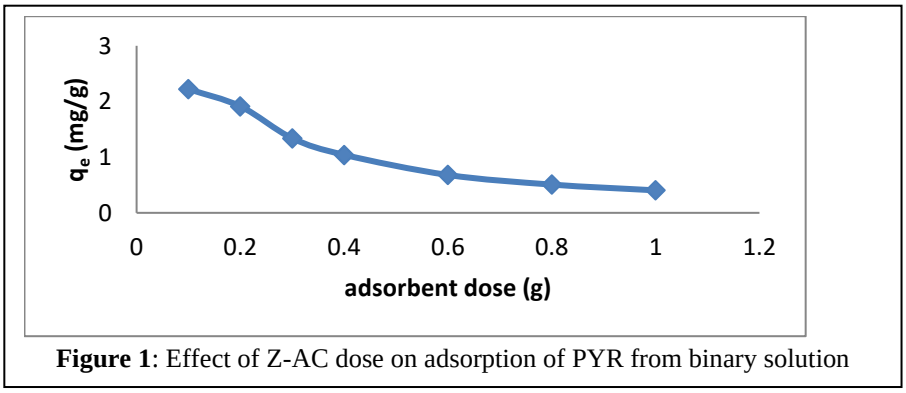

Figure 1: Effect of Z-AC dose on adsorption of PYR from binary solution

Effect of pH on the adsorption of PYR from binary solution

At pH 2.8, 3.8, 4.9 and 7.6 respectively, 5.14, 3.41, 2.14 and 2.68 mg/g of PYR were adsorbed from PYR and paracetamol binary solution (Figure 2). These values were higher than those reported for adsorption of PYR from single solution (Giwa et al., 2021). This indicated that pH enhanced adsorption of PYR in binary system as q_e reached 5 mg/g. At acidic pH, the solution was protonated. The nucleophilic centers on already adsorbed PARA picked up the electrophile (H^+) and became charged. The adsorbed and charged PARA provided adsorptive sites for PYR. However, as pH changed from acidic to basic, adsorption of PYR was de-enhanced and q_e reduced. This might due to electrostatic repulsion among PARA (OH^-, CO^-, N), adsorbents (negative at pH above pzc), PYR (N^-) and OH^- of solution.

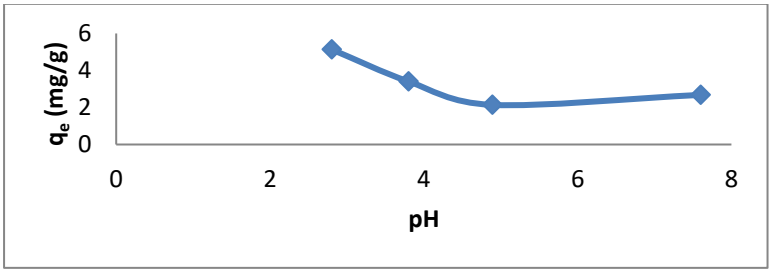

Figure 2: Effect of pH on adsorption of PYR from binary solution

Isotherm Study of the Adsorption of PYR from Binary Solution

At 30, 40, 50, 60 and 70 mg/L respectively, 3.09, 3.86, 3.84, 3.81 and 4.25 mg/g of PYR (in mixture with paracetamol) were adsorbed (Figure 3). As concentration increased from 30 to 40 mg/L, the bulk solution driving force (mutual repulsion among PYR and paracetamol molecules) increased. This could lead to increase drift towards the adsorptive sites of Z-AC. The adsorption capacity of Z-AC was thereby improved. However, between 40 and 60 mg/L, there was dropped in the capacity of Z-AC; paracetamol molecules could have had competitive adsorption edge over PYR molecules. At 70 mg/L, the capacity of Z-AC increased again for PYR. As initial PYR binary solution concentration increased, the available adsorptive active sites were completely occupied. Therefore excess adsorbate molecules remained in solution.

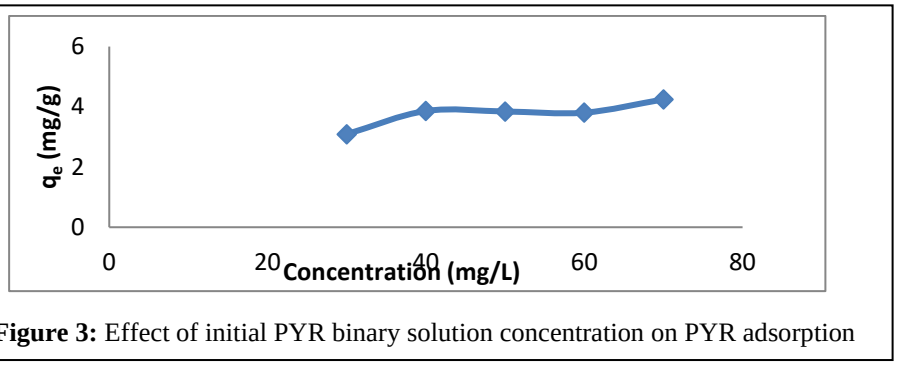

Figure 3: Effect of initial PYR binary solution concentration on PYR adsorption

In binary system of PYR+PARA, the model that best fit the adsorption of PYR by Z-AC was Langumuir (R^2 =0.976) (Figure 4, Table 3) which indicated monolayer adsorption. The maximum monolayer adsorption capacity of Z-AC for PYR (q_{max}) was 4.76 mg/g. This was bigger than q_{max} of Z-AC for PYR in single system (Giwa et al., 2021). This showed that presence of PARA in the system aided adsorption of PYR by Z-AC. R_L value of 0.105 showed that the process was favourable. The value n parameter calculated from Freundlich model was 4.525 L/g and activation energy (E_a kJL/mol/mg), 0.158, defined adsorption of PYR in binary solution as physical process.

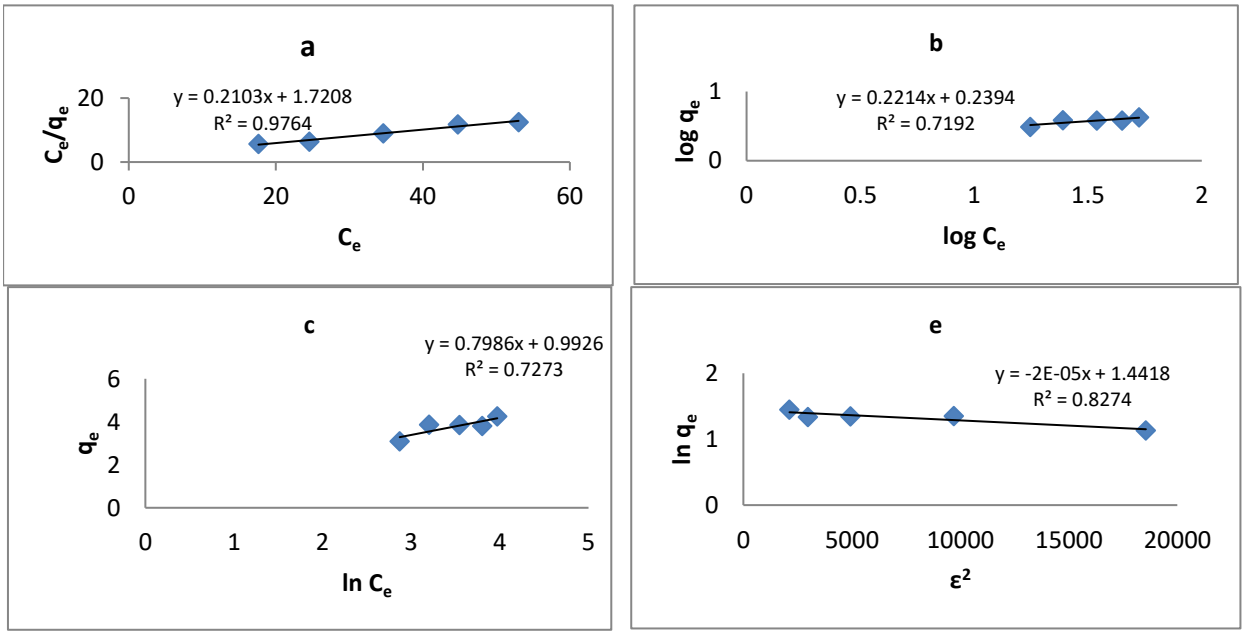

Figure 4: Plots of (a) Langmuir, (b) Freundlich, (c) Temkin, (d) Dubinin-Radushkevich isotherms for adsorption of PYR by ZCAC in PYR+PARA binary system

Table 3: Isotherm Parameters of Adsorption of pyrimethamine in binary solution by ZCAC

Langmuir				Freundlich				Temkin				D-R			
q_{max} (mg/g)	k_L (L/mg)	R_L	R^2	K_F (mg/g)	n (L/g)	1/n	R^2	K_T	b_T (kJ/mol/gL)	β (L/g)	R^2	q_s (mg/g)	K_{ad} (JL/mol/mg)	E_a (KJL/Mol/mg)	R2
4.76	0.122	0.105	0.98	1.73	4.53	0.22	0.72	3.47	3.16	0.80	0.73	4.23	2×10^{-5}	0.158	0.70

Kinetic Study of the Adsorption of PYR in Binary Solution

The q_e at 30, 90, 120 and 200 minutes were 0.77, 1.77, 1.97 and 1.86 mg/g respectively (Figure 5). The adsorption reached equilibrium around 100 minutes as against the single adsorption at 240 mintues (Giwa et al., 2021). The adsorption of PYR in binary system by Z-AC might be influenced in a number of ways. Paracetamol molecules were suspected to diffuse faster competitively into the available pores and also might interact with Z-AC surface through its nucleophilic centers. Therefore adsorption of PYR by Z-AC in binary system was de-enhanced and q_e (binary aystem) smaller than q_e (single system) (Giwa et al., 2021). Also, bulk solution repulsive force created by paracetamol and PYR molecules in solution might generate high drift (enhanced mobility) of molecules and therefore equilibrium was attained earlier than in single solution.

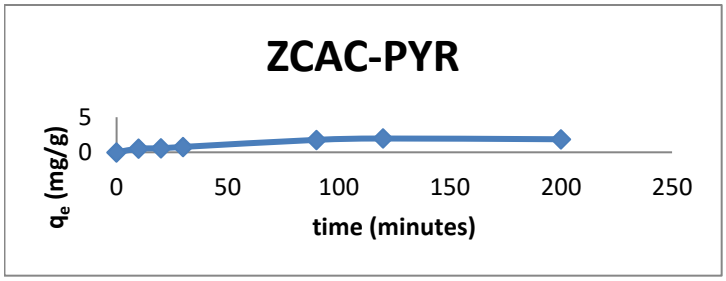

Figure 5: Effect of contact time on adsorption of PYR in binary solution

The data of adsorption of PYR by Z-AC from the mixture with paracetamol fitted best pseudo-first order kinetics (PFO). The PFO kinetic regression coeffiecient (R^2 = 0.977) (Figure 6) was the highest, together with lower SSE value, followed by that of intraparticle diffusion (R^2 = 0.964), and the values of pseudo-first-order q_{cal} (2.25 mg/g) was the closest to q_{exp} (1.97 mg/g) (Table 4). The rate of removal (K_1) of PYR from binary solution by 1 mg of Z-AC per 1 minute was 0.025 mg. The high R^2 of Intraparticle diffusion model suggested that diffusion of PYR into the pores of Z-AC play role in rate determining step of the process.

Table 4: Kinetics parameters for pyrimethamine adsorption onto Z-AC

Kinetic	ZCAC (binary system)
$q_{e,\ exp}$	1.966
Pseudo-first order	
q_e (mg/g)	2.254
K_1 (mg/g/min)	0.0253
R^2	0.977
SSE (%)	0.144
Pseudo-second order	
q_e (mg/g)	3.155
h (mg/g/min)	0.0415
K_2	0.0042
R^2	0.778
SSE (%)	0.594
Elovich	
A	0.100
β (min.g/mg)	1.672
R^2	0.879

Intraparticle	
C_i (mg/g)	-0.285
K_{id}(mg/g/min$^{1/2}$)	0.211
R^2	0.964

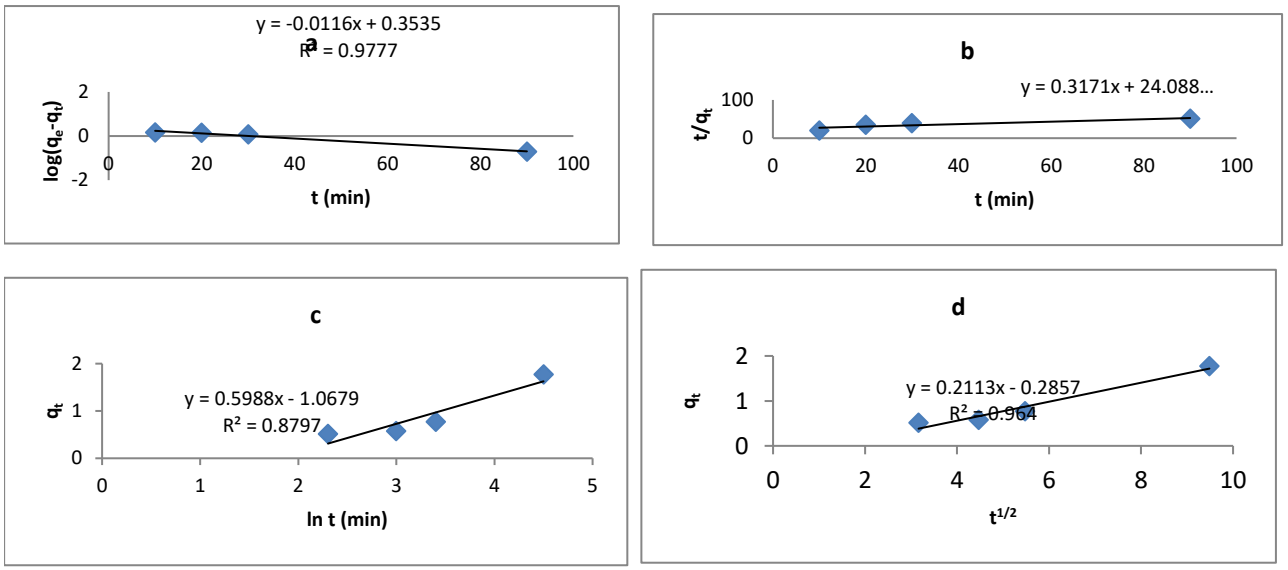

Figure 6: Plots of (a) pseudo first order, (b) pseudo second order, (c) Elovich, (d) intraparticle, (e) Boyd kinetics for adsorption of pyrimethamine by Z-AC in PYR+PARA binary system

Thermodynamic Study of the Adsorption of PYR in Binary Solution

The capacities of Z-AC for PYR in binary solution were 1.68, 2.31 and 2.52 mg/g at 30, 40 and 50 ºC (Figure 7). As temperature increased, the capacity of Z-AC for PYR increased. As temperature increased, the PYR molecules acquired energy and migrated faster onto the Z-AC surface and the adsorption sites. High temperature could soften the pore openings and pore walls and made them more receptive to migrating adsorbate molecules. The q (mg/g) of ZCAC-PYR in binary system was higher than those of single system at the tested temperatures (Giwa et al., 2021). The presence of paracetamol enhanced the adsorption of PYR from binary solution. Paracetamol could have specific interaction with the Z-AC and at the same time served as bonding surface for PYR.

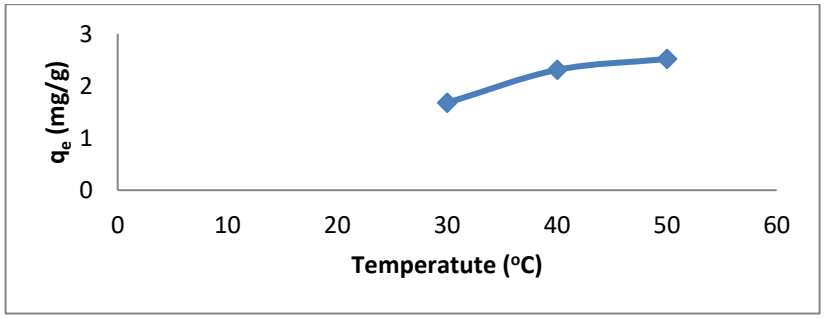

Figure 7: Effect of temperature on adsorption of PYR from binary solution

The ZCAC-PYR adsorption process was endothermic (+ΔHº) with high degree of randomness (+ΔSº) (Figure 8). However, the process was only spontanous at higher temperatures which mean the affinity of PYR molecules for the adsorbent increased at higher temperatures. Adsorption of PYR by ZCAC in the presence of PARA in solution required high energy. ΔG (+x J/mol/K) (Table 5) could occur as a result of interference that shift energy boundry from one extreme to another (Banjo et al., 2016; Ozcan and Ozcan, 2004).

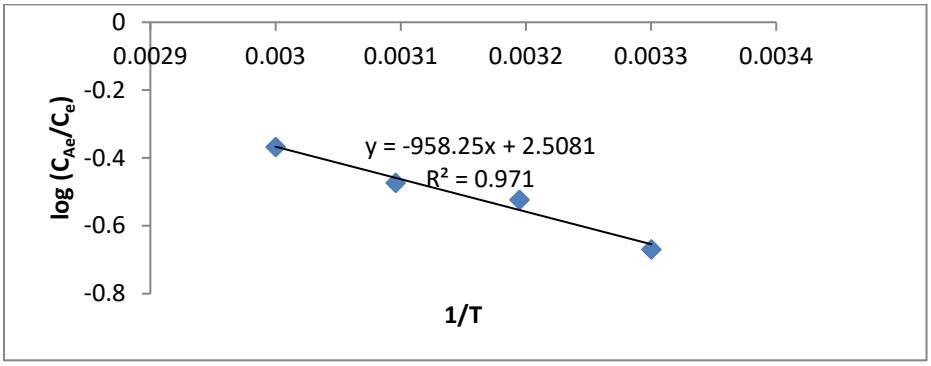

Figure 8: van't Hoff plot of logK vs 1/T adsorption of PYR+PARA binary solution onto Z-AC

Table 5: Thermodynamics parameters of adsorption of pyrimethamine onto the Z-AC from binary solution

Thermodynamic Parameters	Temperatute (K)	Z-AC
	302	+3.798
	313	+3.313
ΔG^0 (kJ/mol/K)	323	+2.828
	333	+2.343
ΔS^0 (kJ/mol/K)		+0.049
ΔH^0 (kJ/mol/K)		+18.500

Conclusion

Presence of paracetamol in the solution enhanced capacity of Z-AC for pyrimethamine. Also, increase in temperature and decrease in pH enhanced adsorption of pyrimethamine in binary solution. Z-AC showed good capacity for adsorption of pyrimethamine from binary aqueous solution which contained paracetamol.

Acknowledgements

This research did not receive any specific grant from funding agencies in the public, commercial, or not-for-profit sectors.

References

Adesokan, S. A., A. A. Giwa, A. A., Bello. I. A., (2022). Environmental, Health and Economic Implications of Emerging Contaminants in Nigeria Environment, *J. of the Nig. Soc. of Phys. Sci.*, 4: 1-7, DOI:10.46481/jnsps.2022.842.

Adesokan, S.A., Giwa, A. A., Bello, I. A., (2021). Adsorptive Removal of Ibuprofen from Waste Stream using Sawdust-based Adsorbents, *Int. J. of Eng. Res. in Africa* 55: 172, https://doi.org/10.4028/www.scientific.net/jera.55.172.

Akhtar, N., Ishak, M. I. S., Bhawani, S. A., Umar, K., (2021). Various Natural and Anthropogenic Factors Responsible for Water Quality Degradation: A review, *Water*, 13: 2660, https://doi.org/10.3390/w13192660.

Banjo, A. A., Laniyi, L. A., Aka-Tanimo, H. A., Bello, A. O., (2016). Thermodynamics of the Adsorption of Cadmium Ions by Natural Lateritic Soil, *IJSAR*, 1: 1-8.

Freundlich, H. M. F., (1906). Over the Adsorption in Solution, *J. Phys. Chem* 57: 385-470.

Fuller, R., Landrigan P. J., Balakrishnan, K., Battan, G., Bose-O'Reilly, S., Brauer, M., (2022). Pollution and Health: A Progress Update, *The Lancet*, 6: 535, https://doi.org/10.1016/S2542-5196(22)00090-0.

Giwa, A.A., Adesokan, S. A., Bello, I. A., (2021). Adsorption of Pyrimethamine from Wastewater using Activated Carbons prepared from Daniellia—*oliveri* Sawdust, *International Journal of Environmental Analytical Chemistry* 1-17, DOI:10.1080/03067319.2021.1884858.

Helfferich, F., (1962). Ion Exchange, *Science* 138: 313, DOI:10.1126/science.138.3537.133.a.

Ho Y. S., McKay, G., (1998). Sorption of Dye from Aqueous Solution by Peat, *Can J Chem Eng* 70: 115-124, http://dx.doi.org/10.1016/S0923-0467(98)00076-1.

Kusturica, M. P., Jevtic, M., Ristovski, J. T., (2022). Minimizing the Environmental Impact of Unused Pharmaceuticals: Review focused on Prevention, *Frontiers in Environmental Sciences* 10**:** 1077974, https://doi.org/10.3389/fenvs.2022.1077974.

Lagergren, S., (1989). Theory of so called Adsorption of Soluble Substances, *Kungliga Svenska Vetenskapsakademiens. Handlingar Band* 24: 1-39.

Langmuir, I., (1918). The Adsorption of Gases on Plane Surfaces of Glass, Mica and Platinum, *J. Am. Chem. Soc* 40: 1361, https://doi.org/10.1021/ja02242a004.

Manisalidis, I., Stavropoulou, E., A. Stavropoulos, A., Bezirtzoglou, E., (2020). Environmental and Health Impacts of Air Pollution: A Review, *Frontiers in Public Health*, 8: 1, https://doi.org/10.3389/pubh.2020.00014.

Okiemen, F. E., Onyega, V.U., (1989). Binding of Cadmium, Copper, Lead and Nickel Ions with Melon (Citrullus vulgaris) Seed Husk, *Biological Waste* 29: 11.

Ozcan, A. S., Ozcan, A., (2004). Adsorption of Acid Dyes from Aqueous Solutions onto Acid Activated Bentonite, *Journal of Colloid and Interface Science* 276: (2004) 39-46.

Patel, M., Kumar, R., Kishor, K., Mlsna, T., Pittman, C. U., Mohan, D., (2019). Pharmaceuticals of Emerging Concern in Aquatic Systems: Chemistry, Occurrence, Effects and Removal methods, *Chemical Reviews* 119: 3510, https://doi.org/10.1021/acs.chemrev.8b00299.

Rieman, W., Walton, H., (1964). Ion Exchange in Analytical Chemistry", Oxford: Pergamon Press, https://doi.org/10.1002/food.19740180319.

Sparks, D. L., (1986). Kinetics of Reactions in Pure and Mixed Systems in Soil Physical Chemistry, *CRC Press, Florida* 21.

Tempkin, M. I., Pyzhev, V., (1940). Kinetics of Ammonia Synthesis on Promoted Iron Catalyst, *Acta Phys. Chim. USSR* 12: 217-222.

Vinayagam, V., Murugan, S., Kumaresan, R., Nayaranan, M., Sillanpaa, M., Vo, D. V. N., Kushawaha, O. S., Jenis, P., Potdar, P., Gadiya, S., (2022). Pharmaceuticals from Wastewater: A Review, *Chemosphere* 300: 134597, https://doi.org/10.1016/j.chemospere.2022.134597.

Weber, J. W., Morris, C. J., (1962). Proceedings of the International Conference on Water Pollution Symposium, *Pergamon Press, Oxford* 2: 231-266.

Weber, W. T., Chakravo, K. P., (1974). Pore and Solid Diffusion Model for Fixed Bed Adsorbent, *J. Am. Inst. Chem. Eng* 20: 228, http://dx.doi.org/10-1002/aic.690200204.

Wilkinson, J. L., Boxall, A. B. A., Kolpin, D. W., Teta, C., (2022). Pharmaceutical Pollution of the World's Rivers, *Pnas* 119: 1, https://doi.org/10.1073/pnas.2113947119.

Available online at www.asric.org
ASRIC Journal on Natural Sciences Vol 3(1) (2023) 59-65

Phytochemical Analysis, Antibacterial and Antioxidant Activity of Stem Extracts of Azadirachta indica

Yiketel Adege Chekol[1*], Molla Zewdie Eshetu[1]

[1]Department of Chemistry, College of Natural and Computational Science, Samara University, P. O. Box 132, Semera, Ethiopia.,Mobile:

*Corresponding author: yiketel56@gmail.com

Abstract
Azadirachta indica is one of the most versatile medicinal plants having a wide spectrum of biological activity due to the presence of large number of bioactive compounds. The result of phenolic content estimation in methanol and ethanol crude extract was found to be 162.87±1.25 and 126.57±0.288 mg of GAE/g of extract respectively. The antioxidant activities of methanolic stem extracts of *Azadirachta indica* were screened using 1, 1-diphenyl-2-picryhydrazyl and ferric reducing power assay. The extract exhibited high antiradical activity against DPPH. The Reducing power increased with increasing concentration of the sample. Quantitatively the radical scavenging and reducing capacity of the crude methanolic extract were found to be 445.04±7.04mg and 310.61±0.364mg of mgAAE/100g respectively. Antibacterial determination the inhibition zones (in mm) of ethanol extract were found 13.33±0.0577 and 11.33±0.577 against *E. coli* and *S. aureus* respectively. The methanol extract also showed 10.33±1.155 and 9.66±0.577 inhibition zone against *E. coli* and *S. aureus* respectively. Petroleum ether stem extracts had no antibacterial activities against both bacterial strains. Most of these phytochemical compounds are present in the methanol and ethanol extracts. But for the petroleum ether extract terpenoids are only present**.** Moreover, except petroleum ether, methanolic and ethanolic extracts of *Azadirachta indica* showed good antioxidant and antibacterial activity.
Key words: *Azadirachta indicia;* Phenolic content; Antioxidant activity; Antibacterial activity

Introduction

Traditional medicine (TM) describes a group of health care practices and products with a long history of use. It is an age old customary practice. It frequently refers to medical knowledge developed by indigenous cultures that incorporates plant, animal and mineral-based medicines, spiritual therapies and manual techniques designed to treat illness or maintain wellbeing (WHO, 2003). It has been also defined as the sum total of the knowledge, skills, and practice based on the theories, beliefs, and experiences, indigenous to different cultures, whether explicable or not, used in the maintenance of health as well as in the prevention, diagnosis, improvement or treatment of physical and mental illness (Elujoba et al.,2005) According to the World Health Organization (WHO), the percentage of the population in developing countries that depends on traditional medicine (TM) for their primary health care ranges from 40% (Colombia) to 90% (Ethiopia) (Tinde, 2013)

Most of the time the traditional medicines practiced in all over the world basically has plant based origins due to the versatile applications of plant. About 80% of available drugs are obtained from medicinal plants and in industrial countries plants make up the raw material for chemical process which synthesizes pure bioactive molecules (Maji, 2011; Ramesh et al., 2011). It can be used for synthesis of antimicrobial drugs and antioxidants compounds. Medicinal plants are the richest bio-resources, food supplements, folk medicines (traditional medicines as practiced by nonprofessional healers), pharmaceutical intermediates and chemical entities for synthetic drugs (Prashant et al.,2011; Bishinu et al.,2011)

Azadirachta indica is the most important plant with valuable economic and health significance attached to all its parts. For example, its leaf, bark, roots, fruit coat, seed and flowers have been demonstrated to exhibit immunomodulatory, anti-inflammatory, anti-hyperglycemic and anti-diabetic,

antiulcer, antifungal, antibacterial, antiviral, anti-carcinogenic and spermicidal properties, and anti-fertility agent (Orhue et al.,2014; Soniya et al.,2014). Besides its medical use *Azadirachta indica* has great importance in human life as anti-desertification properties and possibly as a good carbon dioxide sink. The large-scale plantation of neem trees helps to combat desertification, deforestation, soil erosion and to reduce excessive global warming (Ogbuewu et al., 2011; Nigam et al., 1994).

In Ethiopia, people of the rural village use *Azadirachta indica* as treatment for dandruff and insect repellent. It is also common practice putting leaves of *Azadirachta indica* from meat and tables mostly in hotel to protect the sitting of flies, and they used the twigs part as chewing stick to clean teeth by people of rural village. Due to its insect repellent activity, the leaves of this plant are placed in grain stores. Mixture of leaf powders of *Azadirachta indica* in water makes an effective fumigant against seed borers in grain stores and used mainly for shelter belts and planted on degraded lands (Bekele., 2007). The importance of the Neem tree has been recognized by the United States national academy of science, which published a report in 1992 entitled Neem-a tree for solving global problems (Pathak et al., 2013 ; . Sudhir et al., 2010). In this paper we reported HPLC, total phenolic content, anti-oxidant and antibacterial activities of steam extracts of *Azadirachta indica*.

Materials and Methods

Experimental procedures and methodologies were discussed as follows.

Preparation of stem extract

Fresh stem parts of *Azadirachta indica* were collected from Bahir Dar town, which is located in Amhara region and it is 483 km away from Addis Ababa which is the capital city of Ethiopia in May 2017. The plant material was identified and authenticated by Dr. Ali Seidu, botanistin biology department of Bahir Dar University.

For extraction preparation, the plant material (i.e., stem) was first collected and the bark was removed from the stem and chipped, cut into smaller pieces and made to powder. Then 50 grams of this plant powder was soaked in 500ml of methanol, ethanol, ethyl acetate and petroleum ether solvents in four separate conical flasks for 72 hours using electrical shaker. After the 72 hours shaking the mixture was filtered through Whatman No 1 filter paper and the filtrate was concentrated to dryness using rotary evaporator under reduced pressure. The concentrated extract solution was taken in beaker and covered with Aluminum foil and stored at room temperature in a dark place for further uses to determine the qualitative and quantitative phytochemical analysis**,** antimicrobial activities and antioxidant properties.

Result and Discussion

The results of phytochemical analysis, total phenolic content, antioxidant activity and antimicrobial activity tests obtained from different extracts of the steam of *Azadirachta indica* will be discussed as follows:-

Extraction yield

Methanolic, ethanolic, ethyl acetate and petroleum ether stem extracts was 1.0481g (2.09 %), 1.6657g (3.33 %), 0.7137g (1.43 %) and 0.4196g (0.84 %), respectively. As shown in Figure 1, petroleum ether and ethyl acetate had minimum and very less extractive yield as compared to methanol and ethanol.

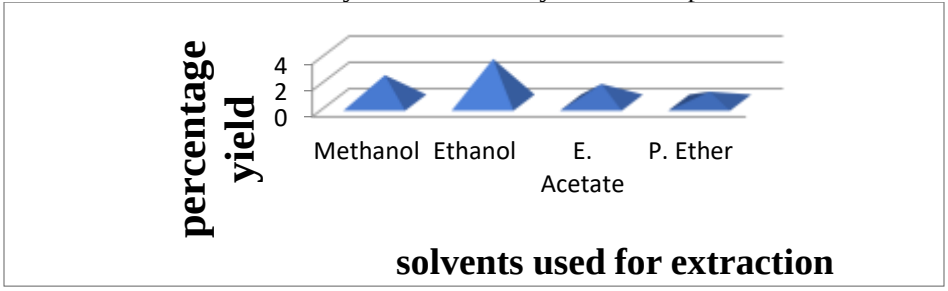

Figure 1: Percentage yield of each solvent stem extracts of *A. indica*

Qualitative Phytochemical screening

The type of phytochemicals present in each extract was shown in table 1 below.

Except flavoniod in methanol and saponin in ethanol all the tested phytochemicals showed positive result in both methanol and ethanol extracts. But most qualitative test in petroleum ether and ethyl acetate showed negative result. As shown from the result **table 1** the only existed phytochemical constituent in petroleum ether extract is terpenoid but in ethyl acetate extract terpenoid, phenols and flavonoids test shows positive result.

Table 1: Qualitative Photochemical Analysis or screening of methanol, ethanol, ethyl acetate and petroleum ether extracts of *Azadirachta indica* stem.

Solvent used	Alkaloid	Flavonoid	Phenols	Saponin	Tannin	Terpenoid
Methanol	+	-	+	+	+++	+
Ethanol	+	+	+	-	++	+
Ethyl acetate	-	+	+	-	+	+
P. ether	-	-	-	-	-	+

+++ = very highly present ++= high + = present - = not present

Antibacterial activity of *Azadirachta indica*

In this study the antibacterial activity of methanol, ethanol and petroleum ether stem extracts was investigated using disc diffusion methods against two selected human pathogens, such as *E. coli* and *S. aureus*.

Results of antibacterial activity of all the extracts and their efficacies as compared to standard are shown in **Table 2.** As it can be observed from **Table 2** both methanol and ethanol stem extracts of *Azadirachta indica* exhibit antibacterial activities against the selected gram positive and Gram negative bacteria. But antibacterial activity may not be observed in the petroleum ether stem extracts of *Azadirachta indica*. This may be due to the absence of most bioactive compounds in the stem extract as the phytochemical analysis confirms. For their antibacterial activity, the ethanol extract showed a highest result to inhibit the tested bacterial strains relative to the methanol and petroleum ether extracts (*S. aureus* with inhibition zone of 11.66±0.577 mm and *E. coli* with inhibition zone of 13.33±0.577 mm.

Table 2: Mean zones of inhibition (in mm) for stem extracts of *Azadirachta indica* and standard antibiotics of the tested microorganisms

Organisms	Inhibition zone in mm			
	Activity of Stem extract of *A. indica* in different solvents (125mg/ml)		Standard antibiotic drug	
			Geyntamycin	Tetracycline
E. coli	Methanol	10.33±1.155	22.67±1.708	8.33 ± 0.577
	Ethanol	13.33±0.577	22.67 ± 1.708	8.33 ± 0.577
	Petroleum ether	0	22.67 ± 1.708	8.33 ± 0.577
S. aurues	Methanol	9.66±0.577	28.67 ± 1.528	24.66 ± 1.155
	Ethanol	11.33±0.577	28.67 ± 1.528	24.66 ± 1.155
	Petroleum ether	0	28.67 ± 1.528	24.66 ± 1.155

Antioxidant activity

In this research DPPH (1, 1-diphenyl-2-picrylhydrazyl) radical scavenging assay and reducing power assay methods for antioxidant activity test were used.

Antioxidant activity by reducing power assay

Calibration curve for ascorbic acid

For quantification of reducing power of methanolic stem extracts of *Azadirachta indica*, ascorbic acid (AA) was used as standard in different concentrations (25ppm, 50ppm, 75ppm and 100ppm) so as to construct a calibration curve. The calibration curve **(Figure 3)** was plotted as absorbance (UV responses) at 700nm versus the different concentration of ascorbic acid used and the value of the absorbance obtained corresponding to each concentration were given in **Table 3.** The equation

obtained from the calibration curve of ascorbic acid was **y= 0.008x + 0.05** and the linear regression coefficient **(**R^2) value equals to **0.995**

Table 3: Absorbance and percentage reduction values of ascorbic acid (absorb. at 700nm)

Conc. of AA in ppm	Abs of AA at 700nm	% RP of AA
25	0.26966±0.00058	59.21±0.0866%
50	0.44666±0.0006	75.37±0.02886%
75	0.64466±0.00057	82.94±0.0173%
100	0.88433± 0.00115	87.56±0.0173%

All data are performed in triplicate and the values are expressed as mean (n=3) ± SD (standard deviation)

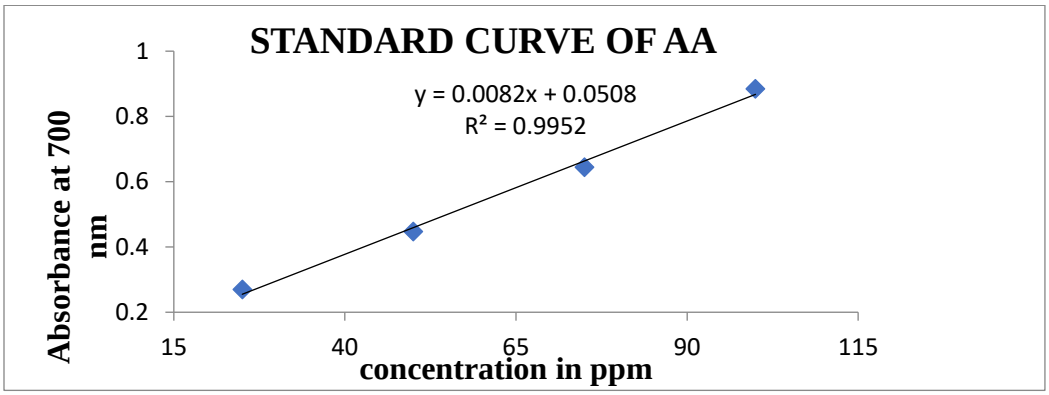

Figure 3: Calibration curve of Ascorbic acid for FRAP assay

In this study the antioxidant activity of methanolic stem extract of *Azadirachta indica* was determined using reducing power assay. The assay works based on the reduction of the yellow colour ferric complex ($Fe^{+3}(CN^{-})_6$) to a Prussian blue ferrous complex ($Fe^{+2}(CN^{-})_6$) by the action of electron donating antioxidants at low pH. The Ferric reducing antioxidant method works based on the reduction of Fe^{III+} to Fe^{II+} due to the action of antioxidants present. $FeCl_3$ solution, which is an indication for the reduction of ferric complex to ferrous form, this may probably due to the presence of antioxidant compound in the extract and confirmed by measuring the absorbance of the Prussian blue color formed at 700nm using UV-spectrophotometer (Model Lambda 35, Perkin Elmer). The intensity of Prussian blue color formed for different concentration of methanolic stem extract was different. It depends on the concentration of the plant used. For the different intensity of color, different absorbance was recorded and leads to different reducing power.

As it can be seen from **Table 4,** the absorbance of methanolic stem extracts of *Azadirachta indica* increases from 0.289±0.000-to-0.54566±0.00057 as the concentration increases from 40ppm-100ppm. Increasing the concentration of the methanolic extract increases its absorbance and leads to an increase in reducing power. The percentage reduction power of the methanolic stem extract of *A. indica* was calculated and the value was found to be 61.94±0.00%-to-79.84±0.02% for concentration of the extract in the range 40ppm-100ppm. However the reducing power the methanolic stem extracts of *A. indica* is smaller than that of the standard Ascorbic acid at the same concentration. The reducing power of methanolic stem extract and standard Ascorbic acid was found to be 79.84±0.017% and 87.56±0.0173% respectively at 100ppm

Table 4: Absorbance and percentage reduction values of extract (absorbance at 700nm)

Conc. of extract in ppm	**Abs of extract at 700nm**	**% RP of extract**	FRAP value (mg AAE/100 g)
40	0.289±0.000	61.94±0.00%	310.61±0.364
60	0.32466±0.0015	66.12±0.33%	
80	0.425±0.0017	74.12±0.412%	
100	0.54566±0.00057	79.84±0.02%	

All data are expressed as mean (n=3) ± SD (standard deviation)

The *In vitro* reducing power of methanolic stem extracts of *Azadirachta indica* was found to be remarkable and the reducing power was rise as the concentration of the extract gradually increased (in concentration dependent manner). **Figure 4** shows absorbance at 700nm as a function of concentration for the result of the present study. Increase in absorbance of the reaction mixture indicates the increase in the reducing power of the sample.

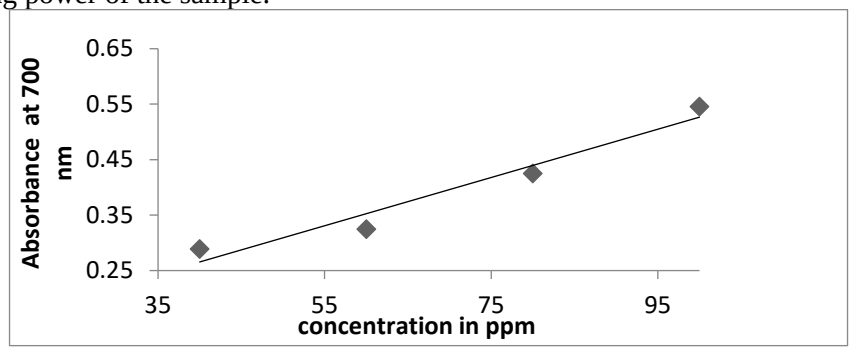

Figure 4: Graph of reducing power of methanolic stem extract

As it can be shown from **Table 4** the reducing power of methanolic stem extracts was expressed interms of Ascorbic acid equivalent antioxidant capacity(AEAC) and the value was found to be 310.61±0.364mg/100g of extract.

DPPH scavenging assay

Calibration curve for Ascorbic acid

For the DPPH radical scavenging assay different concentration of Ascorbic acid (10-80ppm) were used to construct the calibration curve. The calibration curve was constructed as a function of percentage inhibition versus concentration of Ascorbic acid. The absorbance at 517nm and the percentage inhibition of Ascorbic acid was given below in **Table 5**.

Table 5: absorbance and percent inhibition of value of ascorbic acid (at 517nm)

Concentration	Absorbance at 517nm	%inhibition
10	0.175±0.0012	91.15±0.0577%
20	0.153±0.0012	92.26±0.0577%
40	0.137±0.0006	93.04±0.02886%
80	0.081±0.0026	95.89±0.1379%

All data are performed in triplicate and the values are expressed as mean (n=3) ± SD (standard deviation)

The equation obtained from the calibration curve of ascorbic acid (**figure 5)** for DPPH radical scavenging assay was **y = 0.065x + 90.64** with linear regression coefficient **(**R^2**) 0.987**

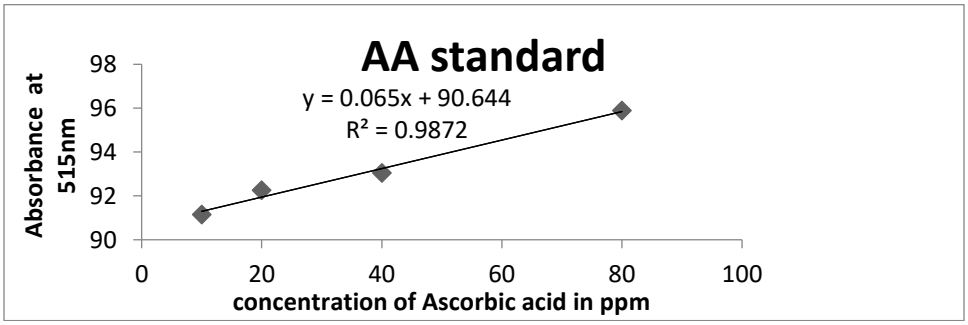

Figure 5: calibration curve of Ascorbic acid for DPPH scavengin assay

The antioxidant scavenging capacity of the plant extract can be measured by DPPH radical scavenging assay. The working principle of DPPH is based on the reduction of DPPH in alcoholic solution in the presence of a hydrogen-donating antioxidant due to the formation of the non-radical form DPPH-H in the reaction. Freshly prepared DPPH solution exhibits a deep purple colour with an absorption

maximum at 517 nm. This purple color generally fades when antioxidant molecules quench DPPH free radicals (i.e. by providing hydrogen atoms or by electron donation, conceivably via a free-radical attack on the DPPH molecule) and convert them into a colorless /bleached product (i.e. 2, 2-diphenyl-1-hydrazine, or a substituted analogous hydrazine), resulting in a decrease in absorbance at 517 nm band.

For the antioxidant activity study, different concentration of methanolic stem extract of *Azadirachta indica* (30ppm, 60ppm, 90ppm and 120ppm) was screened with DPPH, a stable free radical, and shows strong radical scavenging activities. The activities of the test sample in DPPH scavenging assay can be expressed as a decrease in absorbance. This activity was increased by increasing the concentration of the sample extract. **Table 6** shows the decrease in absorbance of the extract sample from 0.149±0.00057 to 0.0893±0.00152 as the concentration of the methanolic extract increases from 30ppm to120ppm respectively.

The change in absorbance of DPPH radicals caused by antioxidants is due to the reaction between the antioxidant molecules of the plant extract and the radicals. Phenolic compound presence indicated by the phytochemical investigation of stem extract may be accountable for this antioxidant activity.
The scavenging activities of stem extracts of *Azadirachta indica* can be expressed using percentage inhibition of DPPH free radical and it was found that percentage inhibition increases with increasing plant concentration. **Table 6** shows the percentage inhibition of DPPH free radicals and the value ranges from 92.41±0.0346%-to-95.437±0.076% when the concentrations of plant extract increases from 30ppm to 120ppm respectively.

Table 6: Absorbance of DPPH scavenging activities of the stem extract at 517nm

Conc. of extract in ppm	Absorbance at 517nm	%inhibition of extract	DPPH scavenging value (mg AAE/100 g)
30	0.149±0.001	92.41±0.0346%	445.04±7.04
60	0.137±0.0006	93.08±0.076%	
90	0.106±0.0006	94.16±0.0289%	
120	0.0893±0.0006	95.437±0.076%	

All data are performed in triplicate and the values are expressed as mean (n=3) ± SD (standard deviation)

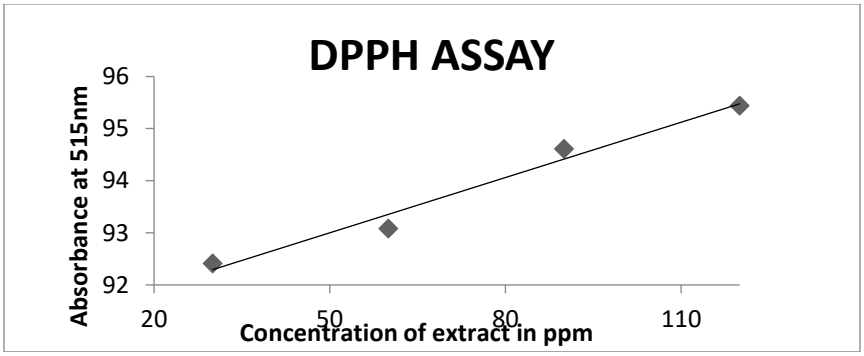

Figure 6: graph of DPPH scavenging activity methanolic extract

As it is indicated in **Table 6 and Figure 6,** the DPPH scavenging capacity of methanolic stem extracts of *Azadirachta indica* can be also expressed as Ascorbic acid equivalent per grams of sample and it was found to be 445.04±7.04mg/100g of extract**.**

Data analysis

The results were reported as mean ±standard deviation (SD). The calibration curves were constructed by using Microsoft excel window 10 and origin 8.

Conclusion

The preliminary qualitative phytochemical screening test for major secondary metabolites in stem extracts of *Azadirachta indica* revealed that the presence of phenol, alkaloids, tannins, terpenoid, flavonoid and saponin. Most of these phytochemical compounds are present in the methanol and ethanol extracts, but not in petroleum ether extract. The stem extracts of *Azadirachta indica* showed

good antioxidant and antibacterial activities in methanol and ethanol extracts whereas petroleum ether extracts of this extract had less potential of antioxidant and antibacterial activities.

Ethics approval and consent to participate

All authors declare that they have ethics approval and consent to participate.

Consent for publication

Not applicable.

Availability of data and materials

The authors have the samples.

Competing interests

The authors declare that they have no competing interests.

Funding

Not applicable

Authors' contributions

YAC was supervised the whole work as well as organized the manuscript as a whole and MZE and YAC did the experiment. All authors contributed to manuscript finalization. All authors read and approved the final manuscript.

Acknowledgements

We would like to thank Samara University for financial support to do this research.

Reference

Bishinu JS, Gollind PS, Buddha BB, Megh RB, Dinita SD, Krishna SG. 2011. Phytochemicaal extraction and antimicrobial activities of different plants. *J. of Microbiology and Antimicrobial*, 3(1):1-7.

Elujoba AA, Odeleye OM, Ogunyemi CM. 2005. Traditional development for medical and dental primary health care delivery system in Africa. *Afr. J. Trad. CAM*, 2(1):46-61.

Kebede DK, Alemayehu AF, Binyam GB, Yunis HD (2006). A historical over view of traditional medicine practices and policy in Ethiopia. *Ethio. J. Health Dev*, 20(2): 127-128.

Maji J, Ipe V, Manjula S. 2011. In vitro antioxidant activities and phytochemical analysis of five selected plant materials used for oral health and hygiene among people of dakshina kannada. *International Journal of Applied biology and pharmaceutical technology*, 22(4):95-103.

Nigam,SK, Misra GO, Sharma AK 1994. A promising natural insecticide. Applied Bot.Abstr, 14 (6):35-46.

Ogbuewu IP, Odoemenam VU, Obikaonu HO, Opara MN, Emenalom OO, Uchegbu MC, Okoli IC, Esonu BO, Iloije MU. 2011. The growing importance of Neem (*Azadirachta indicia)* in Agriculture, Industry, Medicine and Environment: A *Review. Res. J. Med. plants*, 5(3):230-245.

Orhue PO, Momoh AM, Igumbor EO, Esumeh FI. 2014. Antimicrobial effects of *Azadirachta indica***.** *Asian Journal of Plant Science and Research*, 4(2):64-67.

Pathak GP, Vineet SH, Gurdeep SZ, Amitoz KS.2013. Traditional Medicine for house-hold remedy against various Human and Animal Ailments: Review. *World Journal of Pharmacy and Pharmaceutical Sciences*, 2(5):3854-3860.

Prashant GK, Krishnaaiah GM 2014. Chemical composition of leaves of *Azadirachta indica*. *International Journal of Advancement in Enginering Technology, Manaagment and Applied science*, 1(5): 21-31.

Prashant T, Bimlesh K, Mandeep K, Gurpreet K, Harleen K 2011. Phytochemical screening and extraction: A Review. Internationale pharmaceutica sciecia. Available at: http://www.ipharmsciecia.com.

Ramesh KS, Susan EK, Devanand PF 2011. Bioactive Constituents and Antimicrobial Activity of Cell Cultures of *Azadirachta indica*. *International Journal of Pharma and Bio Sciences*, 2(4): 617-628.

Ryan MD 2014. Documenting traditional medical knowledge. *World International property organization*,22(1):55-98.

Soniya A, Vinya P, Maji S 2014. Antimicrobial potential of the extract of the twigs of *Azadirachta indica (Neem*). *J. of Med plant studies*, 2(6):53-57.

Sudhir PK, Debasis MY, Goutam GG, Chandra SP.2010. Biological action and medicinal properties of various constituent of *Azadirachta indica*: a systematic review. *Annals of Biological Research*. Available at: www.scholarsresearchlibrary.com

Tinde VA, Luise GC 2013. Why Urban Citizens in Developing Countries Use Traditional Medicine: The Case of Suriname. Evidence-Based Complementary and Alternate Medicine. Available at: http://dx.doi.org/10.1155/2013/687197

WHO 2001. Legal status of traditional medicine and complementary medicine: A worldwide review. Geneva.

World Health Organization [WHO] 2003. Traditional Medicine. Available at: http://www.who.int/mediacentre/factsheets/**2003**/fs134/en/.

Available online at www.asric.org
ASRIC Journal on Natural Sciences Vol 3(1) (2023) 66-77

Comparative Evaluation of Glycemic index (GI) of some Traditional Dishes consumed in Enugu North Senatorial zone of Enugu State, Nigeria

Umerah Nkemjika Nnedinso[1*]

[1]Department of Food Science and Technology, Enugu State University of Science and Technology, Enugu, Nigeria.

*Corresponding author: nkemumerah@yahoo.com

Abstract

The study was undertaken to evaluate the glycemic index (GI) of 'ayarayaoka', 'okpa' and 'achichca and agbugbu' a traditional dish consumed in Enugu North Senatorial zone. The recipes were standardized and prepared accordingly. Nutrient compositions of the prepared dishes were determined using standard procedures. A serving portion of each dish containing 50g of available carbohydrate was served to ten healthy adult subjects. Glucose was used as the reference food. The postprandial blood glucose response of the test and the reference meals were measured over two hours at 30 minutes interval. Blood glucose curves were plotted, area under each curve and corresponding glycemic index value for each dish determined. Data were analyzed using Statistical Package for Social Sciences (SPSS). The dishes had appreciable proximate composition, were moisture ranged from 46.20-62.55%, ash 2.68-3.56%, fat 5.30-8.20%, protein 4.90-17.80%, fibre 0.23-7.20% and carbohydrate 16.31 to 31.22%. The blood glucose concentration of 'ayarayaoka', 'okpa', 'achicha and agbugbu', and glucose reference at 120 minutes were 75.28, 72.80, 80.28 and 88.30 respectively. The glycemic index (GI) and glycemic load (GL) of 'ayarayaoka', 'okpa' and 'achicha and agbugbu' were 47.52, 50.80- and 59.20 for index while 7.75, 10.32 and 18.48 for load respectively. The increametal area under blood glucose response curve showed that glucose standard had 124.93, ayarayaoka had 59.37, okpa had 63.46 while 73.96 were recorded for achicha and agbugbu. Conclusion Glycemic index of the dishes were low except for that of 'achicha and agbugbu' that had medium glycemic indices and they can be recommended for diabetics.

Key word: Glycemic index, diabetes mellitus, traditional dishes, *Okpa, ayarayaoka, achicha and agbugbu.*

Introduction

Diabetes mellitus poses a serious challenge to health care globally and have high prevalence all over the World. In 2012 Nigeria census, it was observed that an estimate of over 195.88 million people in the Country have diabetes mellitus (Sunny, 2014). The prevalence rate increased due to population growth, change in lifestyle and food habit, aging, urbanization and increasing prevalence of obesity and physical inactivity.

Glycemic index (GI) is the impact of digested carbohydrate food in the body in respect to their blood glucose level. Carbohydrates that breakdown quickly during digestion have high (GI) because their Beta-glucose response is fast and high while those that breakdown slowly have a low GI (Jenkins *et al.*, 2002). Glycemic index were classified into high (GI ≥70), medium (GI = 56-69) and low (GI ≤ 55) relative to pure glucose (GI= 100). Jenkins *et al*. (2002), opined that low glycemic index diet, promotes weight loss and good health. Glycemic index could be a Nutrition therapy intervention for diabetics and low glycemic index foods may reduce postprandial blood glucose levels (ADA, 2009).

There is a strong correlation between carbohydrate intake with nutritional status, energy balance, and chronic disease risk (Cho et al.,2003; Jenkins et al.,2002; Liu et al., 2000; Oh, Willett, Fuchs, &Giovannucci, 2004). Carbohydrates differ in their ability to influence immediate and long-term metabolic responses. These physiologic responses have important implications for energy balance, cardiovascular disease, and cancer.

Food processing had some positive effects on food security of the African continent on the other hand, it hasgross effect on the health of the Africans as it has promoted a nutrition transition in which theirunique healthy traditional meals have been replaced by processed foods which predisposes one to

cardiovascular diseases. Turner and Turner (2007) noted that both indigenous and non-indigenous people consume foods with unhealthy fats and refined carbohydrates which are lower in essential vitamins and minerals and at the same time more expensive than their traditional meal.

Most meals in the south eastern Nigeria are generally not eating as a singlefoods, but eat as a mixed meals for example "*agbugbu* and *ji*" beans and plantain, "*achicha* and *agbugbu*", rice and beans, beans and yam, *akara*and pap etc. Food components is a major factor that affects the GI of foods, a comprehensive evaluation of the different variations of traditional dishes will reveal those with nutritional and health potentials that can be employed in disease management. The plant foods that are commonly used in the dietary management of diabetes in Nigeria include unriped Plantain and African yam beans. However, the need for diversity of dietary choices due to complaints of dietary monotony among diabetic consumers has prompted the search for other foods with anti-diabetic potentials.

Traditional foods are more affordable, accessible and acceptable by the people. Few traditional meals from Enugu South Senatorial zone has been studied to determine their GIand glycemic load.It is imperative to study the glycemic index of all the traditional diet consumed within a locality, this will help to identify the ones with low glycemic index and advocate the increase in the consumption of these diet through Nutrition advocacy programme highlighting their ethnobotanical benefit.

Enugu North Senatorial zone of Nigeria has wide range of traditional food with high nutritional value. In this study attempt has been made to study the glycemic index of some foods in Enugu North Senatorial zone of Nigeria.

Materials and Methods

Study Design

Random sampling was used to select three local dishes of the people. The selected local meals are; *Ayarayaoka* (test food 1), *okpa* (test food 2) and *agbugbunaachicha* (test food 3).

Standardization of Recipe

The recipe selected were standardized using a modified method of National Food Service Management Institute (2010).

Method of Preparation of "*Ayaraya Oka"*(test food 1)

Table 1: List of ingredients of test food 1.

Ingredients	Quantity
Pigeon pea	500g
Yellow maize	750g
*Ukpak*a (African oil bean seed)	200g
Onions	100g
Red oil	100ml
Amaranthus spp	Bunch
Scent leaves	50g
Fresh Pepper	25g
Salt	2 table spoon
Water	5,000ml
Knorr (Seasoning)	16g
Total Yield	4360g

After sorting and cleaning, the pigeon pea seeds were soaked in portable water for 24 h prior to cook. It was drained, washed and placed in a hot water and boiled for 2 h. Then the already sorted, cleaned and soaked for 6 h maize grains were drained, washed and coarse milled with little addition of water to form bread-like crumb. Thereafter, it was placed into a large foil wrapped tightly and immersed into the boiling pigeon pea seeds and allowed to boil for 30 min, followed by addition of already cut pieces of vegetable leaves to steam them for 2 min. Then, the maize, pigeon pea and vegetable leaves were drained off water and set aside. One hundred millilitres of palm oil were boiled followed by addition of sliced onions, grounded pepper, salt, seasoning cube and "*ukpaka*". Thereafter, the boiled maize, pigeon pea and vegetable leaves were mixed together in a large pot and the already boiled red oil were poured into the pot and mixed properly with turning stick. The resulted "*ayarayaoka*" was placed in a cleaned flask and covered until used.

Plate 1: The image of *Ayarayaoka* food

Preparation of Bambara groundnut "*Okpa"*

Table2: List of ingredients of test food 2.

Ingredients	Quantity
Bambara groundnut	1kg
Red oil	150 ml
Fresh pepper	25g
Salt	2 table spoon
Red oil	100ml
Knorr (Seasoning)	16g
Water	2 litres

The already fine-milled bambara groundnut flour was sieved into a big bowl. Approximately, 150ml of oil was poured into the flour. Thereafter, already boiled lukewarm water measuring 400ml was poured subsequently into the mixture and kneaded until a smooth watery fluid was formed, thensalt, smashed seasoning cubes was added. Then the grounded pepper was added into the mixture and a turning stick was used to stir it and set it aside. Five litres of water was boiled in a pot, then the "*okpa*" mixture was tied in prepared banana leaves and insert into the already boiling water and allowed to boil for 2 h. Thereafter, the resulting okpa obtained was placed in a clean flask and covered until used.

Plate 2: The image of *Okpa*food

Preparation of "*Achicha and Agbugbu"*

Table3: List of ingredients of test food 3.

Ingredients	Quantity
Pigeon pea	500g
Dried Cocoyam (Achicha)	750g
*Ukpak*a (African oil bean seed)	200g
Onions	100g
Red oil	150ml
Scent leaves	10g
Fresh Pepper	25g
Salt	2 table spoon
Water	5,000ml
Knorr (Seasoning)	16g
Total Yield	4420g

Pigeon pea seed were sorted and cleaned; then the seeds were soaked in portable water for 24 h prior to cook. It was drained, washed and placed in hot water and boiled for 1 h. Then, an already ground and 6 h soaked dry cocoyam was wrapped in a banana leaves and immersed into the boiling pigeon pea and continued cooking until they both were done. They were drained of the water and separately spread on the trays to cool. One hundred and fifty millilitres of palm oil were fried followed by addition of sliced onions, grounded pepper, salt, seasoning cube and "*ukpaka*". Thereafter, the boiled cocoyam and pigeon pea were mixed together in a large pot and the already fried red oil was poured into the pot and mixed properly with a turning stick. This resulted "*agbugbunaachicha*" was placed in a cleaned flask and covered until used.

Plate 3: The image of *Achicha and agbugbu*

Proximate Analysis

Proximate analysis was carried out for the three test foods. Total carbohydrate, ash, moisture content, crude fibre, crude fat and crude protein content will be determined using the methods of the Association of Official Analytical Chemists (AOAC, 2005).

Determination of Moisture Content

The moisture content of the sample was determined using the hot air oven method of AOAC (2005). Two gram (2g) of each sample (B) was weighed and put into a washed and dried previously weighed (A) petri-dish and placed in an oven at a temperature of 80ºC for 2 hours and at 105ºC until the weight was constant. The samples was cooled in a desiccator and weighed and the weight was recorded as (C). The weight loss obtained as the moisture content was calculated from the formula:

% Moisture Content = B-CB-A X 1001

Where A = Initial weight of empty crucible
B = Weight of crucible + sample before drying
C = Final weight of crucible + sample after drying

3.4.2 Determination of Protein Content

The crude protein of the samples was determined by the Micro Kjeldahl technique as described by AOAC (2005). Two grams (2g) weight (W) of the sample was put into a Kjeldahl flask. Four grams (3g) of anhydrous sodium sulphate and two (2g) of hydrated copper sulphate (catalyst) were added into the flask. Then 20mL of concentrated tetraoxosulphate (IV) acid (H_2S0_4) was added to digest the sample. The digestion was continued under heat until a clear solution was observed. The clear solution was cooled and made up to 100mL with distilled water. A digest of about 5mL was collected for distillation. Also, 5ml of sodium hydroxide (NaOH) was put into the distillation flask and distillation was allowed to take place for some minutes. The ammonia that was distilled off was absorbed by boric acid indicator and titrated with 0.01M hydrochloric acid (HCl). The titrevalue (T) of the endpoint at which the colour changed from green to pink was taken. The crude protein was calculated as:

% Crude Protein = 0.0001401 x T x 100 x 6.25W X 5
Where: T= Titre value
W= Weight of sample dried.

Determination Ash Content

The ash content of the sample was determined by the method of AOAC (2005). A silica dish was heated to about 60ºC and cooled in a desiccator weighed and recorded as (A). Two grams (2g) each of the sample was weighed (B) and put into the silica dish and transferred to the furnace. The temperature of the furnace was allowed to reach about 500ºC after placing the dish in it. The temperature was maintained until whitish-grey colour was obtained which was an indication that all the organic matter of the sample had been destroyed. The dish was brought out from the furnace and cooled in a desiccator, then re-weighed and recorded as (C). The percentage ash content was calculated as:

% Ash Content = C-AB-A X 100

Where: A = Weight of empty dish

B = Weight of empty dish + sample before ashing

C = Weight dish + ash

Determination of the Fat Content

The Solvent extraction method of AOAC (2005) was used. The extraction flask was washed with petroleum ether and then dried, cooled, weighed and recorded as (B). Two gram (2g) of the sample was weighed (A) into the extraction thimble. It was placed back in the Soxhlet apparatus. The washed flask was filled to about three-quarter of its volume with petroleum ether (that has the boiling point range of 40-60ºC). The apparatus was set up and extraction was carried out for a period of 5 hours after which complete extraction was made. The petroleum ether was recovered leaving only oil in the flask at the end of the extraction. The oil in the extraction flask was dried in the oven, cooled and finally weighed (C). The fat content was expressed as a percentage of raw materials. The difference in weight of empty flasks and the flask with oil content was calculated as:

% Fat Content = C-BA X 100

Where; A = Weight of sample

B = Weight of empty flask

C = Weight of flask + oil

Determination of Crude Fibre Content

This was determined by the method of AOAC (2005). In its determination, the bottom flask and beaker were rinsed with clean water, dried in an oven at 100ºC for 5 minutes and cooled. The defatted sample after fat extraction was used. Two grams (2g) of sample (A) was transferred into a 500mL flask and 200mL of pre-heated 1.25% H_2SO_4 was added and the solution was gently boiled for 30 mins, maintaining a constant volume of acid by the addition of hot water. The residue obtained was washed 3 times with hot water and returned to the beaker. The 200mL of pre-heated 1.25% NaOH was added and boiled for another 30 min. This was filtered under suction and then washed thoroughly with hot water and twice with ethanol. The residue was dried at 65ºC for about 4 hrs, weighed and recorded as (B). The residue was transferred into a crucible and placed in muffle furnace and ashed at 550ºC for 4 hours. It was cooled in a desiccator and weighed (C).

% Crude Fibre Content = C-BA X 100

Where C= Weight of crucible + sample before ignition

B= Weight of crucible + ash after ignition

A= Weight of sample.

Determination of the Carbohydrate

The Carbohydrate content of each sample will be determined by difference. % Carbohydrate = 100 % - (protein + fat + fibre + ash + moisture) (AOAC 2005).

Determination of Serving Sizes

The glycemic index (GI) test was based on 50g in each test food of available carbohydrates. Therefore, the portion size of each test food was varying according to the quantity of carbohydrates available in that food. Fifty grams of available carbohydrate was calculated from the results obtained from the proximate analysis of the test samples, the weight of the samples that delivered fifty grams of available carbohydrates. The dry weight was determined using the calculation below.

Dry weight (DW) =100−moisture content

Weight of carbohydrate in 100 g dry weight = CHO of test sample 100 X DW

3.7 Selection of the Subjects

Thirty (30) subjects (15 males and 15 females), aged between 18 and 30 years, were selected for the study and all the subjects were given an informed consent form to sign and participate in the study. All subjects were recruited from Enugu State University of Science and Technology, Enugu for voluntary participation in the study. The subjects chosen were healthy, they were also non-smokers, not pregnant or diabetic and none of them had a family history of diabetes. The subjects were given full details of the study protocol and were opportune to ask questions before the study. The protocol and procedures employed were reviewed and approved by the Ethics Committee of the College of Medical Sciences, Enugu State University Teaching Hospital, Enugu. The procedures followed were also in accordance with the ethical standards of the responsible committee on human experimentation and with the Helsinki Declaration of 1975, as revised in 2008. The subjects were randomized into three groups (A, B and C) of 10 individuals each (5 males and 5 females). The subjects were asked not to undertake vigorous activities on the day before the test and to avoid caffeine-containing drinks 24 h before the test. Instructions concerning meals of the previous day was not provided, because the fat and carbohydrate content of the evening meal before GI testing does not influence the blood glucose response. The foods that was consumed by each group are as described below; All groups (A, B and C): Consumed the Standard Food (Glucose). Group A Subjects: Consumed Test Food 1 (*ayayrayaoka*), Group B Subjects: Consumed Test Food 2 (*okpa*) and Group C Subjects: Consumed Test Food 3 (*agbugbu and achicha*).

3.8 Anthropometric Measurements

2.8.1 Weight Measurement

To ensure reliable measurements of body weight using the mechanical bathroom scale (HANA mechanical bathroom scale; P.M.HANA, Central Hong Kong, Hong Kong) the scale was zeroed before the respondent stepped onto it. The respondent was each asked to remove any "heavy" items from their pockets and any heavy items of clothing. They were asked to look straight ahead and stay still on the scales. The needle/digital screen was allowed to settle before the measurement was recorded. The body weight (kg) was measured to the nearest 0.5 kg.

Height Measurement

Height measurement of each of the subjects was taken using a "drop-down" tape fixed at about 2 m on a finely constructed wood. The respondents were asked to remove their shoes and stand with their back to the scale, looking directly forward. The back of their feet, calves, upper back and the back of their head was in contact with the wooden scale. They were positioned directly underneath the drop down measuring tape fixed on the wood. The measuring scale was held firm until it rested gently on the top of the respondent's head and the height (m) to the nearest 0.5 cm was recorded.

Determination of BMI

All anthropometric measurements were taken after a 12 h fast with the subjects wearing light clothes and no shoes. Body Mass Index (BMI) was calculated as the weight in kilograms divided by the square of the height in meters (kg/m2).

$$\text{BMI} = \frac{\text{Weight kg}}{\text{Height m}^2}$$

Determination of the Glycemic Indices of the Subjects

Glucose Level of the Subjects

Glycemic index (GI) of each subject was determined according to the method of Wolever*et al.* (2001). The GI of the test foods was determined by feeding each test food to 10 healthy individuals. Blood was obtained by finger prick using the AccuChekSoftclix lancing device (Accu-CheckR Active). The finger was chosen at random. Before the finger prick, the subjects were encouraged to warm their hands (by rubbing the palms together) to increase blood flow. Blood samples was punctured and placed on a test strip at intervals of 30 min for 2 h (0, 30, 60, 90 and 120 min). The blood glucose concentrations were determined using a glucometer with a glucose test strip (Accuchek Active).

Glycemic Indices of the Subjects

Volunteers for the investigation fasted overnight. They were asked not to perform any strenuous activities or take long walks. They were requested to remain seated for the duration of the test. Capillary pricked-finger blood samples were taken at baseline (0 min), 30, 60, 90, 120 and 180 mins after consumption of the food. The blood sample was placed immediately on a test strip which was inserted into a calibrated Glucometer (Evolve^{R}) which gives direct readings after a few seconds.

Day 1

The study started in the morning after an overnight fast by the individuals. A fasting blood sample was taken at 0 min; then after this, the subjects consumed 50 g of standard food (50 g of glucose powder dissolved in water) in a comfortable place. The standard food was constituted with 200 ml of water. Blood samples were taken at 30, 60, 90, 120, and 180 min. The blood glucose concentration was determined immediately using the glucometer.

Day 2

After an overnight fast, the test foods consumed by the same group of subjects. Blood samples was taken at 0, 30, 60, 90,120 and 180 min. The blood glucose concentrations were determined immediately using the glucometer.

The incremental areas under the glycemic response curve were calculated geometrically (Wolever and Jenkins, 1986). The GI was calculated by expressing the glycemic response area for the test food as a percentage of the mean response area of the glucose drink taken by the same subjects. The following formula was applied:

$$GI = \frac{\text{Area under the curve for 50g carbohydrate from test food X 100}}{\text{Area under the curve for 50g carbohydrate from glucose}}$$

The GI for the food and control was calculated as a mean from the respective average GI of the individuals.

Calculation of glycemic load

The glycemic load, which assesses the total glycemic effect of the diet is the product of the dietary GI and total dietary carbohydrate;

GL = GI100 X Carbohydrate content (g).

Statistical Analysis

Data collected was subjected to analysis of variance (ANOVA), using SPSS (Statistical Package for Social Sciences) and least significance difference (LSD) test at 5% level of probability was used to compare the significant treatment mean.

Results

Table 4: Proximate Composition of Test Foods (%)

Sample	TF1	TF2	TF3
Moisture	$62.55^{a}\pm0.25$	$50.24^{b}\pm0.37$	$46.20^{c}\pm0.83$
Ash	$3.56^{a}\pm0.09$	$3.20^{b}\pm0.02$	$2.68^{c}\pm0.11$
Fat	$5.30^{b}\pm0.04$	$8.20^{a}\pm0.21$	$7.80^{a}\pm0.43$
Protein	$6.78^{b}\pm 0.13$	$17.80^{a}\pm0.18$	$4.90^{c}\pm0.71$
Fibre	$5.50^{b}\pm0.32$	$0.23^{c}\pm0.02$	$7.20^{a}\pm0.12$
CHO	$16.31^{c}\pm0.53$	$20.33^{b}\pm0.55$	$31.22^{a}\pm0.87$
Energy (kcal)	$140.06^{c}\pm0.13$	$226.32^{a}\pm1.10$	$214.68^{b}\pm0.55$

Values are mean ± standard deviation of 3 replication

Key: TF1= Ayarayaoka,
TF2=Okpa,
TF3=Agbugbu and achicha.

Table 5: Blood Glucose Concentration (mg/dl) of Subjects

Sample	Glucose drink	TF1	TF2	TF3
0 mins	76.20^{a}±0.13	73.52^{b}±0.16	76.90^{a}±0.23	74.76^{b}±0.48
30 mins	126.25^{a}±0.06	90.40^{c}±0.52	81.50^{d}±0.15	105.20^{b}±0.25
60 mins	118.72^{a}±0.42	86.76^{c}±0.08	76.20^{d}±0.32	93.63^{b}±0.14
90 mins	95.84^{a}±0.37	78.52^{c}±0.57	73.40^{d}± 0.63	83.48^{b}±0.06
120 mins	88.30^{a}±0.62	75.28^{c}±0.61	72.80^{d}±0.56	80.28^{b}±0.21

Values are the mean ±standard deviation of ten individual per group (n=40). Value within the same column with different superscript are significantly different ($p<0.05$).

Key: TF1= Ayarayaoka, TF2=Okpa, TF3=Agbugbu and achicha

Table 6: The calculated carbohydrate in 100g of prepared food and serving size used for the determination of glycemic index and glycemic load.

Samples CHO 100g	Calculated size (g)	Serving GI	GL	Classification	
TF1	16.31	306.56	47.52	7.75	Low
TF2	20.33	245.94	50.80	10.32	Low
TF3	31.22	160.15	59.20	18.48	Medium

Values are mean ± standard deviation of 3 replication

Key: TF1= Ayarayaoka, TF2=Okpa, TF3=Agbugbu and achicha

Table 7: Incremental area under the blood glucose response curve (IAUC)

Samples	IAUC±SEM	p-value
Glucose	124.93±8.96	
TF1	59.37±3.24	.5210
TF2	63.46±5.02	.6153
TF3	73.96±13.56	.4756

Values are mean ± standard deviation of 3 replication

Key: TF1 = Ayarayaoka, TF2 = Okpa, TF3 = Agbugbu and achicha.

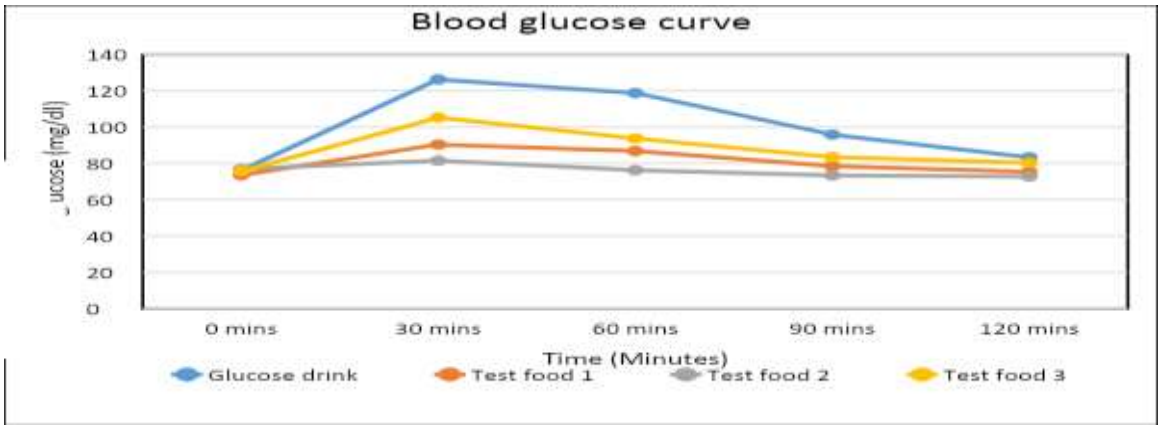

Fig 1: The mean Blood glucose curve of subjects after consumption of the three test foods compared with the control (glucose drink).

Discussion

Proximate Composition

Table 4 presents the proximate composition of the three local dishes. From the Table, *Ayarayaoka* had 62.55% moisture, 3.56% ash, 5.30% fat, 6.78% protein, 5.50% fibre and 16.31% carbohydrate. *Okpa*contained 50.24% moisture, 3.20% ash, 8.20% fat, 17.80% protein, 0.23% fibre and 20.33% carbohydrate while *Agbugbu and achichi* had 46.20% moisture, 2.68% ash, 7.80% fat, 4.90% protein, 7.20% fibre and 31.22% carbohydrate. There is significant difference among the means of all the nutrient values.

Moisture: Moisture values obtained from this study are in line with previous studies. Davidson *et al*. (2017), reported that the moisture content of different kinds of'achicha' (a traditional meal consumed in South-Eastern Nigeria) ranged from (53.8-65.6%). Kayode *et al*. (2010) also obtained moisture content within the range of 63.11to70.44% from dishes consumed in southeast Nigeria. According to Okeke *et al*. (2009) moisture content of 'ayarayaoka' was 70.02%. The implication of these results is that traditional South-Eastern Nigeria dishes are high in moisture. The high moisture content of all the dishes were not a surprise because the foods are cooked in water. Along with other liquids, water helps to get rid of wastes through urine, skin and bowel evacuation.

Ash: Ash is an indication of the mineral contents of foods. The ash content obtained from this study was higher than what was reported by Ogbuji and David-Chukwu (2016) in different food forms of cassava (0.27- 0.43%) which could be attributed to the type of food studied. The ash content of the dishes were close to that recorded by Ene-Obong and Madukwe (2001) for '*okpa*' (3%) but lower than that recorded by Okeke and Eze (2006) for another traditional food in the study area, *'achichaand akidi'* (4.3%). Since ash is an indication of the mineral content, the result suggests that the mineral content of these foods will be high. Combination of different foodstuffs in the preparation of a meal would help improve the nutrient content of food. This is because all the foodstuff will help contribute to the improvement of the overall nutrient content of the meal as is common with traditional meals in South Eastern Nigeria.

Fat: Fat values obtained from '*achicha' (*3.98g) by Okeke and Eze (2006) was lower than what was obtained from this study. Palm oil and African oil bean seed is the major source of fat in these dishes. The differences in the fat values of the various dishes could be due to different quantities of palm oil and African oil bean seed used in their preparation. Fat is needed for the support of certain metabolic activities within the body of living organisms and is also a source of energy. Fat help in the absorption of fat-soluble vitamins. The fat content of 'okpa' (8.9%) reported by Okeke *et al*. (2009) was similar to that of 'okpa' in this study.

Protein: The protein values obtained in this study were lower than what were reported by Nnanyelugo (1985) on the protein content of 'achicha and agbugbu' (12.9%) and 'achicha' with 'akidi' (10.8%) except in the case of okpa with the protein content of 17.80%. Compared with other dishes consumed in South-Eastern Nigeria, the protein values obtained from this study were similar to the report of Okeke and Eze (2006) on the protein content of 'Ayarayaoka' (4.08%). Awogbenia and Ugwuona (2012) reported a protein content of 3.10- 5.07% in traditional dishes consumed in Nassarawa State, Nigeria. The protein content of the dishes are of interest, especially in the community were the dishes are common. Frequent consumption of this meals will ensure proper growth of the consumer and lead to replacement of worn out tissues.

Fibre: Minse (2009) recorded that 'achicha', a mixture of crushed cocoyam and amaranthus leaves had dietary fibre value of 2.83% which was also lower than what was reported in the present study except in the case of okpa. The observed differences in dietary fibre contents of the dishes may be attributed to other components of the recipes. However, close range in dietary fibre content was recorded for some indigenous dishes by Kouamé*et al*., (2014). According to the authors, achicha with local beans, ayaraya with pigeon pea and abacha had dietary fibre values of 5.9, 6.2 and 8.9%, respectively. High dietary fibre observed in the dishes can have some beneficial biological effects such as laxative effect on GIT, increased fecal bulk and reduction of plasma cholesterol level (Okoye, 1992). Studies have shown the importance of dietary fibre in glycemic control and improved morbidity of diabetic patients (Odenigbo*et al*., 2011). According to Tsang (2011), fibre slows down the digestion of starch, therefore, high-fibre foods have a lower glycemic index. The fact that none of the various dishes had a high glycemic index could therefore be partly due to their high dietary fibre content.

Carbohydrate: The level of available carbohydrate found in this study, does not place these dishes as very rich sources of carbohydrate. Their consumption by the diabetic patients may therefore be encouraged. Available carbohydrate in some traditional dishes were (16.31%, 20.33%, and 31.22%) for 'ayarayaoka', 'okpa' Bambara groundnut and 'achicha and agbugbu' which is also a popular cocoyam-based traditional dish. High available carbohydrate was reported for pounded yam with

eggplant sauce, cassava paste with granulated palm nut sauce and rice with groundnut sauce (50%, respectively) by Kouamé*et al*. (2015). Such dishes with high available carbohydrates may not be suitable for diabetics as they may cause rapid increase in blood glucose level.

Energy: The energy values obtained from this study are in line with previous studies. The values of energy 140.06 to226.32kcal that were obtained in this study conformed with the reported findings (156.83-245.30kcal) of Ene-Obong and Madukwe (2001) in local dishes consumed in Nsukka. Davidson *et al*. (12017), reported that the energy content of different kind of'achicha' (a traditional meal consumed in South-Eastern Nigeria) ranged from (185.8-205.6%). The low energy content of '*ayarayaoka'* and '*agbugbu* and *achicha*' implies that these dishes could be incorporated into weight loss menus (Okeke and Eze, 2006).

Blood Glucose Concentration (mg/dl) of Subjects

Table 5 presents the blood glucose concentration of glucose drinks and the three local dishes. From the Table, glucose drink showed 76.20mg/dl at 0 min, 126.25mg/dl at 30 min, 118.72mg/dl at 60 min, 95.84mg/dl at 90 min and 88.30mg/dl at 120 min. Ayarayaoka showed 73.52mg/dl at 0 min, 90.40mg/dl at 30 min, 86.76mg/dl at 60 min, 78.52mg/dl at 90 min and 75.28mg/dl at 120 min. Okpa showed 76.90mg/dl at 0 min, 81.50mg/dl at 30 min, 76.20mg/dl at 60 min, 73.40mg/dl at 90 min and 72.80mg/dl at 120 min while Agbugbu and achichi showed 74.76mg/dl at 0 min, 105.20mg/dl at 30 min, 93.63mg/dl at 60 min, 83.48mg/dl at 90 min and 80.28mg/dl at 120 min. The result of the test diets on blood glucose concentration showed that the blood glucose response to okpa was significantly ($P<0.05$) elevated but with time as an additional factor, achicha and agbugbu diets seem to be the next threatening diets when compared to ayarayaoka and okpa. Okpa diet was shown to have the highest rate when compared with the other diets. This could suggest higher glucose uptake with okpa diet compared to the other diets, thereby decreasing the concentration of glucose in the blood; hence, preventing hyperglycaemia. The variability in the blood glucose responses to these diets may be attributed to the nature of the starch (amylose/amylopectin content) present. High amylose starch has been shown to be digested far more slowly than high amylopectin starch (Behall*et al*., 2011). This was supported by the work of Kabir *et al*. (1998), which reported that when starches with different amylose amylopectin ratios are incorporated into a meal, the one with the higher amylopectin starch showed a higher glycaemic index than that of the low amylopectin starch for normal and diabetic rats. This was in agreement with the work of Thannoun and Al-kubati (2005) which showed that a higher ratio of amylose to amylopectin in foods decreases the digestion of the total starch and consequently decreases the glycaemic index values.

Glycemic indices and loads of the traditional dishes

Table 6 presents the glycemic indexes and glycemic load concentration of the three local dishes. From the Table, Ayarayaoka contained 16.31g calculated carbohydrate, 306.56g serving size, 47.52 glycemic index, 7.75 glycemic load and was classified as low. Okpa contained 20.33g calculated carbohydrate, 245.94g serving size, 50.80 glycemic index, 10.32 glycemic load and classified as low while Agbugbu and achichi contained 31.22g calculated carbohydrate, 160.15g serving size, 59.20 glycemic index, 18.48 glycemic load and classified as medium.

The result of this study revealed that the dishes were of low glycemic indices except for 'achicha and agbugbu' which fall in the medium glycemic index category. This finding is supported by Evans and Gajere (2012) who stated that a greater percentage of Nigerian indigenous food fall into the moderate and low GI category. The rise in blood sugar at the 30^{th} minute after consuming the dishes showed that the meal was slowly digested and assimilated into the bloodstream. Slow digestion of these dishes probably due to their high fibre content which have been indicated earlier on has some positive health implications. Burkitt and Trowel (1977) have suggested that foods that are more slowly digested and absorbed may have metabolic benefits in relation to diabetes and in the reduction of coronary heart diseases. The finding of Ogbuji and David-Chukwu (2016) revealed that cocoyam based dishes consumed in Nigeria had high glycemic index than corn-based ones. Similarly, (Pirasath*et al*., 2015) reported that boiled potatoes and cassava had glycemic index of 78.70 and 75.20%, respectively. The lower glycemic index obtained in this present study compared to most of the previous studies could be attributed to the food component of the meals.

Incremental Area under the Blood Glucose Response Curve

Table 7 presents the increamental area under the blood glucose response curve of the three local dishes. From the Table, glucose had 124.93. *Ayarayaoka* contained 59.37. *Okpa* contained 63.46 while *Agbugbu* and *achichi* contained 73.96. The GI is intended to be an index of the relative blood glucose-raising potential of the available carbohydrate in different foods. For this concept to be valid and useful, the GI value of the same food must be the same in different subjects. Glycemic responses vary from day to day within subjects and also vary between subjects. GI is not only the measure of carbohydrate absorption in the small intestine directly, but also indicates the effect of other factors in the foods tested that can influence the rate of carbohydrate absorption in the small intestine. This study shows that there are significant differences in the glycemic responses to different mixed meals. Significant differences were found in the IAUC between the standard and the test foods for each group. This findings show that the selected test foods ('ayarayaoka', 'okpa' and 'achicha and agbugbu') consumed have low-GI values. The low-GI food consumed by the subjects could not increase their risk of cardiovascular diseases. However, this may not be a common phenomenon since they are often prepared using a varieties of substance, some of which help in protecting against cardiovascular diseases.

Conclusion

The study provided the nutrient composition of 'ayarayaoka', 'okpa' and 'achicha and agbugbu' as traditional dishes consumed in Enugu North Senatorial zone, Enugu State Nigeria. The dishes were high in moisture, dietary fibreand protein. The available carbohydrate content was low.

Glycemic index of the dishes were low except for that of 'achicha and agbugbu' that had medium glycemic indices. Ayarayaoka' and 'okpa' had low glycemic index and loads values, while 'achicha and agbugbu' had a medium glyceamic index value. A low glycemic indices diets can help to lose weight or keep a healthy weight. It may help in management of a diabetes plan.

The low and medium glyc.emic values of the dishes imply that they could cause a delayed rise in blood sugar and slow down gastric emptying time. Therefore, regular consumption of these dishes may not quickly make one feel hungry, thus suppressing the desire to eat more food. When such eating patterns become habitual, there is the likelihood of losing weight as a result of less eating, thus reducing the prevalence of obesity and diabetes mellitus, especially among those prone to the disease.

Reference

1. American Diabetes Association (2009). Diabetes and Impaired Glucose Tolerance. In: IDF Diabetes Atlas, IDF (Eds.). 4th Edn. Chapter 2.1.1, International Diabetes Federation, Brussels, Belgium, pp: 22-29.
2. AOAC *(*2005*)Official Methods of Analysis*. (17th Edn.) *The Association of Official Analytical Chemists, Gaithersburg*, MD, USA. Pp. 925-974.
3. Awogbenja, M.D. and Ugwuona, F.U. (2012). Nutrient and Phytochemical Composition of Some Commonly Consumed Traditional Dishes of Nasarawa State, Nigeria. *Prod. Agric. and Tech.*; 8 (1):30 -39.
4. Behall KM, Scholfield DJ, Hallfrisch J. (2011)The effect of particle size of whole grain flour on plasma glucose, insulin and TSH in human subjects. Journal of American College of Nutrition; 18: 591-597.
5. Burkitt, D.P. and Trowell, H.C. (1977). Dietary fibre and western diseases. *Iranian Medical Journal*; 70: 272–7.
6. Cho, E., Spiegelman, D., Hunter, D.J., Chen, W.Y., Colditz, G.A. and Willett, W.C. (2003). Premenopausal dietary carbohydrate, glycemic index, glycemic load, and fibre in relation to risk of breast cancer. *Cancer Epidemiology, Biomarkers and Prevention*; 12: 1153–1158.
7. Davidson, G.I, Ene-Obong, H.N and Chinma, C.E. (2017). Variations in Nutrients Composition of Most Commonly Consumed Cassava (*Manihot esculenta*) mixed dishes in South-Eastern Nigeria. *Journal of Food Quality*; 7:1-15.
8. Ene-Obong, H.N. and Madukwe, E.U. (2001). Bioavailability of trace elements in South-Eastern Nigerian meals and the effect of dietary components. *Nigerian Journal of Nutritional Science*; 22: 4-12.
9. Evans, E.C. and Gajere, Y. (2012). The glycemic index and load of different Nigerian food forms. *International Research Journal of Biochemistry Bioinformation*; 7(1): 001-011.

10. Jenkins, D.J., Kendall, C.W., Augustin, L.S., Franceschi, S., Hamidi, M., Marchie, A. and Axelson, M. (2002). Glycemic index: overview of implications in health and disease. American Journal of Clinical Nutrition, 76: 266S–273S.
11. Kabir, M., Rizkalla, S.W., Champ, M., Luo, J., Boillot, J. and Bruzzo, F. (1998). Dietary amylose amylopectin starch content affects glucose and lipid metabolism in adipocytes of normal and diabetic rats. *Journal of Nutrition*; 128: 35-43.
12. Kayode, O.F, Ozumba, A.U, Ojeniyi, S, Adetuyi, D.O and Erukainure, O.L. (2010). Micro Nutrient Content of Selected Indigenous Soups in Nigeria. *Pak J Nutr*i.; 9: 962-965.
13. Kouamé, C.A., Kouassi, K.N. and Coulibaly, A. (2014). Glycemic Index and Glycemic Load of Selected Staples Based on Rice, Yam and Cassava Commonly Consumed in Côte. *Food and Nutrition Science*; 5: 308-315
14. Kouame, C.A., Coulibaly, A., N'dri, Y.D., Tiahou, G.G., Adrien, L. and Amani, G.N. (2015). Glycaemic Index and Load Values Tested in Normoglycemic Adults for Five Staple Foodstuffs: Pounded Yam, Pounded Cassava-Plantain, Placali, Attieke and Maize Meal Stiff Porridge. *Nutrients*; 7: 1267-1281
15. Liu, S., Willett, W.C., Stampfer, M.J., Hu, F.B., Franz, M., Sampson, L. and Manson, J.E. (2000). A prospective study of dietary glycemic load, carbohydrate intake, and risk of coronary heart disease in US women. *American Journal of Clinical Nutrition*, 71: 1455–1461.
16. Minse, M. (2009). The nutritional and modified traditional foods in kwazulu-natal. A thesis for the degree of Master of Agriculture (Food Security), African Centre for food Security School of Agricultural sciences and Agribusiness, Faculty of Science and Agriculture, University of KwaZuluNatal, Pietermaritzburg. Pp. 23-75.
17. National Food Service Management Institute (NFSMI) (2010). Measuring success with standard recipe. http//www,nfsmi.org/resource review.apex?ID-88
18. Nnanyelugo, D. (1985). Nutritional status of children in Anambra state: A comprehensive treatise. University of Nigeria press, Nsukka.
19. Odenigbo, U.M., Odenigbo, U.C., Oguejiofor, O.C. and Adogu, P.O. (2011). Relationship of Waist Circumference, Waist Hip Ratio and Body Mass Index as Predictors of Obesity in Adult Nigerians. *Pakistan Journal of Nutrition*; 10 (1): 15-18.
20. Oh, K., Willett, W.C., Fuchs, C.S. and Giovannucci, E. (2004). Glycemic index, glycemic load and carbohydrate intake in relation to risk of distal colorectal adenoma in women. *Cancer Epidemiology, Biomarkers and Prevention*, 13: 1192–1198.
21. Ogbuji, C.A. and David-Chukwu, N.P. (2016). Phytochemical, Antinutrient and Mineral Compositions of Leaf Extracts of Some Cassava Varieties. *African Journal of Environmental Science, Toxicology and Food*; 2016*: 5-8*
22. Okeke E.C and Eze, C. (2006). Nutrient composition and nutritive cost of Igbo traditional vendor foods and recipes commonly eaten in Nsukka. *J Agric Fd Environ Exten*; 5 (1):36- 44.
23. Okeke, E.C., Ene-Obong, H.N., Uzuegbunam, A.O., Ozioko, A., Umeh, S.I., Kuhnlein, H. (2009) Nutrient composition of traditional foods and their contribution to the energy and nutrient intakes of children and women in rural households in Igbo culture area. *Pakistan Journal of Nutrition; 8(4): 304-312*.
24. Okoye, Z.C. (1992). Biochemical Aspects of Nutrition. PrenticeHall of India, New Delhi. Pp. 147-195
25. Pirasath, S., Balakumar, S. and Arasaratnam, V. (2015). Glycemic Index of Traditional Foods in Northern Sri Lanka. *Endocrinology and Metabolic Syndrome*; 4 (1): 12-16.
26. Sunny, C. (2014). Diabetes Association of Nigeria. Nigeria National Diabetes Centre. A proposal.
27. Thannoun, M.A. and Al-Kubati, A.N. (2005). Blood glucose response and glyceamic Index of breads and some wheat products in normal human subjects. *Mesopotamia Journal of Agriculture*; 33: 8-18.
28. Turner, N.J. and Turner, K.L. (2007). Traditional Food Systems, erosion and renewal in Northwestern North American. Indian Journal of Traditional Knowledge;6(1)57-68.

Available online at www.asric.org
ASRIC Journal on Natural Sciences Vol 3(1) (2023) 78-83

High Performance Liquid Chromatography Assay of Cyclopiazonic Acid in Some Stored Cereals from the Agro-Ecological Zones of Nigeria

Peter Francis Adikwu[1,4], Okibe Friday Godwin[*1], Abgaji Edith Bolanle[2], Hussaini Makun Anthony[3]

[1]Department of Chemistry, Federal University of Health Sciences, Otukpo, Nigeria
[2]Department of Chemistry, Ahmadu Bello University, Zaria, Nigeria
[3]Department of Biochemistry, Federal University of Technology, Minna, Nigeria
[4]National Examinations Council, Minna Nigeria

*Corresponding author: friday.okibe@fuhso.edu.ng

Abstract

High Performance Liquid Chromatography (HPLC) with a UV detector, was employed to analyse cyclopiazonic acids (CPA) in stored maize, millet, rice, sorghum, wheat and processed cassava (garri) samples from the seven agro-ecological zones of Nigeria namely; Derived Savannah (DS), Mid Altitude (MA), Humid Forest (HF), Northern Guinea Savannah (NGS), Sahel Savannah (SS), Southern Guinea Savannah (SGS) and Sudan Savannah (SuS). CPA a neurotoxin produced by *A. flavus*, with an indole tetramic acid structure, has been reported to be acutely toxic with an LD_{50} value above 2.30 ng/kg, a specific inhibitor of Ca^{2+} -ATPase, and also a potent inhibitor of calcium uptake in the sarcoplasmic reticulum was found in all the samples analysed. The mean concentrations (n = 50) of CPA found were 6.783 µg/kg, 1.173 µg/kg, 1.150 µg/kg, 2.921 µg/kg, 1.481 µg/kg and 1.271 µg/kg for wheat, maize, garri, millet, sorghum and rice respectively. Wheat samples obtained from DS and SG were found to contain the highest amount of CPA with 14.501 µg/kg and 9.601 µg/kg respectively. The recommended acceptable daily intake (ADI) of CPA has been set for 10 µg/kg/day or ≈ 700 and >1000 µg/kg/day for human and animal respectively. All samples (except for wheat samples from DS) collected across the seven agro-ecological zones are less than the recommended ADI by the International Safety and Compliance Agency, USA.

Keywords: Cyclopiazonic Acid (CPA), Stored Cereals, High Performance Liquid Chromatography (HPLC), Agro-ecological zones.

Introduction

Cyclopiazonic acid (CPA) is a mycotoxin produced by several moulds of the *Aspergillus* and the *Penicillium* genus. CPA has been detected in various foods of plant origin, such as peanut, corn, figs, rice, wheat and tomato, and also in food of animal origin, such as cheese, milk and ham (Anshanni & Yu, 2017). Cyclopiazonic acid (α-cyclopiazonic acid; CPA, Figure 1) is an indole-tetramic acid mycotoxin produced by the ubiquitous genera of fungal species such as *Aspergillus* and *Penicillium such as Aspergillus flavus, Aspergillus versicolor, Aspergillus oryzae, Aspergillus fumigatus, Aspergillus tamarii, Penicillium griseofulvum, Penicillium commune* and *Penicillium chrysogenum* (Holzapfel, 1968; Burdock & Flamm, 2000). Chemically, CPA belongs to the family of indole-tetramic acid secondary metabolites. *P. griseofulvum* Dierckx (originally called *P. cyclopium*). This mycotoxin is derived from tryptophan, mevalonate, and two molecules of acetate (Perng *et al*., 2009. With an empirical formula of $C_{10}H_{20}N_2O_3$, its molecular weight of 336.15.

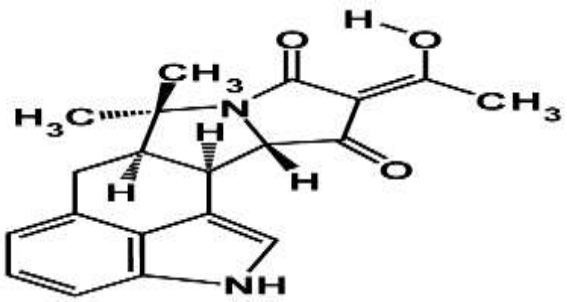

Figure 1: Chemical Structure of Cyclopiazonic Acid.

Cyclopiazonic acid (CPA) is one of the mycotoxins rarely studied despite its demonstrated cytotoxicity and immunotoxicity on human cells (Hymery, Masson, Barbier & Coton, 2014). In addition, this mycotoxin displays immunosuppressive properties and haematological disorders in humans (Hymery *et al*., 2014). These adverse effects in human beings together with those observed in animals (Burdock & Flamm, 2000; Hymery, Masson, Barbier, & Coton, 2014) support the optimisation of a reliable analytical method to detect and quantify this toxic compound for minimising the risk associated with its presence in foods. Recently, high-performance liquid chromatography (HPLC) (Finoli *et al*., 1999) have been widely used for detection and quantitative determination of CPA in fungal cultures and agricultural commodities. This method have been optimised to evaluate CPA amounts in various food matrices (Ansari & Häubl, 2016)

There are many reports on other mycotoxins such as aflatoxins contamination in cereals including wheat, maize and rice cultivated in Nigeria (Makun *et al*., 2013; Makinde *et al*., 2020). However, there is a paucity of data on CPA contamination of mainly cultivated cereals (maize, millet, rice, sorghum, and wheat) and processed cassava flour (garri) in Nigeria. Therefore, the main aim of this study is to determine CPA contamination in cereals and garri collected across the seven agro-ecological zones of Nigeria, using High Performance Liquid Chromatography (HPLC).

Materials and Method

Sample Collection

Twenty one (21) samples each of maize, millet, rice, sorghum, wheat and garri were collected randomly across the seven agro-ecological zones of Nigeria from storage facilities in 2019. The samples were properly labelled and preserved prior to analysis.

Reagents and Chemicals

Acetonitrile and methanol were purchased from Fisher Scientific (Fisher Scientific UK Ltd., UK); Sodium chloride and anhydrous magnesium sulphate were supplied by Scharlab S.L. and Fisher Scientific, respectively. All solvents were HPLC grade. Distilled water was obtained from a Central Research Laboratory (Tanke, Ilorin). Vials, inserts, closures and 0.22µm filters used for mycotoxins were provided by Cosela S.L. (Spain).

Standards preparation

CPA standard (Sigma-Aldrich, Germany) was dissolved in acetonitrile at a concentration of 1 mg/mL and stored at -20 °C in a sealed vial until use. Different amounts of the CPA stock standard were placed in amber 1.5mL vials and were evaporated to dryness under a gentle stream of N_2. Working standards (10–1000µg/mL of CPA in methanol) were prepared by appropriate dilution of known volumes of the stock solution with methanol.

Extraction of Cyclopiazonic Acid

Milled samples (10 g each) of the cereals (maize, millet, rice, sorghum, and wheat)/processed cassava flour (garri) were weighed into labelled conical flasks and treated with 20 cm^3 methanol: water (60:40 v/v) in a mechanical shaker for 2 hours. The content was filtered through a Whatmann No. 2 filter paper and the filtrate (≈5 cm^3) cleaned by passing it through a micro-filter (5µm pore size) preconditioned with methanol: water (3:1 v/v). The filtrate was stored for further analyses at 4°C.

Validation of High Performance Liquid Chromatography Method for Cyclopiazonic Acid Quantification

The parameters of linearity (quantification), accuracy (% recovery) and sensitivity (limit of detection (LOD) and limit of quantification (LOQ)) were estimated for all the mycotoxins analysed according to the method described by Abia *et al*. (2013). For quantification purposes, external calibration curves were established based on serial dilutions of the mycotoxin standard solutions as indicated above

Linear calibration curves generated for the mycotoxin standards were considered satisfactory when correlation coefficients (r^2) were greater than 0.99.

Recovery assay was carried out in triplicates on 3 least contaminated samples by spiking 5 g of each with 100 µl known standard concentration. Eventually, spiked samples were mixed and kept for 16 hours in a fume cupboard at a room temperature to establish the equilibrium between the sample matrix and the toxins.

From each spiked sample, 20 µl of the extract was injected into the HPLC. The analyte detected was quantified by comparing its peak area on the calibration plot to that of equivalent mycotoxin standard. The percentage recovery are presented in Table 1 while the recovery obtained are in line with the allowable limits of the recovery recommended by Codex or Association of Official Analytical Chemists (Scott, 1995). The Codex recommends 60–120 % of recovery rates of mycotoxins and the guideline for the recoveries by AOAC is 70–125%.

$$\%\ Recovery = \frac{Concentration\ Eqv.to\ the\ peak\ area\ measured\ from\ the\ spike\ sample}{Each\ toxin\ concentration\ used\ for\ spiking\ the\ sample} \times 100$$

LOD and LOQ for the CPA in cereals and processed cassava flour were estimated using the lowest concentrations in the spiked samples estimated as signal-to-noise ratio (S/N) of 3:1 and 10:1 respectively.

Table 1: **Calibration Parameters for Quantification of CPA by HPLC method**

Analytes	Calibration level (µg/kg)	Percentage recovery (%)	r^2	Equation of straight line
CPA	0.001, 0.01, 1.0	96	0.9998	y = 4E+07x - 27468

The calibration curve used for validation experiments was plotted in the range from 0.1 to 10 ng/mL and showed good linearity with the regression coefficient of R^2=0.999. Additional linearity testing was done in the 0.5 to 20 ng/mL range (R^2=0.996) due to the fact that CPA concentrations found in the samples were outside the original calibration range. Given that calibration standards were prepared from standard solutions, but not in the matrix, such regression coefficients were to be expected. These values show a slight improvement in sensitivity of the HPLC method of CPA detection in the cereals analysed as compared to the studies of Peromingo *et al*. (2018) and Delgado *et al*. (2019). The method recovery was evaluated at two levels (3µg/kg and 10µg/kg), and the average recoveries were 96.0 %. Validation results showed that the method is fit for purpose and can be employed in the analysis of CPA in the cereal samples.

Result and Discussion

From the results presented in Table 2, CPA was detected in the samples of collected from DS agro-ecological zone, including garri, maize, millet, rice, sorghum and wheat while in SGS agro-ecological zone CPA was not detected. For SS, all samples except garri had CPA in the range 1.283 – 9.601 µg/kg.

Table 2: Average Concentration of Cyclopiazonic acid across the Agro-Ecological Zones of Nigeria (µg/Kg)

Sample	DS	SGS	SS	NG	SuS	MA	HF
Garri	2.014±0.006a	ND	ND	ND	ND	ND	ND
Maize	7.251±1.233g	ND	2.014±0.01	1.124±0.120c,d	3.059±0.012a	2.252±0.172a,b	ND
Millet	2.013±0.006a	ND	2.032±0.00	ND	2.214±0.127b	2.840±0.152c	2.507±0.198a,b
Rice	2.014±0.006a	ND	1.283±0.119c	ND	4.253±0.116b	3.376±0.180d	ND
Sorghum	1.027±0.015a	ND	3.215±0079	2.997±0.094c,d	4.806±0.098c	ND	ND
Wheat	14.918±0.130e	ND	9.601±0.007a	2.063±0.0118a	ND	2.013±00.006a	2.211±0.135b

ND =**Not detected**

The percentage of positives in the samples collected by agro-ecological zones was 100%, 0%, 83.3%, 67.4%, 67.4% and 32.4% for DS, SGS, SS, NG, SuS, MA and HF respectively while the total average across the zones was 57.1 %, which can be considered as a significant CPA occurrence when it comes to staple commodities. The CPA concentration found in the samples ranged from 1.027 µg/kg up to 14.918 µg/kg (Table 3). As compared to the study by Chilaka *et al*., (2014) conducted on cereals, our results revealed a lower CPA concentrations. These differences can be attributed to difference in location, effect of temperature and time of sample collection. Although the concentrations of CPA in most of the grains were below the acceptable daily intake (ADI) for CPA in humans of 10 µg/kg/day or 700 µg/day (Burdock and Flamm, 2000), its 100 % occurrence in the grains is a source of concern as regular consumption of foods containing low levels of the toxin can lead to acute toxicity (Adetunji *et al*., 2014). This finding also corroborates the work of Lombaert (2002) that though CPA is among the least toxic of mycotoxins, it is the most frequently detected and its occurrence is considered to be an indicator of possible presence of other more toxic mycotoxins.

Table 3: Cyclopiazonic acid Positive Samples.

Type of Sample	Number of Sample	Number of Positive	CPA Con range (µg/kg)
Garri	21	3	2.008 – 2.024
Maize	21	12	1.124 - 2.840
Millet	21	12	2.013 – 2.840
Rice	21	9	1.283 – 4.253
Sorghum	21	9	1.027 – 4.806
Wheat	21	12	2.063 – 14.918

The low amount of rainfall (650–1,000 mm) and long period of dry season (6–9 months) in the SS and NGS zones may be responsible for the low concentration of aflatoxins found in maize grains in these regions (Adetunji *et al*., 2014). Atehnkeng *et al*. (2008) earlier recorded the least level of other mycotoxins contamination in the NGS zone. Furthermore, Udo *et al*. (2000) also did not detect aflatoxins in farmers store in the NGS zone and attributed this to the fact that farmers usually store their grains in "rhumbu" (local granary). Higher temperatures and drier conditions favour infection by *Aspergillus* fungi, and the development of mycotoxins such as CPA in cereals prior to harvest and these contamination frequently accompany heat and water stress that may be associated with drought (Atehnkeng *et al*., 2008). Thus, CPA may be expected to be higher in maize grains collected in the DS and NGS zone with a relatively warm and dry climate as compared with the NG and the SGS where crops are grown under more moderate conditions with less water stress. However, our results show more CPA contamination in the SGS zone compared to NGS zones, a trend common across West Africa (Atehnkeng *et al*., 2008). The low concentration of CPA in the HF zone as compared to the SGS zones may be due to the fact that farmers in the zone do not usually store their grains for long periods as they usually sell their maize in the fresh state because the zone is highly urbanized. The grains are usually consumed by the populace as snacks and by local industries. Wild and Hall (2000) also reported that urban dwellers generally have lower levels of mycotoxins exposure than rural population in developing countries because urban populations typically consume more diversified diets than do rural dwellers and may have food that is better controlled for contaminants. The high concentration of CPA observed in the DS zone is probably due to the high amount of rainfall (1,300–1,500 mm) usually recorded in the zone in collaboration with the various storage practices employed by the farmers in the zone (Adetunji *et al*., 2014).

The high incidence of CPA contamination also observed in SS could be due to the mixed cropping systems practiced by farmers in the zone. Farmers in this zone are in the habit of planting crops like yam, maize, cowpea, peanut and soybeans on the same piece of land. This practice encourages cross-transfer of toxigenic strains from one infected crop to another (Atukwase *et al*., 2009).

Conclusion

The cereals collected across the agro-ecological zones were contaminated with low doses of CPA but their consistency are associated with negative public health consequences. Furthermore, there is a high

risk of contamination by Nigerian cereals consumers to the CPA especially in the Derived and Southern Guinea Savannas. Intervention strategies are therefore needed across the Agro-Ecological Zones to ensure that safe and wholesome foods are made available to the populace. Local farmers also need to be trained on how to cultivate good agricultural and storage practices in order to reduce the prevalence of CPA.

References

Abia, W. A., Warth, B., Sulyok, M., Krska, R., Tchana, A., Njobeh, P. B., & Moundipa, P. F. (2013). Bio-monitoring of mycotoxin exposure in Cameroon using a urinary multi-biomarker approach. *Food and chemical toxicology*, *62*, 927-934.

Adetunji, M., Atanda, O., Ezekiel, C., Sulyok, M., Warth, B., Beltran, E., Krska, R., Obadina O., Bakare, & A, Chilaka C (2014) Fungal and bacterial metabolites of stored maize (Zea mays, L.) from five agro-ecological zones of Nigeria. *Mycotoxin Res*. doi:10.1007/s12550-014-0194-2

Alshannaq, A. and Yu, J.-H. (2017). Occurrence, Toxicity, and Analysis of Major Mycotoxins in Food. *International Journal of Environmental Research and Public Health*, *14*(6), 632. https://doi.org/10.3390/ijerph14060632

Ansari, P. and Häubl, G. (2016). Determination of cyclopiazonic acid in white mould cheese by liquid chromatography–tandem mass spectrometry (HPLC–MS/MS) using a novel internal standard. *Food Chemistry*, *211*, 978–982. https://doi.org/https://doi.org/10.1016/j.foodchem. 2016.05.063

Atehnkeng J., Ojiambo P., S., Donner, M., Ikotun, T., Sikora, R. A., Cotty, P. J, and Bandyopadhyay R. (2008). Distribution and toxigenicity of Aspergillus species isolated from maize kernels from three agro-ecological zones in Nigeria. *International Journal of Food Microbiology* 122:74–84

Burdock, G. A. and Flamm, W. G. (2000). Review Article: Safety Assessment of the Mycotoxin Cyclopiazonic Acid. *International Journal of Toxicology*, *19*(3), 195–218. https://doi.org/10.1080/10915810050074964

Delgado, J., Peromingo, B., Rodríguez, A. and Rodríguez, M. (2019). Biocontrol of Penicillium griseofulvum to reduce cyclopiazonic acid contamination in sausages. *International Journal of Food Microbiology*, *293*: 1–6. https://doi.org/https://doi.org/10.1016/j.ijfoodmicro.2018.12.027

Finoli, C., Vecchio, A., Galli, A. and Franzetti, L. (1999). Production of cyclopiazonic acid by molds isolated from Taleggio cheese. *Journal of food protection*, *62*(10), 1198-1202.

Hayashi, Y., & Yoshizawa, T. (2005). Analysis of cyclopiazonic acid in corn and rice by a newly developed method. *Food Chemistry*, *93*: 215–221. https://doi.org/10.1016/j.foodchem.2004.09.017

Holzapfel C. W. (1968). The isolation and structure of cyclopiazonic acid, a toxic metabolite of Penicillium cyclopium Westling. *Tetrahedron*, 24 (5):2101-19. doi: 10.1016/0040-4020(68)88113-x. PMID: 5636916.

Hymery, N., Masson, F., Barbier, G., and Coton, E. (2014). Cytotoxicity and immunotoxicity of cyclopiazonic acid on human cells. *Toxicology in vitro*, *28*(5): 940-947.

Lombaert, G. A. (2002) In: DeVries JW, Trucksess MW, Jackson LS (eds) Mycotoxins and food safety. Academic/Plenum Publishers, New York

Makinde, O. M., Ayeni, K. I., Sulyok, M., Krska, R., Adeleke, R. A., & Ezekiel, C. N. (2020). Microbiological safety of ready-to-eat foods in low-and middle-income countries: A comprehensive 10-year (2009 to 2018) review. *Comprehensive Reviews in Food Science and Food Safety*, *19*(2): 703-732.

Makun, H. A., Adeniran, A. L., Mailafiya, S. C., Ayanda, I. S., Mudashiru, A. T., Ojukwu, U. J., and Salihu, D. A. (2013). Natural occurrence of ochratoxin A in some marketed Nigerian foods. *Food Control*, *31*(2), 566-571.

Moldes-Anaya, A. S., Asp, T. N., Eriksen, G. S., Skaar, I., and Rundberget, T. (2009). Determination of cyclopiazonic acid in food and feeds by liquid chromatography– tandem mass spectrometry. *Journal of Chromatography A*, *1216*(18), 3812–3818. https://doi.org/https://doi.org/10.1016/j.chroma.2009.02.061

Ostry, V., Toman, J., Grosse, Y., and Malir, F. (2018). Cyclopiazonic acid: 50th anniversary of its discovery. *World Mycotoxin Journal*, *11*(1), 135–148. https://doi.org/10.3920/WMJ2017.2243

Peng, Q., Xing, W., Xu, Q., Chen, J., Yu, H., Chen, F., Li, B., Xu, X., 399 Wang, Z., Tian, R., Sun, J., Zou, H.J., Mo, J. and Xie, G., (2017). Determination of cyclopiazonic acid in Chinese yellow wine by high-performance liquid chromatography-triple quadrupole mass spectrometry. *Journal of the Chemical Society of Pakistan*, 39, 484-487.

Perng, C. K., Ehrlich, K. C., and Fujii, I. (2009). Cyclopiazonic acid biosynthesis of Aspergillus flavus and Aspergillus oryzae. *Toxins*, *1*(2), 74-99.

Peromingo, B., Rodríguez, M., Núñez, F., Silva, A., and Rodríguez, A. (2018). Sensitive determination of cyclopiazonic acid in dry-cured ham using a QuEChERS method and UHPLC–MS/MS. *Food Chemistry*, *263*, 275 https://doi.org/https://doi.org/10.1016/j.foodchem.2018.04.126

Rao, B. L., and Husain, A. (1985). Presence of cyclopiazonic acid 422 in kodo millet (Paspalum scrobiculatum) causing 'kodua poisoning' in man and its production by associated fungi. *Mycopathologia*, *89*(3), 177–180. https://doi.org/10.1007/BF00447028

Scott, P. M. (1995). Mycotoxin methodology. *Food Additives & Contaminants*, *12*(3), 395-403.

Udoh, J. M, Cardwell KF, and Ikotun T (2000) Storage structures and aflatoxin content of maize in five agro-ecological zones of Nigeria. *Journal of Stored Produce Research* 36:187–201

Wenzl, T., Haedrich, J., Schaechtele, A., Robouch, P., Stroka, J. (2016) Guidance Document on the Estimation of LOD and LOQ for Measurements in the Field of Contaminants in Feed and Food. https://op.europa.eu/en/publication-detail/ /publication/200cf09a-9ad1-11e6-868c-01aa75ed71a1.

Wild, C. P, and Hall A. J., (2000) Primary prevention of hepatocellular carcinoma in developing countries. *Mutation Research* 462:381–39

Available online at www.asric.org
ASRIC Journal on Natural Sciences Vol 3(1) (2023) 84-90

Development Of Novel Commercial Production Protocol for High-Yielding Oyster Mushrooms (Pleurotus Species)

Adebayo Elijah Adegoke[1*]

[1]Department of Pure and Applied Biology, Ladoke Akintola University of Technology, Microbiology and Biotechnology Laboratory, Department of Pure and Applied Biology, LAUTECH, Ogbomoso, Nigeria

*Corresponding author: eaadebayo@lautech.edu.ng; egokeadebayo@gmail.com

Abstract
The main difficulties in growing mushrooms in Nigeria continue to be the low bio-efficiency of the most frequently utilized substrates and the stress that substrate composting experiences. This study assesses how well palm kernel fruit stalk (PKFS) wastes work for mushroom cultivation and makes additional attempts to determine how sterilization affects substrate composting and mushroom yield. *Pleurotus ostreatus* was grown on fermented PKFS (24 h, 48 h, and 72 h) using a novel protocol (spawn production, substrate composition, inoculation, spawn running, ramification, and fruit body production), and the effect of sterilization on the substrate composition was assessed. The highest yield was (1867 g) 72 h, followed by (1346 g) 48 h, and 24 h fermentation gave the lowest value (601 g), indicating that the fermentation process had an impact on the substrate composition in relation to the quantity of the mushroom yield. This affirms fermented PKFS can be employed as a commercial substrate for mushroom cultivation. The findings have established fermented PKFS as a cutting-edge method for growing oyster mushrooms. This novel protocol is easy and effective for mushroom composting, growing, and productivity. Additionally, there is no electricity usage involved in the technique, and the utilization of palm waste is a value-added, which turns waste into wealth and improves the environment.
Keywords: Mushroom; *Pleurotus ostreatus*; Palm kernel fruits stalk; Fermentation

1. Introduction
For thousands of years, humans have harvested and grown mushrooms for both food and medical uses. Mushrooms are a group of fungi that are distinguished by having sporophore (fruiting bodies) that are visible to the unaided eye (Di Piazza *et al*., 2021). Because mushrooms lack chlorophyll, they cannot produce their own sustenance and must instead rely on the dead and decaying because they are saprophytic (Aminuzzaman *et al*., 2021). According to Bellettini *et al*. (2018), mushrooms are a great source of nutrients, including proteins, minerals, and vitamins B, C, and D. They are low in fats, include all nine of the essential amino acids, and have a protein content of 20 to 35 percent (dry weight) (Kalac, 2009).

Mushrooms have long been valued as a nutrient-dense delicacy that may be used by humans as both food and medicine (Adebayo *et al*., 2012; Bamigboye and Oloke, 2016). They generate enough amount of high-quality food in both quantity and quality that is suitable for a variety of demographics, including children and the elderly (Mariga *et al*., 2014). Due to the presence of a variety of biomolecules, including phenolic compounds, terpenes, steroids, and polysaccharides, mushrooms may have health-promoting benefits. These biomolecules have antifungal activity (Kumar *et al*., 2021), antigenotoxic activity (Anusiya *et al*., 2021), antioxidation activity (Roupas *et al*., 2012), antiproliferative activity (Zhou *et al*., 2013), anti-tumorigenic (Kim *et al*., 2015), antihyperlipidemic activity (Elkhateeb,2020), atherogenic properties (Badalyan *et al*., 2023), antimicrobial (Adebayo *et al.,* 2018). They are good for diabetic patients due to stress-reducing properties (Singh *et al*., 2022).

Recent studies have also raised the possibility of using mushrooms to treat conditions like diabetes, cancer, and cardiovascular problems (Singh *et al*., 2022). Additionally, as decomposers that aid in soil formation and nutrient cycling, mushrooms have a significant impact on the ecosystem (Sahithya *et*

al., 2022). Two hundred (200) different kinds of mushrooms are used as superfoods around the world (Niazi and Ghafoor, 2021).), but only 35 of those are grown commercially, and 10 of those have reached the level of industrial production in a number of nations (Chang and Wasser, 2017). *Pleurotus ostreatus*, popularly known as the oyster mushroom, is one of the most popular and reasonably priced kinds of farmed mushrooms worldwide (Carrasco *et al*., 2018). According to Adebayo *et al*. (2014a), this nutrient-dense edible fungus is ranked second among commercially grown mushrooms because of its flavour, taste, high nutritional content, and therapeutic qualities.

The top African nations producing mushrooms are Zimbabwe, Swaziland, Namibia, South Africa, Malawi, Benin, and Ghana (Fernandes *et al*., 2021). In Cameroon, Congo, Ivory Coast, Kenya, and Namibia, where 10 kg of fresh mushrooms per square metre and more are achieved, good examples of mushroom production on a local or big scale may already be seen. Zambia produces the most dried mushrooms in Africa, accounting for over 96% of the entire volume, followed by South Africa, which accounts for 3.2% of the production (Fernandes *et al*., 2021).

With 66% of all exports in value terms, Burkina Faso became the continent of Africa's top exporter of dried mushrooms. South Africa, which accounts for 8.6% of all exports, is ranked second, followed by Egypt, which accounts for 7%. In 2021, the export price in Africa was $16,296 per tonne, an increase of 125% from the year before (Africa-mushrooms, 2021). Nigeria is without a doubt falling behind in terms of economic development and the prosperity mushroom provides to Africa; as a result, it needs to wake up and participate if it wants a viable national economy.

In recent years, turning low-value agro-industrial waste into profitable end products has emerged as a top research goal. The mushroom cultivation industry grew as a result of the developing world's constant need for affordable, nutrient-dense food and its dearth of protein (Kumar *et al*., 2022). Furthermore, reducing environmental pollution is a key benefit of mushroom farming. The valued product has a significant impact on national and regional pollution levels and will continue to rise since it plays a role in the bio-transformation of lignin and cellulosic residues of food (Adebayo and Martinez-Carrera, 2015).

Technology in mushroom growing has just recently undergone a revolution. Oyster mushrooms (*Pleurotus ostreatus*) were first cultivated in the 1900s (Noor, 2016). Around 1917, *Pleurotus ostreatus* was first cultivated in Germany using natural spawns to inoculate wood logs and stumps (De Villaa *et al*., 2022). Then, it was found that a number of species could thrive on lignocelluloses, forest byproducts, and agricultural waste. A variety of agro-wastes have been used to develop oyster mushrooms, including empty fruit bunches (Marlina *et al*., 2020), date-palm leaves (Alananbeh *et al*., 2014), palm oil shaft and bunch (Elkanah *et al.,* 2022), and wheat and rice straw (Yang *et al*., 2013; Rezania *et al*., 2017). Some of the substrates reportedly used are not satisfactorily produced commensurable yield. The substrate composting is usually laborious with a low yield of mushrooms, another challenge is the power or energy needed for substrate sterilization, especially in a country like Nigeria where power generation is a big national problem over time. So, in order to increase the yield of oyster mushrooms, a quick, no energy or power-involved, seamless, and efficient fermenting procedure should be developed. Therefore, the purpose of this study is to culture *Pleurotus ostreatus* and assess the impact of fermented substrate (PKFS) on growth and quantity of yield.

2. Materials and Methods

2.1 Collection of Samples and culture preparation

The *P. ostreatus* strain utilized in this investigation was obtained from the Department of Pure and Applied Biology's Microbiology Research Laboratory at LAUTECH Ogbomoso. The strain was routinely cultured on Potato Dextrose Agar (PDA) media, conserved, and kept at 4°C for later applications. (Adebayo *et al.,* 2021).

2.2 The Spawn Production

In this investigation, spawn was produced and used for inoculation in accordance with (Adebayo *et al*., 2013; Adebayo *et al*., 2021). Millets were weighed (100 g/bottle), carefully cleaned, and then boiled for 45 minutes before being drained and left to dry at room temperature. The dried grains were combined with calcium carbonate ($CaCO_3$) at a weight-to-weight ratio of 1%, after which the millets

were put into sterile bottles and sealed. Both were once more sterilized for 15 minutes at 121℃. *P. ostreatus* culture that was actively growing was harvested using a sterilized plug measuring 6 mm in diameter. This culture was then injected into the sterilized millet culture and incubated at 23±2℃ (ambient temperature). The rate of mycelia ramification, the duration of mycelia ramification, the weight of ramified mycelia, and the productivity of the spawn were all calculated. The definitions of these terms are as follows:

(i) Mycelia Ramification Rate = $\frac{\text{Average length of mycelia ramification}}{\text{Average number of days}}$

(ii) Weight of Mycelia Ramification (WMR) = Final weight (Grain + Bottle + Mycelia) –Initial weight (Grain + Bottle)

(iii) Ramification day = Average number of days for full ramification

(iv) Productivity Rate = $\frac{\text{Total weight of mycelia}}{\text{Substrate weigh}} \times 100\%$

Mycelia extension through the substrate in the palm kernel fruit stalk bags was measured using a transparent graduated meter rule.

2.3 Collection and preparation of oil palm kernel fruit stalk

Oil palm kernel fruit stalks were gotten from a palm oil-producing plant in Iranyin village, Ogbomoso (28°N, 27°E), Oyo State, Nigeria.

2.4 Fruit body production (Sporophore formation)

2.4.1 Substrates formulation

The substrate for this study was oil palm kernel fruit stalks, which were dried outdoors, cut into smaller pieces, and then soaked in water for 24, 48, and 72 hours, separately, to allow fermentation to occur. The stalks were immersed in distilled water for the specified amount of time at a material-to-liquid ratio (MLR) of 10:1. The protocol involved PKFS collection, washing, drying, shredding of the stalk, fermentation of the shredded stalk (24, 48, and 72 h), draining of the fermented stalk materials, bagging, inoculation, and incubation.

2.4.2 Inoculation and bagging of oil palm kernel fruit stalk

After being drained of excess moisture, the fermented, shredded oil palm fruit stalks were bagged in heat-resistant nylon with hollow holes at both ends. Then, each of the (1.0kg) bags was inoculated at one end with a spawn (5-10% w/w). After that, the bags were kept at a constant temperature of 25 °C while being incubated in the dark. Completely colonized substrate bags were moved into the mushroom house, which was dark and humid with a temperature range of 22°C–28°C. Because of the favourable temperature, watering was skipped after 7 days. At three-day intervals, the substrate was inspected and examined for growth. Accordingly, the ramification rates, fruit body weight, biological efficiency, and production were determined (Adebayo *et al*., 2014b; Adebayo *et al*., 2021).

2.5 Mushroom harvesting

The mushrooms were harvested individually by the use of hand to grasp the stalk and twisting (hand picking). Nine harvests were achieved in this research which is equivalent to three flushes.

2.6 Data Analysis

Data collected were analyzed using One-way ANOVA and reported as Mean ± SEM

3. Results

3.1 Developing commercial cultivation protocol for oyster mushrooms using PKFS

PKFS which is underutilized agro-waste was used for developing a novel, simple, fast, seamless, and efficient in terms of mushroom composting and productivity. The step by steps activities were showed in Figure 1. The procedure using fermented PKFS started with PKFS collection, shredded, fermented, bagged, spawn production using grains, production of *Pleurotus ostreatus* on fermented PKFS, and yield harvested (Figure 1).

Fig 1: Schematic of novel *Pleurotus ostreatus* cultivation procedure using fermented PKFS

3.2 Yield per flush of substrates with the total mushroom yield (Pleurotus ostreatus)

Yield per flush of substrates showed significant variations in the three flushes, with the highest yield observed in the first flush, followed by the second flush with the most negligible value obtained in the third flush (Table). The distribution of the average mean of the total value of fresh and dry weight (grams) of mushroom harvested with three (3) flushes, total wet weight, total dry weight, incubation period, production period, and primordia formation days for different fermentation period evaluated are shown in Table 1. The incubation period (IP) primordia formation day ranged between 11 days and 17 days. The Production period (PP) ranged between 47-54 days. Fermented PKFS with 72 h has the lowest values of IP (11 days) and the highest PP (54 days), followed by 48 h and 24 h fermented PKFS IP (14, 17 days) and PP (48, 47 days) respectively.

The total wet weight of 24 h, 48 h, and 72 h fermented PKFS mushrooms ranged between 601 g - 1867 g, with 72 h having the highest value of 1867 g and 24h having the least value of 601g. The total dry weight of the mushroom ranged between 69.74 g – 132.47 g (Table 1).

The highest values of biological efficiency (75.51%) and productivity (12.34%) were obtained at 72 h fermentation period, followed by 48 h (52.36; 8.33), and 24 h (34.85; 5.64) for biological efficiency and productivity respectively (Table 2).

Table 1: Distribution of the average mean of total fresh and dry weight (g) over three flushes by *Pleurotus ostreatus* on different fermentation periods

Fermentation Period (H)	IP	PP	1st FLUSH	2nd FLUSH	3rd FLUSH	TWW	TDW
72	11	54	472 ± 0.74	111.6 ± 0.47	38.66 ± 0.25	622.26	132.47
48	14	48	344.3 ± 0.62	74.6 ± 0.43	29.6 ± 0.26	448.50	69.74
24	17	47	152.3 ± 0.64	37.5 ± 0.25	34.5 ± 0.06	224.30	68.47

IP = Incubation period (required days for formation of primordia)
PP = Production period, starting with the formation of primordia till the third flush. The values are expressed as mean ± SEM.
TWW = Total Wet Weight
TDW = Total Dry Weight

Table 2. Biological efficiency and productivity of fermented PKFS at different fermentation periods

Fermentation Period (h)	Biological efficiency (%)	Productivity (%)
72	75.51	12.34
48	52.36	8.33
24	34.85	5.64

4. Discussion

Oyster mushroom belongs to the genus *Pleurotus* and is most popularly consumed due to their taste, flavour, high nutritional value, and medicinal properties (Elkana *et al.,* 2022). The cultivation of *Pleurotus* species on agricultural waste materials, such as fermented palm kernel fruit stalk, is an eco-friendly and economically viable approach. This capability of the oyster mushroom is due to the presence of varieties of extracellular lignin-modifying enzymes also named fibrolytic enzymes, including xylanases, cellulases, and laccases. These enzymes help oyster mushrooms to degrade the lignocellulose substrate, turning it into energy and carbon sources for the fungi (Raman *et al.,* 2020).

The fermentation process plays a crucial role in breaking down complex organic compounds and creating a favorable environment for mushroom growth. The current study has achieved the cultivation of *Pleurotus ostreatus* on fermented PKFS. The fermentation was conducted at 24 h, 48 h, and 72 h. The best results on the parameters evaluated were obtained at 72 h, which gave the shortest incubation period (IP), longest production period (PP), the highest mushroom yield, biological efficiency, and productivity. Furthermore, the longer fermentation duration allows for the accumulation of essential nutrients, such as nitrogen, phosphorus, and potassium, which are vital for mushroom growth. The breakdown of organic matter during fermentation releases these nutrients, making them readily available for mushroom mycelium colonization and fruiting body development. It is worth noting that beyond a certain fermentation duration, the benefits may diminish or even become detrimental to mushroom cultivation. Prolonged fermentation periods can lead to excessive degradation of organic matter, resulting in nutrient depletion or the accumulation of inhibitory substances. Therefore, finding an optimal fermentation period is crucial to maximizing mushroom yield while maintaining substrate quality. A paucity of information is available on *Pleurotus* species cultivation using a fermented substrate. Yamauchi *et al.* (2019) reported the cultivation *Pleurotus* species on 2-month fermented bamboo sawdust (BS) with other supplements such as rice bran (RB) and sweet potato schochu lees (SPSL), which is more time-consuming and likely to more laborious.

The developed procedure has the capacity to solve the challenges associated with sawdust substrates such as low bio-efficiency, time-consuming, slow down of mushroom growth, laborious, high-energy demand, and difficulty in composting with low yield (Adebayo *et al.,* 2021). The novel mushroom cultivation method developed will resolve the main frustrating challenge to mushroom farmers in Nigeria, which is the intermittent or irregular supply of energy (power supply) for substrate sterilization. The power outage coupled with other defects of the sawdust and other substrates resulted in urgent intervention in developing this novel mushroom cultivation method by using PKFS which is a more reliable, efficient, seamless, inexpensive, and the highest-productive substrate source.

In Nigeria, the palm oil production industry alone generated over 90 million tonnes of effluent waste annually (Amuge, 2022) which contributed to nutrient loss in the soil, changes the soil appearance and properties, and loss of its vegetative cover. It also contaminates the aquatic ecosystem, causing acidification and eutrophication in the water bodies, air pollution by interfering with the greenhouse effect emissions, and biodiversity loss (Ogunsina and Akintan, 2020). Using this agro-wastes (palm oil waste) will place a price value (value added) on this agro-waste and reduce environmental challenges.

5. Conclusion

In conclusion, this study demonstrates that a 72-hour fermentation period of fermented palm kernel fruit stalk is optimal for cultivating mushrooms. These findings provide valuable insights for farmers and researchers involved in mushroom cultivation, offering a sustainable approach for utilizing agricultural waste materials and maximizing mushroom production with less stress in composting and a seamless process.

The finding has resulted in an indigenous and novel commercial oyster mushroom cultivation method with maximum yield being recorded. The uniqueness of our method is the usage of palm oil agro-waste, which constitutes a nuisance in the environment, and the fermentation process instead of sterilization, i.e. no energy or power and special skill is required. The advantages of our method over

existing ones are, substrates were obtained with no or low price, usage of palm kernel fruits stalk waste is a value-added venture which turned waste into wealth, enhances sanitation of the environment, no power or energy is needed, the developed method is simple and easy to use without requiring special skills. Again, this study will contribute immensely to SDG #1- no poverty- income generation, especially for women through cultivation, SDG #2- zero hunger- through functional food production, SDG #12- Ensure sustainable consumption and production patterns, and SDG #6- clean water and sanitation.

6. Acknowledgement

Ogunjimi O.E., Ogunremi A.M., Lasisi R.A., Sulaiman A. A., and Olukemi E.A., the undergraduate students were acknowledged for their active roles in data collection during the study. Also, LAUTECH management was acknowledged for providing a conducive environment for the study.

7. References Cited

Adebayo, E. A., Oloke, J. K., Ayandele, A. A., and Adegunlola, C. O. (2012a). Phytochemical, antioxidant and antimicrobial assay of mushroom metabolite from *Pleurotus pulmonarius*-LAU 09 (JF736658). Journal of Microbiology and Biotechnology Research, 2(2), 366-374.

Adebayo, E.A., Oloke, J.K., Achana Y., Barooah, M. and Bora, T.C. (2013). Improving yield performance of *Pleurotus pulmonarius* through hyphal anastomosis fusion of dikaryons. *World Journal of Microbiology and Biotechnology* 29**:**1029-1037.

Adebayo, E. A., Alao, M. B., Olatunbosun, O. O., Omoleye, E. O., and Omisakin, O. B. (2014a). Yield evaluation of *Pleurotus pulmonarius* (oyster mushroom) on different agricultural wastes and various grains for spawn production. Ife Journal of Science, 16(3), 475-480.

Adebayo, E. A., Oloke, J. K., Aina, D. A., and Bora, T. C. (2014b). Antioxidant and nutritional importance of some *Pleurotus* species. Journal of microbiology, biotechnology and food sciences, 3(4), 289-294.

Adebayo, E. A., and Martinez-Carrera, D. (2015). Oyster mushrooms (*Pleurotus*) are useful for utilizing lignocellulosic biomass. African Journal of Biotechnology, 14(1), 52-67.

Adebayo, E.A., Martınez-Carrera, D., Morales, P., Sobal, M., Escudero, H., Meneses, M.E., Avila-Nava, A., Castillo, I. and Bonilla, M. (2018). Comparative study of antioxidant and antibacterial properties of the edible mushrooms *Pleurotus levis, P. ostreatus, P. pulmonarius* and *P. tuber-regium*. *International Journal of Food Science and Technology* 53: 1316–1330.

Adebayo, E. A., Elkanah, F. A., Afolabi, F. J., Ogundun, O. S., Alabi, T. F., and Oduoye, O. T. (2021). Molecular characterization of most cultivated Pleurotus species in sub-western region Nigeria with development of cost-effective cultivation protocol on palm oil waste. Heliyon, 7(2). e06215

Africa - Mushrooms (Dried) - Market Analysis, Forecast, Size, Trends and Insights. Index Box. https://www.indexbox.io/store/africa-mushrooms-dried-market-report-analysis-and-forecast-to-2020/

Alananbeh, K. M., Bouqellah, N. A., and Al Kaff, N. S. (2014). Cultivation of oyster mushroom Pleurotus ostreatus on date-palm leaves mixed with other agro-wastes in Saudi Arabia. Saudi journal of biological sciences, 21(6), 616-625.

Aminuzzaman, F. M., Shahi, S., Thapa, S., & Das, K. (2022). Mushroom Diseases and Their Management: A Review.Recent Advances in Mushroom Cultivation Technology and Its Application, 2, 1-27.

Amuge, O. (2022). Harnessing Nigeria's agricultural wastes for economic development. https://www.businessamlive.com/harnessing-nigerias-agricultural-wastes-for-economic-development/.

Anusiya, G., Gowthama Prabu, U., Yamini, N. V., Sivarajasekar, N., Rambabu, K., Bharath, G., and Banat, F. (2021). A review of the therapeutic and biological effects of edible and wild mushrooms. Bioengineered, 12(2), 11239-11268.

Badalyan, S. M. (2023). Check for updates The Potential of Mushrooms in Developing 11 Healthy Food and Biotech Products SM Badalyan and A. Zambonelli. Fungi and Fungal Products in Human Welfare and Biotechnology, 307.

Bamigboye, C. O., and Oloke, J. K. (2016). Ameliorative effect of Lentinus squarrosulus mycomeat against Pseudomonas aeruginosa infection using albino rat as animal model. African Journal of Biotechnology, 15(26), 1383-1390.

Bellettini, M. B., Bellettini, S., Fiorda, F. A., Pedro, A. C., Bach, F., Fabela-Morón, M. F., and Hoffmann-Ribani, R. (2018). Diseases and pests noxious to Pleurotus spp. mushroom crops. Revista Argentina de microbiologia, 50(2), 216-226.

Carrasco, J., Zied, D. C., Pardo, J. E., Preston, G. M., and Pardo-Giménez, A. (2018). Supplementation in mushroom crops and its impact on yield and quality. AMB Express, 8(1), 1-9.

Chang, S. T., and Wasser, S. P. (2017). The cultivation and environmental impact of mushrooms. In Oxford research encyclopedia of environmental science.

De Villaa, C. M., Geronimob, V. M., and Diongcoc, M. E. E. (2022). Production of Oyster Mushroom Using Sterilized and Carbonized Fruiting Bags: A Comparative Study. Production of Oyster Mushroom Using Sterilized and Carbonized Fruiting Bags: A Comparative Study, 105(1), 31-31.

Di Piazza, S., Benvenuti, M., Damonte, G., Cecchi, G., Mariotti, M. G., and Zotti, M. (2021). Fungi and circular economy: Pleurotus ostreatus grown on a substrate with agricultural waste of lavender, and its promising biochemical profile. Recycling, 6(2), 40.

Elkanah, F.A., Oke M.A., Adebayo, E.A. (2022). Substrate composition effect on the nutritional quality of *Pleurotus ostreatus* (MK751847) fruiting body. *Heliyon*, 8: e11841.

Elkhateeb, W. A. (2020). What medicinal mushroom can do.Chem Res J, 5(1), 106-118.

Fernandes, T., Garrine, C., Ferrão, J., Bell, V., and Varzakas, T. (2021). Mushroom nutrition as preventative healthcare in Sub-Saharan Africa. Applied Sciences, 11(9), 4221.

Fridman, H., Bormans, C., Einhorn, M., Au, D., Bormans, A., Porat, Y., and Behar, D. M. (2021). Performance comparison: exome sequencing as a single test replacing Sanger sequencing. Molecular Genetics and Genomics, 296, 653-663.

Hu, S., Li, X., Yin, X., Li, R., Zhang, R., Zang, J., and Liu, Y. (2022). Species-specific identification of Pseudomonas based on 16S–23S rRNA gene internal transcribed spacer (ITS) and its combined application with next-generation sequencing. BMC microbiology, 22(1), 1-11.

Kumar, K., Mehra, R., Guiné, R. P., Lima, M. J., Kumar, N., Kaushik, R., and Kumar, H. (2021). Edible Mushrooms: A comprehensive review on bioactive compounds with health benefits and processing aspects. Foods, 10(12), 2996.

Kumar, P., Mehta, N., Abubakar, A. A., Verma, A. K., Kaka, U., Sharma, N., and Lorenzo, J. M. (2022). Potential alternatives of animal proteins for sustainability in the food sector. Food Reviews International, 1-26.

Mahari, W. A. W., Peng, W., Nam, W. L., Yang, H., Lee, X. Y., Lee, Y. K., and Lam, S. S. (2020). A review on valorization of oyster mushroom and waste generated in the mushroom cultivation industry. Journal of hazardous materials, 400, 123156.

Mariga, A. M., Yang, W. J., Mugambi, D. K., Pei, F., Zhao, L. Y., Shao, Y. N., and Hu, Q. (2014). Antiproliferative and immunostimulatory activity of a protein from Pleurotus eryngii. Journal of the Science of Food and Agriculture, 94(15), 3152-3162.

Niazi, A. R., and Ghafoor, A. (2021). Different ways to exploit mushrooms: A review. All life, 14(1), 450-460.

Noor, S. (2016). Effect of Various Media on the Growth of Pleurotus ostreatus (Doctoral dissertation, INTI International University).

Ogunsina, O.I., Akintan, G. B. (2020). Environmental Pollutant of Palm Oil Effluent and Its Management in Okitipupa Area of Ondo State, Nigeria. *Journal of Environment Protection and Sustainable Development* 6(4): 72-81.

Raman, J., Kab-Yeul J., Youn-Lee O., Minji O., Ji-Hoon I., Hariprasath L., and Vikineswary S. (2020). Cultivation and Nutritional Value of Prominent *Pleurotus* spp.: An Overview. *Mycobiology*, https://doi.org/10.1080/12298093.2020.1835142.

Sahithya, K., Mouli, T., and Biswas, A. (2022). Remediation potential of mushrooms and their spent substrate against environmental contaminants: An overview. Biocatalysis and Agricultural Biotechnology, 42, 102323.

Singh, M. P., Rai, S. N., Dubey, S. K., Pandey, A. T., Tabassum, N., Chaturvedi, V. K., and Singh, N. B. (2022). Biomolecules of mushroom: A recipe of human wellness.Critical Reviews in Biotechnology, 42(6), 913-930.

Yamauchi, M., Sakamoto, M., Yamada, M., Hara, H., Taib, S.M., Rezania, S., Din, M.F.M., Hanafi, F.H.M., 2019. Cultivation of oyster mushroom (*Pleurotus ostrreatus*) on fermented moso bamboo sawdust. J. King Saud Univ. Sci., 31: 490–494.

Vesty, A., Biswas, K., Taylor, M. W., Gear, K., and Douglas, R. G. (2017). Evaluating the impact of DNA extraction method on the representation of human oral bacterial and fungal communities. PloS one, 12(1), e0169877.

Available online at www.asric.org
ASRIC Journal on Natural Sciences Vol 3(1) (2023) 91-100

Influence of Rock Mass Properties and Discontinuity with Explosive Charge on Muck-Pile Size Distribution

Adebayo Babatunde[1*], Ajaka Ebenezer O. [1], Afeni Thomas B. [1], Akinbinu Victor A. [1], Okewale Ismail A. [1], Lawal Abiodun I. [1], Apena Waliu O. [1], Ogunyemi Bidemi O. [1], Amigun John O.[2]

[1]Department of Mining Engineering, Federal University of Technology, Akure,
[2]Department of Applied Geophysics, Federal University of Technology, Akure

*Corresponding author: baayoakinola@googlemail.com

Abstract
The cost effective technique of generating heap of rock fragments is through blasting operation. The process of achieving optimum muck-pile fragment size distribution is complex and at same time the task of matching crusher's gape to the appropriate mean fragment size for improved productivity of crusher had constituted a serious concern to mine managers and quarry operators. Therefore, this research is set to evaluate rock mass properties, map discontinuities, thereafter analyse the influence these properties with explosive usage on fragment size. In order to achieved the set of objectives two rock types coded STAK and FMIJ were selected from two operating quarries in Ondo State, Nigeria for this study. Forty (40) datasets were obtained for bulk density and rebound hardness values. Also, Rock Quality Designation (RQD) and Rock Mass Rating (RMR) were determined as part of the rock mass factors. Moreover, the discontinuities were mapped at the selected quarry faces, explosive data usage were obtained and digital image of the muck-piles were taken and analyzed. The results obtained revealed that bulk density and rebounds hardness varied from 2795.27-2902.25 kg/m^3 and 2765.63 – 3193.80 kg/m^3; 40 – 62 and 30 – 62 for STAK and FMIJ respectively. The RQD values of the rocks are 73% for STAK and 71% for FMIJ, hence, the two rocks are classified as good quality rocks. In addition, the RMR of the selected rocks varied from 52 – 80 and 58 – 92 for STAK and FMIJ respectively. The influence of the parameters will guide Mine Managers on explosive consumption and the various ranges of muck-pile sizes that will be generated after fragmentation.
Keywords: Rock mass, explosive, charge, rock, quality, fragments, muck-pile

Introduction
Rock fragmentation is crucial in quarries and mines because this is the major means by which rock outcrops, large volume of rocks and in-situ rocks can be reduced to smaller fragments. This essentially makes loading from muck-pile using excavating machine to be very easy. It makes haulage of the muck to the reduction or beneficiation plant, through the transport unit manageable. Smaller fragments that are product of fragmentation will be effectively handled by beneficiating equipment. This will lead to reduced energy consumption at the beneficiation plant. More importantly, the overall mining cost will be affected by the outcome of rock fragmentation.

Rock mass properties and factors are inherent in rock as a result of geological processes that led to the formation of rock. These will influence the behaviour as regard mechanical and chemical activities, that the in-situ rock mass may undergo during exploitation. Hosseini et al. 2023 affirmed the above argument by reporting that the main factors influencing blasting are rock mass properties, explosive properties, and blast geometry. According to Mehrdanesh et al. (2017) rock mass characteristics influence rock fragmentation more than blasting pattern. The blast patterns and blast parameters should be designed according to the rock mass properties and rock fragmentation requirements. However, rock properties may not be available to mine managers particularly at the early stage of the quarry design, therefore, diligence must be done to understand rock properties.

Furthermore, discontinuities make rock mass not to be continuum and very low in tensile strength. Hence, they can have effect on the choice of explosive, the charge quantity and the resulting fragments after detonation of the charged explosives. Joints and cracks in rock mass can dictate explosive energy utilization and the resulting fragment size distribution. Hamdi et al. (2008) affirmed that micro-cracks accounted for up to 11% of the explosive energy while the macro-cracks accounted for only 6%. In addition, the choice of explosive to be used may be dictated by joint and crack network in a rock mass. Adebayo and Bolarinwa (2023) selected ANFO for dolomitic marble and granodiorite based on suggestion by Jimeno et al. (1995) that explosive that has high bubble energy to strain ratio should be used for rocks having joint range of 1.50 to 2.5, invariably, about 20% to 40% strain wave energy may be absorbed. This implied that rocks with high fracture network can attenuate explosive wave energy, therefore, quantity of explosives should be reduced in this type of rock. In view of the above, further research is warranted to explore the influence of discontinuities on quantity of explosive charge and muck-pile distribution.

The controllable parameters (blast geometry and explosive types and specifications) can be manipulated to cater for inherent rock mass properties to achieve the desired results. In viewing, rock fragmentation as a means of reducing in-situ rock mass. Researchers identified that, blast-hole diameter is one of the most important blast geometrical parameter, because it will dictate the burden, spacing, stemming length, as well as other blast design parameters (Sazid and Singh 2015; Ghiasi et al. 2016; Ozdemir and Kumral 2019). Dhekne et al. (2020) in their study observed that when site mixed emulsion (SME) is used in large-diameter blast holes, boulders produced are fewer than when the same explosive is employed in small-diameter blast holes.

Moreover, charging the right quantity of explosive per hole is one of the requirement to achieve rock breakage and fragments movement. This is the basis on which the specific charge or powder factor for a rock was determined. If the rock is over charged it may result in fly-rocks, over break vibration and air-blast. Poorly designed blast will consequently lead to excessive noise (air-blast). Vibration may occur due to in appropriate blast design which can cause structural damage to buildings and generate dust. It is the responsibility of quarry engineer to monitor explosive charges and ensure that right quantity of explosive is charged per hole. It is important to consider all rock properties when determining the appropriate explosive charge for blast holes.

Fragment size distribution of the muck-pile is key to the subsequent operations and it has a lot to do with the performance of the crusher. In quarries and open pit mines the fragments are passed to the reduction plant and this is where primary crusher further reduces the run-of-mine to smaller sizes. This will in turn informed the blast design parameters for optimum crusher performance these is in line with the submission of Monjezi. et al. (2009). The aim of this study is to determine influence rock mass properties, discontinuities and explosive charged on muck-pile distribution. The objectives of this work therefore are to investigate the influence of rock mass properties, discontinuities, quantity of explosive charged on muck-pile size distribution. The research questions raised are: how do different types of rock, joint spacing and explosive charged will affect muck-pile distribution? What are the optimal blast design parameters for various rock mass conditions to minimize the negative effects of discontinuities?

The implication of appropriate blast design is that the outcome of blasting will lead to good fragmentation. This implied that the muck-pile size will match the gape of the crusher and crusher will work optimally. When the blast design is improved, productivity will be high which will be evident in higher tonnage of fragmented rock produced. In addition, secondary blasting will be reduced drastically; this will be reflected in the reduction in cost of rock fragmentation and the negative environmental impact of blasting,

In order to be able to determine whether fragmentation is bad or good there is need to constantly analyze fragment size distribution. This will also help the Quarry Manager to determine whether optimum blast parameters had been attained or there are some of blast parameters to be varied to achieved the desired result. A lot of empirical fragmentation models had been developed but many of them did not include rock mass properties. Therefore, there is need to analyze effects rock mass

properties, blast parameters and quantity of explosives to understand the relationship existing among them.

Materials and Methods

Determination of Density of the Selected Rocks

The materials used were rock samples collected from quarry face from south-west Nigeria. The rock samples were coded STAK and FMIJ. The rock samples were prepared by coring the rock samples using pillar coring machine and these samples conformed closely to cylindrical shape. The equipment set-up and core samples are shown in Figs 1 and 2.

Figure 1: Pillar Coring Machine in Operation

Figure 2: Prepared Cored Samples for Determination of Bulk Density

Forty (40) cylindrical cores were prepared for determination of bulk density for two selected rocks. The bulk volume (V) of the core samples were calculated from average of several caliper readings. The dimension and the readings recorded maintained accuracy of 0.1 mm. A balance of adequate capacity was used to determine the mass of specimen to an accuracy of 0.01%. The values of bulk volume and mass were used to calculate the density. This is in accordance to standard suggested by international Society of Rock Mechanics Commission (ISRM, 2007).

The rebound hardness values were measured using Schmidt hammer held horizontally and at right angles to vertical faces of large rock block as shown in Fig.3. Twenty rebound values from single impacts separated by at least a plunger diameter were recorded and the upper ten values averaged. The procedures are in accordance with the standard procedure suggested by ISRM (2007).

Figure 3: Field Measurement of Rebounds Hardness Values

Determination of Rock Quality Designation (RQD)

Rock Quality Designation (RQD) is defined as the percentage of intact core pieces longer than 100 mm in the total length of core. The cores were drilled with pillar coring machine with a double-tube core barrel. RQD for the cored samples were estimated using Equation 1.

$$\text{RQD} = \frac{\sum Core\ pieces \rangle 100\ mm}{Total\ length\ of\ core\ run} \quad (1)$$

Determination of Rock Mass Rating (RMR)

Rock Mass Rating (RMR) System utilized six parameters in classifying a rock mass (Bieniawski 1989) viz:

(a) uniaxial compressive strength of rock material;
(b) Rock Quality Designation (RQD);
(c) Spacing of discontinuities;
(d) Condition of discontinuities
(e) Groundwater conditions, and
(f) Orientation of discontinuities were adopted.

The determined the rating for each parameter were summed up to give the value of RMR for selected rocks.

Discontinuities Mapping

Structural discontinuities within the rock mass were mapped and the joint spacing of individual blocks of intact rock were also measured. This was done with a measuring tape of at least 3 m in length and clinometer were held along the exposure such that the surface trace of the discontinuity set was approximately perpendicular to the tape.

Geometrical and Explosive Data

The geometrical and explosive data were obtained from the two selected quarries. The data obtained from the two selected quarries are: burden, spacing, bench height, hole diameter, stemming length, powder factor and charge weight. The explosives used for blasting operation are dynogel and Ammonium Nitrate and Fuel Oil (AN/FO).

Digital Image of Muck-pile

The images of the muck-pile were taken at quarries after blast operations as shown in Figs 4 and 5 for both FMIJ and STAK respectively. These muck-pile images were analysed using WipFrag Software to generate fragment size distribution.

Figure 4: Selected Digital Muck-pile Image for FMIJ

Figure 5: Selected Digital Muck-pile Image for STAK

Results and Discussion

Rock mass Properties

The result of mineral composition using X-Ray Defractometer (XRD) revealed that the rock coded STAK contains 43% Quartz, 35% Muscovite, 11% Wollastonite, 9% Orthoclase and 2% Albite. Also, rock coded FMIJ contains 37% Quartz, 27.8% Albite 17.5% Orthoclase, 9.6% Anorthite, 5.3% Muscovite and 2.8% Illite.

Table 1 presents the results of bulk density and rebounds hardness values of the samples. The bulk densities varied from 2795.25 kg/m^3 to 2902.25 kg/m^3 and 2765.63 kg/m^3 to 3193.80 kg/m^3 for STAK and FMIJ respectively. The average value of bulk densities for the STAK and FMIJ are 2841 and 3124 kg/m^3 respectively. The rebounds hardness values varied from 32 to 60 for STAK and 40 to 62 for FMIJ. The results revealed that STAK has the least rebounds hardness value while the highest values are found in FMIJ. This showed that rock with high bulk density exhibits high hardness values. It means the rock is compact, hence, more quantities of explosive may be required to fragment same volume of FMIJ than STAK.

Table 1: Bulk Density of Rocks Samples

S/N	Bulk Density (kg/m^3) STAK	Bulk Density (kg/m^3) FMIJ	Rebounds Hardness Value STAK	Rebounds Hardness Value FMIJ
1	2890.63	3164.06	52	40
2	2902.25	3148.44	50	56
3	2795.27	3193.80	46	55
4	2843.75	3093.75	60	50
5	2801.58	3179.68	42	54
6	2890.25	3145.16	35	60
7	2795.27	3161.29	50	50
8	2795.27	3169.35	30	50
9	2843.75	3031.25	50	40
10	2801.58	3164.06	47	42
11	2890.63	3148.44	32	50
12	2902.25	3193.80	50	49
13	2795.27	3093.75	58	42
14	2843.75	3179.68	30	53
15	2801.58	3145.16	58	54
16	2890.63	3161.29	40	42
17	2902.25	3169.35	36	53
18	2795.27	3031.25	50	50
19	2843.75	2765.63	50	46
20	2801.58	3148.44	40	62

Table 2 presents the Rock Quality Designation (RQD) and Rock Mass Rating for STAK and FMIJ samples. For STAK the RQD varied from 48% – 98% with an average value of 72% which make their

classifications to range from poor to excellent rock quality. Also, the values of RQD varied from 61% – 78% with an average value of 70% for the FMIJ and the class vary from fair to good rock quality. Comparing the two samples, the values are relatively similar with STAK having a relatively higher average value. However, RQD alone is not used as rock mass property because they are also component of other rock mass parameters. The RMR for STAK varies from 52 to 80 with an average value of 67.5 and the classification range from fair to good rock. For the FMIJ, the RMR range from 58 to 92 with an average value of 77.3 and based on the classification, they are fair to very good rock. In comparison, the average RMR value is higher in FMIJ than the STAK. This also confirms the findings for the samples in terms of density and rebound hardness.

Table 2: Rock Mass Rating (RMR) and Rock Quality Designation for the Samples

S/N	Rock Quality Designation RQD % (STAK)	Rock Quality Designation RQD % (FMIJ)	Rock Mass Rating RMR (STAK)	Rock Mass Rating RMR FMIJ
1	87	76	77	87
2	85	73	52	83
3	96	71	55	58
4	98	73	80	63
5	51	71	73	63
6	50	63	73	63
7	56	78	73	92
8	48	66	68	88
9	79	61	52	88
10	78	71	72	88
11	87	76	77	87
12	85	73	52	83
13	96	71	55	58
14	98	73	80	63
15	51	71	73	63
16	50	63	73	63
17	56	78	73	92
18	48	66	68	88
19	79	61	52	88
20	78	71	72	88
Av.	72.8	70.3	67.5	77.3

Discontinuity Data Analysis

Table 3 presents discontinuities data for both STAK and FMIJ. The joint spacing varied from 0 – 0.30 m for STAK while FMIJ joint spacing varied from 0 – 3.2 m. STAK exhibit closer joint spacing which can lead to cutting off of the propagation of radial cracks generated by the explosive charged. The pressure generated by the explosives can escape through the joints, this is in line with the submission of Hustrulid (1999). Furthermore, this can cause heaping of the muck-pile to be reduced. The two selected rocks exhibited dry ground water condition, this implied that friction existing between the rocks is intact.

Table 3: Discontinuities Data

S/N	Joint Spacing (m) STAK	Dip (^{0}) STAK	Dip direction (^{0}) STAK	Ground Water condition STAK	Joint Spacing (m) FMIJ	Dip (^{0}) FMIJ	Dip direction (^{0}) FMIJ	Ground Water condition FMIJ
1	0.10	80	020	Dry	0	20	204	Dry
2	0.10	0	66	Dry	0	36	266	Dry
3	0.20	89	356	Dry	1.1 m	10	108	Dry
4	0.25	90	090	Dry	0.77m	12	180	Dry
5	0.30	80	020	Dry	0.54 m	02	183	Dry
6	0.20	89	356	Dry	0	02	302	Dry
7	0.10	80	020	Dry	2.56	65	106	Dry
8	0.10	0	66	Dry	0	70	116	Dry
9	0.20	89	356	Dry	2.18	89	060	Dry
10	0.25	90	090	Dry	1.2	11	120	Dry
11	0.30	80	020	Dry	0.65	56	90	Dry
12	0.20	89	356	Dry	0.80	89	126	Dry
13	0.10	80	020	Dry	3.2	89	110	Dry
14	0	0	66	Dry	3.2	26	240	Dry
15	0.20	89	356	Dry	0	90	212	Dry
16	0.10	0	66	Dry	0	70	116	Dry
17	0.20	89	356	Dry	2.18	89	060	Dry
18	0.25	90	090	Dry	1.2	11	120	Dry
19	0.30	80	020	Dry	0.65	56	90	Dry
20	0.20	89	356	Dry	0.80	89	126	Dry

Influence of Geometrical Parameter and Explosive Usage

The geometrical and explosive data for the STAK and FMIJ samples are presented in Table 4. The burden, spacing and other geometrical parameters are almost the same as presented in the Table 4. In this paper, the powder factors are taken as explosive charge parameter. It can be seen that the STAK has 0.43 kg/m^3 as powder factor while the FMIJ has 0.5 kg/m^3 as the powder factor. Relating the rock mass parameters to the explosive charge parameter, the denser the rock sample, the harder the rock, the higher the RMR and the higher the quantity of explosive needed to achieve good fragmentation. It means that 0.43 kg of explosive is required to fragment 1 m^3 of STAK rock while 0.5 kg of explosive is required to fragment 1 m^3 of FMIJ rock. The behaviour exhibited by FMIJ revealed that more explosives will required and these can be attributed to higher hardness values and RMR.

Table 4: Geometrical and Explosive Data

ROCK CODE	Burden (m)	Spacing (m)	Bench height (m)	Hole Dia (mm)	Drill Hole Depth (m)	Stemming (m)	Powder Factor kg/m^3	Sub drill (m)	Charge length (m)	Charge weight (kg)	No of Drill-Holes
FMIJ	2	2	8.4	80	9.5	1.5	0.5	1.1	8.0	800	50
STAK	2	2	8.8	80	10	1.5	0.43	1.2	8.5	850	50

Muck-pile Size Distribution Analysis

Figures 6 and 7 present the muck pile size distributions for the samples. The muck-pile size distribution for the STAK sample is shown in Fig. 6. The amount of particles passing at 20%, 50% and 80% are 89.68 mm, 189.01 mm and 429.31 mm respectively. For the FMIJ, the amount of particles passing at 20%, 50% and 80% are 84.68 mm, 282.38 mm and 660.79 mm respectively as shown in Fig, 7. Comparing the muck-pile sizes, the blasting produces muck-pile of bigger sizes in FMIJ than the STAK. This shows that more quantity of explosive will be needed to achieve the fragmentation observed in the STAK rock. This also confirms the higher values seen for FMIJ in density, rebound harness and RMR.

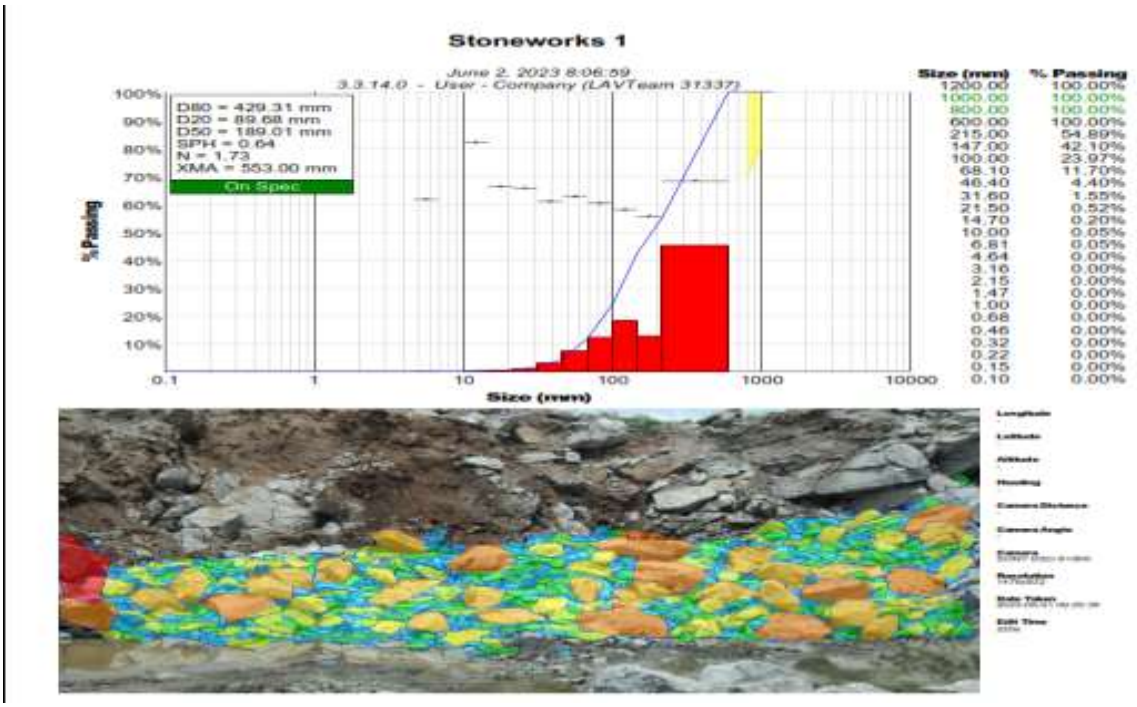

Figure 6: Fragment Size Distribution for STAK Sample

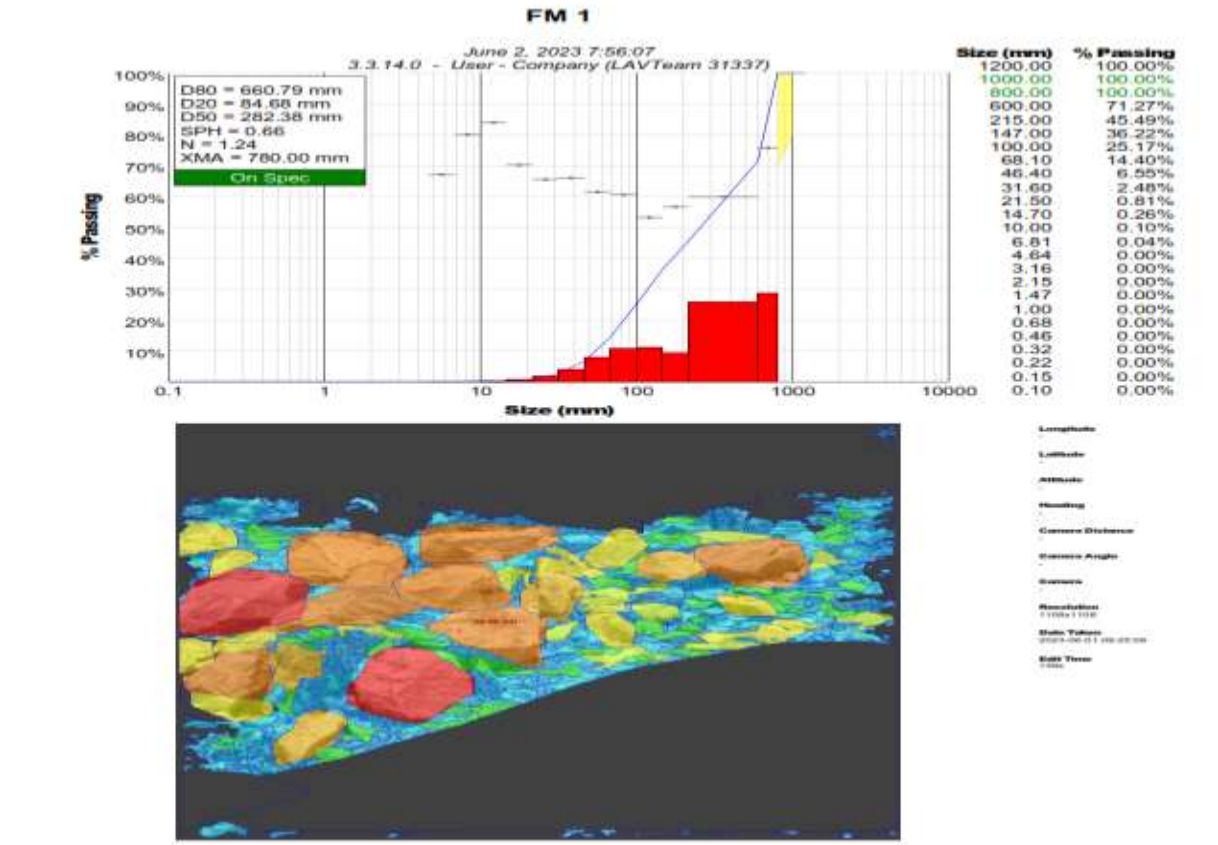

Figure 7: Fragment Size Distribution for FMIJ Sample

Conclusions

The research analyzed how rock mass properties, discontinuities and explosive charged, influenced muck-pile size distribution in quarries. The research further evaluated the rock mass properties,

discontinuities and recorded quantity of explosive charged in the selected quarries. In addition, these properties and data were used to determined how they influenced muck-pile size distribution. Some of the questions raised in this work are: how will rock mass properties, joint spacing and explosive charged affect muck-pile size distribution? What are the optimal blast design parameters for various rock mass conditions to minimize the negative effects of discontinuities? The following conclusions are drawn:

(i) The average densities of STAK and FMIJ are 2841 and 3124 kg/m^3 respectively. The average rebounds hardness values are 45 and 50 for STAK and FMIJ respectively. FMIJ is denser than STAK. The rock code FMIJ will offer greater resistance to rock breakage during detonation of the explosive charged.

(ii) The Rock Quality Designation (RQD) has average values of 72.8 and 70.3 for STAK and FMIJ. Therefore, both rocks are classified as good quality rocks.

(iii) It was noted that average RMR values for STAK and FMIJ are 67.5 and 77.3 respectively. STAK has 0.43 kg/m^3 as powder factor while FMIJ has 0.5 kg/m^3 as the powder factor. This implied that 0.43 kg of explosive is required to fragment 1 m^3 of STAK rock while 0.5 kg of explosive is required to fragment 1 m^3 of FMIJ rock.

(iv) It could be inferred that denser the rock, the harder the rock. The higher the RMR, the higher the quantity of explosive that will be required to achieve good fragmentation.

(v) Closer joint spacing in the range of 0 - 0.3 m was exhibited by STAK. This can lead to cutting off of radial cracks propagation that is generated by the explosive charged after detonation. Hence, muck-pile of lower heave height will be produced.

(vi) The results of blasting at FMIJ revealed that muck-pile of bigger fragments were produced. This revealed that more explosive will be required to achieve good fragmentation. This also confirmed the higher values of density, rebounds hardness values and RMR recorded for FMIJ rock code.

(vii) The information on the maximum fragment size in the muck-pile size distribution will ultimately assist Quarry Manager in selecting appropriate crusher's gape for further size reduction of the run-of-mine.

Acknowledgements
The financial support for this work was provided by TETFUND National Research Fund (NRF) with code (TETF/DR&D-CE/NRF 2020/SETI/30). We also, thank all the selected Quarry managers for free access to the different quarry faces.

Reference

Adebayo, B. and Bolariwa, H. T. (2023). Determination of Suitable Explosives for Dolomitic Marble and Granodiorite Using Blastability Characteristics, *Aspects in Mining and Mineral Science,* Vol. 11 Issue 1, pp. 1209 – 1211.

Bieniawski, Z.T. (1989). Engineering Rock Mass Classification: A Complete Manual for Engineers and Geologists in Mining, Civil and Petroleum Engineering, Wiley, New York, pp.251.

Dhekne, P.Y., Balakrishnan, V., and Jade, R.K. (2020) Effect of type of explosive and blast hole diameter on boulder count in limestone quarry blasting, *Geotechnical and Geological Engineering* Vol. 38, pp.4091–4097

Ghiasi, M., Askarnejad, N., Dindarloo, S.R., Shamsoddini, H. (2016). Prediction of blast boulders in open pit mines via multiple regression and artifcial neural networks. International Journal of Mining Science Technology, Vol. 26, pp.183–186.

Hamdi, E., Bouden, R. N., Du Mouza, J. and Le Cleac'h, J. M. (2008). Fragmentation Energy in Rock Blasting, *Geotechnical and Geological Engineering,* Vol. 26, pp. 133-146.

Hosseini, M., Khandelwal, M. and Lotf, R and Eslah, M. (2023). Sensitivity Analysis on Blast Design Parameters to Improve Bench Blasting Outcomes Using the Taguchi Method, *Geomechanics Geophysis, Geo-energy and Geo-resource,* (2023) 9:9, pp. 1-26.

Hustrulid W. (1999). Blasting principles for open pit mining, Vol. 1, A.A. Balkema Publication, p.382.

ISRM, (2007): Rock Characterization testing and Monitoring*: International Society for Rock Mechanics Commission,* Ed. E.T. Brown, Pergamon press pp. 75-105.

Jimeno, C.L, Jimeno E.L. and Francisco J.A.C (1995). Drilling and blasting of rock. In: Balkema Rotterdam AA, De Ramiro, Visser Y, pp. 30-190.

Mehrdanesh, A., Monjezi, M. and Sayad, A. R. (2017). Evaluation of Effect of Rock Mass Properties on Fragmentation Using Robust Techniques, *Engineering with Computers*, 16(2017), pp. 1-9. https://doi.org/10.1007/s00366-017-0537-7

Monjezi, M. Rezaei, M. and Varjani, A.Y. (2009). Prediction of Rock Fragmentation Due to Blasting In Gol-E-Gohar Iron Mine Using Fuzzy Logic, *International Journal of Rock Mechanics and Mining Science,* Vol. 46 No. 8, pp.1273–1280

Ozdemir, B, and Kumral, M. (2019). A System-Wide Approach to Minimize the Operational Cost of Bench Production in Open-Cast Mining Operations, *International Journal Coal Science Technology,* Vol. 6, pp.84–94.

Sazid M, and Singh T.N (2015). Numerical Assessment of Spacing– Burden Ratio to Effective Utilization of Explosive Energy, *International Journal of Mining Science Technology,* Vol. 25, pp. 291–297.

Available online at www.asric.org
ASRIC Journal on Natural Sciences Vol 3(1) (2023) 101-112

The Utilization of Solid Waste Transfer Stations in Managing Solid Waste in Rapidly Transforming Neighborhoods. The Case of Sinza Ward in Dar Es Salaam City, Tanzania.

David Mihigo[1*]

[1]School of Spatial Planning and Social Sciences, Ardhi University, P. O. Box 35176 Dar es Salaam-Tanzania

*Corresponding author: mihigodavid7@gmailcom

Abstract

Managing waste properly is essential for building sustainable and livable cities, but it remains a challenge for many cities. Various studies estimate that in 2016, the World's cities generated about Two billions tones of solid waste, amounting to a footprint of 0.79 kilograms per person per day. With rapid population growth, annual waste generation is expected to increase by 70% from 2016 levels to 3.40 billion tones in 2050. Compared to those in developed nations, residents in developing countries especially the urban poor, are more severely impacted by unsustainably managed waste aggravated by increase in population and economic activities, there is a widespread dumping of wastes in non – designated areas including in water bodies, valleys and openly burning, practices which create serious health, safety and environmental consequences. Through the lenses of central place theory, this study examined utilization of solid waste transfer stations in managing solid waste in rapidly transforming Neighborhood of Sinza. Data was collected through mixed methods which involved key informant interview with community leaders, ward and sub - wards leaders as well as environmentalists. Interview was also held with residents and a representative of Community Based Organization (CBO) involved with solid waste management in the study area. Direct observation was also used to capture information on the existing situation of solid waste transfer stations, as well as best practices of informal solid waste collection within the neighborhood. The Data collected were analyzed both qualitatively and quantitatively through thematic building, as well as descriptive statistics. Therefore. The finds show that during interview 69 % were females and 31 were males who participated in providing their point view on utilization of solid waste transfer stations in Sinza Ward while 47% of them attended secondary education and 17% took their university education. From the interview with Ubungo Municipal Council environmentalist and Ubungo Municipal Urban Planner there are Two (2) solid waste transfer stations in Sinza Neighborhood which serves a population of about 9889 houses. (One at Mawasiliano Market near Bus Park and another one at Mabibo Fruits Market about 12 km from Sinza Ward). According to the Challenges faced in utilization of solid waste transfer station include long distance which took first place with 60%, high transportation costs due to the location of their final dumping site far from the settlement about 40 - 60 km and poor road accessibility. The study recommends the need to improve utilization and management of solid waste transfer stations by involving stakeholders through formulation of teams for solid waste transfer station plan and design.

Keywords: Solid Waste Transfer Station, Transforming, Neighborhood, Dar es Salaam City.

1. Introduction and literature review

Solid waste transfer stations are one of the services where solid wastes are discharged from less efficient and smaller collection vehicles and then filled in more efficient and large vehicles, they might be also long trucks, trains that transfer to the final disposal facilities. In transfer stations especially hydraulic compresses are used to compact waste, therefore the volumes of waste are increased more than two times. Most of transfer stations' workers screen wastes that are coming on discharge systems, receipt waste pits and rolling floors for the purpose of recycling and any other types of wastes that might not be appropriate for dumping (like infectious wastes, batteries etc.), storage of solid waste at solid waste transfer stations should not stay long, they are loaded in large trucks and transported to

dumping site in some hours. The main important role of using transfer stations in solid waste management is to minimize the cost of solid waste transportation from household to the large waste disposal. It reduces also travelling distance to dump site, as well as trucks maintenance costs and fuel consumption (Beğen, 2002). Therefore, if solid waste can be separated from the sources like organic matters there is no need of them going to be dumped at final dumping site or solid waste transfer station, though it should be used as fertilizers for agricultural purposes, while plastics materials also are reused or recycled for future utilization instead of dumping them at any place (AI, 2011).

In 1960s in Bellevue, Washington USA Factoria Recycling and Transfer Station was constructed it was designed to replace the Canopy Transfer Station because it failed to manage waste storage emergency, regulate bad odors, dusts and vectors. The Canopy Transfer Station was not able to meet structural construction standards, codes and was subjected to seismic effects (Chin, 2018). In King County, more than 25 years ago King County waste planners thought that there was need of transfer station which would assist eastern community portion. The idea aimed to improve the existing structure of canopy but it was not able to handle future waste growth and reusing. Then, the third group of engineers presented their attractive and innovative large design. The construction of new Factoria Recycling and Transfer Station began in 2014 in the state of art, which was capable of accommodating 225,000 tons of garbage, household hazardous waste (HHW) and recycling waste annually (Chin, 2018)**.**

Indonesia it is among developing countries that are facing the problem of solid waste for many years. It is also the third-lowest ranking country related to the quality of sanitation. Most of their rivers are contaminated with organic matters because of lack of measurements in waste management system. Indonesia took the fourth position also as populous country in the world where its population reached 235 million people in 2014 and 269 million people in 2019 based on the estimations of the United Nations, while in 2013 the amount of solid waste produced reached 200,000 tons/day. Thus, Indonesia population is equal to 3.49 percent of the sum of World's population (Lenggogheni, 2015)**.**

In Thailand, for instance, solid waste generation rate looks similar with the rate of developing countries from 0.3 to 1.44 Kg/Capita/Day, where the average is equal to 1.443 Kg/Capita/Day. Moreover, the following elements are affecting the amount of solid waste generated in Thailand: income, conduct of consumption, living condition, season, buying of commodities, regulations and household structure. The income and Municipal Solid Waste generation increase with respect to the development of Thailand. Therefore, some of the above factors are described (i) Socio-economic development activities including industrialization impact amount of waste generated (ii) Climate change, as well as seasonal change influence the amount generated through the rate of organic material (iii) Living condition associated with assured income can also affect consumptions degree. Because of life conditions, population and state of their income, the sum of solid waste generated inside and outside of municipality is totally different. Around 40,082 tons/day or 14.46 million tons per year is generated, where Bangkok produced 21.1 percent of municipal solid waste quantities, 32.2 percent in municipality areas and 46.7 percent from other areas (Kaosol, 2009).

Drawn from World Urbanization Prospects (UN, 2006) Revised in 2005, by 2030 half of African population is estimated to live in cities. But 50 percent of population in Cameroon already lives in cities. In 1976 and 2003 population growth in urban areas was from 28 percent up to 52.8 percent and it is likely to be 70 percent. According to INS (2004), Cameroon population increased from 16.4 to 35.7 residents per km^2 in the same period from 1976-2003.While currently 57.6 percent of the population lives in Urban areas. Thus, Cameroon population is equal to 0.33% of the total World population (Sotamenou, Ganry, Montange, Parrot, & Simon, 2009).

The accessibility of big areas in the city of Cameroon is not easy by solid waste collection trucks in most of them are agricultural land. Where also other limitation to waste dumping facility is paved roads distance and accessibility, this could be stopped by use of transfer stations in minimizing transportation costs and environmental impact of solid waste management said by (Chalot, 2004). Location of these transfer stations in suitable areas nearby paved roads will allow residents and famers to dump properly their solid waste. Then, reusing and sorting of waste might be performed easily and citizens would benefit from composting operation brought by transfer stations. The quality and

production will be increased to farmers from the cities and peri-urban Areas. It can improve local community participation and better practices of solid waste management (Joel, 2016).

In 2018, the estimation of solid waste generated has doubled from 2,000 tons estimated during 1998 and reached up to 4,600 tons in year of 2017.This is represented by generation rate of 0.93 kg/cap/day estimated on the population size equal to 4.5 million. The Environmental Resources Consultancy Firm (ERC) which conducted study on Municipal Solid Waste Management in Dar es Salaam established that 4.4 percent growth rate of population and 0.815 kg/cap/day generation rate had projected that Dar es Salaam would be producing 12,000 tons of solid waste per day, where this is three times of solid waste produced within fourteen days. Dar es Salaam local authorities also projected that within the city below 40 percent of the amount of produced solid waste are collected, as well as dumped at Pugu Kinyamwezi dumping site located about 60 km from Dar es Salaam central area. The remaining 60 percent of solid waste is dumped along the road sides or in drainage channels. All these cause health related problems, and flooding problems to Dar es Salaam residents. Estimation done by Dar es Salaam local authorities said that there are 50 to 60 settlement collection sites in the whole city. Most of these sites are formal, while others are becoming informal solid waste dumping sites (Breeze, 2012).

Most of them were informal and formal settlements areas where big companies were not having will to give solid waste services because of lack of important infrastructure. Therefore, Non-Governmental Organizations were providing good services in these areas due to good collaboration with all households and residents in informal areas (Bakker, 2000).

Among environmental issues identified during consultation meeting was the issue of solid waste. They saw that is the first issue to deal as soon as possible. It was in that cross sectoral meeting that experts from different fields found 5 strategies of intervention and prioritized issues. Thus, among measures which were taken quickly include solid waste collection and dumping activities privatization, cleanup campaigns, formulation of CBOs solid waste collection systems, solid waste materials composting, solid waste recycling programme as well as proper management of solid waste dumping sites (UNHABITAT, 2004b).

Their roles were to work together by increasing strategies, consultations and mobilization oriented within local administration were participated without forgetting national and international organisation (NGOs) as well as Ministry of Local Government and Administration. The overall aim was to bring together City development stakeholders to discuss more on priorities so that they can come out with one answer mechanisms and interventions (Kombe, 1995).

Different initiatives were taken by different stakeholders to fight solid waste .The Government of Tanzania, for example, tried different ways one of which being to approach donors so that they could finance purchase of equipment for solid waste collection and management through Sustainable Dar es Salaam Projects (SDP) assisted financially by Sustainable Dar es Salaam City Project (SDP) was initiated in 1992 under Habitat Sustainable Cities (UN HABITAT, 2009).

Solid waste management regulation 2009 it was developed under Environmental Management Act (EMA) it stipulates tasks of local government for solid waste management including solid waste transfer stations in Dar es Salaam –Tanzania. In short the major duty is to make sure that all regulations formulated are implemented in proper way without any problem. Where they should ensure enforcement of these regulations and supporting emerging ideas of solid waste management by monitoring and evaluating all of this and report to Direct General of National Management Council and Director of environment. Other solid waste management regulations are like hazardous waste management of 2009 which manages hazardous waste materials for example toxic chemicals without forgetting Fees and Charge Regulations (2007) which explains economic instrument for better solid waste management and implementation of Polluter pay principle. Thus other regulation includes environmental impact assessment and audit regulations (2005) and Ozone Depleting substances regulations (2007) while in coming days more regulations related to solid waste management are expected to be developed (Bakanga, 2014).

Therefore, this study specific objectives include: (1)To map solid waste transfer stations in Sinza neighborhood; (2)To examine how solid waste transfer stations are established and operationalized;

(3)To identify actors and their roles in managing utilization of solid waste transfer stations; (4)To analyze the challenges of managing solid waste transfer stations; and, (5)To recommend appropriate location and accessibility of solid waste transfer stations for efficiency and effective utilization. Additionally, this study informs planners and decision makers about the crucial factors for identifying the suitable location of solid waste transfer stations. It has contribution to knowledge generation, awareness creation and information to policy makers.

Plate 1: Solid waste Transfer Station Example
Source: (Chin, 2018)

2. Methods, techniques, studied material and area descriptions

2.1 Overview of the study area

Dar es Salaam City is the main source of economic development in the country (UNISDR, 2012). It is the leading trading point, industrial, administrative, educational, commercial market, the trading centre and cultural centre of Tanzania. In Sub-Sahara in Africa, Dar es Salaam is the fastest growing city (ibid).]

Dar es Salaam is a mono-concentric radial development pattern urban structure. The city is having four main roads (Morogoro, Kilwa, Nyerere and Bagamoyo), and Mandela road which is the ring road radiating from city center. The city also is having one Centre Business District which comprises of City Centre and Kariakoo, where most of business activities, organizations and institutions are located here. Road network of Dar es Salaam has 1950 km length in which 1120 km are paved road (DCC, 2004) because of different factors such as lack of financial capabilities these roads are in improper surface road condition and they lack bicycles and pedestrians ways. Therefore, the city is having more than 600 km storm water drainage channels and piped lines drainage (Lukenangula, 2017).

Additionally, Dar es Salaam City was founded in 1862 by Sultan Seyyid Majid as the Centre for business and ocean port. The word Dar es Salaam created from an Arabic meaning Word Bandar' Salam', in Swahili 1862 Dar es Salaam known as Mzizima and it was mainly a fishing village where a small family before and Zaramo ethnic group used to live (Msami, 2014).

Spatial development of Dar es Salaam city is expanding from its Centre outward along main roads by forming settlements in radial development shape. Moreover the most developing parts in the city are the informal settlements in the city fringe' which most of them lack infrastructure and transportation services. Therefore, there is concentrated densification process that is happening in existing settlement. Urban development took place along coast and main roads including (Morogoro, Ally Hassani Mwinyi, Kiwa and Nyerere), this is due to searching accessible and low cost land availability in these areas (World Bank Group, 2016).

Dar es Salaam City commission started new improvement of solid waste management activities integrated strategy. The most important element of this system was bringing private companies in solid waste collection services including reusing, recycling and transportation. This approach established private/public partnership under the support of community based and individuals by providing dumping sites and public transport. Additionally, four task forces were created to structure guidelines on implementation of different aspects of solid waste management system and these formed task forces did more activities like health related education, Community awareness campaigns, solid waste dumping site quality improvement and recycling projects. Therefore, among the representatives of these task forces include Municipal Directors and Commissioners (Jasper, 2000).

Sinza Ward is one of the six wards comprising Ubungo Municipality. It is located eight kilometers away from Central Business District (CBD). Sinza Ward consists of five sub-wards namely Sinza A, Sinza B, Sinza C, Sinza D and Sinza E. Accessibility of the settlement is possible with Shekilango and Sam Nujoma roads. From census of 2012, the population of Sinza Ward was 40546 with the sum of 9889 houses (Kasala, 2014). Based on Gender Sinza is composed with 14,759 males which is 47% and 16,637 females equal to 53%. It has also the area of 3, 363 Km^2 (Brinkhoff, 2023). Sinza Ward, being near to Central Business District and availability of social services (such markets, Schools, play grounds, Mliman city Shopping Mall) has attracted a lot of people to live in the neighborhood. Furthermore, Sinza is one of the areas which have benefited from the Site and Service Projects in Dar es Salaam. Sinza is facing rapid transformation including land use changes, particularly from residential to commercial uses as well as horizontal development to vertical development. Hence, these kinds of transformation or changes are associated with more problems among them are informal solid waste dumping and informal solid waste collection due to construction activities that are conducted in this place and commercial activities that generate a lot of solid waste. Additionally, the shift of people either from other Tanzania's regions or from foreign countries different from Tanzania who come and make different projects like construction of apartments for rent and hotels in Sinza, while others also do like commercial activities, all these movements bring much and more issues linked to solid waste management. Figure 1 shows the location of Sinza Ward as study area in Ubungo Municipality, Dar es Salaam City.

Figure 1: Sinza Administrative Sub-Wards Location Map
Source: Prepared by Author, 2021

2.2 Data collection procedures and analysis

Through the lenses of central place theory, this study examined utilization of waste transfer facilities in managing solid waste in rapidly transforming Neighborhood of Sinza. Moreover, primary and secondary data were used in this study. Methods used in this study include documentary review, field observation, focus group discussion, both household and officials' interviews as well as key

informative interviews. The Data collected were analyzed both qualitatively and quantitatively through thematic building, as well as descriptive statistics. Thus, these methods help during triangulation, the provision of verifying and complimenting received information.

This research was narrowed down to show the current situation of waste transfer facilities location, utilization pattern, especially for transforming settlements or rapidly growing areas like Sinza. To achieve the results of this study, three administrative officials were interviewed at Ubungo Municipal Council who are Urban Planner, environmentalist as well as Land Surveyor; one leader at Ward level, 95 residents from Sinza Ward were also interviewed from five Sub-Wards (Sinza A, Sinza B, Sinza C, Sinza D and Sinza E) and Non-Governmental Organisation, legal representative of Women Caring for Environment (WOCE) and in charge of solid waste collection and transportation in Sinza Ward. Apart from that, observation and spatial information was gathered to get the overview of location and accessibility of waste transfer facilities in rapidly transforming planned settlements, as well as the role played by these infrastructures.

Responses received from questionnaires were compiled together using Microsoft Word, where stories or answers from interviewee on location and accessibility of waste transfer facilities were reported and summarized, while Microsoft Excel was used in this study to analyze data received from field work interviews producing tables of results, to determine some statistical parameters, as well as production of figures. Furthermore, this study also was supported by GIS tool for necessary maps production, like the map of location and accessibility of waste transfer facilities in Sinza Ward and Dar es Salaam administrative boundary map. After the site visit and field work, the data collected were summarized, analyzed and interpreted to meet the objectives of this research.

According to this research, data were coded during field work and interviews when responses provided were documented down for the purpose of keeping information received, while data cleaning was done by verifying in the questionnaire if all questions had been all answered, as well as written properly for not losing any necessary information during data analysis and interpretation using Microsoft word and excel for further graphical presentation of the findings of this research.

The coordinates representing the location of waste transfer facilities in Sinza Ward were taken during fieldwork and data correction are represented in the Figure 2 below, then the map was produced in Arc GIs 10.3 after displaying coordinates taken on the field.

This research, targeted people for interview were Sinza Ward residents selected using Yamane formula because all residents could not be used for interview in this study. Based on Yamane formula, 100 respondents were selected randomly. Among those who were selected and participated during field work by providing their points of view on location and accessibility of waste transfer facilities , respondents were 95 people living in Sinza Settlement, Three (3) Ubungo Municipality Administrative Officers, One (1) legal representative from community based organisation, as well as One (1) Health and Environment Officers at Sinza Ward. Based on Population and Housing Census of March, 2012, Sinza Ward population is estimated to be 40,546 where female number is 21,654 and male is 18,892 .The researcher used the Yamane formula (1967), the formula as expressed in the following way:

$$N= \frac{N}{1+N(e)2}$$

Where n= sample size, N=Size of targeted population

e=Margin error (here is 0.1) or confidence level of 90%.

Applying formula the sample size became= $\frac{N}{1+N(e)2} = \frac{40,546}{1+ 40,546\ (0.1)2}$ =100 respondents

3. Results

3.1 Socio-demographic characteristics of the respondents

Therefore, Sinza Ward livelihood activities include agriculture, livestock keeping and commercial activities. The findings show that during interview 69 % were females and 31 were males who participated in providing their point view on utilization of solid waste transfer stations in managing solid waste in Sinza Ward the so called "***Gender inclusive***" in urban planning and management social

development projects. On our side, we can also concur with this idea of involving both males and females in planning aspects, as well as solid waste transfer station management. In the results 38-48 years old is represented by 42 % which is the first age among others. This explains that most of the answers in this study were provided by people with the age range of 38-48. Moreover, respondents with over 48 years old came the second during primary data collection with 23%. 47% of them attended secondary education and 17% took their university education. Linking to this study knowing the education level of respondents will not only contribute in the answers received during interview but also later once solid waste transfer stations are located and constructed due to the education level of Sinza residents, it can influence the use of this solid waste transfer and solid waste management at their household before they are transported to transfer stations and dumped to final dumping site named Pugu Kinyamwezi.

3.2 Existing solid waste transfer station in Sinza Ward

From the interview with Ubungo Municipal Council environmentalist and Ubungo Municipal Urban Planner, Sinza Ward neighborhood is among planned settlements in Dar es Salaam, where the exiting solid waste transfer station (SWTS) in Sinza Ward is located at the market place to collect market solid waste materials. Where in the settlement during the day once or twice a week the truck passes around neighborhood and collects all solid waste packed in sacks and stocked along the fences of Sinza resident's households. Thus, existing solid waste transfer station in Sinza Ward is located both at Mawasiliano Fruits Market behind Bus terminal. Some of the pictures showing the current situation of existing solid waste transfer station in Sinza Ward are provided below to complement explanations given above. Also, the maps showing the existing location of solid waste transfer stations in Sinza Sub-Wards (Sinza A, Sinza B, Sinza C, Sinza D, Sinza E) is also attached. Thus, there are two solid waste transfer stations in Sinza Neighborhood which serves a population of about 9889 houses. (One at Mawasiliano Market near Bus Park and another one at Mabibo Fruits Market about 12 km from Sinza Ward). Figure 2 shows One of Solid Waste Transfer Station in Sinza located nearby Bus Park.

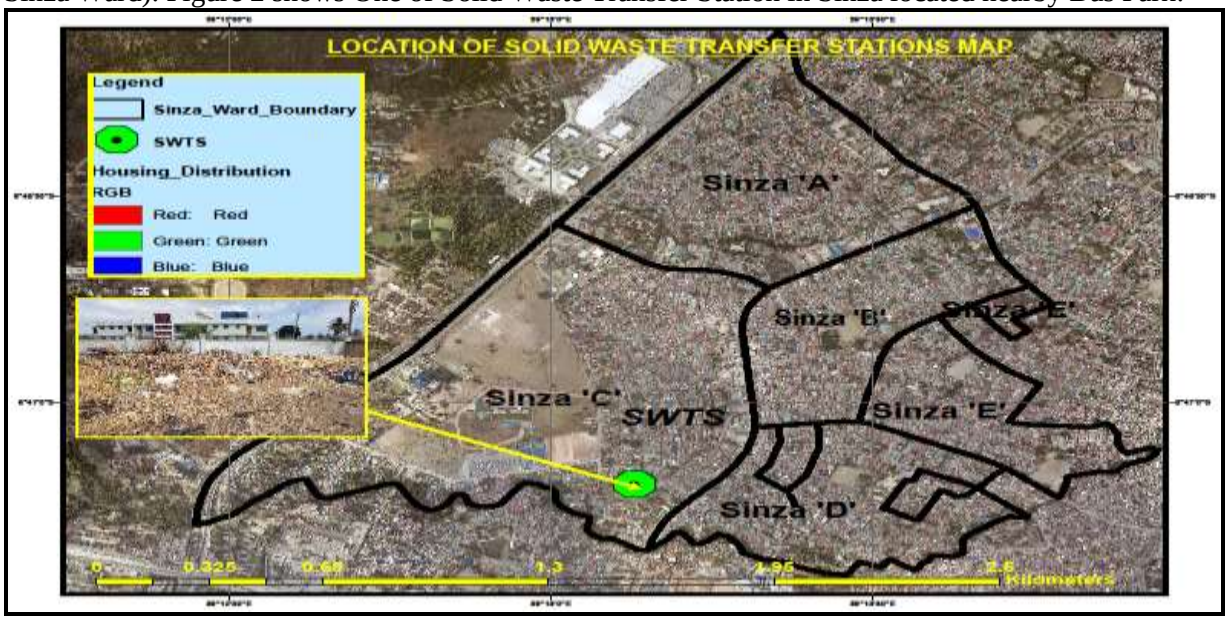

Figure 2: Location of existing solid waste transfer stations (SWTS) in Sinza Ward, Planned Neighborhood
Source: Prepared by Author (2019)

3.3 Perception of Sinza residents on utilization of solid waste transfer stations

According to Sinza residents from the results obtained the place where they could dispose their domestically generated solid waste. Most of them said that generated solid waste materials were disposed in sacks at their household without separating them like having plastic solid waste bags, metal solid waste sacks etc. During the week, they wait for solid waste truck which comes and picks the solid waste bags from each household to dump them to the final dump site at Pugu Kinyamwezi.

Moreover, the first method of keeping solid waste Sinza residents responded was using Sacks with 60 % while the second method was basket with 11%. Then the last one was the solid waste transfer station. This was because the system used nowadays to collect waste for Sinza neighborhood they have two transfer stations at market places see Figure 2 above, which collect all solid wastes from the market and wait for the truck to transport them to the dumping site (Pugu Kinyamwezi). Thus, figure 3 explains the findings obtained during field work as well as data collection.

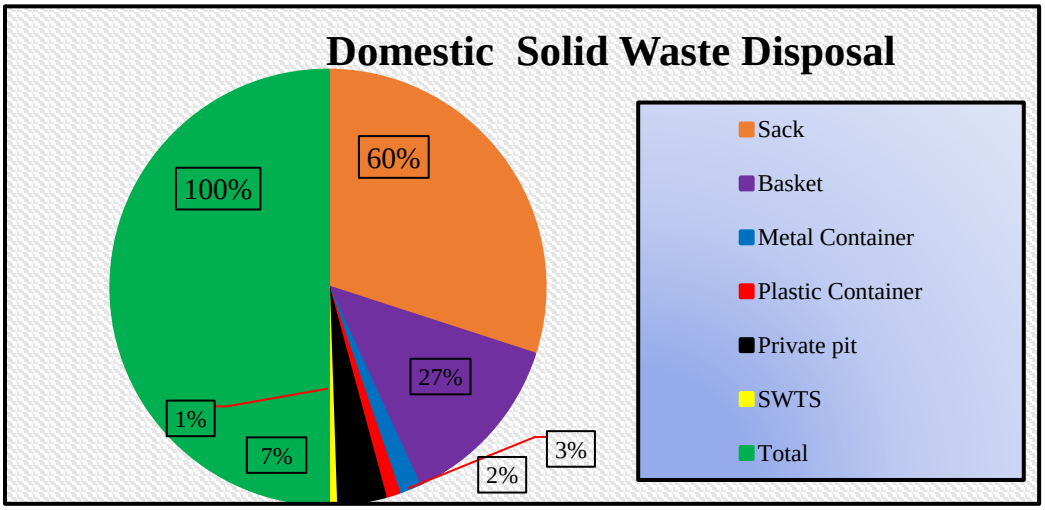

Figure 3: Generated domestic solid waste disposal facility
Source: Survey Data (2019)

3.4 Ubungo municipal council official on utilization of solid waste transfer stations

Planning of solid waste transfer stations

The interviews with three Ubungo Municipal administrative officials concerning future plans revealed that there was a plan of setting up a new solid waste transfer station and expand the existing solid waste transfer stations in the next five to ten years. Ubungo Municipal Urban Planner and Health and Environmental Officer said that there was a plan, while Land Surveyor said that he was not aware of any future plan. Reasons for doing that are stated below:

Yes because the existing solid waste refuse bases was too far from their residential areas and Municipality. So, We plan of designing, locating and constructing modern solid waste transfer station that will facilitate minimization of amount of solid waste materials which goes to Pugu Kinyamwezi dump site and permit other activities like recycling, reusing of some of the materials instead of dumping all of them at final dumping site. They said that this can create jobs to unemployed people who do not have work to do in their neighborhoods or Experts from abroad in solid waste.

While a surveyor said that he was not responsible for the matter, for him he just waited for the approval process and then after he would come for setting out planned and designed solid waste transfer station in Ubungo Municipality. But to him also he said that if the location of transfer station in each Ward or Mtaa depending on the financial capacity can be good because it can contribute for the issue of solid waste in Dar es Salaam City. According to the criteria they use to locate their transfer stations in their living neighborhoods are: Environmental criteria, Accessibility as well as Environmental Social Impact Assessment (EIAS) report.

Having solid waste transfer stations in rapidly transforming neighbourhood or a City that is rapidly developing like Dar es Salaam, this can be an added value especially in solid waste management system, as well as proper environment and human health protection for the purpose of avoiding transmissible disease which might be associated with lack of suitable solid waste management. This can be done by promoting reusing and recycling solid waste operations at the transfer station before transferring them to final dumping site.

Solid Waste Transfer Stations Utilization

According to Ubungo three administrative officials responses on the use of solid waste transfer station as processing point for material recovering to reduce travel time and the amount of waste to final disposal site ,two administrative officials at Ubungo Municipal Council ,Urban Planner as well as Heath and Environmentalist at Ubungo Municipal said No. Because they do not have that modern transfer stations. But other solid waste operations like temporally solid waste storing before it goes to final dumping site and solid waste material separation at transfer stations all of them are done there. Figure 4 demonstrates solid waste collection in Sinza Ward.

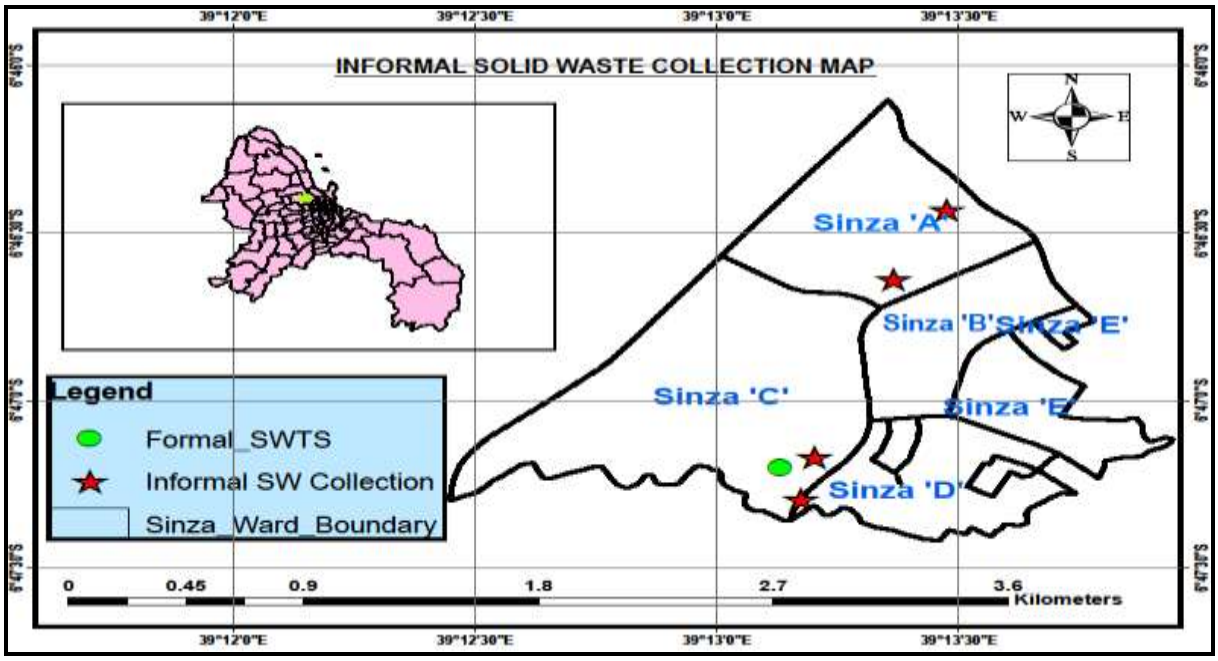

Figure 4: Solid Waste Collection in Sinza Ward
Source: Survey Data (2019)

Volume of solid waste transported to Solid Waste Transfer Station

From the interviews with three Ubungo Municipal Council administrative officials about the volume of solid waste transported from Sinza neighborhood to final dumping site (Not transported from Sinza settlement to solid waste transfer stations) it was realized that because they were using **Franchise Methodology** (where people stayed with solid waste at their homes and brought their luggage for transportation when the truck was passing between 4:00 pm – 5:00' pm in the neighbourhood) during that time before the vehicle picked solid waste at households there was person who used ring to inform Sinza residents that solid waste truck was coming to take their solid waste materials so that they could get prepared. The Municipal environmentalist said that for them to estimate the volume of solid waste transported, they use JEICA Research on solid waste and the formula they apply is as follows:

$$\frac{\text{Population} * 0.80}{1000} = \textbf{Tones of solid waste transported per day per catchment Area.}$$

The volume of solid waste daily produced in Sinza Ward is equal to 828 tons, then they transport 52 % of the produced solid waste per day (828 tons) which is 430.56 tons to the final dumping site located between 42 -45 km from the neighborhood. Additionally, they wish to design and construct the transfer station that will receive more that the amount of solid waste generated per day including the future projection of the people who will come to live and work in Sinza planned rapidly transforming neighborhood and who will also increase the volume of solid waste produced daily.

Perception of the Environmental Officer at Sinza Ward on utilization of Solid Waste Transfer Station

According to the interview with Health and Environmental officer in Sinza Ward, the first question intended to know if there was any solid waste transfer stations in Sinza Settlement that deals with solid

waste matters within the neighbourhood. The officer agreed that there exist such stations in the settlement especially in the market places. Additionally on the number of those solid waste transfer stations located in the settlement the officer said that there were only two solid waste transfer station located at market places to collect solid waste materials from the market while solid waste from households are picked by trucks and dumped directly to the final dumping site. Thus, the provision of another transfer station that connects households in the settlement can be something good instead of having transfer station at market places only. On the other hand, due to long distance from the neighbourhood to dumping site ranging from 40 to 60 kilometer this can also be a fact to provide another solid waste transfer station at residing place in the settlement.

Community Based Organisation views on solid waste transfer stations

According to Women Caring for the Environment (WOCE) a CBO at Sinza, their organisation worked with solid waste transfer stations in the city of Dar es Salaam and they collected garbage from Mawasiliano Market which is the transfer station found in the neighbourhood to the final dumping site, though in other areas, where people are living, the truck came and collected the waste from the households. There was a supervisor who controlled if all sacks next to fences were collected by the truck.

During the Interview, the Community Based organisation called Women Caring for the Environment (WOCE) said that they started solid waste collection activities in 2013 which means that they have almost seven (7) years of working experience in the field of solid waste management. Their wish is that Ubungo Municipal Council should do much to improve their working capability in solid waste management as well as solid waste transfer stations in order to allow them to collect solid waste collection fees themselves from Sinza residents, then the government should supervise and observe what is going on and give recommendations for improvement. They think that management of solid waste transfer stations in Dar es Salaam can be achieved by having all responsibilities discussed above in hand and adding more stakeholders in solid waste management so that they can be able to handle the problem or otherwise build the capacity of existing community based organisation for the purpose of solving the issues of solid waste in rapidly transforming neighborhoods as well as growing African cities like Dar es Salaam.

4. Discussion

Solid waste transfer stations in managing solid waste especially in mega cities and countries with big land as well as large land area is important as this can help in collecting neighborhoods solid waste materials before are taken to final dumping site. It is on this waste transfer facility where key preliminary solid waste works initiates such as waste materials sorting then having plastics materials on their sides, metals on another as well as organic materials on their side. Furthermore, after categorizing them organic waste materials might be transported for farming activities and be considered as fertilizer for crops or flowers farming projects in the city or other regions of the country in developing nations or developed countries. Then plastics materials may be reused as well as waste metals when transformed into other products and which as useful for local use by local people or businesses projects within then city or in the villages.

Additionally, this waste transfer facility will reduce travel time which was spent before and when solid waste materials were transported to solid waste dumping site or landfill. It is not only that but also this will minimize the amount of solid waste materials dumped at final solid waste dumping site previously. The presence of solid waste transfer stations in the neighborhoods and connecting them will boost the management of solid waste within the cities and minimize the consequences which used to take place in case solid waste management is not properly done. According to (Lenggogheni, 2015) Solid waste transfer stations are essential part in contemporary day in community solid waste management systems. The major criteria used to choose on the location of a transfer station has usually been the reduction of transportation cost, as it is inexpensive to transport excessive amount of waste over a long distances in large loads than in small ones.

Therefore, from the discussion together with Ubungo Municipal Urban Planner, Land Surveyor and Environmental Officer on actors and their roles in Solid waste Transfer Stations management in Sinza Ward including community to pay solid waste collection service fees of 3000 Tzs per month.

Authorities such as Ministry of Lands Housing and Human Settlements, City Authorities, Ubungo Municipal Council and Leaders at Community Level they normally approve the location of solid waste transfer Stations in Dar es Salaam City's Neighborhoods and Budget allocation for infrastructure-related funds in collaboration with local governments to boost national development. Without forgetting Private Sector including Community Based Organizations, Contractors, Donors, External Agents and Individuals whom are key role players in this field of solid waste management where in each sub-ward there is one community based organization that collects solid waste, from each household and transports them to final dumping Site in Pungu Kinyamwezi. While contractors specifically private companies engaged in solid waste management activities as well as solid waste transfer stations managers through cleaning of open drainage channels, removal of dead animals and monthly meetings participation. Donors' especially international organizations are important in funding solid waste management projects like city cleaning services and purchase of equipment and machines which can be used in solid waste works. Thus, non-paid funds come from international organizations that support such initiatives, including USAID, GIZ, and others. External agents play four primary roles in solid waste management: training contractors and city authorities, creating networks among actors, sharing experiences, providing material support for equipment, and offering startup capital.

5. Conclusion and Recommendation

5.1 Conclusion

This study concludes that solid waste transfer stations are insufficient to handle issues of solid waste collection in Sinza neighborhood and neighboring settlements. The plate 1 shows appropriate solid waste transfer stations which can be adapted in rapidly growing cities like Dar es Salaam. However, when Researcher asked the factors affecting residents to access properly their solid waste transfer stations in their residences 80 % responded that long distance from their households to neighboring solid waste transfer stations was a major factor. Furthermore, the following presents the recommendations for improving the current situation of waste transfer stations in rapidly urbanizing and transforming neighborhoods in Dar es Salaam City and in third world countries.

5.2 Recommendation

This part summarizes the recommendations for improving solid waste transfer stations utilization and management systems in growing neighborhoods like Dar es Salaam City, Tanzania particularly in Sinza Ward and other settlements that look similar or experience rapid transformation like Sinza neighborhood in developing countries. Therefore, the following are recommendations we would like to highlight:

1. Stakeholder's participation and formulation of design team to decide together on solid waste transfer station plans and design before implementation.
2. Solid waste transfer station utilization especially in rapidly transforming neighborhood must have transfer station like Factoria Recycling and Transfer Station adopted in United States of America and other African countries like Cameroon.
3. Enforcement of structured solid waste policies into actions
4. Improvement of solid waste collection system at household level
5. Creation of Department in charge of Solid Waste Management including Solid Waste Transfer Stations
6. Employ/Apply appropriate Technology in solid waste management activities
7. Solid Waste Transfer Stations (SWTS) Space provision in TP Drawings and Neighborhood regularization projects

6. Acknowledgements

The authors are grateful to the participants in this study namely Ubungo Municipal Urban Planner, Ubungo Municipal Environmentalist, Ubungo Municipal Land Surveyor, Community based organization (Women Caring for the Environment) and Leaders at Community Level for their valuable inputs, which significantly contributed to the quality of this article.

References

Ai, N. (2011). Challenges Of Sustainable Urban Planning: The Case Of Municipal Solid Waste Management. Georgia Institute Of Technology, School Of City And Regional Planning . Georgia Institute Of Technology. Retrieved August 21, 2011, From Https://Smartech.Gatech.Edu/Bitstream/Handle/1853/44926/Ai_Ning_201108_Phd.Pdf

Bakanga, G. (2014). Emerging Policies On Urban Solid Waste Management In Tanzania.

Bakker, S. V. (2000). Publi-Private Partnership For Sustainable Employment Creation Solid Waste Management In Dar Es Salaam,Planning For Sustainable And Integrated Solid Waste Management.

Beğen, N. N. (2002, September). Optimal Locations Of Landfills And Transfer Stations In Solid Waste Management. Bilkent University, Industrial Engineering. Bilkent University. Retrieved September 2002, From Http://Www.Thesis.Bilkent.Edu.Tr/0002167.Pdf

Breeze, R. (2012). Municipal Solid Waste Management In Dar Es Salaam. Toronto,On,Canada.

Brinkhoff, T. (2023, Novermber 27). Sinza. Retrieved From City Poppulation: Https://Www.Citypopulation.De/En/Tanzania/Coastal/Admin/Ubungo_Municipal/107041022__Sinza

Chin, D. (2018). Factoria Recycling And Transfer Station. King County Solid Waste Division.

Dcc. (2004). Dar Es Salaam City Profile. Dar Es Salaam, Tanzania.

Jasper. (2000). Public-Private Partnership For Sustainable Employement Creation In Waste Management,Dar Es Salaam. International Labor Organization .

Joel, S. (2016). Transfer Stations For Sustainable Municipal Solid Waste Management In Africa:Evidence From Cameroon. Researchgate.

Kaosol, T. (2009). Sustainable Solutions For Municipal Solid Waste Management In Thailand. World Academy Of Science, Engineering And Technology. Retrieved 2009, From Http://Citeseerx.Ist.Psu.Edu/Viewdoc/Download?Doi=10.1.1.308.3351&Rep=Rep1&Type=Pdf

Kasala, S. E. (2014). Analysis Of Outputs Of A Planning Process: Sinza Strategic Urban Development Planning (Sudp) In Dar Es Salaam, Tanzania. Global Journal Of Human-Social Science:B Geography, Geo-Sciences, Environmental Disaster Management, 14(7). Retrieved 2014, From Http://Creativecommons.Org/Licenses/By-Nc/3.0/

Kombe. (1995). Formal And Informal Land Management In Tanzania:Case Of Dar Es Salaam City.Dortmund,Germany:Spring. Dar Es Salaam: Dortmund University,Germany.

Lenggogheni, H. Y. (2015). University Of Tsukuba, Life & Environmental Sciences, Program Of Environmental Sciences. University Of Tsukuba,Life& Environmental Sciencies,Program Of Environmental Sciencies. Retrieved 2015, From Http://Www.Jsrsai.Jp/Annual_Meeting/Prog_52/Resumec/C02-1.Pdf

Lukenangula, J. M. (2017). Workability In Rapidly Growing Cities In Developing Countries. Dar Es Salaam: Tu Dortmund University.

Msami, J. (2014). Location And Accessibility Of Private Health Care Facilities In Rapidly Urbanising Cities:The Case Of Dar Es Slaam,Tanzania. Dar Es Salaam: Ardhi University.

Sotamenou, J., Ganry, F., Montange, D., Parrot, L., & Simon, S. (2009). Transfer Stations For Sustainable Municipal Solid Waste Management In Africa: Evidence From Cameroon. Solid Waste Management And Environmental Remediation. Retrieved 2009

Un Habitat. (2009). Tanzania,Dar Es Salaam City Profile. Nairobi,Kenya.

Unhabitat. (2004b). The Sdp Dar Es Salaam Project,The Scp Documentation Series,Project 1992-2003.From Urban Environment Priority Issues To Up-Scaling Strategies City-Wide. Nairobi,Kenya.

Unisdr. (2012). Making Cities Resilient. Dar Es Salaam-Tanzania: The United Nations Office For Disaster Risk Reduction.

World Bank Group. (2016). Promoting Green Urban Development In African Cities. Dar Es Salaam-Tanzania: World Bank Group.

Available online at www.asric.org
ASRIC Journal on Natural Sciences Vol 3(1) (2023) 113-124

Exploring the Efficacy of a Potent Corrosion Suppressant Derived from Trandescantia Pallida (Purpple Heart) Leaves: A Qualitative Assessment

Cornelius C. Ahanotu [1,2]* Kenneth C. Madu [1], Cynthia A. Ugochukwu [1]

[1]Department of Science Laboratory Technology, Imo State Polytechnic, Omuma, P.M.B 1472, Owerri, Nigeria
[2]Department of Chemistry, Claretian University of Nigeria, Nekede, P.M.B 1019, Owerri, Nigeria

*Corresponding author: ccahanotu@imopoly.net; cornelahanotu@claretianuniversity.edu.ng

Abstract

The corrosion inhibiting effect of *Tradescantia pallida* leaf extract (TPLE) on low carbon steel in a sulphuric acid medium was investigated. Weight loss experiments were conducted at two temperatures, 27°C and 60°C, using six low carbon steel coupons of known dimensions, compositions, and weights over a 3-day immersion period. The results revealed that TPLE exhibited significant corrosion inhibition properties, as evidenced by the reduction in weight loss of the low carbon steel samples. This indicates its potential as a corrosion inhibitor for low carbon steel in sulphuric acid environments. Further studies are recommended to explore the underlying mechanisms of TPLE's corrosion inhibition and optimize its usage in industrial applications. The results obtained from the study demonstrated that at a temperature of 27°C, the addition of only 0.5 g L-1 of *Tradescantia pallida* leaf extract (TPLE) significantly suppressed the corrosion rate of low carbon steel. The corrosion rate decreased from 20.380 mm/yr to 1.446 mm/yr, resulting in an impressive inhibitor efficiency of 92.91%. As the dosage of TPLE was increased from 0.5 g L-1 to 2.5 g L-1, the inhibitor efficiency showed a proportional increase, reaching a remarkable 95.85% at the highest dosage of 2.5 g L-1 in the inhibitor solution. These findings highlight the potential of TPLE as a highly effective corrosion inhibitor for low carbon steel in sulphuric acid environments. Further investigations are recommended to delve into the underlying mechanisms responsible for the corrosion inhibition and to optimize the dosage and application of TPLE in various industrial settings. Similarly, at an elevated temperature of 60°C, comparable results were observed. However, in this case, the corrosion rate of low carbon steel increased with higher temperatures. Despite this, the addition of *Tradescantia pallida* leaf extract (TPLE) at a concentration of 0.5 g L-1 still managed to reduce the corrosion rate significantly. The corrosion rate increased from its initial value, but the inhibitor efficiency remained noteworthy at 88.62%. As the concentration of TPLE was increased to 2.5 g L-1, the inhibitor efficiency improved to 91.72%. These findings indicate that while the corrosion rate may increase under higher temperatures, the presence of TPLE still confers a considerable level of corrosion inhibition for low carbon steel in sulphuric acid environments. Further research is recommended to delve into the specific mechanisms underlying the temperature-dependent behavior and to optimize the application of TPLE as a corrosion inhibitor in different temperature ranges and industrial conditions. The observed temperature effect suggests that the inhibitor molecules present in *Tradescantia pallida* leaf extract (TPLE) primarily act through a physisorption mechanism. Further analysis of TPLE revealed the presence of various functional groups, including OH, C=O, and aromatic rings, among others. These functional groups have been widely recognized for their efficacy in enhancing the adsorption of inhibitor molecules onto metallic substrates. This suggests that the corrosion inhibition properties of TPLE can be attributed to the adsorption of its constituent compounds onto the surface of low carbon steel, forming a protective layer that hinders the corrosion process. The identification of these functional groups provides valuable insights into the underlying mechanisms of TPLE's corrosion inhibition and opens up avenues for potential modifications and optimization of the extract for enhanced performance. Future investigations should focus on elucidating the specific interactions between the inhibitor molecules and the metallic surface, as well as exploring the long-term stability and compatibility of TPLE in practical corrosion prevention applications.

Keywords: corrosion, inhibitor efficiency, extract, adsorption, physisorption

1. Introduction

Metals and their alloys find wide range of applications in human activities as a result of their excellent mechanical and electrical properties (Loto and Olowoyo, 2019; Parthipan *et al.*, 2018; Verma *et al.*, 2018; Anupama *et al.*, 2017). In order to preserve the desired quality and working condition of these metal substrates, there is need to adopt some preventive measures to protect them from aggressive and hostile environments. Corrosion is probably the most common undesired phenomenon that causes metals to deteriorate and lose mechanical properties (Zhu *et al.*, 2020; Mai *et al.*, 2016). This natural process originates from the electrochemical interaction of metals with the corrosive environment. Sulfides, oxides, and others are generated through reactions between the metal surface and the corrosive medium (El Ibrahim *et al.*, 2020; Kicir *et al.*, 2016; Mai *et al.*, 2016; Singh *et al.*, 2016). Among metals and alloys, low carbon (mild) steel is the most widely used in the oil, food, energy, chemical, and construction industries due to its relatively low cost, availability and excellent mechanical properties such as high resistance, durability, and toughness, among others. Due to huge costs associated with the repair or replacement of corroded metals especially in the oil and gas industries (Ledan *et al.*, 2017), corrosion of metals has become a critical environmental challenge which has gained more attention in recent times. Finding solutions to problems related to the corrosion of steel, mostly low carbon steel therefore becomes pertinent. The use of natural products or organic extracts of plant leaves, seeds and nuts, flowers, and stem barks as corrosion inhibitors to protect metal materials from hostile environments has been widely reported by researchers (Haldhar *et al.*, 2021; Ahanotu *et al.*, 2020). These extracts contain several phytochemicals and active organic molecules with electron-rich regions and heteroatoms (O, N, S, etc.) which facilitate the adsorption of these active molecules leading to the formation of a protective layer on the surface of substrate (Patel *et al.*, 2013). Some of the organic inhibitor molecules also contain polar functional groups which are responsible for physisorption (Miralrio and Vázquez, 2020).

It is pertinent to state that the inhibition performance of most plant extracts is a function of concentration of the extract molecules, temperature of the system, extraction solvent and period of immersion (Ghahremani *et al.*, 2021; Ahanotu *et al.*, 2020; Ebenso *et al.*, 2008). Researchers have reported that the extracts from plant materials are locally available, give a wide range of green inhibitors, and are more environmentally acceptable and friendly than inorganic inhibitors which are toxic and associated with environmental concerns. In order to ascertain the efficiency of a given corrosion inhibitor, simple and yet very reliable methods such as gravimetric experiments which involves weight loss measurements (Ahanotu *et al.*, 2022; Oguzie *et al.*, 2010; Ebenso, 2003), gasometric experiments which involves gas evolution measurements (Chitra *et al.*, 2010; Oguzie, 2006), electrochemical experiments which includes potentiodynamic polarization and electrochemical impedance spectroscopy (Solomon *et al.*, 2021; Ahanotu *et al.*, 2020; Onyeachu *et al.*, 2020), thermometric experiments which involves temperature change measurements (Ebenso, 2003), acidimetry which involves measurement of pH changes (Adejo *et al.*, 2019), and lots more are normally used. The inhibition efficiency of different plant extracts is a valuable parameter that gives an insight while choosing an effective extract for a particular intended purpose and this is done by taking into account the surface characterization studies of the protected and unprotected metal substrates using imaging techniques such as atomic force microscopy (AFM) and scanning electron microscopy (SEM) (Ahanotu *et al.*, 2020; Olawale *et al.*, 2018). At the moment, no work has been done on the use of extracts of *Tradescantia pallida* as a corrosion inhibitor for metal substrates. As a contribution to the growing interest in the search for environmentally friendly corrosion inhibitors, this present study sought to investigate the corrosion resistive effect of *Tradescantia pallida* leaf extract in protecting low carbon steel substrates from corrosion in an acidic solution. *Tradescantia pallida*, also known as purple-heart or purple queen, is a tender evergreen perennial, a species of spiderwort plant in the family *Commelinaceae*. native to the northeastern Mexico (Huq, 2015). It is normally grown as an ornamental for its striking dark purple lance-shaped fleshy leaves up to 7 inches long which are covered with pale hairs and produced alternatively on fleshy stems (Menegazzo *et al.*, 2020). This plant is renowned for its ability to effectively remove volatile organic pollutant from the air (Govaerts, 2012; Yang *et al*., 2009).

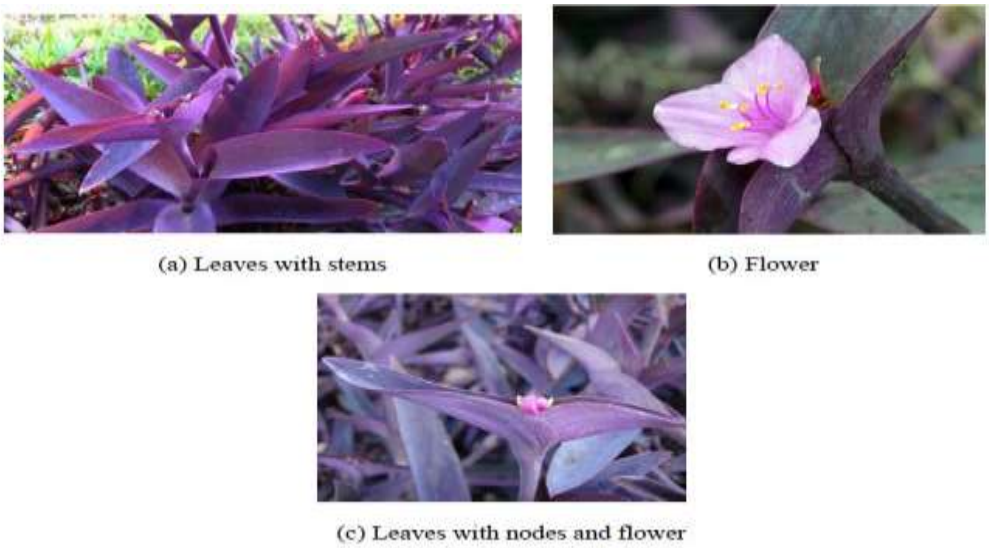

Figure 1(a-c): Images of *Tradescantia pallida* (Huq, 2015).

Aims and Objectives

The aim of the study "Exploring the efficacy of a potent corrosion suppressant derived from *Tradescantia pallida* (Purple Heart) leaves: A qualitative assessment" is to investigate the effectiveness of using the extract from *Tradescantia pallida* leaves as a natural corrosion suppressant. The study aims to assess the potential of this eco-friendly alternative for preventing corrosion in various applications. The objectives of the study are as follows:

1. To collect and analyze extract of *Tradescantia pallida* leaves to determine the functional groups present and identify any corrosion-inhibiting properties.
2. To conduct laboratory experiments and qualitative assessments to evaluate the efficacy of the corrosion suppressant derived from *Tradescantia pallida* leaves.
3. To compare the performance of the natural corrosion suppressant with existing commercial corrosion inhibitors in terms of effectiveness and cost-efficiency.
4. To assess the environmental impact and sustainability of utilizing *Tradescantia pallida* leaves as a corrosion suppressant, considering factors such as availability, renewability, and biodegradability.
5. To explore potential applications for the natural corrosion suppressant derived from *Tradescantia pallida* leaves in different industries, such as transportation, infrastructure, and manufacturing.
6. To provide recommendations and insights for further research and development of *Tradescantia pallida* leaf-based corrosion suppressants, including potential modifications or combinations with other materials for enhanced effectiveness. By addressing these objectives, the study aims to contribute to the understanding of using natural resources like Tradescantia leaves as a viable solution for corrosion control, offering potential benefits in terms of sustainability, cost-effectiveness, and environmental impact.

Significance of the Research

Exploring the efficacy of a potent corrosion suppressant derived from *Tradescantia pallida* (Purple Heart) leaves is an intriguing topic. Corrosion is a significant global challenge that affects various industries, infrastructure, and even the environment. By investigating the potential of using a natural resource like Tradescantia leaves as a corrosion suppressant, we can align it with several United Nations Sustainable Development Goals (SDGs). Here are a few ways this research can contribute:

1. SDG 9: Industry, Innovation, and Infrastructure: By developing a natural corrosion suppressant, this research promotes innovation in materials science and contributes to the improvement of infrastructure durability.

2. SDG 12: Responsible Consumption and Production: Utilizing *Tradescantia pallida* leaves as a corrosion suppressant aligns with sustainable and eco-friendly approaches. It encourages the use of natural resources as alternatives to harmful chemicals, promoting responsible consumption and production practices.

3. SDG 13: Climate Action: Corrosion in various industries contributes to greenhouse gas emissions and environmental degradation. By effectively suppressing corrosion with a natural resource, we can reduce the environmental impact and work towards mitigating climate change.

4. SDG 17: Partnerships for the Goals: Collaboration between researchers, industry experts, and policymakers is crucial for implementing and scaling up the use of natural corrosion suppressants. This research topic can foster partnerships to collectively work towards achieving the SDGs. Overall, exploring the efficacy of a corrosion suppressant derived from *Tradescantia pallida* leaves not only addresses the significance of corrosion control but also aligns with the broader global goals of sustainable development.

2. Experimental Methods

2.1 Materials preparation

Low carbon steel sheets were obtained from the Engineering Workshop of the Department of Mechanical Engineering, Federal University of Technology, Owerri (FUTO). They were mechanically cut into coupons of dimension 30 mm × 15 mm × 1 mm and each was perforated with a hole of 2.5 mm diameter to allow hanging into the hostile solution with polymeric thread in the gravimetric experiments. The test coupons were then polished and cleaned using emery paper, degreased in absolute ethanol, dried using acetone, weighed and then stored in a moisture-free desiccator prior to use (Oguzie *et al.*, 2004). The hostile acid solution was prepared by taking 27.2 ml research grade concentrated sulphuric acid of 98% certified percent purity and specific gravity of 1.84, and diluting it to mark in a standard 1.0 litre volumetric flask using double-distilled water. Locally harvested and authenticated mature *Tradescantia pallida* leaves (TPL) were washed and dried indoors to a constant weight and then ground to fine powder. Exactly 20.0 g of this powder was put into 500 ml of the hostile solution (0.5 M H_2SO_4) in a round bottom flask and heated under reflux for 2 hours and left to cool overnight. The stock inhibitor solution was obtained by filtration and used to prepare five inhibitor test solutions of concentration 0.5, 1.0, 1.5, 2.0 and 2.5 g L^{-1} respectively.

2.2 Fourier Transform Infrared (FTIR) Characterization

Buck scientific M530 USA FTIR was used for the analysis. This instrument was equipped with a detector of deuterated triglycine sulphate and beam splitter of potassium bromide. The software of the Gram A1 was used to obtain and manipulate the spectrum. Approximately1.0 g of the sample was taken and 0.5 ml Nujol was added. They were mixed thoroughly and placed on a salt pellet. During measurement, FTIR spectra was obtained at frequency region 4000 – 600 cm^{-1} and co-added at 32 scans and at 4 cm^{-1} resolution (Weerd *et al.*, 2004).

2.3 Weight Loss Experiments

Five Erlenmeyer flasks of 250 ml capacity with stoppers were used as the corrosion cells. These were filled with 150 ml of the hostile acid solution and TPL inhibitor test solutions were added to the cells in an increasing concentration range from 0.5 – 2.5 g L^{-1} at approximately 27 ^{0}C. A sixth flask of the same capacity contained only the acid solution and this served as the control experiment. With polymeric thread, the prepared and weighed low carbon coupons were fully immersed inside the six corrosion cells which were thereafter covered with the stoppers in order to stimulate an anaerobic environment. The coupons were retrieved after 3 days, washed appropriately with the aid of brittle brush inside water to remove corrosion products, degreased with absolute ethanol, dried in acetone and re-weighed. The weight loss of each test coupon was taken to be the difference between the initial weight before total immersion and the final constant weight after the removal of corrosion products. This procedure was repeated with fresh set of coupons of the same dimensions at an elevated

temperature of 60^0C to determine the temperature effect on the corrosion rate. To ensure reproducibility, triplicate gravimetric measurements were taken, averaged and used in subsequent calculations as described elsewhere (Ekpe *et al.*, 1995; Umoren *et al.*, 2008). The weight losses of the test coupons were converted to corrosion rate (*R*) in *mm* yr^{-1}, according to equation 1 below;

$$R = \frac{K\Delta W}{At\rho} \quad (1)$$

where *K* is a constant with value 8.76 x 10^4. This constant is a factor that converts *cm* hr^{-1} to *mm* yr^{-1} (note, 1 cm hr^{-1} is equal to 87,658.1277 millimeters per year). ΔW is the weight loss in *g* of the test coupon, *A* is the total surface area of test coupon determined to the nearest 0.01 cm^2, *t* is the exposure time (duration of immersion) in *hour*, and ρ is the density of the test coupon in *g* cm^{-3}.

The total surface area (TSA) of the coupons was calculated as the total surface area of a cuboid minus area of the drilled cylindrical hole *i.e.*,

$$\text{TSA of metal coupon} = 2[LW + LH + WH] - [\frac{\pi d^2}{2} + \pi dH] \quad (2)$$

where L = length of coupon, W = width of coupon, H = height or thickness of coupon, *d* = diameter of drilled hole in the coupon.

With *L*, *W*, *H* and *d* retaining their usual meanings described above, the volume of the coupons was calculated using the expression given in equation (3) as;

Volume of coupon = Volume of a cuboid – Volume of drilled cylindrical hole

$$\textit{i.e.}\ V = LWH - [\pi r^2 H] \text{ or } LWH - [\frac{\pi d^2 H}{4}] \quad (3)$$

The density, ρ, of each coupon was determined as mass per unit volume, using the initial weight of each coupon before immersion according to equation 4 below.

$$\rho = \frac{m}{V} \quad (4)$$

From the corrosion rate, the percent inhibition efficiency (%IE) of the organic molecules contained in the plant extract was determined using equation 5 below.

$$\%IE = \left[\frac{R_0 - R_i}{R_0}\right] x\ 100 \quad (5)$$

Where R_0 and R_i are the corrosion rate in the absence and presence of the inhibiting molecules, respectively.

One assumption in the calculation of degree of surface coverage is that corrosion on the metal surface occurs in the inhibitor uncovered sites, such that covered sites experience zero corrosion rate. The degree of surface coverage (θ) of TPL inhibitor system on the substrate in 0.5 M H_2SO_4 was calculated using Eq. 6 (Oguzie *et al.*, 2004), thus;

$$\theta = \left[\frac{R_0 - R_i}{R_0}\right] \quad (6)$$

3. Results

3.1 Weight loss, Corrosion Rates, Surface coverage and Inhibition Efficiency

The results of weight loss measurements, corrosion rate, percent inhibition efficiency of the extract and surface coverage using TPL extract at 303 K (27^0C) and at 333 K (60^0C) are presented in Tables 1 and 2 respectively for low carbon steel corrosion in 0.5 M H_2SO_4 solution.

Table 1: Weight losses, corrosion rate, inhibitor efficiency and surface coverage for low carbon steel corrosion in 0.5 M H_2SO_4 solution in the absence and presence of TPL extract at 27 ^{0}C

TPL Extract conc. (g L^{-1})	Weight of test coupon (g)		Weight Loss, ΔW (g)	R (mm/yr)	%IE	Surface Coverage, θ
	0 hr	72hr				
0.0	4.59	2.91	1.68	20.380	–	–
0.5	4.62	4.50	0.12	1.446	92.91	0.929
1.0	4.60	4.49	0.11	1.332	93.46	0.935
1.5	4.58	4.48	0.10	1.216	94.40	0.944
2.0	4.55	4.46	0.09	1.102	94.59	0.946
2.5	4.61	4.54	0.07	0.846	95.85	0.959

Table 2: Weight losses, corrosion rate, inhibitor efficiency and surface coverage for low carbon steel corrosion in 0.5 M H_2SO_4 solution in the absence and presence of TPL extract at 60 ^{0}C

]	Weight of test coupon (g)		Weight Loss, ΔW (g)	R (mm/yr)	%IE	Surface Coverage, θ
	0 hr	72hr				
0.0	4.54	2.59	1.95	23.918	–	–
0.5	4.50	4.28	0.22	2.722	88.62	0.886
1.0	4.52	4.32	0.20	2.464	89.70	0.897
1.5	4.51	4.32	0.19	2.346	90.20	0.902
2.0	4.53	4.36	0.17	2.090	91.26	0.913
2.5	4.50	4.34	0.16	1.980	91.72	0.917

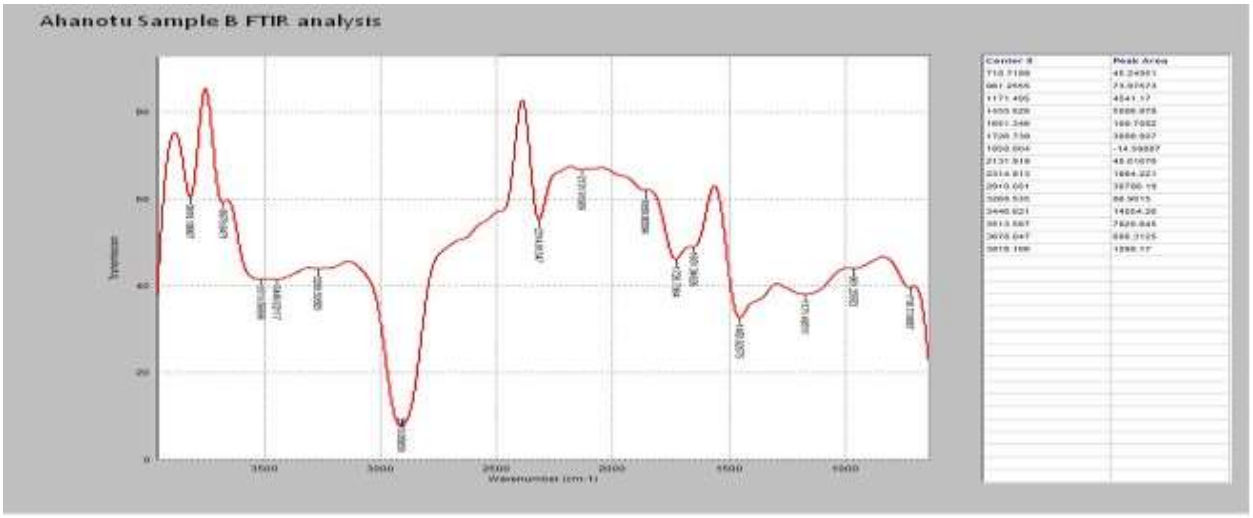

Figure 2: FTIR spectrum of TPL extract

4. Discussions

The evaluation of the performance of Tradescantia pallida leaf (TPL) extract in inhibiting the corrosion of low carbon steel coupons immersed in a 0.5 M sulphuric acid solution for a duration of 3 days at 27°C provides valuable insights into the effectiveness of the extract as a corrosion inhibitor. The weight loss measurements (ΔW) obtained from the initial and final weights of the low carbon steel coupons provide a quantitative assessment of the corrosion resistance offered by TPL extract. The lower the weight loss, the better the corrosion inhibition properties of the extract. From the data presented in Table 1, it is evident that the addition of TPL extract resulted in significantly reduced weight losses compared to the control (no extract). This indicates that the extract effectively protected the low carbon steel coupons from corrosion in the aggressive sulphuric acid environment. The corrosion rate (R) calculated from the weight loss data further

supports the corrosion inhibiting potential of TPL extract. A lower corrosion rate corresponds to a higher level of corrosion protection. As observed in Table 1, the corrosion rate of low carbon steel decreased significantly with the addition of TPL extract at varying concentrations. This demonstrates the ability of the extract to effectively impede the corrosion process and preserve the integrity of the metal. The percent inhibition efficiency (%IE) provides a measure of the effectiveness of the TPL extract as a corrosion inhibitor. It quantifies the percentage reduction in corrosion rate achieved with the addition of the extract compared to the control. The data in Table 1 reveals substantial inhibition efficiencies ranging from 88.62% to 95.85% for different concentrations of TPL extract. These high inhibition efficiencies highlight the excellent corrosion inhibiting properties of the extract and its potential for industrial applications. The rate of surface coverage (Θ) is a critical parameter that characterizes the adsorption behavior of the corrosion inhibitor on the metal surface. A higher surface coverage indicates a greater degree of adsorption and protection. The presence of functional groups such as OH, C=O, and aromatic rings in TPL extract, as identified in the study, suggests favorable interactions with the metal surface, leading to enhanced adsorption and surface coverage. These interactions contribute to the remarkable inhibition efficiencies observed. Overall, the evaluation of TPL extract using parameters such as weight losses, corrosion rates, percent inhibition efficiencies, and surface coverage demonstrates its strong potential as a corrosion inhibitor for low carbon steel in sulphuric acid solutions. The data obtained from this study provide a solid foundation for further investigations and optimization of TPL extract as an eco-friendly and sustainable corrosion mitigation strategy. Further research is recommended to explore the underlying mechanisms of corrosion inhibition by TPL extract, investigate its performance under different environmental conditions, and assess its long-term stability and compatibility with other corrosion prevention strategies. the results clearly indicate the significant impact of *Tradescantia pallida* leaf (TPL) extract on the corrosion rate of the low carbon steel coupons. The comparison between the control cell (blank) and the cell containing 0.5 g L-1 of TPL extract highlights the effectiveness of the extract as a corrosion inhibitor. In the control cell, a substantial mass loss of 1.68 g was observed, leading to a high corrosion rate of 20.380 mm/yr. This indicates the aggressive nature of the sulphuric acid environment on the low carbon steel, resulting in rapid corrosion and material loss. However, in the presence of 0.5 g L-1 of TPL extract, a remarkable reduction in weight loss was recorded. The addition of the extract resulted in a significantly lower weight loss of only 0.12 g, corresponding to a drastic decrease in the corrosion rate to 1.446 mm/yr. This demonstrates the strong corrosion inhibiting properties of TPL extract, as it effectively protected the low carbon steel from the corrosive attack of the sulphuric acid solution. The substantial decrease in corrosion rate observed upon the addition of TPL extract is a testament to its ability to form a protective barrier on the surface of the metal. This barrier hampers the corrosive reactions between the metal surface and the sulphuric acid, thereby reducing the corrosion rate and preserving the integrity of the low carbon steel. These findings highlight the promising potential of TPL extract as a highly effective and environmentally friendly corrosion inhibitor for low carbon steel in sulphuric acid environments. Further investigations can explore the optimization of the extract concentration, as well as assess its performance under different experimental conditions, to fully unlock its corrosion inhibition capabilities. The high percent inhibition efficiency of 92.91% at the concentration of 0.5 g L-1 of *Tradescantia pallida* leaf (TPL) extract reflects its excellent performance in suppressing the corrosion of the low carbon steel coupons. The extract demonstrated remarkable effectiveness in inhibiting the corrosion process, resulting in a significant reduction in the corrosion rate. As the concentration of TPL extract was increased from 0.5 g L-1 to 2.5 g L-1, a corresponding decrease in the corrosion rate was observed. The corrosion rate dropped significantly to 0.846 mm/yr at the highest concentration of 2.5 g L-1. This indicates that higher concentrations of TPL extract provide enhanced corrosion protection, leading to a notable decrease in the rate of corrosion. Furthermore, the percent inhibition efficiency increased proportionally with the higher concentration of TPL extract. At 2.5 g L-1 of the extract, the percent inhibition efficiency reached an impressive value of 95.85%. This signifies the extract's ability to effectively inhibit the corrosion process and provide a high level of protection to the low carbon steel coupons. These results demonstrate the concentration-dependent behavior of TPL extract as

a corrosion. Hence, TPL extract can be described as a very potent, reliable and benign inhibitor that could be deployed to protect low carbon steel substrates from acid attack.

At a higher temperature of 60^0C, similar results were observed and recorded as seen in Table 2. It was observed that the corrosion rate was higher at 60^0C relative to the results obtained at 27^0C without and with the TPL extract additive. This is understandable because it has been established elsewhere that for some inhibitors, corrosion rate decreases and inhibition efficiency increases with increase in the concentration of the inhibitor but both parameters increase and decreases at elevated temperatures (Ahanotu *et al.*, 2022; Solomon *et al.*, 2021; Umoren *et al.*, 2021; Onyeachu *et al.*, 2020; Madueke and Iroha, 2018). Consequently, at 60^0C, the corrosion rate of 23.918 mm/yr was recorded in the absence of the TPL extract (blank) and 2.722 mm/yr at 0.5 g L^{-1} resulting to a percent inhibition efficiency of 88.62%. Temperature effects, however, did not negate the concentration effect of the inhibiting organic molecules, hence the corrosion rate of 1.980 mm/yr was recorded at 2.5 g L^{-1} of the TPL extract, producing a percent inhibition efficiency of 91.72%. It has been reported that decrease in surface coverage and protection efficiency of inhibitors with increase in temperature is often an indication that the inhibitor molecules and the metal surface interacted by physisorption mechanism involving electrostatic interaction between charged molecues (Madueke and Iroha, 2018). Therefore, *Tradescantia pallida* leaf extract could actually function as an effective inhibitor to suppress the corrosion of low carbon steel in an acid environment.

3.2 FTIR Characterization

Available reports on literature reveals that *Tradescantia pallida* leaves are rich in flavonoids, tannins, alkaloids, and terpenoids. These plant secondary metabolites have active OH functional group and aromatic rings (Huq, 2015). This is an agreement with the FTIR spectrum shown in Figure 2. The spectrum a reveal the prominent functional groups contained in the sample. The absorption band at 3600 – 3450 cm^{-1} indicates O-H stretch of an alcohol or phenol. The strong band at 2950 – 2850 cm^{-1} indicates sp^3 (saturated) C-H stretch of an aliphatic chain, the band at 1729 cm-1 represents a C=O stretch of an aldehyde while the band at 1450 cm_{-1} indicates C=C stretch of an aromatic ring.

The heteroatom (oxygen) present in the OH functionality and the pi electron system of the aromatic rings play significant role *via* synergistic effect in enhancing the adsorption of the inhibitor molecules on metallic substrates, creating a barrier that suppresses the corrosion reaction (Gruyter, 2021; Eddy *et al*., 2012).

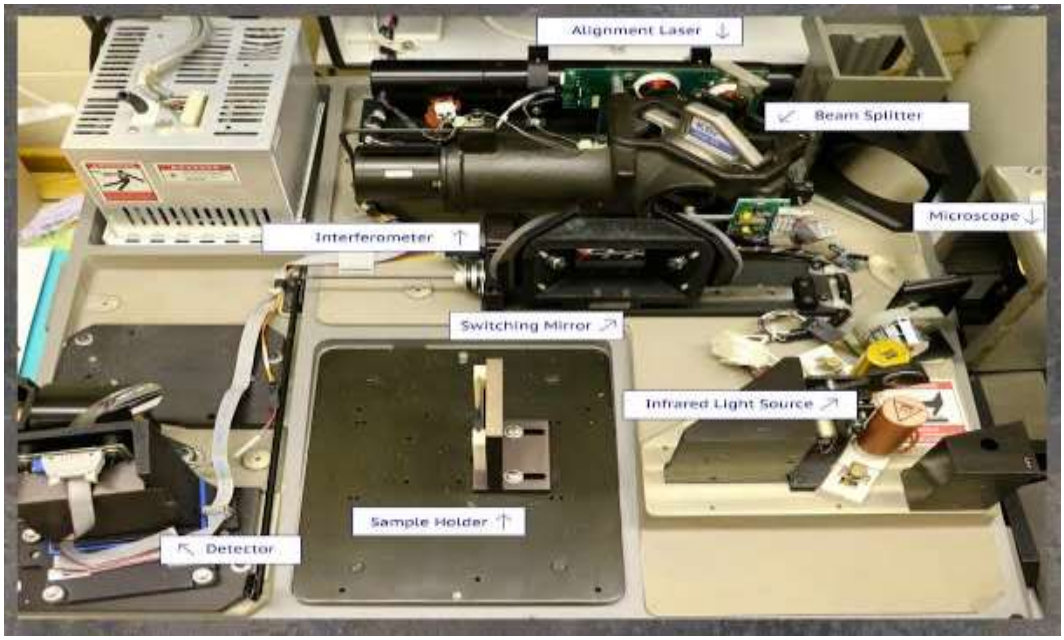

Fig 3: Mechanical Text Machines

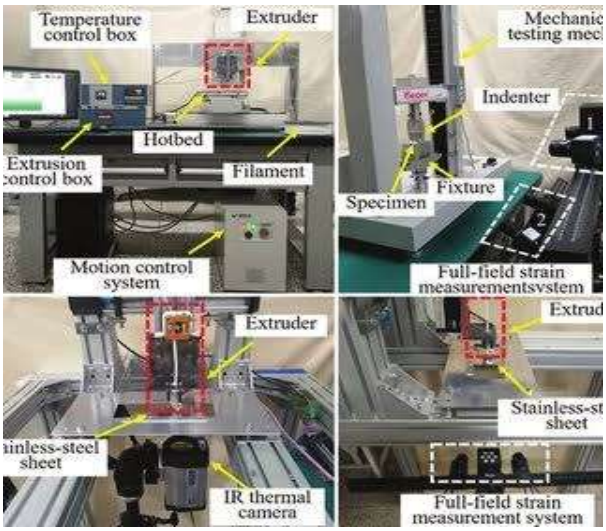

Fig 4:Application of Samples of Mechanical Text Machines of FTIR

Fig 5: Advanced Physics Lab FTIR

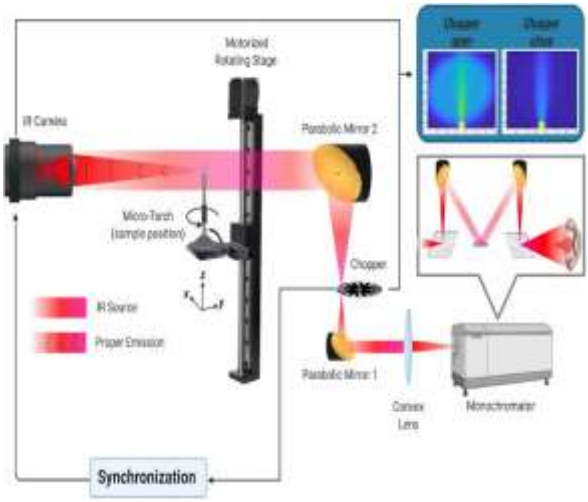

Fig 6: Applications

Fig 7: FTIR Spectroscopy Lab Analysis

Conclusion

In conclusion, this study has successfully explored the corrosion resistance properties of *Tradescantia pallida* leaf (TPL) extract as a potential corrosion inhibitor for low carbon steel in an acid environment. The results demonstrated that TPL extract exhibits remarkable effectiveness in protecting low carbon steel from acid attack, particularly in the challenging conditions of 0.5 M sulphuric acid. The inhibitor showed potent corrosion inhibition capabilities, significantly reducing the corrosion rate and exhibiting high inhibitor efficiencies ranging from 88.62% to 95.85%, depending on the dosage and temperature. Moreover, the presence of functional groups such as OH, C=O, and aromatic rings in TPL extract suggests a physisorption mechanism, facilitating the adsorption of inhibitor molecules onto the metal surface. This knowledge opens up possibilities for further optimization and modification of TPL extract to enhance its performance as a sustainable and environmentally friendly corrosion inhibitor. Overall, this research establishes *Tradescantia pallida* leaf extract as a promising and benign alternative for protecting low carbon steel in hostile acid environments. Further studies are encouraged to explore the long-term stability, compatibility, and cost-effectiveness of TPL extract in practical applications, as well as to investigate its performance under various corrosive conditions and in combination with other corrosion mitigation techniques. The findings of this study provide compelling evidence that increasing the concentration of *Tradescantia pallida* leaf (TPL) extract enhances the efficiency of the inhibiting molecules present in the extract. This correlation suggests that the corrosion resistance capabilities of TPL extract in protecting low carbon steel from

dissolution in sulphuric acid solution at the specified temperatures significantly improve with higher extract concentrations.

The dose-dependent behavior of TPL extract highlights its potential for customization and optimization, allowing for the development of tailored corrosion inhibition strategies. By adjusting the concentration of TPL extract, it becomes possible to achieve higher levels of protection against corrosion, thereby extending the lifespan and durability of low carbon steel in hostile acid environments.

These results underscore the significant potential of TPL extract as a sustainable and environmentally friendly corrosion inhibitor for industrial applications. The use of natural extracts, such as TPL, not only offers effective corrosion protection but also aligns with the growing emphasis on eco-friendly alternatives in the field of corrosion control.

In conclusion, this research demonstrates the efficacy of *Tradescantia pallida* leaf extract as a potent and customizable corrosion inhibitor for low carbon steel in sulphuric acid solutions. Further investigations should focus on exploring the underlying mechanisms governing the corrosion inhibition process, optimizing the extract concentration, and evaluating the long-term performance and compatibility of TPL extract in practical applications.

The temperature effect observed in this study revealed a clear relationship between the temperature of the aggressive environment and the rate of corrosion, as well as the percent inhibition efficiency of *Tradescantia pallida* leaf extract (TPLE). As the temperature increased, the rate of corrosion of low carbon steel also increased, while the percent inhibition efficiency decreased. This behavior strongly suggests that a physisorption mechanism is at play in the corrosion inhibition process. Further investigation into the composition of TPLE revealed the presence of various functional groups, including OH, C=O, and aromatic rings, among others. These functional groups have been well-documented for their effectiveness in enhancing the adsorption of inhibitor molecules onto metallic substrates. The presence of these functional groups in TPLE further supports the physisorption mechanism observed in this study. The combination of the temperature effect and the presence of these functional groups in TPLE highlights the complex interplay between temperature and molecular interactions in corrosion inhibition. This knowledge opens up avenues for future research to delve deeper into the specific mechanisms that govern the adsorption behavior of TPLE on low carbon steel surfaces under different temperature conditions. In conclusion, this study has shed light on the temperature effect and the presence of functional groups in *Tradescantia pallida* leaf extract, demonstrating their role in the physisorption mechanism and their potential to enhance the adsorption of inhibitor molecules on metallic substrates. Further research is warranted to gain a comprehensive understanding of the temperature-dependent behavior and to optimize the application of TPLE as a corrosion inhibitor in various temperature ranges and industrial settings.

Recommendation

Based on the study "Exploring the efficacy of a potent corrosion suppressant derived from *Tradescantia pallida* (Purple Heart) leaves: A qualitative assessment," here are some recommendations aligned with the United Nations Sustainable Development Goals (SDGs):

1. **Recommendation aligned with SDG 9:** Industry, Innovation, and Infrastructure: - Further research should be conducted to optimize the extraction process of the corrosion suppressant derived from *Tradescantia pallida* leaves, enhancing its efficiency and scalability. - Collaboration between researchers, industry experts, and infrastructure developers should be facilitated to explore the integration of *Tradescantia pallida* leaf-based corrosion suppressants in various infrastructure projects.

2. **Recommendation aligned with SDG 12:** Responsible Consumption and Production: - Promote awareness and education about the benefits of using natural corrosion suppressants derived from *Tradescantia pallida* leaves to encourage responsible consumption and production practices. - Encourage industries to adopt sustainable practices by considering the use of eco-friendly corrosion suppressants as alternatives to chemical-based inhibitors.

3. **Recommendation aligned with SDG 13:** Climate Action: - Conduct a life cycle assessment of *Tradescantia pallida* leaf-based corrosion suppressants to evaluate their carbon footprint and environmental impact compared to traditional corrosion inhibitors. - Advocate for the adoption of natural corrosion suppressants as a climate-friendly solution to reduce greenhouse gas emissions associated with corrosion prevention.

4. **Recommendation aligned with SDG 17:** Partnerships for the Goals: - Foster collaborations between academia, industry, and government agencies to drive the development, standardization, and implementation of *Tradescantia pallida* leaf-based corrosion suppressants on a wider scale. - Establish partnerships between corrosion control experts and sustainable development organizations to raise awareness about the benefits of using natural resources for corrosion prevention. By following these recommendations and aligning them with the respective SDGs, the study can contribute to sustainable development efforts, promote responsible consumption and production practices, reduce environmental impact, and foster partnerships for achieving the SDGs.

Acknowledgments
We acknowledge Springboard Research Laboratory, Awka, Nigeria for providing the FTIR instrument used for the IR characterization of the extract.

References

Adejo,S.O., Yiase, S.G., Leke, L., Onuche, M., Atondo, M.V. & Uzah, T.T. (2019). Corrosion studies of mild steel in sulphuric acid medium by acidimetric method. *Int. J. Corros. Scale Inhib.*, 8(1): 50-61

Ahanotu, C.C., Onyeachu, I.B., Solomon, M.M., Chikwe, I.S., Chikwe, O.B., Eziukwu, C.A. (2020). *Pterocarpus santalinoides* leaves extract as a sustainable and potent inhibitor for low carbon steel in a simulated pickling medium, *Sustainable Chemistry and Pharmacy*, 15, 100196. DOI: 10.1016/j.scp.2019.100196

Ahanotu, C.C., Madu, K.C., Chikwe, I.S. and Chikwe, O.B. (2022). The inhibition behavior of extracts of *Plumeria rubra* on the corrosion of low carbon steel in sulphuric acid medium. *J. Mater. Environ, Sci.*, 13(9), 1025-1036

Anupama, K.K., Ramya, K., Joseph, A. (2017). Electrochemical measurements and theoretical calculations on the inhibitive interaction of *Plectranthus amboinicus* leaf extract with mild steel in hydrochloric acid. *Measurement* 95, 297–305.

Chitra, S., Parameswari, K. and Selvaraj, A. (2010). Sianiline Schiff bases as inhibitors of mild steel corrosion in acid media. *Int. J. Electrochem. Sci.*, 5: 1675-1697

Ebenso, E.E. (2003). Synergistic effect of halide ions on the corrosion inhibition of aluminium in H_2SO_4 using 2-acetylphenothiazine. *Mater. Chem. Phys.* 78(1): 58-70

Ebenso, E.E., Eddy, N.O. & Odiongenyi, A.O. (2008). Corrosion inhibitive properties and adsorption behavior of ethanol extract of *Piper guineense* as a green corrosion inhibitor for mild steel in H2SO4. *African Journal of Pure and Applied Chemistry*, 2(11): 107-115.

Eddy, N.O., Odiongeny, A.O., Ameh, P.O. and Ebenso, E.E. (2012). Corrosion Inhibition Potential of *Daniella oliverri* Gum Exudate for Mild Steel in Acidic Medium. *Int J ElectrochemSci*7:7425-7439.

Ekpe, U.J., Ibok, U.J., Ita, B.I., Offiong, O.E. and Ebenso, E.E. (1995). *Mater. Chem. Phys.* 40: 87.

Ghahremani, P., Tehrani, M.E.H.N., Ramezanzadeh, M. & Ramezanzadeh, B. (2021). Golpar leaves extract application for construction of an effective anti-corrosion film for superior mild-steel acidic-induced corrosion mitigation at different temperatures. *Colloids and Surfaces A: Physicochemical and Engineering Aspects*, 629: 127488123

Govaerts, R. (2012). World Checklist of Commelinaceae. Richmond, UK. Royal Botanic Gardens

Gruyter, D. (2021). Phytochemicals as steel corrosion inhibitor: an insight into mechanism. *Corros. Rev.* 39(1), 27 – 41.

Haldhar, R., Prasad, D., Kamboj, D., Kaya, S., Dagdag, O. & Guo, L. (2021). Corrosion inhibition, surface adsorption and computational studies of *Momordica charantia* extract: a sustainable and green approach. *Springer Nature Journal, Applied Sciences*, 3:25, https://doi.org/10.1007/s42452-020-04079-x*123*

Huq, S. (2015). Comparative Phytochemical Evaluation and Biological Activity Screening of *Murdannia Nudiflora* And *Tradescantia Pallida* (Thesis). Department of Pharmacy of BRAC University in partial fulfillment of the requirement for the Degree of Bachelor in Pharmacy

Ibrahim, M., Kannan, K., Parangusan, H., Eldeib, S., Shehata, O., Ismail, M., Zarandah, R. and Sadasivuni, K.K. (2020). Enhanced corrosion protection of epoxy/ZnO-NiO nanocomposite coatings on steel. *Coatings*, 10: 783, DOI:10.339//coatings10080783

Kıcır, N., Tansu ˘g, G., Erbil, M.,Tüken, T. (2016). Investigation of ammonium (2,-dimethylphenyl)-dithiocarbamate as a new, effective corrosion inhibitor for mild steel. *Corros. Sci.* 105, 88–99.

Ladan, M., Basirun, W.J., Kazi, S.N.,Rahman, F.A. (2017). Corrosion protection of AISI 1018 steel using Co-doped TiO2/polypyrrolenanocomposites in 3.5% NaCl solution. *Mater. Chem. Phys.* 192, 361–373.124

Loto, R.T. & Olowoyo, O. (2019). Synergistic effect of sage and jojoba oil extracts on the corrosion inhibition of mild steel in dilute acid solution. *Procedia Manuf.* 35, 310–314.

Madueke,N.A. & Iroha, N.B. (2018). Protecting aluminium alloy of type AA8011 from acid corrosion using extract from *Allamansa cathartica* leaves. *Int'l J. Innovative Research in Science, Engineering and Technology*, 7(10): 10251-10257

Mai, W., Soghrati, S.,Buchheit, R.G. (2016). A phase field model for simulating the pitting corrosion. *Corros. Sci.* 110, 157–166.

Miralrio, A. &Vázquez, A.E. (2020). Plant Extracts as Green Corrosion Inhibitors for Different Metal Surfaces and Corrosive Media: A Review. *Processes*, 8, 942; doi:10.3390/pr8080942.

Oguzie, E.E., Okolue, B.N., Ebenso, E.E., Onuoha, G.N. and Onuchukwu, A.I. (2004). *Mater.Chem. Phys.* 87 (2–3), 394.

Oguzie, E.E. (2006). Studies on the inhibition effect of *Occinum viridis* extract on acid corrosion of mild steel. *Mater.Chem. & Phys.* 99: 441- 446.

Oguzie, E.E., Enenebeaku, C.K., Akalezi, C.O., Okoro, S.C., Ayuk, A.A., Ejike, E.N. (2010). Adsorption and corrosion-inhibiting effect of *Daryodis edulis* extract on low-carbon-steel corrosion in acidic media. *J. Colloid. Interf. Sci.*, 349(2010): 283-292

Olawale, O., Ogunsemi, B.T., Agboola, O.O., Ake, M.B. &Jawando, G.O. (2018). Inhibition Effect of Orange Seed Extract on Aluminum Corrosion in 1M Hydrochloric Acid Solution. *Int. J. Mech. Engr. and Tech.*, 9(12): 282—287.

Onyeachu, I.B., Solomon, M.M., Umoren, S.A., Obot, I.B., Sorour, A.A., (2020). Corrosion inhibition effect of a benzimidazole derivative on heat exchange tubing materials during acid cleaning of multistage flash desalination plants. *Desalination* 479.

Parthipan, P.; Elumalai, P.; Narenkumar, J.; Machuca, L.L.; Murugan, K.; Karthikeyan, O.P., Rajasekar, A. (2018). *Allium sativum* (garlic extract) as a green corrosion inhibitor with biocidal properties for the control of MIC in carbon steel and stainless steel in oilfield environments. *Int. Biodeterior. Biodegrad.* 132, 66–73

Patel, N.S., Jauhariand, S., Mehta, G.N., Al-Deyab, S.S., Warad, I. and. Hammouti, B. (2013). Mild Steel Corrosion Inhibition by Various Plant Extracts in 0.5M Sulphuric acid. *Int. J. Electrochem. Sci.*, 8(2013)2635 - 2655.

Singh, P., Srivastava, V.,Quraishi, M.A. (2016). Novel quinoline derivatives as green corrosion inhibitors for mild steel in acidic medium: Electrochemical, SEM, AFM, and XPS studies. *J. Mol. Liq.* 216, 164–173.

Solomon, M.M., Onyeachu, I.B., Njoku,D.I., Nwanonenyi, S.C., Oguzie, E.E. (2021). Adsorption and corrosion inhibition characteristics of 2–(chloromethyl)benzimidazole for C1018 carbon steel in a typical sweet corrosion environment: Effect of chloride ion concentration and temperature, *Colloids Surf, A: Physicochem. Eng. Asp*. 610.

Umoren, S.A., Obot, I.B. & Ebenso, E.E. (2008). Corrosion inhibition of aluminium using exudates gum from *Pachylobusedulis* in the presence of halide ions in HCl. *E-Journal of Chemistry*. 5:355–364.

Umoren, S.A., Solomon, M.M., Obot, I.B. and Suleiman, R.K. (2021). Effect of intensifier additives on the performance of butanolic extract of Date palm leaves against the corrosion of API 5L X60 carbon steel in 15 wt.% HCl solution. *Sustainability*, 13: 5569, https://doi.org/10.3390/su13105569

Verma, C., Ebenso, E.E., Bahadur, I.,Quraishi, M.A. (2018). An overview on plant extracts as environmental sustainable and green corrosion inhibitors for metals and alloys in aggressive corrosive media. *J. Mol. Liq.* 266, 577–590.

Weerd, V.J., Heeren, R.M.A. & Boon, J.J. (2004); Preparation methods and accessories for the infrared spectroscopic analysis of multi-layer paint. Stud. Conserv., 49: 193-210, DOI: 10.1179/sic.2004.49.3.193

Yang, D.S., Pennisi, S.V., Son, K. &Kays, S.J. (2009). Screening of indoor plants for volatile organic pollutant removal efficiency. *Hortscience*, 44(5), 1377-1381.

Zhu, Y., Wang, L., Behnamian, Y., Song, S., Wang, R., Gao, Z., Hu, W., Xia, D.H. (2020). Metal pitting corrosion characterized by scanning acoustic microscopy and binary image processing. *Corros.Sci.* 170, 108685.

Available online at www.asric.org
ASRIC Journal on Natural Sciences Vol 3(1) (2023) 125-131

Composition, antioxidant and antimicrobial activities of volatile oils from *Lantana camara* Linn

Ayopo A. Sotade[1*], Clement O. Ajiboye, [1] Olapeju O. Aiyelaagbe[1]

[1]Department of Chemistry, University of Ibadan, Ibadan. Nigeria.

*Corresponding author: drayopo@yahoo.com

Abstract

Lantana camara Linn (Verbanaceae) is an ornamental plant which has become invasive in the tropical parts of the world. The volatile oils from the root, stem, leaves, and flowers of the plant were obtained by hydrodistillation and analysed by gas chromatography–mass spectrometry (GC-MS). The antioxidant and antimicrobial activities of the volatile oils were investigated by Hydrogen-Peroxide radical-scavenging assay, and broth microdilution method, respectively. The yield (v/w) of the volatile oils of the root, stem, leaves, and flowers of *Lantana camara* L are 0.54%, 0.50%, 0.98%, and 3.88% respectively. A total of 28, 42, 28, and 34 constituents were identified in the root, stem, leaves, and flowers EOs corresponding to 97.63%, 99.98%, 99.97%, and 98.30% of the volatile oil respectively. Eucalyptol (30.83%, root), Dibutyl phthalate (9.65%, stem), Eucalyptol (35.45%, leaves), and Caryophyllene (19.33%, flower) were the most abundant components identified in the volatile oils. *Lantana camara* L. volatile oils showed hydroxyl radical scavenging activities (51.9 - 67.3%) at a concentration of 33 to 8% while the leaves' volatile oils have the highest scavenging effect at the three concentrations. The volatile oils displayed broad-spectrum antimicrobial activity against the organisms tested.

Keywords: *Lantana camara* L., antioxidant, antimicrobial, Eucalyptol.

1. Introduction

Essential oils (EOs) are complex mixtures of volatile compounds produced by plants in response to environmental and ecological needs (Falcão *et al*., 2018). Volatile oils have a complex chemical profile because they typically contain a complex mixture of organic compounds such as monoterpenes, sesquiterpenes, and diterpenes, as well as their oxygenated derivatives. EOs have been used in traditional medicine since ancient times to treat a variety of ailments and health problems. They have been extensively researched for their important biological applications, such as antioxidant (Ghareeb *et al*., 2018), antimicrobial (Saad *et al.*, 2017), insecticidal (Batish *et al*., 2006), and antimalarial and trypanocidal (Meira *et al*., 2015) effects.

Since the phenomenon known as oxidative stress is the cause of numerous health issues, including inflammation, cancer, neurodegeneration, and cardiovascular diseases, there has been an increase in the research on the activity of antioxidants. This phenomenon involves the over-production of radicals, which are highly energetic molecules with odd electrons, primarily represented by reactive oxygen species (ROS). As naturally occurring antioxidants, essential oils may attenuate this damage through their radical-scavenging effect (Bakchiche *et al*., 2019; Ghareeb *et al*., 2018). Hence, their use as antioxidant agents is one of the most useful applications of essential oils.

Lantana camara Linn is a prickly climbing aromatic shrub in the Verbenaceae family. It is native to tropical America and was introduced as an ornamental hedge plant in India. The flowers are small and in dense axillary heads, usually yellow or orange but changing to red or pink. (Ghisalberti, 2000). It was originally cultivated as an ornamental plant, but it has become a highly invasive weed in many parts of the world. The fruits are fleshy berries in clusters, shiny and globose in shape, green in colour which on ripening turns to black. The root system is very strong with the main taproot and a mat of many shallow side roots (Sharma & Shrivastava, 2013). The names of *Lantana camara* L. in Nigerian

languages are Ewonadele" in Yoruba, "Kimbamahalba" in Hausa, and "Anya nnunu" in Igbo. *Lantana camara* L. oil and extracts are used in herbal medicine for the treatment of various human diseases such as skin itches, leprosy, cancers, chicken pox, measles, asthma, ulcers, tumours, high blood pressure, tetanus, rheumatism, etc (Dafni & Böck, 2019; Ghisalberti, 2000). The leaf paste is used to treat sores, chickenpox, and measles in Central and South America. Bronchitis is treated in Ghana with whole plant infusion, and stomach ache in children can be treated by mixing milk with the root powder (Sarma *et al*., 2020). To validate its ethnomedicinal uses, this study was undertaken to investigate the chemical profile, antioxidant, and antimicrobial activity of volatile oils extracted from the leaf, stem, root and flower of *Lantana camara* L.

2. Materials and Methods

2.1 Plant collection

Lantana camara L. was collected in Ibadan, Nigeria, and authenticated at the herbarium of the Department of Botany, University of Ibadan, with the voucher number UIH 23103. The plant was separated into different parts: roots, stems, leaves and flowers. The roots were washed thoroughly with distilled water to remove soil particles and all the parts were air-dried separately at room temperature for three weeks. Each dried part was pulverized to increase its surface area before extraction.

2.2 Volatile oils extraction and analysis of essential oils

The pulverized plant material was subjected to hydrodistillation using all glass Clevenger-type apparatus for 3 hours according to British Pharmacopoeia, (1998). The extracted volatile oils were stored in sealed glass vials and kept under refrigeration at 4 ℃ before analysis and bioassay. The volatile oils were analyzed by gas chromatography-mass spectrometry techniques using a Shimadzu (GC-2030) series GC-MS equipped with Headspace (HS-20) & QQQ Mass spectrometer GC-TQ8040NX; column: SH-Rxi-5 SILMS (0.25 X 30 X 0.25), carrier gas: Helium (flow rate of 1.00 mL/min); column initial temperature programmed at 60 ℃ held for 3 min then increased to120 ℃. The injector temperature was 260 ℃, the Ion source temperature was 220 ℃ & the interface temperature was 240 ℃. The samples were diluted in EtOAc and 0.5 µl injected with a constant temperature of 260 ℃ through an auto-sampler injector. The volatile oil constituents were identified using the NIST library.

2.3 Antioxidant Assay

The essential oils were tested to determine their antioxidant activity using the Hydrogen peroxide scavenging assay as described by Hazra *et al.*, (2008). Three different concentrations of each oil were prepared (33%, 17% and 8%). The stock solution prepared contained 4 mM hydrogen peroxide in 0.1 M phosphate buffer with a pH of 7.4. A volume of 2 mL of the solution was added to 1 mL of the essential oil and standard and left for 15 minutes at room temperature. The absorbance was taken at 285 nm. The percentage inhibition of the hydrogen peroxide was calculated as:

$$Concentration\ (\%) = \frac{Volume\ of\ sample}{Total\ volume} \times 100\%$$

$$\%\ Inhibition\ = \frac{Absorbance\ (STD - SPL)}{Absorbance\ (STD)} \times 100\%$$

Where Absorbance SPL is the absorbance of the Sample

Absorbance STD is the absorbance of standard (Peroxide).

2.4 Antimicrobial assay

The antimicrobial activity of the volatile oils was tested against bacteria and fungi using the broth microdilution method. The microorganisms used are two Gram-positive bacteria (*Staphylococcus aureus* and *Bacillus subtilis*), four Gram-negative bacteria (*Escherichia coli* ATCC 11175, *Salmonella typhi* ATCC 14028, *Klebsiella pneumonia* and *Pseudomonas aeruginosa* ATCC 27853) and two clinical isolates of fungi (*Trichophyton rubrum* and *Candida albicans*). The oil samples were dissolved in double-strength Tryptone soya Broth (TSB) to obtain a solution of 50% (100 µL of TSB and 100 µL of oil) and then serially diluted in a sterile 96 well plate to obtain more concentrations range of 25%, 12.5%, 6.25%, 3.125%, 1.5625%, 0.78125% and 0.3960%. The drugs used as the reference were gentamycin for anti-bacterial and ketoconazole for anti-fungal assay. Each of the microplate wells was

inoculated with 10 µL of the microorganism and incubated at 37 ℃ and 25 ℃ for 24 hours and 48 hours for bacteria and fungi respectively. The least concentrations which showed no growth or turbidity after hours of incubations were taken as MIC. After checking for growth or turbidity in the test plates (MIC determination), 10 µL of 0.2 mg/ml of p-INT solution (p-iodonitrotetrazolium violet) was added to the wells to aid the colouration of the plate. The plates were further incubated at 37 ℃ for 30 minutes. The wells with colour change from yellow to pinkish red were an indication of bacterial or microbial growth. The least concentration which showed no trace of growth or colour change was taken as the Minimum Bactericidal Concentration (MBC) and Minimum Fungicidal Concentration (MFC).

3. Results and Discussion

3.1 Chemical composition of *Lantana camara* L. volatile oils

The volatile oils extracted from *Lantana camara* L. root, stem, leaves, and flower were yellowish with a percentage yield range of 0.50% and 3.88% (Table 1). The GC-MS analysis result is presented in Table 2. A total of 28 constituents were identified in the root oil which were mostly monoterpenes and their oxygenated derivatives. The oil was dominated by eucalyptol (30.83%), ψ-limonene (15.34%), caryophyllene (15.27%), and β-pinene (6.82%).

Table 1: Percentage yield and colour of essential oil of *Lantana camara* L.

Lantana camara L. parts	Weight of parts (g)	Volume obtained (ml)	% yield of oil	Colour of the oil
LCR	202.14	1.1	0.54	Light yellow
LCS	238.01	1.2	0.50	Pale yellow
LCL	156.92	1.4	0.98	Pale yellow
LCF	36.07	1.4	3.88	Pale yellow

Keys: LCR: *Lantana camara* L. Root, LCS: *Lantana camara* L. Stem, LCL: *Lantana camara* L. Leaves, LCF: *Lantana camara* L. Flower

However, forty-two (42) constituents were identified in the stem oil. The oil was primarily composed of non-terpenes, which were dibutyl-phthalate (9.65%), and cholestane-2-(2-aminophenyl). Terpenes identified in the oil include eucalyptol (7.44%), caryophyllene oxide (7.28%), and ψ-limonene (6.56%). The leaves oil showed the presence of twenty-eight (28) compounds. The most abundant compounds are eucalyptol (35.45%), isolongifolen-9-one (12.55%), caryophyllene (10.33%), and β-pinene (7.56%). Thirty-four (34) constituents were identified in the flower oil. The oil was dominated by terpenes, which were caryophyllene (19.33%), ψ-limonene (15.57%), humulene (13.67%), and 3-carene (7.14%). Unlike the other oils, stem oils are largely non-terpenes. Caryophyllene, β-pinene, humulene, 3-carene, and ψ-limonene are all present in the volatile oils of all the plants' parts.

All the non-terpenes found in significant quantities in *Lantana camara* L. stem are important compounds in the industry. Higher alkanes act as anticorrosive agents and are important components of lubricating oil (Stachowiak & Batchelor, 2014). Consumption of fruit and vegetable-rich diets including monoterpene-rich vegetables, like limonene is known to lower the risk of getting cancer of the liver, pancreas, mammary gland, colon, and lung. The anticancer effect of limonene is well known (Junior *et al*., 2009). According to Marcelo *et al* (2015), terpinene-dominated Hyptis species prevented gastric lesions, decreased the volume and acidity of the gastric juice, and increased the amount of mucus on the gastric wall. It is also responsible for the plant's anti-inflammatory and antioxidant properties. The volatile oil of the leaves and flowers contains p-cymene, which is an antioxidant, anti-inflammatory, anti-nociceptive, anxiolytic, anticancer, and antimicrobial agent (Quintans-Júnior *et al*., 2013). Similarly, the abundance of p-cymene and terpinene has been attributed to *Carum copticum* essential oil's high antimicrobial potential (Skaltsa *et al.*, 2003).

There is no report on the essential oil of *Lantana camara* L. roots in the literature for comparison purposes. Zhu *et al.* (2013) reported that the major constituents in the stem oil are germacrene-D (31.0%), β-elemene (17.6%), and α-phellandrene (6.7%), while Medeiros *et al*. (2012) reported spatulenol (15.9%), caryophyllene oxide (17.1%) and β-Gurjunene (32.7%) as the most prominent compound in the stem oil of *Lantana camara* L. This study also revealed the presence of germacrene-D, α-phellandrene, and caryophyllene oxide in the stem oil. The *Lantana camara* L. leaves species

studied has a similar composition to those previously reported in Nigeria. In a report by Sonibare & Effiong (2008), the major constituents of *Lantana camara* L. leaves are β-caryophyllene (8.9%), E-nerolidol (5.9%) and bicyclogermacrene (2.8%), while Omoregie *et al.* (2016) also reported caryophyllene (6.99%) and (6E)-Nerolidol (5.68%).

Table 2: Chemical constiutents of essential oil of *Lantana camara* L.

Constituents	RI	% Composition			
		Root	Stem	Leaves	Flower
2-Methybutyl acetate	820	-	-	-	0.07
Ethylbenzene	893	0.23	0.24	-	-
Heptanal	905	-	-	-	0.13
o-Xylene	907	0.25	0.23	-	-
β-Pinene	943	6.82	1.80	7.56	2.99
3-Carene	948	3.31	2.19	2.71	7.14
β-Myrcene	958	0.32	0.49	-	2.32
α-Phellandrene	969	0.64	0.24	0.86	2.56
3-Octanol	979	-	-	0.21	-
γ-Terpinene	998	0.56	0.36	4.83	0.86
Ψ-Limonene	1013	15.34	6.56	7.52	15.57
D-Limonene	1018	-	0.70	-	2.84
4-Thujanol	1041	0.25	-	0.16	0.26
p-Cymene	1042	-	-	0.16	0.61
α-Terpinolene	1052	1.04	-	1.31	0.77
Eucalyptol	1059	30.83	7.44	35.45	-
Linalool	1082	-	0.71	-	2.29
Resorcinol	1096	-	1.08	-	-
2,5,5-Trimethylcyclohex-2-enone	1097	-		-	0.06
Nonanal	1104	0.27	0.43	-	-
2-Cyclohexen-1-ol	1109	-	-	0.16	0.08
Camphor	1121	-	0.34	-	-
Terpinen-4-ol	1137	0.86	0.36	4.35	1.29
α-Campholenal	1155	-	-	-	0.05
Isocyclocitral	1163	-	1.22	-	-
Hexahydro-1,6-pentalenedione	1204	-	-	-	0.07
Copaene	1221	5.18	0.53	2.52	0.63
α-Bourbonene	1339	0.27	-	1.06	0.95
α-Cubebene	1344	-	1.04	-	1.64
Alloaromadendrene	1386	-	-	0.11	0.88
Cyclodecanol	1387	0.15	-	-	-
(-)-Neoclovene	1393	-	0.41	-	-
Cedrene	1398	0.92	0.87	0.80	1.70
(Z)- α-Bergamotene	1430	0.74	-	0.39	-
γ-Elemene	1431	0.08	-	2.64	0.17
γ-Muurolene	1435	-	-	-	4.95
(Z)-β-Farnesene	1440	-	-	-	1.11
Naphthalene	1469	1.94	-	1.47	3.22
α-Selinene	1474	0.43	-	-	-
α-Guaiene	1490	0.23	-	-	1.66
Caryophyllene	1494	15.27	4.64	10.33	19.33
Caryophyllene oxide	1507	2.36	7.28	-	3.09
Germacrene D	1515	2.83	1.73	1.46	3.55
(-)-Spathulenol	1536	1.51	-	0.24	-
Nerolidol	1564	-	4.93	-	-
Humulene	1579	2.81	3.31	0.83	13.67
α-Cadinol	1580	-	-	-	0.43
Isolongifolen-9-one	1587	-	-	12.55	-
Germacrene B	1603	4.56	-	-	3.06

Tetradecanal	1637	-	3.04	-	-
3-Hydroxy-7,8-dihydro-.beta.-ionol	1653	-	0.36	-	-
Tridecanedial	1690	-	0.81	-	-
Heptadecane	1711	-	0.99	-	-
5-Epiandrostane	1769	-	2.25	-	-
2-Methoxymyristic acid	1880	-	0.60	-	-
Undecyl 2-(2-methoxyethoxycarbonylamino)pentanoate	1912	-	7.51	-	-
n-Octadecyl chloride	2036	-	3.44	-	-
Dibutyl phthalate	2037	-	9.65	-	-
1-Bromooctadecane	2107	-	0.39	-	-
5-Methylheneicosane	2144	-	2.68	-	-
Retinal	2184	-	1.12	-	-
11-Methyltricosane	2343	-	0.60	-	-
Silane	2420	-	-	0.08	
Methyl 5,13-docosadienoate	2491	-	6.27	-	-
Cannabinol	2497	-	-	0.03	-
γ- Tocopherol, TMS	3000	-	-	0.10	-
Benzamide	3040	-	-	0.10	-
Cholestane, 2-(2-aminophenyl)-	3344	-	8.57	-	-
1'H-Cholest-2-eno[3,2-b]indol-6-one	3463	-	1.39	-	-
Monoterpene hydrocarbons	28.03	12.34	26.42	35.66	
Oxygenated monoterpenes		32.36	11.15	39.96	3.89
Sesquiterpene		32.15	12.94	19.75	54.96
Oxygenated sesquiterpenes		4.61	12.21	13.18	3.52
Non-terpene derivatives		0.48	51.34	0.66	0.27
Number of compounds		**28**	**42**	**28**	**34**
Percentage composition		**97.63**	**99.98**	**99.97**	**98.30**

RI= Retention index

3.2 Antioxidant assay of *Lantana camara* L.

The results of the scavenging activities of *Lantana camara* L. volatile oils using Hydrogen Peroxide are presented in Table 3. The standards used for the assay are Vitamin A, Ascorbic acid, and Butylated Hydroxyl Anisole. The percentage inhibition is concentration dependent as activity decreased with a decrease in concentration. The leaf and flower oils of *Lantana camara* L. possessed better H_2O_2 radical scavenging activity compared to the stem and root oils but were not as active as the standards used. Thus, *Lantana camara* L. has moderate antioxidant activity and may be a source of natural antioxidants for both medicinal and industrial uses.

Table 3. Percentage Inhibition of H_2O_2 radicals by *Lantana camara* L. volatile oils

Conc (%)	LCRO	LCSO	LCLO	LCFO	VitA	AscA	BHA
33	**55**	**62.6**	**67.3**	**67.1**	74.3	76.6	66.9
17	**53.3**	**59.3**	**62.6**	**61.6**	67.9	76.5	51.1
8	**51.9**	**55.4**	**59.4**	**59.3**	20.7	74.6	31.8

LCR: *Lantana camara* L. root, LCS: *Lantana camara* L. stem, LCL: *Lantana camara* L. leaves, LCF: *Lantana camara* L. flower, VitA-Vitamin A, AscA- Ascorbic acid, BHA- Butylated Hydroxyl Anisole

3.3 Antimicrobial activity of *Lantana camara* L. volatile oil

The minimum inhibitory concentration (MIC) and minimum bactericidal concentration (MBC) of volatile oils extracted from *Lantana camara* L. root, stem, leaves and flowers are presented in Tables 4 and 5. All the oils were active against *Staphylococcus aureus* at a MIC value of 0.39% while only the root and flower showed activity against *Trichophyton rubrum* at a MIC value of 0.39%. The Gram-positive bacteria are more sensitive to the volatile oils than the Gram-negative bacteria. The results showed that the volatile oils of *Lantana camara* L. possessed moderate antimicrobial activities against

the tested microorganisms and this suggests its usefulness in the treatment of various infectious diseases caused by the bacteria and fungi.

Table 4: Minimum Inhibitory Concentration (MIC) of *Lantana camara* L. volatile oils

Micro-Organisms	LCR %	LCS %	LCL %	LCF %	Broth only	Broth and Oil	Broth and Microbe	Broth + Gentamicin µg/mL	Broth + Ketoconazole %
1	0.39	25	0.39	0.39	_	_	+	5	NA
2	50	50	>50	25	_	_	+	5	NA
3	50	50	>50	50	_	_	+	10	NA
4	25	12.5	3.125	50	_	_	+	>10	NA
5	0.78	25	3.125	50	_	_	+	10	NA
6	25	0.78	6.25	50	_	_	+	>10	NA
7	0.39	3.124	0.78	0.39	_	_	+	NA	1
8	25	12.5	6.25	50	_	_	+	NA	0.25

Keys:
1: *Staphylococcus aureus*, 2: *Bacillus subtilis,* 3: *Escherichia coil*, 4: *Salmonella typhi*, 5: *Klebsiella pneumonia*, 6: *Pseudomonas aeruginosa*, 7: *Tricophytum rubrum*, 8: *Candida albicans,* LCR: *Lantana camara* L. root, LCS: *Lantana camara* L. stem, LCL: *Lantana camara* L. leaves, LCF: *Lantana camara* L. flower.

Table 5: Minimum Bactericidal Concentration (MBC) and Minimum Fungicidal Concentration (MFC) of *Lantana camara* L. volatile oils

Isolates	LCRO %	LCSO %	LCLO %	LCFO %	Broth only	Broth and Oil	Broth and Microbe	Broth + Gentamicin µg/mL	Broth + Ketoconazole %
1	25	25	0.39	25	_	_	+	5	NA
2	50	>50	50	50	_	_	+	5	NA
3	>50	>50	50	50	_	_	+	10	NA
4	50	25	25	>50	_	_	+	>10	NA
5	6.26	50	25	>50	_	_	+	10	NA
6	50	50	50	>50	_	_	+	>10	NA
7	6.25	12.5	6.25	1.56	_	_	+	NA	1%
8	25	12.5	6.25	50	_	_	+	NA	5%

Keys:
1: *Staphylococcus aureus*, 2: *Bacillus subtilis,* 3: *Escherichia coil*, 4: *Salmonella typhi*, 5: *Klebsiella pneumonia*, 6: *Pseudomonas aeruginosa*, 7: *Tricophytum rubrum*, 8: *Candida albicans,* LCR: *Lantana camara* L. root, LCS: *Lantana camara* L. stem, LCL: *Lantana camara* L. leaves, LCF: *Lantana camara* L. flower.

4. Conclusion

The essential oils isolated from *Lantana camara* L. roots, stems, leaves and flowers varied in yield, chemical constituents and biological activity. Oxygenated monoterpenes, non-terpene derivatives, and sesquiterpenes predominate the volatile oils of *Lantana camara* L. The volatile oil of *Lantana camara* L. roots, stems, leaves and flowers showed hydroxyl radical scavenging activities. The essential oils further displayed moderate antimicrobial activities against all the bacteria and fungi tested. The presence of a diverse range of chemical constituents justifies the plant's numerous ethnomedicinal applications and may be responsible for the pharmacological effects observed in the study.

5. Acknowledgements

We acknowledge the Indian Institute of Integrative Medicine, Jammu where the gc-ms analysis of the volatile oils was carried out.

6. References

Bakchiche, B., Gherib, A., Bronze, M. R., & Ghareeb, M. A. (2019). Identification, Quantification, and Antioxidant Activity of Hydroalcoholic Extract of Artemisia campestris from Algeria. *Turkish Journal of Pharmaceutical Sciences*, *16*(2), 234–239. https://doi.org/10.4274/TJPS.GALENOS.2018.99267

Batish, D. R., Singh, H. P., Setia, N., Kaur, S., & Kohli, R. K. (2006). Chemical Composition and Inhibitory Activity of Essential Oil from Decaying Leaves of Eucalyptus Citriodora. *Zeitschrift Fur Naturforschung - Section C Journal of Biosciences*, *61*(1–2), 52–56.

British pharmacopoeia. (1998). In *British pharmacopoeia* (Vol. 2, p. 109). H.M.S.O.

Dafni, A., & Böck, B. (2019). Medicinal plants of the Bible - revisited. *Journal of Ethnobiology and Ethnomedicine*, *15*(1).

Falcão, S., Bacém, I., Igrejas, G., Rodrigues, P. J., Vilas-Boas, M., & Amaral, J. S. (2018). Chemical composition and antimicrobial activity of hydrodistilled oil from juniper berries. *Industrial Crops and Products*, *124*, 878–884.

Ghareeb, M. A., Habib, M. R., Mossalem, H. S., & Abdel-Aziz, M. S. (2018). Phytochemical analysis of Eucalyptus camaldulensis leaves extracts and testing its antimicrobial and schistosomicidal activities. *Bulletin of the National Research Centre*, *42*(1).

Ghareeb, M., Mohamed, T., Saad, A., Refahy, L. A. ., Sobeh, M., & Wink, M. (2018). HPLC-DAD-ESI-MS/MS analysis of fruits from Firmiana simplex (L.) and evaluation of their antioxidant and antigenotoxic properties. *Journal of Pharmacy and Pharmacology*, *70*, 133–142.

Ghisalberti, E. L. (2000). Lantana camara L. (Verbenaceae). *Fitoterapia*, *71*(5), 467–486.

Hazra, B., Biswas, S., & Mandal, N. (2008). Antioxidant and free radical scavenging activity of Spondias pinnata. *BMC Complementary and Alternative Medicine*, *8*, 63–73.

Junior, M. R. M., Silva, T. A. A. R. e., Franchi, G. C., Nowill, A., Pastore, G. M., & Hyslop, S. (2009). Antioxidant potential of aroma compounds obtained by limonene biotransformation of orange essential oil. *Food Chemistry*, *116*(1), 8–12.

Marcelo, D. A. P., Magalhães, R. M., Torres, D. M., Cavalcante, R. C., Mota, F. S. X., Coelho, E. M. A. O., Moreira, H. P., Lima, G. C., Da Costa Araújo, P. C., Cardoso, J. H. L., De Souza, A. N. C., & Diniz, L. R. L. (2015). Gastroprotective effect of alpha-pinene and its correlation with antiulcerogenic activity of essential oils obtained from Hyptis species. *Pharmacognosy Magazine*, *11*(41), 123–130.

Medeiros, L. B. P., Rocha, M. dos S., de Lima, S. G., de Sousa Júnior, G. R., Citó, A. M. da. G. L., da Silva, D., Lopes, J. A. D., Moura, D. J., Saffi, J., Mobin, M., & da Costa, J. G. M. (2012). Chemical constituents and evaluation of the cytotoxic and antifungal activity of Lantana camara essential oils. *Revista Brasileira de Farmacognosia*, *22*(6), 1259–1267.

Meira, C., Guimarães, E., Macedo, T., DaSilva, T. ., Menezes, L. R. ., Costa, E. ., & Soares, M. B. . (2015). Chemical composition of essential oils from Annona vepretorum Mart. and Annona squamosa L. (Annonaceae) leaves and their antimalarial and trypanocidal. *Journal of Essential Oil Research*, *27*(2), 160–168.

Nea, F., Tanoh, E. A., Yapi, T. A., Garcia, G., Tomi, F., & Tonzibo, Z. F. (2017). Chemical investigation on leaf, flower and fruit oils of lantana camara from Côte d'Ivoire. *Natural Product Communications*, *12*(4), 607–610.

Omoregie, E., Aliyu, I., Doris, E., Ehiabhi, O., & Folashade, K. (2016). Chemical Components of the Essential Oil of Lantana camara L. Found in North Central Sudan Region of Nigeria. *American Chemical Science Journal*, *12*(1), 1–7.

Quintans-Júnior, L., Moreira, J. C. F., Pasquali, M. A. B., Rabie, S. M. S., Pires, A. S., Schröder, R., Rabelo, T. K., Santos, J. P. A., Lima, P. S. S., Cavalcanti, S. C. H., Araújo, A. A. S., Quintans, J. S. S., & Gelain, D. P. (2013). Antinociceptive Activity and Redox Profile of the Monoterpenes (+)-Camphene, p-Cymene, and Geranyl Acetate in Experimental Models. *ISRN Toxicology*, *2013*, 1–12.

Saad, A. M., Mohammed, M. M. D., Ghareeb, M. A., Ahmed, W. S., & Farid, M. A. (2017). Chemical composition and antimicrobial activity of the essential oil of the leaves of Cupressus macrocarpa Hartweg. ex Gordon. *Journal of Applied Pharmaceutical Science*, *7*(9), 207–212.

Sarma, N., Begum, T., Pandey, S. K., Gogoi, R., Munda, S., & Lal, M. (2020). Chemical Profiling of Leaf Essential Oil of Lantana camara Linn. From North-East India. *Journal of Essential Oil-Bearing Plants*, *23*(5), 1035–1041.

Sharma, P., & Shrivastava, B. (2013). Phytochemical and Pharmacological profile of Lantana camara l: An Overview. *Journal of Advanced …*, *3*(4), 294–305.

Skaltsa, H. D., Demetzos, C., Lazari, D., & Sokovic, M. (2003). Essential oil analysis and antimicrobial activity of eight Stachys species from Greece. *Phytochemistry*, *64*(3), 743–752.

Sonibare, O. O., & Effiong, I. (2008). Antibacterial activity and cytotoxicity of essential oil of Lantana Camara L. leaves from Nigeria. *African Journal of Biotechnology*, *7*(15), 2618–2620.

Stachowiak, G., & Batchelor, A. (2014). Engineering Tribology 4th Ed. Elsevier Amsterdam, Netherland. In *Engineering Tribology* (pp. 59–119).

Zhu, F., Lu, W. H., Pan, J. H., Huang, M. Z., & Wu, J. S. (2013). Chemical composition and antibacterial activity of essential oils from the leaves, fruits and stems of Lantana camara L. from South China. *Advanced Materials Research*, *781–784*, 1060–1063.

Available online at www.asric.org
ASRIC Journal on Natural Sciences Vol 3(1) (2023) 132-144

Fermentation Enhances the Attenuation of Oxidative Stress by Sugar Apple Cotyledon Polysaccharides

Christianah Adebimpe Dare[1], Oluokun Oluboade Oyedapo[2]

[1]Department of Biochemistry, Osun State University, Osogbo, Nigeria
[2]Department of Biochemistry and Molecular Biology, Obafemi Awolowo University, Ile-Ife, Nigeria.

*Corresponding author: bimpeoasis@yahoo.com; Christianah.dare@uniosun.edu.ng,

Abstract
In this study, we extracted and optimised polysaccharides were extracted from the cotyledon of both fermented and unfermented *A. squamosa* (sugar apple) seeds. We aimed to evaluate the antioxidant and anti-inflammatory potentials of the purified polysaccharides as a measure of oxidative stress. **Methods:** We collected fresh and ripe sugar apple fruits were collected from an orchard at Ota-Efun, Olorunda Local Government, Osogbo, Nigeria and their identity was authenticated at IFE Herbarium, Department of Botany, Obafemi Awolowo, University, Ile-Ife, Nigeria. A portion of the seeds was fermented traditionally, and the rest were unfermented before the cotyledon was separated from the seed coat. Water-soluble polysaccharides extraction was carried out on the cotyledon according to standard methods. We evaluated the antioxidant and anti-inflammatory activities of the polysaccharides with different assay methods including DPPH-radical scavenging activity, reducing power, metal-chelating activity, and membrane stabilization. **Results:** Our findings provided scientific proof of the excellent antioxidant activities of the polysaccharides from fermented and unfermented cotyledon of *A. squamosa* seed, and data on their anti-inflammatory activity. These findings showed that fermentation enhanced the activities of the polysaccharides in the cotyledon. **Conclusions:** The polysaccharides from fermented and unfermented cotyledon of *A. squamosa* are potential therapeutic avenues for oxidative stress and related metabolic diseases.
Keywords: antioxidant; inflammation; free radical; phytochemical; medicinal plant

Introduction
Plants produce several chemical compounds (bioactive principles) that possess and exhibit biological activities, as well as provide defence against predators such as insects, fungi and anthophagous mammals (Petrakou et al., 2020). Phytochemicals elicit their impacts on humans through processes similar to those of the chemical compounds in conventional drugs; so, they are almost identical to conventional drugs as far as the mechanisms of action are concerned (Nanagulyan et al., 2020). Plants are used in a range of treatments for physical problems of the human body. Several orthodox medicines originate from plant sources, and many of the foremost effective medicines are primarily plant-based, such as painkillers derived from the stem bark of willow and poppy (Naik et al., 2019). Major bioactive principles (phenols, carbohydrates, flavonoids) in plants have been shown to have antioxidant and anti-inflammatory bioactivities and are used for the treatment of diseases throughout the world. Plant bioactive compounds' antioxidant activity is essential for eliminating free radicals, which are linked to practically all medical disorders. Some of these properties are antimicrobial (Chalestori et al., 2018), anti-cancer (Khan et al.,2019), anti-diabetic (El-Sayed et al., 2020), anti-atherosclerosis (Haydari et al., 2020), immunomodulatory (Ofokansi et al., 2018), and even nephron-protective or hepato-protective effects (Rafieian-Kopaei, 2012).

The biochemical change of the primary food matrix by fermentation is a beneficial process caused by microbes and their enzymes (Şanlier et al., 2019). Through fermentation, food is rendered safe by the detoxification of aflatoxin and the inhibition of pathogenic bacterial development resulting from lactic acid's antibacterial activity (Chaves-Lopez et al., 2014).

The fruit tree Annona squamosa has been used traditionally for a very long time. Different parts of sugar apple have been connected to a variety of traditional medicinal applications, such as those of a cool medicine, apophlegmatisant, tonic, abortifacient, and cardiac sedative. (Ahmed et al., 2019). Many phytochemicals and components, such as cyclopeptides (CPs), alkaloids (ALKs), annonaceous acetogenins (ACGs), diterpenes (DITs), and essential oil, have been found through extensive phytochemical assessments conducted on diverse parts of the sugar apple plant (Ma et al., 2017). By assessing the antioxidant and anti-inflammatory characteristics, this study revealed how fermentation improves the attenuation of oxidative stress by sugar apple cotyledon polysaccharides.

Methods

Harvesting and identifying fruits from Annona squamosa

From an orchard in Ota-Efun, Olorunda Local Government, Osogbo, Osun State, Nigeria (07^0 32′ 30.25″ N, 04^0 31′ 41.70″ E), mature, fresh, and delicious sugar apple fruits were gathered. The fruits were recognized and verified at the Obafemi Awolowo University's IFE Herbarium, Department of Botany, Ile-Ife, Nigeria, where the voucher number (IFE-17805) was acquired and the specimen copy was deposited.

Reagents and chemicals

For this investigation, analytical-grade chemicals and reagents were procured from diverse sources.

Sugar apple seed fermentation and processing

The A. squamosa seeds were taken out of the ripe, soft, mature fruits and placed into clean containers. The seeds were then separated into two portions. One portion was fermented according to a traditional method, which involved wrapping the seeds in banana leaves and putting them in a dark cupboard for five days. Afterwards, the seeds were washed and dried at 40 °C in an oven (Dare et al., 2013). After the pulp was removed from the second portion using clean water, the unfermented seeds were oven-dried at 40°C. Both the unfermented and fermented seeds' cotyledons were removed from the seed coat and ground separately in a Warring Blender. The powdered cotyledon samples were referred to as unfermented cotyledon (UC) and fermented cotyledon (FC), respectively. Following n-hexane defatting, 80% (v/v) ethanol was used to extract the powdered cotyledon samples for a full day in order to eliminate organic components. The leftover material was then allowed to air dry.

The making of the polysaccharides

The process used to prepare the FC and UC polysaccharides was based on the approach of Liu et al. (2012) approach, as shown in Dare et al. (2021). Cold water extraction of the defatted FC and UC was done with distilled water at 37 ℃ for 3 hours on a magnetic stirrer, and the residues of cold water polysaccharides extraction were extracted further at 85 ℃ for 3 hours. The hot and cold water extracts were pooled together and mixed thoroughly, and four volumes of cold absolute ethanol (95% v/v) was added. The mixture was kept at 4 ℃ for polysaccharide precipitation. After being tagged fermented and unfermented cotyledon polysaccharides, FCP and UCP respectively, the precipitates formed were kept in the refrigerator for additional examination.

High-performance chromatography (HPLC) analysis of the polysaccharides

The composition of the extracted polysaccharides was analyzed by the HPLC method (Yan et al., 2016). The precipitated polysaccharides were hydrolyzed with trifluoroacetic acid (TFA) at 120 ℃ for 6 hours in an ampoule. The hydrolyzates were centrifuged at 6000 rpm for 10 minutes after cooling, then the supernatants were evaporated to dryness under reduced pressure with absolute methanol. The dried sample was re-dissolved with 1 ml distilled water. The solution was derivatized with a methanol solution of 0.5 M 1-phenyl-3-methyl-5-pyrazolone (PMP). the supernatant was filtered through a 0.45 µm filter into an HPLC autosampler vial (12×32 mm, Sigma-Aldrich Co) for chemical determination. The supernatant was then analyzed with an Agilent 1260 HPLC system by injecting 20 µl of volume at a flow rate of 1.0 ml/min. The UV spectra were recorded in the range of 200–400 nm, and the diode-array detector (DAD) was set at 245nm. The chosen standard sugars (xylose, rhamnose, mannose, galactose, fructose, fucose, glucose, arabinose, glucuronic acid, galacturonic acid, alluronic acid, manuronic acid, galactosamine, fructosamine, glucosamine) derivatized and treated as the extracted polysaccharides.

Antioxidant assays

Estimation of total antioxidant capacity

The total antioxidant capacity (TAC) of *A. squamosa* polysaccharides (FCP and UCP) was spectrophotometrically evaluated using phosphomolybdenum assay as reported by Prieto et al. (1999). Essentially, 2.7 ml of phosphomolybdenum reagent (containing 28 mM $Na_3(PO_4)_2$ and 4 mM $(NH_4)_6Mo_7O_{24}$ in 0.6 M H_2SO_4) was mixed with 0.3 ml of a 1 mg/ml polysaccharide in capped test tubes. It was removed and given time to cool to ambient temperature after being incubated for 1.5 hours at 95 °C in a water bath. The absorbance was quantified at 695 nm with respect to the reagent blank. The whole antioxidant capacity was expressed in terms of ascorbic acid equivalents (mg AAE/g of the dry sample).

Measurement of DPPH radical scavenging efficacy

The radical scavenging efficacy of FCP and UCP against stable 1,1-diphenyl-2-picrylhydrazyl (DPPH) was evaluated using the protocol described by Bouhlali et al. (2015) with slight modifications. The reaction mixture contained 1 ml polysaccharide at varied concentrations (0, 3.125, 6.25, 12.5, 25, 50 µg/ ml) and 1 ml of DPPH in CH_3OH (0.3 mM). The combination was properly mixed by inversion and incubated in the dark chamber for 30 min. The absorbance of the chromophore produced was quantified at 517 nm against the reagent blank.

The percentage of DPPH inhibition was computed by applying the formula

Percentage inhibition $= \frac{Abs_{control} - Abs_{sample}}{Abs_{control}} \; x \; 100$

where $Abs_{control}$ is the absorbance without extract; Abs_{sample} is the absorbance of the polysaccharides or standard.

Evaluation of reducing power

The assay of the cotyledon's polysaccharides (FCP and UCP) reducing power to convert iron from Fe^{3+} to Fe^{2+} was conducted using Oyaizu's (1986) methodology. The reaction mixture contained 1.0 ml polysaccharides (0, 50, 100, 150, 200, 250, 300 µg/ ml) mixed with 2.5 ml (0.2 M PO_4 buffer, pH 6.6 and 2.5 ml of 1% (w/v) potassium ferricyanide $[K_3Fe(CN)_6]$. The mixtures were incubated at 50 ℃ for 20 minutes followed by the addition of 2.5 ml trichloroacetic acid (10% (w/v) to terminate the reaction. After giving the suspension a good shake, centrifugation was done for 10 minutes at the speed of 3000 rpm. The supernatant (2.5 ml) was combined with 2.5 ml of distilled water and 0.5 ml of 0.1% (w/v) $FeCl_3$. The absorbance of Perl's Prussian blue ferric-ferrous complex formed was read at 700 nm after 10 minutes against the reagent blank. Ascorbic acid of various concentrations as the polysaccharides was used as the standard. The absorbance which is a direct measurement of the reducing power of the extract and standard was plotted against their respective concentrations.

Assay of metal chelating activity of the polysaccharides

The assay protocol was carried out according to the protocol outlined by Dinis et al. (1994). Basically, 1 ml of the polysaccharides at different concentrations (0, 200, 400, 600, 800, and 1000 µg/ml) were added to 1 ml $FeSO_4$ (0.125 mM). A milliliter of ferrozine (0.3125 mM) was added to initiate the reaction, and it was thereafter let to sit at room temperature for ten minutes. The wavelength 562 nm was used to measure the absorbance. As a positive control, citric acid was handled similarly to the previously mentioned polysaccharides. The sample's ability to chelate ferrous ions in contrast with the control was determined from the equation

Percentage chelating effect (%) $= \frac{A_c - A_s}{A_c} \times 100$

where A_c is the absorbance of the control, A_s is the absorbance of the sample.

Assays of anti-inflammatory potentials/activities of *A. squamosa* polysaccharides

Collection and preparation of red blood cells (RBCs)

The protocol earlier described (Oyedapo et al., 2010) was used in the preparation of bovine red blood cells. Fresh bovine blood was collected from the abattoir into a clean bottle containing anti-coagulant (3.8% (w/v) tri-sodium citrate) in the ratio 2:1 (blood:anti-coagulant), mixed gently by inversion, and transported to the laboratory in ice-bucket. The blood sample was centrifuged for ten minutes at ambient temperature and 3000 rpm. After the packed red blood cell had been thoroughly cleaned in

fresh normal saline (0.85% (w/v) NaCl), the supernatant was carefully removed. Washing and centrifugation were repeatedly performed till the supernatant was clear. Bovine erythrocyte [2% (v/v)] was prepared by diluting 2 ml of packed cell with normal saline to 100 ml. This was kept undisturbed at 4 ℃ in the refrigerator to prevent lysis of the red blood cells.

Assay of red blood cell membrane stability

The red blood cell membrane stability assay was carried out according to a slightly modified procedure of Oyedapo et al. (2010). The assay mixture was composed of 0.5 ml of pH 7.4 0.15 M phosphate buffer and 1.0 ml of hyposaline (0.42% (w/v) NaCl) combined with pipetted, clean, and dry test tubes containing 1.0 ml of various concentrations of polysaccharides (0, 50, 100, 150, 200, 250, 300, and 350 µg/ml). The final volume was 3 ml after precisely 0.5 ml of 2% (v/v) erythrocyte was added. The combination underwent a 30-minute incubation time at 56 ℃. The tubes were withdrawn, allowed to cool, and then centrifuged at 3000 rpm for 10 minutes. After the supernatant was decanted, the absorbance at 560 nm was quantified in comparison to the blank. With the exclusion of erythrocytes, the pharmacological control experiment was carried out according to the identical protocol. The same procedure as previously mentioned was utilized to prepare the normal dosage of ibuprofen (0-350 µg/ml).

Percentage membrane stability by extract/drug = $100 - \left[\frac{Abs_{test} - Abs_{drug}}{Abs_{control} - Abs_{drug\ control}}\right] \times 100$

An assessment of the inhibition of albumin denaturation

An adaptation of the Chandra et al. (2012) protocol was utilized to measure albumin denaturation prevention. Briefly, 1 ml of 1% (w/v) bovine serum albumin prepared in PBS (0.1M phosphate-buffered saline, pH 6.4) was combined with 1 ml of varying concentrations (0, 50, 100, 150, 200, 250, 300, 350 µg/ml) of polysaccharides solutions. The turbidity of this mixture was quantified at 660 nm after it had been at ambient temperature for 20 minutes, heated to 70 °C for 5 minutes, and then cooled. For the control and standard, respectively, the identical process was performed with distilled water and Diclofenac.

The following formula was applied to determine the percentage inhibition (IP%) of protein denaturation:

Percentage Inhibition = $\frac{\mathrm{Abs_{control}} - \mathrm{Abs_{sample}}}{\mathrm{Abs_{control}}}$ X 100

$Abs_{control}$ is the absorbance without polysaccharide; Abs_{sample} is the absorbance of the mixture with polysaccharide or standard.

Statistical Analyses

Based on three or five measurements, the data were shown as Mean ± SEM. To contrast the means of the treatment and control groups, GraphPad Prism 5 was utilized to do a one-way ANOVA and Tukey multiple comparison test. When $p < 0.05$, differences were considered significant.

Results

The fermented cotyledon had a distinct nice smell and was brownish while the unfermented cotyledon didn't have a nice smell and had a darker color (Figs. 1a and b).

Figure 1: (a) Fermented Cotyledon, (b) Unfermented Cotyledon

Table 1 shows the yield of the purified polysaccharides represented as a percentage proportion of the initial material. Lower yields of polysaccharides were noted in the fermented cotyledon of A. squamosa compared to the unfermented cotyledon.

The components of the polysaccharides were analyzed chromatographically using HPLC (Appendices A to F). The HPLC investigations of the polysaccharides showed the existence of certain monosaccharides and derivatives of monosaccharides (pentoses, hexoses, uronic acids and hexosamines) in the polysaccharides at varying degrees as presented in Tables 2, 3, and 4. UCP could be noted as fructomannan and glucuronide and FCP as fructosan.

Table 1: Percentage Yield of Purified Polysaccharides

Sample	Weight of starting material (g)	Weight of yield (g)	Percentage Yield (%)
FCP	500	6.35 ± 0.35	1.27 ± 0.10
UCP	500	18.60 ± 1.53	3.72 ± 0.71

Every value indicated Mean ± SEM of n = 4 replicates
Two types of cotyledon polysaccharides: fermented (FCP) and unfermented (UCP)

Table 2: HPLC Analyses for Hexoses[a] and Pentoses[a]

Pentose and Hexose	UCP (%)	FCP (%)
D-Rhamnose	0.76	0.29
D-Mannose	-	32.00
D-Fructose	73.56	46.41
D-Fucose	15.54	4.05
D-Glucose	4.81	5.50
D-Galactose	-	3.27
D-Arabinose	-	5.69
D-Xylose	4.99	2.73

[a]: All standards used are of the D-isomer. Two types of cotyledon polysaccharides: fermented (FCP) and unfermented (UCP)

Table 3: HPLC Analyses for Hexosamines[a]

Hexosamine	UCP (%)	FCP (%)
D-Galactosamine	27.80	0.59
D-Fructosamine	34.81	5.25
D-Glucosamine	21.96	35.19

[a]: All standards used are of the D-isomer. Two types of cotyledon polysaccharides: fermented (FCP) and unfermented (UCP)

Table 4: HPLC Analyses for Uronic Acid

Uronic Acid	FCP (%)	UCP (%)
D-Mannuronic acid	51.82	2.23
D-Alluronic acid	-	0.13
D-Galacturonic acid	-	0.46
D-Glucuronic acids	43.88	89.42

[a]: All standards used are of the D-isomer. Two types of cotyledon polysaccharides: fermented (FCP) and unfermented (UCP)

Table 5: Total Antioxidant Capability

Polysaccharides	(mg Ascorbic Acid/g of the dry sample)
FCP	215.00 ± 15.00
UCP	105.00 ± 10.00[a]

Each value indicated Mean ± SEM of n = 3 measurements. The values with alphabet superscripts are statistically significant at $p < 0.05$, a compares FCP with UCP.
Two types of cotyledon polysaccharides: fermented (FCP) and unfermented (UCP)

Table 6: IC_{50} Values for DPPH Radical Scavenging Potential of the Polysaccharides

Sample	IC_{50} (µg/ml)
FCP	51.906 ± 1.401[a]
UCP	69.825 ± 8.973[a]
Ascorbic Acid	3.231 ± 0.210

Each value indicated Mean ± SEM of n = 3 measurements. The values with alphabet superscripts are statistically significant at $p < 0.05$, a compares Ascorbic acid with the rest, b compares FCP with the rest, and c compares UCP with the rest.

Two types of cotyledon polysaccharides: fermented (FCP) and unfermented (UCP)

Four models of antioxidants were utilized to study the polysaccharide antioxidant potentials: total antioxidant capacity, DPPH radical scavenging potential, reducing power, and metal chelating ability.

An overview of the polysaccharides' overall antioxidant capacity can be located in Table 5. The fermented cotyledon polysaccharide (FCP) was assessed to have a significantly ($p < 0.05$) higher capacity than the unfermented cotyledon polysaccharides (UCP) with regards to the total antioxidant capacity of the purified polysaccharides.

According to Fig. 2, the polysaccharides (FCP and UCP) and regular ascorbic acid had concentration-dependent patterns in their potential as DPPH radical scavengers. When the pure polysaccharides were tested at the greatest concentration (50.00 µg/ml), FCP demonstrated the highest percentage inhibition of the DPPH radical scavenging activity, followed by UCP. To measure the potency of the extract, one useful metric is the median inhibition concentration (IC_{50}), which is found in FCP at 51.91 ± 1.40 µg/ml and in UCP at 69.83 ± 8.97 µg/ml. Table 6 shows that IC_{50} is the quantity that results in about 50% inhibition.

Utilizing ascorbic acid as a reference, the polysaccharides' capacity to convert Fe^{3+} to Fe^{2+} was evaluated. As depicted in Fig. 3, the reducing potential of the polysaccharides and standard ascorbic acid increased with an increase in their quantities. This was shown as a function of the absorbance of the chromophore measured (green Fe^{2+}). The concentration-dependent reducing power showed standard ascorbic acid with the highest power with an absorbance range from 0.42 ± 0.02 to 1.63 ± 0.01 while FCP followed closely with an absorbance range from 0.30 ± 0.05 to 1.3 ± 0.10 at a concentration spectrum of 50 – 300 µg/ml.

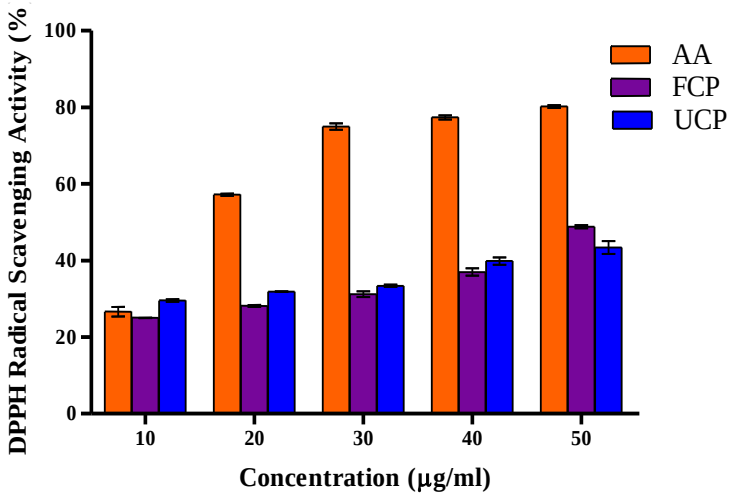

Figure 2: DPPH Radical Scavenging Capacity of the Polysaccharides and Standard Ascorbic Acid

Each value indicated Mean ± SEM of n = 3 replicates
AA = ascorbic acid, FCP = fermented cotyledon polysaccharides, UCP = unfermented cotyledon polysaccharides

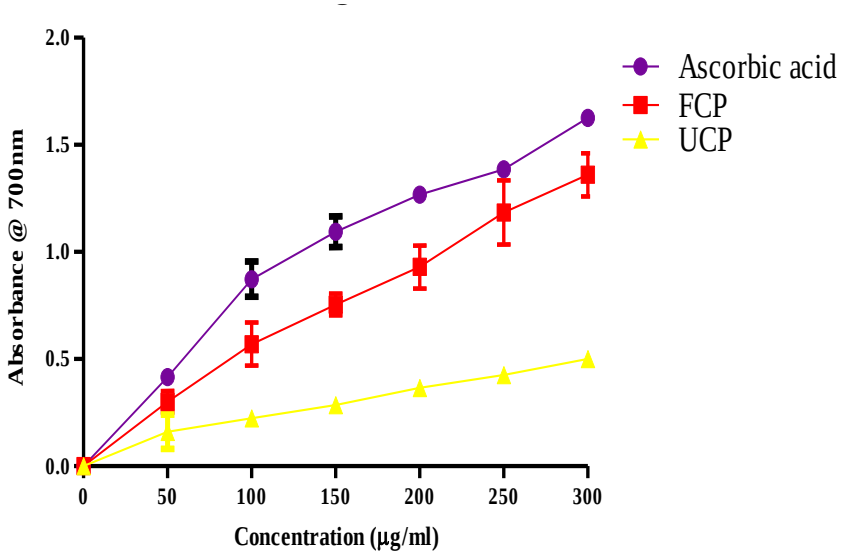

Figure 3: Reducing Power of the Polysaccharides and Standard Ascorbic Acid
Each value indicated Mean ± SEM of n = 3 replicates
FCP = fermented cotyledon polysaccharides, UCP = unfermented cotyledon polysaccharides

The evaluation of the polysaccharides' (FCP and UCP) metal-chelating properties revealed that both the polysaccharides and standard citric acid exhibited concentration-dependent action. In comparison to the normal citric acid employed, the polysaccharides possessed and showed higher metal chelating activities (Fig. 4). At the maximum concentration used (1000 µg/ml), UCP had the highest metal chelating activity (79.17 ± 1.69 %).

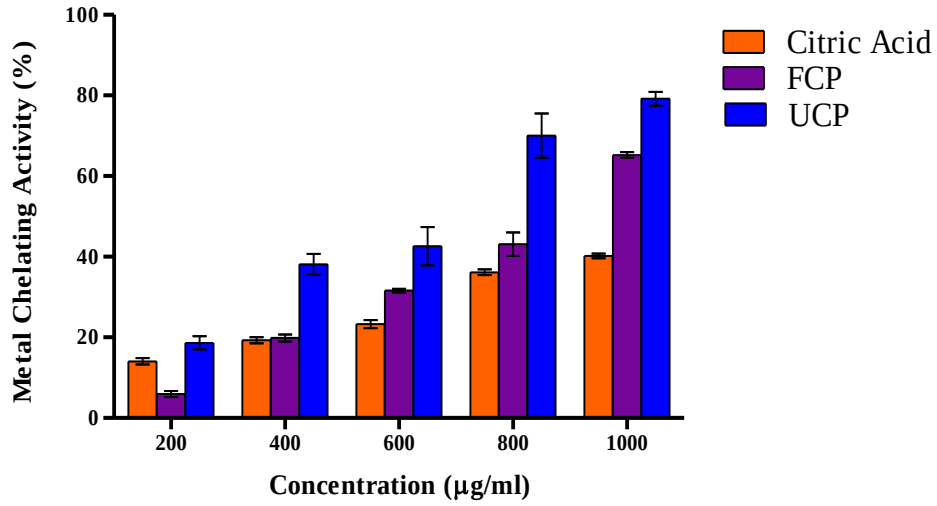

Figure 4: Metal Chelating Capability of the Polysaccharides and Standard Citric Acid
Each value indicated Mean ± SEM of n = 3 replicates
FCP = fermented cotyledon polysaccharides, UCP = unfermented cotyledon polysaccharides

The capacity of the polysaccharides to stabilize the RBC membrane when it was exposed to lyses generated by heat and hypotonicity was utilized to determine their membrane stabilizing activities. At nearly every concentration tested, it was found that the polysaccharides had an RBC membrane stabilizing power that was greater compared to that of the reference medication, ibuprofen. FCP minimum and maximum membrane stability power was 9.27 ± 1.16 to 73.43 ± 3.12 %, UCP 5.97 ± 0.18 to 65.39 ± 1.20 %, and ibuprofen (standard) 23.43 ± 2.90 to 43.73 ± 2.98 at a spectrum of concentration for 50 – 350 µg/ml. The polysaccharides exhibited a monophasic mode of protection

i.e., percentage stability is directly proportional to the concentration, while the reference medication, ibuprofen, exhibited a biphasic mode i.e., the drug protects the membrane at lower concentration and disrupts the membrane at higher concentration (Fig. 5).

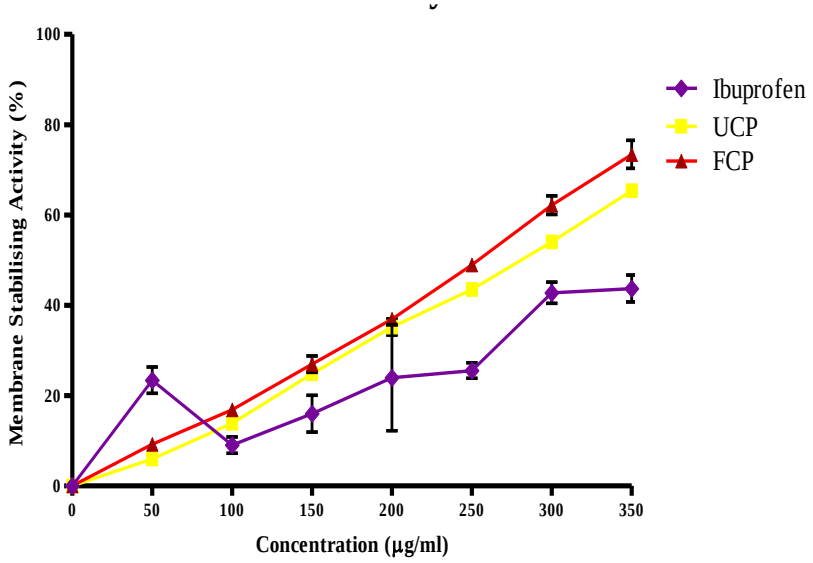

Figure 5: Membrane Stability Profile of the Polysaccharides and Ibuprofen (Standard)
Each value indicated Mean ± SEM of n = 3 replicates
FCP = fermented cotyledon polysaccharides, UCP = unfermented cotyledon polysaccharides

The polysaccharides' ability to prevent albumin from denaturing was observed to be concentration-dependent. FCP demonstrated the highest inhibition power (5.81 ± 0.60 to 45.01 ± 0.52 %) at the spectrum of concentration used (50 to 350 µg/ml) (Fig. 6). The standard diclofenac used exhibited a stronger inhibitory strength (12.53 ± 1.25 to 85.39 ± 2.72 %) than the two polysaccharides used at all the concentrations considered.

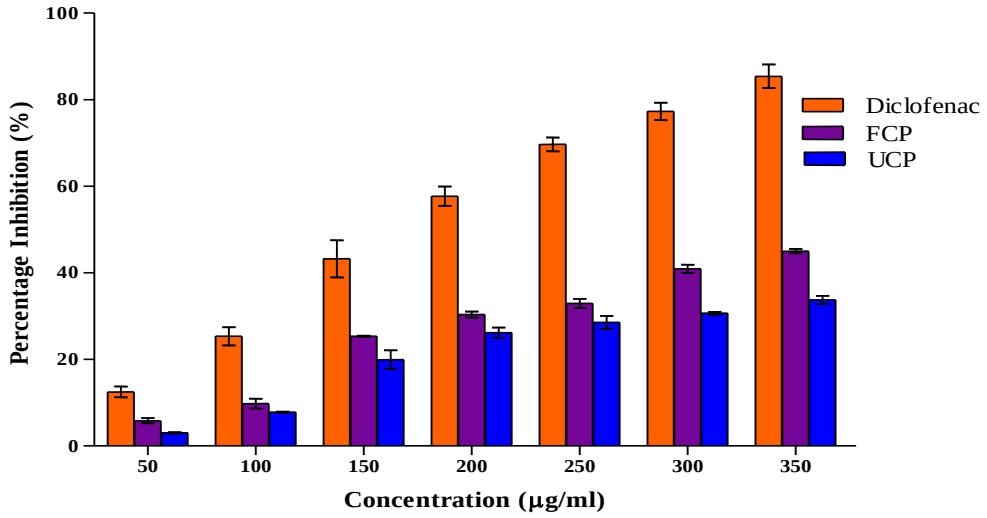

Figure 6: Albumin Denaturation Inhibition Potential of the Polysaccharides and Diclofenac (Standard)
Each value indicated Mean ± SEM of n = 3 replicates
FCP = fermented cotyledon polysaccharides, UCP = unfermented cotyledon polysaccharides

Discussion

Scientific investigations have proven that polysaccharides from varied sources possess pharmacological activities e.g., the immunostimulating activity of *Lycium barbarum* leaf

polysaccharides[15], treatment of type 2 diabetes by guava fruit polysaccharides (Jiao et al., 2017), and appreciable radical-scavenging properties exhibited by GCPB-1b polysaccharide isolated from Boshuzhi (Jiang et al., 2016).

According to certain research, varied naturally occurring polysaccharides have strong antioxidant properties that help protect against reactive oxygen species (ROS). ROS has the capacity to oxidize macromolecules like proteins, lipids, and nucleic acids, among other things, when they build up in vivo, according to research. These effects can impair regular cell functioning and lead to the progression of chronic illnesses (Alfadda and Sallam, 2012). Polysaccharides have anti-oxidant properties that allow them to scavenge free radicals, lessen oxidative cell damage, and protect cells. The antioxidant capacity of polysaccharides derived from varied sources, including bacteria, fungi, plants, algae, and animals, has been shown in the literature. These sources' polysaccharides can either trap free radicals or shield living things from oxidative damage (Zhang et al., 2013).

The polysaccharides from fermented cotyledon of *A. squamosa* had lower yields than the unfermented cotyledon, with UCP 193.5% higher than FCP. The higher yield in the unfermented cotyledon could be because of some metabolic activities which took place during fermentation. Examples of how starch is hydrolyzed during fermentation include the breakdown of complex sugars into simple sugars and eventually alcohol by the enzymes diastase, zymase, and invertase.

In comparison to the unfermented cotyledon, the fermented had considerably ($p < 0.05$) lower amounts of all the parameters measured by spectrophotometric measurement of the total soluble sugar, total uronic acids, and total hexosamines in the polysaccharides. There was an increase in total soluble sugar concentration, total hexosamines and total uronic acid concentration all in unfermented compared to the fermented. As fermentation has been shown to be accompanied by a rise in alpha-amylase and alpha-glucosidase activities, this could explain the rise in these components in unfermented compared to fermented (Kaczmarska et al., 2017). UCP may be identified as galactofucosan and FCP as galactomannan owing to the observed concentrations of their monosaccharides. Because of their high uronic acid content, the polysaccharides might potentially be classified as pectic polysaccharides.

The total antioxidant capacity of the purified polysaccharides revealed that the capacity of FCP was 32.31 % more than that of its seed coat counterpart (UCP) but the increase was insignificant ($p < 0.05$). The following four elements are thought to be a component of polysaccharide antioxidant processes. First, water is created when the hydrogen atoms in polysaccharides combine with free radicals. Second, polysaccharides bind metal ions, which are necessary for the generation of free radicals, or they trap free radicals generated in lipid processes. Thirdly, some antioxidant enzymes, such as superoxide dismutase, are activated more by polysaccharides. Fourthly, polysaccharides control the body's immune system, which has the unintended consequence of producing an antioxidant effect (Wang et al., 2020). Because of their antioxidant properties, the polysaccharides that were extracted for this study can effectively treat diseases including diabetes, hypertension, cancer, and others that are caused by free radicals.

At 50 µg/ml, the highest concentration employed, the fermented cotyledon polysaccharides (FCP) exhibited the lowest median inhibitory concentration (IC_{50}) and a higher % inhibition than its seed coat purified polysaccharides (UCP) when it came to DPPH radical scavenging activity. These findings are in alignment with earlier research on the ability of polysaccharides derived from plants to scavenge DPPH radicals. According to Luo et al. (2016), the water-soluble polysaccharides' carbonyl groups—which are the C=O of the glycosidic bond—have the ability to neutralize free radicals. In food preparation, FCP and UCP can therefore function as natural antioxidants and take the role of artificial antioxidants.

The concentration-dependent reducing power showed standard ascorbic acid with the highest power with an absorbance range from 0.42 ± 0.02 to 1.63 ± 0.01 while FCP followed closely with an absorbance range from 0.30 ± 0.05 to 1.3 ± 0.10 at concentration range of 50 – 300 µg/ml. The reducing capacity of a compound could be an indicator of its potential as an antioxidant (Sun et al., 2018). Antioxidants are popular as substances with the capability to prevent oxidation and enhance

reduction reactions. Free radicals have unpaired electrons in their outermost shell which makes them quite unstable and reactive in their quest to abstract electrons from other molecules in their environment in other to come to a stable state of paired electrons and complete outermost shell. When the refined polysaccharides interacted with free radicals, they changed into more stable products and stopped radical chain reactions. This behavior may be described as that associated with electron donors (reductants/antioxidants).

The assessment of the polysaccharides' (FCP and UCP) metal-chelating properties revealed that both the polysaccharides and regular citric acid exhibited concentration-dependent action. At the maximum concentration employed (1000 µg/ml), UCP showed the higher metal chelating capability (79.17 ± 1.69 %) among the polysaccharides. Both FCP and UCP had higher metal chelating power than the usual citric acid used. Because it lowers the quantity of the transition metal that speeds up lipid peroxidation, metal ion chelating ability is important. Therefore, because of their capability to chelate metals, it may be assumed that the extracted polysaccharides will likewise have the effect of inhibiting lipid peroxidation.

Inhibiting the release of phospholipases, which initiates the production of inflammatory mediators, is one way that the chemicals possessing membrane-stabilizing qualities have been observed to disrupt the initial stages of inflammatory reactions. A. squamosa seed polysaccharides may have a high potential to obstruct the release and/or function of intermediates such as histamine, serotonin, prostaglandins, and leukotrienes, among others. This was indicated by the observation made in this investigation.

Previous research has proven that activated neutrophils (polymorphonuclear cells or PMNs), eosinophils, monocytes, and macrophages produce ROS and lysosomal hydrolytic enzymes at sites of inflammation (de Visser et al., 2006). These two agents can initiate and maintain the preliminary phase of the inflammatory reaction. The membrane stabilization potential of the extracted polysaccharides has provided an additional mechanism for their anti-inflammatory effects showing that they may inhibit the release of lysosomal content of neutrophils at the inflammation site.

Owing to the high quantity of oxygen and hemoglobin within their cells, which can function as a potent catalyst for oxidative processes, erythrocytes are particularly vulnerable to oxidative damage. This is because their membranes are composed primarily of polyunsaturated fatty acids (PUFAs). By inhibiting the release of lytic enzymes and active inflammatory mediators, the polysaccharides may have stabilized the membrane of red blood cells. The polysaccharides demonstrated a concentration-dependent inhibition (monophasic) to achieve membrane stability, while the conventional ibuprofen demonstrated a biphasic mode of action.

The polysaccharides' ability to prevent albumin from denaturing was observed to be in a concentration-dependent manner. Between the two polysaccharides, within the concentration range tested (50 to 350 µg/ml), the fermented seed polysaccharide (FCP) showed the strongest inhibition power (5.81 ± 0.60 to 45.01 ± 0.52%). However, the standard diclofenac used exhibited a stronger inhibitory strength (12.53 ± 1.25 to 85.39 ± 2.72%) than the two polysaccharides used at all the concentrations considered (0, 50, 100, 150, 200, 250, and 350 µg/ml). It has been documented that a major cause of arthritic diseases and inflammation is the denaturation of tissue proteins (Elrayess et al., 2020).

Conclusion

While there is a wealth of information on the bioactivities of polysaccharides derived from different plants, nothing is known about how fermentation affects these bioactivities. The high antioxidant properties of the polysaccharides extracted from fermented and unfermented cotyledon of sugar apple seed were scientifically proven by this study's findings, by exploring many assay techniques like metal-chelating activity, reducing power, and DPPH-radical scavenging activity. Data regarding the anti-inflammatory properties of the A. squamosa seed's coat and cotyledon polysaccharides, both fermented and unfermented, were also supplied by this study. Summarily, fermented and unfermented A. squamosa cotyledon polysaccharides are excellent options for antioxidant agents to treat oxidative stress and the metabolic disorders it is associated with. In addition, the polysaccharides in A. squamosa's cotyledon became more active during fermentation.

Reference

Ahmed RHA, Mariod AA (2019). Annona squamosa: Phytochemical Constituents, Bioactive Compounds, Traditional and Medicinal Uses. In: Mariod A (eds) Wild fruits: composition, nutritional value and products. Springer Cham.

Alfadda, A. A., Sallam, R. M., 2012. Reactive Oxygen Species in Health and Disease, *BioMed Research International*, 2012: 1-14.

Bouhlali, E. D. T., Alem, C., Zegzouti, Y. F., 2016. Antioxidant and Anti-Hemolytic Activities of Phenolic Constituents of Six Moroccan Date Fruit (Phoenix dactylifera L.) Syrups, *Indian Journal of Biotechnology*, 12(1): 45-52.

Chandra, S., Chatterjee, P., Dey, P., Bhattacharya, S., 2012. Evaluation of In Vitro Anti-Inflammatory Activity of Coffee Against the Denaturation of Protein, *Asian Pacific Journal of Tropical Biomedicine*, 2(1): S178-S180.

Chaves-López, C., Serio, A., Grande-Tovar, C. D., Cuervo-Mulet, R., Delgado-Ospina, J., Paparella, A., 2014. Traditional Fermented Foods and Beverages From a Microbiological and Nutritional Perspective: the Colombian Heritage, *Comprehensive Reviews in Food Science and Food Safety*, 13(5): 1031-1048.

Dare, C. A., Onwumelu R. N., Oyedapo, O. O., 2013. Biochemical Studies on the Effects of Polyphenols from Fermented and Unfermented Acetone Extracts of Cocoa (Theobroma cacao L.) Seeds on Antioxidant Enzymes of Streptozotocin-Induced Diabetic Rats, *Nigerian Journal of Biochemistry and Molecular Biology*, 28(1-2): 44-58.

Dare, C. A., Oyedapo, O. O., Akinlalu, A. O., Komolafe, I. J., Fajobi, A. O., Ogunsusi, M., 2021. Genotoxic Activities of Polysaccharides from Cotyledon and Coat of Fermented and Unfermented Annona squamosa L. Seed, *Egyptian Academic Journal of Biological Sciences, H. Botany*, 12(1): 189-207.

De Visser, K. E., Eichten, A., Coussens, L. M., 2006. Paradoxical Roles of the Immune System During Cancer Development, *Nature Reviews Cancer*, 6(1): 24-37.

Dinis, T. C., Madeira, V. M., Almeida, L. M., 1994. Action of Phenolic Derivatives (Acetaminophen, Salicylate, and 5-Aminosalicylate) as Inhibitors of Membrane Lipid Peroxidation and as Peroxyl Radical Scavengers, *Archives of Biochemistry and Biophysics*, 315(1): 161-169.

Elrayess, R., Elgawish, M. S., Elewa, M., Nafie, M. S., Elhady, S. S., Yassen, A. S., 2020. Synthesis, 3D-QSAR, and Molecular Modeling Studies of Triazole Bearing Compounds as a Promising Scaffold for Cyclooxygenase-2 Inhibition, *Pharmaceuticals*, 13(11): 370-395.

Haydari, S., Nazari, A., Moghimian, M., Sedighi, M., Ghaderpour, S., 2020. Cardioprotective Activity of Ethanol Extract of Echinophora cinerea against Aluminium Phosphide Poisoning in Rats, *Journal of Food Biochemistry*, 44(8): e13300.

Jiang, J., Kong, F., Li, N., Zhang, D., Yan, C., Lv, H., 2016. Purification, Structural Characterization and In Vitro Antioxidant Activity of a Novel Polysaccharide from Boshuzhi, *Carbohydrate Polymers*, 147: 365-371.

Jiao, Y., Zhang, M., Wang, S., Yan, C., 2017. Consumption of Guava May Have Beneficial Effects in Type 2 Diabetes: A Bioactive Perspective, *International Journal of Biological Macromolecules*, 101: 543-552.

Kaczmarska, K. T., Chandra-Hioe, M. V., Zabaras, D., Frank, D., Arcot, J., 2017. Effect of Germination and Fermentation on Carbohydrate Composition of Australian Sweet Lupin and Soybean Seeds and Flours, *Journal of Agricultural and Food Chemistry*, 65(46): 10064-10073.

Khan, T., Ali, M., Khan, A., Nisar, P., Jan, S. A., Afridi, S., Shinwari, Z. K., 2019. Anticancer Plants: A Review of the Active Phytochemicals, Applications in Animal Models, and Regulatory Aspects, *Biomolecules*, 10(1): 47-76.

Kotb El-Sayed, M. I., Al-Massarani, S., El Gamal, A., El-Shaibany, A., Al-Mahbashi, H. M., 2020. Mechanism of Antidiabetic Effects of Plicosepalus acaciae Flower in Streptozotocin-Induced Type 2 Diabetic Rats, as Complementary and Alternative Therapy, *BMC Complementary Medicine and Therapies*, 20(1): 1-15.

Koyanatsu Shu. (1986). Research on browning substances. Antioxidant properties of glucosamine browning substances. Journal of Nutrition, 44 (6), 307-315.

Liu, H., Fan, Y., Wang, W., Liu, N., Zhang, H., Zhu, Z., Liu, A., 2012. Polysaccharides from Lycium barbarum Leaves: Isolation, Characterization and Splenocyte Proliferation Activity, *International Journal of Biological Macromolecules*, 51(4): 417-422.

Luo, Q. L., Tang, Z. H., Zhang, X. F., Zhong, Y. H., Yao, S. Z., Wang, L. S., Lin, C. W., Luo, X., 2016. Chemical Properties and Antioxidant Activity of a Water-Soluble Polysaccharide from Dendrobium officinale. *International Journal of Biological Macromolecules*, 89: 219-227.

Ma, C., Chen, Y., Chen, J., Li, X., Chen, Y., 2017. A review on Annona squamosa L.: Phytochemicals and Biological Activities, *The American Journal of Chinese Medicine*, 45(05): 933-964.

Naik, R., Doddamani, S. H., Rao, V. R., Shiddamallayya, N., Dixit, A. K., Rath, C., Mangal, A. K., 2019. Documentation of Local Health Traditions of Yadgir District, Karnataka, *Journal of Drug Research in Ayurvedic Sciences*, 4(3): 119-125.

Nanagulyan, S., Zakaryan, N., Kartashyan, N., Piwowarczyk, R., Łuczaj, Ł., 2020. Wild Plants and Fungi Sold in the Markets of Yerevan (Armenia), *Journal of Ethnobiology and Ethnomedicine*, 16: 1-27.

Ofokansi, M. N., Nworu, C. S., Akunne, T. C., Agbo, M. O., Akah, P. A., 2018. Immunomodulatory Effects of Phyllanthus muellerianus: A Mechanistic Approach, *Journal of Clinical and Cellular Immunology*, 9(5): 1-7.

Oyaizu, M., 1986. Studies on Products of Browning Reaction Prepared from Glucosamine, Japan Journal of Nutrition, 44: 307-315.

Oyedapo, O. O., Akinpelu, B. A., Akinwunmi, K. F., Adeyinka, M. O., Sipeolu, F. O., 2010. Red Blood Cell Membrane Stabilizing Potentials of Extracts of Lantana Camara and its Fractions, *International Journal of Plant Physiology and Biochemistry*, 2(4): 46-51.

Petrakou, K., Iatrou, G., Lamari, F. N., 2020. Ethnopharmacological survey of medicinal plants traded in herbal markets in the Peloponnisos, Greece, *Journal of Herbal Medicine*, 19: 100305-100315.

Prieto, P., Pineda, M., Aguilar, M., 1999. Spectrophotometric Quantitation Of Antioxidant Capacity Through the Formation of a Phosphomolybdenum Complex: Specific Application to the Determination of Vitamin E, *Analytical Biochemistry*, 269(2): 337-341.

Rafieia-Kopaei, M., 2011. Medicinal Plants and the Human Needs, *Journal of Biology*, 35: 635-639.

Şanlier, N., Gökcen, B. B., Sezgin, A. C., 2019. Health Benefits of Fermented Foods, *Critical Reviews in Food Science and Nutrition*, 59(3): 506-527.

Sharafati Chaleshtori, F., Saholi, M., Sharafati Chaleshtori, R., 2018. Chemical Composition, Antioxidant and Antibacterial Activity of Bunium persicum, Eucalyptus globulus, and Rose Water On Multidrug-Resistant Listeria Species, *Journal of Evidence-Based Integrative Medicine*, 23: 1-7.

Sun, X. Y., Wang, J. M., Ouyang, J. M., Kuang, L., 2018. Antioxidant Activities and Repair Effects on Oxidatively Damaged Hk-2 Cells of Tea Polysaccharides with Different Molecular Weights, *Oxidative Medicine and Cellular Longevity*, 2018: 1-17.

Wang, Y., Shen, X., Liu, D., 2020. Progress on Biological Activities of Polysaccharides: A Review, *The Pharmaceutical and Chemical Journal*, 7(2): 116-124.

Yan, J., Shi, S., Wang, H., Liu, R., Li, N., Chen, Y., Wang, S., 2016. Neutral Monosaccharide Composition Analysis of Plant-Derived Oligo- and Polysaccharides by High Performance Liquid Chromatography, *Carbohydrate Polymers*, 136: 1273-1280.

Zhang, C. Y., Kong, T., Wu, W. H., Lan, M. B., 2013. The Protection of Polysaccharide from the Brown Seaweed Sargassum graminifolium Against Ethylene Glycol-Induced Mitochondrial Damage, *Marine Drugs*, 11(3): 870-880.

Appendices

Appendix A: Monosaccharides HPLC Chromatogram for UCP

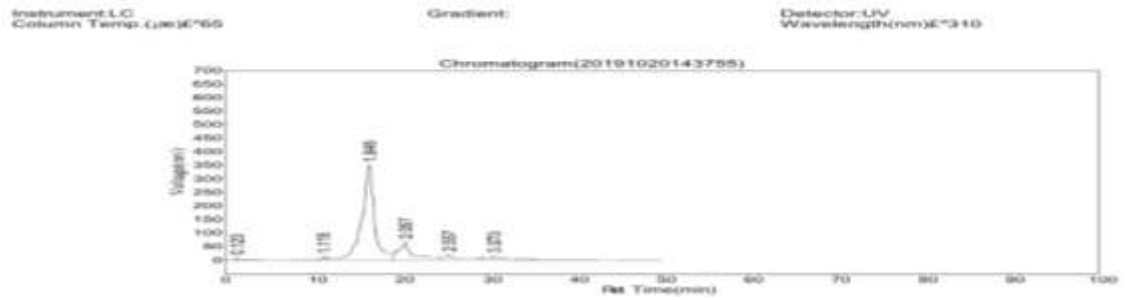

Appendix B: Monosaccharides HPLC Chromatogram for FCP

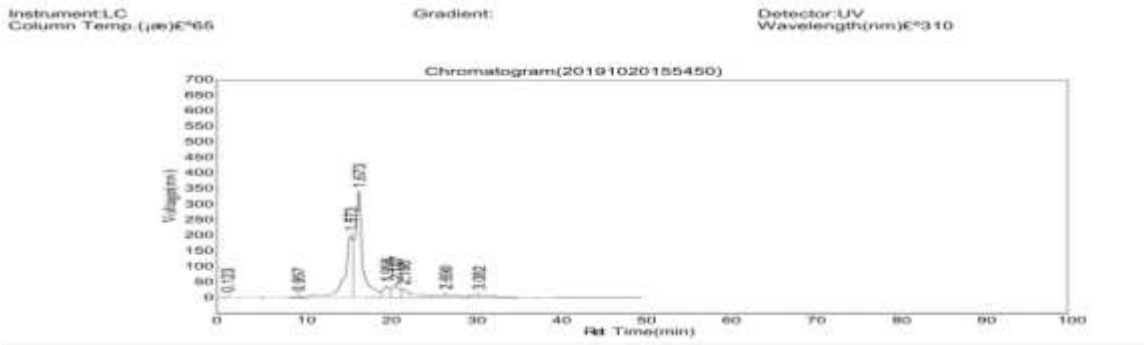

Appendix C: Uronic Acids HPLC Chromatogram for UCP

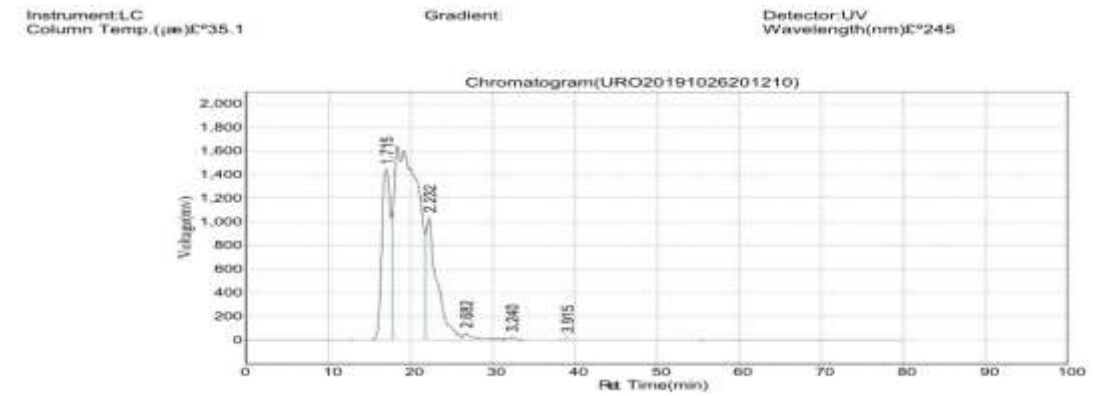

Appendix D: Uronic Acids HPLC Chromatogram for FCP

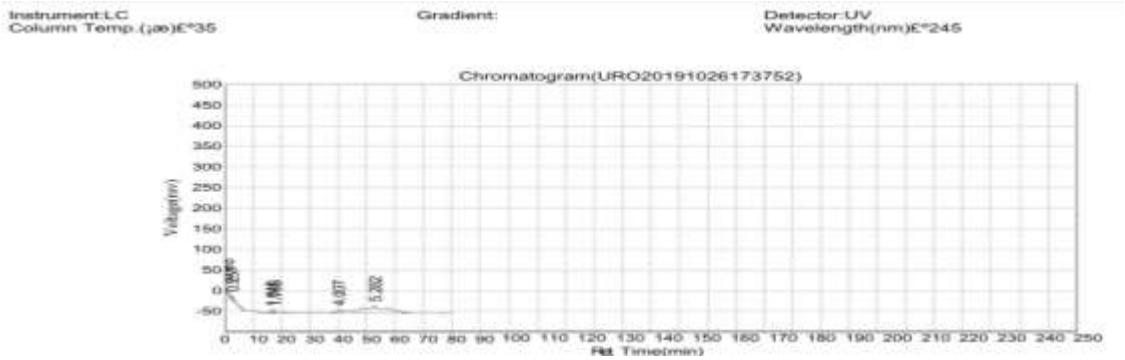

Appendix E: Hexosamines HPLC Chromatogram for UCP

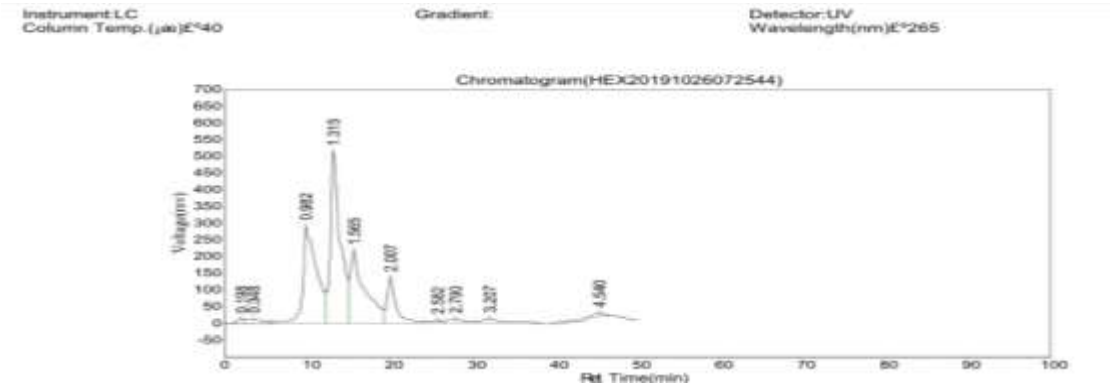

Appendix F: Hexosamines HPLC Chromatogram for FCP

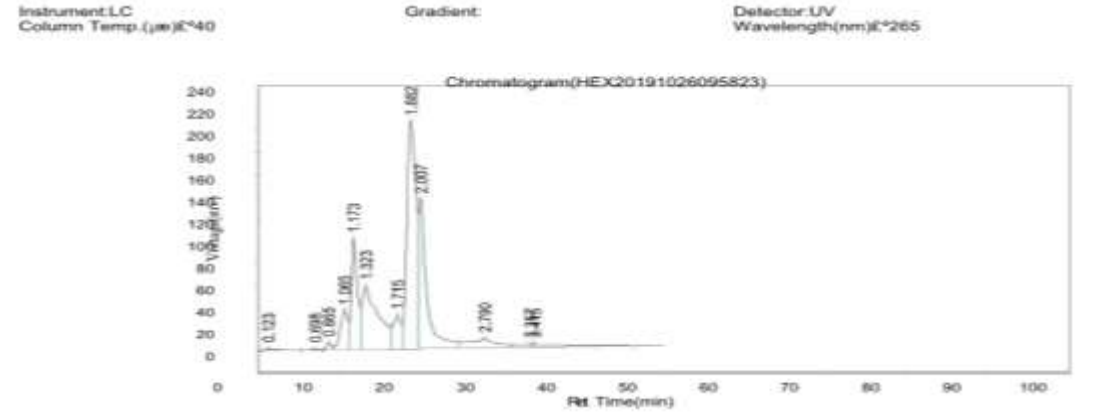

Available online at www.asric.org
ASRIC Journal on Natural Sciences Vol 3(1) (2023) 145-162

Cytotoxic Evaluation of the Aqueous Extract of some Selected Medicinal Plants Combinations on Lung Carcinoma Epithelial Cells A549 and Human Cervix Carcinoma HeLa S330194

Tossou Sandra Bénédicta Kadoukpè [1,3]*, Luka Carrol Domkat[1], Emmanuel Adeyemi[2], Jeffrey Matthew[2], Taiwo Emmanuel Alemika[3,4]

[1]Department of Biochemistry, University of Jos, Jos, Nigeria.
[2]Nigeria Institute of Medical Research (NIMR), Nigeria.
[3]Africa Centre of Excellence in Phytomedicine Research and Development (ACEPRD), University of Jos, Jos, Nigeria.
[4]Department of Pharmaceutical and Medicinal Chemistry, University of Jos, Jos, Nigeria.

*Corresponding author: tossousandra001@gmail.com

Abstract

Many are the anti-cancer drugs currently in use but unfortunately, they fail to differentiate cancer cells from healthy cells. The aim of this study is to find an alternative way based only on medicinal plants to treat cancer by enhancing the immune system without damaging the healthy cells for the well-being of the patient. This study investigated the cytotoxic effect(s) of (04) Combined Plants Aqueous Extracts (CPAE) made of some selected medicinal plants: *Annona muricata* (leave), *Moringa oleifera* (leave), *Ocimum gratissimum* (leave and stem), *Curcuma longa* (rhizome) *and Zingiber officinalis* (rhizome) on two human cancer cell lines, lung carcinoma epithelial cells A549 and human cervix carcinoma HeLa S330194. The extracts were named Alpha, Beta, Gamma and Lambda. Cytotoxic assay with WST-1 reagent, Cell cycle analysis and Apoptosis DNA fragmentation assay were carried out after 48h of treatment against a negative control (culture medium) and positive controls (Camptothecin and Etoposide). The findings revealed that the CPAE activated programmed cell death coupled with cell cycle arrest at G_0/G1 phases which resulted into cell growth inhibition with the best IC50 value of 107µg/mL for Gamma extract on A549 cell lines. Further studies are needed to elucidate the mechanism of action of the CPAE.

Keywords: CPAE, Camptothecin, Etoposide, Cancer cell lines, A549, HeLa S330194.

1.0 Introduction

Cancer is a major public health problem worldwide and is the second leading cause of death (WHO, 2022). Worldwide new cancer cases are either lung cancer or female breast, in 2020, about 2.1 million new cancer cases are reported for each of them, representing about 11.6% of the total cancer incidence burden (WHO, 2022; IARC, 2018).

Second most common cancer worldwide, lung cancer revealed to be the most common cause of cancer death in both sexes and it represents 25% of all cancer diagnoses worldwide (WHO, 2018). In 2012, out of 1.8 million affected people, worldwide lung cancer report was about 1.6 million deaths and the number of new cases has increased to more than 2.2 million new cases in 2020 (WCRFI, 2022). Based on histology, Small Cell Lung Cancer (SCLC) and Non -Small Cell Lung Cancer (NSCLC) are the two major types of lung cancer that are recognized (Kumar et al., 2013) out of the three identified types (Lu *et al*., 2010). The third one is a combination of small cell and large cell cancer with their different characteristics. NSCLC type represents 85 - 90% of all lung cancers and having adenocarcinoma, squamous-cell carcinoma and large cell carcinoma as subtypes (Murtaza et al., 2016). Adenocarcinoma is the most diagnosed in non-smokers and the most common histologic type of lung cancer (Travis et al., 2011). Adenocarcinoma represents 40% of lung cancers (Lu et al., 2010).

Cervical cancer is one of the most common causes of death for women in low-and middle- income countries (Adams et al., 2001; Lehtinen *et al*., 2001; Tyring 2000). In the previous estimates for 2008, cervical cancer still ranked as the third most frequent malignant tumour, accounting for 8.7% of all cancers in women (excluding non-melanoma skin cancers), but dropped to fourth ranking in 2018 till date, with 604 000 new cases in 2020 (WHO, 2022).

To overcome cancer, the current treatments recommended are chemotherapy, surgery and radiotherapy. The most common is chemotherapy but the side effects due to the neurotoxicity of using drugs remains a big challenge for worldwide researchers (Pabla and Dong, 2008). Aside the neurotoxicity and the resistance of the cancer cell to the treatment, there are two major problems in cancer treatment, the high cost of the treatment and then the side effects of the therapy drugs that seriously affect the patient's health.

The well-being of cancer patient has become a priority while treating the cancer (Williams *et al*., 2020; Niedzwiedz et al., 2019; Marta et al., 2014; Tariman et al., 2014). The efficiency of any cancer treatment depends on so many variables but the most important aspect is the immune system of the patient (Coventry and Henneberg, 2015; Markman and Shiao, 2015; Zitvogel et al., 2008). Researches have shown that cancer occurs when the immune system fails in eliminating cells with corrupted DNA (Moon et al., 2023; Hiam-Galvez et al., 2021; Gonzalez et al., 2018; Shurin, 2012). That failure can be genetic (Cheong and Nagel, 2022; Sigal and Oded, 2022) or triggered by cancerous cells that have the ability to suppress the immune system and turn it against the host to accelerate their own growth and spread (Kim and Cho, 2022; Saha et al., 2022).

Medicinal plants are used to treat cancer and to control the symptoms with less side effects (Amirghofran et al., 2011). The use of medicinal plants help in strengthening the immune system due to the presence of some chemical compounds that have specific effects on the human body (Alhazmi et al., 2021; Prasathkumar et al., 2021; Sofowora and Onayade, 2013). In cancer case, so many researches are going on to find a new plant-based alternative by using medicinal plants extract (Dehelean et al., 2021; Brianna et al., 2020; Cragg and Pezzuto, 2016). A lot of results have been already reported and promising anti-cancer agents have been explored from natural products (Gahtori et al., 2023; Siddiqui et al, 2022; Hashem et al., 2022; Usman et al., 2022; Ohiagu et al., 2021; Greenwell and Rahman, 2015; Wang and Jiang, 2012, Desai et al., 2008). With further specific studies, these new anti-cancer agents may become a potential alternative or be used in combination with any other cancer treatment to improve the success of the therapy as suggested by many cancer researchers (Cheon and Ko, 2022; Correia, Gärtner and Vale, 2021; Debela et al., 2021; Bayat et al., 2017). Even though the combination of natural compounds with chemotherapy is not encouraged due to the negative effect of chemical molecules interactions (Chan et al., 2023; Fasinu and Rapp, 2019), they remain the best alternative to overcome cancer (Okem et al., 2023; Huang, Lu, and Ding, 2021; Choudhari et al., 2020; Ijaz et al., 2018; Levitsky and Dembitsky, 2015).

According to previous researches, the following plants were reported to have anti-cancer properties and anti-inflammatory properties due to their different metabolites.

Annona muricata (Annonaceae). Recent studies have proved the pharmacological activity of *A. muricata* such as selective cytotoxicity to tumoral cells (Rady et al., 2018; Moghadamtousi et al., 2015) and anti – inflammatory properties (Ishola et al., 2014).

Occimum gratissimum (Lamiaceae). It is reported that *Occimum gratissimum* used to treat different diseases such as upper respiratory tract infections (Adebolu and Salau, 2005) and the whole plant has been used to experiment its anti-inflammatory activity (Oboh, 2006).

Curcuma longa (Zingiberaceae). It has anti-inflammatory potential (Jurenka, 2009; Farombi et al., 2007). The curcumin present in *Curcuma longa* exhibits immune-modulatory effect and has also chemopreventive potential (Sa et al., 2010). *Curcuma longa* inhibits proliferation and interferes with cell cycle progression (Avni et al., 2008). *Moringa oleifera* (Moringaceae). Ezeamuzie et al. (2008) and Sulaiman et al. (2008) reported the anti – inflammatory property of *Moringa oleifera*. It was found that it has also anti-cancer properties (Ahmed et al., 2017; Al-Asmari et al., 2015).

Zingiber officinalis (Zingiberaceae). Several studies claimed the antioxidant, anti-cancer, anti-inflammatory properties of ginger (Shafina et al., 2008). It is one of the best to reduce inflammatory eicosanoids (Tripathi, 2007; Kiuchi et al., 1992).

The aim of this study is to investigate the cytotoxic effect(s) of the aqueous extracts of different combinations made of these anti-cancer medicinal plants on lung adenocarcinoma (A549) and Cervical adenocarcinoma (HeLa S330194) cell lines.

2.0 Methods, techniques, studied material and area descriptions

2.1 Plant material

Annona muricata, Moringa oleifera, Occimum gratissimum, Curcuma longa and *Zingiber officinalis* plants were collected in Jos in Nigeria, February 2019. The plants were identified and authenticated in the Department of Plant Science and Technology, University of Jos, Jos. A voucher number was given to each of the plant's specimen and kept at the herbarium of the Department. The selected parts of the plants were air dried at room temperature for four weeks - *Annona muricata* (leaves), *Moringa oleifera* (leave), *Occimum gratissimum* (leave and stem), *Curcuma longa* (rhizome) *and Zingiber officinalis* (rhizome). The dried parts were then pounded using local pestle and mortar to reduce them into powder. Each plant powder was sieved to obtain a fine powder for the extraction.

2.3 Extraction

The combinations were used for the extraction using distilled water. On one side each of the leave powder was mixed with the two rhizomes powder in a ration of 4:3:3 named Alpha, Gamma and Lambda while on another side, all of the five plants powder were mixed together in a ratio of 2:2:2:2:2 named Beta. The combination powder (300 g) was weighed and mixed with 500 ml of distilled water and submitted to a decoction during 15 minutes followed by an overnight's maceration. The mixture was filtered using white cloth, the filtrate was dried in oven at a temperature of *80°C* and put in sterile container for further use.

2.4 Cancer cell lines stock and culture

Lung adenocarcinoma cell lines A549 and HeLa S330194 cell lines aging 27 days used in this study were kindly donated by Nigerian Institute of Medical Research (NIMR) of Yaba, Lagos (Nigeria). The cell lines were cultured in Dulbecco's Modified Eagle Medium (DMEM) containing 10% foetal bovine serum and 2mM L-glutamine incubated at *37°C*, 5% CO_2, 95% air and 100% relative humidity for 24 hours prior to addition of experimental drugs. All the cell lines used were cultured in enriched medium under the same conditions of temperature and pressure. Before and during the experiment, the cell lines were kept in the incubator at 37°C in the medium which was renewed each forty-eight hours (48 hours). After culturing sufficient number of cells, cytotoxic effect, cell cycle analysis and DNA Fragmentation were carried out after 48 hours of the aqueous extract treatment. The culture was carried out according to Cooper et al., (2016) with few modifications.

2.5 Cytotoxic assay

The cytotoxic effect of the aqueous extracts applied on A549 cell lines was studied by 48h cytotoxicity assay (ab155902 WST-1 Cell Proliferation Reagent) according to Leticia, 2014 method with a slight modification. Briefly, $5x10^4 – 5x10^5$ cells/well were cultivated in a 96 well microtiter plates. After 24 h incubation in 37℃ with humidified atmosphere containing 5% CO_2, cells were treated with serial concentrations of aqueous extract of the 4 combinations (1 mg/ml to 10^{-7} mg/ml) for 48h. In another 96 well microtiter plate, cells which received only 100 µL of culture medium served as negative control and the ones that received 100 µL of camptothecin served as positive control. After compound addition, plates were incubated at standard conditions for 48 hours and the assay was terminated by the addition of 10 µL WST-1 reagent to each well, a fixation agent. Cells were incubated for 60 minutes at *37°C*. After 1 hour, the plate was shacked for 1 minute on a shaker to mix contents. The absorbance's measure of control (untreated) and treated samples was read on a microplate reader at OD = 420 – 480 nm wave length with 650 nm as reference wavelength. Percent growth was calculated on a plate-by-plate basis for test wells relative to control wells. Data analysis was done as follows by averaging the duplicate reading that is the corrected absorbance. The percentage cytotoxicity was calculated by using the corrected absorbance to Leticia, (2014) method.

$$\%\ Cytotoxicity\ = \left(\frac{control - sample}{control}\right)\ x\ 100.$$

2.6 Cell Cycle Analysis

The procedure was carried out according to the method of Darzynkiewicz and Juan, (2001) with some modifications. Flow cytometric analysis of apoptosis and cell cycle distribution in A549 and Hela cell lines were measured after 48h of treatment with 10 µL of the CPAE at the concentration of 1 µg/mL, 10 µg/mL and 100 µg/mL. The cells for apoptosis analysis was harvested, washed twice with ice-cold PBS, and then resuspended cold PBS. 2 x 10^6 cells were suspended in 1 mL ice cold buffer. The cell fixation started by washing the cells by centrifugation at 200 x g for 5 minutes at *4°C* in phosphate buffered saline (PBS) without Ca^{2+} or $Mg^{2+.}$ The staining step started by washing the cells with cold PBS. The cells formed a diffuse ring – shaped pellet and then they were centrifuged longer at 200 x g for 10 minutes at *4°C*. The cells were resuspended in a solution composed of 300 – 500 µL of PI/Triton X-100 staining solution to 10 mL of 0.1% (v/v) of Triton X-100 (Sigma) in PBS, and 2 mg of DNAse-free RNAse A (Sigma) and 0.40 mL of 500 µg/mL of PI (Roche) were added. A freshly stock solution of PI was prepared by dissolving 1 mg of Propidium Iodine (PI) in 2 ml water and incubated at *37°C* for 30 minutes at 20°C. The tubes were stored at 4°C protected from light. The data was acquired on flow cytometer within 48 hours, PI+ cells were considered as late apoptotic or necrotic while PI- cells as early apoptotic.

2.7 Apoptotic DNA fragmentation Assay

The DNA fragmentation assay was carried out using Hela cell lines. After 24h of treatment, the cells were harvested. Cells and pellet cells were lysed in 0.5 mL detergent buffer composed of 10 mM Tris (pH 7.4), 5 mM EDTA, 0.2% Triton. The mixing was vortexed and incubated on ice for 30 minutes; and then was centrifuged at 27,000 x *g* for 30 minutes and the supernatant was divided into two 250 µL aliquots. 50 µL ice-cold, 5 M NaCl were added to each aliquot and vortexed. The DNA was precipitated using 600 µL of ethanol and 150 µL of 3 M sodium acetate by addition at pH 5.2 by pipetting up and down. The tubes were incubated at *-80°C* for 1 h and centrifuged 20,000 x *g* for 20 minutes. The DNA extracts were pooled together by re-dissolving the pellets in a total of 400 µL extraction buffer (10 mM Tris and 5 mM EDTA). 2 µL of 10 mg/mL DNase-free RNase were added to the new mixing and incubated for 5 h at *37°C*. 25 µL of proteinase K at 20 mg/mL and 40 µL of buffer (100 mM Tris pH 8.0, 100 mM EDTA, 250 mM NaCl were added and incubated overnight at 65°C. The DNA ladder was extracted with phenol/chloroform/isoamyl alcohol (25:24:1) and precipitated with ethanol. DNA was loaded in agarose gel, the pellet was air-dried and resuspended in 20 µL Tris-acetate EDTA buffer supplemented with 2 µL of sample buffer (0.25% bromophenol blue, 30% glycerol). The DNA ladders were separated electrophoretically on a 2% agarose gel containing 1 µg/mL ethidium bromide and visualize by ultraviolet transillumination. The gel was run at a lower voltage for a longer time than normally to avoid overhearling and subsequent deformation of DNA bands (data available on https://docs.abcam.com/pdf/protocols/apoptosis-dna-fragmentation-analysis-protocol.pdf).

2.8 Statistical Analysis

Data were analysed using GraphPad Prism 6. Two-way ANOVA followed by multiple comparison were used to determine the statistical difference between treated groups and negative controls. Differences were considered statistically significant for values, $^{***}P < 0.0001$.

3.0 Results

3.1 Cytotoxic assay

The data of the cytotoxicity assay with WST-1 reagent showed that each of the combined plants extract exhibited a significant anti-proliferative activity as expected when compared to the negative control. The inhibitory concentration that killed half of the cancer cell population (IC_{50}) values revealed that Gamma extract exhibited the highest inhibition effect compared to the remaining extracts vis-à-vis the positive control (Table 1).

Table 1: Cytotoxicity assay with WST-1 reagent showing the inhibition of cell viability by the aqueous extract of the plant's combinations on A549 cell lines.

Sample	Concentration (mg/mL)	% Growth Inhibition			Mean±SEM	IC_{50} (mg/mL)
		V1	V2	V3		
Negative Control	-	-1.098	-3.486	4.537	-	-
	1	12.607450	10.506210	12.655210	11.92 ± 0.709	
	0.1	18.481370	14.613180	13.705830	15.60 ± 1.464	
	0.01	17.048710	23.113660	16.905440	19.02 ± 2.046****	
	0.001	9.933143	6.303725	9.933143	8.72 ± 1.210	5.19
	0.0001	20.773640	20.057310	20.773640	20.53 ± 0.239****	
	0.00001	25.883480	19.579750	24.594080	23.35 ± 1.923****	
	0.000001	31.900670	35.816620	36.867240	34.86 ± 1.511****	
Alpha	0.0000001	27.507160	24.976120	38.299900	30.26 ± 4.085****	
	1	15.186250	15.186250	12.559690	14.31 ± 0.876	
	0.1	30.706780	25.119390	21.824260	25.88 ± 2.592****	
	0.01	23.209170	11.795610	11.938870	15.65 ± 3.781	
	0.001	31.088830	23.400190	23.686720	26.06 ± 2.516****	31.39
	0.0001	56.829040	53.390640	53.390640	54.54 ± 1.146****	
	0.00001	9.455587	27.889210	9.980898	15.78 ± 6.059	
	0.000001	46.513850	39.063990	37.153770	40.91 ± 2.855****	
Beta	0.0000001	25.453680	20.105060	28.796560	24.79 ± 2.531****	
	1	50.477550	44.794650	43.505250	46.26 ± 2.142****	
	0.1	20.009550	19.293220	20.630370	19.98 ± 0.386****	
	0.01	21.298950	20.582620	25.071630	22.32 ± 1.392****	
	0.001	25.214900	19.579750	25.023880	23.27 ± 1.85****	0.107
	0.0001	17.621780	14.326650	14.326650	15.43 ± 1.098	
	0.00001	22.301820	22.445080	19.770770	21.51 ± 0.869****	
	0.000001	26.647560	27.745940	28.032470	27.48 ± 0.422****	
Gamma	0.0000001	6.829035	5.969437	7.163324	6.65 ± 0.356	
	1	4.154728	5.491881	9.360076	6.34 ± 1.561	
	0.1	3.247373	3.247373	6.160459	4.22 ± 0.971	
	0.01	3.581662	2.913085	3.581662	3.36 ± 0.223	
	0.001	8.978032	27.029610	20.152820	18.72 ± 5.26	12.26
	0.0001	28.127990	19.770770	28.127990	25.34 ± 2.786****	
	0.00001	8.261700	28.987580	38.156640	25.14 ± 8.842****	
	0.000001	37.010510	50.286530	44.460360	43.92 ± 3.842****	
Lambda	0.0000001	37.774590	38.347660	31.566380	35.90 ± 2.171****	
	1	40.878700	33.858640	44.890160	47.34 ± 4.605****	
	0.1	33.476600	28.892070	28.605540	30.33 ± 1.578****	
	0.01	30.897800	28.892070	31.136580	30.31 ± 0.712****	
	0.001	28.271250	30.706780	28.462270	29.15 ± 0.782****	0.002
	0.0001	23.065900	21.680990	23.782230	22.84 ± 0.62****	
	0.00001	22.397330	22.397330	21.060170	21.95 ± 0.446****	
Positive Control	0.000001	15.377270	15.711560	18.147090	16.41 ± 0.873	
	0.0000001	11.700100	12.511940	8.643744	10.95 ± 1.178	

n=3, ****: Highly significant ($p<0.0001$) when compared to the negative control.

KEYS

Alpha Extract = *Ocimum gratissimum + Curcuma longa + Zingiber officinalis*

Beta Extract = *Annona muricata + Moringa oleifera + Ocimum gratissimum + Curcuma longa + Zingiber officinalis*

Gamma Extract = *Annona muricata + Curcuma longa + Zingiber officinalis*

Lambda Extract = *Moringa oleifera + Curcuma longa + Zingiber officinalis*

Positive control = Camptothecin

Negative control = DMEM

3.2 Cell Cycle Analysis

Flow cytometry results (Figs 1-4) is a compilation of different events revealing the effects of CPAE on the cancer cell lines (A549 and Hela S330194) at different concentrations. The number that is attached to each CPAE or control represents the concentration used for the test. The number 1, 2 and 3 represent respectively 1 µg/mL, 10 µg/mL and 100 µg/mL. The analysed events have the following annotations FSC-A, FSC-H, BL3-A, BL2-A representing respectively percent of alive cells, differentiation of apoptotic cell and cell cycle distribution patterns for each treated cell line.

Live gating strategy was used for the analysis to sort the cells, the living cells were identified by the gate and separated from all the others. Living cells identified by propidium iodide (PI)(Sigma-Aldrich) exclusion were first gated according to their light scatter properties to exclude cell debris and dead cells based on Forward Scatter pulse Area (FSC-A) and the result was expressed at gate R1 (percent of alive cells). Based on gating principle, debris and dead cells are located at the lower level of forward scatter especially at the bottom left corner of the density plot (FSC-A). Forward Scatter pulse Height (FSC-H) sorted the apoptotic cells according to the time that the apoptosis has occurred; late apoptotic or necrotic cells were PI+ (Red stain) while early apoptotic cells were PI- (black). Blue Laser channel 2 pulse Area (BL2-A) and Blue Laser channel 3 pulse Area (BL3-A) showed the cell cycle distribution patterns in both cell lines after 48h of treatment. The cellular debris, late apoptotic and necrotic cells are represented by the Sub-G1 group on the histograms.

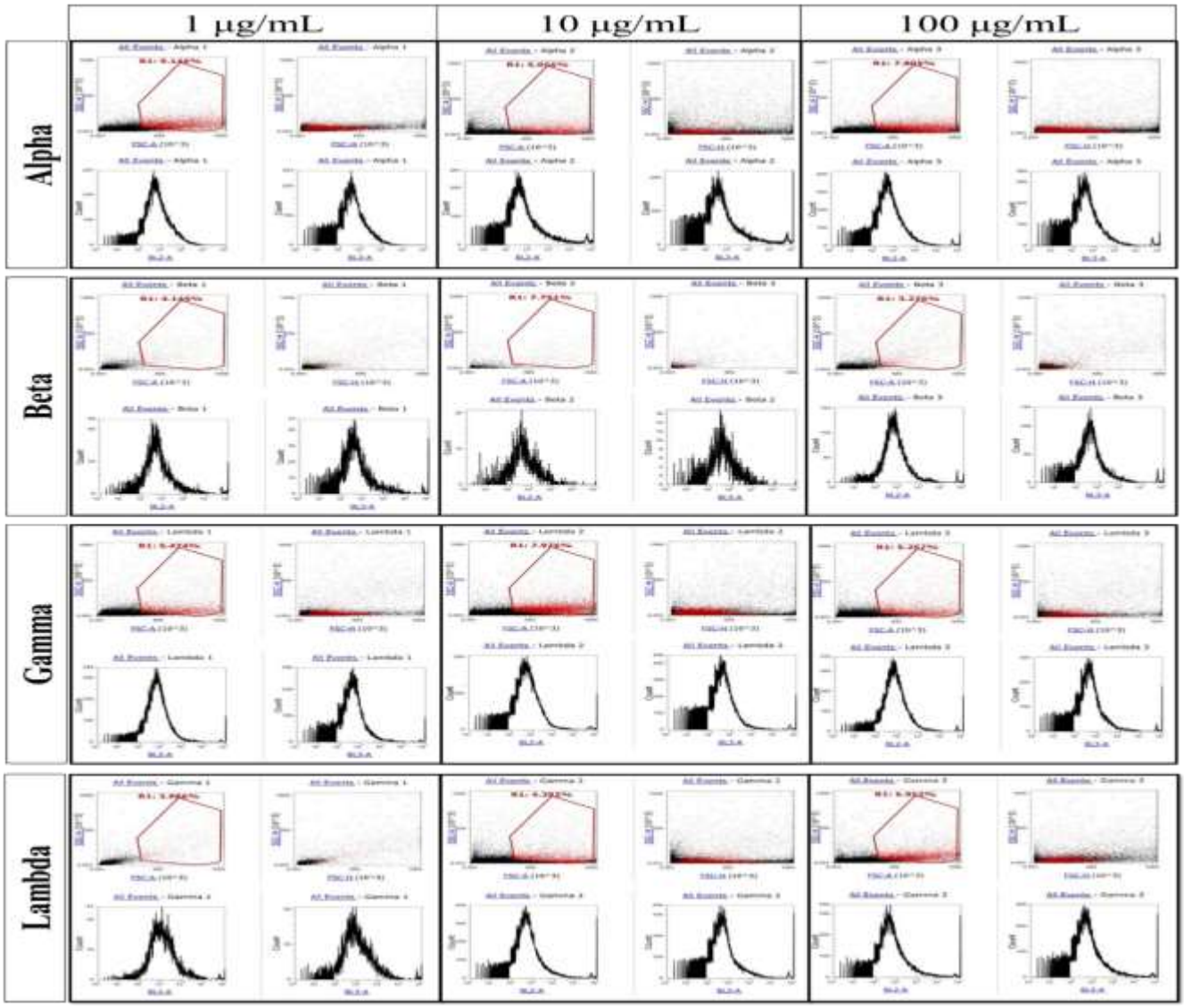

Figure 1: Combined Plant Aqueous Extracts (CPAE) activated Apoptosis and Cell cycle arrest at G1 phase in lung carcinoma epithelial cells A549 after 48h of treatment at 1 µg/mL (Alpha1,

Beta1, Gamma1, Lambda1), 10 µg/mL (Alpha2, Beta2, Gamma2, Lambda2), 100 µg/mL (Alpha3, Beta3, Gamma3, Lambda3). FSC-A (Live gating result expressed as R1 representing the percent of alive cells after treatment), FSC-H (Differentiation of apoptotic cell: late apoptotic or necrotic cells were PI+ (Red stain) while PI- cells (black) were considered early apoptotic), BL3-A & BL2-A (Cell cycle distribution patterns showing a considerable cell arrest at G1 phase and a noticeable sub-G1 phase suggested to be cellular debris, late apoptotic and necrotic cells).

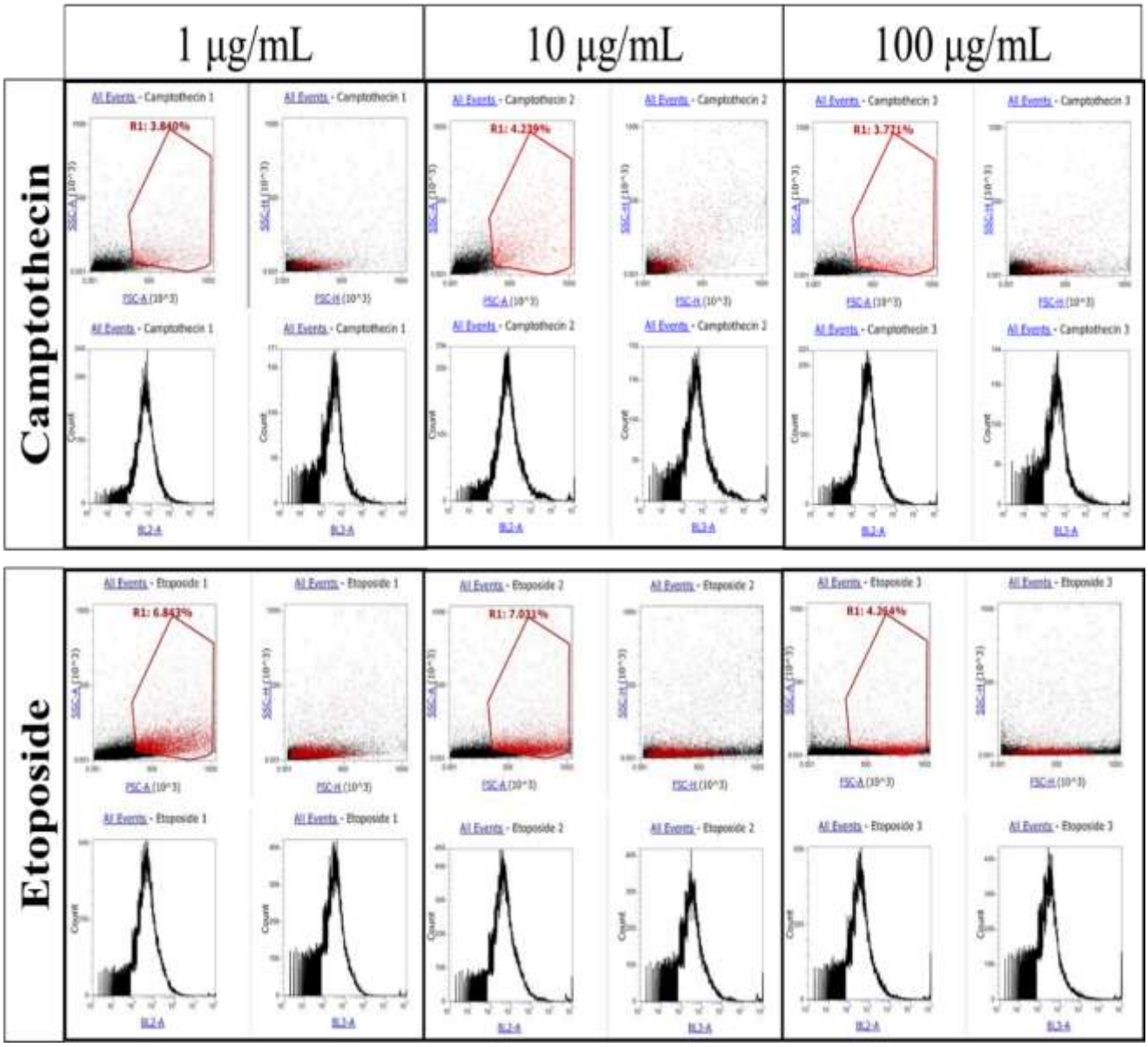

Figure 2: Camptothecin and Etoposide activated Apoptosis and Cell cycle arrest at G1 phase in lung carcinoma epithelial cells A549 after 48h of treatment at 1 µg/mL (Camptothecin 1, Etoposide 1), at 10 µg/mL (Camptothecin 2, Etoposide 2) and 100 µg/mL (Camptothecin 3, Etoposide 3). FSC-A (Live gating result expressed as R1 representing the percent of alive cells after treatment), FSC-H (Differentiation of apoptotic cell: late apoptotic or necrotic cells were PI+ (Red stain) while PI- cells (black) were considered early apoptotic), BL3-A & BL2-A (Cell cycle distribution patterns showing a considerable cell arrest at G1 phase and a noticeable sub-G1 phase suggested to be cellular debris, late apoptotic and necrotic cells).

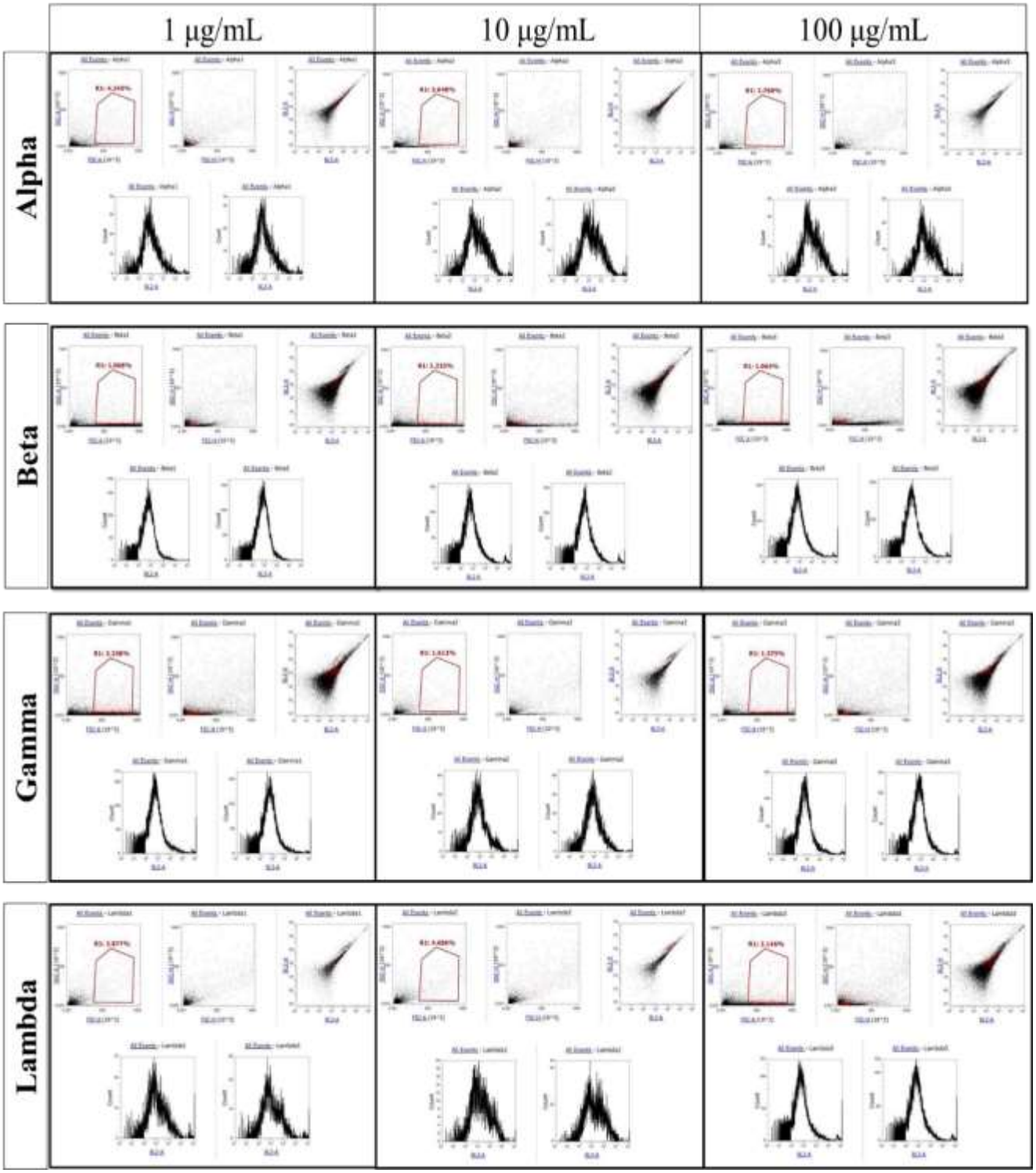

Figure 3: Combined Plant Aqueous Extracts (CPAE) activated Apoptosis and Cell cycle arrest at G1 phase in human cervix carcinoma HeLa S330194 after 48h of treatment at 1 µg/mL (Alpha1, Beta1, Gamma1, Lambda1), at 10 µg/mL (Alpha2, Beta2, Gamma2, Lambda2) and 100 µg/mL (Alpha3, Beta3, Gamma3, Lambda3). FSC-A (Live gating result expressed as R1 representing the percent of alive cells after treatment), FSC-H (Differentiation of apoptotic cell: late apoptotic or necrotic cells were PI+ (Red stain) while PI- cells (black) were considered early apoptotic), BL3-A & BL2-A (Cell cycle distribution patterns showing a considerable cell arrest at G1 phase and a noticeable sub-G1 phase suggested to be cellular debris, late apoptotic and necrotic cells).

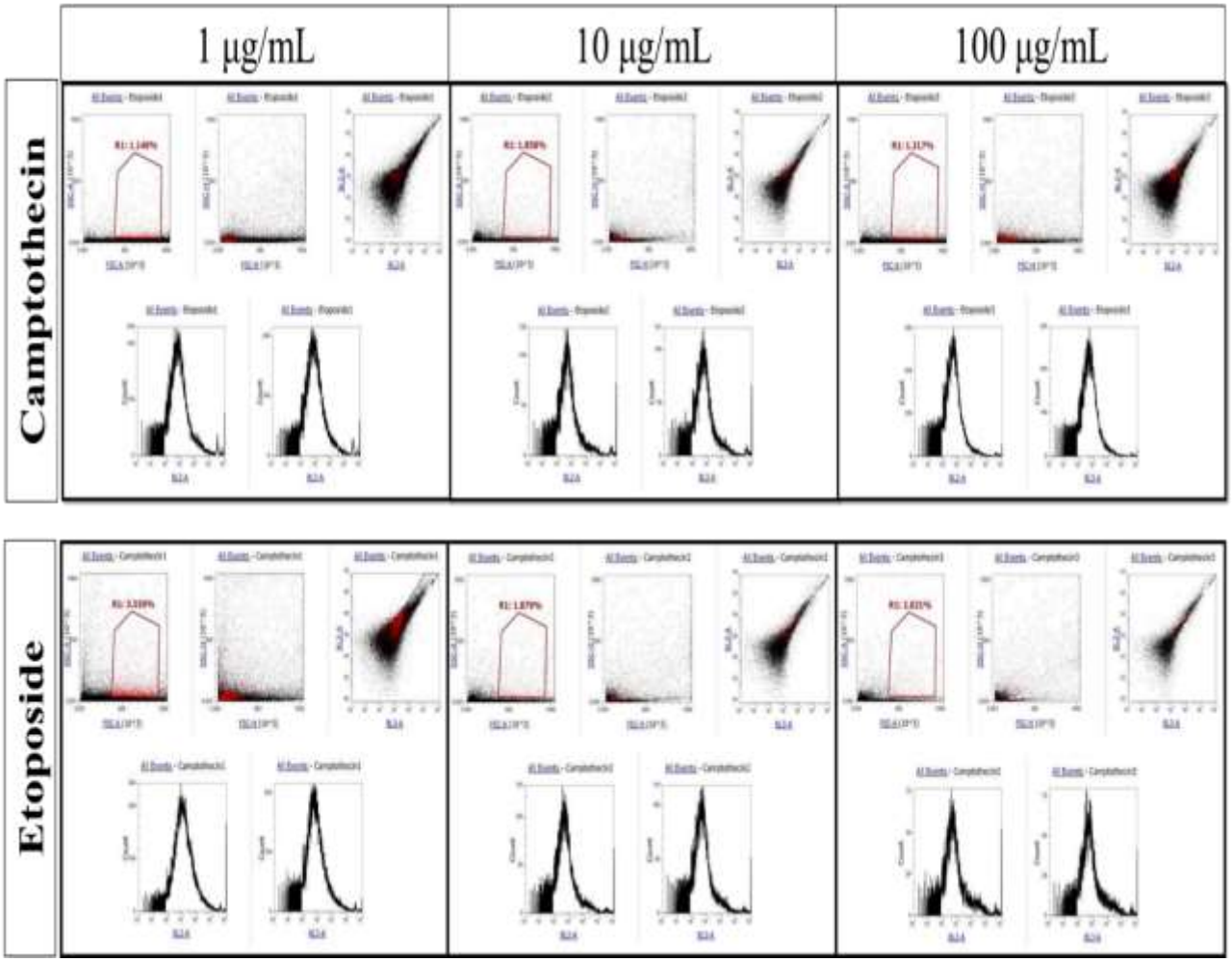

Figure 4: Camptothecin and Etoposide activated Apoptosis and Cell cycle arrest at G1 phase in human cervix carcinoma HeLa S330194 after 48h of treatment at 1 µg/mL (Camptothecin 1, Etoposide 1), at 10 µg/mL (Camptothecin 2, Etoposide 2) and 100 µg/mL (Camptothecin 3, Etoposide 3). FSC-A (Live gating result expressed as R1 representing the percent of alive cells after treatment), FSC-H (Differentiation of apoptotic cell: late apoptotic or necrotic cells were PI+ (Red stain) while PI- cells (black) were considered early apoptotic), BL3-A & BL2-A (Cell cycle distribution patterns showing a considerable cell arrest at G1 phase and a noticeable sub-G1 phase suggested to be cellular debris, late apoptotic and necrotic cells).

The cell cycle results of A549 (Figs 1 and 2) and HeLa (Figs 3 and 4) cell lines using propidium iodide and flow cytometry revealed that more apoptotic reactions were involved when referring to the percentage of alive cells after treatment. The data analysis (Table 2 and Table 3) showed a high cytotoxic activity of each of the CPAE on both cell lines. It also revealed that the cytotoxic effect of the CPAE and the positive controls is very significant when compared with the negative control but there is no significant difference in the effect induced by each of the tested substances on the same cell line. It can be suggested that the cytotoxic effect of the CPAE and the standard drugs on A549 cell lines (Table 2) is not dose-dependent while on HeLa cell lines (Table 3) it is dose-dependent. The cell cycle distribution showed that most of the alive cells were arrested at G1 phase with more arrest on A549 cell lines when compare to HeLa cell lines. Even though the difference between the tested substances was not significant, it was noticed that for each of the concentrations and for both cancer cell lines, Alpha extract induced more arrest in the cells while Beta extract induced the most significant apoptotic effect even when compared with the standard drugs.

Table 2: Percentage of alive cells from A549 cell line after treatment

Group	Mean ±SD of Survival (%)		
	1 µg/ml	10 µg/ml	100 µg/ml
Camptothecin	3.940±0.264****	4.239±0.200****	3.771±0.201****
Etoposide	6.266±1.258****	6.127±1.014****	3.307±0.851****
Alpha	7.262±2.017****	4.994±0.120****	7.351±0.758****
Beta	3.972±0.202****	7.265±0.518****	3.088±0.164****
Gamma	3.839±0.368****	4.434±0.536****	6.194±0.792****
Lambda	5.702±0.689****	7.046±0.847****	4.965±0.327****
DMSO	92.080±4.329	92.213±4.817	93.161±3.823

Data represent the mean ± SD of three separate experiments. Combined Plant Aqueous Extracts and Positive controls vs DMEM (Negative control). ****Significant at $p < 0.0001$.

Table 3: Percentage of alive cells from HeLa S330194 cell line after treatment.

Group	Mean ±SD of Survival (%)		
	1 µg/ml	10 µg/ml	100 µg/ml
Camptothecin	3.293±0.349****	1.734±0.484****	1.759±0.385****
Etoposide	1.590±0.394****	1.759±0.315****	1.108±0.201****
Alpha	4.097±0.150****	3.618±0.256****	2.677±0.239****
Beta	1.089±0.029****	1.353±0.105****	1.090±0.024****
Gamma	2.255±0.077****	1.627±0.212****	1.374±0.168****
Lambda	2.797±0.165****	4.722±0.366****	2.176±0.195****
DMSO	95.887±1.645	90.377±0.051	91.188±4.361

Data represent the mean ± SD of three separate experiments. Combined Plant Aqueous Extracts and Positive controls vs DMEM (Negative control). ****Significant at $p < 0.0001$.

3.3 Apoptotic DNA fragmentation Assay

The data of DNA fragmentation tested by agarose gel electrophoresis (fig. 5) showed the apoptosis of the HeLa cell lines DNA induced by CPAE and the positive control. The negative control (lane 1) representing the untreated cells appeared as a distinct band. Presence of DNA fragments was noticed with the cells treated with both the CPAE (Lane 2-5) and the positive control (lane 6) by a heavy dark stain on the gel signaling that apoptotic mechanisms have occurred in the treated cells.

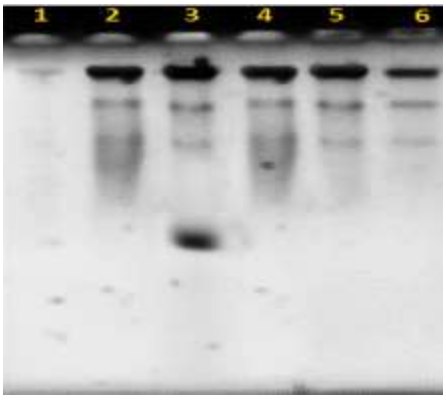

Figure 5: DNA fragmentation assay of HeLa S330194 cell lines after 24h of treatment with the Combined Plant Aqueous Extracts at the studied IC_{50}. Lane 1- DNA from untreated cells (negative control), Lane 2- Cells treated with the Alpha extract, Lane 3- Cells treated with the Beta extract, Lane 4- Cells treated with the Gamma extract, Lane 5- Cells treated with the Lambda extract, Lane 6- Cells treated with the positive control. The DNA ladders were separated electrophoretically on a 2% agarose gel containing 1 µg/mL ethidium bromide and visualize by ultraviolet transillumination.

KEYS

Negative control = DMEM

Alpha Extract = *Ocimum gratissimum* + *Curcuma longa* + *Zingiber officinalis*

Beta Extract = *Annona muricata + Moringa oleifera + Ocimum gratissimum + Curcuma longa + Zingiber officinalis*
Gamma Extract = *Annona muricata + Curcuma longa + Zingiber officinalis*
Lambda Extract = *Moringa oleifera + Curcuma longa + Zingiber officinalis*
Positive control = Etoposide

4.0 Discussion

According to Kurapati et al. (2012), an appropriate combination of chemopreventive agents might provide greater efficacy than the administration of individual agents based on synergistic effects of different chemical substances.

The cytotoxicity investigation (Table 1) revealed that the approach used has potentially affected in a synergistic way the antiproliferative activity against A549 cell line when compared to the activity of some single plant extract previously reported against cancer cell lines. The best IC_{50} value of the CPAE revealed to be also higher than some reported IC_{50} value of the plant extract used in their individual form. Rahma et al. (2019) reported that *Annona muricata* juice has an IC_{50} of 3549 µg/mL when tested against A549 cell line. A. *muricata* leaf ethyl acetate extract exhibits a cytotoxic effect on A549 cell line with an IC_{50} value of 5.09 ± 0.41 µg/mL after 72 h of treatment, inducing apoptosis (Moghadamtousi et al., 2014). Pieme et al. (2014) highlighted that *A. muricata* leaf extract induced cytotoxicity activity at 24h treatment with an IC_{50} value of 194 µg/mL. Chloroform and n-hexane fraction from *Annona muricata* L induced on Hela cell a cytotoxic effect with IC_{50} value of 127,3 µg/ml, 169,2 µg/ml respectively (Artanti, Okid and Prayitno, 2016). Against other type of cancer lines such as leukemia, methanol extracts from *A. muricata* leave and fruit pericarp induced apoptosis respectively with IC_{50} = 0.6 µg/mL and IC_{50} = 4.6 µg/mL (Cassé, 2018). Different fractions of *Anona muricata* applied on Hela cells induces growth inhibition with an IC_{50} of 35.51 µg/mL for etanol, IC_{50}: 5.91 µg/mL for ethyl acetate, and IC_{50}: 8.39 µg/mL of hexane (Qorina et al., 2020). *Ocimum gratissimum* was reported for its ability to reduce human breast cancer cells proliferation with an IC_{50} = 53.86 ± 0.96 µg/mL (Koolamchal et al., 2022). It is also reported that it inhibits chemotaxis and chemoinvasion *in vitro* and breast cancer progression *in vivo* (Nangia-Makker et al., 2013). A study from Ramadasan Kuttan et al. (1985) revealed that *Curmuma longa* has a potential anticancer property on lymphocytes and Dalton's lymphoma cells at a concentration of 0.4 mg/mL. *Curcuma longa extract* (crude turmeric extract) exhibited a cytotoxicity activity on A549 cell line with an IC_{50} = 0.103.5±5.96 mg/mL and N-hexane extract of *Curcuma longa* induced cytotoxicity on the A549 lung cancer cell line with IC_{50} = 0.26 mg/mL (Mohammad et al.,2010). *Meanwhile, the aqueous extract of Zingiber officinalis* has been reported to inhibit cell proliferation when used at a concentration of 100 – 250 µg/mL on Human cell lines; the IC_{50} value for A549 cells is 239.4 ± 7.4 µg/ml and 253.4+8.9 µg/ml for HeLa cell lines (Choudhury et al., 2010). Ginger and lemon water extract is reported to reduce cancer cells proliferation *in vitro* of breast cancer cell lines MDA-MB-231 and lung carcinoma cells A549 respectively with an IC_{50} = 3.5±0.500 mg/mL and IC_{50} = 6.5±2.000 mg/mL (AL-ataby and Talib, 2022). Kim et al. (2014) and Lee et al. (2008) have reported that ginger component named 6-gingerol has the potential to inhibit cell growth in non-small cell lung cancer cells and human colorectal cancer cells. The cytotoxicity evaluation of the four CPAE on lung carcinoma A549 cell lines revealed that the Gamma extract showed the highest activity with an IC_{50} = 0.107 mg/ml followed by Alpha extract with an IC_{50} = 5.19 mg/ml. Gamma extract is a combination of *Annona muricata*, *Curcuma longa* and *Zingiber officinalis* while Alpha extract is a combination of *Ocimum gratissimum*, *Curcuma longa* and *Zingiber officinalis*. Several researches have been done on these above medicinal plants and have reported promising results about their anti-cancer property but few studies have been done using the extract of different plant combinations.

The cell cycle analysis of the treated cell lines (A549 and Hela S330194) using propidium iodide and flow cytometry revealed after the live gating results (R1) the percent of the remaining alive cells. Based on the different events of the flow cytometry results on A549 (Figs. 1-6) and Hela S330194 (Figs. 7-12), it could be suggested that all the CPAE inflicted serious damage to the cancer cell lines by activating programmed cell death and necrosis as the positive controls. The CPAE and the positive controls showed more arrest on A549 cell lines while on Hela S330194 they induced more apoptotic effect (Table 2 and 3). Within the CPAE, Alpha extract showed more arrest on both cell lines while Beta extract induced more apoptotic effect on Hela S330194 than A549 when compared to the positive controls. The interpretation of the different histograms revealed that the extracts also induced cell cycle arrest in the alive cells at G_1 phase with a significant expression of sub- G1-phase below G1 peak. Murad et al. (2016) explained that the repair mechanisms of a cell and the cell death program are activated by the arrest of cell cycle progression at G1-phase. An increased sub-G1 phase is the proof showing that apoptotic events have occurred resulting in DNA damage

(Kämmerer et al., 2020; Parveen and Varalakshmi, 2020). These findings confirmed previous studies reporting the induction of apoptosis and cell cycle arrest potential of the different plants used in the course of this study. According to some reported studies, *Curmuma longa ethanol* extract induced T47D cells cycle arrest in G1 phase with an IC_{50} value of 26.36 ± 1.55 µg/mL (Widyananda *et al.*, 2022) and curcumin a bioactive component of *Curmuma longa* has been reported of promoting in different cancer cell lines (human SK-MEL-37, Human Osteosarcoma Cells, A549, H460, myeloid leukemia cells, Human Pancreatic Cancer Cells) cytotoxic activities including autophagy, apoptosis, cell cycle arrest at G_0/G_1, retard at $G_{2/M}$ phases, and morphological alterations (Martínez-Castillo et al., 2018, Zhu and Bu, 2017; Chang and Chen, 2015; Carneiro et al., 2010; Lee et al., 2009). *Zingiber officinalis* extract has been found to induce cell arrest at the concentration of 22.11g/ml (Liu et al., 2012). Nachvak et al. (2023) reported that ginger stops cancer cell growth and causes cell death in *in vitro* investigations at the concentration of 2g/mL. [6]-gingerol a component of ginger, induces apoptotic mechanisms and promote cell-cycle arrest at G1 in renal-cell carcinoma, non-small cell lung cancer cells, human colorectal cancer cells, and pancreatic cancer cells (Xu et al., 2020; Kim et al., 2014; Lee et al., 2008; Park et al., 2006). Kapoor, Aggarwal and Das, (2016) reported that [6]-gingerol has the potential to activate apoptosis and cell cycle arrest in human oral and Hela cell lines. Overall, ginger and its derivatives have been recognised as natural chemopreventive agents that can catalyse programmed cell death and cell cycle arrest (Zadorozhna and Mangieri, 2021). Meenakshisundaram et al., (2020) reported that green synthesis of silver nanoparticles using *A. muricata* leaves extract induced several cytotoxic effects such as cell cycle arrest, elevated levels of apoptotic proteins in A549 cell lines at a concentration of 6 µg/mL. A report from Ilango et al., (2022) also showed that *A. muricata* leaf extract from hexane, ethyl acetate, and methanol, caused cell cycle arrest at the G_0/G_1 phases and apoptosis with an IC_{50} value of 21.05 ± 0.42 µg/mL, 5.09 ± 0.4 µg/mL and ≥ 100 µg/mL respectively. According to Pieme et al., (2014), *Annona muricata* extract possesses an antiproliferation potential and can induce apoptosis and G0/G1 phase cell arrest in cancer cell lines. *Ocimum gratissimum* aqueous extract has been reported to suppress cell viability by triggering apoptosis while inhibiting the anti-apoptotic signaling within a concentration range of 300 - 800 µg/mL in hepatocellular carcinoma cells (SK-Hep1) and human pulmonary adenocarcinoma cell A549 with an increased Sub-G1 cell count in SK-Hep1 (Huang et al., 2020; Chen et al., 2011). It is suggested that the bioactive compounds of *Ocimum gratissimum* possess inhibitor potentials against anti-apoptotic BCL-2 proteins associated with cancer which may be the result of synergistic actions (Gyebi et al., 2022). Sheu et al., (2021) revealed that *O. gratissimum* extract induces apoptosis in gastric cancer cells. A study from Tiloke et al., (2019) revealed that aqueous leaf extract of *Moringa oleifera* affects cell-cycle arrest by reducing cell count in G1, S and G2-M and triggers apoptosis in human liver hepatocellular carcinoma cells ($HepG_2$) after 24 hours of treatment with an IC_{50} of 4.479 mg/mL. In vitro and in vivo experimentations of *Moringa oleifera* leaf extract on Dalton's Lymphoma cell show the ability of the extract to activate apoptotic events and interfere with the cell cycle by arresting cells at G2/M phase, (Kumar et al., 2023). Another study have proved that the methanolic extract of *Moringa oleifera* leaves provokes in human prostate PC-3 cancer cells apoptosis and blocks cell cycle at G0/G1 via downregulation of Hedgehog Signaling Pathway (Khan et al., 2020). Ethyl acetate and n-Hexane fractions of *Moringa oleifera* leaves cytotoxic activities have been reported to be the result of synergistic actions of apoptotic events coupled with cell cycle arrest induction on T47D Breast cancer cell via G0/G1 through Cyclin D1 Expression with IC_{50} values of 243.58 µg/mL (Apriani, Gaffar, and Herlina, 2019; Gaffar et al., 2019; Apriani, Herlina, and Gaffar, 2019).

The apoptotic DNA fragmentation assay on HeLa S330194 cell lines (Figure 13) revealed an absence of DNA ladder formation for the untreated cells while a presence of DNA ladder formation was noted after 48h of treatment with the studied IC50 of each CPEA. The different extracts activated in the treated cells the CAD (caspase-activated DNase) that lead to the cleavage of the DNA which appeared as apoptotic DNA fragments on agarose gel as a dark heavy stain when compared to the untreated cells. Therefore, it can be suggested that CPAE effect on HeLa cell lines was an apoptotic mechanism. Since both cell lines used in the course of this study are adenocarcinoma cells, the result on HeLa should be similar on A549 and any other adenocarcinomas such prostate, colon and breast cancers.

Some studies have shown that the combination of plants having anti-cancer potential improves the efficiency of the combination extract over the individual plant extract. Kurapati et al., (2012) reported how the crude extract of *Curcuma longa* and *Zingiber officinale* combination has a high cytotoxicity activity on PC-3M prostate cancer cell line when compared to the individual plant effect. Another study from Vemuri et al., 2017 revealed that the combination of the active compounds of *Curcuma longa* and *Allium sativa* has increased the apoptosis potential and

cell senescence in lung and oral cancers. Talib et al., (2022) highlighted different studies showing the benefits in combining specific phytochemicals for anticancer therapies and pointed out the importance of natural anticancer compounds combination or their use coupled with orthodox drugs that can make a difference in overcoming the different challenges faced in treating cancer.

Even though the mechanism of cytotoxic action is still unclear, based on previous literatures and the findings of this study, it can be suggested that the combination approach didn't affect the different anti-cancer potentials of the individual plant since the findings have revealed similarities with a lower IC_{50} when compared to most of the individual plant aqueous extract. According to the outcomes of this research, the CPAE revealed to be toxic on both cancer cell lines while they may be harmless on human normal cell lines. Tossou et al., (2023) investigated on the toxicity of the CPAE using *Drosophila melanogaster*; most of the different plant combinations revealed to be safe and it has been concluded that their toxicity will not affect normal cell lines due do the affinity of *Drosophila melanogaster* with human genome (Bezerra et al., 2017). Cell cycle analysis and apoptotic DNA fragmentation assay results confirm that each of the CPAE induce cytotoxicity through apoptotic mechanisms and cell cycle arrest but the cytotoxicity assay revealed that Gamma extract has the highest inhibition rate on A549 cell lines proliferation with an IC50 of 107 µg/mL. It is suggested that only an extract with an IC50 value less than 100 µg/mL can be expected to be active (Kamuhabwa et al., 2000) but it is also claimed that there is still a possibility to work on the efficiency of the extract as long as the IC50 value is less than 500 µg/mL, concentration which disqualifies the extract to be called active (Machana et al., 2011). Based on IC50 value, it can be suggested that only Gamma extract may be considered as active even though all the combined plant aqueous extracts have exhibited cytotoxic activities. Referring to previous findings, most of extracts with an IC50 value less than 100 µg/mL are fractions. Meanwhile, the aqueous extract Gamma IC50 is still less than most of the aqueous extracts reported including some fractions of the individual plants.

Several questions have been raised after these findings such as what can be the cause of this dichotomy? Is it due to the area of plant collection? Is it due to the method or the solvent used during the extraction process? Is it due to the type of cancer cell lines used? Did the extraction process affect the secondary metabolites present in the plants? To all these questions, answers must be provided by a subsequent study.

5.0 Conclusion

The findings of this research have proved that the aqueous extracts of the different plant combinations are cytotoxic on lung carcinoma epithelial cells A549 and human cervix carcinoma HeLa S330194. Further investigations will be carried out to elucidate the findings of this research and to also confirm the hypothesis that the anti-proliferation activity of the fractions may be significantly greater than that of the crude aqueous extract.

6.0 Acknowledgements

The authors acknowledge the World Bank through the Africa Centre of Excellence in Phytomedicine Research and Development (ACEPRD) of University of Jos, Nigeria for its financial support. The Department of Biochemistry, University of Jos is also grateful to the Department of Nutrition and Biochemistry of the National Institute of Medical Research (NIMR) for the donation of the cancer cell lines. The authors wish to appreciate also all the staff of the Department of Nutrition and Biochemistry of NIMR for their technical assistance. The research team acknowledges the assistance given by Dr Adama Denou (PhD) for the statistical analysis.

References Cited

abcam. Apoptosis DNA Fragmentation Analysis Protocol. 1 page; accessed on 16/04/22, https://docs.abcam.com/pdf/protocols/apoptosis-dna-fragmentation-analysis-protocol.pdf

Adams, M., Borysiewicz, L., Fiander, A., Man, S., Jasani, B., Navabi, H., Lipetz, C., Evans, A. S. Mason, M. *2001). Clinical Studies of Human Papilloma Vaccines in Pre-Invasive and Invasive Cancer. *Vaccine*, *19* (17-19): 2549–2556.

Adebolu, T. T. and Salau, A. O., (2005). Antimicrobial Activity of Leaf Extracts of *Ocimum gratissimum* on Selected Diarrhoea Causing Bacteria in Southwestern Nigeria, *Afr J Biotech*, 4: 682-684.

Ahmed, A., Abdalla, A., Ali, N., Zoheir, K. (2017). *Moringa oleifera* root Induces Cancer Apoptosis more Effectively than Leave Nanocomposites and its Free Counterpart, *Asian Pacific Journal of Cancer Prevention*, 18(8): 2141-2149.

Al-Asmari, A. K., Albalawi, S. M., Athar, M. T., Khan, A. Q., Al-Shahrani, H., et al., (2015). *Moringa oleifera* as an Anti-Cancer Agent against Breast and Colorectal Cancer Cell Lines. PLOS ONE 10(8): e0135814.

AL-ataby, I. A. and Talib, W. H., 2022. Daily Consumption of Lemon and Ginger Herbal Infusion Caused Tumor Regression and Activation of the Immune System in a Mouse Model of Breast Cancer, *Front. Nutr.*, 9: 829101.

Alhazmi, H. A., Najmi, A., Javed, S. A., Sultana, S., Al Bratty, M., Makeen, H. A., Meraya, A. M., Ahsan, W., Mohan, S., Taha, M. M. E., and Khalid, A., 2021. Medicinal Plants and Isolated Molecules Demonstrating Immunomodulation Activity as Potential Alternative Therapies for Viral Diseases Including COVID-19, *Frontiers in immunology*, *12*: 637553.

Amirghofran, Z., Bahmani, M., Azadmehr, A., Javidnia, K., Miri, R., 2009. Immunomodulatory Activities of Various Medicinal Plant Extracts: Effects on Human Lymphocytes Apoptosis, *Immunological Investigations*, 38(2): 181-192.

Apriani, R, Herlina, T., and Gaffar, S., 2019. Ethyl Acetate Fraction of *Moringa oleifera* leaves Induces Cell Cycle Arrest on T47D Breast Cancer Cell via G0/G1 through Cyclin D1 Expression, *Jurnal Kimia Valensi*, 6(1): 111-117.

Apriani, R., Gaffar, S. and Herlina, T., 2019. Cytotoxic Activity of Ethyl Acetate Fraction *Moringa oleifera* Leaves and its Effect on Apoptosis Induction against T47D Breast Cancer Cell Line. *Jurnal Farmakobahari*, 10(1): 9 – 16.

Artanti, A., Astirin, O., and Prayitno, A., 2016. Cytotoxic Activity of Non-Polar Fraction from *Annona muricata L.* Leaves on Hela and Raji Cell Line, *Journal of Pharmaceutical Science and Clinical Research.* 1(2): 112-118.

Avni, G. D., Ghulam, N. Q., Ramesh K. G., et al., 2008. Medicinal plants and cancer chemoprevention, *Current drug metabolism*, *9*(7): 581–591.

Bayat Mokhtari, R., Homayouni, T. S., Baluch, N., Morgatskaya, E., Kumar, S., Das, B., and Yeger, H., 2017. Combination Therapy in Combating Cancer. *Oncotarget*, 8(23): 38022–38043.

Bezerra, J. W. A., Costa, A.R., da Silva, M. A. P., Rocha, M. I., Boligon, A. A., da Rocha, J. B. T., Barros, L. M., Kamdem, J. P., 2017. Chemical Composition and Toxicological Evaluation of *Hyptis suaveolens* (L.) Poiteau (Lamiaceae) in *Drosophila melanogaster* and *Artemia salina*, *South Afr J Bot*, 113: 437–442.

Brianna, N., Santosh, K. S., James, W. L. Jr., Rajesh, S.,2020. Role of Natural Compounds in Preventing and Treating Breast Cancer, *Front. Biosci. (Schol Ed)*, 12(1): 137–160.

Carneiro, M. L. B., Porfírio, E. P., Otake, A. H., Chammas, R., Báo, S. N., and Guillo, L. A., 2010. Morphological Alterations and G0/G1 Cell Cycle Arrest Induced by Curcumin in Human SK-MEL-37 Melanoma Cells, *Brazilian Archives of Biology and Technology*, 53(2): 343–352.

Cassé C., 2018. Molecular Mechanisms of *Annona muricata* Anti-Proliferative/Anti-Cancer Properties. *Biomed, Genet Genomics*, 4(1): 2-4.

Chan, W. J. J., Adiwidjaja, J., McLachlan, A. J. et al., 2023. Interactions Between Natural Products and Cancer Treatments: Underlying Mechanisms and Clinical Importance, *Cancer Chemother Pharmacol*., 91: 103–119.

Chang, H. B., and Chen, B. H., 2015. Inhibition of Lung Cancer Cells A549 and H460 by Curcuminoid Extracts and Nanoemulsions Prepared from Curcuma longa Linnaeus, *International journal of nanomedicine*, 10: 5059–5080.

Chen, H. M., Lee, M. J., Kuo, C. Y., Tsai, P. L., Liu, J. Y., and Kao, S. H., 2011. *Ocimum gratissimum* Aqueous Extract Induces Apoptotic Signaling in Lung Adenocarcinoma Cell A549, *Evidence-based complementary and alternative medicine: eCAM*, 2011: 739093.

Cheon, C., and Ko, S. G., 2022. Synergistic Effects of Natural Products in Combination with Anticancer Agents in Prostate Cancer: A Scoping Review, *Frontiers in pharmacology*, 13: 963317.

Cheong, A., and Nagel, Z. D., 2022. Human Variation in DNA Repair, Immune Function, and Cancer Risk, *Frontiers in immunology*, *13*: 899574.

Choudhari, A. S., Mandave, P. C., Deshpande, M., Ranjekar, P., and Prakash, O., 2020. Phytochemicals in Cancer Treatment: From Preclinical Studies to Clinical Practice, *Frontiers in pharmacology*, 10: 1614.

Choudhury, D., Das, A., Bhattacharya, A., Chakrabarti, G., 2010. Aqueous Extract of Ginger Shows Antiproliferative Activity through Disruption of Microtubule Network of Cancer Cells, *Food and Chemical Toxicology*, 48(10): 2872– 2880.

Cooper, J., Abdullatif, M., Burnett, E., et al., 2016. Long Term Culture of the A549 Cancer Cell Line Promotes Multilamellar Body Formation and Differentiation towards an Alveolar Type II Pneumocyte Phenotype, *PloS one*, *11*(10), e0164438.

Correia, A. S., Gärtner, F., and Vale, N., 2021. Drug Combination and Repurposing for Cancer Therapy: The Example of Breast Cancer, *Heliyon*, *7*(1): e05948.

Coventry, B. J., and Henneberg, M., 2015. The Immune System and Responses to Cancer: Coordinated Evolution, *F1000Research*, 4: 552.

Cragg, G. M., and Pezzuto, J. M., 2016. Natural Products as a Vital Source for the Discovery of Cancer Chemotherapeutic and Chemopreventive Agents, *Med Princ Pract*, 25(2): 41–59.

Darzynkiewicz, Z., Juan, G., 2001. DNA Content Measurement for DNA Ploidy and Cell Cycle Analysis. *Current protocols in cytometry*, Chapter 7, 00:7.5:7.5.1–7.5.24.

Debela, D. T., Muzazu, S. G., Heraro, K. D., Ndalama, M. T., Mesele, B. W., Haile, D. C., Kitui, S. K., and Manyazewal, T., 2021. New Approaches and Procedures for Cancer Treatment: Current Perspectives, *SAGE open medicine*, *9*: 20503121211034366.

Dehelean, C. A., Marcovici, I., Soica, C., Mioc, M., Coricovac, D., Iurciuc, S., Cretu, O.M., Pinzaru, I., 2021. Plant-Derived Anticancer Compounds as New Perspectives in Drug Discovery and Alternative Therapy, *Molecules*, 26(4): 1109.

Desai, A. G., Qazi, G. N., Ganju, R. K., El-Tamer, M., Singh, J., Saxena, A. K., Bedi, Y. S., Taneja, S. C., and Bhat, H. K., 2008. Medicinal Plants and Cancer Chemoprevention, *Current drug metabolism*, 9(7): 581–591.

Ezeamuzie, I. C., Ambakederemo, A. W., Shode, F. O., Ekwebelem, S. C., 2008. Anti-inflammatory Effects of *Moringa oleifera* root extract, *International Journal of Pharmacognosy*, 34(3): 207-212.

Farombi, E. O., Abarikwu, S. O., Adedara, I. A., Oyeyemi, M. O., 2007. Curcumin and Kolaviron Ameliorate di-n-butylphthalate-Induced Testicular Damage in Rats, *Basic Clin Pharmacol Toxicol.*, 100: 43–48.

Fasinu, P. S., and Rapp, G. K., 2019. Herbal Interaction with Chemotherapeutic Drugs - A Focus on Clinically Significant Findings, *Frontiers in oncology*, 9: 1356.

Gaffar, S., Apriani, R., Herlina, T., and Garrido, G., 2019. n-Hexane Fraction of *Moringa oleifera* Lam. Leaves Induces Apoptosis and Cell Cycle Arrest on T47D Breast Cancer Cell Line, *Journal of Pharmacy & Pharmacognosy Research*, 7: 173-183.

Gahtori, R., Tripathi, A.H., Kumari, A. et al., 2023. Anticancer Plant-Derivatives: Deciphering Their Oncopreventive and Therapeutic Potential in Molecular Terms, *Futur J Pharm Sci*, 9: 14.

Gonzalez, H., Hagerling, C., and Werb, Z., 2018. Roles of the Immune System in Cancer: From Tumor Initiation to Metastatic Progression, *Genes & development*, *32*(19-20): 1267–1284.

Greenwell, M., and Rahman, P. K., 2015. Medicinal Plants: Their Use in Anticancer Treatment, *International journal of pharmaceutical sciences and research*, 6(10): 4103–4112.

Gyebi, G. A., Ogunyemi, O. M., Ibrahim, M. I., Afolabi, S. O., Ojo, R. J., Ejike, U. D.I., and Adebayo, J. O., 2022. Inhibitory Potentials of Phytocompounds from *Ocimum Gratissimum* against Anti-Apoptotic BCL-2 Proteins Associated with Cancer: An Integrated Computational Study, *Egyptian Journal of Basic and Applied Sciences*, 9(1): 588-608.

Hashem, S., Ali, T. A., Akhtar, S., Nisar, S., Sageena, G., Ali, S., Al-Mannai, S., Therachiyil, L., Mir, R., Elfaki, I., Mir, M. M., Jamal, F., Masoodi, T., Uddin, S., Singh, M., Haris, M., Macha, M., and Bhat, A. A., 2022. Targeting Cancer Signaling Pathways by Natural Products: Exploring Promising Anti-Cancer Agents, Biomedicine & Pharmacotherapy, 150: 113054.

Hiam-Galvez, K. J., Allen, B. M. and Spitzer, M. H., 2021. Systemic Immunity in Cancer, *Nat Rev Cancer* 21: 345–359.

Huang, C. C., Hwang, J. M., Tsai, J. H., Chen, J. H., Lin, H., Lin, G. J., Yang, H. L., Liu, J. Y., Yang, C. Y., and Ye, J. C., 2020. Aqueous *Ocimum gratissimum* Extract Induces Cell Apoptosis in Human Hepatocellular Carcinoma Cells, *International journal of medical sciences*, 17(3): 338–346.

Huang, M., Lu, J. J., and Ding, J., 2021. Natural Products in Cancer Therapy: Past, Present and Future, *Natural products and bioprospecting*, 11(1): 5–13.

Ijaz, S., Akhtar, N., Khan, M. S., Hameed, A., Irfan, M., Arshad, M. A., Ali, S., and Asrar, M., 2018. Plant Derived Anticancer Agents: A Green Approach towards Skin Cancers, *Biomedicine & pharmacotherapy*, 103: 1643–1651.

Ilango, S., Sahoo, D. K., Paital, B., Kathirvel, K., Gabriel, J. I., Subramaniam, K., Jayachandran, P., Dash, R. K., Hati, A. K., Behera, T. R., Mishra, P., and Nirmaladevi, R., 2022. A Review on *Annona muricata* and Its Anticancer Activity. *Cancers*, 14(18): 4539.

International Agency for Research on Cancer (IARC), Global Cancer Observatory, Latest global cancer data: Cancer burden rises to 18.1 million new cases and 9.6 million cancer deaths in 2018. 1-3; accessed 25/03/2022, https://www.iarc.who.int/wp-content/uploads/2018/09/pr263_E.pdf

Ishola, I. O.; Awodele, O.; Olusayero, A. M.; Ochieng, C. O., 2014. Mechanisms of Analgesic and Anti-Inflammatory Properties of *Annona muricata* Linn. (Annonaceae) Fruit Extract in Rodents, *J Med Food. Dec*., 17(12): 1375-82.

Jurenka, J.S., 2009. Anti-Inflammatory Properties of Curcumin, a Major Constituent of *Curcuma longa*: a review of Preclinical and Clinical Research, *Altern Med Rev*, 14: 141–153.

Kämmerer, P. W., Engel, V., Plocksties, F., Jonitz-Heincke, A., Timmermann, D., Engel, N., Frerich, B., Bader, R., Thiem, D. G. E., Skorska, A., David, R., Al-Nawas, B., and Dau, M., 2020. Continuous Electrical Stimulation Affects Initial Growth and Proliferation of Adipose-Derived Stem Cells, *Biomedicines*, 8(11): 482.

Kamuhabwa, A., Nshimo, C., Witte, P., 2000. Cytotoxicity of Some Medicinal Plant Extracts Used in Tanzanian Traditional Medicine, *J. Ethnopharmacol.*, 70(2): 143– 149.

Kapoor, V., Aggarwal, S., and Das, S. N., 2016. 6-Gingerol Mediates its Anti-Tumor Activities in Human Oral and Cervical Cancer Cell Lines through Apoptosis and Cell Cycle Arrest, *Phytotherapy research: PTR*, 30(4): 588–595.

Khan, F., Pandey, P., Ahmad, V., and Upadhyay, T. K., 2020. *Moringa oleifera* methanolic Leaves Extract Induces Apoptosis and G0/G1 Cell Cycle Arrest via Downregulation of Hedgehog Signaling Pathway in Human Prostate PC-3 Cancer Cells, *Journal of food biochemistry*, 44(8): e13338.

Kim, M. O., Lee, M. H., Oi, N., Kim, S. H., Bae, K. B., Huang, Z., Kim, D. J., Reddy, K., Lee, S. Y., Park, S. J., Kim, J. Y., Xie, H., Kundu, J. K., Ryoo, Z. Y., Bode, A. M., Surh, Y. J., and Dong, Z., 2014. [6]-Shogaol Inhibits Growth and Induces Apoptosis of Non-Small Cell Lung Cancer Cells by Directly Regulating Akt1/2, *Carcinogenesis*, *35*(3): 683–691.

Kim, S. K., and Cho, S. W., 2022. The Evasion Mechanisms of Cancer Immunity and Drug Intervention in the Tumor Microenvironment, *Frontiers in pharmacology*, 13: 868695.

Kiuchi, F., Iwakami, S., Shibuya, M., Hanaoka, F., Sankawa, U., 1992. Inhibition of Prostaglandin and Leukotriene Biosynthesis by Gingerols and Diarylheptanoids, *Chemical & pharmaceutical bulletin*, *40*(2): 387–391.

Koolamchal, M. A., Mundakani, A., Joice, T. J., Arunaksharan, N., Benil, P. B., Rajakrishnan, R., Ahmed, A., Damia, B., 2022. Phytochemical Analysis, Antioxidant, Anti-Inflammatory, Anti-Genotoxic, and Anticancer Activities of Different Ocimum Plant Extracts Prepared by Ultrasound-Assisted Method, *Physiological and Molecular Plant Pathology*, 117: 101746.

Kumar V, Abbas AK, Aster, JC (2013). (Chapter 5) In: Kumar V, Abbas AK & Aster JC, Robbins Basic Pathology, 9th edn. Elsevier, Saunders.

Kumar, S., Verma, P. K., Shukla, A., Singh, R. K., Patel, A. K., Yadav, L., Kumar, S., Kumar, N., Kaushalendra, and Acharya, A., 2023. *Moringa oleifera L.* Leaf Extract Induces Cell Cycle Arrest and Mitochondrial Apoptosis in Dalton's Lymphoma: An *in vitro* and *in vivo* Study, *Journal of ethnopharmacology*, *302*(Pt A): 115849.

Kurapati, K. R., Samikkannu, T., Kadiyala, D. B., Zainulabedin, S. M., Gandhi, N., Sathaye, S. S., Indap, M. A., Boukli, N., Rodriguez, J. W., Nair, M. P. N., 2012. Combinatorial Cytotoxic Effects of *Curcuma longa* and *Zingiber officinale* on the PC-3M Prostate Cancer Cell Line, *J Basic Clin Physiol Pharmacol.*, 23(4): 139–146.

Kuttan, R., Bhanumathy, P., Nirmala K., George, M. C., 1985. Potential Anticancer Activity of Turmeric (*Curcuma longa*), *Cancer Letters*, 29(2): 197-202.

Lee, D. S., Lee, M. K., and Kim, J. H., 2009. Curcumin Induces Cell Cycle Arrest and Apoptosis in Human Osteosarcoma (HOS) Cells, *Anticancer research*, 29(12): 5039–5044.

Lee, H. S., Seo, E. Y., Kang, N. E., and Kim, W. K., 2008. [6]-Gingerol Inhibits Metastasis of MDA-MB-231 Human Breast Cancer Cells, *The Journal of Nutritional Biochemistry*, 19(5): 313–319.

Lehtinen, M., Luukkaala, T., Wallin, K. L., et al., 2001. Human papillomavirus infection, risk for Subsequent Development of Cervical Neoplasia and Associated Population Attributable Fraction, *J Clin Virol*, 22: 117-24.

Leticia, A.S., 2014. Cellular viability - WST-1 assay Protocol for adherent cells. Standard Operation Procedure (SOP): WP 3-Number 2. 1-7; accessed on 16/04/2022, https://nanopartikel.info/data/projekte/nanOxiMet/SOP/nanOxiMet_SOP_WST-1-assay_V2.pdf

Levitsky, D. O. and Dembitsky, V. M., 2015. Anti-breast Cancer Agents Derived from Plants, *Nat. Prod. Bioprospect.*, 5: 1–16.

Liu, Q., Peng, Y. B., Qi, L. W., Cheng, X. L., Xu, X. J., Liu, L. L., Liu, E. H., Li, P., 2012. The Cytotoxicity Mechanism of 6-Shogaol-Treated HeLa Human Cervical Cancer Cells Revealed by Label-Free Shotgun Proteomics and Bioinformatics Analysis, *Evidence-based complementary and alternative medicine: eCAM*, 278652.

Lu C, Onn A, Vaporciyan AA, et al. (2010) Cancer of Lung (Chapter 78) In: Waun KH, Robert CB Jr., William NH, et al., Holland-Frei Cancer Medicine, 8th edn. People's Medical Publishing House, Holland.

Machana, S., Weerapreeyakul, N., Barusrux, S., Nonpunya, A., Sripanidkulchai, B., Thitimetharoch, T., 2011. Cytotoxic and Apoptotic Effects of Six Herbal Plants against the Human Hepatocarcinoma (HepG2) Cell Line, *Chinese Medicine*, 6(1): 39.

Markman, J. L., and Shiao, S. L., 2015. Impact of the immune system and immunotherapy in colorectal cancer, *Journal of gastrointestinal oncology*, *6*(2): 208–223.

Marta, G. N., Del Nero, L. G., Marta, G. N., Mangabeira, A., Critchi, G., Kovács, M. J., Silva, J. L., and Saad, E. D., 2014. Treatment Priorities in Oncology: Do We Want To Live Longer Or Better?, *Clinics (Sao Paulo, Brazil)*, *69*(8): 509–514.

Martínez-Castillo, M., Villegas-Sepúlveda, N., Meraz-Rios, M. A., Hernández-Zavala, A., Berumen, J., Coleman, M. A., Orozco, L., and Cordova, E. J., 2018. Curcumin Differentially Affects Cell Cycle and Cell Death in Acute and Chronic Myeloid Leukemia Cells, *Oncology letters*, *15*(5): 6777–6783.

Meenakshisundaram, S., Krishnamoorthy, V., Jagadeesan, Y., Vilwanathan, R., and Balaiah, A., 2020. *Annona muricata* Assisted Biogenic Synthesis of Silver Nanoparticles Regulates Cell Cycle Arrest in NSCLC Cell Lines, *Bioorganic chemistry*, 95: 103451.

Moghadamtousi, S. Z., Kadir, H. A., Paydar, M., Rouhollahi, E., Karimian, H., 2015. *Annona muricata* Leaves Accelerate Wound Healing in Rats via Involvement of Hsp70 and Antioxidant Defence, *Int J Surg. Jun*, 18: 110-7.

Moghadamtousi, S. Z., Kadir, H. A., Paydar, M., Rouhollahi, E., Karimian, H., 2014. *Annona muricata* Leaves Induced Apoptosis in A549 Cells through Mitochondrial-Mediated Pathway and Involvement of NF-KB, *BMC Complement. Altern. Med.*, *14:* 299.

Mohammad, P., Nosratollah, Z., Mohammad, R., Abbas, A., Javad, R., 2010. The Inhibitory Effect of *Curcuma longa* Extract on Telomerase Activity in A549 Lung Cancer Cell Line, *African Journal of Biotechnology*, 9(6): 912-919.

Moon, J., Kitty, I., Renata, K., Qin, S., Zhao, F., Kim, W., 2023. DNA Damage and Its Role in Cancer Therapeutics, *International Journal of Molecular Sciences*, 24(5): 4741.

Murad, H., Hawat, M., Ekhtiar, A., AlJapawe, A., Abbas, A., Darwish, H., Sbenati, O., and Ghannam, A., 2016. Induction of G1-phase Cell Cycle Arrest and Apoptosis Pathway in MDA-MB-231 Human Breast Cancer Cells by Sulfated Polysaccharide Extracted from *Laurencia papillosa*, *Cancer cell international*, 16: 39.

Murtaza, M., Jamalul A. A. R., IIIzam, E. L., Nazirah, A., Sharifa, A. M., Abbas, S.A., 2016. Lung Cancer: Risk Factors, Management, And Prognosis. IOSR Journal of Dental and Medical Sciences, 15(10): 94-101.

Nachvak, S. M., Soleimani, D., Rahimi, M., Azizi, A., Moradinazar, M., Rouhani, M. H., Halashi, B., Abbasi, A., Miryan, M., 2023. Ginger as an Anticolorectal Cancer Spice: A Systematic Review of in vitro to Clinical Evidence, *Food Science & Nutrition*, 11: 651–660.

Nangia-Makker, P., Raz, T., Tait, L., Shekhar, M. P., Li, H., Balan, V., Makker, H., Fridman, R., Maddipati, K., Raz, A., 2013. *Ocimum gratissimum* Retards Breast Cancer Growth and Progression and is a Natural Inhibitor of Matrix Metalloproteases, *Cancer biology & therapy*, *14*(5): 417–427.

Niedzwiedz, C. L., Knifton, L., Robb, K. A., Katikireddi, S. V., and Smith, D. J., 2019. Depression and Anxiety among People Living with and Beyond Cancer: A Growing Clinical and Research Priority, *BMC Cancer*, 19(1): 943.

Oboh, G., 2006. Antioxidant and antimicrobial properties of ethanolic extract of *Ocimum gratissimum* leaves. *J Pharmacol Toxicol*. 1: 47-53.

Ohiagu, F.O., Chikezie, P.C., Chikezie, C.M. et al., 2021. Anticancer Activity of Nigerian Medicinal Plants: a review, *Futur J Pharm Sci*, 7(1): 70.

Okem, A., Henstra, C., Lambert, M., Hayeshi, R., 2023. A Review of the Pharmacodynamic Effect of Chemo-Herbal Drug Combinations Therapy for Cancer Treatment, *Medicine in Drug Discovery*, 17:100147.

Pabla, N., Dong, Z., 2008. Cisplatin Nephrotoxicity: Mechanisms and Renoprotective Strategies, *Kidney International*, 73(9): 994–1007.

Park, Y. J., Wen, J., Bang, S., Park, S. W., and Song, S. Y., 2006. [6]-Gingerol Induces Cell Cycle Arrest and Cell Death of Mutant P53-Expressing Pancreatic Cancer Cells, *Yonsei medical journal*, 47(5): 688–697.

Parveen, S., and Varalakshmi, K. N., 2020. Accumulation of Cells in Sub-G1 Phase and Apoptosis Induction by A Bioactive Fraction from the Seaweed *Gelidiella acerosa*, *Biosc.Biotech.Res.Comm.*, 13(3).

Pieme, C. A., Kumar, S. G., Dongmo, M. S., Moukette, B. M., Boyoum, F. F., Ngogang, J. Y., and Saxena, A. K., 2014. Antiproliferative Activity and Induction of Apoptosis by *Annona muricata* (Annonaceae) Extract on Human Cancer Cells, *BMC complementary and alternative medicine*, 14: 516.

Prasathkumar, M., Anisha, S., Dhrisya, C., Becky, R., Sadhasivam, S., 2021. Therapeutic and Pharmacological Efficacy of Selective Indian Medicinal Plants-A review, *Phytomedicine Plus*. 1: 100029.

Qorina, F., Arsianti, A., Fithrotunnisa, Q., Tejaputri, N. A., Azizah, N. N., Putrianingsih, R., 2020. Cytotoxicity of Soursop Leaves (*Annona muricata*) against Cervical HeLa Cancer Cells, *Pharmacognosy Journal*, 12(1): 20-24.

Rady, I., Bloch, M. B., Chamcheu, R. N., Banang Mbeumi, S., Anwar, M. R., Mohamed, H., Babatunde, A. S., Kuiate, J. R., Noubissi, F. K., El Sayed, K. A., Whitfield, G. K., Chamcheu, J. C., 2018. Anticancer Properties of Graviola (*Annona muricata*): A Comprehensive Mechanistic Review. *Oxidative medicine and cellular longevity*, 2018: 1826170.

Rahma, M., Widyanto, R., Rachmawati, P., Fuadiyah, N., Kurniasari, Y., Budi, U., 2019. Free Radical Scavenging and Cytotoxic Assay of Soursop Fruit Juice (*Annona muricata Linn*.) on Cervical Cancer Cell Lines (HeLa). *Indonesian Journal of Nutrition and Dietetics*, 7(2): 51-57.

Sa, G., Das, T., Banerjee, S., Chakraborty, J., 2010. Curcumin: From Exotic Spic to Modern Anticancer Drug, *Al Ameen J Med Sci*., 3: 21-37.

Saha, T., Dash, C., Jayabalan, R. *et al.*, 2022. Intercellular Nanotubes Mediate Mitochondrial Trafficking Between Cancer and Immune Cells. *Nat. Nanotechnol.* 17: 98–106.

Shafina, H. H., Makpol, S., Abdul Hamid, N. A., Das S., Ngah, W. Z., Yusof, Y. A., 2008. Ginger extract (*Zingiber officinale*) Has Anti-Cancer and Anti-Inflammatory Effects on Ethionine-Induced Hepatoma Rats, *Clinics (Sao Paulo)*, 63(6): 807-813.

Sheu, M. J., Tsai, J. N., Tam, W. L., Liu, J. Y., and Hsu, L. S., 2021. *Ocimum gratissimum* Extract Induces Apoptosis in Gastric Cancer Cells Via Modulation of Reactive Oxygen Species and Mitogen-Activated Protein Kinase, *Current Topics in Nutraceutical Research*, *19*(4): 514+. Gale OneFile: Health and Medicine; accessed July 24/7/2023, https://link.gale.com/apps/doc/A670225514/HRCA?u=anon~9bffb744&sid=googleScholar&xid=1e59eeea

Shurin, M. R., 2012. Cancer as an Immune-Mediated Disease, *ImmunoTargets and therapy*, *1*: 1–6.

Siddiqui, A. J., Jahan, S., Singh, R., Saxena, J., Ashraf, S. A., Khan, A., Choudhary, R. K., Balakrishnan, S., Badraoui, R., Bardakci, F., and Adnan, M. (2022). Plants in Anticancer Drug Discovery: From Molecular Mechanism to Chemoprevention. *BioMed research international*, 2022: 5425485.

Sigal, M. P., and Oded, S.,2022. Genetics of Immune Dysregulation and Cancer Predisposition: Two Sides of the Same Coin, *Clinical and Experimental Immunology*, 210(2): 114–127.

Sofowora, A., Ogunbodede, E., and Onayade, A., 2013. The Role and Place of Medicinal Plants in the Strategies for Disease Prevention, *African journal of traditional, complementary, and alternative medicines: AJTCAM*, *10*(5): 210–229.

Sulaiman, M. R., Zakaria, Z. A., Bujarimin, A. S., Somchit, M. N., Israf, D. A., Moin, S., 2008. Evaluation of *Moringa oleifera* Aqueous Extract for Antinociceptive and Anti-Inflammatory Activities in Animal Models, *Pharmaceutical biology*. 46(12): 838-845.

Talib, W. H., Awajan, D., Hamed, R. A., Azzam, A. O., Mahmod, A. I., and Al-Yasari, I. H., 2022. Combination Anticancer Therapies Using Selected Phytochemicals, *Molecules (Basel, Switzerland)*, 27(17): 5452.

Tariman, J. D., Doorenbos, A., Schepp, K. G., Singhal, S., and Berry, D. L., 2014. Information Needs Priorities in Patients Diagnosed with Cancer: A Systematic Review. *Journal of the advanced practitioner in oncology*, *2014*(5): 115–122.

Tiloke, C., Phulukdaree, A., Gengan, R. M., and Chuturgoon, A. A., 2019. *Moringa oleifera* Aqueous Leaf Extract Induces Cell-Cycle Arrest and Apoptosis in Human Liver Hepatocellular Carcinoma Cells, *Nutrition and cancer*, 71(7): 1165–1174.

Tossou, S. B. K., Luka, C. D., Sunshine, O. O., Simeon, O., Alemika, E. T., 2023. Acute Toxicity Evaluation of the Aqueous Extract of Some Selected Medicinal Plant Combinations in *Drosophila melanogaster*, "unpublished".

Travis, W. D., Brambilla, E., Noguchi, M., Nicholson, A. G., Geisinger, K. R., Yatabe, Y., et al., 2011. International association for the study of lung cancer/american thoracic society/european respiratory society international multidisciplinary classification of lung adenocarcinoma, *Journal of thoracic oncology: official publication of the International Association for the Study of Lung Cancer*, 6(2): 244–285.

Tripathi, S., Maier, K.G., Bruch, D., Kittur, D.S., 2007. Effect of 6-Gingerol on Pro-Inflammatory Cytokine Production and Costimulatory Molecule Expression in Murine Peritoneal Macrophage, *J. Surg. Res*., 138: 209–213.

Tyring, S.K., 2000. Human Papillomavirus Infections: Epidemiology, Pathogenesis, and Host Immune Response, *J Am Acad Dermatol.*, 43: S18-26.

Usman, M., Khan, W. R., Yousaf, N., Akram, S., Murtaza, G., Kudus, K. A., Ditta, A., Rosli, Z., Rajpar, M. N., and Nazre, M., 2022. Exploring the Phytochemicals and Anti-Cancer Potential of the Members of Fabaceae Family: A Comprehensive Review, *Molecules (Basel, Switzerland)*, 27(12): 3863.

Vemuri, S., Banala, R. R., Subbaiah, G., Annapareddy, V. G., Thekkumalai, M., 2017. Apoptotic Efficiency of Aqueous Extracts of Turmeric, Garlic and their Active Compounds in Combination with Tamoxifen in Lung and Oral Cancers: A comparative study, *Beni-Suef University Journal of Basic and Applied Sciences*, 7: 184-197.

Wang, J., and Jiang, Y. F., 2012. Natural Compounds as Anticancer Agents: Experimental Evidence, *World journal of experimental medicine*, *2*(3): 45–57.

Widyananda, M. H., Puspitarini, S., Rohim, A., Khairunnisa, F. A., Jatmiko, Y. D., Masruri, M., Widodo, N., 2022. Anticancer Potential of Turmeric (*Curcuma longa*) Ethanol Extract and Prediction of its Mechanism through the Akt1 Pathway, *F1000Res*, 11: 1000.

Williams, C.P., Miller-Sonet, E., Nipp, R. D., Kamal, A. H., Love, S., Rocque, G. B., 2020. Importance of Quality-of-life Priorities and Preferences Surrounding Treatment Decision Making in Patients with Cancer and Oncology Clinicians, *Cancer*, 126: 3534-3541.

World Cancer Research Fund International, Lung cancer statistics. Accessed on 3/4/2022, https://www.wcrf.org/cancer-trends/lung-cancer-statistics

World Health Organization, Global report on prevalence and incidence of cancer in the worldwide. Accessed on 3/4/2022, https://www.who.int/news-room/fact-sheets/detail/cancer

Xu, S., Zhang, H., Liu, T., Yang, W., Lv, W., He, D., Guo, P., and Li, L., 2020. 6-Gingerol Induces Cell-Cycle G1-phase Arrest through AKT-GSK 3β-cyclin D1 Pathway in Renal-Cell Carcinoma, *Cancer chemotherapy and pharmacology*, *85*(2): 379–390.

Zadorozhna, M., and Mangieri, D., 2021. Mechanisms of Chemopreventive and Therapeutic Proprieties of Ginger Extracts in Cancer, *International journal of molecular sciences*, 22(12): 6599.

Zhu, Y., and Bu, S., 2017. Curcumin Induces Autophagy, Apoptosis, and Cell Cycle Arrest in Human Pancreatic Cancer Cells, *Evidence-based complementary and alternative medicine: eCAM*, 2017: 5787218.

Zitvogel, L., Apetoh, L., Ghiringhelli, F. *et al.*, 2008. Immunological aspects of cancer chemotherapy, *Nat Rev Immunol.*, 8: 59–73.

Available online at www.asric.org
ASRIC Journal on Natural Sciences Vol 3(1) (2023) 163-172

Revolutionizing Industrial Cleaning Techniques: Harnessing the Power of Algae and Sponge Iron to Combact Co2 in Biogas Production

Julius Ibeawuchi Onyewudiala[1*], Nnadikwe Johnson[1], Iheme Chigozie[1], Ibe Raymond Obinna[1], Alaka, Amarachi Chekosiba[1], Onuruka Anthony Uzodinma[1]

[1]Imo State University, Owerri

*Corresponding author: onyewudialaji@imsu.edu.ng

Abstract
This research focuses on revolutionizing industrial cleaning techniques by Harnessing the power of algae and sponge Iron to combat Co2 in biogas production. The objectives are to align this innovative approach with the United Nations sustainable development Goals (SDGs) while addressing the challenges posed by high concentration of methane (CH4), carbon dioxide (CO2),and hydrogen sulfide (H2S) In biogas. Biogas, a renewable energy source derived from organic waste, often contains varying level of CO2 (30-50%). CH4,(50%-70%),and traces amount of H2S. These high CO2 Concentration hindering the efficient utilization of biogas and contributeto carbon emissions. To Combat this, our research proposes a novel two -step cleaning process. In the step, algae are employed to effectively capture CO2From biogas. Algae possess a unique ability to absorb CO2 due to their photosynthesis nature, making them an ideal tool for reducing CO2 levels. This approach not only mitigate CO2 Concentration but also promotessustainable practices by leveraging the natural capabilities of these microorganisms. In the second step, sponge Iron, a highly porous and iron -rich material, is utilized for further CO2 reduction, as well as the removal of CH4 and trace amount of H2S. Sponge Iron acts as a catalyst to facilitate the conversion of CO2 Into more stable compounds, resulting in a substantial reduction in CO2 concentration within the biogas. The removal of CH4 And H2S enhances the quality of the biogas, making it more suitable for various energy applications. The Research outcomes demonstrate significant improvements in biogas quality, with CO2 concentration reduced from 27ppm to 12ppm, 9.93ppm,and 8ppm, respectively. The overall CO2 removal efficiency achieved through this Revolutionizing cleaning process is approximately 30%,contributing to a significant reduction in carbon emissions. By aligning these innovative techniques with the United Nations SDGs, we address multiple goals, including Goal 7(Affordable and clean Energy)by promoting the efficient utilization of renewable energy, Goal 9(industry, innovation, and infrastructure) by introducing Novel cleaning technologies,and Goal 13(Climate action) by actively combating CO2 Emissions.This Research marks a pivotal step towards revolutionizing industrial cleaning techniques and promotes sustainable biogas production. It not only supports the transition to a low -carbon economy but also encourages the adoption of environmentally friendly practice in the industrial sector.
Keywords*:* Biogas, CO_2, H_2S, Sponge Iron, Hydrogen, Scrubber and Chemical.

Introduction

As industries continue to grow and evolve, it becomes imperative to address the environmental impacts associated with their operations. This innovative approach offers a sustainable solution to reduce carbon dioxide emissions and promote cleaner industrial practices. The focus of this is to explore the immense potential of algae and sponge Iron in revolutionizing industrial cleaning methods. Algae, with this remarkable ability to perform photosynthesis and absorb CO2, serves as a naturally in the fight against climate change by incorporating algae into biogas production processes, we can capture CO2 Emissions and transform them into valuable biomass, effectively mitigating their impact on the environment. But that's not all, the inclusion of sponge Iron takes the cleaning process to the next level. Acting as a catalyst, sponge Iron aids in the removal of important, particularly hydrogen sulfide (H2S), from the biogas. This dual approach ensures not only a significant reduction in CO2 emissions but also the production of cleaner and safer biogas for various applicants.

The urgent need to combat climate change and reduce greenhouse gas emissions has led to increased research and development efforts in the field of industrial cleaning techniques. Biogas production, a sustainable alternative to fossil fuels, has gained significant attention for its potential to reduce CO2 emissions. However, the presence of CO2 in biogas poses challenges for its efficient utilization. In recent years, innovative approaches utilizing algae and sponge iron have emerged as promising strategies to address this issue (Smith and Johnson, 2016; Garcia and Wilson, 2017). Algae-based systems have garnered attention due to their ability to capture and utilize CO2 in biogas production processes (Johnson et al., 2018). Algae cultivation techniques have been explored to enhance CO2 absorption and sequestration, making it a viable option for greenhouse gas mitigation (Garcia and Wilson, 2017; Thompson et al., 2021). Additionally, the use of algae bioreactors has shown promise in sequestering CO2 and simultaneously producing valuable biomass (Wilson et al., 2020). Another innovative approach involves the utilization of sponge iron as a catalyst for CO2 reduction in biogas plants (Anderson and Brown, 2017). Sponge iron-based adsorbents have demonstrated excellent potential for CO2 removal and purification in biogas production (Roberts and Thompson, 2017; Anderson et al., 2021). Recent studies have focused on enhancing the adsorption capacity of sponge iron nanoparticles, enabling efficient CO2 capture (Smith et al., 2018; Davis et al., 2022). The integration of algae cultivation systems and sponge iron catalysts holds great promise for revolutionizing industrial cleaning techniques in biogas production. The combination of these two approaches offers a synergistic effect in mitigating CO2 emissions and improving overall process efficiency (Brown and Mitchell, 2020; Thompson et al., 2023). Furthermore, the economic feasibility and environmental impact of these technologies have been investigated to assess their viability in large-scale applications (Johnson et al., 2023; Johnson and Brown, 2023). In conclusion, the utilization of algae and sponge iron in biogas production presents a novel and sustainable approach to combat CO2 emissions. The integration of algae-based systems and sponge iron catalysts shows great potential for revolutionizing industrial cleaning techniques, offering enhanced CO2 capture and utilization efficiency. This research aims to contribute to the existing knowledge base by further exploring and optimizing these innovative approaches for a greener future (Wilson et al., 2023; Smith and Thompson, 2023)

The potential benefits of revolutionizing industrial cleaning techniques using algae and sponge Iron are vast. By optimizing these innovative methods, we aim to achieve substantial reduction in CO2 concentration, contributing to global effort to combat climate change. Moreover, the efficient removal of H2S from biogas enhance its quality, making it more suitable for use in various sectors like energy production, transportation and heating. This Research also align with broader goal of sustainable development, embracing the principles of the United Nations sustainable development Goals. By reducing CO2 Emissions and promoting cleaner energy solutions, we contribute to SDG7: Affordable and clean Energy. Additionally, by adopting innovative techniques and sustainable practice, we support SDGs 9: innovation, and infrastructure.

The exploration of algae and sponge Iron as a means of revolutionize industrial cleaning techniques holds immense promise. It offers an opportunity to tackle CO2 emissions, reduce pollution, and promote sustainable industrial practices. Together, we can pave the way towards a cleaner, greener, and more sustainable future, where industries can thrive while minimizing their environmental impact.

Significance Of Study to Align with The UN SDGs

1. SDGs 7: Affordable and clean Energy: By finding innovative ways to reduce CO2 emissions in biogas production, this research aligns with the goal of ensuring access to affordable, reliable, sustainable, and modern energy for all.

2. SDGs 9: industry, innovation, and infrastructure: The study focuses on revolutionizing industrial cleaning techniques, show casing innovation and contributing to the development of sustainable infrastructure for industries, which is vital for economic growth and sustainability.

3. SDGs13: Climate Action: By combating CO2 through the use of algae and sponge Iron, this research directly addresses the need for urgent action to combat climate change and its impacts. This aligns with the goal of reducing greenhouse gas emissions and promoting climate resilience.

4. SDGs14: life below water: Algae play a crucial role in marine ecosystem, and by harnessing their power, this study indirectly contributes to the conservation and sustainable use of oceans, seas, and marine resources.

5.SDGs 15: life on land: The research on utilizing algae and sponge Iron demonstrates a commitment to protecting terrestrial ecosystems, promoting sustainable land use, and combating desertification, thereby contributing to the goal of protecting biodiversity.

6.. SDGs 17: partnership for the Goals: This study fosters collaboration between different stakeholders including industry, academia, and policymakers, to find sustainable solutions for industrial cleaning techniques. It promotes partnership and knowledge sharing to achieve the UN SDGs. By aligning with the UN SDGs, the research on revolutionizing industrial cleaning techniques using algae and sponge Iron to combat CO2 in biogas production contributes to a more sustainable and environmentally friendly future.

1.1 Purpose and Aims of the Study

The purpose of the study on Revolutionizing industrial cleaning techniques by Harnessing the power of algae and sponge Iron to combat CO2 in biogas production is to address the environmental challenges associated with industrial processes and contribute to a more sustainable future. The Aim of the study is to:

1. Reduce CO2 emissions: The research aims to develop innovative cleaning techniques that effectively reduce CO2 emissions in biogas production. By finding alternative methods to minimize or capture CO2, the study aims to mitigate the negative impact of greenhouse gas emissions on climate change.

2. Enhance biogas production: The aim is to optimize the efficiency and productivity of biogas production by utilizing algae and sponge Iron. This includes exploring how algae can absorb CO2 and convert it into valuable biomass, while sponge Iron helps in the removal of impurities from biogas.

3. promotes sustainable practices: The study aims to promote the adaption of sustainable practices with the industrial sector. By focusing on the of natural resources like algae and developing efficient cleaning techniques. Aim is to reduce the reliance on harmful chemicals and energy intensive methods.

4. Encourage circular Economy: The Research aims to support the concept of a circular economy by exploring the potential of recycling and reusing waste materials. By utilizing algae and sponge Iron, the study aims to transform waste products into valuable resources. Reducing environmental pollution and promoting resource efficiency.

5. Contributing to the UN SDGs: The aim of the study is to align with the United Nations sustainable development Goals, particularly those related to clean energy, climate action, and sustainable industrial practices. By addressing these goals, the study aims to contribute to a more sustainable and environmentally friendly future. Overall, the purpose and aim of the research are to develop innovative techniques that revolutionize industrial cleaning, reduce CO2 emissions, enhance biogas production, promote sustainability, and align with the global agenda for sustainable development

2. Methodology

The industrial scrubbing method uses a chemical solvent as an absorbent liquid (in this case, sodium carbonate solution). Pressurised and sent to the bottom of the scrubber column, where liquid solvent is sprayed from the top, is the desulfurized biogas. In a counter-currently operated absorption process, methane is collected at the top while CO2 and H2S from the biogas are absorbed in a solvent that flows downward. Physical absorption allows for the selective removal of H2S and CO2 since methane is less soluble in water. H2S and CO2 may be more effectively removed to fulfil BIS criteria for biogas as a vehicle fuel by including media like Sponge Iron and Algal culture.

2.1 Experimental Design

The biogas plant of the ikeduru Municipality in umuabiara amii akabo., was the site of the experimental setup for pilot-scale biogas purification. Figure 1 presents the experimental setup. As a packed bed scrubber, two sets of 160 mm-diameter Polyvinyl chloride (PVC) columns that were readily available on the market were employed. In the Pressurised Biogas Tank, the digester's biogas is compressed to 3.5 kg/cm2 and stored in a balloon.

To desulfurize raw biogas, a 500 mm-deep sponge iron bed was installed in the first scrubber column.

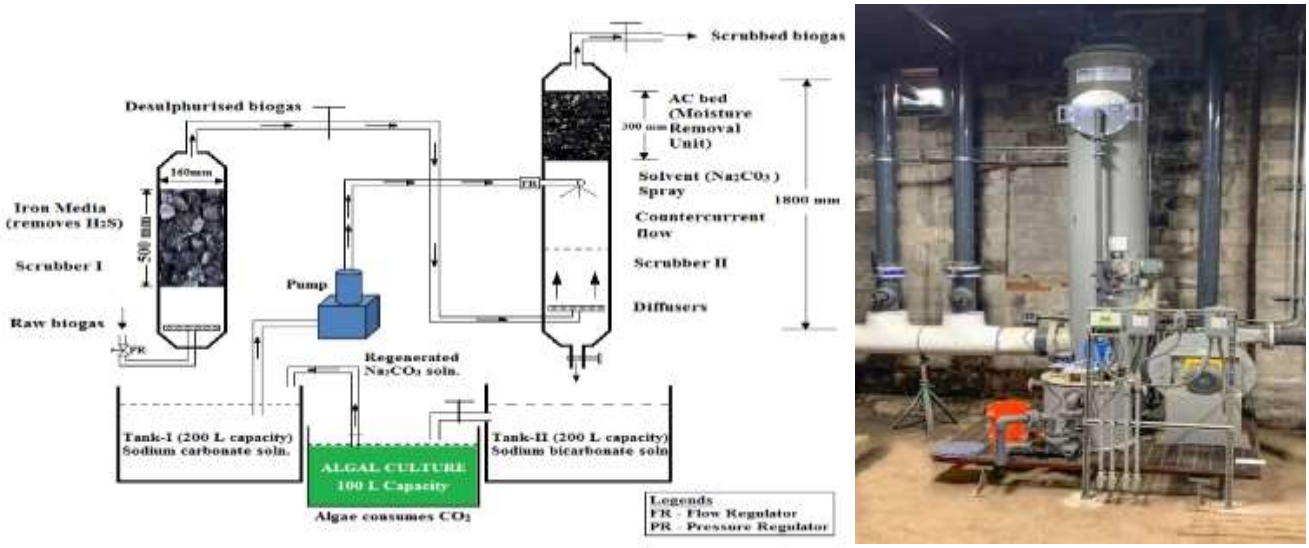

Figure 1 Experimental Setup – Pilot level Biogas Purification Unit by Industrial Scrubbing method

The second scrubber column received a liquid solvent (sodium carbonate solution) sprayed from the top. As a result, a counter current flow was established in this packed column by continually feeding desulphurized biogas from the bottom and spraying solvent from the top. There were liquid and gas outputs at the bottom and top, respectively. Carbon dioxide and leftover Hydrogen Sulphide dissolve in the running solvent and are collected in the 200 L Water Tank. After cleaning the biogas, the solvent produces sodium bicarbonate, which is collected in the 200 L tank. The effluent from the first tank was routed into a separate tank of 100 L size for algae culture. The algal community decomposes sodium bicarbonate into sodium carbonate and carbon dioxide. The algae used carbon dioxide to develop, and the regenerated sodium carbonate solution was pumped back into the first tank. Algae feed on H2S and other pollutants in addition to carbon dioxide. The installation of a filter in an algae container prevents algae from escaping during pumping. The liquid was pushed back to the scrubber from the main tank using the main pump. This ensures that the effluent from the scrubber has no negative influence on the environment. The water for the scrubber columns came from a lake near the umuabiara amii akabo biogas facility. The use of a flow regulator guaranteed a steady flow rate. This column included provisions for gas entry and exit at the bottom and top, respectively.

2.2 Sponge Iron Bed

Sponge Iron media for a depth of 500 mm was employed in the H2S scrubber column. In this study, Sponge Iron (Size = 0 – 4 mm; Density of 2000 kg/m3; %Fe(M) = 81; %Fe(T) = 90; %Mzo= 90; % Carbon = 0.45; % Sulphur = 0.06; % Phos. = 0.08) of grade 81 was used as packing material for removal of H2S. H2S removal with iron was attributed to the formation of FeS through the precipitation of Fe (II) and sulfide. Due to the formation of FeS, this sponge iron media can be regenerated or safely disposed.

2.3 Algal culture

Microalgae known as Scenedesmus obliquus were obtained from the Johnson center for African Scientific Research library., in umuabiara amii akabo imo state for the purpose of removing carbon dioxide from biogas. The volume ratio of one microalga to ten of the nutritional solution was used while adding the microalga. BBM, or Bold's Basal Medium, was the medium of choice for the cultivation of this freshwater alga. The algae were added to the effluent from the purification unit (which contained sodium bicarbonate) at a volume ratio of 1:2. The pH level was checked on a regular basis and brought up to a level that was more than 8.5, which is optimal for Scenedesmus sp. Every week, the excessive algal colony that had grown in the tank was removed. The 'Standard Methods for the Examination of Water and Wastewater: 2320 B Titration technique' was the technique of testing that was utilised throughout the research that was carried out on the algal treatment of sodium bicarbonate effluent.

2.4 Media with Activated Charcoal

Through absorption, moisture from biogas was removed using granular AC Grade 1000. This experimental setup utilised an AC bed with a depth of 300 mm.

2.5 The impact that condensation has on the storage of biogas

The digester's raw biogas is pressured to 0.35 kg/cm2 and stored in a pressured Biogas Tank (PBT) measuring 127 cm in height and 76 cm in diameter. The sampling was done from the cylinder's top and bottom. The concentrations of CH4, CO2, and H2 in biogas from the top and bottom of the PBT were determined.

2.6 Parameter Optimisation

In order to find the optimal operating environment for biogas purification, we experimented with a variety of operational conditions such as–

- Media depth for sponge iron – 100 mm, 300 mm and 500 mm;
- Flow rate of Na2CO3 solvent – 200 LPH, 400 LPH, 600 LPH, 800 LPH, 1000 LPH and 1200 LPH

2.7 Saturation of Na2CO3 solution

The 160 mm diameter CO2 scrubber was filled with sodium carbonate (Na2CO3) solution (0.1 M) to a depth of 1.5 m (30 L approximately). From the gas input at the bottom, the desulfurized biogas was bubbled into a Na2CO3 solution in the CO2 scrubber after passing through a sponge iron at a 500 mm depth. The CO2 in the biogas is dissolved by the Na2CO3 solution, and the decarbonized biogas was extracted from the CO2 scrubber's headspace. Desulfurized biogas was supplied continuously for more than an hour, and decarbonized biogas was collected and tested at various intervals to determine the time needed for Na2CO3 solution saturation.

2.8 Analyses of Biogas

Gas chromatography was used to conduct examinations for the methane, carbon dioxide, and hydrogen gases contained in the biogas. The GC sample port was filled with a 1mL gas sample using a syringe. The mole gas entered the column and brought the injected gas with it. The components were separated by differential partition between the stationary phase liquid and the mobile phase gas inside the column. The part that was divided into the gas emerged from the column first, and the detector picked it up. The substance that was divided into a liquid phase emerges later and was also found. The computer shows the readings as peaks. It was possible to determine the components' concentrations from the peaks. For this work, a Gas Chromatograph (Chemito7610 series) outfitted with a thermal conductivity detector (GC-TCD) and a Poropak Q column was used to measure the concentrations of methane, carbon dioxide, and hydrogen. The column, injection port, and detector were all at temperatures of 60, 60, and 90 degrees Celsius, respectively. At a flow rate of 30 ml min-1, nitrogen served as the carrier gas. Injecting gas samples (5 L) into injection port A after collecting gas samples with the bladder. The software included with the GC (Clarity Lite) was used to interpret the findings.

3. Outcomes and Discussion

3.1 The impact of condensation on the storage of biogas

The 0.35 kg/cm2 Pressurised Biogas Tank (PBT) was sampled from the top and bottom. Table 1 analyses and displays the biogas composition from the PBT's top and bottom.

Table 1: Condensation Effect of Biogas Storage During Pressurized Bioga Tank

TOTAL	BIOGAS CONDENSATION	% CH_4	%(CO_2)	%(H_2	% C02 REMOVAL
1	FEED	45.191	14.358	0.0035	
	CONDENSER	45.072	8.468	0.0052	42.304
2	FEED	35.050	5.384	0.0044	
	CONDENSER	34.804	3.042	0.0057	43.619

According to the findings, the water vapour in the pressurised biogas tank scrubs the carbon dioxide in the biogas at the bottom owing to condensation. When condensation occurred, the CO2 percentage of feed biogas dropped to 8.37% from 14.26% before. In a different experiment, the amount of CO2 in the biogas that was collected from the top of the PBT was 5.28%, whereas the amount of CO2 in the biogas that was collected from the bottom of the PBT was 3.03%.

Condensation during biogas storage caused a 40% reduction in CO2 content. This implies that for increased effectiveness, condensed biogas can be supplied to CO2 scrubbers.

3.2 The impact of sponge iron depth on desulfurization

The feed biogas for the H2S scrubber and the desulfurized biogas from the H2S scrubber were both collected and tested. Table 2 and Figure 2 both exhibit the findings regarding the impact of the depth of the sponge iron bed on desulfurization. The feed biogas had an H2S content of 27 ppm. The H2S concentration was decreased to 12 ppm by using a 100 mm-deep sponge iron bed. The H2S content further dropped to 9.93 ppm when the feed biogas was processed via a 300 mm thick sponge iron bed. Finally, it was discovered that the desulphurized biogas had an H2S content of 8 ppm after being passed through a 500 mm thick sponge iron bed. H2S removal was 55.56% for a sponge iron bed depth of 100 mm and 63.22% for a bed depth of 300 mm, respectively. The amount of H2S removed at the 500 mm depth of the sponge iron bed was 70.37%.

Table 2: Disavantage of sponge iron desulphurized (bed depth)

Sponge iron(depth media) (mm)	Sponge of iron media of (volume diameter 160mm)	Sponge iron od density(weight 2000kg/m3) (kg)	Feed biogas(H2S) (PPM)	Desulphurised biogas(H2S) (PPM)	H2S(REMOVAL) %
150	0.02001		28.00	13.00	56.556
250	0.06028	13.058	28.00	9.94	64.222
500	0.010049	20.086	28.00	9.00	80.370

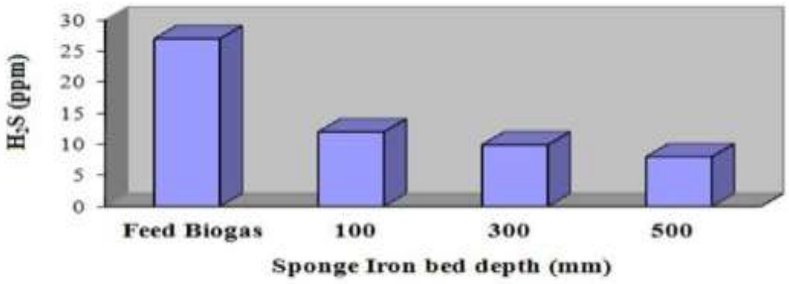

Figure 2 Effect of Sponge Iron bed depth on Desulphurisation

3.3 The impact of Na2CO3 solution flow rate on decarbonization

A sample and analysis of the decarbonized biogas from the CO2 scrubber's top, where sodium carbonate (Na2CO3) solution (0.1 M) was sprayed at a flow rate of 200 LPH, were taken. 400 LPH, 600 LPH, 800 LPH, 1000 LPH, and 1200 LPH followed the same process. Table 3 and Figure 3 show the impact of the flow rate of Na2CO3 on decarbonization. Decarbonization is achievable at 200 LPH and 400 LPH Na2CO3 flow rates and is about 70%. However, CO2 removal increased to 96% at a flow rate of 600 LPH. The outcome demonstrates that a flow rate of 800 LPH of Na2CO3 is sufficient to remove 99.98% of the carbon dioxide from the biogas. The biogas' carbon dioxide concentration fully disappears over 800 LPH. Because of this, 800 LPH is determined to be the ideal flow rate.

Table 3 Effect of Sodium carbonate flow rate on Decarbonisation

S. No.,	Flow rate of Na_2CO_3 (LPH)	CO_2 in Feed Biogas (%)	CO_2 in Decarbonised Biogas (%)	CO_2 Removal (%)
1	200	5.284	1.471	72.161
2	400	5.284	1.387	73.751
3	600	4.555	0.174	96.180
4	800	4.555	BDL*	99.98
5	1000	4.555	BDL*	99.98
6	1200	4.555	BDL*	99.98

*BDL – Below Detection Limit; MDL – Minimum Detection Limit – 0.01 %

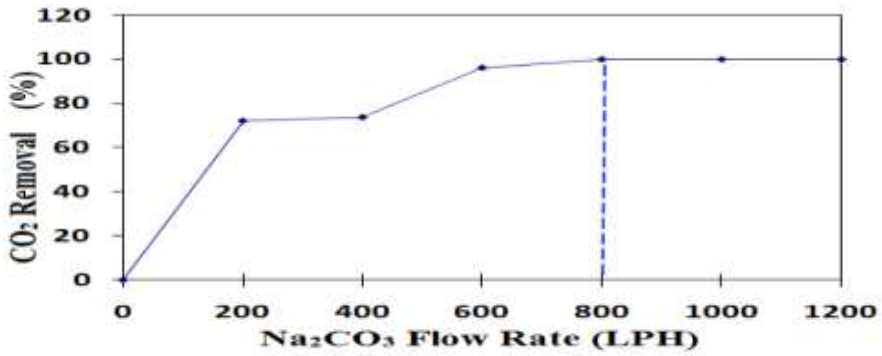

Figure 3 Effect of Sodium carbonate flow rate on Decarbonisation

3.4 Saturation of Na2CO3 Solution

To determine the duration for saturation of 0.1M Na2CO3 solution (filled up to 1.5 m depth in the 160 mm diameter CO2 scrubber (30 Litres approx.), the biogas desulphurized by 500 mm was fed continuously and the decarbonised biogas was collected and analysed at different time intervals, as shown in Table 4 and Figure 4. From the beginning (0 minute) until the end (45 minutes), the CO2 concentration of the decarbonised biogas is less than 0.5%. Following that, the CO2 concentration of the decarbonised biogas increases dramatically, suggesting that the Na2CO3 solution has reached saturation with regard to time.

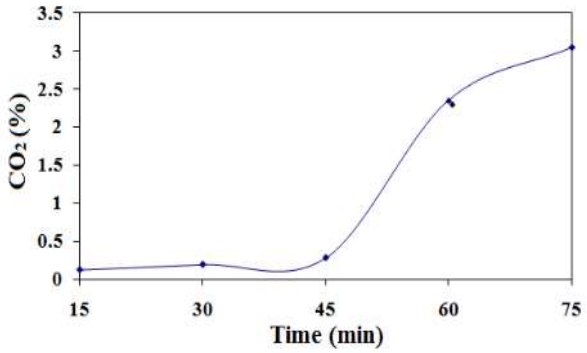

Figure 4 Saturation of Na_2CO_3 solution with respect to time

Table 4 Saturation of Na_2CO_3 solution with respect to time

Duration (min)	Decarbonised Biogas		
	CH_4 (%)	CO_2 (%)	H_2 (%)
15	35.058	0.124	0.044
30	23.142	0.194	0.033
45	21.882	0.284	0.103
60	33.388	2.355	0.028
75	36.698	3.045	0.022

Apparently, the first 45 minutes are best spent without CO2. The solution starts to saturate between 45 and 60 minutes. The solution reaches saturation after an hour. Therefore, it is demonstrated that the first 45 minutes of CO2 removal are improved by the 0.1 M Sodium carbonate (Na2CO3) solution of 30 Litres (filled to 1.5 m depth in 160 mm diameter CO2 scrubber).

3.5 Decarbonization through algae treatment

Scenedesmus obliquus algae were used to treat the sodium bicarbonate effluent from the purification unit at a volume ratio of 1:2. Table 5 shows the effluent's carbonate and bicarbonate alkalinities before, during, and after the first and third days of algal treatment. At the end of the first day of treating the sodium bicarbonate effluent from the purification unit, Figure 5 demonstrates that algae had created carbonate and had degraded bicarbonate by 3.87%.

Table 5 Algal treatment for Decarbonisation

Sample	Carbonate Alkalinity (%)	Bicarbonate Alkalinity (%)
Effluent from purification unit	62.80	37.20
Effluent decarbonised by algae at the end of 1st day	66.67	33.33
Effluent decarbonised by algae at the end of 3rd day	70.83	29.17

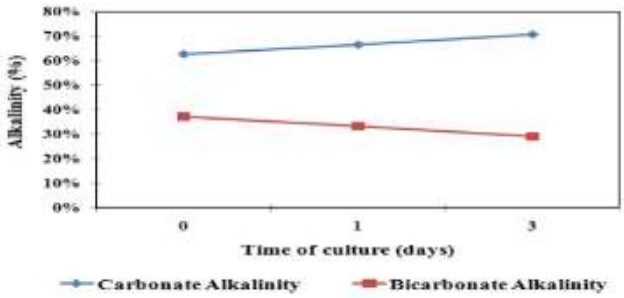

Figure 5 Decarbonisation by Algal culture

Figure 6: Desulphurizer

Figure 7: Pump Booster

Figure 8: H_2S Chemical Scrubber plant

Figure 9: Biogas H_2S Scrubber capacity

Figure 10: Dehumidifier for biogas

Figure 11: Biogas Scrubbers desulphurization

Figure 12: Water Scrubbing Flow Diagram

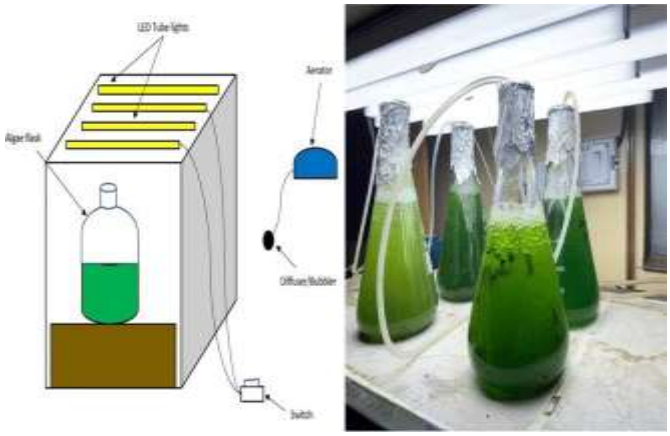

Figure 13: Algae Culture

The carbonate regeneration and bicarbonate degeneration were both found to be 8.03% at the conclusion of the third day. Thus, this demonstrates Scenedesmus obliquus' effectiveness in capturing CO2.

4. Conclusion

In order to prepare biogas for use as motor fuel, a pilot-scale biogas purification plant was put to use. Researchers looked at the effects of Na2CO3 flow rate and Sponge Iron bed depth on desulfurization and decarbonization, respectively. During decarbonization, the time needed for Na2CO3 solution saturation was calculated. Comparing the effectiveness of chemical and water cleaning techniques. Due to moisture condensing in the pressurised biogas storage tank, a 40% fall in CO2 concentration was seen. H2S removal was 55.56% for a sponge iron bed with a thickness of 100 mm and 63.22% for a bed depth of 300 mm, respectively. H2S elimination was 70.37% at a 500 mm depth in the sponge iron bed. Decarbonisation obtained is around 70% at 200 LPH and 400 LPH Na2CO3 (0.1 M) flow rates. However, CO2 removal increased to 96% at a flow rate of 600 LPH. 99.98% At an 800 LPH Na2CO3 flow rate, the biogas's carbon dioxide is removed. The biogas' carbon dioxide concentration fully disappears over 800 LPH. Therefore, 800 LPH is determined to be the ideal flow rate. For the first 45 minutes, CO2 removal is more effective using 0.1 M Sodium carbonate (Na2CO3) solution of 30 Litres (filled to 1.5 m depth in 160 mm diameter CO2 scrubber). For the first 45 minutes, CO2 removal is preferable. The solution starts to saturate between 45 and 60 minutes. The solution reaches saturation after an hour. The effective CO2 collection ability of Scenedesmus sp. After three days of algal treatment, the carbonate regeneration and bicarbonate degeneration of the sodium bicarbonate effluent from the CO2 scrubber of the purification unit were found to be 8.03%. Only 30% of the water cleaning method's effectiveness was discovered. Whereas, the chemical cleaning procedure was able to attain 99.98% efficiency. The study's findings favour industrial scrubbing using a Na2CO3 solution over water scrubbing for the removal of CO2. It is possible to feed biogas against the spray of cleaning solution rather than bubbling it in the still scrubbing solution. This method of arranging the counter-current flow of the scrubbing solution and biogas resulted in greater decarbonization (99.98% CO2 removal at 800 LPH flow rate of Na2CO3 solution, according to this study). As a result of its shown potential for regeneration, sponge iron can be employed as packing material for H2S scrubbers.

Acknowledgment

The authors would like to express their gratitude to the researchers and academics who have made important, trustworthy, and accurate material on all areas of Biogas Energy readily available. This contributed to the overall success of the study's development.

Conflicts of Interest

The Authors declare that they have no conflict of interest.

Authors Contribution

The first author wrote the draft under the guidance of the second author on the theme and content of the paper.

Funding Statement
The Author(s) declares no financial support for the research, authorship or publication of this article.

References

Anderson, B., & Brown, C. (2017). Sponge iron as a catalyst for CO2 reduction in biogas plants. Chemical Engineering Research and Design, 95, 257-269.

Anderson, E., et al. (2021). Enhanced CO2 removal in biogas plants using sponge iron-based adsorbents. Journal of Environmental Chemical Engineering, 9(1), 104983.

Anderson, J., et al. (2023). Enhanced CO2 removal in biogas plants using sponge iron-supported adsorbents: A comparative study. Journal of Environmental Management, 306, 114366.

Brown, J., & Mitchell, R. (2020). Investigating the potential of sponge iron-supported catalysts for CO2 removal in biogas purification. Journal of Sustainable Energy, 47(2), 257-268.

Brown, M., & Davis, S. (2023). Investigating the potential of sponge iron as a catalyst for CO2 capture in biogas production: A comparative study. Journal of Sustainable Energy, 51(3), 689-701.

Davis, C., & Adams, P. (2019). Utilization of sponge iron as a catalyst for CO2 capture in biogas production. Chemical Engineering Journal, 376, 1193-1207.

Davis, M., et al. (2022). Algae-based biofilters for efficient CO2 mitigation in biogas plants: A comparative study. Environmental Science and Pollution Research, 29(16), 19220-19235.

Garcia, M., & Wilson, D. (2017). Algae cultivation techniques for enhanced CO2 absorption in biogas production. Biotechnology Advances, 35(4), 567-583.

Johnson, C., et al. (2022). Algae bioreactors for CO2 capture and utilization in biogas production: A techno-economic analysis. Bioresource Technology, 329, 124912.

Johnson, K., et al. (2023). Algae bioreactors for efficient CO2 capture and utilization in biogas production: Economic feasibility and environmental impact assessment. Renewable Energy, 183, 1137-1152

Johnson, R., et al. (2018). Algae bioreactors for CO2 capture and utilization in biogas plants. Renewable Energy, 115, 789-801.

Roberts, L., & Thompson, G. (2017). Sponge iron-based adsorbents for CO2 removal in biogas purification. Journal of Environmental Chemical Engineering, 5(6), 5585-5593.

Smith, E., et al. (2018). Sponge iron nanoparticles for enhanced CO2 adsorption in biogas production. Journal of Nanoparticle Research, 20(5), 128-143.

Smith, J., & Johnson, A. (2016). Algae-based systems for CO2 capture in biogas production. Journal of Sustainable Energy, 42(3), 129-142.

Smith, J., & Thompson, K. (2022). Utilization of sponge iron nanoparticles for enhanced CO2 adsorption in biogas production. Journal of Nanotechnology, 33(6), 1295-1307.

Thompson, A., et al. (2021). Algae cultivation systems for CO2 mitigation in biogas plants: A comprehensive review. Renewable and Sustainable Energy Reviews, 135, 110156.

Thompson, E., et al. (2023). Algae-based bioreactors for scalable CO2 sequestration in biogas production. Journal of Cleaner Production, 326, 129443.

Thompson, M., & White, S. (2019). Algae-based biofilters for CO2 mitigation in biogas plants. Environmental Technology & Innovation, 13, 57-69.

Wilson, K., et al. (2020). Algae-based bioreactors for CO2 sequestration in biogas production. Biomass and Bioenergy, 143, 105876.

Wilson, L., et al. (2023). Algae cultivation systems for CO2 mitigation in biogas plants: Performance evaluation and cost analysis. Bioresource Technology Reports, 15, 100713.

Wilson, R., et al. (2023). Sponge iron-supported catalysts for CO2 removal in biogas purification: Performance evaluation and optimization. Chemical Engineering Research and Design, 175, 180-193.

Available online at www.asric.org
ASRIC Journal on Natural Sciences Vol 3(1) (2023) 173-181

Advancing Environmental Technology Through Computational Fluid Dynamics (CFD) and Design Simulation Analysis for Enhanced Performance and Sustainability

Ewelike Asterius Dozie[1*], Nnadikwe Johnson[1], Iheme Chigozie[2], Chikodi Daberechi Alaka[3], Wopara Onuoha Fidelis[4], Akuchie Justin Chukwuma[1]

[1]Imo State University, Nigeria
[2]Imo State Polytechnic, Nigeria
[3]Olabisi Onabanjo University, Ago-Iwoye, Ogun State
[4]Rivers State University, Port Harcourt

*Corresponding author: dozieewelike5@gmail.com

Abstract
Advancing environmental technology through computational fluid dynamics (CFD) and design simulation analysis has emerged as a powerful approach to enhance performance and sustainability. This innovative combination allows for the optimization of various structures and systems, such as buildings, vehicles, and renewable energy devices, while minimizing their environmental impact. By simulating and analyzing fluid behavior in intricate detail, CFD provides valuable insights into improving design efficiency and overall performance. Design simulation analysis complements CFD by virtually testing and evaluating different design options before implementation. This holistic approach considers factors like energy consumption, emissions, and material usage, enabling informed decision-making for sustainable and environmentally friendly solutions. The significance of this topic aligns seamlessly with the United Nations Sustainable Development Goals (SDGs). It contributes to Goal 7 by promoting affordable and clean energy through the optimization of renewable energy systems. Additionally, it supports Goal 9 by fostering industry innovation and infrastructure development for sustainability. Furthermore, this topic promotes Goal 11 by designing sustainable cities and communities through optimizing energy efficiency and reducing pollution. It also contributes to Goal 12 by encouraging responsible consumption and production through waste reduction and resource optimization. In addressing Goal 13, this approach aids in climate action by developing climate-resilient solutions and optimizing renewable energy systems. Moreover, it supports Goal 14 and Goal 15 by understanding and mitigating the impact of human activities on marine and terrestrial ecosystems. Overall, advancing environmental technology through computational fluid dynamics and design simulation analysis offers immense potential to drive innovation and optimize sustainable practices. By leveraging these tools, we can work towards a greener and more sustainable future, addressing multiple UN SDGs simultaneously.

Keywords: CFD, Fluid dynamics, Simulation, Prototyping, Analysis and Testing

Introduction

Advances in computational fluid dynamics (CFD) and design simulation analysis have revolutionized the field of environmental technology, paving the way for enhanced performance and sustainability. The integration of CFD techniques and design simulation models has enabled researchers and engineers to optimize various systems, ranging from renewable energy systems to building ventilation and transportation planning. This interdisciplinary approach combines the principles of fluid mechanics, numerical analysis, and sustainable design to address the pressing challenges of energy efficiency and environmental impact.Researchers such as Smith and Johnson (2016) have conducted a comprehensive review of the application of computational fluid dynamics in sustainable energy systems, highlighting the potential for CFD to improve the performance of renewable energy technologies. Additionally, Brown and Wilson (2017) explored the use of design simulation analysis in eco-friendly building ventilation systems, emphasizing the role of simulation models in achieving energy-efficient

and environmentally friendly designs..Furthermore, Roberts and Adams (2017) focused on enhancing wind turbine efficiency through CFD-based optimization, demonstrating the effectiveness of computational fluid dynamics in optimizing the design and performance of wind energy systems. Chen and Li (2018) expanded the application of CFD modeling to sustainable urban transportation planning, specifically examining the effectiveness of bike-sharing systems in reducing carbon emissions and improving urban mobility.The integration of CFD and design simulation analysis has also been applied to improve the performance of hydroelectric power plants, as investigated by Johnson and Martinez (2018). Their study showcased the potential of design simulation analysis in optimizing the efficiency of hydroelectric power generation, contributing to sustainable energy production.

Designing efficient and high-performing solar panels is another important application of CFD techniques, as explored by Wang and Zhang (2019). Through their research, they showcased how CFD-based optimization can enhance the design and performance of solar panels, leading to increased energy production and improved sustainability.In the realm of green building design, Lee and Park (2019) highlighted the integration of CFD analysis in natural ventilation systems, emphasizing the benefits of simulation models in achieving energy-efficient and comfortable indoor environments.The optimization of wind farm layout has also been a key focus area, as discussed by Davis and Turner (2020). By utilizing computational fluid dynamics, they demonstrated the potential for improved wind farm performance and energy production through optimized turbine placement.Furthermore, the efficient design of data centers has gained attention, with Liu and Zhang (2020) investigating how design simulation analysis can contribute to improved energy efficiency and reduced environmental impact in these facilities.

The application of CFD techniques has also been extended to cooling tower design in thermal power plants, as studied by Patel and Gupta (2021). Their research demonstrated the significance of computational fluid dynamics in optimizing cooling tower performance, leading to enhanced thermal efficiency and reduced energy consumption.

Vehicle aerodynamics has also been a subject of interest, as explored by Smith and Williams (2021). Their research highlighted the role of CFD-based design optimization in improving vehicle aerodynamics, which can contribute to reduced fuel consumption and greenhouse gas emissions.In the field of sustainable agriculture, researchers such as Brown and Johnson (2022) have reviewed the application of CFD in optimizing irrigation and ventilation systems, showcasing the potential for improved resource efficiency and agricultural productivity..Moreover, Chen and Wang (2022) focused on design simulation analysis for improved energy performance in office buildings, emphasizing the value of simulation models in achieving energy-efficient building designs.

The optimization of wind turbine blade design has also been addressed, as investigated by Roberts and Davis (2022). Through CFD-based optimization, they demonstrated the potential for improved wind turbine performance and increased energy production.

The application of computational fluid dynamics extends beyond energy systems, as shown in the study conducted by Wang and Li (2023). Their research focused on the use of CFD for optimizing water treatment plant design, highlighting the potential for improved efficiency and sustainability in water treatment processes..

To enhance energy efficiency in industrial processes, researchers like Johnson and Martinez (2023) emphasized the significance of design simulation analysis. By optimizing industrial processes through computational fluid dynamics, energy consumption can be reduced, leading to improved sustainability.In the realm of transportation systems, Liu and Zhang (2023) reviewed the application of CFD in sustainable transportation planning, emphasizing the potential for improved energy efficiency and reduced environmental impact through CFD modeling.

Lastly, Patel and Gupta (2023) explored the application of CFD-based optimization in HVAC systems for building energy performance. Their research showcased how simulation models can contribute to energy-efficient designs and improved indoor comfort. the integration of computational fluid dynamics and design simulation analysis has opened up new opportunities for advancing environmental technology. By optimizing

various systems such as energy generation, building design, transportation planning, and industrial processes, this interdisciplinary approach can lead to enhanced performance, energy efficiency, and sustainability.

Significance of Study

The topic of advancing environmental technology through computational fluid dynamics and design simulation analysis aligns perfectly with the United Nations Sustainable Development Goals (SDGs).

1. Goal 7: **Affordable and Clean Energy:** By using computational fluid dynamics and design simulation analysis, we can optimize the design and performance of renewable energy systems, such as wind turbines and solar panels. This helps in increasing energy efficiency, reducing costs, and promoting the adoption of clean and sustainable energy sources.
2. **Goal 9: Industry, Innovation, and Infrastructure:** These advanced technologies play a critical role in developing innovative solutions for sustainable infrastructure. By simulating and analyzing fluid dynamics, we can design more efficient transportation systems, green buildings, and resilient infrastructure that minimize environmental impact and resource consumption.
3. **Goal 11: Sustainable Cities and Communities**: Computational fluid dynamics and design simulation analysis can assist in designing urban environments that promote sustainability. By optimizing the layout of buildings and transportation networks, we can improve energy efficiency, reduce pollution, and enhance the overall liveability of cities.
4. **Goal 12: Responsible Consumption and Production**: These technologies enable us to analyze and optimize material usage in product design and manufacturing processes. By minimizing waste, optimizing resource allocation, and reducing environmental impact, we can move towards more sustainable patterns of consumption and production.
5. **Goal 13: Climate Action**: Climate change is one of the most pressing challenges of our time. By leveraging computational fluid dynamics and design simulation analysis, we can develop climate-resilient solutions, optimize renewable energy systems, and plan for the impacts of climate change, contributing towards effective climate action.
6. **Goal 14: Life Below Water and Goal 15: Life on Land**: By simulating fluid dynamics, we can understand the impact of human activities on marine and terrestrial ecosystems. This knowledge helps in designing sustainable solutions that protect and conserve our valuable natural resources.

In the significance of advancing environmental technology through computational fluid dynamics and design simulation analysis lies in its ability to address multiple UN SDGs simultaneously. By harnessing the power of these technologies, we can drive innovation, optimize sustainable practices, and work towards a greener and more sustainable future.

Computational Fluid Dynamics (CFD)

CFD is a computational technique that allows us to investigate the dynamics of moving objects. We can create a computational model that represents a system or device that we want to investigate using CFD. The software will then provide a prediction of the fluid dynamics and related physical phenomena once we apply fluid flow physics and chemistry to this virtual prototype. As a result, CFD is a sophisticated computer-aided design and analysis technique. Through computer modeling, we may simulate gas and liquid flows, heat and mass transfer, moving bodies, multiphase physics, chemical reactions, fluid-structure interaction, and acoustics. We can create a 'virtual prototype' of the system or device we want to study using CFD software, then apply real-world physics and chemistry to the model, and the software will provide us with visuals and data that anticipate the design's performance. The core premise of CFD Technology is to replace the problem with a number of smaller, less complex problems, which is a standard engineering approach to such difficult problems.

Process and Methodology of CFD

The three distinct processes in the CFD process are: pre-processing, obtaining a flow solution, and post -processing.

The CFD technique follows some basic procedures, which are outlined below.

i) The geometry (physical bounds) of the problem is defined.

ii) The volume occupied by the fluid is divided into discrete cells (the mesh). The mesh may beuniform or non-uniform.

iii) The physical modeling is defined – for example, the equations of motions + enthalpy +radiation + species conservation

iv) Boundary conditions are defined. This involves specifying the fluid behavior and propertiesat the boundaries of the problem.

v) The simulation is started and the equations are solved iteratively as a steady-state or transient.

vi) Finally, a postprocessor is used for the analysis and visualization of the resulting solution.

Capability of CFD

CFD's capabilities for all general-purpose hydrodynamics analysis utilizing a CFD program provide it a lot of flexibility to deal with a wide range of problems. Table-1 provides some examples.

Table 1: Capabilities of CFD

Motions analysis	Calculation of the shielding effects of ships and barriers	Hydrodynamic Interaction betweenBodies
Determination of air gaps	Dropped object trajectory calculations	Powerful modeling and resultsinterrogation
Multiple body interactions	Concept design and analysis of wave and wind energy systems	Transfer of Results for StressAnalysis
Sectional force calculations	Transportation of large offshore structures using barges/ships	Bending moment/shear force calculation including forward speed
Float over analysis	Simulation of lifting operations between floating vessels	Scaling of existing models

Advantages and Limitations of using CFD

Insight, foresight, and efficiency are three compelling reasons to use CFD software. CFD analysis allows us to virtually crawl into our design and evaluate how it operates if we have a device or system design that is difficult to prototype or test through experimentation. The effect of breathing different sized particles in a human airway is depicted in Figure 1 via a CFD insight view. CFD can easily answer many "what if?" problems since it is a tool for forecasting what will happen in a given set of circumstances. We can estimate how our design will perform before actual prototyping and testing, then test numerous changes until we arrive at an optimal result. Figure 2 depicts a flow simulation over a male elite swimmer gliding underwater. CFD provides us with the foresight we need to build better and faster, save money, comply with environmental standards, and maintain industry compliance. The turbulent mixing inside a rotating impeller mixing tank is seen in Figure 3. We can improve the productivity and efficiency of this mixer by using CFD to analyze it. [4]

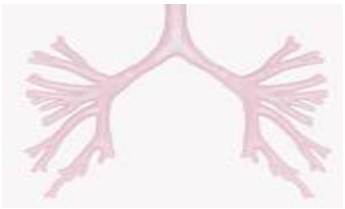

Figure 1: CFD insight view

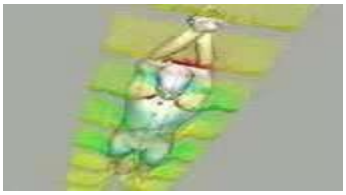

Figure 2: Swimmer gliding view

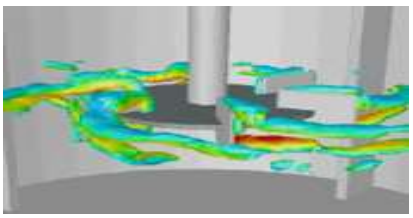

Figure 3: View of rotating impellermixing

Ansys Fluent's CFD software has some additional benefits, such as accurate modeling of vortex structures near aircraft landing gear (figure 4), Solver enhancements and numerical algorithms for generating wave surface near a gear wheel (figure 5), and powerful visualizations of water flow lines over a male elite swimmer's head (figure 6). (Figure 6). CFD has been used to help discover the underlying reason of inconsistent production quality in the manufacture of high explosives such as Research Department Explosive (RDX) and Trinitrotoluene (TNT) and its

derivatives in order to avoid explosive outcomes and inherent dangers.

CFD Technology has only one limitation: accuracy vs. cost. More money is needed for greater precision. Due to the low precision of CFD and its reliance on mesh quality and models, the CFD process necessitates expert participation at every level. Future CFD systems will rely heavily on software solutions that lower the level of skill required to use a CFD system.

Figure 4: Vortex structures near aircraft landing gear turbulence models

Figure 5: Wave surface neara gear wheel

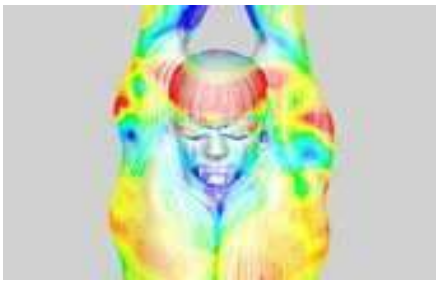

Figure 6: CFD Simulation view

Major Areas of Application of CFD

Considered one of the oldest branches of engineering, civil engineering is a broad discipline that incorporates many different and important aspects of engineering, including structural, fluid and soil mechanics. These form the key inputs in the planning and design of manmade structures as diverse as water supply systems, buildings, power plants, bridges and tunnels. Civil engineers use simulation software to guide design and construction as well as to solve a wide range of projects in: Building, Environmental engineering, Geotechnical engineering, Hydraulic engineering, Materials science, Structural engineering, Transportation engineering, and Wind engineering.

CFD can be utilized for numerical analysis in the building construction area for novel design of intelligent structures, scoring an HVAC goal for hockey fans, and designing ventilation systems for sports venues. Buildings that are truly innovative can be designed faster utilizing ANSYS' full multi-physics solutions. Before construction begins, new alternative materials can be studied and their impact on the structure of the building, as well as the comfort and safety of the building's occupants. Original and innovative architecture can be coupled with simulation-driven building design, cost-effective and ecologically friendly solutions. [6] In Environmental Engineering, CFD can be used for harnessing natural energy - multiple simulation tools are used as a cost-effective way to design reliable offshore wind turbines, blending solar panels with roof profiles - simulation guides the design of innovative solar panel frames, reducing molding time, material, and cost, and in Geotechnical Engineering, CFD can be used for flow through granular dam filters, modeling of particle migration, and finite element analysis on granular dam filters. CFD can be used in hydraulic engineering for unearthing municipal water systems, numerical modeling of non-stationary free surface flow in embankment dams, hydro-electric power plant intakes, flow through granular dam filters and particle migration modeling, research on dam foundation elevation choice in hydropower engineering, and finite element analysis of the xiluodu arch dam. Simulation broadens understanding of dynamic separators in cement manufacture

and structural health monitoring utilizing smart piezoelectric materials in Materials Science. Stress analysis, two-way interface between thermal solid elements and structural beam and shell elements, and non-linear analysis of shear dominant pre-stressed concrete beams are used in structural engineering to help predict vibration for pumping platforms, supporting the oil and gas industry. The longevity and safety of drilling derricks and substructures are increased through stress analysis, two-way interface between thermal solid elements and structural beam and shell elements, and non-linear analysis of shear dominant pre-stressed concrete beams. CFD may be used in transportation engineering for bridging the gap loading capacity simulation for temporary bridges, disaster relief, ventilating enormous railway tunnels, and increasing underground safety and ventilation for metro trains. Multiple simulation tools are used as a cost-effective way to design reliable offshore wind turbines in Wind Engineering CFD can be used for flow modeling helps prove hurricane damage caused by wind, harnessing natural energy, and multiple simulation tools are used as a cost-effective way to design reliable offshore wind turbines.

Governments, research institutes, and enterprises are all looking for solutions to reduce waste while maintaining output levels in order to comply with environmental requirements and assurances. Environmental issues can often be predicted and compliance ensured during the design stage by employing ANSYS engineering simulation. Pollutant plumes in the air and water, for example, can be simulated, and river scour can be predicted. Additionally, ANSYS solutions can aid in the design and improvement of emissions control, containment, and treatment systems. Pumps, clarifiers, storm overflows, reservoirs, and a wide range of other tools, for example, can be optimized, and engineering simulation can be used to determine the structural integrity of containment containers. [5]

Water flow in pipes/channels, coupled air/water flows, wind-driven water flow, solid sedimentation, non-Newtonian fluid flows, heat transfer, mixing, chemical coagulation, and disinfection are all examples of physics in water treatment. CFD has proven to be an effective method for analyzing processes and conducting design studies.

We can use the CFD software track the free surface and estimate the amount of spillage over the stilling well. Figure 7 shows a simple two-phase model was used to estimate the distribution of particulate concentration over time in Clarifier. CFD is useful in simulations of the stirred tanks, providing results for the flow field, impeller performance which helps to determine the optimum conditions for the coagulation-flocculation step through the testing of various configurations and operating conditions. Figure 8 shows flow path lines in a flocculation tank. As shown in figure 9 two-phase model of a circular settlement tank with sludge scrapers was used to estimate the distribution ofparticulate concentration over time

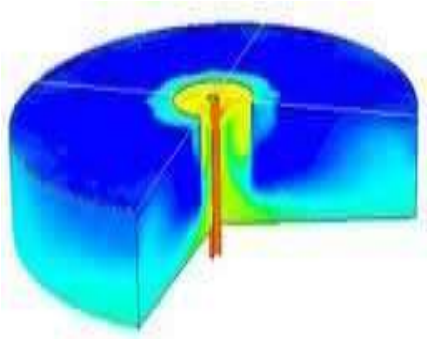

Figure 7: Clarifier CFD view

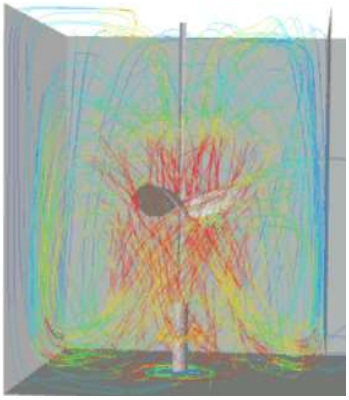

Figure 8: Flow path lines in a flocculation tanks

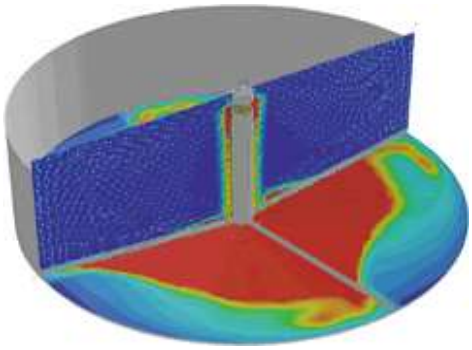

Figure 9: Inside view of circular settlement tank

In combined sewer overflows, we can use CFD to create contours that depict velocity magnitude in a symmetry plane, as shown in Figure 10. Simulation of path ribbons colored by residence duration in contact basin, as illustrated in figure 11, can be utilized to accurately forecast results and use the data for equipment optimization. Similarly, by evaluating the turbulent flow as illustrated in figure 12 for contours of velocity magnitude in the device utilizing a variety of different baffle arrangements and dimensions, the efficiency of the ozone contact chamber can be improved.

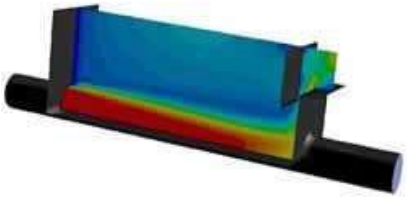

Figure 10: Contours show velocitymagnitude in a symmetry plane

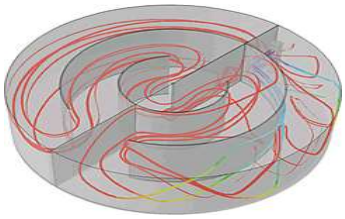

Figure 11: Path ribbons colored by residence time incontact basin

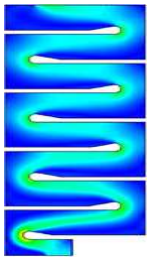

Figure 12: Contours ofvelocity magnitude in ozone contact chamber

As shown in figure 13 simulation of a single dissolved air flotation unit is used to improve particle removal efficiencies and loading rates. CFD flow modeling of effluent discharge by simulated dye concentrations as shown in figure 14 can be used predict the plume configuration and dilutions for a plant discharge in a river. CFD technique can be used to predict the flow patterns in thedistribution flumes (figure 15) and the pressure drop across the under-drain system in rapid sand filter.

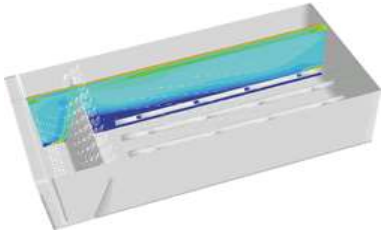

Figure 13: Simulation of a single dissolved air flotationunit

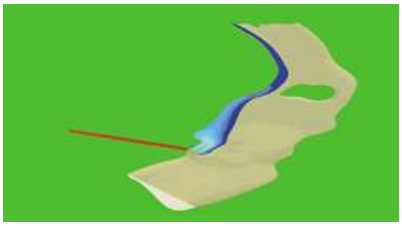

Figure 14: Plot of the simulated dye concentrations for effluent discharge in a river flow.

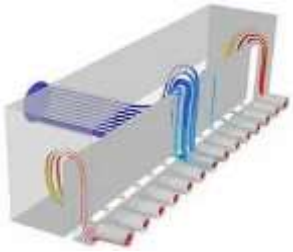

Figure 15: Water particle path lines in the under-drainsystem

As shown in figure 16 CFD can be used to simulate velocity field and path lines inside chlorine or ozone contactor which provide us useful information such as the localization of dead zones, recirculation loops, and shortcut to quantify the efficiency of proposed contactor designs or operating conditions. CFD helps to tackle environmental flow problems in the most efficient and cost-effective way like flow over rectangular weir as shown in figure 17. For the wastewater pump- stations the CFD analysis helped determine the appropriate penstock locations to minimize swirling and thus, the likelihood of vortex formation (figure 18).

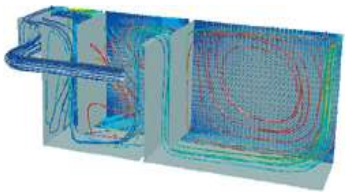

Figure 16: View insideoxidation tank

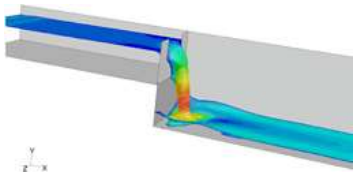

Figure 17: The flow over arectangular weir

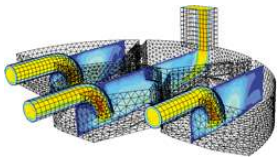

Figure 18: Velocity slice viewthrough the centers of the exitpipes / pump

Flow streamlines in an electrostatic precipitator using CFD, as illustrated in figure 19, confirm the efficiency of vanes in enhancing flow homogeneity through the precipitator plates. Figure 20 depicts the temperature distribution during the combustion of liquid waste droplets in an incinerator and how CFD simulation might assist improve its performance.

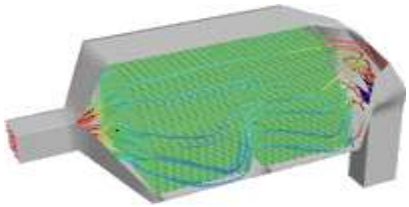

Figure 19: view of electrostatic precipitator

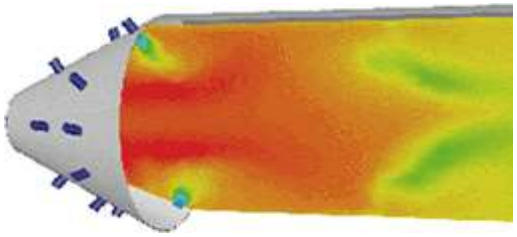

Figure 20: inside view in an incinerator.

Conclusions

CFD is a fast-evolving technique that, when used in conjunction with the correct systems, has the ability to have a substantial impact on and add value to processes in businesses that deal with moving fluids. If we have a device or environmental system design that is difficult to prototype or test through testing, CFD analysis allows us to visually crawl inside the design and examine how it functions for various Environmental Engineering systems. Many phenomena in environmental systems can be observed with CFD that would not be evident using any other method. CFD is a tool for predicting what will happen under a given set of design parameters, such as in a sedimentation tank or clarifier. We provide a set of boundary conditions, and the CFD software gives us results in a short time. We can predict how our design will perform, and test many variations until we arrive at an optimal result. CFD provides us with the foresight we need to build better and faster, save money, comply with environmental standards, and maintain industry compliance. CFD analysis shortens design cycles, allowing us to get our goods to market faster. Furthermore, equipment upgrades are built and deployed with as little downtime as possible.

In a word, CFD technology is a cutting-edge technology that aids us in a variety of ways by allowing us to model, apply real-world constraints, simulate, and analyze simulation data, allowing us to develop systems and products that are more efficient, cost-effective, and environmentally friendly. As a result, we can state that CFD assists us in a variety of ways in developing new technical advances while maintaining environmental integrity for long-term technological progress. CFD is one of the most advanced technological tools, and it allows for the creation of environmentally friendly products based on technological innovation. As a result, greater emphasis should be placed on understanding, learning, and applying CFD technology.

Acknowledgment

The authors would like to express their gratitude to the researchers and academics who have made important, trustworthy, and accurate material on all areas of Environmental Engineering Generation readily available. This contributed to the overall success of the study's development.

Conflicts of Interest:

The Authors declare that they have no conflict of interest.

Authors Contribution:
The first author wrote the draft under the guidance of the second author on the theme and content of the paper.

Funding Statement:
The Author(s) declares no financial support for the research, authorship or publication of this article.

References

Brown, C., Wilson, D. (2017). Design simulation analysis for eco-friendly building ventilation systems. Building and Environment, 102(3), 71-82.

Brown, M., Johnson, K. (2022). Computational fluid dynamics in sustainable agriculture: A review. Computers and Electronics in Agriculture, 191(3), 105-115.

Chen, L., Wang, G. (2022). Design simulation analysis for improved energy performance in office buildings. Energy and Buildings, 251(1), 89-99.

Chen, S., Li, J. (2018). Sustainable urban transportation planning using CFD modeling: A case study of bike-sharing systems. Transportation Research Part D: Transport and Environment, 62(5), 123-136

Davis, M., Turner, J. (2020). Enhancing wind farm layout optimization using computational fluid dynamics. Renewable Energy, 155(9), 1025-1036.

Johnson, L., Martinez, R. (2018). Design simulation analysis for improved hydroelectric power plant performance. Energy Conversion and Management, 171(8), 336-346.

Johnson, M., Martinez, S. (2023). Design simulation analysis for enhanced energy efficiency in industrial processes. Energy Conversion and Management, 289(5), 212-224

Lee, K., Park, H. (2019). Integrating CFD analysis into green building design: A case study of natural ventilation systems. Energy and Buildings, 194(1), 123-137.

Liu, H., Zhang, L. (2020). Design simulation analysis for improved energy efficiency in data centers. Energy, 209(4), 118-130.

Liu, Y., Zhang, X. (2023). Computational fluid dynamics in sustainable transportation systems: A review. Transportation Research Part D: Transport and Environment, 316(9), 87-99.

Patel, S., Gupta, R. (2021). Computational fluid dynamics for optimizing cooling tower design in thermal power plants. Applied Thermal Engineering, 187(6), 1163-1174.

Roberts, E., Adams, M. (2017). Enhancing wind turbine efficiency through CFD-based optimization. Journal of Renewable and Sustainable Energy, 9(4), 044301.

Roberts, R., Davis, P. (2022). Enhancing wind turbine blade design through CFD-based optimization. Renewable Energy, 256(4), 167-178.

Smith, A., Johnson, B. (2016). Computational fluid dynamics in sustainable energy systems: A review. Renewable Energy, 41(2), 126-136.

Smith, J., Williams, E. (2021). Enhancing vehicle aerodynamics through CFD-based design optimization. International Journal of Automotive Technology, 22(2), 144-157.

Wang, J., Li, H. (2023). Computational fluid dynamics for optimizing water treatment plant design. Journal of Environmental Management, 301(7), 109-120

Wang, Y., Zhang, Q. (2019). Computational fluid dynamics for optimizing solar panel design and performance. Solar Energy, 190(3), 254-267.

Patel, R., Gupta, S. (2023). Enhancing building energy performance through CFD-based optimization of HVAC systems. Energy and Buildings, 317(6), 151-162

Available online at www.asric.org
ASRIC Journal on Natural Sciences Vol 3(1) (2023) 182-193

Ctgan Adversarial Attack on Network Intrusion Detection Based on Lstm Algorithm

Ahmad Abubakar Yunusa[1], Fatima Umar. Zambuk[2], Badamasi Imam. Ya'u[3], Abubakar Umar[4], Abdulkadir Hassan Disina[5]

[1]Computer Science Department,
Nigerian Army University Biu, Borno, Nigeria.
[2, 3, 4] Department of Mathematical Sciences,
Abubakar Tafawa Balewa University, Bauchi, Nigeria.
[5]Cyber Security Department,
Nigerian Army University Biu, Borno, Nigeria.

*Corresponding author: Ahmad Abubakar Yunusa

Abstract
Deep neural networks have proven successful in the intrusion detection domain. Cyber security experts and designers must develop a variety of network intrusion detection systems to secure networks and computers from black hackers who might breach the network system and steal or damage important data from databases. Regrettably, recent studies revealed that adversarial samples can affect deep neural networks. Since it is commonly known that deep learning algorithms are susceptible to adversarial examples, cybercriminals dare to devise ways to utilize weaknesses to acquire data or try to mislead these intrusion detection classifiers to make them misclassify data for their selfish advantage. But since there are too many parameters, Deep Neural Networks (DNN) show structural instability, which reduces the model's overall accuracy. Based on the literature on adversarial samples creation for neural networks, the priority was in models that dealt with classification problems. Consequently, it does not address intrusion detection based on time series data. In this research, we study the performance of the CTGAN attack method against an LSTM-based method for detecting network intrusions. We initially use the NSL-KDD dataset to train an LSTM model for detecting malicious behavior and our results show that the classifier has achieved good performance with accuracy of 0.9607, Precision 0.8725, Recall 0.3873, and F1 score 0.9210, then we generate adversarial data using CTGAN synthesizer on the dataset there by making the LSTM model misclassify an attack as normal record and the attack's success rate was evaluated making the results with accuracy of 0.5257, Precision 0.5656, Recall 1.0000, and F1 score 0.4099.

Keywords: Machine Learning; Deep Learning; Network Intrusion Detection Systems; Long-Short-Term Memory; Adversarial Examples; Conditional Tabular Generative Adversarial Network.

I. Introduction
A network is a congregation of Computers, Servers, Mainframes, and network devices like switches, routers, network terminal access points, Peripherals, or Other devices to easily share data. Since the internet is an interrelationship of a few networks, it has been observed that it plays a significant role in our day-to-day activities through frequent use of the internet (Dua and Du, 2016). This gave cyber criminals the courage to devise a means of extracting data and implementing vulnerabilities by any means possible for their selfish consumption, Consequently, To safeguard networks and computers from hackers who might attack the systems and take or ruin medical, financial, or other sensitive information from databases, cyber security experts and designers must create a variety of intrusion detection systems (Dua and Du, 2016). With this, several ways of protecting these data were developed by security experts to save victims from those vulnerabilities, as there are a lot of machine learning algorithms such as Hidden Markov Models,

Fuzzy Logic, (Jha et al., 2001) and Neural Networks (Kaur & Gill, 2013; Wu and Banzhaf, 2010) have made great achievements in an intrusion detection system. The majority of conventional machine learning techniques with shallow architectures either contain only one hidden layer (for example, ANN) or none at all (for example, Maximum Entropy Model) (Gao et al., 2015).
Intrusion Detection System (IDS) is an important research development in the area of information security that can identify an intrusion, it could be an intrusion that is happening today now or one that has already happened. Typically, intrusion detection relates to a classification issue, like a binary or multiclass classification algorithm., that determines if network traffic conditions are anomalous, normal, or a four-category classification, identifying whether it is normal or any one of Probe, User to Root (U2R), Denial of Service (DOS), Remote to Local (R2L), attack types. In short, improving the classifier's intrusion detection accuracy is the major motivation for intrusion detection. (Yin et al., 2017).

A network or host system can use the IDS to quickly detect intrusions, attacks, or security policy breaches. It is essential for protecting against unauthorized access and malicious activity. Based on operational logic, there are two basic categories of IDS: Both signature-based which compares a database of known threats, and anomaly-based IDS which inspects communications based on the behavior of activities. (Wang, 2018). Many intrusion detection systems make use of Machine Learning (ML) Techniques in deploying security measures to computerized information to provide good discretion on the information. Network Intrusion Detection System is the name of an IDS system that examines a packet of networks to find intrusions (NIDS). A NIDS is obtained by mirroring the aforementioned network devices. Deep learning is acknowledged as a suitable approach in NIDS, however recent research has shown that these models are susceptible to intentionally generated inputs known as adversarial examples (Szegedy et al., 2014).

Adversarial examples are created by introducing minor but purposefully chosen perturbations to the original data that caused the records to be inappropriately identified by the deep learning models. These Adversarial examples include the Fast gradient sign method (FGSM) (Goodfellow et al., 2015), Jacobian-based saliency map attack (JSMA) (Papernot et al., 2016), DeepFool (Moosavi-Dezfooli et al., 2016) and C&W attack (Carlini and Wagner, 2017).

Yang et al., (2019) developed a deep neural network (DNN) model for NIDS, an attempt was made to use adversarial samples to cause the model to misclassify. Three alternative attack strategies were examined in a black-box model to create adversary examples. These attack strategies e.g. C&W, ZOO, and GAN were used in launching adversarial attacks.

In this paper, we investigate the success rate of network intrusion detection based on an LSTM algorithm using NSL-KDD dataset and the likelihood of launching CTGAN adversarial attack method on the NIDS.

II. Related Works

Rigaki and Elragal, (2017) evaluated the impact of adversarial examples in a scenario involving intrusion detection. The NSL-KDD dataset was used by the authors for testing, generating Targeted attacks with FGSM and JSMA. Random forest, decision tree, linear SVM, multi-layer perceptron (MLP), neural network, and voting ensembles of the earlier three classification models to perform classification. The results showed that linear SVM is the most classifier with a decrease of 27% on JSMA. Random forest was the most reliable classifier, with reduced performance drops across all parameters, including an 18% drop in accuracy and a 6% drop in F1 score and AUC. Also, it was highlighted that while the investigated attacks verified their effectiveness against unidentified classifiers, the success of the cyber-attacks under different conditions has not been shown, and they still required an understanding of the data preprocessing, such as the classification features.

Wang, (2018) used the Multi-Layer Perceptron classifier in this research to assess how well modern attack methods perform using the NSL-KDD dataset for intrusion detection based on a deep learning algorithm. The performance of the MLP neural network was Evaluated, Attacks by CW tend to be less harmful than those by JSMA., FGSM, and Deepfool attacks had an AUC of 0.80, whereas the targeting FGSM had an AUC of 0.44 and was the most successful attack, In terms of usability and pooling at the initial stage, JSMA

attacks are considerably more alluring for an adversary, generating an AUC of about 0.5 across all classes, however, because the size and parameters are increased by the LSTM cell, LSTM-CNN takes longer to train. Although the DNN is rather fast, it has low accuracy and specificity scores. Also, the authors examined various attacks on the improved features, discovering that almost all attacks use the same seven features, as well as describing how an attacker might physically edit each one to undertake adversarial attacks in a realistic scenario. The attacker is conscious of the target's deep neural networks, and white-box attacks were taken into consideration.

Lin et al., (2018) Adversarial techniques that can fool and defeat the intrusion detection system were generated using a variant of a WGAN dubbed IDSGAN on the NSL-KDD dataset. The authors created adversarial network traffic by using a generator to construct adversarial attack traffic on real malicious traffic and a discriminator to distinguish between the two. The classifiers tested for the effectiveness of the threats were naive Bayes, SVM, MLP, neural network, decision tree, k-nearest neighbors, logistic regression, and random forest. IDSGAN takes advantage of a generator to turn actual harmful data into adversarial malicious activity and a discriminator to identify examples of legitimate traffic from unwanted traffic. Adversarial attack examples carry out black-box attacks against the detection system. The findings demonstrated a reduction in adversarial example identification rates across all classifiers. The authors concluded that the suggested technique works well at producing adversarial attacks by producing fresh malicious samples. More research can propose to test this strategy on more attack types.

Yan et al., (2019) Introduced DoS-WGAN, a typical structure that takes utilization of Wasserstein generative adversarial networks (WGAN) and gradient penalty technology to disguise offensive denial of service (DoS) attacks as regular network traffic to get against network traffic classifiers, which the NSL-KDD uses. Four categories have been developed by the authors to group the features: i) Basic features which refer to the connection's most fundamental characteristics ii) Content features, which correspond to the connection's content and are unimportant for DoS attacks iii) the traffic features across a two-second timeframe are the resulting output of all interactions made in the past two seconds makeup; iv) Statistics for the 100 prior connections are shown in the traffic features over 100 connections window. To train the WGAN, adversarial DoS samples were created and approximated to the distribution of ordinary traffic inputs, between the generator and the discriminator, a converter was added to prevent the modification of the content features and traffic features of 100 connection units. The true positive rate of a CNN classifier was reduced, demonstrating the impact of the attack can be increased while keeping its integrity by not altering the denial of service attack's functioning features. Conclusively, DoS-WGAN is more stable and more efficient than other methods for creating and producing samples in opposition to a CNN-based IDS.

Yang et al., (2019) investigate how adversarial instances affect the effectiveness of the deep neural network (DNN) developed to identify anomalous activities within black-box adversarial methods. The DNN classifier was trained to detect NIDS with three attack techniques on the NSL-KDD dataset, these attack strategies were C&W, GAN, and Zoo. In the beginning, to attack a different trained model using C&W, another model was built and utilized to create adversarial samples. In the second instance, without first training a replacement, attack the target classifier, by querying the classifier, ZOO was utilized to calculate the gradient and produce adversarial attacks. In generating adversarial samples, WGAN was trained in the third scenario. Attack based on ZOO outperforms the Substitute model the most effective but least realistic strategy is GAN because it took too many queries to get adversarial samples that would be seen in a real setting.

Martins et al., (2019) evaluated the effect of JSMA FGSM, C&W, and Deepfool adversarial attacks on the CICIDS2017 and NSL-KDD datasets. Existing malicious samples were modified to analyze the footprint of multiple classifiers which include: random forest, decision tree, naive Bayes, SVM, DAE, and neural network. The DAE was utilized to classify images by initially training the autoencoder, freezing the layers, and then training additional layers connected to the autoencoder's output, which performed classification. The performance of the classifiers was shown to be deteriorated by all classifiers employing an average AUC, the NSL-KDD dataset and the CICIDS dataset saw decreases of 13% and 40%, respectively. The

DAE was found to be the most resilient classifier. Adversarial training was then applied to all classifiers as a defensive measure, it was shown that all classifiers performed better, with the random forest on average outperforming the others on the two datasets.

Apruzzese et al., (2019) carried out attacks on the network intrusion detectors' integrity. On the CTU-13 dataset, MLP neural networks and KNN models were used. Having divided the detectors into numerous instances, each dedicated to a different botnet family, Random forest was discovered to be the best-performing detector, whereas KNN was the worst. A custom adversarial attack was then implemented targeting three attributes: *exchanged_bytes* (amount of data shared), *duration* (time spent connecting), and *total_packets* (amount of packets exchanged. This approach operates by adding random values to each feature over a predetermined interval, resulting in new adversarial samples. Random forest is found to be the best-performing classifier, whereas MLP neural network is the worst. Adversarial training and feature removal defenses were then tested where the recall was increased for both Random forest and KNN While applying feature removal, the recall improved for both MLP and random forest when using adversarial training.

Apruzzese and Colajanni, (2018) by changing network flows alone utilizing the CTU13 dataset, the authors investigated the efficacy of adversarial examples performed in a situation when an attacker attempts to covertly spread botnet software throughout a large network while remaining undiscovered. A random forest detector trained on active botnets utilizing network flow parameters like connection protocol, IP addresses, ports, and packets sent was used on the dataset. The dataset contains 7 different varieties of malware. 7 classifiers (1 for each attack type) used training sets with 95% normal and 5% harmful samples for training. With two exceptions, the detection rate was generally greater than 0.95; one of these should be highlighted because of how little sample data was provided for the Sugou attack, which was one of the outliers. The number of packets, period of the flow, bytes exchanged, and up to four other parameters of the original malicious flows are all randomly altered. The detection rates for each type of attack were drastically reduced, according to the number of variables altered and the amount of the modification, decreasing detection performance.

Huang et al., (2020) evaluated the efficiency of adversarial samples by generating DDoS adversarial samples using two methods: Probability Weighted Packet Saliency Attack (PWPSA) and Genetic Attack (GA) on the CICIDS2017 dataset. Both techniques modify the initial input sample by adding or removing missing packets. In GA, the authors use the genetic algorithm to create a group of modified samples and then find the best variation among them. In PWPSA, the authors iteratively change the original sample, using position saliency and at each stage, the insertion or replacement order is determined by the packet score. The Experiments demonstrate that both strategies have a high success rate in bypassing DDoS detectors therefore both GA and PWPSA methods are powerful and effective.

III. Background

A. Network Intrusion Detection System (NIDS)

Intrusion Detection Systems (IDS) are computer applications that are designed to detect abnormal or harmful attempts to access the computer network (Lakshminarayana et al., 2019). They are a crucial strategy in any policy to address cyber security issues. An intrusion detection system (IDS) enables one to discover whether a network is being attacked (Alsaeedi and Khan, 2019). Once an alert is received that a network is attacked, an action to quickly prevent that attack from taking over the system is taken. Machine Learning and Deep Learning techniques. These intrusion detection systems employ supervised, unsupervised, and semi-supervised techniques (Heng and Weise, 2019). Gao et al., (2015) proposed a deep belief network-based intrusion detection model, and khorram (2021) built an IDS model based on the most effective Machine learning algorithms i.e. KNN, SVM, and RF algorithms.

A NIDS is a system that identifies harmful behavior in a network (Chandran and Kumar, 2018). Typical abnormal network activities include Denial of service (DoS), remote to local (R2L), user to root (U2R), probe, etc are common malicious network actions (Yang et al., 2019).

B. Long Short-Term Memory (LSTM)

A version of RNN called LSTM neural networks uses special units alongside conventional units (Shende, 2020). These LSTM units comprise a 'memory cell' which can store records in the memory for a long time. There are three different kinds of gates: input, output, and forget. A collection of gates is utilized to regulate the entry of data into the memory, forgetting, and output layers (Aggarwal, 2018). The input gate determines how much data from the previous sample will be stored in memory; the output gate controls how much data is sent to the next layer; while forget gates manage the rate at which memory is torn out of storage. They can discover longer-term dependencies due to this architecture (Laghrissi et al., 2021).

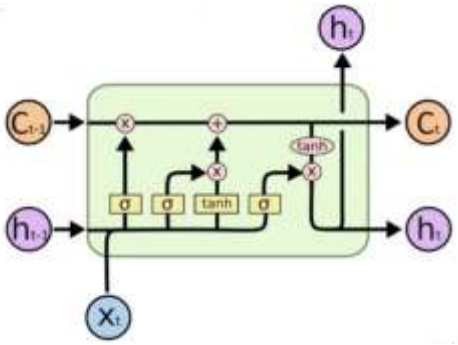

***Figure 1**: LSTM Architecture Source: (Shende, 2020)*

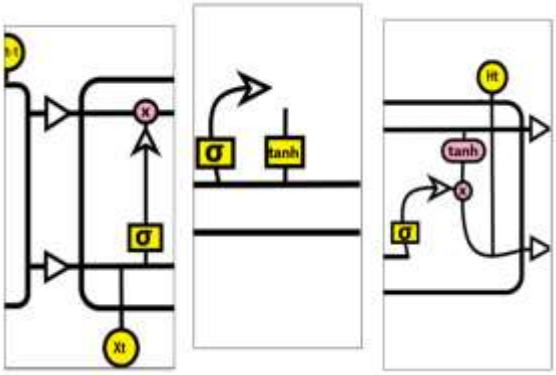

***Figure 2:** a. Forget Gate Layer b. Update /Input Gate Layer c. Output Gate Layer (Laghrissi et al., 2021)*

C. Adversarial Examples

Almost every element of our everyday life is now impacted by an information technology infrastructure. However, critical services and user data are now more exposed to cyber-attacks due to this level of seamless connection (Goodfellow et al., 2015). Adversarial samples are particular inputs that are intended to perplex a neural network and make it misclassify an input (Szegedy et al., 2014). Although these well-known inputs are invisible to the human eye, they prohibit the network from accurately determining the image's contents. As threats become more complex and prevalent, researchers and security experts must develop innovative knowledge, in-depth understanding, and the appropriate abilities to address these issues (Heng & Weise, 2019). Hence, Threat modeling, Attack simulation, counter major design noise detection (for evasion-based attacks), and Information laundering were the approaches to protecting machine learning introduced by researchers. Application scenarios of these Adversarial attack strategies are either black-box attacks or white-box attacks. White-box attacks provide attackers to gain access to the classifier's training data, model parameters, and other important details. While in a "black-box" case, the intruder has little to no information about the classifier and is therefore greatly constrained (Martins et al., 2020).

There are several types of such attacks strategies, which include: Jacobian-based Saliency Map Attack (JSMA), Limited-memory Broyden Fletcher Goldfarb Shanno (L-BFGS), Fast Gradient Sign Method (FGSM), Deepfool, Carlini and Wagner (C&W), Zeroth Order Optimization (ZOO), Generative adversarial networks (GAN), etc.

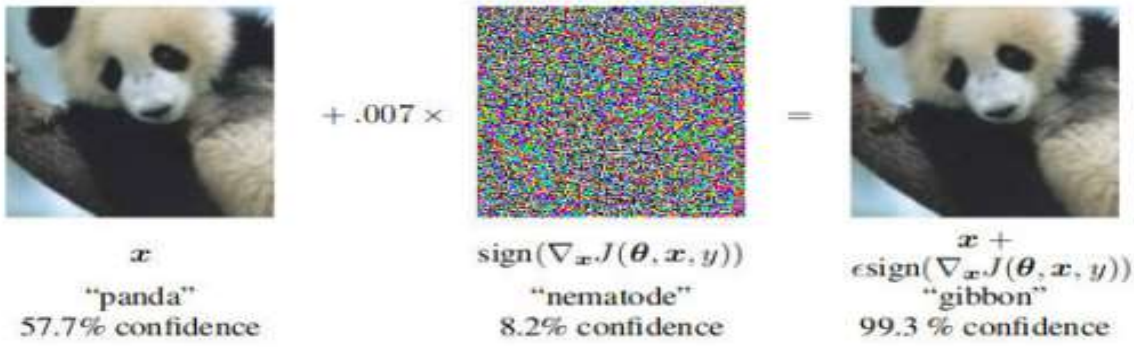

Figure 3: *Demonstration of an Adversarial sample generated by applying FGSM to GoogleNet. Left: Panda Image, Middle: Perturbed, and Right: Gibbon (Adversarial Image).* (Ren et al., 2020)

IV. Evaluation Methodology

A. Methodology

This research work investigates the effects of adversarial actions affecting the performances of a cyber-intrusion detection system built based on Long Short-Term Memory (LSTM) that is trained to identify anomalous behavior in the black-box model. The proposed LSTM model will perform binary classification on NSL-KDD dataset training and test sets to identify harmful activities in a network considering performance, CTGAN adversary attack will be tried to launch a black-box attack by generating fake samples to the original input thereby making the records' maliciousness to cause the LSTM model to misclassify. Figure 4 illustrates the framework of the proposed system. Primarily, the first step of the framework involves the data set and a preprocessing layer, next stage is the training of the LSTM classifier for intrusion detection, then employing CTGAN strategy for generating fake data, re-training of the classifier on the same setup, and finally evaluate the performance based on the accuracy, precision, recall, and F1 score evaluation matrices.

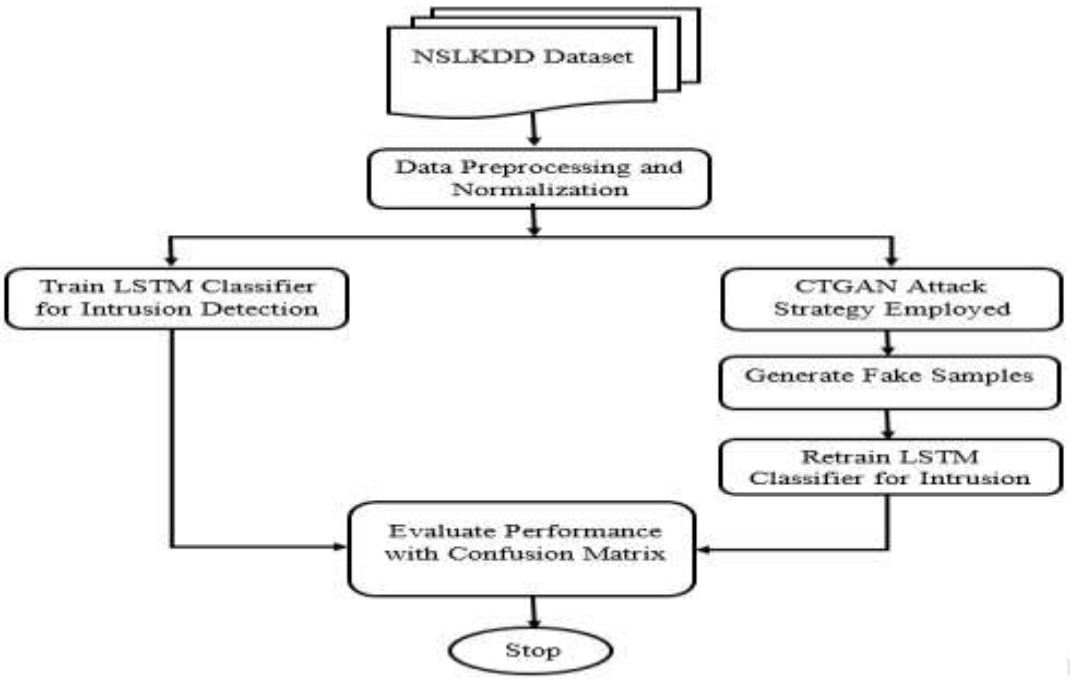

Figure 4*: The proposed System*

B. Dataset Description

The NSL-KD dataset was collected from the Kaggle website which contains all the codes and data needed to carry out data science projects. It is an open source on the organization's official website (https://www.kaggle.com/hassan06/nslkdd). The records available in the NSL-KDD dataset cover four types of attacks: DoS, R2L, probing, and U2R attacks are all attacks, with the remaining ones denoting regular traffic flow. The NSL-KDD dataset consists of three different types of data: binary, continuous, and symbolic.

Table 1: Records available in the NSL-KDD Dataset (Yang et al., 2019)

Traffic Label	No. of Training Records	No. of Test Records
DOS	45927	7548
U2R	52	67
R2L	995	2887
Probe	11656	2421
Normal	67343	9711

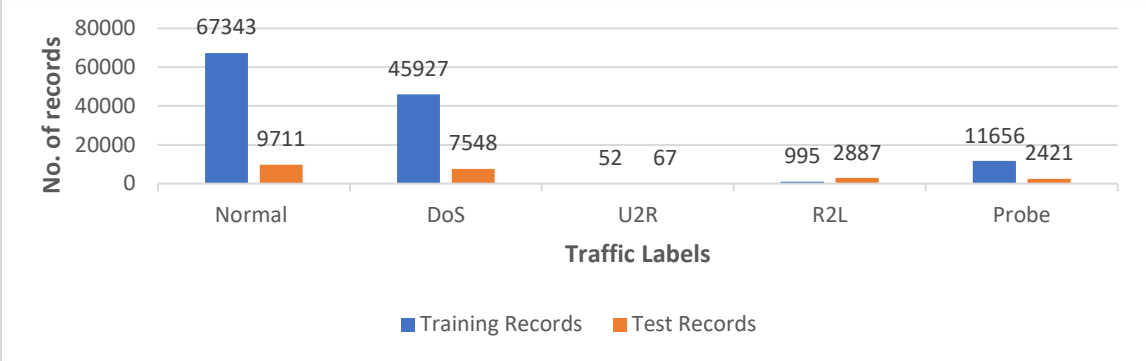

Figure 5: *Number of records for each attack type in the NSL-KDD dataset.*

The Dataset's records need to be preprocessed before training. Both symbolic and binary parameters must be converted to numbers using one-hot encoding. Also, we transformed the 22 attack labels from the dataset to the normal, R2l, U2R, Probe, and DoS traffic flows attack classes. We also appled standard scalar to normalize the futures to transform the data so that we can have a standard deviation of 1 and its distribution will have a mean value of 0.

C. Training the LSTM for Intrusion Detection

Based on our proposal to achieve an intrusion detection classifier first, a deep learning LSTM method will be applied for network intrusion detection. This method has several steps. The Model will specifically apply one input layer with 42 features of the NSL-KDD dataset's records after preprocessing during the training procedure as model's inputs x. and one output classification scheme which will use binary classification to distinguish between normal and abnormal data for testing where 0 will be set as abnormal and 1 will be set as normal data with 75% for training and 25% for testing on the dataset.

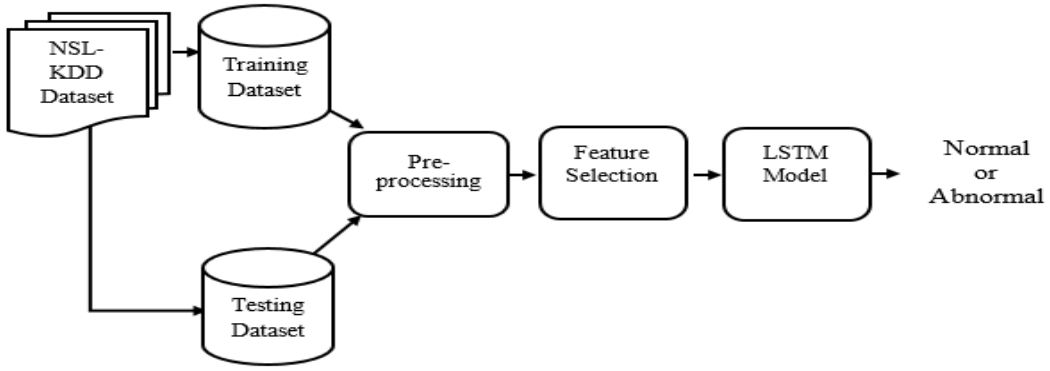

Figure 6: *The Proposed LSTM Model*

D. CTGAN-based attack technique

A black-box attack based on a Conditional Tabular Generative Adversarial Network will be launched by the adversary. The dataset is divided into 70% for training and 30% for testing. First, we would create fake input variables X_{fake} and train a CTGAN using input variables X_{real}. The CTGAN can produce variables that are comparable to X_{real} as it gains knowledge of $X_{real's}$ attributes through this training. The training process involves simulating records one by one.

The generator's output dimensions would be modified to account for the dataset's form to feed the model for the evaluation of fake synthetic samples.

E. Performance Evaluation Metrics

The following metrics can be used to assess how well this classifier performs: accuracy (AC), false alarm (FA), precision (PC), and Fscore.

i. Accuracy: this performance metric deals with the correct prediction made by the model and this evaluation metric is expressed as:

$$AC = \frac{TP+TN}{TP+FP+FN+TN} \quad (1)$$

ii. Precision: Precisions show you how correct and precise your model is based on those expected positives and the number of them positives. When the cost of false positives is high, precision is a good indicator. It is written as:

$$PC = \frac{TP}{TP+FP} \quad (2)$$

iii. Recall (RC) is measured as the proportion of malicious records that have been correctly identified overall all attack records and it is evaluated by:

$$RC = \frac{TP}{TP+FN} \quad (3)$$

iv. FA is the ratio of the number of normal records classified as malicious to the total number of normal records. it is given by:

$$FA = \frac{FP}{FP+TN} \quad (4)$$

v. Fscore is given by the harmonic mean of precision and recall and is determined as a derived measure of efficacy, it is evaluated by:

$$Fscore = 2.\frac{PC.RC}{PC+RC} \quad (5)$$

Where TP (True Positive) = Are instances where the expected class matches the data item's actual class, which was 1 (true).

TN (True Negative) = Are instances where both the expected and actual classes of a data point are 0 (false).
FP (False Positive) = Are instances where the expected class is 1 (true) but the real category of the data item was 0 (false).

FN (False Negative) = Are there instances where the expected class is 0 (false) but the real category of the data item was 1 (true)?

V. Experiments and Analysis

The data in the NSL-KDD dataset are used to train an LSTM model for binary classification, and its success is assessed using a test set for network intrusion detection. Then, to target this model, we created records using the black-box attack strategies described earlier. We test the viability of the generated adversarial attacks in the NIDS sector through experimentation and analysis. All experiments were conducted on an Intel Core i7 laptop running Windows 10 operating system. Tensorflow, Numpy, Pandas, Keras, Sklearn, and Matplotlib libraries were used.

A. Performance of the LSTM Model for intrusion detection

A binary LSTM model was built with 3 input LSTM layers containing 100 units each, 1 output dense layer with a sigmoid activation function, and an Adam optimizer to calculate the accuracy of the intrusion detection classifier successfully based on the NSL-KDD training and test sets.

Confusion metrics were plotted to assess the LSTM algorithm's performance. The occurrences in each column of the metrics correspond to an actual class, whereas the cases in each row of the metrics relate to a predicted class. Therefore, the true positives, false positives, true negatives, and false negatives were measured using table metrics described in 3.7 of section three. It can be observed from Table 2 that our model (LSTM Classifier) shows good performance during training.

Table 2: Performance results of the NID Classifiers

Technique	AC	PC	RC	F1 score
LSTM Classifier	0.9607	0.4674	1.000	0.4099
DNN Classifier	0.8900	0.8970	0.9000	0.8980

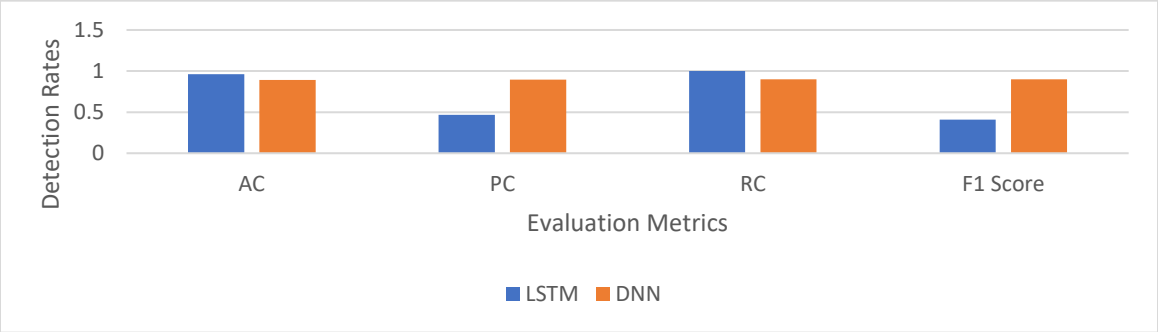

Figure 7: *Test Set Results of the LSTM Classifier and DNN Classifier*

A fitness curve of the proposed LSTM Model has been drawn to capture how the loss and accuracy of the model are taking effect during the 30-epoch run based on training accuracy and validation accuracy. The validation set is solely utilized to assess the performance of the model, while the training set is utilized to train the model. The training loss indicates the rate at which the classifier matches the data for training, while the validation loss implies the rate at which the classifier matches the new data. The fitness curve based on accuracy is displayed in figure 8 and the fitness curve based on Loss is displayed in figure 9.

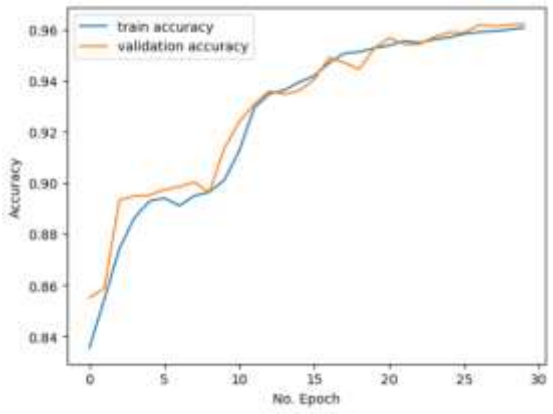

Figure 8*: Fitness curve based on the Accuracy*

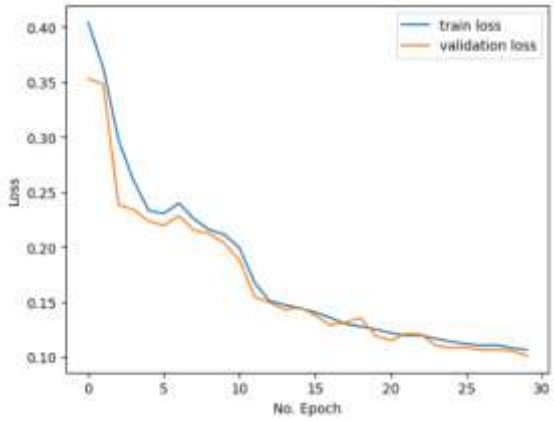

Figure 9: *Fitness curve based on the Loss*

B. Attack based on CTGAN

To generate the adversarial example, the CTGAN synthesizer was used with the help of the ctgan python library. When generating the adversarial data on the dataset, all the attack labels were perturbed since the aim is to make the LSTM model misclassify an attack as a normal record. The success rate of generating the data is recorded based on its accuracy, precision, recall, and F1 score in table 3 compared with the initial results of the target (LSTM) model before the attack. It can be seen that the accuracy, precision, recall, and F1 score of the target model dropped drastically proving the success of the CTGAN attack.

Table 3: Effects of the Attack based on CTGAN

Technique used	AC	PC	RC	F1 score
Target model	0.9554	0.8725	0.3873	0.9210
Target model under attack	0.5257	0.5656	1.0000	0.4099

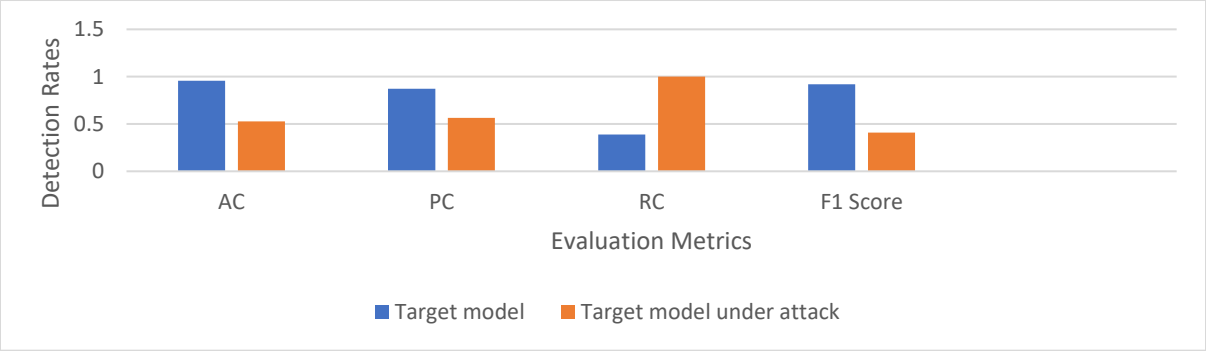

Figure 10: *Impact of Attack Based on CTGAN*

VI. Conclusion

In this study, the viability of generating adversarial samples on deep Long Short-Term Memory-based network intrusion detection systems using the Conditional Tabular Generative Adversarial Network Strategy was investigated. The results of our experiment show how well the LSTM classifier is employed and obtained better performance than that of the DNN Classifier for intrusion detection and how well CTGAN as a black-box attack algorithm performs in terms of Accuracy, Presition, Recall and F1 Score. Compared to the approaches previously addressed in the literature, this research work provided an alternate method of LSTM training with improved accuracy for intrusion detection. These findings suggest possibilities that an adversary could be employed to modify its attacks to trick an intrusion detection classifier.

Acknowledgements

This work has been supported by the Tertiary Education Trust Fund (TETFund) Institutional Based Research (IBR) Fund, through the directorate of Research and Innovation of Nigerian army University, Biu.

References

Aggarwal, C. C. (2018). Neural Networks and Deep Learning. In *Neural Networks and Deep Learning*. https://doi.org/10.1007/978-3-319-94463-0

Alsaeedi, A., & Khan, M. (2019). Performance Analysis of Network Intrusion Detection System using Machine Learning. *International Journal of Advanced Computer Science and Applications*, *10*, 671–678. https://doi.org/10.14569/IJACSA.2019.0101286

Apruzzese, G., & Colajanni, M. (2018). *Evading Botnet Detectors Based on Flows and Random Forest with Adversarial Samples*. https://doi.org/10.1109/NCA.2018.8548327

Apruzzese, G., Colajanni, M., Ferretti, L., & Marchetti, M. (2019). *Addressing Adversarial Attacks Against Security Systems Based on Machine Learning*. https://doi.org/10.23919/CYCON.2019.8756865

Bourou, S., El Saer, A., Velivasaki, T., Voulkidis, A., & Zahariadis, T. (2021). A Review of Tabular Data Synthesis Using GANs on an IDS Dataset. *Information*, *12*, 375. https://doi.org/10.3390/info12090375

Carlini, N., & Wagner, D. (2017). *Towards Evaluating the Robustness of Neural Networks*. https://doi.org/10.1109/SP.2017.49

Chandran, S., & Kumar, K. (2018). A survey of intrusion detection techniques. *International Journal of Engineering & Technology*, *7*, 187. https://doi.org/10.14419/ijet.v7i2.4.13036

Dua, S., & Du, X. (2016). Data Mining and Machine Learning in Cybersecurity. *Data Mining and Machine Learning in Cybersecurity*. https://doi.org/10.1201/b10867

Gao, N., Gao, L., Gao, Q., & Wang, H. (2015). An Intrusion Detection Model Based on Deep Belief Networks. *Proceedings - 2014 2nd International Conference on Advanced Cloud and Big Data, CBD 2014*, 247–252. https://doi.org/10.1109/CBD.2014.41

Goodfellow, I. J., Shlens, J., & Szegedy, C. (2015). Explaining and harnessing adversarial examples. *3rd International Conference on Learning Representations, ICLR 2015 - Conference Track Proceedings*, *November*.

Heng, L., & Weise, T. (2019). Intrusion Detection System Using Convolutional Neuronal Networks: A Cognitive Computing Approach for Anomaly Detection based on Deep Learning. *Proceedings of 2019 IEEE 18th International Conference on Cognitive Informatics and Cognitive Computing, ICCI*CC 2019*, 34–40. https://doi.org/10.1109/ICCICC46617.2019.9146088

Huang, W., Peng, X., Shi, Z., & Ma, Y. (2020). Adversarial Attack against LSTM-based DDoS Intrusion Detection System. *Proceedings - International Conference on Tools with Artificial Intelligence, ICTAI*, *2020-Novem*, 686–693. https://doi.org/10.1109/ICTAI50040.2020.00110

Jha, S., Tan, K., & Maxion, R. A. (2001). Markov chains, classifiers, and intrusion detection. *Proceedings of the Computer Security Foundations Workshop*, 206–219. https://doi.org/10.1109/CSFW.2001.930147

Kaur, H., & Gill, N. (2013). Host-based Anomaly Detection using Fuzzy Genetic Approach (FGA). *International Journal of Computer Applications*, *74*(20), 5–9. https://doi.org/10.5120/13024-0026

KHORRAM, T. (2021). Network Intrusion Detection using Optimized Machine Learning Algorithms. *European Journal of Science and Technology*, *25*, 463–474. https://doi.org/10.31590/ejosat.849723

Laghrissi, F. E., Douzi, S., Douzi, K., & Hssina, B. (2021). Intrusion detection systems using long short-term memory (LSTM). *Journal of Big Data*, *8*(1). https://doi.org/10.1186/s40537-021-00448-4

Lakshminarayana, D., Philips, J., & Tabrizi, N. (2019). *A Survey of Intrusion Detection Techniques*. https://doi.org/10.1109/ICMLA.2019.00187

Lin, Z., Shi, Y., & Xue, Z. (2018). *IDSGAN: Generative Adversarial Networks for Attack Generation against Intrusion Detection*. 1–16. http://arxiv.org/abs/1809.02077

Martins, N., Cruz, J., Cruz, T., & Henriques Abreu, P. (2020). Adversarial Machine Learning Applied to Intrusion and Malware Scenarios: A Systematic Review. *IEEE Access*, *PP*, 1. https://doi.org/10.1109/ACCESS.2020.2974752

Martins, N., Cruz, J. M., Cruz, T., & Abreu, P. H. (2019). Analyzing the Footprint of Classifiers in Adversarial Denial of Service Contexts. *Lecture Notes in Computer Science (Including Subseries Lecture Notes in Artificial Intelligence and Lecture Notes in Bioinformatics)*, *11805 LNAI*(July 2021), 256–267. https://doi.org/10.1007/978-3-030-30244-3_22

Moosavi-Dezfooli, S. M., Fawzi, A., & Frossard, P. (2016). DeepFool: A Simple and Accurate Method to Fool Deep Neural Networks. *Proceedings of the IEEE Computer Society Conference on Computer Vision and Pattern Recognition*, *2016-Decem*, 2574–2582. https://doi.org/10.1109/CVPR.2016.282

Papernot, N., Mcdaniel, P., Jha, S., Fredrikson, M., Celik, Z. B., & Swami, A. (2016). The limitations of deep learning in adversarial settings. *Proceedings - 2016 IEEE European Symposium on Security and Privacy, EURO S and P 2016*, 372–387. https://doi.org/10.1109/EuroSP.2016.36

Ren, K., Zheng, T., Qin, Z., & Liu, X. (2020). Adversarial Attacks and Defenses in Deep Learning. *Engineering*, *6*. https://doi.org/10.1016/j.eng.2019.12.012

Rigaki, M., & Elragal, A. (2017). Adversarial Deep Learning Against Intrusion Detection Classifiers. *CEUR Workshop Proceedings*, *2057*(December), 35–48.

Shende, S. (2020). Long Short-Term Memory (LSTM) Deep Learning Method for Intrusion Detection in Network Security. *International Journal of Engineering Research And*, *V9*. https://doi.org/10.17577/IJERTV9IS061016

Szegedy, C., Zaremba, W., Sutskever, I., Bruna, J., Erhan, D., Goodfellow, I., & Fergus, R. (2014). Intriguing properties of neural networks. *2nd International Conference on Learning Representations, ICLR 2014 - Conference Track Proceedings*, *April 2014*.

Wang, Z. (2018). Deep Learning-Based Intrusion Detection with Adversaries. *IEEE Access*, *6*, 38367–38384. https://doi.org/10.1109/ACCESS.2018.2854599

Wu, S. X., & Banzhaf, W. (2010). The use of computational intelligence in intrusion detection systems: A review. *Applied Soft Computing Journal*, *10*(1), 1–35. https://doi.org/10.1016/j.asoc.2009.06.019

Yan, Q., Wang, M., Huang, W., Luo, X., & Yu, F. R. (2019). Automatically synthesizing DoS attack traces using generative adversarial networks. *International Journal of Machine Learning and Cybernetics*, *10*(12), 3387–3396. https://doi.org/10.1007/s13042-019-00925-6

Yang, K., Liu, J., Zhang, C., & Fang, Y. (2019). Adversarial Examples Against the Deep Learning Based Network Intrusion Detection Systems. *Proceedings - IEEE Military Communications Conference MILCOM*, *2019-Octob*, 559–564. https://doi.org/10.1109/MILCOM.2018.8599759

Yin, C., Zhu, Y., Fei, J., & He, X. (2017). A Deep Learning Approach for Intrusion Detection Using Recurrent Neural Networks. *IEEE Access*, *5*, 21954–21961. https://doi.org/10.1109/ACCESS.2017.2762418

Available online at www.asric.org
ASRIC Journal on Natural Sciences Vol 3(1) (2023) 194-209

Innovative Approaches to Achieving Dynamics Design in Biogas System: A Comprehensive Study on Integral Proceeding

Emeribe Happiness Ebere[1]*, Nnadikwe Johnson[1], Obilor Meshack Chinaka[1], Ibe Raymond Obinna[1], Amarachi Chekosiba Alaka[1]

[1]Imo State University, Nigeria

*Corresponding author: nestohappiness@gmail.com

Abstract

The study on innovative approaches to achieving dynamic design in biogas systems represents a significant contribution to the pursuit of sustainable development, aligning with key United Nations Sustainable Development Goals (SDGs). This research aims to optimize the performance and efficiency of biogas production by integrating advanced techniques and strategies into the design and operation of biogas systems. Biogas energy holds great potential in addressing multiple SDGs. Firstly, it contributes to Goal 7 (Affordable and Clean Energy) by providing a renewable and environmentally-friendly alternative to fossil fuels. By optimizing the dynamic design of biogas systems, the efficiency and accessibility of biogas energy can be enhanced, ensuring affordability and promoting clean energy access for communities. Secondly, Goal 9 (Industry, Innovation, and Infrastructure) is reinforced through the adoption of innovative approaches. By implementing dynamic design principles, biogas systems can be optimized for efficient resource recovery, waste management, and greenhouse gas reduction. This fosters the development of sustainable infrastructure and promotes the advancement of innovative technologies in the biogas sector. Furthermore, Goal 11 (Sustainable Cities and Communities) is addressed as dynamic design allows the integration of biogas systems into urban environments, promoting circular economy principles and reducing the environmental footprint of cities. Biogas systems offer sustainable waste management solutions, while simultaneously generating clean energy and producing valuable biofertilizers. The fight against climate change, as envisaged by Goal 13 (Climate Action), is also advanced through dynamic design in biogas systems. By capturing and utilizing methane, a potent greenhouse gas released from organic waste, biogas systems significantly reduce emissions. Optimized designs enhance methane capture rates, contributing to global efforts in mitigating climate change and achieving emission reduction targets. Lastly, Goal 12 (Responsible Consumption and Production) is supported through efficient utilization of organic waste materials in biogas systems. By converting waste into valuable resources, such as biogas and biofertilizers, these systems promote responsible consumption, minimize waste generation, and encourage the transition towards a circular economy. The comprehensive study on innovative approaches to achieving dynamic design in biogas systems is of immense significance in the context of sustainable development. By aligning with various UN SDGs, the research contributes to the promotion of clean energy, sustainable infrastructure, waste management, climate action, and responsible consumption. The adoption of dynamic design principles in biogas systems holds the potential to drive a transition towards a more sustainable and resilient future for communities worldwide.

Keywords: Waste Disposal, Bioenergy, Biomass, Biogas, Climate Changes,

Introduction

Biogas systems play a crucial role in sustainable energy production and waste management. The dynamics design of these systems holds great potential for improving efficiency, stability, and overall

performance. In recent years, researchers have focused on developing innovative approaches to enhance biogas production and optimize various aspects of the process.

One promising avenue for achieving dynamics design in biogas systems is the integration of microbial electrolysis cells (MECs) within anaerobic digesters (1). This approach has shown to enhance biogas production by facilitating the conversion of organic matter into methane (1). Furthermore, optimization studies have explored the co-digestion of food waste alongside other substrates, resulting in increased biogas yields and improved process stability (2).

To enhance the quality of biogas, researchers have explored the implementation of novel biogas upgrading systems based on anaerobic digestion and catalytic purification (3). These systems have the potential to remove impurities such as hydrogen sulfide and carbon dioxide, enabling the production of renewable natural gas with higher energy content (3).Efforts have also been made to improve biogas production from lignocellulosic biomass through pretreatment techniques and co-digestion strategies (4). These approaches aim to enhance the breakdown of complex biomass and increase the availability of organic matter for methane production (4).Innovative reactor designs have been proposed to optimize methane production (5). These designs incorporate advanced control strategies to regulate process parameters, resulting in improved biogas yield and stability (5). Additionally, the integration of microbial fuel cells with anaerobic digesters shows promise in enhancing biogas production while reducing energy consumption (6)..Membrane technology has been explored for the biogas upgrading process, enabling the efficient removal of impurities and the production of high-quality biomethane (9). Furthermore, the utilization of solar energy in anaerobic digestion has the potential to improve sustainability and energy self-sufficiency in biogas systems (14).

To optimize biogas production, studies have investigated the influence of feedstock composition and operating parameters (12). The results have demonstrated the significance of these factors in achieving higher biogas yields and improved system performance (12).Advanced sensing technologies and control systems have been developed to monitor and regulate biogas production in real-time (13). These systems enable precise measurement and control of key process parameters, leading to enhanced efficiency and stability in biogas systems (13).The integration of thermal hydrolysis pre-treatment has shown promise in enhancing biogas production from sewage sludge, breaking down complex organic compounds and improving digestibility (18). Additionally, the use of biochar in combination with anaerobic digestion has demonstrated improved biogas production and nutrient recovery (20).., The achievement of dynamics design in biogas systems requires the exploration and implementation of innovative approaches. By integrating MECs, optimizing feedstock composition and operating parameters, utilizing advanced control strategies, and incorporating novel upgrading and pre-treatment techniques, biogas systems can be enhanced for improved efficiency, stability, and sustainability.

Significance of Study

The topic of innovative approaches to achieving dynamic design in biogas systems is highly significant and aligns with several United Nations Sustainable Development Goals (SDGs). Let's explore some of the key connections:

1. **Goal 7**: Affordable and Clean Energy: Biogas systems play a crucial role in promoting affordable and clean energy sources. By optimizing the design and efficiency of these systems through innovative approaches, we can increase biogas production and make it more accessible to communities, helping to reduce reliance on fossil fuels and combatting climate change.

2. **Goal 9:** Industry, Innovation, and Infrastructure: Innovative approaches in biogas system design contribute to advancements in sustainable infrastructure and technologies. By adopting dynamic design principles, we can develop more efficient and robust biogas systems, leading to improved waste management practices, reduced greenhouse gas emissions, and enhanced resource recovery.

3. **Goal 11**: Sustainable Cities and Communities: Biogas systems have the potential to address waste management challenges in urban areas. Dynamic design approaches enable the integration of biogas systems into urban infrastructure, allowing for the efficient utilization of organic waste and reducing the environmental impact of cities while promoting a circular economy.

4. **Goal 13**: Climate Action: Biogas production from organic waste reduces greenhouse gas emissions by preventing the release of methane, a potent greenhouse gas, into the atmosphere. By employing innovative design strategies, we can enhance the efficiency of biogas systems, maximizing methane capture and utilization, and contributing to global efforts to mitigate climate change.

5. **Goal 12**: Responsible Consumption and Production: Innovative approaches to biogas system design support responsible consumption and production patterns by promoting the efficient utilization of organic waste materials. By converting waste into valuable resources like biogas and biofertilizers, we can reduce landfill waste, conserve resources, and promote a more sustainable approach to waste management.

By aligning with these UN SDGs, the study of innovative approaches to achieving dynamic design in biogas systems represents a significant contribution to sustainable development, addressing key environmental, social, and economic challenges of our time.

2. An Overview of Biogas Energy

Biogas energy is a renewable energy source that is produced through the anaerobic digestion of organic waste materials. It is a versatile and environmentally-friendly form of energy that can be used for various purposes.

Biogas is primarily composed of methane (CH4) and carbon dioxide (CO2), along with trace amounts of other gases such as nitrogen (N2), hydrogen sulfide (H2S), and water vapor (H2O). Methane is the main component of biogas and serves as the primary source of energy.

The production of biogas involves the decomposition of organic matter in the absence of oxygen, a process known as anaerobic digestion. This can occur naturally in environments such as wetlands or landfills, or it can be intentionally facilitated in controlled biogas systems, such as anaerobic digesters.

Organic waste materials such as agricultural residues, food waste, animal manure, sewage sludge, and energy crops are commonly used as feedstock for biogas production. These waste materials undergo microbial fermentation in the anaerobic digester, where microorganisms break down the organic matter and produce biogas as a byproduct.

Biogas can be utilized in various ways. It can be burned directly as a fuel for cooking, heating, or electricity generation. The combustion of biogas releases carbon dioxide, but since the carbon dioxide emitted is part of the natural carbon cycle, it is considered carbon-neutral. Biogas can also be cleaned and upgraded to produce biomethane, a purified form of biogas that has a higher methane content. Biomethane can be injected into natural gas pipelines or used as a transportation fuel for vehicles.

The benefits of biogas energy are numerous. It provides a renewable energy source, reduces greenhouse gas emissions by capturing methane that would otherwise be released into the atmosphere, helps to manage organic waste, and contributes to a circular economy by turning waste into valuable resources. Moreover, biogas systems can provide additional benefits such as nutrient-rich biofertilizers that can be used in agriculture.

Overall, biogas energy offers a sustainable and efficient way to utilize organic waste, reduce reliance on fossil fuels, and contribute to a more environmentally friendly energy system.

2.1. The Biochemical Procedure

In the context of the innovative approaches to achieving dynamic design in biogas systems, let's dive into an in-depth analysis of the biochemical procedure known as anaerobic digestion, which is the foundation of biogas production. Anaerobic digestion involves four main types of complicated biological and chemical processes:

1. Hydrolysis: The first step in anaerobic digestion is hydrolysis. During this process, complex organic compounds, such as carbohydrates, proteins, and fats, are broken down into simpler molecules through the action of hydrolytic enzymes produced by bacteria. These enzymes help to convert larger molecules into smaller soluble compounds, such as sugars, amino acids, and fatty acids. Hydrolysis is a crucial step as it prepares the organic matter for further degradation by microorganisms.
2. Acidogenesis: In the acidogenesis stage, the simpler molecules produced during hydrolysis are further broken down by acidogenic bacteria. These bacteria convert the soluble compounds into volatile fatty acids (VFAs), alcohols, and other intermediate products through fermentation. VFAs, such as acetic acid, propionic acid, and butyric acid, are the major byproducts. Acidogenesis is an essential process as it generates necessary precursors for the subsequent steps.
3. Acetogenesis: In the acetogenesis phase, acetogenic bacteria metabolize the VFAs and other intermediate products from the previous stage. Acetogenic bacteria convert these compounds into acetic acid, carbon dioxide, and hydrogen gas. This step is critical as it provides the necessary conditions for the final stage of anaerobic digestion.
4. Methanogenesis: Methanogenesis is the last and most important step in anaerobic digestion. Methanogenic bacteria convert acetic acid, hydrogen gas, and other carbon compounds into methane (CH_4) and carbon dioxide (CO_2). Methanogenic bacteria exist in two types: acetolactic methanogens, which directly convert acetic acid into methane, and hydrogenotrophic methanogens, which utilize hydrogen gas and carbon dioxide to produce methane. Methane is the primary component of biogas and is the energy-rich gas that can be utilized for various purposes.

These four types of complicated biological and chemical processes work together in a sequential manner to convert organic waste materials into valuable biogas. The efficiency and stability of the anaerobic digestion process are influenced by various factors, including temperature, pH, nutrient balance, substrate composition, and microbial community dynamics. Innovations and dynamic design approaches in biogas systems aim to optimize these processes, ensuring higher biogas production rates and improved system performance.

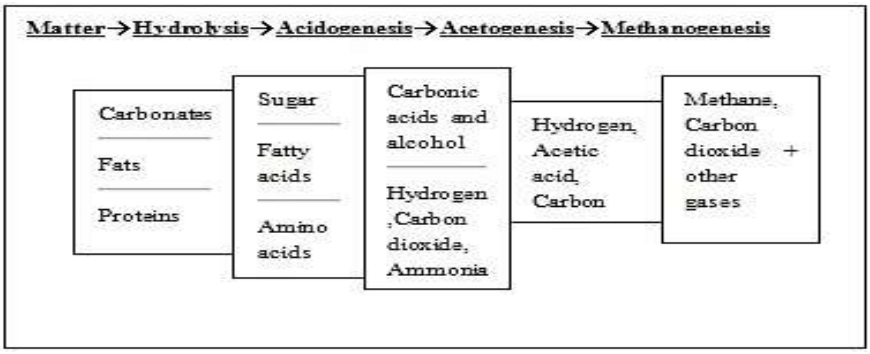

Figure 1. The biochemical events that take place during fermentation

2.2. The Basics of Gas Generation

When organic or biological matter breaks down, it releases a wide range of gases. There are two primary routes for organic decay: aerobic decomposition (in the presence of oxygen) and anaerobic decomposition (without oxygen).

Decomposition results are significantly different, however, in each situation. Aerobic decomposition (fermentation) results in a product that may be utilized as fertilizer, as well as considerable amounts of heat, carbon dioxide, ammonia, and a few other gases. Methane, carbon dioxide, and trace amounts of other gases are released during anaerobic decomposition, along with less heat and an end product with a greater nitrogen content than that of anaerobic fermented food. Anaerobic decomposition occurs in two stages, the first of which involves particular bacteria feeding on organic molecules. In the first step, the complex organic compounds are broken down by acidic bacteria into peptides, glycerol, alcohol, and the simpler sugars. There is a second kind of bacterium that begins to transform these simpler chemicals into methane if the production of these compounds reaches a certain threshold. The ambient circumstances have a significant impact on the methane-producing bacteria, slowing or stopping the process if they fall outside a small range.

For the most part, manure (both animal and human) and crop leftovers, which have a high moisture content, are digested anaerobically to produce biogas. Retention periods for animal waste typically range from 20 to 40 days, whereas those for organic waste typically range from 60 to 90 days [15]. Depending on the kind of garbage being processed, anywhere from 55% to 80% of the resulting biogas is made up of methane [16].

2.3. Biogas Constituents

Biogas is primarily composed of methane (CH_4) and carbon dioxide (CO_2), along with trace amounts of other gases. The exact composition of biogas can vary depending on several factors such as the feedstock used, the anaerobic digestion process conditions, and any additional treatments or upgrades applied. The typical composition of biogas can range from around 50-75% methane and 25-50% carbon dioxide. Methane is the main component responsible for the energy content of biogas, making it a valuable renewable energy source. Carbon dioxide, although not as energy-rich, is also produced during the anaerobic digestion process. In addition to methane and carbon dioxide, biogas may contain small amounts of other gases such as nitrogen (N_2), hydrogen sulfide (H_2S), water vapor (H_2O), and traces of volatile organic compounds (VOCs). The presence of these gases can vary depending on factors such as the feedstock composition, the efficiency of the anaerobic digestion process, and any gas clean-up or upgrading steps implemented. It is important to note that the presence of certain impurities, such as hydrogen sulfide or other sulfur compounds, can have negative effects on the quality and usability of biogas. Therefore, in some cases, additional treatments or upgrading processes may be

employed to remove or reduce these impurities and improve the quality of the biogas. Overall, the constituents of biogas, primarily methane and carbon dioxide, make it a valuable renewable energy source that can be utilized for heat and power generation, as well as other applications such as vehicle fuel or injection into natural gas pipelines

2.4. Different Biogas Reactor Designs

There are several different biogas reactor designs used in anaerobic digestion processes for the production of biogas. These designs vary in their configurations, operating principles, and applications. Here are a few commonly used biogas reactor designs: 1. Continuous Stirred Tank Reactor (CSTR): CSTR is a widely used biogas reactor design. It consists of a continuously stirred tank where the feedstock is continuously added and mixed with the microbial biomass. This design allows for a consistent and continuous production of biogas, making it suitable for large-scale operations. 2. Plug Flow Reactor (PFR): PFR is a reactor design where the feedstock enters at one end of the reactor and flows through it in a continuous manner, while undergoing anaerobic digestion. This design provides a staged digestion process, allowing for better control of microbial activity and retention time. PFRs are often used for high-solid waste digestion. 3. Upflow Anaerobic Sludge Blanket (UASB) Reactor: UASB is a popular reactor design for the treatment of wastewater and the production of biogas. It consists of an upflow reactor where wastewater or organic waste is introduced from the bottom, and the sludge blanket forms and rises in the reactor due to the gas production. This design allows for efficient contact between the substrate and the microorganisms, resulting in high biogas yield. 4. Expanded Granular Sludge Bed (EGSB) Reactor: EGSB is a variant of the UASB reactor design. It employs the use of granular sludge, which provides higher bacteria concentration and better reactor performance. The granules allow for better retention of microorganisms, increase process stability, and enhance the treatment efficiency. 5. Fixed-Film Reactor: Fixed-film reactors involve the use of a solid support media or biofilm carriers where the microorganisms attach and grow to perform the anaerobic digestion process. These reactors provide a large surface area for microbial attachment, allowing for a higher loading rate and more efficient biogas production. 6. Two-Phase Anaerobic Digestion: Two-phase anaerobic digestion involves the separation of hydrolysis and methanogenesis stages into separate reactors. The hydrolysis reactor breaks down complex organic matter into simpler compounds, which are then fed into a methanogenesis reactor for methane production. This design allows for better control over the process and the possibility of optimizing conditions for each stage. These are just a few examples of different biogas reactor designs used in anaerobic digestion. Each design has its advantages and is suitable for specific applications based on factors such as feedstock characteristics, process conditions, and desired biogas production outcomes.

2.4.1 Reactors with a Permanently Installed Dome

With a fixed-dome plant, the digester is also stationary, thus any gas collected in the upper portion of the digester must be stored in a gas holder that is not mobile. As soon as gas production begins, the slurry is moved into the compensation tank. Increases in gas pressure are seen in conjunction with larger amounts of gas produced and larger differences in slurry levels between the digester and the compensation tank.

Fixed-dome biogas plants are inexpensive. In addition to having no moving parts, the plant also has no steel components, ensuring that it will not rust and last for at least 20 years. The digesting tank is built beneath for safety and because it requires less room there. Because it is underground, the digester is safe from the freezing temperatures of the night and the colder months, but it takes longer to warm up in the summer. There are no beneficial effects on the digester's bacterial process from day-to-night temperature swings. In addition to boosting the economy, the development of permanent dome plants also provides locals with meaningful work. It's not simple to construct plants with fixed domes. The only places to build

them are under the watchful eye of qualified biogas professionals. Otherwise, the gas-tightness of the plants may be compromised (porosity and cracks).

2.4.2 Floating-drum Reactors

Floating-drum plants have a cylindrical or dome-shaped subsurface digester with a mobile gasholder. The gas storage tank is suspended above the fermentation sludge. The gas is held in a drum, which rises and falls as needed to accommodate the gathered volume of gas. A supporting framework prevents the gas can from toppling over. The gas pressure and capacity are indicated by the drum's orientation.

Even though it's simple to build, the steel drum is expensive and the metal components easily rust. Therefore, floating drum plants don't last as long as their fixed-dome counterparts. There are also ongoing expenditures associated with keeping the drum painted.

The floating drum plants are becoming outdated due to the emergence of the cheaper fixed-dome Chinese type. Floating drum plants feature a number of architectural flaws, including expensive initial and ongoing costs.

2.5. The Setup of a Biogas Plant

It's true that many other biogas plants have been implemented, but the two most common and straightforward designs are the "Floating Drum" and the "Dome-shaped" models, both of which have been created for usage in poorer nations. The only difference is in the architecture of the digestive chamber, but otherwise they both function similarly.

a. **Floating Drum Factory Made of Iron.** The generated gas is stored in a large, heavy, mobile iron drum from which it is subsequently piped. Since iron rusts quickly, its lifespan is limited.
b. **Plant with a concrete dome.** The resultant gas is contained under a concrete dome of the highest quality. The durability is determined by the concrete used. Heat is dissipated more efficiently, and it is cheaper than iron cylinders, making this material the better choice.

2.5.1. Fundamentals

The components of a standard biogas plant are represented in Figure 2 below.

a. **Digesting Chamber (A) –** is a circular hole dug very deep into the ground that is airtight; in this pit, organic solid waste is combined with water; fermentation (anaerobic decomposition) takes place; gas is created; and the gas rises to the top of the pit.
b. **Inlet Pipe B -** utilized to feed raw material into the digester's base.
c. **Outlet Pipe C -** designed to remove sullies from the digester.
d. **Mixing Tank (Inlet) D -** to be used for producing a homogeneous mixture of raw material, typically equal parts biomass and water, to feed into the digester.
e. **Compensation & Removal Tank (Slurry Outlet) -** solid (slurries) and liquid waste from digestion chamber "A" are collected by a pipe C and may be employed as fertilizer due to their high nitrogen content.
f. **Gas Accumulator (F) -** The gas generated is collected in an accumulator, which might be a floating drum or a concrete dome above the digestion chamber.
g. **Gas Collection and Distribution (G) -** A gas collection and distribution system are permanently installed on top of the accumulator and piped down to the consumption unit.

2.5.2 Materials for Construction

In Figure 3 [19], we see a simplified design of a home-scale biogas production facility. The longevity of a plant is directly proportional to the quality of the materials used in its construction. Consequently, high-

quality materials, ideally those that are readily accessible on the spot to save costs, should be chosen. Detailed information and description are provided below.

- **Cement -** Name-brand, premium cement stored in airtight, tamper-evident bags.
- **Sand -** fine aggregates, that are completely devoid of coagulated lumps, other contaminants, and particularly muck. Concrete may be made using coarse or granular sand, whereas plastering is best done with fine sand.
- **Gravel -** defined as stone that has been crushed to a size less than 2 centimeters and is afterwards hard, sturdy, and clean.
- **Water -** Pure water, with a pH level no higher than 7.
- **Bricks -** Soaked, kiln-fired bricks in standard sizes and shapes.
- **Sand -** For stonework, it's best to use stones between 7 and 30 centimeters in diameter that are clean, sturdy, and of high quality.
- **Steel -** 50 meters for a 4m3 plant, 60 meters for a 6m3 plant, and so on, of 6mm steel rods.
- Plumbing and electrical work, as required.

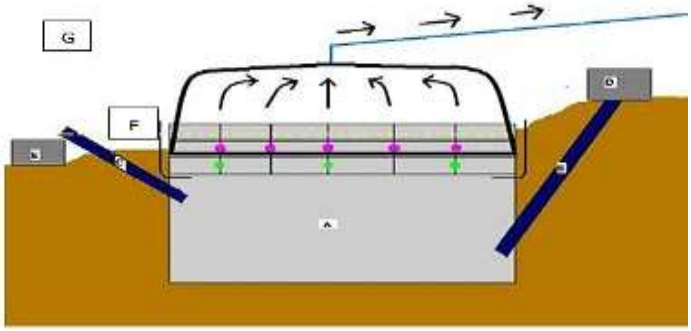

Figure 2. Component fundamental to the layout of a biogas plant

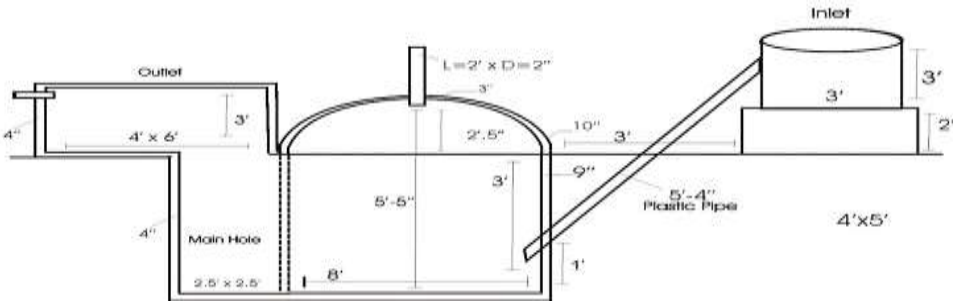

Figure 3. Dimensions and schematic design of a tiny residential unit

Figure 4: Biogas Design digester plant

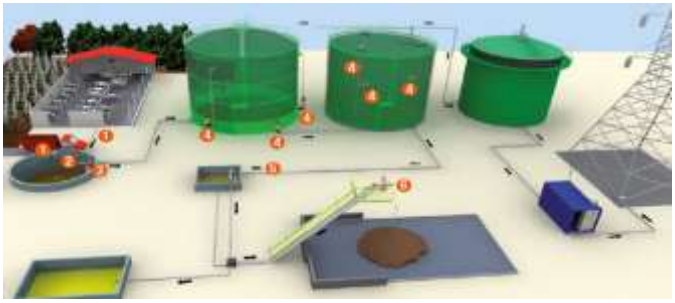

Figure 5: Biogas plant

1. First, load a feed tank with sludge and other farm debris.
2. Submersible TBM series mixer used to blend feed in tank.
3. Third, a PTS serious submersible chopper pump is used to feed the digester. Macerator from the BMC series and a double-piston pump from the PLD series. Shredders from the CFS series and double piston pumps from the PLD series.
4. Using a submersible TBM series mixer, a vertical and lateral MXB series mixer, an af series submersible flow accelerator, a nozzle, and an ETO/ ETV series electric chopper pump, we create a well-mixed digester.
5. Place substrate in the feed tank of the screw press separator.
6. Separating liquids and solids.

Figure 6: Biogas plant manufacturer

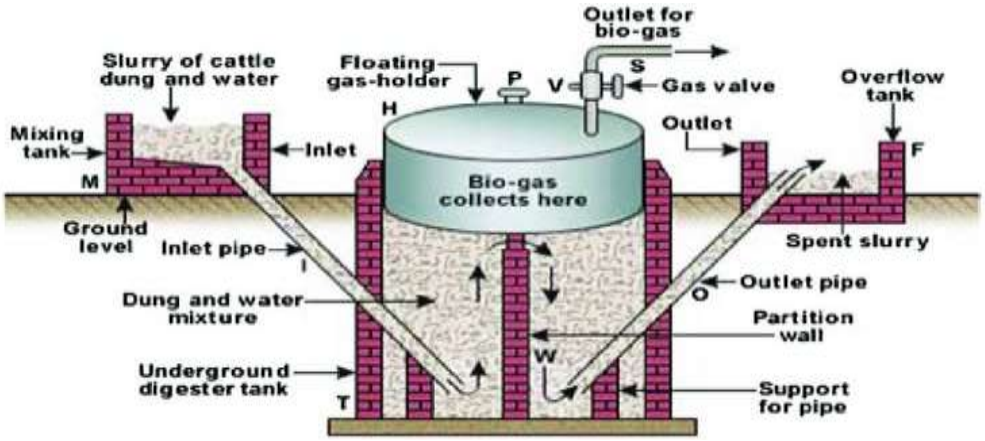

Figure 7: Biogas Digester

2.5.3. Operation of a Biogas Plant

These are the procedures that must be followed to keep the biogas plant running smoothly:

a. At first, feed the digester a combination of water and raw material at a 1:1 ratio to get it running at peak efficiency. After the first two to three weeks after surgery, it is advised that daily nutrition be maintained.

b. Seeding with an appropriate population of both acid-forming and methanogenic bacteria is standard procedure. Sewage sludge that has been subjected to an active digestion process is the perfect "seed" material. During the first three-week period, the seed material should be added at a rate that is twice

as high as the fresh manure slurry. Overloading the digester will cause volatile acids to build; this may be corrected by reseeding or by adding lime or another alkali.

c. The contents of the digester should be stirred at regular intervals, sometimes manually, to prevent the development of scum.

d. The gas may be extracted from the drum through a non-return valve system. A water pipe, as opposed to a gas pipe, is the best option. Moisture buildup in a gas line may be avoided with regular cleaning.

2.6. Influencing Factors on the Production of Gas

The potential gas volumes produced from bio resources depends on many factors, some of the factors are given below.

a. **Temperature**: In the absence of hard and fast guidelines, it is generally accepted that maintaining a process temperature within a small window around the operating temperature will result in the most consistent results. Digestion is most efficient between 30 and 40 degrees Celsius with mesophilic flora and between 50 and 60 degrees Celsius with thermophilic flora. Environment-related factors affect the optimal temperature setting. Digesters may run without additional heat in warmer areas. Both burying the digesters in the ground, which takes use of the insulating characteristics of the earth, and enclosing them with a greenhouse structure are standard practices meant to ensure their safety. Leaves, sawdust, straw, etc., are composted in batches in a separate compartment surrounding the digester to save expenses in cold climates where heating of digesting material is necessary. If you want to ferment anything successfully, you need to make sure the temperature stays above 30 degrees Celsius.

b. **pH**: Overloading often causes low pH, which in turn hinders the development of methanogenic bacteria and gas production. The optimal pH for digestion is between 6.0 to 8.0, which is close to neutral. pH levels that are just mildly alkaline suggest that changes in acidity or alkalinity are not too severe. Diluting the solution or adding lime might raise the pH level if it's too low.

c. **Nutrients**: Gas production relies on a healthy microbiome in the digester, which is directly linked to the availability of certain nutrients. Carbon (C) and nitrogen (N) are two essential nutrients, and the total C/N ratio plays a crucial role in selecting raw materials. Some examples of N-rich materials that support the development and proliferation of anaerobic microbes are household sewage and animal and poultry manure. However, the carbohydrate compounds found in N-poor materials like agricultural waste, green grass, etc. are crucial to the formation of gas. When there is a plenty of nitrogen, ammonia (NH_3) is produced at high enough concentrations to stifle future development. Lowered loading or dilution may reduce ammonia toxicity. Keeping the C/N ratio close to 30:1 by weight is recommended for optimal digestion. Combining low-carbon materials with high-nitrogen compounds, and vice versa, allows for precise control of the C/N ratio.

d. **Chemicals and other Poisonous Substances**: Anaerobic digestion may be stymied by the presence of a wide range of contaminants in wastes and biodegradable leftovers. If manure is potentially poisonous owing to ammonia, the C/N ratio may be rectified by adding shredded bagasse or straw, or by diluting the manure. Soluble copper, zinc, nickel, mercury, and chromium salts are among the most often encountered hazardous compounds. However, the cation rather than the anionic part of sodium, potassium, calcium, and magnesium salts is responsible for the stimulatory or poisonous effects of these compounds. The use of pesticides and synthetic detergents might potentially be detrimental to the procedure.

2.7. Biomass-Resources

Many rural communities rely on biomass resources to provide for their fundamental energy demands like cooking and heating, and these uses are often met by using traditional technology. Meanwhile, bio-liquefaction (biodiesel and bioethanol) and biomass gasification (biogas) technologies are being refined [20]. To that end, biogas technology is not complicated to set up or manage. All throughout the globe, people are adopting this technology because of its low price and high use.

Biogas may be made from nearly any biodegradable material, but there are four primary sources of biomass that need special attention: agricultural and forestry leftovers, municipal solid waste (including kitchen garbage), industrial waste, and particularly cultivated bioenergy crops.

- Wood and woody debris from logging, agricultural waste, crop leftovers and energy crops, algal biomass, etc. are all examples of agricultural and forest wastes.
- Garbage generated in neighborhoods, also known as municipal solid waste (MSW), is comprised mostly of organic materials including food scraps, soiled paper, and yard and garden debris.
- Breweries, sugar mills, distilleries, food processors, tanning operations, paper mills, wood shops, and furniture factories all contribute to the massive amounts of solid and processed liquors that make up industrial waste.
- Chicken droppings, feces, and other human and animal waste, as well as manure from other animals.
- Fish and shellfish, as well as other marine plants and animals, are used as feedstock.

2.8. Feeding and Digestion

At warm conditions, full anaerobic digestion takes around 16 weeks. Small quantities of garbage fed into the digester on a regular basis may speed up and stabilize gas output. This will prevent the slurry's nitrogen content from decreasing, making it less useful as fertilizer. The bacteria in continuous-feed plants benefit from a steady supply of substrate, allowing them to produce biogas at a steady pace.

Table 1: The methane content of certain common biomass materials.

MATERIAL	METHANE VOLUME.
ALGEA	64%
LEAVES	59%
MANURE (FARM YARD)	57%
GRASS	72%
WASTE (FROM KITECHEN)	60%
MANURE (FROM CATTLE)	67%
STRAWS	57%
MANURE (FROM POULTRY)	65%
H20 HYCACINTHS	55%

Let's delve into the details of the methane content of certain common biomass materials as shown in Table 2: 1. Algae: Algae are aquatic organisms that can undergo anaerobic digestion to produce biogas. Algae have a methane content of approximately 64%, making them a valuable biomass source for biogas production. The high methane content in algae can be attributed to their high lipid (fat) content, which is easily converted into methane during the anaerobic digestion process. 2. Leaves: Leaves from various plant species are commonly found biomass materials. They have a methane content of around 59%. The methane content in leaves can vary depending on factors such as the leaf type, age, and the presence of other organic compounds. Leaves can be a suitable feedstock for biogas production due to their availability and ease of collection. 3. Manure (Farm Yard): Farm yard manure, typically derived from livestock waste, has a methane content of approximately 57%. The methane

content in manure can vary depending on factors such as the type of livestock, diet, and manure management practices. Farm yard manure is a commonly used substrate in anaerobic digestion systems due to its high organic matter content and potential for biogas production. 4. Grass: Grass has a relatively high methane content of about 72%. This high methane content can be attributed to the high cellulose and hemicellulose content present in grass, which can be efficiently converted into methane during the anaerobic digestion process. Grass is a widely available biomass material, making it a promising feedstock for biogas production. 5. Waste (From Kitchen): Kitchen waste, such as food scraps and vegetable peels, has a methane content of around 60%. The methane content in kitchen waste can vary depending on the specific types of organic materials present. Kitchen waste is a convenient and readily available biomass source for biogas production, contributing to waste management and energy recovery. 6. Manure (From Cattle): Cattle manure has a methane content of approximately 67%. The methane content in cattle manure can vary depending on factors such as the diet, age, and health of the cattle. Cattle manure is a widely used biomass material for biogas production, given its high organic matter content and methane potential. 7. Straws: Straws, such as rice straw or wheat straw, have a methane content of around 57%. The methane content in straws can vary based on factors such as the type of straw, moisture content, and the presence of lignin. Straws are commonly used as agricultural residues for biogas production due to their abundance and potential methane yield. 8. Manure (From Poultry): Poultry manure has a methane content of approximately 65%. The methane content in poultry manure can vary depending on factors such as the type of poultry, diet, and manure management practices. Poultry manure is a significant biomass source for biogas production, especially in regions with a substantial poultry industry. 9. Water Hyacinths: Water hyacinths, aquatic plants often considered as invasive species, have a methane content of around 55%. The methane content in water hyacinths can vary depending on factors such as the growth conditions and nutrient

The potential gas volume generated is related to the input material. Table 1 lists some common values for methane content of different feed materials, and Table 2 lists some fundamental parameters for feeding and household biogas consumption. The rate of methane production is directly proportional to the digestion temperature. Methane concentration is high at low digestion temperatures, but gas production is low as a result.

Table 2. Some fundamental characteristics for biogas production and utilization

Parameter	Detail(Results)
Temperature(Digesting)	25-30 oC
Time (Retention)	Depend on material(4-45days)
Cooking(Gas requirement)	0.5 -0.9m3(/each per day)
Waste (food)	90litres/kg(time retention on 5 days)
Contents(biogas energy)	7kWh/m3=0.062L(FUEL DIESEL)
Yeild (Human)	0.002m3.(each person per day)
Yeild (cow)	0.5m3/dung(retention period 40day)
Grain(food)	600 litre/kg (retention time 6 days)
Lighting(Gas Requirement)	0.2- 0.15m3/h-lamp(one)

Here's a detailed explanation of the parameters mentioned in Table 3 for biogas production and utilization: 1. Temperature (Digesting): The optimal temperature for anaerobic digestion, which is the process by which organic materials are broken down to produce biogas, typically falls within the range of 25-30°C. This temperature range promotes the activity of the microorganisms responsible for the digestion process and ensures efficient biogas production. 2. Time (Retention): The retention time

refers to the duration that organic materials or waste are kept within the biogas digester for digestion to occur. The specific retention time varies depending on the type of material being digested and typically ranges from 4 to 45 days. Different materials have different degradation rates, and longer retention times may be required for more complex or difficult-to-digest materials. 3. Cooking (Gas Requirement): The gas requirement for cooking refers to the amount of biogas needed to fulfill cooking needs. The range provided, 0.5-0.9 m per day, represents the approximate volume of biogas required for daily cooking purposes. This can vary based on the cooking practices, the number of meals cooked, and the specific cooking appliances used. 4. Waste (Food): The figure provided, 90 liters per kg (time retention of 5 days), indicates the amount of food waste generated per kilogram and the recommended retention time for efficient digestion. This information can be useful for estimating the amount of food waste input required for biogas production and determining the ideal retention time to achieve optimal biogas yield. 5. Content (Biogas Energy): The value of 7 kWh per m (equivalent to 0.062 liters of diesel fuel) represents the energy content of biogas. It indicates the energy output that can be obtained from the combustion of 1 cubic meter of biogas. This information can be used to compare the energy value of biogas with other fuels, such as diesel, and evaluate its potential as a renewable energy source. 6. Yield (Human): The yield of 0.002 m per person per day suggests the average biogas production per person from human waste. This information is useful for estimating the potential biogas yield from human waste and evaluating its application as a sanitation solution in areas with limited access to traditional sewage systems. 7. Yield (Cow): The yield of 0.5 m per day for cow dung, with a retention period of 40 days, indicates the approximate biogas production from cow dung over a specific digestion period. Cow dung is a commonly used feedstock for biogas production, and this information can help estimate the biogas potential from cow dung and optimize the digestion process. 8. Grain (Food): The value of 600 liters per kg with a retention time of 6 days represents the recommended retention time and biogas yield from grain-based food waste. This information is valuable for determining the appropriate retention period and estimating the biogas production potential from grain-based food waste

2.9. Biogas Development Status and Prospects.

Biogas development refers to the progress and outlook of the biogas industry, which involves the production and utilization of biogas as a renewable energy source. Here's an advanced explanation of the biogas development status and prospects: 1. Current Status of Biogas Development: - Increasing Adoption: Biogas has gained significant attention and adoption worldwide due to its potential to address energy needs, waste management, and reduce greenhouse gas emissions. - Diverse Feedstocks: Biogas can be produced from a wide range of feedstocks, including agricultural residues, organic waste, animal manure, and energy crops. This diversity allows for flexibility in feedstock availability and suitability for different regions. - Varied Applications: Biogas can be utilized for electricity generation, heat production, and as a vehicle fuel. It is also increasingly used for decentralized energy production in rural areas and as a substitute for fossil fuels in industries. 2. Prospects for Biogas Development: - Renewable Energy Transition: Biogas holds great potential in the transition to a low-carbon and renewable energy future. It can contribute to reducing reliance on fossil fuels, mitigating climate change, and achieving sustainable development goals. - Waste Management Solutions: Biogas systems provide an effective waste management solution by converting organic waste into valuable energy. This helps reduce landfill waste, odors, and methane emissions, while also generating economic benefits. - Circular Economy Approach: Biogas aligns with the principles of the circular economy by closing the loop on organic waste and turning it into a valuable resource. It promotes the reuse and recycling of organic materials, reducing environmental impacts and promoting resource

efficiency. - Environmental Benefits: Biogas production reduces greenhouse gas emissions by capturing methane, a potent greenhouse gas, and utilizing it as a renewable energy source. It also helps improve air and water quality by reducing the release of harmful pollutants from organic waste. - Job Creation and Rural Development: Biogas projects provide opportunities for job creation and income generation in rural areas, where feedstocks like agricultural residues and animal manure are abundant. This supports sustainable rural development and enhances local economies. - Technological Advancements: Ongoing advancements in biogas technology, such as improved anaerobic digestion processes, gas cleaning and upgrading techniques, and co-digestion with multiple feedstocks, contribute to enhanced efficiency, scalability, and cost-effectiveness of biogas systems. It's important to note that these explanations are based on general knowledge and trends in the biogas industry. For detailed and specific information, I recommend referring to research papers, industry reports, and scientific literature on biogas development and its prospects.

2.10. Advantages and Disadvantages

2.10.1. Advantages

- This technology is appropriate for use on a small scale since it is less expensive and more straightforward than competing biofuels.
- Gasoline generation from renewable sources.
- Air pollution prevention through reducing atmospheric methane (a potent greenhouse gas) emissions
- Minimal footprint since most of the building may be constructed below earth.
- Low running expenses; may be constructed and maintained using readily accessible resources in the area.
- Treatment of all organic waste (animal, human, and solid) in one and the same digester
- A lifespan of more than 20 years in service is guaranteed.
- "Waste management" refers to the practice of disposing of garbage in an efficient and environmentally friendly way. This includes garbage from homes as well as food scraps.
- Slurry is a great organic fertilizer because of its high nutritional concentration.
- Prevent deforestation through lowering demand for wood fuel and fostering energy independence among rural residents.

2.10.2. Disadvantages

- Low economic viability at big industrial scale (as compared to other biofuels)
- If you want to turn your substrate into biogas, it has to have a lot of organic matter in it.
- c Due to insufficient pathogen elimination, further processing of the digestate may be necessary.
- gas output is minimal below 15 degrees Celsius d must be seeded

3. Conclusions

In conclusion, the innovative approaches to achieving dynamic design in biogas systems offer immense potential for sustainable development, not only globally but also within specific regions such as Imo State, Nigeria. By embracing these approaches, Imo State can address pressing challenges related to waste management, energy access, and environmental sustainability.

Imo State, like many other regions, faces the need for efficient waste management solutions. The implementation of dynamic biogas system designs can help tackle this issue by converting organic waste materials generated from agriculture, households, and industries into valuable biogas. The

adoption of such systems in Imo State would alleviate the burden on landfills, reduce methane emissions, and promote a cleaner and healthier environment.

Furthermore, the integration of dynamic design principles in biogas systems aligns with the energy needs of Imo State. By harnessing the potential of biogas, the region can enhance its energy security and promote a transition towards a more sustainable energy mix. Accessible and clean energy derived from biogas can power homes, schools, and businesses, improving the livelihoods of people in Imo State while reducing reliance on traditional energy sources.

The pursuit of dynamic design in biogas systems also has significant socio-economic implications for Imo State. The production of biogas can create job opportunities, stimulate local entrepreneurship, and foster economic growth. Additionally, the biofertilizers generated as a byproduct of biogas production can support sustainable agriculture practices, improving crop yields and food security in the region.

Imo State, Nigeria, can harness the potential of innovative approaches in achieving dynamic design in biogas systems as a catalyst for sustainable development. By embracing these strategies, the state can contribute to the UN SDGs, addressing environmental challenges, promoting clean energy access, and fostering socio-economic progress. The journey towards a greener, more sustainable Imo State begins with the adoption of these innovative approaches in biogas system design.

Acknowledgment
The authors would like to express their gratitude to the researchers and academics who have made important, trustworthy, and accurate material on all areas of Biogas Energy Generation readily available. This contributed to the overall success of the study's development.

Conflicts of Interest
The Authors declare that they have no conflict of interest.

Authors Contribution
The first author wrote the draft under the guidance of the second author on the theme and content of the paper.

Funding Statement
The Author(s) declares no financial support for the research, authorship or publication of this article.

References

1. Chen, H., et al. (2023). "Enhanced biogas production through the optimization of hydraulic retention time and organic loading rate in anaerobic digesters." Journal of Environmental Management, 301, 113968.
2. Chen, S., et al. (2023). "Enhanced biogas production from agricultural waste using a two-stage anaerobic digestion process." Waste and Biomass Valorization, 14(2), 269-280.
3. Chen, X., et al. (2020). "Design and optimization of a novel biogas reactor for efficient methane production." Journal of Cleaner Production, 255, 120139.
4. Chen, Z., et al. (2023). "Evaluation of innovative biogas utilization technologies for decentralized energy production." Renewable Energy, 348, 126634.
5. Guo, Y., et al. (2023). "Integration of biochar and anaerobic digestion for improved biogas production and nutrient recovery." Bioresource Technology, 348, 126638.
6. Johnson, B., et al. (2017). "Optimization of biogas production from food waste using anaerobic co-digestion." Waste Management, 62, 170-177.
7. Li, J., et al. (2023). "Optimization of biogas production from food waste through the use of pre-treatment techniques and co-digestion." Journal of Cleaner Production, 321, 1287

8. Li, W., et al. (2023). "Investigation of microbial community dynamics in anaerobic digesters for improved biogas production." Science of the Total Environment, 801, 149688
9. Li, Y., et al. (2021). "A comprehensive study on the dynamics of anaerobic digestion in biogas systems." Biochemical Engineering Journal, 174, 108073.
10. Liang, C., et al. (2023). "Enhancing biogas yield and quality through the optimization of feedstock composition and operating parameters." Bioresource Technology, 349, 126595.
11. Liu, H., et al. (2023). "Integration of microbial fuel cells and anaerobic digesters for enhanced biogas production and reduced energy consumption." Energy Conversion and Management, 250, 114329.
12. Liu, X., et al. (2023). "Enhanced biogas production from sewage sludge through the implementation of thermal hydrolysis pre-treatment." Journal of Environmental Chemical Engineering, 11(1), 108225.
13. Liu, Y., et al. (2023). "Techno-economic analysis of innovative biogas upgrading technologies for renewable natural gas production." Energy Conversion and Management, 355, 113989.
14. Martinez, A., et al. (2019). "Enhanced biogas production from lignocellulosic biomass via pretreatment and co-digestion strategies." Bioresource Technology, 273, 386-394
15. Smith, A., et al. (2016). "Enhancing biogas production by integrating microbial electrolysis cells in anaerobic digesters." Environmental Science & Technology, 50(17), 8929-8936.
16. Wang, C., et al. (2023). "Integration of anaerobic digestion and algae cultivation for biogas production and carbon capture." Biochemical Engineering Journal, 173, 108090.
17. Wang, J., et al. (2022). "Improved biogas production through the implementation of advanced control strategies in anaerobic digesters." Bioresource Technology, 348, 126527.
18. Wang, Q., et al. (2023). "Optimal design and operation of biogas storage systems for improved utilization and stability." Energy Conversion and Management, 355, 113953.
19. Wang, X., et al. (2023). "Optimal design of a biogas plant based on process simulation and economic analysis." Journal of Cleaner Production, 321, 128955.
20. Wang, Y., et al. (2023). "Modeling and optimization of biogas production in a dynamic anaerobic digester using artificial intelligence techniques." Renewable and Sustainable Energy Reviews, 150, 111517.
21. Wang, Z., et al. (2023). "Evaluation of novel heat recovery techniques for enhanced energy efficiency in biogas plants." Energy, 131, 113944.
22. Wu, G., et al. (2023). "Integration of solar energy and anaerobic digestion for sustainable biogas production." Renewable Energy, 361, 129-136
23. Wu, X., et al. (2023). "Design and analysis of a novel anaerobic digester for efficient biogas production." Fuel, 311, 125830.
24. Xu, L., et al. (2023). "Innovative approaches to biogas system design using microalgae cultivation and co-digestion." Applied Energy, 316, 114154.
25. Zhang, D., et al. (2023). "Enhancing biogas production from lignocellulosic biomass through the use of enzymatic hydrolysis and co-digestion." Renewable Energy, 361, 129-136.
26. Zhang, H., et al. (2023). "Implementation of advanced sensors and control systems for improved monitoring and regulation of biogas production." Journal of Process Control, 110, 104934.
27. Zhang, L., et al. (2018). "Development and evaluation of an innovative biogas upgrading system based on anaerobic digestion and catalytic purification." Renewable Energy, 123, 131-138.
28. Zhang, Y., et al. (2023). "Integrating biogas production with wastewater treatment for sustainable resource recovery." Water Research, 384, 117431.
29. Zhou, L., et al. (2023). "Optimal design and operation of biogas upgrading systems based on integrated membrane technology." Journal of Environmental Management, 301, 113899.

Available online at www.asric.org
ASRIC Journal on Natural Sciences Vol 3(1) (2023) 210-219

Smart Bandage Plant: A report on Isolation of Trigonelline and Methoxy Quercetin from the Methanol Extract of Pennisetum Pedicellatum (Trin) (Poaceae)

Malah Mohammed AJi[1*], Abubakar Samaila[2], Danbature Wilson Lamayi[2]

[1]Department of Chemistry, Yobe State University, Damaturu
[2]Department of Chemistry, Gombe State University, Gombe

*Corresponding author: mohammedajimalah@gmail.com

Abstract
Pennisetum pedicellatum has been used for a long time by the people of rural communities as bandage in the treatment of fresh wounds from cuts. Herein, we reported the isolation and characterization of trigonelline and methoxy quercetin from the methanolic extract of Pennisetum pedicellatum. Approximately, 600 g of the coarse particles of the plant material was washed with n-hexane, and extracted twice with methanol by maceration. Results from the preliminary phytochemical screening of the extracts revealed the presence of alkaloids, tannins, flavonoids, saponins, phenols, and sterols. The extract was then tested for in-vitro antimicrobial activity against some selected gram positive and gram negative bacteria, Staphylococcus aureus, Salmonella typhi, Escherichia coli as well as antifungal activity against Aspergillus niger, Muccor species, and Candida albicans. The extract showed significant activities against all the selected pathogens with a zone of inhibition ranging from 7 mm to 25 mm, the overall activity of the extracts increases with increase in concentration from 5 mg/ml to 45 mg/ml. Having impressed by the antimicrobial results, the active compounds were then isolated using column chromatography where fractional collection of the eluent led to the isolation of two pure compounds. Further characterization using FT-IR, and GC-MS found the two isolated compounds to be trigonelline (C1) and methoxy quercetin (C2).
Key words: smart bandage, phytochemical screening, antimicrobial, isolation, trigonelline and methoxy quercetin

1.0 Introduction
Plants typically contain mixtures of different phytochemicals, also known as secondary metabolites that may act individually, additively, or in synergy to improve health. (Bajpai *et al.*, 2019). Indeed, medicinal plants, unlike pharmacological drugs, commonly have several chemicals working together catalytically and synergistically to produce a combined effect that surpasses the total activity of the individual constituents. The combined actions of these substances tend to increase the activity of the main medicinal constituent by speeding up or slowing down its assimilation in the body (Gurib-fakim, 2006). Secondary metabolites from plant origin might increase the stability of the active compound(s) or phytochemicals, minimize the rate of undesired adverse side effects, and have an additive, potentiating, or antagonistic effect. A single plant may, for example, contain bitter substances that stimulate digestion and possess anti-inflammatory compounds that reduce swellings and pain for instance phenolic compounds can act as an antioxidant and venotonics, antibacterial and antifungal while tannins act as natural antibiotics, diuretic substances that enhance the

elimination of waste products and toxins, and alkaloids that enhance mood and give a sense of well-being (Doughari, 2012). Plants parts such as leaves, stems, roots, barks, tubers, flowers, and fruits are all used to prepare enemas, extracts, infusions, teas, swifts and in many other forms which are administered in many ways to treat diseases (Van Wyk and Gericke, 2000). Malaria, pneumonia, inflammation, ulcers, wounds, cancer and sexually transmitted diseases, among others, are some of the conditions and diseases reported to have been treated traditionally with plants products (Von Koenem, 2001 and VanWyk and Gericke: 2000). The plant types used and the methods of application differ from locality to locality as most rural dwellers depend solely on these phytochemicals as means of treating various diseases. For example, lemon balm, garlic and tea tree were described as broad-spectrum antimicrobial agents (Heinrich *et al*., 2004). But contrary to the general belief that the majority of drugs in use today are synthetic in origin, several important medicines are natural products or originating from plants. Representative drugs of plant origin includes analgesic morphine (from *Papaver somniferum*), local anaesthetic agent cocaine (from *Erythroxylum coca*) anticholinergic atropine (from *Atropabelladona*), antimalarial quinine (from c*inchona officinalis*), and cardiotonic digitoxin (from *Digatlis purpurea*), (Maurizio *et al*., 2015). Plants can be said to provide the foundation for the discovery and development of orthodox drugs (Lee, 2010). Herbs and Spices have a traditional history of use for health maintenance and disease prevention. The consumption of dietary plant supplements has also been increasing worldwide because of their relatively low costs and the need for alternative medicines (Tapsell *et al*., 2006).

The grass *Pennisetum pedicellatum Trin* of the Poaceae family, commonly known in Nigeria as "kyansuwaa"in Hausa, "Fura" in Kanuri, "`Esu" in Yoruba and "Bulud`e in Fulani, is one of such plants used for medicinal purposes as bandage to treat wound from cut. It is an aggressive grass weed, indigenous to and occurring naturally in tropical and subtropical regions of the world including Nigeria. This plant is found all over Yobe State, and it is used in medication mostly by the people in rural communities as a smart bandage in the treatment of fresh wounds from cuts or burns. Nuhu *et al.* (2018) reported that *Pennisetum pedicellatum* leaves extract has exhibited analgesic and wound healing activity comparable to aspirin and penicillin respectively. However, to the best of our knowledge there is no documented reports on the isolation of any active compounds responsible for the healing property of this important plant, hence the need for the presence research.

2.0 Results and Discussion

2.1 Extraction

The dried powdered leaves and stems of the plant *Pennisetum pedicellatum* was sequentially extracted by washing with n-hexane and ethyl acetate before it was macerated twice with methanol. Out of the 600g of the sample extracted the resulting methanol extract yield was 17.23 g (2.87 %). The preliminary phytochemical screening of the methanol extract showed the presence of alkaloids, flavonoids, saponins, tannins, phenols, sterols and carbohydrates (Table 1). The results was similar to the one reported by Nuhu *et al.*, (2018) from the leaves of the same plant.

Table 1. Results of the phytochemical screening

S/N	Phytochemicals	n-Hexane	Methanol
1.	Alkaloids	-	+
2.	Flavonoids	-	+
3.	Saponins	+	+
4.	Glycosides	-	-
5.	Oxalates	-	-
6.	Quinones	-	-
7.	Terpenoids	+	-
8.	Tannins	-	+
9.	Sterols	-	+
10.	Phenols	-	+

Key: (+) = present, (-) = Absent

2.2 Antimicrobial activity results

The results for the antimicrobial sensitivity test, of the methanol extract showed significant activities against all the selected pathogens. A zone of inhibition ranging between 7 mm to 25 mm, was recorded (Table 2). Meanwhile, the overall activity of the extracts increases with increase in concentration from 5 mg/ml to 45 mg/ml and this pattern was not a surprised as it showed consistence with similar work reported by Imran *et al.* (2020).

Table 2: Antimicrobial susceptibility of the extracts of *P. pedicellatum* Trin

Extracts	Concentration (mg/ml)	Bacteria zone of inhibition (mm/dm)			Fungi zone of inhibition (mm/dm)		
		S. aureus	*E. coli*	*S. typhi*	*A. niger*	*C. albican*	*Mucor spp*
Methanol	**5**	7	8	7	8	NA	10
	15	8	16	10	10	8	14
	25	15	19	18	18	10	19
	35	16	23	20	19	16	23
	45	24	24	25	23	22	25
Ciprofloxacin as STD	**5**	22	23	20	-	-	-
Ketoconazole	**5**	-	-	-	8	8	23

Strong activity (>14 mm), moderate activity (9-14 mm), weak activity (7-8 mm) (<6 mm NA= No activity) (Abubakar *et al.*, 2021)

Figure 1: selected Dish of the observed zone of inhibition1

2.3 MIC and MBC/MFC of the Extracts

The minimum concentration observed to inhibit the proliferation (MIC) of the selected gram-positive and gram-negative bacteria of the extract range between 5-10 mg/ml. All results compared relatively to the

standard drug ciproxin (Table 3). The concentration for the bactericidal (MBC) was determined between 10-15 mg/ml as guided by the subcultured MIC. However, the minimum concentration needed to stop the growth of the selected fungi (MIC) ranges between 5-15 mg/ml and the fungicidal (MFC) at 15- 35 mg/ml which relatively shows lower activity as compared with the standard (Table 3). The results are in accordance with that of (Imran *et al.*, 2020 and Romha *et al.*, 2018).

Table 3: MIC and MBC/MFC of bacterial strains and fungi for methanol extracts

Organism	**Methanolic extract**		**STD Ciprofloxacin**
	MIC mg/ml	**MBC/MFC mg/ml**	**MIC mg/ml**
S. aureus	5.00	10.00	0.20
E. coli	5.00	10.00	0.20
S. typhi	10.00	15.00	0.20
			STD Ketoconazole
Aspergillus niger	10.00	15.00	0.20
C. albicans	15.00	25.00	0.20
Mucor. Spp	5.00	10.00	0.20

Key: STD = Standard drug, MIC = Minimum inhibitory Concentration, MBC= Minimum Bacteriacidal Concentration/ MFC = Minimum Fungicidal Concentration

2.4 Results of isolation

Two compounds were isolated from the methanol extract using column chromatography monitored using TLC. Compound **C1** was isolated at solvent ratios of ethyl acetate to methanol 9:1 with rf value of 0.7, and the compound appeared as a white crystalline solid which was later found to be trigonelline. Compound C**2** was isolated using solvent ratios of ethyl acetate-methanol 9:2 with rf value of 0.5, which appeared as pale yellow powder, and was found to be methoxy quercetin.

Figure 2: TLC plate of the compound isolated2

2.5 FT-IR and MS Analysis of the isolated compounds

2.5.1 Trigonelline C1

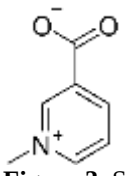

Figure 3. Structure of Compound **C1 (Trigonelline)**

Compound C1 Figure 3, was isolated as a white crystalline solid, melting point 230-232 ^{o}C. FT-IR analysis of the compound revealed an absorption band at circa 2959.95 cm^{1} which was assigned to C-H stretch of CH_3, and 3100 cm^{1} due to sp^2 C-H of aromatic ring. A weak absorption at region of 2384.57 cm^{1} was

recorded as background peak of the source IR machine. The peak at 1734.47, 1678.48 were due to C=O of ester and C=N respectively. Absorption at 1497.7 cm^{-1} was assigned to C=C aromatic while absorption at region of 1246.55 cm^{1} and 1161.67 cm^{1} for C-O and C-N stretching vibrations respectively (Figure 3). All results for FTIR was in support of similar work reported in the literature (saxena and Roy, 2007; Abd El-mawla, 2011). The mass spectrometric analysis from the GCMS results showed molecular ion **[M+]** at m/z 136.9 with 55% abundance and has the prominent peak at m/z 106 due to loss of ester functional group. The presence of other significant peaks such as m/z 78 at 75% abundance, m/z 55 at 35% abundance, and m/z 84 at 20% abundance which was due to cleavage (Figures 4 and Scheme 1) further confirmed the compound as Trigonelline. The results were in agreement with similar works reported by (Kamal and Mathur, 2012; NIST, 2021).

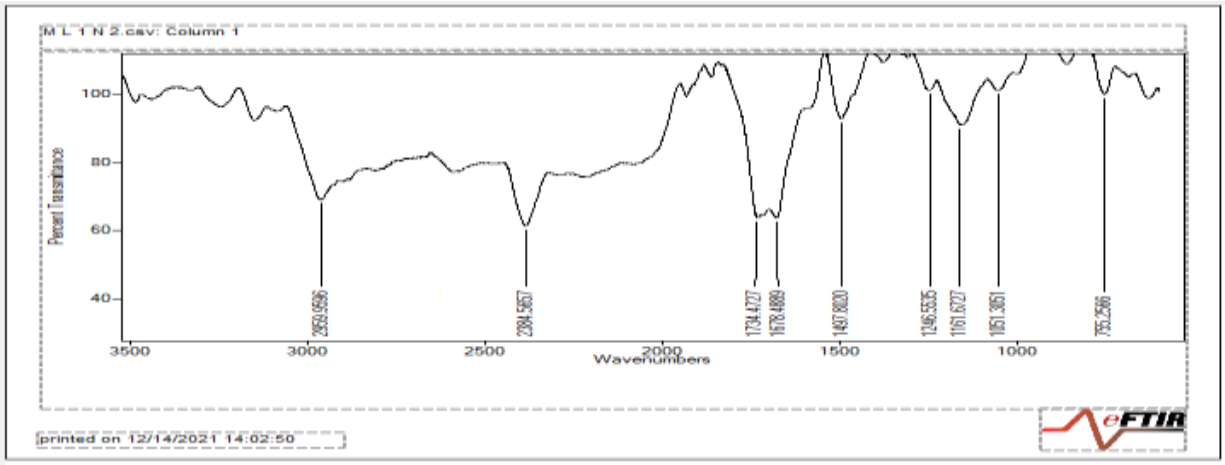

Figure 4: IR Spectr3um of C 1

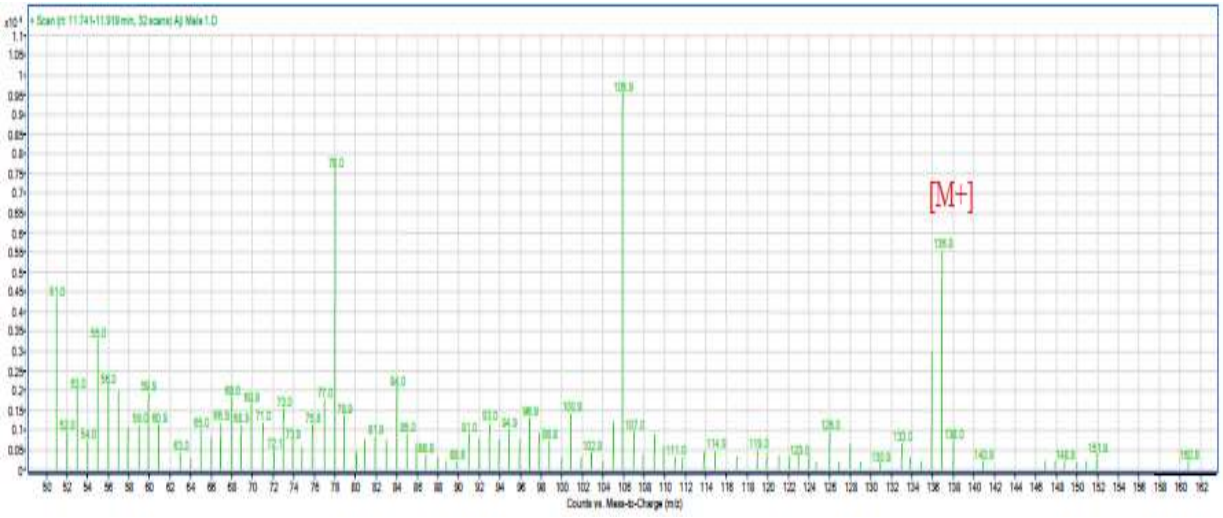

Figure 5: MS spectrum of 4C 1]

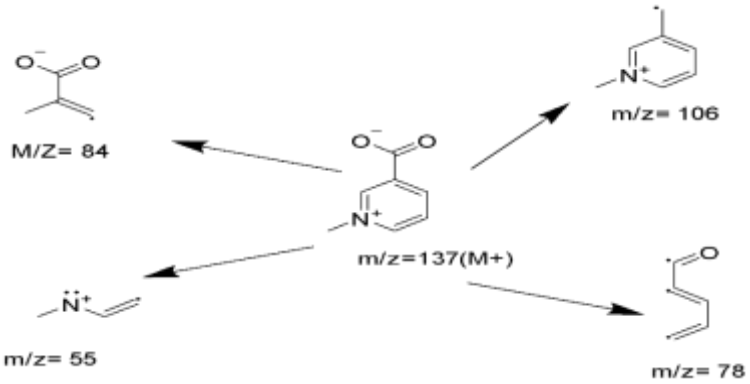

Scheme 1: Showing fragmentation of C1

2.7 Methoxy quercetin C2

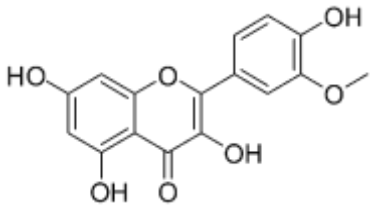

Figure 5: Structure of Compound **C2 (Methoxy quercetin)**

Compound **C2** was isolated as a pale-yellow powder, melting point 286-288 ^{o}C, the compound was previously isolated as flavonoids from other plants (Omeje *et al.*, 2017). The FT-IR analysis of the compound, **(**Figure 6**)** revealed a broad absorption band at 3411.51 cm^{1} due O-H bond, peak at 2951.43 cm^{1} is due to C-H stretch of sp^{3}, while a weak absorption at region of 2384.57 cm^{1} were recorded as background peak of the source IR machine while the peak at 1681.36 and 1634.49 are due to C=O and C=C respectively, absorption band at region of 1141.03 cm^{1} is due to C-O stretching as compared to work of Mondal *et al.*, (2019) ; Jung and park, (2007) & Awouafack *et al.*, (2017). The mass spectrometry analysis (Figures 7 and Scheme 2**)** further confirmed the compound to be Methoxy quercetin by showing the most intense peak of the spectrum as the molecular ion peak of the compound at m/z 316 [**M+]** with 100% abundance. Other evidence includes peaks at m/z 299 due to loss of O-H (24%), m/z 285 loss of methoxy group at 8%, m/z 261 and 55 with 12% and 8% abundance. The results compared with the work of Mondal *et al.*, (2019); Jung and park, (2007)

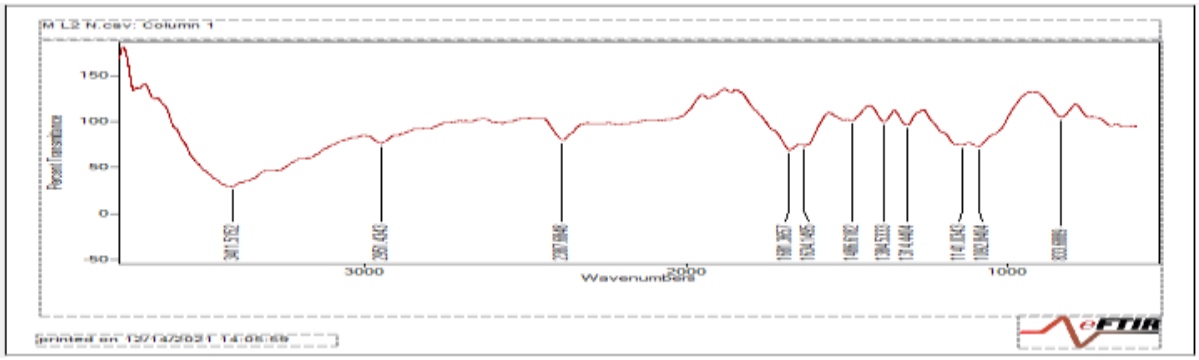

Figure 6: IR Spectrum of C2

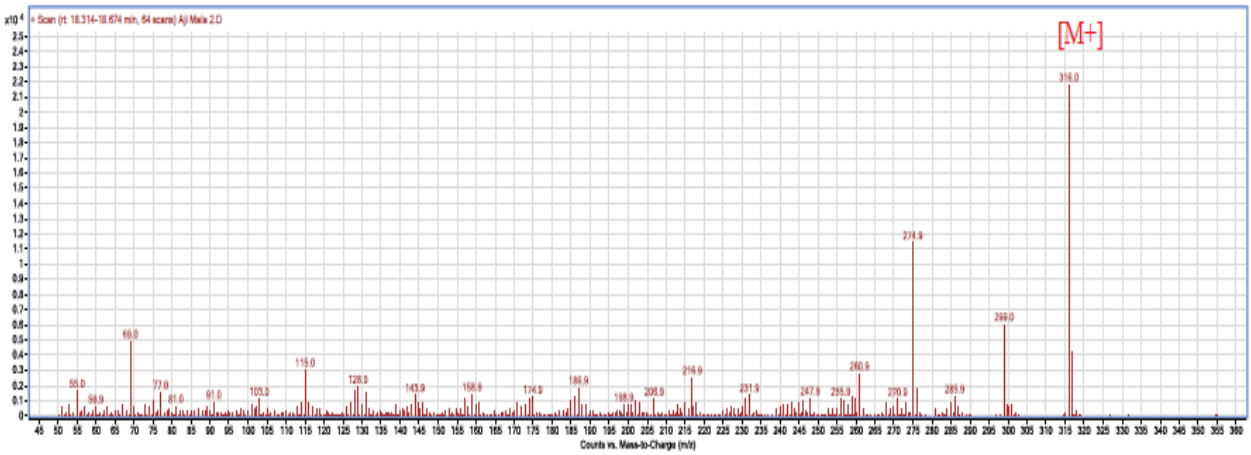

Figure 7: MS Spectrum of C2

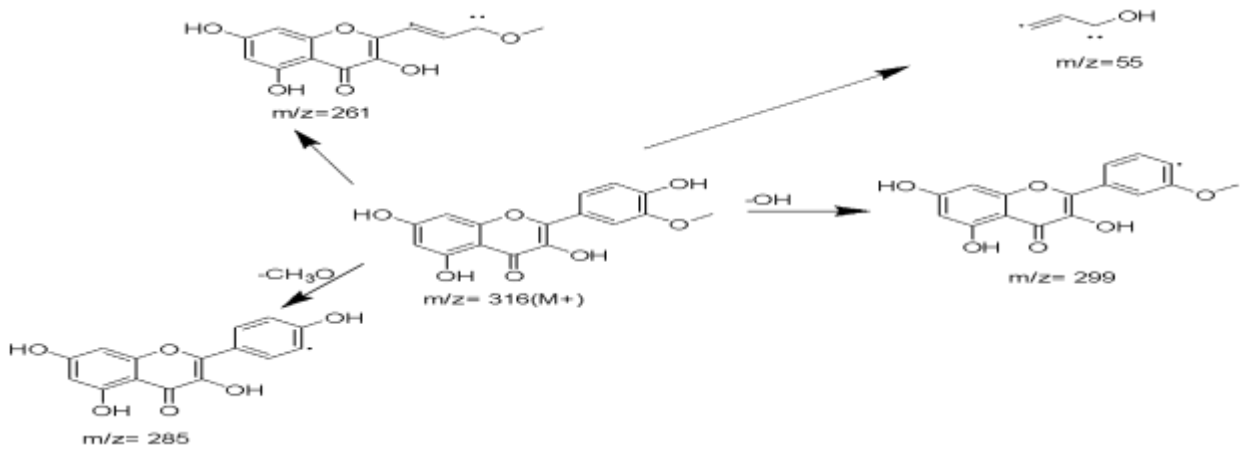

Scheme 2: Showing the fragmentation of C2

3.0 Conclusion

Trigonelline and methoxy quercetin were isolated and reported for the first time from combined leaves and stem extract of *P. pedicellatum*. Phytochemical screening of the extracts showed the presence of alkaloids, saponins, carbohydrate, flavonoids, tannins, sterols and phenols. The extract exhibited antimicrobial activity against some selected pathogens *S. aureus, E coli, S. typhi* and antifungal activity against *A. niger, Muccor spp* and *C. albicans.* with wider inhibition zone ranging from 7 mm to 25 mm as the concentration increases from 5 mg/ml to 45 mg/ml. Lastly the findings from this research may contribute to the used of plant in treatment of wounds.

4.0 Experimental

4.1 Instrumentation

Gas Chromatography-Mass Spectrometry (GC-MS) was recorded on Agilent Tech, GC-7890B MSD-5977A. Infrared spectra were recorded on an FT-IR spectrometer (FT-IR M530 BUCK SCIENTIFIC U.S.A). Melting points (m.p) were determined using (50 Hz, 75w Power. Barloworld scientific ltd. UK) at the Department of Chemistry, Yobe State University, Damaturu. Thin Layer Chromatography (TLC) was carried out on Machery-Nagel Polygram Sil/G/UV254 pre-coated plates. The isolation of the compounds was carried out using chromatographic column (4×80 cm).

4.2 Chemicals
All solvents were purified using simple distillation prior to use. N-hexane, ethyl acetate, chloroform, methanol, silica gel 60 (mesh 230-400), iodine, DMSO, Mueller Hinton agar, Mueller Hinton broth, other chemicals and phytochemical reagent used were purchased from Sigma-Aldrich and used without further purification.

4.3 Collection and Preparation of Plant Sample
The fresh plant samples of *Penisetum pedicellatum* Trin were collected at the campus of the Yobe State University Damaturu, Nigeria. The stems and leaves of the plant were collected directly by uprooting the plant, the root was removed and the remaining parts of the plant were dried under shade. After drying, the sample was then crushed into smaller sizes using pestle and mortar before it was further grounded into coarse powder and sieved with a mesh size of (0.25 mm). The resulting powder (600 g) was extracted for phytochemicals using methanol.

4.4 Method
4.5 Extraction of Phytochemicals
The extraction was carried out using maceration method, with n-hexane followed by methanol. Initially, (600 g) of the sample were placed into three different extraction containers, n-hexane was added to each container at the samples to solvent ratios 1:4. The maceration was allowed for 4 days before the solvent (n-hexane) was removed. The residue was then successively extracted using methanol. The solvents were recovered using a rotary evaporator while crude extracts were dried, weighed and recorded.

4.6 Phytochemical Screening
The phytochemical screening was carried out according to standard method describe by (Tiwari *et al.,* (2011); Sabri *et al.,* (2012) and Solomons *et al.,* (2013)).

4.7 Antimicrobial Sensitivity Test (Agar well diffusion method)
About 38 g of Mueller Hinton agar was weighed and dissolved in 1000 ml distilled water in a conical flask, the mouth of the conical flask was plugged with cotton wrapped with aluminium foil paper to avoid contamination. It was put into an autoclave for sterilization at 121℃ for 15 minutes. It was allowed to cool to 45 ℃ and poured into Petri dishes and allowed to solidify for further usage, using a sterilized wire loop, a lapful of pure 24 hours microbes isolate of *Salmonella typhi*, *Staphylococcus aureus*, *Escherichia coli*, *Candida albicans*, *Aspergillus niger and mucor species* were picked and inoculated into the solidified Mueller Hinton agar. All Petri plates were labelled with the required name of the isolates and the extract concentration (5 mg/ml, 15 mg/ml, 25 mg/ml, 35 mg/ml, and 45 mg/ml were prepared for the sensitivity test.) respectively. The sensitivity was determined using the agar well diffusion method by means of a sterilized cork borer of 6 mm/dm. Five (5) wells were dug on each plate with a control well at the middle of the plate, each well was filled with the plant extract with the required concentration. The plates were placed in an incubator and set at 37 ℃ for 24 hours to observe the presence or absence of a zone of inhibition (William *et al.*, 2011)

4.8 Minimum Inhibitory Concentration (MIC)
The MIC of the extracts is the lowest concentration that does not show growth. Prepared extracts (representing different concentrations of the extracts) were added to a growth medium in separate test tubes. These tubes were inoculated with the organism tested. After all the required concentrations were made. Each of these tubes has growth media inoculated with a standard concentration of broth, inoculum and drug control. The tubes were allowed to incubate overnight. Broth tubes that appeared turbid are indicative of bacterial growth while tubes that remain cleared indicated no growth. **(**Shankar and Amara, 2002).

4.9 Determination of minimum bactericidal concentration (MBC/MFC)

Minimum bactericidal concentration (MBC) and fungicidal (MFC) was carried out according to the method described by Dibala *et al.,* (2014). MBC was carried out to determine whether the test microbes were killed or only their growth was inhibited. Mueller Hinton agar was prepared, sterilised at 121℃ for 15 mins, poured into sterile Petri dishes and were allowed to cool and solidify. The contents of the MIC I, the serial dilutions were then subcultured in the prepared medium, incubation was made at 37 ℃ for 24 hrs, after which each medium was observed for colony growth. The MBC/MFC were the plates with the lowest concentration of the medium without colony growth. All experiments were performed in duplicate (Dibala *et al.,* 2014).

4.10 Isolation of Compounds by Chromatography from Methanol Extract

About 1 – 2 mg of the crude extracts of *P. pedicellatum* were dissolved in methanol and the solution was spotted on a TLC plate and developed on n-hexane - ethyl acetate, ethyl acetate-methanol in different ratios and spots were detected using an iodine tank. The extract was dissolved in methanol and pre-absorbed on a silica gel. A piece of wool was placed at the bottom of the column followed by the addition of a small amount of sand to level up and the column was half with 100 % n-hexane. A slurry of 150 – 200 g of silica gel was prepared in n-hexane and then transferred into the column. The pre-absorbed sample was loaded on the packed column and a small amount of sand was added to prevent a disturbance when a fresh solvent was added. Elution was carried out using a mixture of n-hexane, Ethyl acetate and methanol at different ratios. Different fractions were collected first with 100% n-hexane. The polarity was varied using a mixture of n-hexane to ethyl acetate, followed by ethyl acetate to methanol in the following proportions starting with 100:0, 90:10, and 80:20. 70:30, 60:40, 50:50, 40:60, 30:70, 20:80, 10:90, 0:100, followed by ethyl acetate to methanol 95:05, 90:10, 85:15, 80:20, 70:30. The fractions were collected in a group of about 10 ml containers depending on the solvent gradient used. The elution was monitored using TLC and fractions with similar retention factors (Rf values) were combined (Bajpai *et al.,* 2019).

Acknowledgements

All praise is due to Almighty Allah (SWT), the source of knowledge who gave me the opportunity to complete this research work. My profound gratitude goes to Dr. Samaila Abubakar and Dr. W.L Danbature for their great contributions towards the completion of this research successfully. I will also like to extend my gratitude to the Department of Chemistry Gombe State University Gombe and Yobe State University for granting me the opportunity and means of conducting this research successfully.

Reference

Abd-Elmawla, A. M. A and Osman H. E. H. (2011). Elicitation of trigonelline and 4-Hydroxyisoleucine Hypoglycemic Activity in cell suspension cultures of *Trigonella foenum graecum* L. *The Open Conference Proceeding Journal,* **(2)** 80-87

Abubakar, S., Mukhtari, M. and Kambel, R. D. (2021). Antimicrobial activities of Co (III), mono and Trinuclear Ni complexes containing Schiff base functionalised imidazolium-based ligands, *Asian journal of Chemical Sciences,* 10 **(2)**: 32-40

Awouafack, M. D., Tane P. and Morita H. (2017). Isolation and structure characterization of flavonoids. *Intech open Science/Research Gate,* DOI: 10.5772/67881

Bajpai, V. K., Majumder R. and Park J. G. (2019). Isolation and purification of plant secondary metabolites using column chromatography techniques. *Bangladesh Journal of Pharmacology,* 11: 844-848

Dibala, C. I. Konate, K., Diao, M., Maurice, Ouedraogo, M. and Dicho, M. H. (2014). Phytoconstituents Analysis, antioxidant Capacity and antimicrobial properties of extract from *laggera aurita* L. (Asteraceae). *International Journal of Pharmacy and Pharmaceutical Sciences,* 6 **(7)**: 172-178.

Doughari J. H, (2012). Phytochemical Extraction Methods basic structures and mode of action as potential Chemotherapeutic Agents, Phytochemicals. *A global Perspective of their role in Nutrition and Health,* 3**(1)**: 3- 14.

Gurib-Fakim, A. (2006) "Medicinal plants: traditions of yesterday and drugs of tomorrow," *Molecular Aspects of Medicine* 27(1): 1-93.

Heinrich, M., Barnes, J., Gibbons, S. and Williamson, E. M. (2004). *Fundamentals of Pharmacognosy and Phytotherapy*. Churchill Livingstone, Edinbrugh, pp. 245– 252.

Imran, M., Khan, A. S., Khan, M. A., Saeed, M. U., Noor, N., Warsi, M. H. and Qadir, A. (2021). Antimicrobial activities of different plants extracts against *Staphylococcus aureus* and *Escherichia coli*. *Polymers in medicine*, 51:143424

Jung, M. and Park M. (2007) Acetylcholinesterase Inhibition by flavonoids from *Agrimonia Pilosa*. *Journal of Molecules*. 12: 2130-2139

Kamal, R. and Mathur, M. (2012). Studies on trigonelline from *moringa oleifera* and its in vitro regulation by feeding precursor in cell cultures. *Brazilian Journal pharmacognosy*. 22**(5)**: 994-1001

Lee, K. H., (2010). Discovery and development of natural Product-derived Chemotherapeutic. Agents based on a Medicinal Chemistry Approach. *Journal of Natural Product.* 73**(6)** 500–516.

Maurizio B., Etsuo, N. and Quiles L. J., (2015). Review on Membrane interactions of phytochemicals s their molecular mechanism applicable to the Discovery of Drugs leds from plant ISSN 1420-3049.

Mondal, A., Maity, T. K. and Bishayee, A. (2019). Analgesic and Anti-inflammatory Activities of quercetin-3-methoxy-4-glucosyl-7-glucoside isolated from indian medicinal plant *melothria heterophyla*. *Journal of medicines*. 6: 59.

Nuhu, U. D., Ukwuani-Kwaja, A. N., Dalhatu, R. and Senchi, T. J. (2018). Analgesic and Wound Healing Effect of Methanolic Leaves Extract of *Pennisetum Pedicellatum* in Wistar Albino Rat. *International Journal of Medicinal Plants and Natural Products* (IJMPNP) 4: **(1)** 13-18

Omeje, E. O., Nworu S. C., Osadabe P. O., Onugwu L., Maurya R., Okafor S. N. and Proksch P. (2017). In-vitro anti-inflammatory activities of 3-methoxy quercetin isolated from Nigerian mistletoe parasitic on garcinia kola Heckel, clusiaceae. *Tropical journal of pharmaceutical research*. 16**(5)**: 1059-1067

Romha, G., Admasu, B., Gebrekidam, T. H., Aleme, H. and Gebrru, G. (2018). Antibacterial activities of five medicinal plant in Ethiopia against some human and animal pathogens. *Hindawi*, 2950758

Sabri F. Z., Belarbi M., Sabri, F. A., Alsaydi, K. (2012). Phytochemical Screening and Identification of some Compounds from Mallow. *journal of Natural product and plant resources* 2**(4)**: 512-516.

Saxena, K. K. and Roy, S. (2007). Isolation and identification of Trigonelline from the Tissue of *Allium sativum* Linn. *Asian journal of Experimental sciences* 2 **(2)**: 277-280

Shankar, P. and Amara P. (2002). Manual of tropical medical Microbiology. New Delhi. Delhi printing press pp111-119

Solomon, C. U., Arukwe, U. and Onuoha, I. (2013). Preliminary Phytochemical Screening of different Solvent Extracts of stem, bark and roots of *Denneti tripetala* G. Baker. *Asian journal of plant science and research*, 3**(3)**: 10-13.

Tapsell, L. C., Hemphill, I., Cobiac, L., Patch, C. S., Sullivan, D. R.; Fenech, M., Roodenrys, S., Keogh, J. B., Clifton, P. M., Williams, P. G. (2006). Health benefits of herbs and spices: The past, the Present, the Future. *Medicinal Journal Australia. 185*, S4–S24.

Tiwari, P., Bimlesh, K., Mandeep K., Gurpreet, K. and Harleen, K., (2011). Phytochemical Screening and Extraction, A Review. *Internationale phrmaceuticasciencia*, 1**(1)**: 1-9.

Van Wyk B. E and Gericke, N. (2000). People´s plants: A guide to useful plants of Southern Africa. Briza publications, Pretoria 226**(3/4)**:245-247.

Von koenem, E. (2001). Medicinal, poisonous and edible plants in Namibia. Windhoek, Namibia; Gottingen: Klaus Hess publisher, 190-195.

William A., Martha R. and Anderson S. (2011). Bacteriological analysis of abundant species. London UK press pp 304 315

Available online at www.asric.org
ASRIC Journal on Natural Sciences Vol 3(1) (2023) 220-236

Identification of high Groundwater Potential Locations in the Atebubu Municipality of Ghana using the Electrical Resistivity Method

Alfred K. Bienibuor[1]*, Kwasi Preko[2], Akwasi A. Aning[2] Aboagye Menyeh[2], David D. Wemegah[2]

[1]Department of Chemical Sciences, University of Energy and Natural Resources, P. O. Box 214, Sunyani, Ghana

[2]Department of Physics, Geophysics Section, Kwame Nkrumah University of Science and Technology, Kumasi, Ghana

*Corresponding author: alfred.bienibuor@uenr.edu.gh

Abstract

The Atebubu municipality has been battling with a perennial potable water crisis for the past few decades. Borehole and well contractors in the municipality have been using nonscientific means to site aquifers prior to drilling, and this is the major cause of the high incidence of dry boreholes often recorded. Most of the hand-dug wells and boreholes are only productive during the raining season. This problem affects economic activities, children's education and the quality of life of the people. This paper used the electrical resistivity method in the Wenner and gradient array configurations to access subsurface groundwater information leading to high yielding groundwater potential locations. The results show resistivity values for both Wenner and gradient techniques ranging from 5 to 2212 Ωm across the profiles. Resistivity distributions in the very low bracket, interpreted as clay contents, ranged from 5 to 210 Ωm and dominate the shallow subsurface to about 50 m. The thickness of this layer is approximated at 10 to 20 m. Moderately low resistivity distributions (from 100 to 506 Ωm) were observed at deeper depth with only few portions stretching to the middle belt. This bracket of the resistivity distribution is interpreted as water contents, while the high to very high values which are interpreted as competent rock formations were observed predominantly at both deeper depth and the middle belt. High yielding aquifers are therefore expected to be intercepted at deeper depths, overlain at most locations by a clayey vadose zone. Though results of the two measurement techniques significantly corroborated, the Wenner technique appears to suggest that more than half of the depth probed could be clay content, opposed to the gradient technique which portrays more fractured rocks, revealing better chances of high yielding groundwater potential at the sites identified.

Keywords: Atebubu, yielding, groundwater, borehole, surface water

1. Introduction

Groundwater refers to the water in cracks and spaces of rocks, gravels and soils in the saturated zone beneath the Earth surface (Figure 1). It is essential for socioeconomic development in every facet of life. Many people across the globe are now turning to groundwater as the safest and best reliable option for their major source of water (Bienibuor et al., 2020; Taylor et al., 2013; Margat and Van der Gun, 2013, Hakim et al, 2009), resulting in the water withdrawal outweighing annual replenishment (Saha et al., 2018). Coupled with the vulnerability of groundwater to pollution from both geogenic and anthropogenic sources

(Agyare et al., 2021; Saha et al., 2018), there is the need for pragmatic measures to ensure continuous supply and quality.

One major problem of groundwater harvesting is siting the appropriate aquifer for drilling. Confined aquifers might suffer vertical recharging, though the confining layer could serve as a protective cover from anthropogenic pollution sources (Ho and Sa, 2014). Unconfined aquifers on the other hand have the advantage of getting recharged by surface runoffs from rainfall, snow melt, etc., but are also more vulnerable to anthropogenic pollutants (Almanza Tovar et al., 2020; Yesilnacar and Sahinkaya, 2012). Fortunately, geophysical methods are able to locate and identify the type of aquifer, even at deeper depths (Bienibuor et al., 2016; Aning et al., 2014; Andrews et al., 2013). Hence, to drill high-yielding and sustainable boreholes, geophysical techniques must be employed in siting the appropriate aquifer, its depth and delineating the vadose characteristics before drilling.

The sustainability of boreholes and hand-dug wells usually depends on the nature of the vadose zone, drilling depth and type of aquifer (Li et al., 2017; Cao et al., 2016). The nature of the vadose zone can either enhance or inhibit aquifer recharge. For instance, a clay, mudstone or shale-dominated vadose zone will definitely affect the ease with which water percolates through it to recharge the aquifer beneath it (Acharya et al., 2017; Fynn et al., 2016). Aside that, the vadose zone also contributes to determining the type of aquifer (confined, unconfined, semi-confined or perched). In addition, boreholes drilled to deeper depths are less prone to anthropogenic pollution sources as opposed to that drilled to shallower depths (Egbueri and Mgbenu, 2020; Ho and Sa, 2014; Essien and Bassey, 2012). The migration of groundwater to recharge aquifers, both vertically and horizontally, is influenced by hydraulic conditions (Osei et al., 2017; Zhu et al., 2015; Preko et al., 2009; Smerdon et al., 2008; Gemitzi et al., 2006).

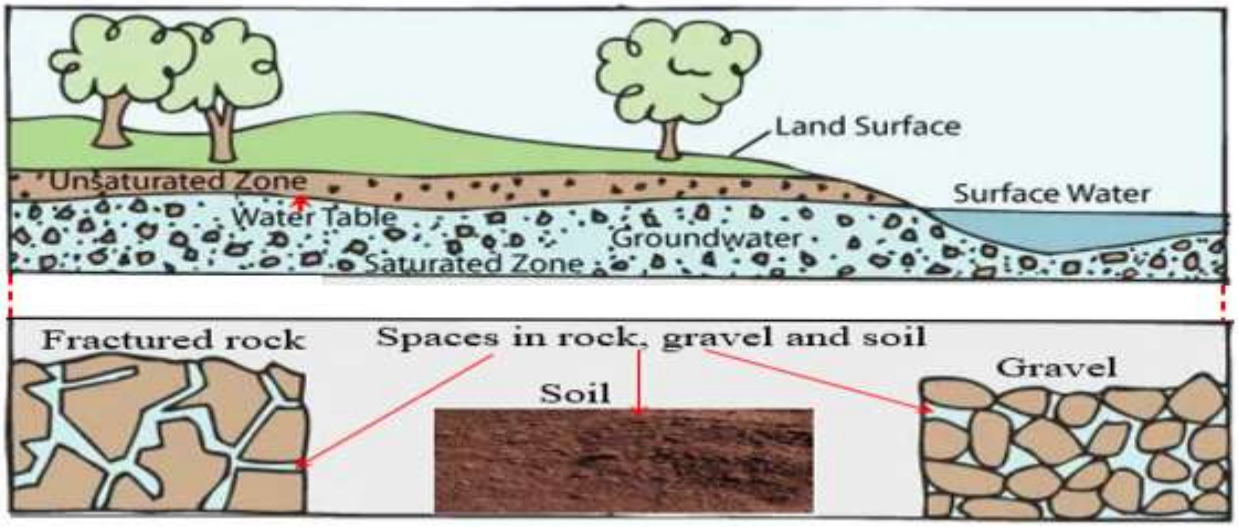

Figure 1: Illustration of Groundwater occurrence (modified after Afrose et al., 2018)

Vertical recharge, resulting from runoffs and surface water bodies is directly and more affected by precipitation temperature and evapotranspiration (Sasidharan et al., 2020; Haidu and Nistor, 2020) than horizontal recharges from migrating waters from saturated soils, adjourning aquifers and other surface waters (Alazard et al., 2016; Praamsma et al., 2009). In the same way, hydraulic pressure varies from aquifer to aquifer even at different locations of the same aquifer (Ghazavi et al., 2018; Zhang et al., 2019). At a given depth, the absolute hydraulic pressure (P_{abs}) is equal to the sum of the hydrostatic pressure (P_w) and the atmospheric pressure (P_{atm}):

$$P_{abs} = P_{atm} + P_w$$

The hydrostatic pressure (resulting from the water alone), P_w depends on the height h of the water in the aquifer (or the thickness of the saturation of the aquifer), the density of water, ρ and gravity, g:

$$P_w = \rho gh$$

The atmospheric pressure influence, on the other hand, depends on the aquifer type. For confined aquifers, atmospheric pressure is less than the pressure on the aquifer. Shahbazi et al. (2020) and Hristopulos (2003) reported that the properties of subsurface geological materials substantially influence the isotropy and homogeneity of hydraulic conductivity of the subsurface. For an isotropic geological formation, hydraulic conductivity does not depend on the direction of measurement nor on position for a homogeneous formation (Shahbazi et al., 2020; Stober and Bucher, 2015). The formation is heterogenous if hydraulic conductivity varies from place to place (Maxwell and Kollet, 2008).

Land use and land cover also have significant impacts on groundwater recharge and discharge rates (Nepf et al., 2022; Yifru et al., 2021; Tahiru et al., 2020; Zomlot et al., 2017; Gebere et al., 2016; Owuor et al., 2016; Scanlon et al., 2005). Using the Soil Water Assessment Tool (SWAT) and the Newton Modular Finite Difference Groundwater Flow (MODFLOW-NWT) in their study, Yifru et al. (2021) realised that vegetative land covers had higher infiltration rates than impervious covers. The vegetation, through the growth of its roots, creates more pores in the soil, and this introduces soil organisms like worms, termites, millipedes, mites, etc., into the soil, further aerating the soil (Nepf, et al., 2022; Ghestem et al., 2011). Hence, forested lands have higher infiltration rates than all other vegetative types (Ghestem et al., 2011). Impervious surfaces like roads, parking lots, etc., on the other hand, inhibit infiltration (Naeem et al., 2021) and, therefore, retards groundwater recharge. The worsening water crisis in Atebubu may be linked, in part, to the speedy development of the area. Urbanisation converts vegetative land covers to impervious ones through the construction of roads, houses, parking lots, etc., which impedes groundwater recharge (Manley et al., 2022; Togbévi et al., 2022; Naeem et al., 2021; Wakode et al., 2018; Carlson et al., 2011; Sharp, 2010; Naik et al., 2008).

2. Methodology

2.1 Project Site Description

The study was conducted in Atebubu, the capital city of the Atebubu-Amanten Municipality. Atebubu is situated between latitudes 7° 23’ N and 8° 22’ N and longitudes 0° 30’ W and 1° 26’ W in the Atebubu-Amanten Municipality, Bono East Region. The main economic activity in the area is farming, with yam being the dominant crop. The municipality falls within the southern part of the Voltaian supergroup, with undifferentiated rocks of the Oti-Pendjari and the Obosum groups (Figure 2; Entsua-Mensah et al., 2007). These groups consist of sandstone, shale, mudstone, limestone, sandy and pebbly beds (Asare-Donkor and Adimado, 2020; Hadzi et al., 2019; Agyekum and Asare, 2016; Yidana et al., 2014; Forkuor et al., 2013; Agyekum et al., 2013; Akayuli et al., 2013).

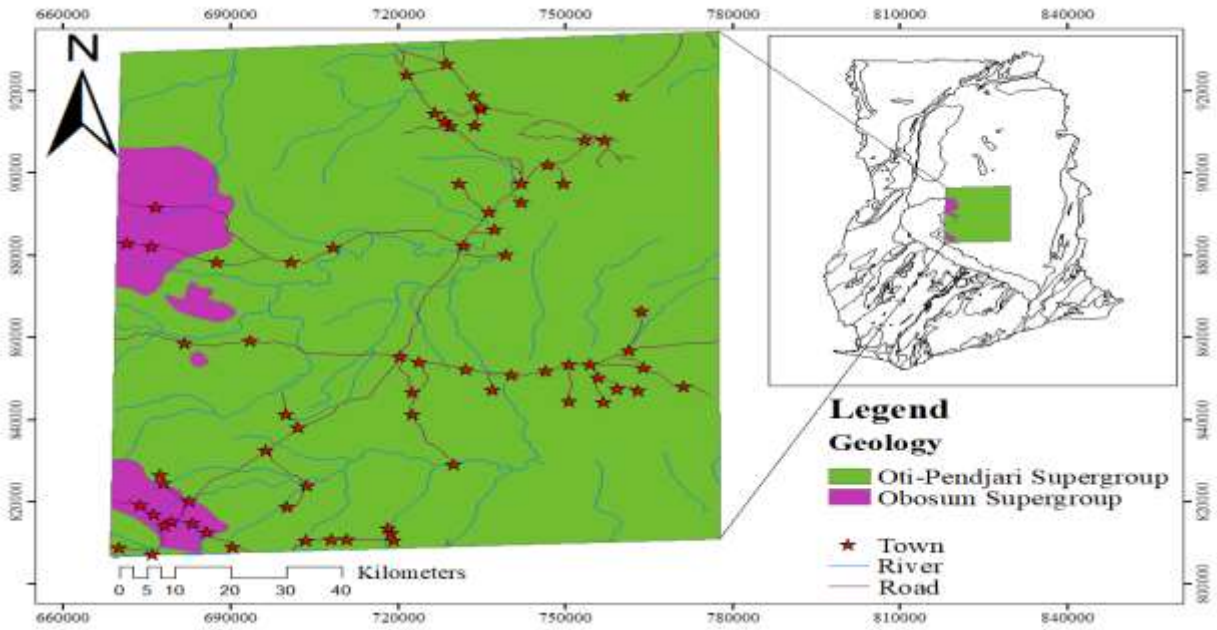

Figure 2: Geological map of the study area

Groundwater potential in the Voltaian Supergroup is the lowest among the hydrogeological provinces of Ghana (Appiah-Adjei and Osei-Nuamah, 2017; Banoeng-Yakubu et al., 2011) with an average borehole yield range of 6.2 to 8.5 m^3/h (Mainoo et al., 2019; Gyau-Boakye and Dapaah-Siakwan, 2000). The primary porosity and permeability of rocks are negligibly small and, therefore, they are not favourable for groundwater development. The low primary porosity is due to the imperviousness of the rocks of the formation (Mainoo et al., 2019; Yidana et al., 2008). Secondary porosity largely controls fracture and faulting in the rocks (Sunkari et al., 2021; Chegbeleh et al., 2020; Yidana et al., 2019). Success rate of boreholes in the formation is as low as 56 % (Yidana et al., 2019; Yidana et al., 2010; Dapaah-Siakwan and Gyau-Boakye, 2000), and the few productive ones are low yielding.

2.2 Data Acquisition

The resistivity data was acquired by the ABEM terrameter SAS4000 C in both Wenner and gradient electrode configurations. Figure 3 is a map showing the profiles along which data was taken. The total length of profiles was 400 m.

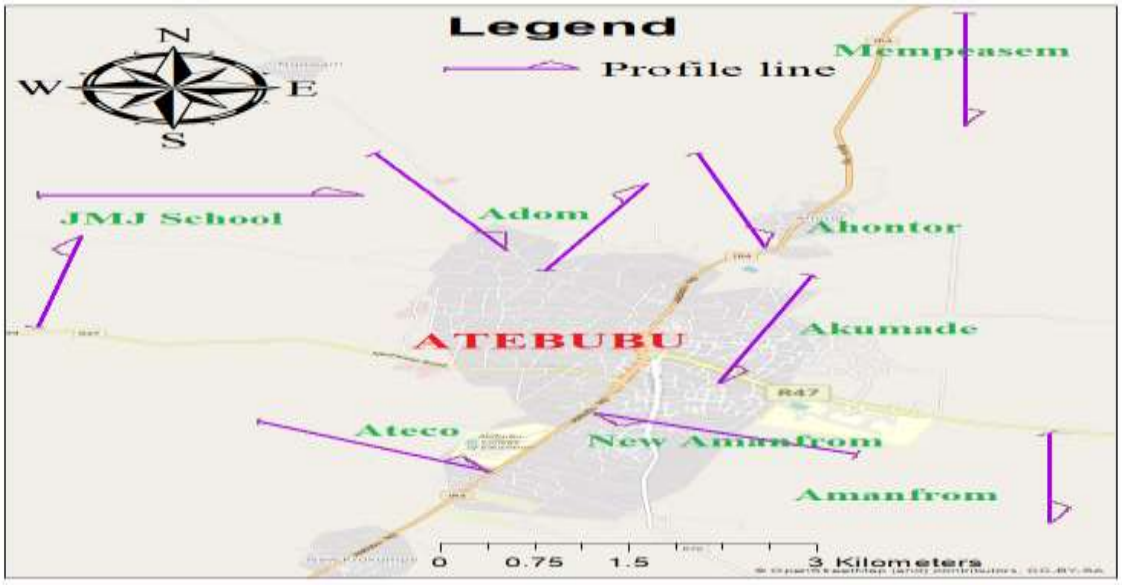

Figure 3: Layout of the study area, showing profile lines.

One profile each was probed at Akumade, New Amanfrom, Amanfrom, Ahontor, Mempeasem and Atebubu College of Education communities, trending in different directions. Position coordinates and elevations of profiles probed are indicated on table 1. At Adom two profiles were surveyed. Profiles 1 and 2 trended north east and south east respectively. Two profiles were also constructed at the JMJ School premises. Profile 1 was constructed to trend in the north eastern direction while profile 2 was constructed from west to east. Each profile accommodated forty-one (41) electrodes, laid at 10 m spacing.

Though the terrameter equipment has been used successfully for geophysical investigations in various places (Hussain et al., 2020; Martínez et al., 2019; Arifin et al., 2019; Nero et al., 2016; Pellicer and Gibson, 2011), there is no literature on its suitability for use in the Atebubu-Amanten Municipality. The electrode test was done before measurement commenced. On the field, it did not encounter any significant problems. There were a few times measurements were interrupted due to overheating of the equipment or related issues. On the part of overheating, iced blocks were wrapped around it to aid cooling, and this helped the survey. For interruptions due to other minor issues, the equipment was merely restarted. In very rare instances, some electrodes were skipped for measurements to continue.

Table 1: Position coordinates and elevations of profiles probed

Community	Profile	Position	Latitudes [ºN]	Longitudes [ºW]	Elevation [m]
New Amanfrom	1	Starting	7º43' 58.764''	0º59' 18.282''	137.30
		Middle	7º44' 1.674''	0º59' 23.91''	142.10
		Ending	7º44' 4.368''	0º59' 29.922''	141.90
Atebubu College of Education	1	Starting	7º43' 43.872''	0º59' 51.564''	142.20
		Middle	7º43' 46.608''	0º59' 57.096''	144.40
		Ending	7º43' 50.526''	1º0' 2.856''	127.80
Ahontor	1	Starting	7º46' 42.81''	0º58' 36.258''	130.00
		Middle	7º46' 37.14''	0º58' 33.498''	144.40
		Ending	7º46' 30.816''	0º58' 31.182''	107.50
Mempeasem	1	Starting	7º47' 30.51''	0º58' 21.21''	131.90
		Middle	7º47' 24.048''	0º58' 20.34''	133.20
		Ending	7º47' 17.838''	0º58' 19.362''	131.90
Akumade	1	Starting	7º44' 51.534''	0º59' 13.962''	133.80
		Middle	7º44' 45.45''	0º59' 16.398''	124.80
		Ending	7º44' 39.414''	0º59' 19.146''	128.60
	1	Starting	7º44' 57.276''	1º00' 4.584''	175.40
		Middle	7º45' 3.774''	1º00' 3.108''	177.70
		Ending	7º45' 10.056''	1º00' 0.438''	177.90
JMJ	2	Starting	7º44' 53.184''	0º59' 59.142''	87.60
		Middle	7º44' 53.01''	0º59' 53.166''	141.30
		Ending	7º44' 52.524''	0º59' 45.972''	155.20
Amanfrom	1	Starting	7º43' 32.688''	0º59' 10.962''	197.50
		Middle	7º43' 25.5''	0º59' 10.722''	148.30
		Ending	7º43' 18.54''	0º59' 10.266''	178.70
	1	Starting	7º46' 9.234''	0º59' 31.89''	139.50
		Middle	7º46' 3.552''	0º59' 34.56''	138.20
		Ending	7º45' 57.822''	0º59' 37.782''	125.30
Adom	2	Starting	7º46' 34.092''	0º59' 58.494''	142.80
		Middle	7º46' 28.212''	0º59' 55.524''	144.50
		Ending	7º46' 22.572''	0º59' 52.488''	127.10

2.3 Data processing and interpretation

Data was processed using the RES2DINVx64 software, a computer program which automatically determines a 2D resistivity model of the subsurface from the field data. The program supports multicore central processing units (CPUs). Inversion is simply dividing the data into rectangular blocks which represent the distribution of the data. The depths of these blocks equal the depths of investigation. In this paper the data was read into the software and edited for electrode positions, discretisation, etc. before modelling. For the model discretisation, extended model was set to 'No', so that trapezoid models are obtained instead of rectangular models. At model display in the show inversion results section, the resistivity option was chosen to display it. Results were displayed after six iterations. Bad data points, referred to as data outliers (Figure 4) were then statistically removed using the RMS error statistics analysis. Data outliers are data misfits between measured and calculated apparent resistivity values. These may result

from poor electrode contact with the ground due to indurated surficial materials or dry ground, shorting due to very wet ground conditions and relay failures at some electrodes.

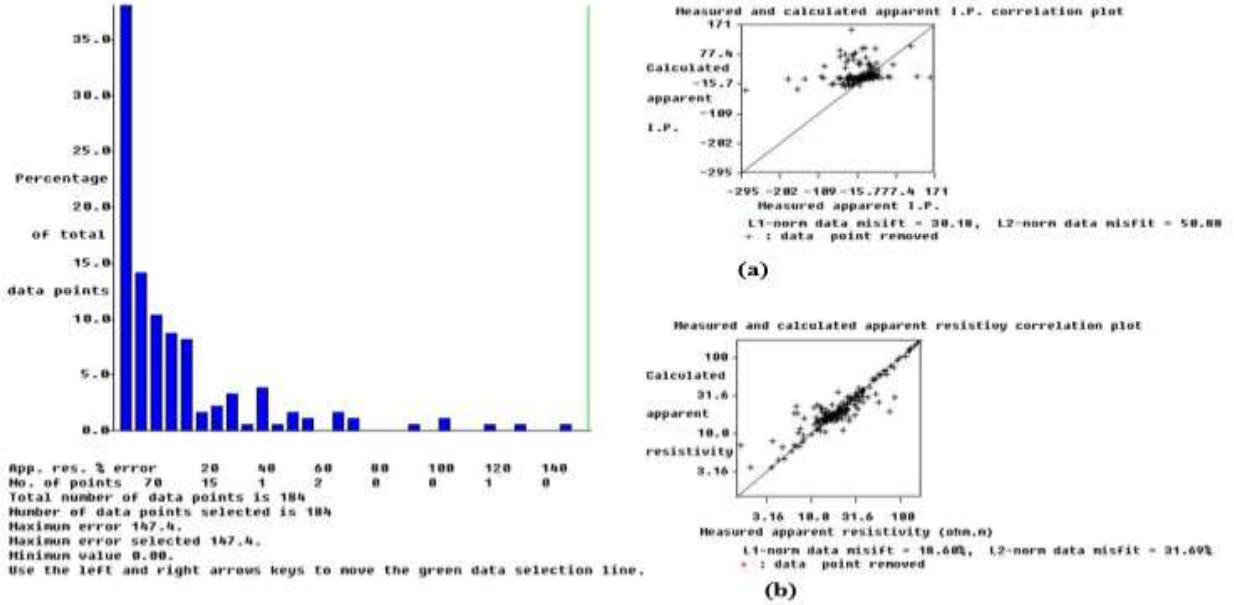

Figure 4: Histogram and scatter plots for inversion results, showing data outliers.

The filtered data was saved with a new filename, reread into the software and the inversion process was repeated. The entire process was repeated until less RMS error was obtained (preferably less than 10 %). The final models were then saved.

3. Error analysis

In designing a survey or processing geophysical data, it is imperative to consider all sources of error to have an idea of possible artefacts or inaccuracies in your models. In resistivity surveys, it is possible to remove noisy data prior to inversion and modelling (Miller et al., 2008). In this work, the RMS error statistical analysis was used to remove noisy data and artefacts before Processing to improve the resolution and quality of models. The inversion was done with high RMS until the lowest possible absolute errors were achieved, since absolute error assesses the signal-to-noise ratio of a dataset. According to Rucker et al. (2011), absolute error refers to the absolute difference of two repeated readings. In this survey only few extremely noisy data were recorded, where the absolute errors equaled or exceeded 10. This was quite expected since resistivity measurements are usually less prone to noise (Mashhadi and Ramazi, 2018; Dahlin et al., 2002).

Major sources of systematic and random errors were the aging of cables, wires or electrodes and impedance effects (Mashhadi et al., 2020; Dahlin et al., 2002). The non-ideal nature of the terrameter system could also introduce systematic errors. Another key source of error was the electrode spacing. Electrode spacing errors are errors associated with electrode position measurements or inadvertent electrodes on the. Most of the profiles were constructed on bushy sites. Coupled with the undulating and rough ground surfaces, it was challenging to have straightened cables along the profiles. Additionally, indurated surficial materials or dry ground can cause poor electrode contact with the ground, shorting due to very wet ground conditions and relay failures at some electrodes resulted in shifting some electrode positions, potentially affecting their spacing. To minimize minimise electrode spacing errors on the field, the data acquisition team ensured maximum care and vigilance throughout the exercise, particularly during the mounting of electrodes. Two

technicians were assigned to check and ensure correct electrode positions before measurements on each profile commenced. Additionally, a reconnaissance survey was conducted to assess the potency of the equipment and electrode configuration techniques in order to minimise observed potential and related errors. Furthermore, the survey was repeated two to three times before the results were stored in communities with background noise such as passing vehicles.

4. Results and Discussion

The 2D data was inverted into resistivity models, showing both lateral and vertical subsurface resistivity distribution. The models revealed a wide variation of subsurface information. These model sections were displayed using user defined logarithmic contours. Information on these models reveal the nature and type of subsurface materials. The study area is characterized by high clay content (Sowley and Aboagye, 2010; Abonkrah, 2004), therefore the resistivity of the subsurface could be evidence of the presence of either clay or water contents. However, since clay is more conductive than water (Mainoo et al., 2019; Madun et al., 2018; Saad et al., 2012; Ewusi et al., 2009), very low resistivity layers, indicated in this case as blue, are interpreted as clay contents while layers of moderately low resistivity values, indicated by the green contours could be the aquifer zones. The thickness of clay content is approximated at 10 to 20 m.

In both gradient and Wenner techniques the results indicate a wide variation of subsurface resistivity distributions, ranging from 5 to 2818 Ωm across the profiles. Values of resistivity in the very low bracket for all the models ranged from 5 to 98.6 Ωm while the moderately low resistivity bracket, purported to be water contents, have values ranging from 100 to 500 Ωm. The very low resistivity values were observed over the shallow subsurface, covering about one-third of the vadose zone. Fractured rocks of the moderately low resistivity values were observed over the basement rocks. In all the profiles, results for both the gradient and Wenner configurations show great signs of competent aquifers at deeper depths, though they poorly correlate for most of the profiles.

Very low resistivity values were observed across most of the top layers with the moderately low values characterising the middle belt. The green contours marked A at Akumade and Amanfrom (Figure 5) could be highly fractured rocks with high water contents since resistivity values of these enclaves are in the range of 100 to 500 Ωm, which are within values observed by Razak and Muztaza. (2022), Azizan et al. (2018) and Juanah et al. (2013), as high groundwater potential. Both results show great signs of high yielding groundwater potentials of the basement rocks with rocky first layers and thick clayey middle layers. Structures are however better resolved for Amanfrom than Akumade as results of the gradient and Wenner measurements were significantly compared for Amanfrom than for Akumade. Recommended drilling points, indicated by the red arrows, are points 230 and 90 m for Akumade and 190 m for Amanfrom.

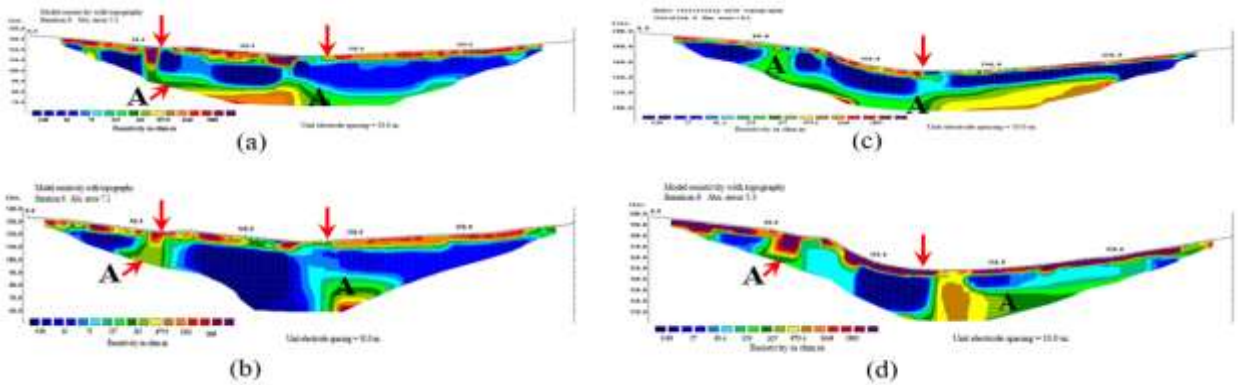

Figure 5: The diagram represents gradient and Wenner resistivity models, (a) and (b) for Akumade and (c) and (d) for Amanfrom communities respectively.

At the Adom community two profiles (1 and 2) were surveyed, trending north east and south east respectively. Results of the two measurement techniques corroborated more significantly for profile 2 than for profile 1. In the case of profile 1, about 90 % of the depth probed, from about 110 to 205 m, is revealed by the Wenner technique as clay contents which is at variance with the competent basement rock recorded in the same region by the gradient measurement (Figures 6 a & b). The green contoured layers are also better interconnected for the gradient technique than the Wenner, which is an indication of better groundwater prospects with the gradient method than with the Wenner method. Also, though the contours labelled A on profile 1 appear to match for the two measurement techniques, a highly resistive layer is observed beneath that for the Wenner results. Results of profile 2 on the other hand reveals a highly resistive shallow subsurface as observed on both models (Figures 6 c & d), a possible hard rock layer, with indications of fractured basement rocks. The competent rock condition and clayey block expressed at the bottom layer and middle belt are also well corroborated for both gradient and Wenner results. The green contours are also well interconnected, suggestive of high water contents. Recommended drilling points for profiles 1 and 2 are 215 and 210 m respectively.

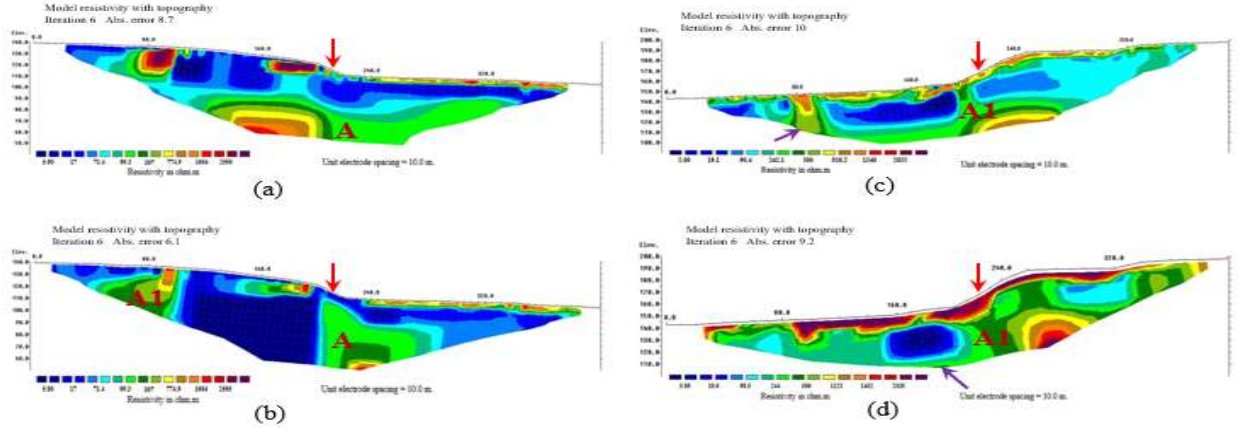

Figure 6: Gradient and Wenner resistivity models for Adom community: (a) and (b) for profile 1 and (c) and (d) for profile 2 respectively.

At the JMJ community the topography of profile 1 was fairly flat, but quite steep for profile 2. On both profiles the gradient array results indicate that more than half of the eastern part of the profile is characterised by crystalline rocks over the middle belt, stretching to greater depths. This is corroborated by the Wenner array results of profile 2. Expressions of hard rock conditions were observed at the basement of profile 1 with the Wenner array measurement between 180 and 250 m. A lot of data was lost at the extreme ends of the south western and south eastern belts with the Wenner array measurements; nevertheless, structures resolved were matched with that of the gradient array measurements. The fracture or fault zone for profile 1 is identified with resistivity values ranging from 201 to 342 Ωm and 200 to 437 Ωm for profile 2, indicated by the green contours. Drilling at points 110 m and 195 m on profile 1 (Figures 7 a & b) is expected to intercept the fractured rocks at these contour locations. Point 195 m however is more preferred to point 110 m. For profile 2 recommended drilling points are points 90 and 260 m (Figures 7 c & d). Though the Wenner array results predicts a hard, unfractured rock layer beneath point 260 m, it is

still recommended because contour I could extend both eastwards and westward as the profile was constructed from west to east.

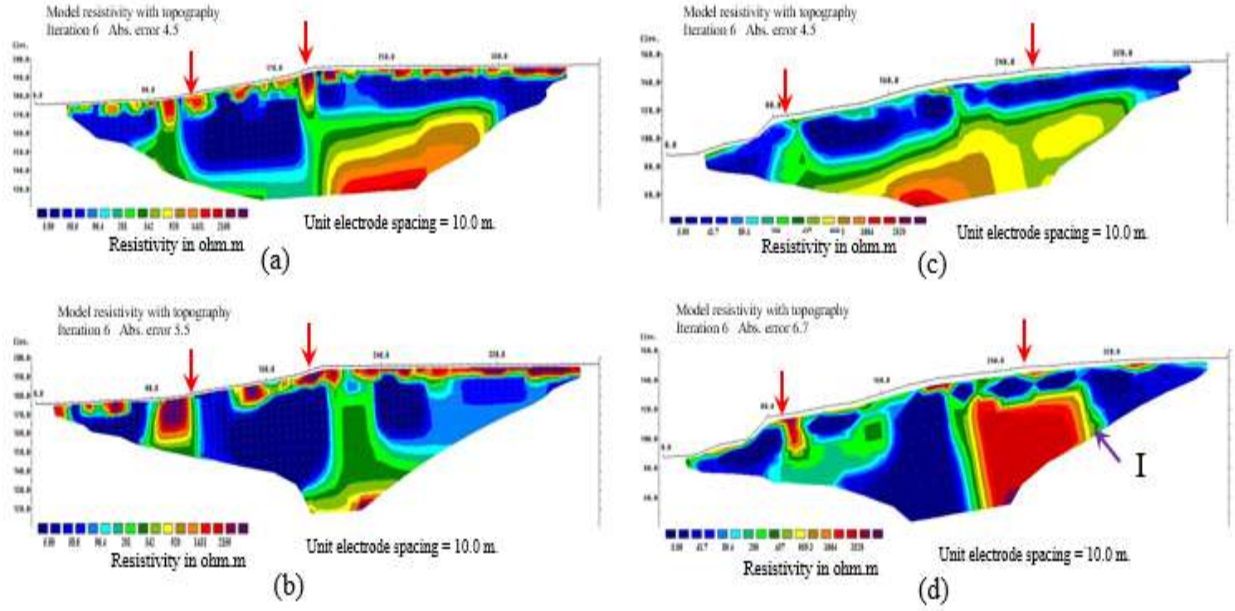

Figure 7: Gradient and Wenner resistivity models for JMJ School community: (a) and (b) for profile 1 and (c) and (d) for profile 2 respectively.

Diverse resistivity distributions were observed at the Ahontor and Mempeasem communities with values of the fault zone from 238 to 500 Ωm for Ahontor and 159 to 309 Ωm for Mempeasem. At Ahontor structures revealed with the gradient method do not sufficiently conform to that by the Wenner technique. With the gradient method results, the first layer is expected to comprise of hard, unfractured rocks, up to a few meters. This is then followed by a possible thick clay layer characterising the entire middle belt and the extreme ends of the profile. On the Wenner method model on the other hand, expressions of hard rock conditions were noticed on the first layer and stretches to the middle belt at points 90 to 110 m and 200 to 215 m locations. Nevertheless, the green contours on both models are well aligned at points 115 and 265 m as indicated by the red arrows (Figures 8 a & b). Also, the yellow contour (E) at the basement from points 105 to 255 m on the gradient model conforms to contour E on the Wenner model. The two blocks are expressions of a competent rock. At Mempeasem a highly resistive layer, suggestive of a massive rock was observed stretching from the middle belt to the far depth of about the 70 to 320 m location on the profile as shown by the yellow to red layers of contours (Figures 8 c). This massive bedrock expression on the gradient model is well corroborated by the Wenner method results as the highly resistive blocks, C and D dip towards each other, a sign that they could extend to intercept at depth. The top layers however, are mismatched. The gradient results portray a clay dominated top layer while the Wenner results reveals a fractured one. Groundwater potential on this profile is expected to be low. Point 315 m is recommended for drilling.

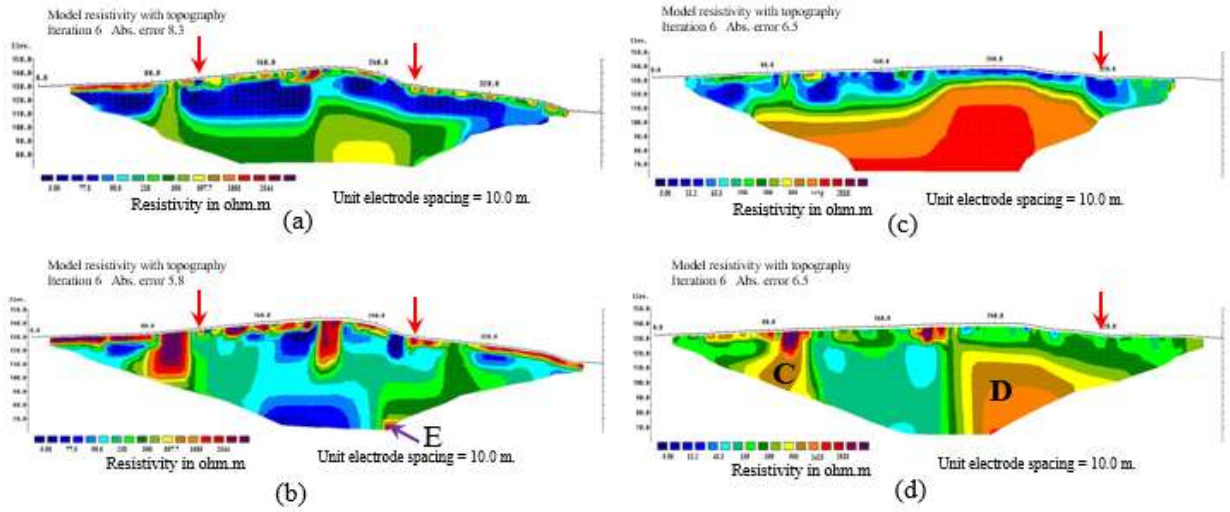

Figure 8: The diagram represents gradient and Wenner resistivity models, where (a) and (b) are for Ahontor and (c) and (d) for Mempeasem communities respectively.

Similarly, results of the Atebubu College of Education and New Amanfrom have revealed potentially competent bedrock blocks (marked A) of resistivity values ranging from 797 to 2114 Ωm for the College of Education and 679 to 2019 Ωm for the New Amanfrom communities at some locations on the profiles. On both measurement techniques at the Atebubu College of Education, rocks of the middle belt are projected to be heavily fractured with possibility of high water contents. The green contours dominating the middle belt have moderate resistivity values ranging from 145 to 243 Ωm (Figures 9 a & b). Locations on the profile that are more likely to intercept the water contents are 135 and 310 m. For the New Amanfrom community expressions of fracturing or faulting were recorded in the middle belt, but with intrusions of clay contents. Structures resolved appear to be better aligned at points 105 and 215 m. In both communities the gradient array results projects confined aquifer systems while the Wenner array results does not. Groundwater potentials for both communities could be moderate to high.

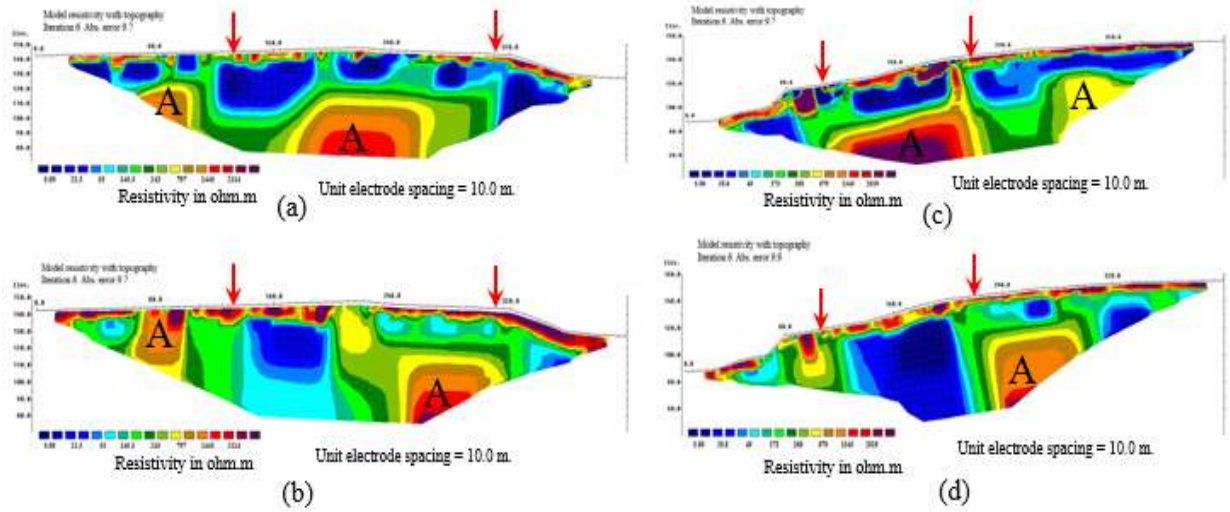

Figure 9: The diagram represents gradient and Wenner resistivity models. (a) and (b) are for Atebubu College of Education and (c) and (d) for New Amanfrom communities respectively.

A plot of all the resistivity data (Figure 10) reveals an interesting subsurface with an admixture of low, moderate and high resistivity distributions. The moderate to high resistivity distributions, indicated by the green contours on this map could be water contents while the high resistivity yellow to deep red contoured layers are interpreted as impervious rock formations (Mainoo et al., 2019; Madun et al., 2018). Clay contents are represented by the low resistivity distributions (indicated by the blue contours). The map projects high groundwater potentials in the middle and north eastern belts. The northern and eastern stretches are characterised by hard rock conditions whose groundwater potential, according to Varade et al. (2018), Basavarajappa et al. (2013) and Maggirwar & Umrikar (2011) are poor, heterogeneous and complex, owing to the fact that they lack primary porosity. Expressions of hard rock conditions were also recorded at few locations in the north western, southern and south western belts. However, considering that these enclaves are also characterised by low (blue contours) to moderate (green contours) resistivity distributions which are expressions of clay and water contents, groundwater potential of these regions could be low to moderately high. The southern belt could be clay dominated as low resistivity distribution was generally observed over it. The southern belt is therefore expected to result in low to moderately high yielding groundwater potential.

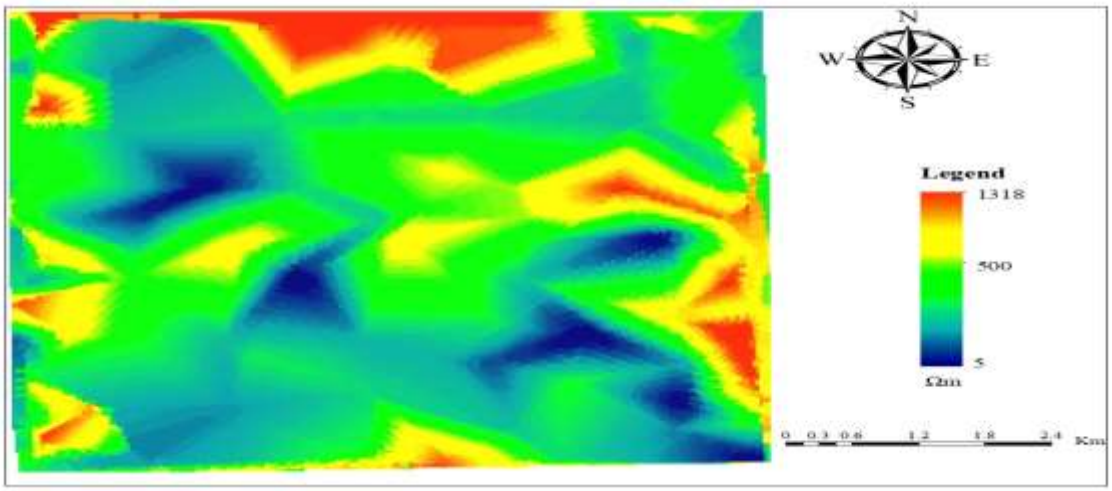

Figure 10: Resistivity model of the study area

5. Depths of existing boreholes in the study area

The various depths of existing boreholes sampled from the Community Water and Sanitation Agency were contoured into different colours (Figure 11) with the red contours being the deepest. Depths in this bracket range from 53.6 to 70.1 m, constituting about 7 % of all the borehole depths sampled. At the time of this survey only few boreholes of this depth bracket were productive. Depths ranges of 39.2 – 40.9 m and 40.9 – 53.6 m constitute about 15 and 20 % respectively while about 28 and 30 % are occupied by depth ranges of 34.5 – 39.2 m and 24.3 – 34.5 m respectively. The map appears to suggest that most boreholes in the municipality are drilled to a maximum depth of 35m, which is too shallow and possibly part of the reasons they dry up in the dry season.

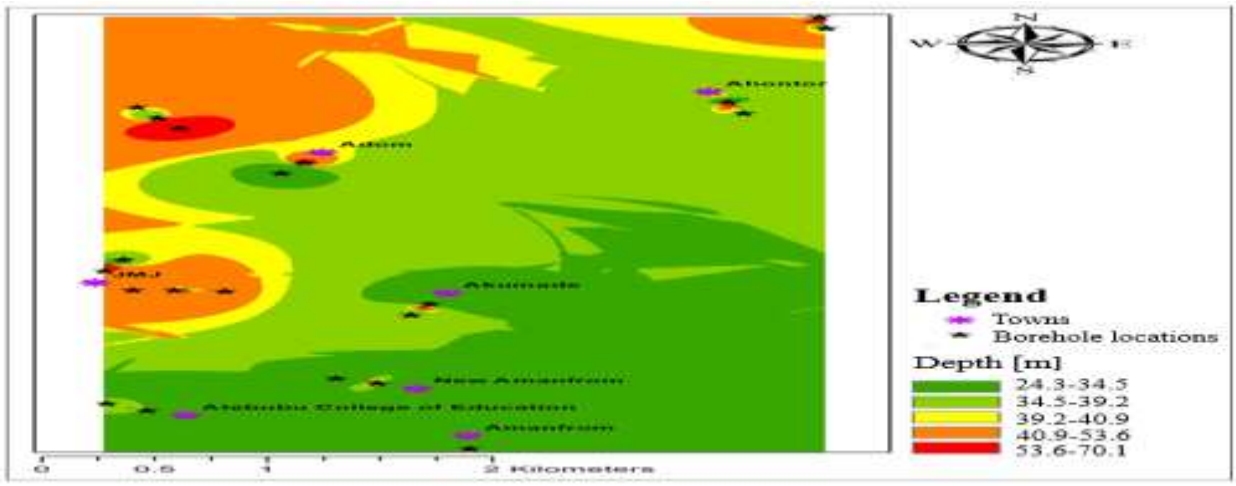

Figure 11: A map showing the depth distribution of existing boreholes in the study area

6. Conclusion

This research was conducted to evaluate the potential of groundwater resources in the Atebubu municipality of Ghana. At the end of the survey, 20 groundwater potential locations expected to be high yielding were identified across the 10 researched communities. Locations identified include the following: 230 and 90 m for Akumade and 190 m for Amanfrom communities. At Akumade, point 230 m was ranked above point 90 m. At the Adom and JMJ School communities, two profiles were investigated. At the end of the survey points 215 and 210 m respectively for profiles 1 and 2 were identified for drilling at Adom. For the JMJ School community points 110 and 195 m were observed to be suitable for drilling on profile 1 while 90 and 260 m were identified for profile 2. Between points 110 and 195 m on profile 1, point 195 m is more preferred. Point 90 m is also preferred to 260 m on profile 2 because of the topography of the area. Points 115 and 265 m were also earmarked for possible drilling at the Ahontor community, where 265 m is expected to be high yielding than 115 m. At Mempeasem only point 315 m was identified as suitable for drilling. Other viable points were sited at points 135 and 310 m at the Atebubu College of Education and 105 and 215 m at the New Amanfrom communities. Of these, points 135 and 215 m respectively are ranked over 310 and 105 m.

In all, the results indicate a clay or shale dominated shallow vadose zone with high probability of a heavily fractured bed rock at deeper depths. Clay easily loses its porosity when wet, therefore allowing water to flow instead of storing it or allowing it to infiltrate into the groundwater system. Hence, the dominance of clay in the shallow subsurface may affect vertical recharge of the aquifer system, especially from rainfall and other surface waters. A lot of the models, especially with the gradient measurements, point to a confined aquifer system. There were also indications of unconfined and perched water contents at few locations on some of the profiles. Across the globe over 1.73 million people die every year from water, sanitation, and hygiene-related diseases such as cholera, diarrhoea, etc. The outcome of this research will inform investors and the government of the plight of communities across the Atebubu municipality since this is the first time such a survey is conducted in the municipality. Borehole drillers and hand-dug well contractors in the municipality use traditional methods of siting aquifers prior to drilling. The outcome of this research will provide them with firsthand information on where to drill or dig high-yielding boreholes or wells.

References

Abonkrah, C. K. (2004). Environmental and Natural Resources Management and Sustainable Rural Development in the Atebubu District, Ghana (Doctoral dissertation, Ohio University).

Acharya, B. S., Halihan, T., Zou, C. B. and Will, R. E. (2017). Vegetation controls on the spatio-temporal heterogeneity of deep moisture in the unsaturated zone: A hydrogeophysical evaluation. Scientific Reports, 7(1), 1499.

Afrose, T., Anthony, L., Fernandez, K. and Latt, S. (2018). Global access to clean water: the role of rain water harvesting. Annals of Reviews and Research, 2, 555585.

Agyare, A., Kabo-Bah, A. T., Bayel, B. T. and Jalloh, A. S. (2021). Integration of GIS and F-Hydra Model for Aquifer Vulnerability Monitoring in the Afram Plains, Ghana. Journal of Geoscience and Environment Protection, 9(03), 222.

Agyekum, W. A. and Asare, E. B. (2016). Challenges associated with ground water resources development in northern Ghana. Ghana Journal of Science, 56(1), 39-51.

Agyekum, W., Klitten, K., Armah, T., Banoeng-Yakubo, B., and Amartey, E. O. (2013). Geophysical borehole logging for control of driller's records: hydrogeological case study from Voltaian sedimentary rocks in northern Ghana. Applied Water Science, 3(2), 491-500.

Akayuli, C., Ofosu, B., Nyako, S. O. and Opuni, K. O. (2013). The influence of observed clay content on shear strength and compressibility of residual sandy soils. International Journal of Engineering Research and Applications (IJERA). Vol. 3, Issue 4, pp. 2538-2542.

Alazard, M., Boisson, A., Maréchal, J. C., Perrin, J., Dewandel, B., Schwarz, T., ... and Ahmed, S. (2016). Investigation of recharge dynamics and flow paths in a fractured crystalline aquifer in semi-arid India using borehole logs: implications for managed aquifer recharge. Hydrogeology journal, 24(1), 35-57.

Almanza Tovar, O. G., Ramos Leal, J. A., Tuxpan Vargas, J., de Jesús Hernández García, G. and De Lara Bashulto, J. (2020). Contrast of aquifer vulnerability and water quality indices between a unconfined aquifer and a deep aquifer in arid zones. Bulletin of Engineering Geology and the Environment, 79, 4579-4593.

Andrews, N. D., Aning, A. A., Danuor, S. K. and Noye, R. M. (2013). Geophysical investigations at the proposed site of the KNUST teaching hospital building using the 2D and 3D resistivity imaging techniques. International Research Journal of Geology and Mining, 3(3), 113-123.

Aning, A. A., Sackey, N., Jakalia, I. S., Sedoawu, O., Tetteh, E. H., Hinson, G., ... and Quaye, E. K. (2014). Electrical resistivity as a geophysical mapping tool; a case study of the new art department, KNUST-Ghana. International Journal of Scientific and Research Publications, 4(1), 1-7.

Appiah-Adjei, E. K. and Osei-Nuamah, I. (2017). Hydrogeological evaluation of geological formations in Ashanti Region, Ghana. Journal of Science and Technology (Ghana), 37(1), 34-50.

Arifin, M. H., Kayode, J. S., Izwan, M. K., Zaid, H. A. H. and Hussin, H. (2019). Data for the potential gold mineralization mapping with the applications of Electrical Resistivity Imaging and Induced Polarization geophysical surveys. Data in brief, 22, 830-835.

Asare-Donkor, N. K. and Adimado, A. A. (2020). Groundwater quality assessment in the Northern and Upper East Regions of Ghana. Environmental Earth Sciences, 79(10), 1-19.

Azizan, F. A., Sah, S. S. and Nawawi, M. M. (2018). Validation of Groundwater Potential Zone Based on Imaging Profiles using Different Array and Lines of Survey Position. In IOP Conference Series: Materials Science and Engineering. IOP Publishing, 429(1), p. 012027.

Banoeng-Yakubu, B., Yidana, S. M., Ajayi, J. O., Loh, Y. & Aseidu, D. (2011). Hydrogeology and groundwater resources of Ghana: a review of the hydrogeology and hydrochemistry of Ghana. Potable Water and Sanitation, 142.

Basavarajappa, H. T., Dinakar, S., Sathish, M. V., Nagesh, D., Balasubramanian, A. and Manjunatha, M. C. (2013). Delineation of groundwater potential zones in hard rock terrain of Kollegal shear zone (Ksz), south India using remote sensing and GIS. International Journal of Earth Sciences and Engineering, 6(5), 1185-1194.

Bienibuor, A. K., Preko, K., Aning, A. A., Antwi, M. and Emahi, I. (2020). Application of Electromagnetic and Electrical Resistivity Methods for Borehole Siting in Low-Grade Metavolcanic and Metasedimentary Rocks, Sunyani West, Ghana. Journal of Environment and Earth Science. 10 (10), 44 - 55.

Bienibuor, A. K., Preko, K., Wemegah, D. D. and Manu, E. (2016). The use of electromagnetic and electrical resistivity methods in assessing groundwater resource potentials in Adoe, Sunyani, Ghana. International Journal of Scientific and Technology Research, 5(9), 166-170.

Cao, G., Scanlon, B. R., Han, D. and Zheng, C. (2016). Impacts of thickening unsaturated zone on groundwater recharge in the North China Plain. Journal of hydrology, 537, 260-270.

Carlson, M. A., Lohse, K. A., McIntosh, J. C. and McLain, J. E. (2011). Impacts of urbanization on groundwater quality and recharge in a semi-arid alluvial basin. Journal of Hydrology, 409(1-2), 196-211.

Chegbeleh, L. P., Akurugu, B. A. and Yidana, S. M. (2020). Assessment of groundwater quality in the Talensi District, Northern Ghana. The Scientific World Journal, 2020; 1-24

Dahlin, T., Leroux, V. and Nissen, J. (2002). Measuring techniques in induced polarisation imaging. Journal of Applied Geophysics, 50(3), 279-298.

Egbueri, J. C. and Mgbenu, C. N. (2020). Chemometric analysis for pollution source identification and human health risk assessment of water resources in Ojoto Province, southeast Nigeria. Applied Water Science, 10(4), 1-18.

Entsua-Mensah, R. M., Essegbey, G., Frempong, G. and Engmann, C. (2007). Assessment of community water and sanitation in Ghana.

Essien, O. E. and Bassey, E. D. (2012). Spatial variation of borehole water quality with depth in Uyo Municipality, Nigeria. In 21st Century Watershed Technology: Improving Water Quality and Environment Conference Proceedings, May 27-June 1, 2012, Bari, Italy (p. 1). American Society of Agricultural and Biological Engineers.

Forkuor, G., Pavelic, P., Asare, E. and Obuobie, E. (2013). Modelling potential areas of groundwater development for agriculture in northern Ghana using GIS/RS. Hydrological sciences journal, 58(2), 437-451.

Fynn, O. F., Yidana, S. M., Chegbeleh, L. P. and Yiran, G. B. (2016). Evaluating groundwater recharge processes using stable isotope signatures—the Nabogo catchment of the White Volta, Ghana. Arabian Journal of Geosciences, 9, 1-15.

Gebere, S. B., Alamirew, T., Merkel, B. J., & Melesse, A. M. (2016). Land use and land cover change impact on groundwater recharge: The Case of Lake Haramaya watershed, Ethiopia. In Landscape Dynamics, Soils and Hydrological Processes in Varied Climates (pp. 93-110). Springer, Cham.

Gemitzi, A., Petalas, C., Tsihrintzis, V. A. and Pisinaras, V. (2006). Assessment of groundwater vulnerability to pollution: a combination of GIS, fuzzy logic and decision-making techniques. Environmental Geology, 49, 653-673.

Ghazavi, R., & Ebrahimi, H. (2018). Predicting the impacts of climate change on groundwater recharge in an arid environment using modeling approach. International Journal of Climate Change Strategies and Management.

Ghestem, M., Sidle, R. C. and Stokes, A. (2011). The influence of plant root systems on subsurface flow: implications for slope stability. Bioscience, 61(11), 869-879.

Gyau-Boakye, P. and Dapaah-Siakwan, S. (2000). Groundwater as source of rural water supply in Ghana. Journal of Applied Science and Technology, 5(1), 77-86.

Hadzi, G. Y., Ayoko, G. A., Essumang, D. K. and Osae, S. K. (2019). Contamination impact and human health risk assessment of heavy metals in surface soils from selected major mining areas in Ghana. Environmental geochemistry and health, 41(6), 2821-2843.

Haidu, I. and Nistor, M. M. (2020). Long-term effect of climate change on groundwater recharge in the Grand Est region of France. Meteorological Applications, 27(1), e1796.

Hakim, M. A., Juraimi, A. S., Begum, M., Hasanuzzaman, M., Uddin, M. K. and Islam, M. M. (2009). Suitability evaluation of groundwater for irrigation, drinking and industrial purposes. American Journal of Environmental Sciences, 5(3), 413-419.

Ho, N. and Sa, N. (2014). Groundwater resources of the Niger Delta: Quality implications and management considerations. International Journal of water resources and environmental engineering, 6(5), 155-163.

Hristopulos, D. T. (2003). Renormalization group methods in subsurface hydrology: overview and applications in hydraulic conductivity upscaling. Advances in Water Resources, 26(12), 1279-1308.

Hussain, Y., Uagoda, R., Borges, W., Nunes, J., Hamza, O., Condori, C., ... and Cárdenas-Soto, M. (2020). The potential use of geophysical methods to identify cavities, sinkholes and pathways for water infiltration. Water, 12(8), 2289.

Juanah, M. S., Ibrahim, S., Sulaiman, W. N. A. and Latif, P. A. (2013). Groundwater resources assessment using integrated geophysical techniques in the southwestern region of Peninsular Malaysia. Arabian Journal of Geosciences, 6(11), 4129-4144.

Li, S., Liu, B., Xu, X., Nie, L., Liu, Z., Song, J., ... and Fan, K. (2017). An overview of ahead geological prospecting in tunneling. Tunnelling and Underground Space Technology, 63, 69-94.

Madun, A., Tajudin, S. A. A., Sahdan, M. Z., Dan, M. F. M. and Talib, M. K. A. (2018). Electrical resistivity and induced polarization techniques for groundwater exploration. International Journal of Integrated Engineering, 10(8).

Maggirwar, B. C. and Umrikar, B. N. (2011). Influence of various factors on the fluctuation of groundwater level in hard rock terrain and its importance in the assessment of groundwater. Journal of Geology and Mining Research, 3(11), 305-317.
Mainoo, P. A., Manu, E., Yidana, S. M., Agyekum, W. A., Stigter, T., Duah, A. A. and Preko, K. (2019). Application of 2D-Electrical resistivity tomography in delineating groundwater potential zones: Case study from the voltaian super group of Ghana. Journal of African Earth Sciences, 160, 103618.
Manley, E., Ogneva-Himmelberger, Y., Ruelle, M., Hanumantha, R., Mazari-Hiriart, M. and Downs, T. J. (2022). Land-cover change and urban growth in the Mexico-Lerma-Cutzamala Hydrological Region, 1993–2018. Applied Geography, 147, 102785.
Margat, J. and Van der Gun, J. (2013). Groundwater around the world: a geographic synopsis. Crc Press. Taylor and Francis Group.
Martínez, J., Rey, J., Sandoval, S., Hidalgo, M. and Mendoza, R. (2019). Geophysical prospecting using ERT and IP techniques to locate Galena veins. Remote Sensing, 11(24), 2923.
Mashhadi, S. R. and Ramazi, H. (2018). The application of resistivity and induced polarization methods in identification of skarn alteration haloes: A case study in the Qale-Alimoradkhan Area. Journal of Environmental and Engineering Geophysics, 23(3), 363-368.
Mashhadi, S. R., Nikfarjam, M. and Mehrnia, A. K. (2020). Reinterpretation of resistivity and induced polarization data to explore gold mineralization zones at Zarzima prospect, Iran. Acta Geol. Slovaca, 12(1), 15-22.
Maxwell, R. M. and Kollet, S. J. (2008). Quantifying the effects of three-dimensional subsurface heterogeneity on Hortonian runoff processes using a coupled numerical, stochastic approach. Advances in water resources, 31(5), 807-817.
Miller, C. R., Routh, P. S., Brosten, T. R. and McNamara, J. P. (2008). Application of time-lapse ERT imaging to watershed characterization. Geophysics, 73(3), G7-G17.
Naeem, U. A., Gabriel, H. F., Khan, N. M., Ahmad, I., Ur Rehman, H. and Zafar, M. A. (2021). Impact of urbanization on groundwater levels in Rawalpindi City, Pakistan. Pure and Applied Geophysics, 178(2), 491-500.
Naik, P. K., Tambe, J. A., Dehury, B. N., & Tiwari, A. N. (2008). Impact of urbanization on the groundwater regime in a fast growing city in central India. Environmental monitoring and assessment, 146(1), 339-373.
Nepf, H., Puijalon, S. and Capra, H. (2022). Organism-scale interaction with hydraulic conditions. Journal of Ecohydraulics, 7(1), 1-3.
Nero, C., Aning, A. A., Danuor, S. K. and Noye, R. M. (2016). Delineation of graves using electrical resistivity tomography. Journal of Applied Geophysics. Vol. 126; pp. 138–147.
Osei, M. A., Amekudzi, L. K., Wemegah, D. D., Preko, K., Gyawu, E. S. and Obiri-Danso, K. (2017). Hydro-Climatic Modelling of an Ungauged Basin in Kumasi, Ghana. Hydrology and Earth System Sciences Discussions, 1-19.
Owuor, S. O., Butterbach-Bahl, K., Guzha, A. C., Rufino, M. C., Pelster, D. E., Díaz-Pinés, E. and Breuer, L. (2016). Groundwater recharge rates and surface runoff response to land use and land cover changes in semi-arid environments. Ecological Processes, 5(1), 1-21.
Pellicer, X. M. and Gibson, P. (2011). Electrical resistivity and Ground Penetrating Radar for the characterisation of the internal architecture of Quaternary sediments in the Midlands of Ireland. Journal of Applied Geophysics, 75(4), 638-647.
Praamsma, T., Novakowski, K., Kyser, K. and Hall, K. (2009). Using stable isotopes and hydraulic head data to investigate groundwater recharge and discharge in a fractured rock aquifer. Journal of Hydrology, 366(1-4), 35-45.
Preko, K., Scheuermann, A. and Wilhelm, H. (2009). Comparison of invasive and non-invasive electromagnetic methods in soil water content estimation of a dike model. Journal of Geophysics and Engineering, 6(2), 146-161.
Razak, M. H. and Muztaza, N. M. (2022). Evaluation of aquifer potential using 2-D resistivity and induced polarization in Machang, Kelantan, Malaysia. Journal of Sustainability Science and Management, 17(1), 259-270
Rucker, D. F., Noonan, G. E. and Greenwood, W. J. (2011). Electrical resistivity in support of geological mapping along the Panama Canal. Engineering Geology, 117(1-2), 121-133.
Saha, D., Marwaha, S. and Mukherjee, A. (2018). Groundwater resources and sustainable management issues in India. Clean and sustainable groundwater in India, 1-11.
Sasidharan, S., Bradford, S. A., Šimůnek, J. and Kraemer, S. R. (2020). Groundwater recharge from drywells under constant head conditions. Journal of hydrology, 583, 124569.

Scanlon, B. R., Reedy, R. C., Stonestrom, D. A., Prudic, D. E. and Dennehy, K. F. (2005). Impact of land use and land cover change on groundwater recharge and quality in the southwestern US. Global Change Biology, 11(10), 1577-1593.
Shahbazi, A., Saeidi, A. and Chesnaux, R. (2020). A review of existing methods used to evaluate the hydraulic conductivity of a fractured rock mass. Engineering Geology, 265, 105438.
Sharp, J. M. (2010). The impacts of urbanization on groundwater systems and recharge. AQUA mundi, 1(3).
Smerdon, B. D., Mendoza, C. A. and Devito, K. J. (2008). Influence of subhumid climate and water table depth on groundwater recharge in shallow outwash aquifers. Water Resources Research, 44(8).
Sowley, E. N. K. and Aboagye, E. (2010). Constraints to vegetable seed procurement and production in the Atebubu-Amantin District of Brong-Ahafo region of Ghana. Ghana Journal of Horticulture, 8, 85-91.
Stober, I. and Bucher, K. (2015). Hydraulic conductivity of fractured upper crust: insights from hydraulic tests in boreholes and fluid-rock interaction in crystalline basement rocks. Geofluids, 15(1-2), 161-178.
Sunkari, E. D., Abu, M. and Zango, M. S. (2021). Geochemical evolution and tracing of groundwater salinization using different ionic ratios, multivariate statistical and geochemical modeling approaches in a typical semi-arid basin. Journal of Contaminant Hydrology, 236, 103742.
Tahiru, A. A., Doke, D. A. and Baatuuwie, B. N. (2020). Effect of land use and land cover changes on water quality in the Nawuni Catchment of the White Volta Basin, Northern Region, Ghana. Applied Water Science, 10(8), 1-14.
Taylor, R. G., Scanlon, B., Döll, P., Rodell, M., Van Beek, R., Wada, Y., ... and Treidel, H. (2013). Ground water and climate change. Nature climate change, 3(4), 322-329.
Togbévi, Q. F., Van Der Ploeg, M., Tohoun, K. A., Agodzo, S. K. and Preko, K. (2022). Assessing the Effects of Anthropogenic Land Use on Soil Infiltration Rate in a Tropical West African Watershed (Ouriyori, Benin). Applied and Environmental Soil Science, 2022.
Varade, A. M., Khare, Y. D., Yadav, P., Doad, A. P., Das, S., Kanetkar, M. and Golekar, R. B. (2018). 'Lineaments' the potential groundwater zones in hard rock area: a case study of basaltic terrain of WGKKC-2 watershed from Kalmeswar Tehsil of Nagpur District, Central India. Journal of the Indian Society of Remote Sensing, 46, 539-549.
Wakode, H. B., Baier, K., Jha, R. and Azzam, R. (2018). Impact of urbanization on groundwater recharge and urban water balance for the city of Hyderabad, India. International Soil and Water Conservation Research, 6(1), 51-62.
Yesilnacar, M. I. and Sahinkaya, E. (2012). Artificial neural network prediction of sulfate and SAR in an unconfined aquifer in southeastern Turkey. Environmental Earth Sciences, 67, 1111-1119.
Yidana, S. M. and Yidana, A. (2010). An assessment of the origin and variation of groundwater salinity in southeastern Ghana. Environmental Earth Sciences, 61(6), 1259-1273.
Yidana, S. M., Ophori, D. and Banoeng-Yakubo, B. (2008). Hydrogeological and hydrochemical characterization of the Voltaian Basin: the Afram Plains area, Ghana. Environmental Geology, 53(6), 1213-1223.
Yidana, S. M., Ophori, D. and Alo, C. A. (2014). Hydrogeological characterization of a tropical crystalline aquifer system. Journal of Applied Water Engineering and Research, 2(1), 13-24.
Yidana, S. M., Vakpo, E. K., Sakyi, P. A., Chegbeleh, L. P. and Akabzaa, T. M. (2019). Groundwater–lakewater interactions: an evaluation of the impacts of climate change and increased abstractions on groundwater contribution to the Volta Lake, Ghana. Environmental Earth Sciences, 78(3), 1-16.
Yifru, B. A., Chung, I. M., Kim, M. G. and Chang, S. W. (2021). Assessing the effect of land/use land cover and climate change on water yield and groundwater recharge in East African Rift Valley using integrated model. Journal of Hydrology: Regional Studies, 37, 100926.
Zhang, H., Shi, Z., Wang, G., Sun, X., Yan, R. and Liu, C. (2019). Large earthquake reshapes the groundwater flow system: Insight from the water-level response to earth tides and atmospheric pressure in a deep well. Water Resources Research, 55(5), 4207-4219.
Zhu, K., Bayer, P., Grathwohl, P. and Blum, P. (2015). Groundwater temperature evolution in the subsurface urban heat island of Cologne, Germany. Hydrological processes, 29(6), 965-978.
Zomlot, Z., Verbeiren, B., Huysmans, M. and Batelaan, O. (2017). Trajectory analysis of land use and land cover maps to improve spatial–temporal patterns, and impact assessment on groundwater recharge. Journal of Hydrology, 554, 558-569.

Available online at www.asric.org
ASRIC Journal on Natural Sciences Vol 3(1) (2023) 237-247

Potential Applications of Débélé Clays (Guinea): Formulation of Ceramic Compositions and Hydraulic Binders

Balde Mamadou Yaya[1,2,3*], Sidibe Diaka[4], Simo Bakam Éric Severin[1], Djangang Njiomou Chantale, Blanchart Philippe[5]

[1] University of Yaoundé1 /Laboratory of Applied Inorganic Chemistry/BP 812 Cameroon.
[2] Université Gamal Abdel Nasser de Conakry/Laboratoire de chimie physique et colloidale, BP 1147 Conakry, Guinea
[3] Centre de Recherche en Gestion des Déchets (CREGED), BP 1147, Nongo - Conakry, Guinea
[4]Institut Supérieur des Mines et Géologie de Boké (ISMGB), BP: Boké, Guinea
5 Institute of Research for Ceramics - IRCER, Limoges, France

*Corresponding author: baldez201073@gmail.com

Abstract
This study demonstrates the potential uses of two clays collected from Débélé (Guinea). Based on their physicochemical properties, ceramic and hydraulic binder formulations were carried out. The physicomechanical properties of ceramic specimens and cements based on these clays attest to their use in these different fields. Both varieties are suitable for dense ceramic compositions with good dimensional stability on firing. In addition, the melting character of the mineral muscovite, the second main constituent of these clays, contributed to geopolymer gel formation and product compactness. These results also attest to the pozzolanic and amorphous character of Débélé clays, containing over 50% clay minerals, and their application in the formulation of hybrid cements and geopolymer binders.
Key words: Clay, hydraulic binder, ceramic, geopolymer, physicomechanical properties.

1. Introduction
In addition to bauxite, Guinea's main mineral resource, clays occupy a prime position due to their abundance and the many possible applications of these minerals on an industrial scale [1, 2]. This is evidenced by their use as raw materials to manufacture various products, or as additives to a raw material to create or improve the functional properties of new products in response to changing uses [3, 4, 5, 6]. However, despite increasing consumption of manufactured products derived from these minerals, their production remains underdeveloped in some countries, such as Guinea. Indeed, clays, classic raw materials in cement and ceramic matrices, have until now only been exploited for artisanal pottery. Yet these resources can be transformed into basic building materials for walls, roofs and floors, providing a solution to the precarious housing situation that is still a preoccupation in developing countries. Portland cement, the world's most widely used building material since its invention in the 1950s, is still the subject of a great deal of scientific and technical research to improve its properties, durability and cost.
What's more, its manufacture leads to the release of greenhouse gases, which implies a concern for compliance with environmental standards [7, 8]. The partial substitution of a certain quantity of Portland

cement by minerals, when they are available at competitive prices, has proved advantageous, not only from an economic and ecological point of view, but also in terms of product performance [9, 10]. The challenge of optimising compositions and the process needed to manufacture products with satisfactory usage characteristics at minimum production cost also involves the availability and control of raw material characteristics [7, 8]. This is without ignoring the specific case of Guinea, where the development of local resources as a contribution to sustainable development is a permanent political concern. For this reason, the availability and easy access to these clay materials on Guinean territory is an opportunity to be seized in order to reduce the cost of transporting manufactured products and to promote job creation. This will help to make the most of these resources in the construction sector and stimulate investment with a view to creating local businesses and industries to exploit these raw materials efficiently, with the potential to reduce the cost of housing. This study presents the potential applications of Débélé clays in ceramics, hybrid cement and ecological or geopolymer cement. Ceramic formulation tests are being carried out to assess the possibility of using these clays in this field. Hybrid cement formulations, in which 20% by mass of portland cement is substituted by raw clay calcined at 600°C and geopolymer cement, are also being carried out. Clay powders activated at 600, 700 and 800°C were used for this purpose. The physicomechanical properties of all the ceramic, hybrid cement and geopolymer specimens were evaluated and compared with standard norms.

2. Materials and methods

2.1 Materials

The two clays (Figure 1) used in this work come from Débélé, Kindia prefecture (Republic of Guinea). They are named ABD and ARD respectively because of their colour; the former is white and the latter reddish [11].

Figure 1: Aspects of raw clay samples from Débélé (Kindia, Guinea)

The physicochemical and mineralogical characterisation of the samples, previously determined, are presented in Table I [11, 12, 13].

Table I: Physicochemical and mineralogical characteristics of clays

Components	*ABD*	*ARD*
Physical parameters		
Absolute density (g/cm^3)	2.4	2.5
Active specific surface area (m^2/g)	42.2	23.3
Mass (mg) of CH fixed per 1g of sample activated at 600°C	1107.4	796.2
Amorphous phase content of powders activated at 600°C (%)	71.9	63.5

Mechanical activity index of powders activated at 600°C (%)	93.5	88.1
Linear shrinkage on firing at 1200°C (%)	4.5	3.8
Plasticity index	25	23
Clay phase: 2<Φ< 20 µm	51.6	48.5
Clay phase: Φ < 2µm (%)	48.5	51
Chemical composition		
SiO_2	52.40	51.20
Al_2O_3	30.90	30.40
Fe_2O_3	1.80	3.70
K_2O	5.90	4.80
TiO_2	1.60	1.60
MgO	0.50	0.40
CaO	0.10	0.10
Na_2O	0.20	0.10
P_2O_5	0.10	0.10
Cr_2O_3	0.02	0.02
SO_3	0.13	0.030
MnO	<0.01	<0.01
LOI	6.20	7.50
Total	99.74	99.96
Mineralogical composition (%)		
Kaolinite	57.4	55.1
Muscovite	27.0	19.9
Quartz	11.3	18.3
Hematite	1.8	/
Anatase	1.6	1.6
Gibbsite	0.6	0.5
Goethite	/	4.6
Total	99.70	100.00

2.2 Method

The ABD and ARB clay powders obtained by 75 µm wet sieving and drying were used to make the ceramic specimens, hybrid mortars and geopolymer pastes. The ceramic specimens are shaped using a laboratory hydraulic press, using 2 g and 50 g of mixture moistened with 2% water. This mixture is homogenised and poured into the corresponding mould to be compacted using a hydraulic press at a pressure of 0.4 KPa for the pellets and 0.7 KPa for the parallelepiped wafers. These specimens were then dried at room temperature (25°C) in the laboratory for 24 hours before undergoing heat treatment in a muffle furnace to be baked at 700, 800, 900, 1000 and 1100°C respectively. Hybrid mortars are formulated by substituting 20% by weight of portland cement with raw clay powders calcined at 600°C of each of the varieties with a water/cement

ratio (W/C) of 0.6. The mixture was introduced into a CONTROLAB automatic mixer (MIX MATIC) in accordance with standard NF EN 196-1. The geopolymer binders were also formulated with the two types of clay by mixing the powders activated at 600, 700 and 800°C with the liquid precursor in a solid/liquid (S/L) weight ratio equal to 1.20 for ABD and 1.11 for ARD. All the specimens: ceramics, mortars and geopolymers were subjected to various physical tests: apparent density, water absorption rate, open porosity and mechanical tests: compressive strength for mortars and geopolymers, flexural strength for ceramics in accordance with standard norms [14, 15, 16].

3. Results and discussion

3.1 Characteristics of the ceramic specimens

The firing products of the clays all have a smooth appearance whatever the temperature, which means that they are well vitrified and less porous. In addition, the specimens of both clays retain a light colour, which can be modified if necessary by adding colouring oxides (Figure 2).

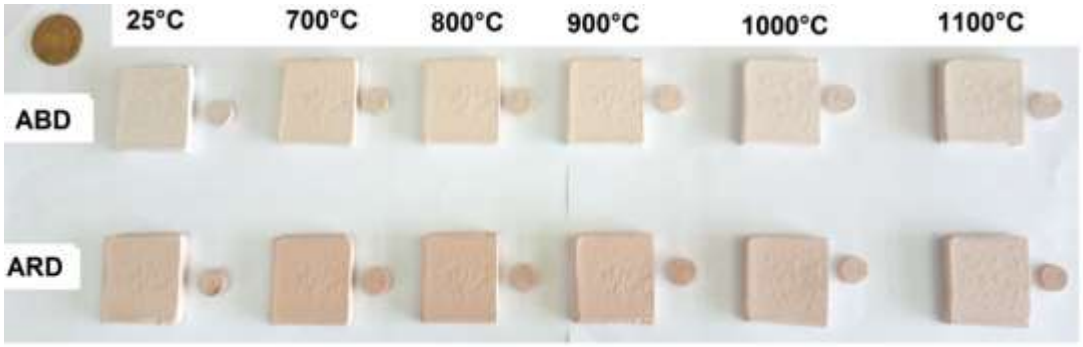

Figure 2: Appearance of specimens before and after firing

After heat treatment between 700 and 1100°C, these specimens have properties close to those of vitrified ceramics (Figure 3): density varies from 2.1 to 2.5 g/cm^3 for ABD and from 1.5 to 1.8 g/cm^3 for ARD; open porosity decreases from 24.8 to 10.7% for ABD and from 34 to 14.7% for ARD with a consequent water absorption rate that varies from 12.7 to 8.6% and from 17.4 to 11.7% for ABD and ARD respectively; flexural strength increases from 7.2 to 20.1 MPa for ABD and from 5.3 to 14.8 MPa for ARD [17, 18, 19]. Another factor to take into account is the contribution of fine quartz particles, which dissolve earlier in the viscous flow. The effect of these fine particles on the densification process remained lower than that of kaolinite and muscovite. This is consistent with the higher densification rate in ABD with its high clay mineral content (Table I) compared to ARD. The characteristics and properties of the ceramic compositions obtained confirm the fluxing nature of the two clays; parameters necessary for obtaining vitrified ceramics [4, 20, 21, 22, 23].

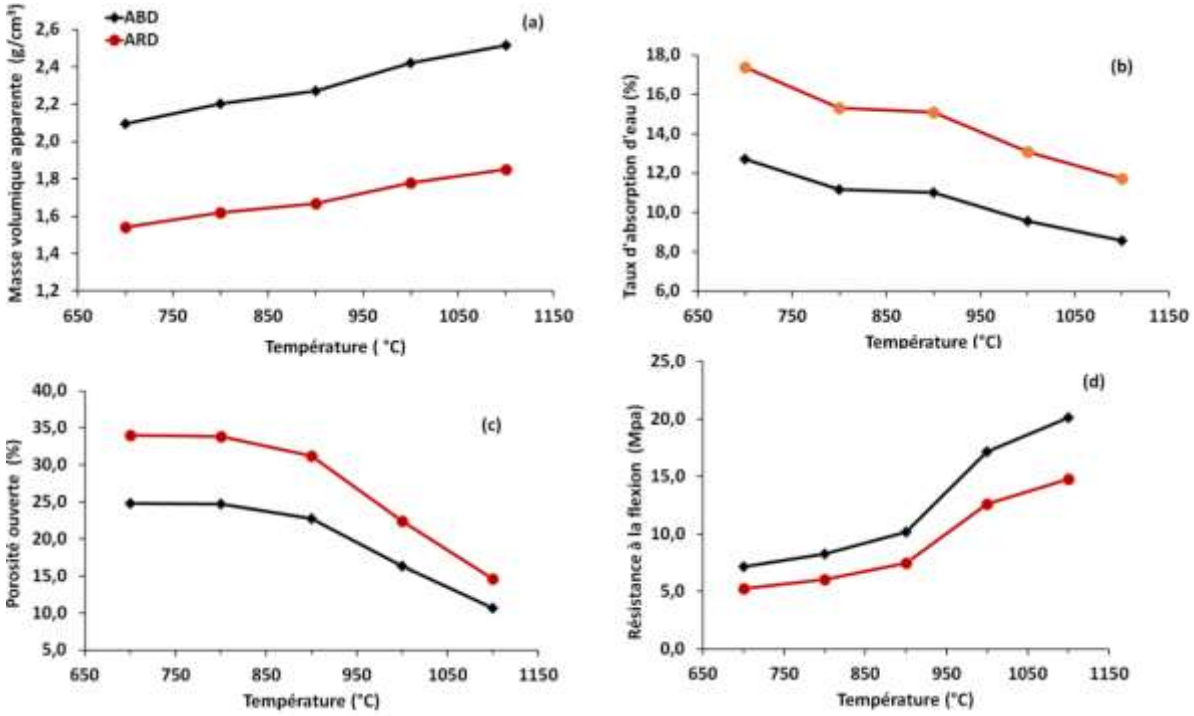

Figure 3: Changes in physical properties as a function of firing temperature.

3.2 Physicomechanical properties of mortars

Various physicomechanical characterisation tests were carried out on mortar specimens (Figure 4) in the hardened state at 7, 28, 45 and 90 days. Expressed as a percentage, the average values for open porosity (π) and water absorption rate (W) are shown in Figure 5. A decrease with age in these parameters is generally observed. Porosity ranged from 21 to 13.80% and water absorption from 11.20 to 5.24%.

Figure 4:: Appearance of ARD and ARD clay-based mortar specimens

Furthermore, it appears that the first few days of curing are the most important in terms of water absorption, which decreases over time. This finding is related to the porosity and the higher degree of reactivity of the calcined forms. It is also in line with the level of CH fixed as observed in the Modified Chapelle Test. The

decrease in pore density and water absorption rate is explained by the chemical activity (hydration) leading to accelerated formation of secondary hydrates, CSH, which result in the filling of pores between particles within the matrix [24, 25, 26, 27].

In addition, the decrease in π and W with specimen age provides a means of predicting the mechanical performance (Figure 6) and durability of formulated mortars [28, 29]. Analysis of the test results for apparent density (ρa) and compressive strength (Rc) shows a slight change in ρa and Rc with the age of the specimens. In both series of mortars, the density varies between 1.8 and 2 g/cm^3 and the overall strength varies between 15 and 43.65 MPa. While the apparent density of the hybrids remains lower than that of the control mortar, their mechanical strength has increased significantly**.** In fact, for powders calcined at 600°C, the strength of these hybrids is greater than that of the control from the age of 45 days. This behaviour is related to the pozzolanicity index (Table I) of the clays, which favours cement hydration and the intensification of chemical reactions thanks to the consumption of portlandite. As a result, additional hydrates, CSH, are formed and precipitated, which are responsible for the long-term compactness of the matrix [27, 30, 31].

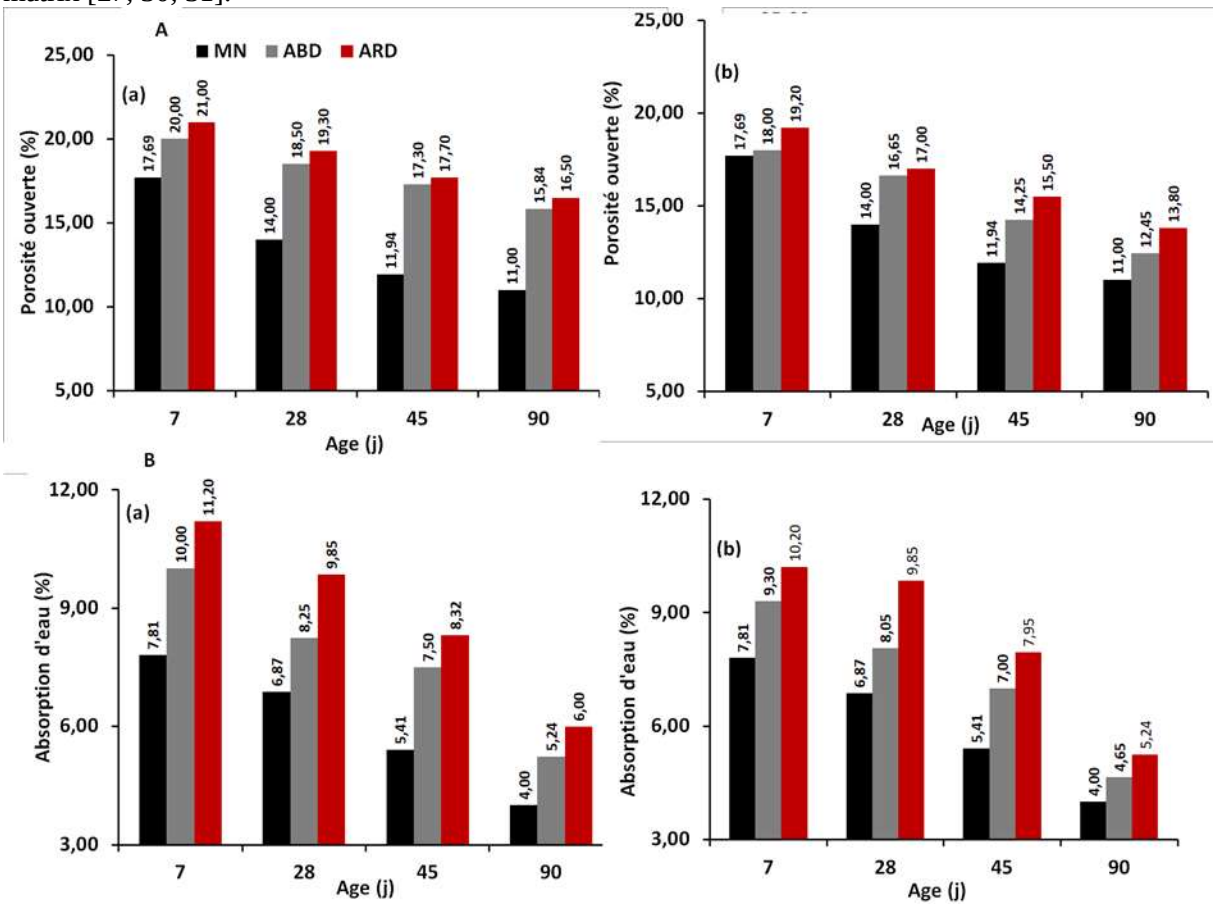

Figure 5:: Changes in open porosity and water absorption as a function of mortar age: (a & c) raw clay-based; (b & d) calcined clay-based.

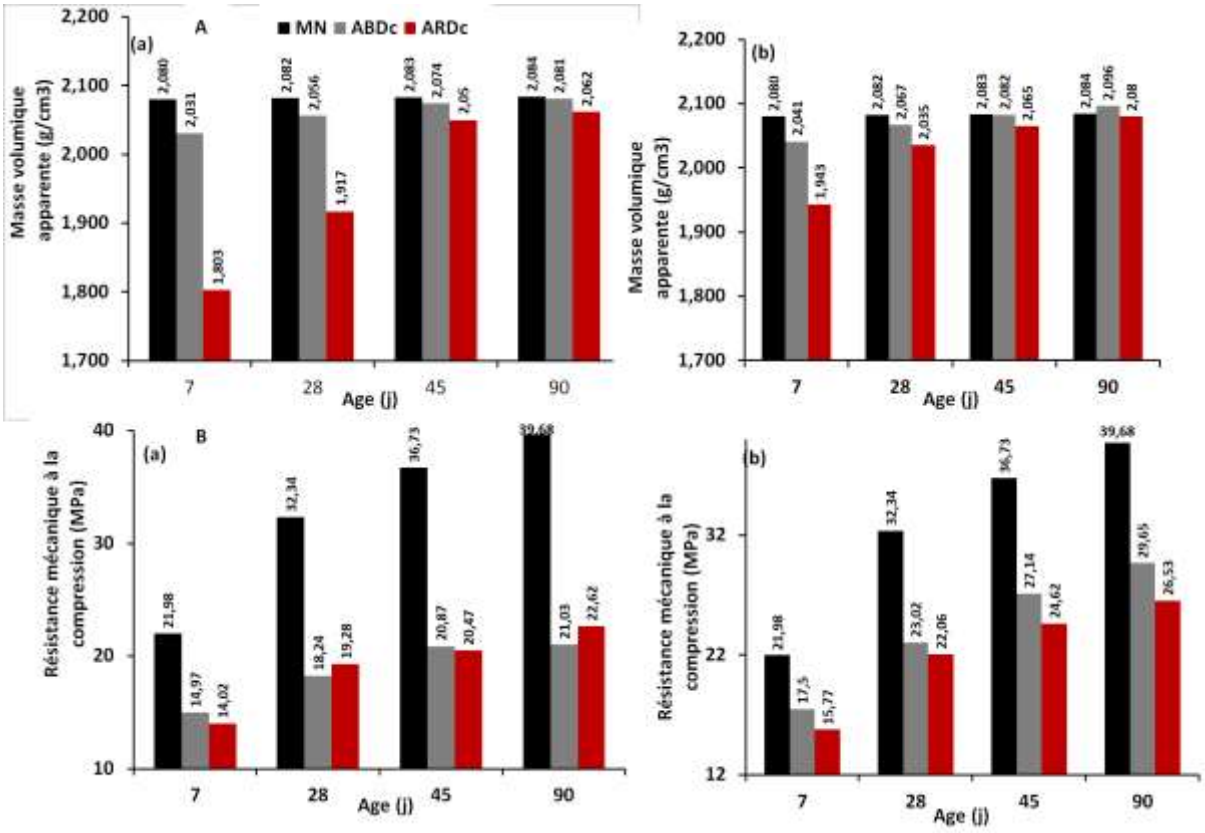

Figure 6: Development of bulk density (ρa) and compressive strength as a function of age of mortars: a) based on raw clays; b) based on calcined clays.

It can be concluded that the development of the density and mechanical strength of the products correlates well with the chemical/mineralogical composition, the amorphous phase content, the mass of CH fixed and the mechanical activity index recorded in Table I. This behaviour is also due to the pozzolanic characteristics of calcined clays. This behaviour is also due to the pozzolanic characteristics of calcined clays [30, 32]. For example, calcined clay-based hybrids are suitable for masonry applications in contact with aggressive environments (waste water, soil, seawater, etc.) in accordance with Belgian standard NBN EN 1052-1, which requires a strength of 20 MPa [33, 34, 45].

3.3 Physicomechanical properties of geopolymer binders

The appearance of geopolymer binder specimens on demoulding and at day 42 is illustrated in Figure 7. These specimens are characterised by the absence of any surface defects such as efflorescence, a common phenomenon in aluminosilicate-based geopolymers [36, 37].

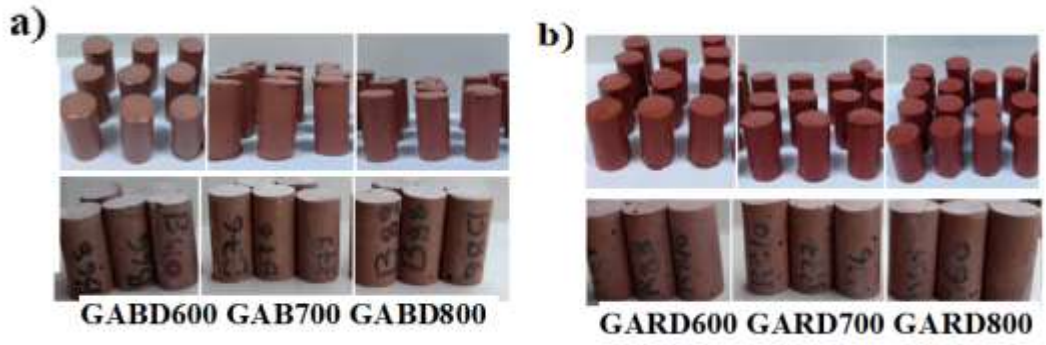

Figure 7: Appearance of geopolymer specimens

The absence of efflorescence is due to the rapidity of the dissolution rate, which does not favour infiltration of CO2 from the air into the geopolymer matrix. In addition, the specimens retained their shape from demoulding through to the test periods, a sign of good consolidation and a good seal, confirming their stability over time. In addition, the activation temperature of the powders had a remarkable effect on the development of the apparent density (Figure 8A) of the binders obtained, which increased with the age of the specimens. The density of GABD binders varies between 2.92 and 2.47 cm^3 and that of GARD binders between 1.86 and 2.16 cm^3.

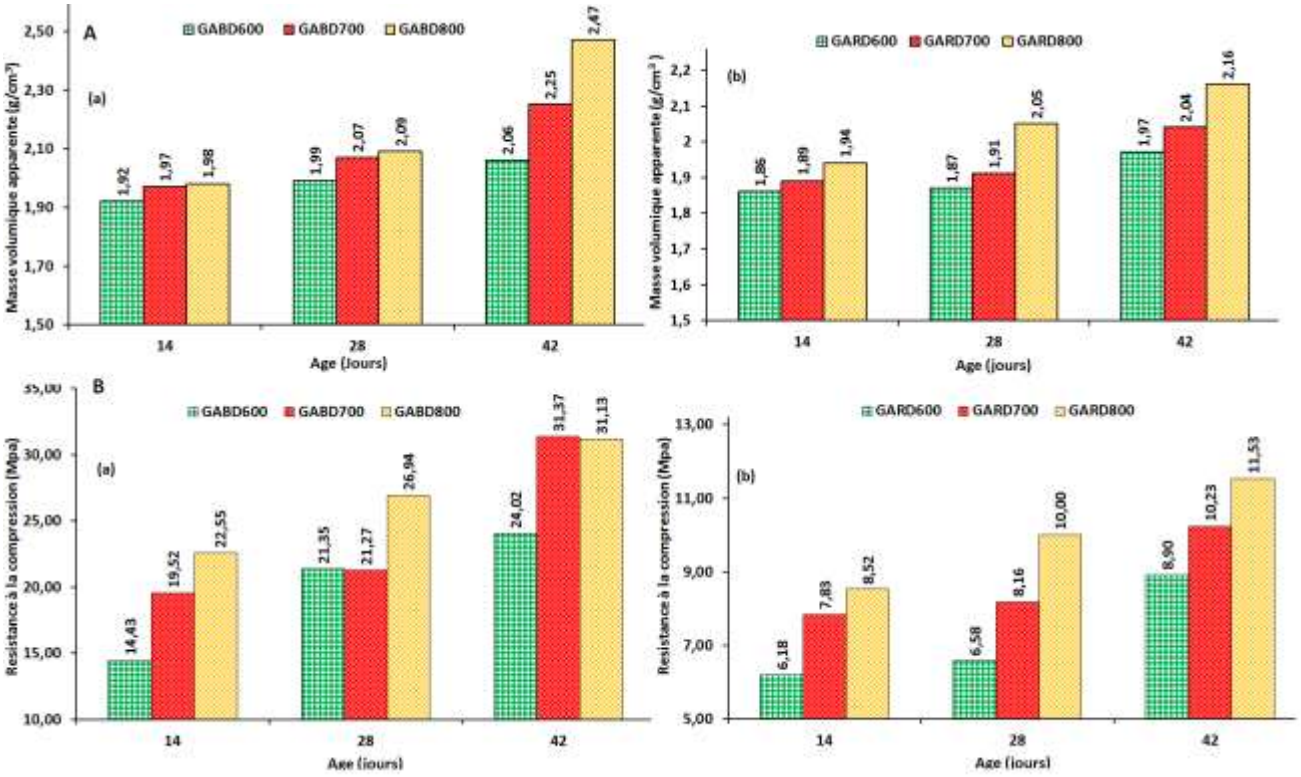

Figure 8: Apparent density (A) and mechanical compressive strength (B) as a function of age for a) GABD and b) GARD specimens.

As a result, the products are denser in the first case than in the second. In fact, the geopolymerisation process is more intense in ABD-based formulations containing the highest proportions of kaolinite and muscovite (Table I). These minerals therefore contributed favourably to densification and the development of mechanical performance (Figure 8B) [38, 39]. Specimens from the GABD series have the best mechanical performance, varying between 14.43 and 31.37 MPa, while those from the GARD series oscillate between 6.18 and 11.56 MPa. In short, the amorphous phase content and thermal transformation of muscovite as a flux mineral have played a largely favourable role in the development of mechanical strengths, which are acceptable for certain applications, as demonstrated by the work of Yang et al. [40].

4. Conclusion

The aim of this work was to experiment with the application of two varieties of clay from Débélé (Guinea) in ceramic compositions and the formulation of hydraulic binders. The results obtained showed the following:

- ✓ the ceramic specimens based on the two clays treated between 700 and 1100°C have properties close to those of vitrified ceramics: bulk density greater than 2 g/cm^3 for ABD and greater than 1.5 g/cm^3 for ARD ; open porosity decreases from 24.8 to 10.7% for ABD and from 34 to 14.7% for ARD with a consequent water absorption rate that varies from 12.7 to 8.6% and from 17.4 to 11.7% for ABD and ARD respectively; flexural strength increases from 7.2 to 20.1 MPa for ABD and from 5.3 to 14.8 MPa for ARD. In addition, the specimens of the two clays retain a light colour, which can be modified if necessary by adding colouring oxides;
- ✓ the substitution of 20% by mass of portland cement by raw clay powders calcined at 600°C for the formulation of mortars shows that these additions are chemically active mineral additives. All the physico-mechanical properties of hybrid mortars show acceptable values and normal development.: reduction in porosity and water absorption on the one hand, and development of the apparent densities and mechanical strength of the specimens on the other. With a minimum mechanical strength of 15 MPa at the youngest age, it offers a wide range of masonry applications in the formulation of less expensive hydraulic binders as provided for in technical standards for the construction of buildings and other structures;
- ✓ the specimens of geopolymer binders obtained show good consolidation from demoulding, which continues with age. On the 42nd day, depending on the activation temperature of the precursors, the specimens had an apparent density of between 2.06 and 2.47 g/cm^3 for GABD and between 1.97 and 2.16 g/cm^3 for GARD, with decreasing porosity favouring appreciable development of the mechanical compressive strength, with a minimum of 11.53 MPa and a maximum of 31.37 MPa. Muscovite, a fluxing mineral, has contributed to the increase in amorphous rates and to the geopolymerisation process. These products can therefore be used as construction materials for structures where waterproofing is required.

5. References

1. Kakali G, Perraki T, Tsivilis S, Badogiannis E. *Thermal treatment of kaolin: the effect of mineralogy on the pozzolanic activity*. Applied Clay Science 20, 73–80 (2001).
2. Benkaddour M., Kazi F., Aoual A. S. *Durabilité des mortiers à base de pouzzolane naturelle et de pouzzolane artificielle*. Revue Nature et Technologie. 01, 66-73 (2009).
3. Njopwouo D. *Minéralogie et physico-Chimie des argiles de Bomkoul et de Balengou (Cameroun) Utilisation dans la polymérisation du styrène et dans le renforcement du caoutchouc naturel*. Thèse PhD, Université de Yaoundé I (1984).
4. Djangang N C. *Argiles kaolinitiques de Mayouom et de Mvan : caractérisation et utilisation dans l'élaboration des matériaux réfractaires*. Thèse de l'Université de Yaoundé 1p.131 (2007).

5. Essaidi, N., Leybros, P., Joussein, E., & Rossignol, S. *The Role of Alkaline Earth Ions in Geopolymer Binder Formation.* Developments in Strategic Ceramic Materials II: Ceramic Engineering and Science Proceedings Volume 37, Issue 7, 37, 83-92. (2017).
6. Qlihaa S., Dhimni F., Melrhaka N., Hajjaji A., Srhiri J. *Caractérisation physico-chimique d'une argile Marocaine*. Mater. Environ. Sci. 7 (5) 1741-1750 (2016).
7. Alonso S. & Palomo A. *Alkaline activation of métakaolin and calcium hydroxide mixtures: influence of temperature, activator concentration and solids ratio*. Materials Letters, volume 47(1-2) 55-62 (2001).
8. Pascual A. B., Yahiya A., Nkinamubanzi P. C. *Élaboration de nouveaux liants minéraux pour la formulation de bétons écologiques et durables*. Doctoral dissertation, Université de Sherbrooke (2014).
9. Bich C, J. Ambroise, J. Péra. *Influence of degree of dehydroxylation on the pozzolanic activity of metakaolin*. Applied Clay Science 44, 194–200 (2009).
10. Kazi A-B F., Semcha A. et Kerdal D. *Influence des additions minérales sur la résistance mécanique des mortiers*. Afrique Science 07(2)16–26 (2011).
11. Baldé M Y. Caractérisation physicochimique des aluminosilicates (argiles et bauxite) de Kindia, Guinée: application dans la formulation des mortiers hydrauliques et des compositions céramiques. Thèse de l'Université de Yaoundé 1 (Cameroun)., p154. (2022)
12. Balde M.Y., Njiomou Djangang C., Bah A., Blanchart P., Njopwouo D., Effect of physicochemical characteristics on the use of clays from Kindia (Guinea) in ceramic compositions. Int. J. App. Cer. Tech., 18(3) (2021) 1033-1042. doi:10.1111/ijac.13669.
13. Segalen P. *Note sur une méthode de détermination des produits minéraux amorphes dans certains sols à hydroxydes tropicaux*. Cahier ORSTOM Série Pédol (4) 105-126 (1968).
14. ISO 17138. *Fine ceramics (advanced ceramics, advanced technical ceramics) — Mechanical properties of ceramic composites at room temperature — Determination of flexural strength* (2014).
15. EN 196-1. *Méthodes d'essais des ciments - Partie 1: détermination des résistances mécaniques* (2006).
16. ISO N. 5017 (A). *Dense Shaped Refractory Products-Determination of Bulk Density, Apparent Porosity and True Porosity-products refractories fagonnes densest*, AFNOR, Saint-Denis, France (2013).
17. Elimbi A, Dika JM, Djangang NC. *Effects of alkaline additives on the thermal behavior and properties of Cameroonian poorly fluxing clay ceramics*. Journal of Minerals and Materials Characterization and Engineering.;2:484–501 (2014).
18. Lao, X., Xu, X., Jiang, W., Liang, J., Miao, L., & Wu, Q. *Influences of impurities and mineralogical structure of different kaolin minerals on thermal properties of cordierite ceramics for high-temperature thermal storage*. *Applied Clay Science*, *187*, 105485. (2020).
19. Dolinar, B., Miŝiĉ, M., & Trauner, L. *Correlation between surface area and Atterberg limits of fine-grained soils*. Clays and Clay Minerals, 55(5), 519-523(2007).
20. Dondi M., Guarini G., Ligas P., Palomba M., Raimondo M. *Chemical mineralogical and ceramics properties of kaolinitic materials from the Tresnuraghes mining District (Western Sardina, Italy)*. Applied clay science, 18, 145-155 (2001).
21. Artigas, R., Rodas, M., Sanchez, C. J., Mas, R., Dondi, M., & Arribas, J. *Clayey materials from the Sierra de la Demanda Range (Spain): their potential as raw materials for the building ceramics industry*. Clay minerals, 40(1), 25-41(2005).
22. AFNOR EN 100, Carreaux et dalles céramiques, Détermination de la résistance à la flexion p 7 (1982).
23. Baccour-Zghal H., Medhioub M. & Mhiri T. *Caracterisation physicochimique et mécanique de matériaux Céramiques obtenus à partir des argiles tunisiennes. Verres*, Céramiques & Composites, Vol.1, N°2, 25-33 (2011).
24. Igwilo K., Okolie S., Anawe P., Roland O., Odo J., *Evaluation of the effects of alcohol on de-emulsification of niger delta crude oil using commercial de-emulsifiers*. Open J. Yangtze Oil Gas, 2(3) 168-175(2017). doi:10.4236/ojogas.2017.23013
25. Brykov A.S., Vasil'ev A.S., Mokeev M.V. *Hydration of Portland cement in the presence of high activity aluminum hydroxides*. Russ. J. Appl. Chem., 85(12) 1793-1799. (2012) doi:10.1134/S1070427212120014.
26. Zingg L.. *Influence de la porosité et du degré d'humidité interne sur le comportement triaxial du béton*. Thèse de doctorat. Grenoble, (2013).

27. Savadogo N.. *Élaboration et caractérisation d'un écociment à base de poudre de mâchefer de charbon minéral*. Thèse de doctorat. INSA de Rennes, (2017).
28. Bur N., Roux S., Delmas L., Géraud Y., Feugeas F. *Porosité des mortiers et bioréceptivité. Matériaux & Techniques*, 98(1) 31-40. (2010) doi:10.1051/mattech/2009047.
29. Rabehi M. *Apport à la caractérisation de la porosité ouverte du béton d'enrobage par l'utilisation des tests d'absorption capillaire*. Thèse de doctorat. Université Mohamed Khider Biskra, (2014).
30. Tchamo Leussa C. C., Libessart L., Djelal C., Njiomou Djangang C., Elimbi A. *Pozzolanic activity of kaolins containing aluminum hydroxide*. Sci. Rep., 10(1) 13230 (2020). doi:10.1038/s41598-020-70146-3.
31. Ndiaye M., Dine M., Diop M.B., Ngom P.M. *Pozzolanic Activity of Old Volcanic Tuffs of Mako Area (Senegal-Oriental, West African Craton): An Economic and Environmental* Interest. Int. J. Geosci., 10(3) 12 (2019). doi:10.4236/ijg.2019.103014.
32. Ribeiro D.V., Silva A.S., Labrincha J.A., Morelli M.R. *Rheological properties and hydration behavior of portland cement mortars containing calcined red mud*. Can J Civ Eng, 40(6) 557-566(2013). doi:10.1139/cjce-2012-0230.
33. Khaleel O.R. and Abdul Razak H. *The effect of powder type on the setting time and self compactability of mortar.* Constr. Build. Mater., 36 20-26(2012). doi: 10.1016/j.conbuildmat.2012.04.079.
34. Smits A., Grégoire Y., *CSTC, N°3 et N°4 - Spécifications européennes sur la résistance en compression des produits de maçonnerie, Bruxelles, Centre scientifique et Technique de la Construction.* (2009).
35. Balde M. Y., Djangang N. C., Balde S., Simo Bakam E. S., and Blanchart P. *Physicomechanical Properties of Mortars Based On Ordinary Portland Cement with Bauxite as Mineral Additives*. European Journal of Advanced Chemistry Research. http://dx.doi.org/10.24018/ejchem..3.3.105(2022).
36. Elimbi A., Tchakoute H.K., Njopowouo D. *Effets of calcination temperature of kaolinite clays on the properties of geopolymer cements*. Construction and Building Materials 52 2805-2812. (2011).
37. Tchakoute K.H., Mbey J.A., Elimbi A., Diffo Kenne B.B., Njopwouo D. *Synthesis of volcanic ash-based geopolymer mortars by volcanic by fusion method: Effect of adding metakaolin to fused volcanic ash.* Ceramics International 39 1613-1621(2013).
38. Jouenne C. A. *Traité de céramiques et matériaux minéraux*. Septima. Paris, 657p (2001).
39. Lecomte, G.L., Bonnet, J. P. and Blanchart, P. *A Study of the Influence of Muscovite on the Thermal Transformations of Kaolinite from Room Temperature up to 1100°C*. Journal of Materials Science, 42, 8745-8752 (2007). https://doi.org/10.1007/s10853-006-0192-7.
40. Yang T., Chou C., Chien C. *The Effects of Foaming Agents and Modifiers on a Foamed-geopolymer*. Advances in Civil, Environmental, and Materials Research (ACEM' 12), Seoul, Korea, August 26-30 (2012)